BCEE2

Conference Proceedings

The Second International Conference on Buildings, Construction & Enviromental Engineering

BCEE2

October 17-18, 2015 - Beirut, Lebanon

Vol. III, Geotechnical & Geological Engineering

The 2nd International Conference of Buildings, Construction and Environmental Engineering (BCEE2-2015)

SUPREME COMMITTEE

1. **Prof. Amin D. Thamir, UOT, Iraq/ Chair**
2. **Prof. Ryiad H. Hadi, UOT, Iraq**
3. **Prof. Makram Suidan, AUB, Lebanon**
4. **Prof. Mohamed Harajli, AUB, Lebanon**
5. **Eng. Estabraq I. El-Showq, MOCH, Iraq**
6. **Eng. Ibrahem Mustafa, Mayoralty of Baghdad, Iraq**
7. **Eng. Raad A. Abdulamir, MOWR, Iraq**
8. **Eng. Fouad A. Hamid, NIC, Iraq**

INTERNATIONAL ADVISORY COMMITTEE

1. **Prof. Riadh S. Al-Mahaidi, Swinburne University, Australia/Chair**
2. **Prof. Muthana H. Al-Dahan, University of Missouri, USA**
3. **Prof. Husham Al-Mansour, National Research Council, Canada**
4. **Prof. Tom Schanz, Ruhr University Bochum, Germany**
5. **Prof. Siamak Yazdani, North Dakota State University, USA**
6. **Prof. Andrzej M. Brandt, Polish Academy of Sciences, Poland**
7. **Prof. Caijun Shi, Hunan University, China**
8. **Prof. Namir K. Al-Saoudi, Australia**
9. **Prof. Hanaa A. Yousif, University of Akron, USA**
10. **Prof. Mohamed N. Hadi, University of Wollongong, Australia**

ORGANIZING COMMITTEE

1. **Prof. Ryiad H. Hadi, UOT, Iraq / Chair**
2. **Assoc. Prof. Ghassan Chehab, AUB, Lebanon/Co-Chair**
3. **Prof. Tareq S. Hadi, UOT, Iraq/ Co-Chair**
4. **Assist. Prof. Issam Srour, AUB, Lebanon**
5. **Assist. Prof. George Saad, AUB, Lebanon**
6. **Assist. Prof. Faris H. Mohammed, UOT, Iraq**
7. **Assist. Prof. Hasan H. Joni, UOT, Iraq**
8. **Assist. Prof. Mohammed A. Mahmoud, UOT, Iraq**
9. **Ms. Zakeya Deeb, AUB, Lebanon/ Exec Admin Assist**
10. **Mr. Helmi EL Khatib, AUB, Lebanon**

LOCAL SCIENTIFIC COMMITTEE

1. **Prof. Shakir A. Salih, UOT, Iraq / Chair**
2. **Prof. Emu. Kaiss F. Sarsam, UOT, Iraq**
3. **Prof. Hussain H. Karim, UOT, Iraq**
4. **Prof. Nabeel A. Jadoo'a, UOT, Iraq**
5. **Prof. Hisham K. Ahmed, UOT, Iraq**
6. **Prof. Aqeel Al-Adili, UOT, Iraq**
7. **Prof. Abdulrazzaq T. Ziboon, UOT, Iraq**
8. **Prof. Mohammed Y. Fattah, UOT, Iraq**
9. **Prof. Abdulhameed M. Jawad, UOT, Iraq**
10. **Assoc. Prof. Shadi Najjar, AUB, Lebanon**
11. **Assist. Prof. Abbas K. Zidan, UOT, Iraq**
12. **Assist. Prof. Waleed A. Abbas, UOT, Iraq**
13. **Assist. Prof. Hasan A. Omran, UOT, Iraq**
14. **Assist. Prof. Falah H. Rahil, UOT, Iraq**
15. **Assist. Prof. Mahmoud S. Mahdi, UOT, Iraq**
16. **Assist. Prof. Maan S. Hassan, UOT, Iraq**
17. **Dr. Hussain L. Zamil, MOWR, Iraq**
18. **Dr. Suhair K. Al-Habbobi, MOCH, Iraq**
19. **Eng. Ammar M. Abdulrassol, NIC, Iraq**
20. **Assist. Prof. Nisreen S. Mohammed, UOT, Iraq / Rapporteur and Secretary**
21. **Dr. Wael Shawky Abdulsahib, UOT, Iraq / Rapporteur and Secretary**

SPONSORS OF THE CONFERENCE

Our thanks and appreciation to the supporting points of the Conference

Ministry of Higher Education and Scientific Researches, Iraq

Hanwha Engineering and Construction Bismayah Project, Iraq

Veolia For Water Technology CO. France

Fugro - Maps, Lebanon

Al-Tariq Engineering Bureau for Pile Testing Iraq

PREPARATION COMMITTEE OF THIS BOOK

1. **Prof. Dr. Aqeel Al-Adili**
2. **Dr. Wael Shawky Abdulsahib**
3. **Dr. Bassman R. Muhammad**
4. **Eng. Luay Yaly**

REVIEWERS OF THIS TOPIC

1. **Prof. Dr. Hussein H. Karim**
2. **Prof. Dr. Saad Farhan Ibrahim**
3. **Prof. Dr. Raid R. Al-Omari**
4. **Prof.Dr. Aqeel Al-Adili**
5. **Prof. Dr. Mohammed Y. Fattah**
6. **Dr. Mahmoud Rasheed**
7. **Dr. Nahla Salim**
8. **Ass. Prof. Husam H. Baqir**
9. **Dr. Falah Hassan Rahil**
10. **Dr. Mohammed Abdulateef**
11. **Dr. Qassyun Saad Aldeen**
12. **Dr. Abbas Fadhel Ibrahim**
13. **Dr. Ameen Ibrahim**
14. **Dr. Anwar Luay Al-Obeydi**
15. **Dr. Bushra S. Zbar**
16. **Dr. Haifa Abd Rassol Ali**
17. **Dr. Karim H. Al-Helo**
18. **Dr. Khalid R. Mahmoud**
19. **Dr. Madhat Shakir**
20. **Dr. Mahdi Obaid Karkosh**
21. **Dr. Mahmoud D. Ahmed**
22. **Dr. Mohammed Shakir Alshakarchi**
23. **Dr. Mustafa A. Yousif**
24. **Dr. Namir G. Ahmed**
25. **Dr. Yasir M. Al-Badran**
26. **Dr. Zina Walled**
27. **Dr. Mahmoud T. Ahmed**
28. **Dr. Qassyun Saad Aldeen**

Table of Contents

The Behavior of Conical Shell Foundation under Dynamic Loads

Prof. Dr. Mohammed Y. Fattah [(1)] **Asst. Prof. Dr. Waleed A. Waryosh [(2)]**
Dr. Mohammed A. E. Al-Hamdani [(1)]

1. Building and Construction Engineering Department, University of Technology, Baghdad.
2. Civil Engineering Department, College of Engineering, Al-Mustansiriyah University, Baghdad.

Abstract— **Shell foundations present an economical alternative solution to the conventional plane foundations in case of heavy loads to be transmitted to low–bearing capacity soil. Shell foundations reveal high bearing capacity values which make them suitable in soft or weak soils. At the same time, these foundations are thin which makes the failure in concrete preceding the soil failure. Therefore, it is intended to improve concrete quality to increase its load carrying capacity and develop the shell foundation behavior to be close to conventional foundations.**

Reactive Powder Concrete (RPC) is an ultra-high strength, low porosity material with high cement and silica fume contents and steel fibers. In this study, conical shell footings are prepared which are composed of reactive powder concrete. Five values of steel fiber volume fractions of 0, 0.5%, 1.0%, 1.5%, and 2.0% were used in casting the shells, in order to study the effect of steel fiber content on the shear strength. Taking into consideration the aspect ratio of the fibers used and the type of concrete mix, a maximum of 2.0% fiber content was used in which the fibers were found to achieve a practical and uniform distribution within the fresh and hardened concrete. The finite element software ANSYS-Ver. 11 is used in the analysis. Harmonic option is used as a type of load that is applied as a function of time. It was concluded that the increase of thickness of the conical footing with and without ring beam will reduce vertical displacement due to increase the rigidity of footing but the footing with ring beam has more rigidity than footing without ring beam. The vertical displacement decreases with the increase of shell foundation thickness by about (4, 5, 6)% for (15 mm) shell thickness and for the three amplitudes of dynamic load (30 kN, 40 kN, 50 kN) and then increases obviously in the case of (20 mm) thickness by about (6, 11, 15) more than the (10 mm) thickness; the reference case, for the three amplitudes of dynamic load due to increase of self-weight of the shell foundation.

Keywords: Conical shell, footing, reactive powder concrete, dynamic, finite elements.

I. INTRODUCTION

he concept of shell footing is not new in foundation design, Tconsidering past constructions using inverted brick arch foundation. The use of inverted brick arches as foundation or footing has been in practice in many parts of the world for a long time. Shells in modern foundation engineering are however relatively new. Shell footings have been found to be economical foundations in areas having high material to labor cost ratio. Shell footing has greater load carrying capacity compared with flat shallow foundations. Moreover, shells are essentially thin structures, thus structurally more efficient than flat structures. This is an advantage in situations involving heavy super structural loads to be transmitted to weaker soils (Vesic, 1975).

Shell footing in foundation engineering however is limited to a few geometries, such as conical, pyramidal, hyper, spherical and triangular footings (Vesic, 1975).

Shell foundations have been employed as an alternative for the conventional flat shallow foundations and have proven to provide economical advantage. They have shown considerably improved performance in terms of ultimate capacity and settlement characteristics. However, despite conical shell foundations are frequently used in industry, the theoretical solutions for bearing capacity of these footings are available for only triangular shell strip foundations. The benefits in design aspects can be achieved through theoretical solutions considering shell geometry.

The engineering behavior of a conical shell foundation on mixed soils was investigated experimentally and theoretically by Colmenares et al. (2014). The failure mechanism was obtained by conducting laboratory model tests. Based on that, the theoretical solution of bearing capacity was developed and validated with experimental results, in terms of the internal angle of the cone. In comparison to the circular flat foundation, the results show 15% increase of ultimate load and 51% decrease of settlement at an angle of intersection of 120. Based on the results, the design chart of modified bearing capacity coefficients for conical shell foundation was proposed.

Dynamic forces are present in every engineering problem although they are only considered to be significant in a few specific scenarios. The most high profile situation is when an engineered structure is subjected to earthquake induced loading. Finite element is the most commonly accepted analysis tool for solution of engineering problems.

Effective pre and post processing capabilities make modeling and interpretation of results simple.

It is relatively easy to incorporate changes, if any, and repeat the analysis without much loss of time. Viewing of animated mode shapes and dynamic response makes understanding of the dynamic behavior of the machine foundation system relatively simpler. The objective of this study is to present a better understanding of the behavior of shell foundations and assess the margin of safety that such footing possesses against failure. In this study, the behavior of shell foundation and the soil underneath is simulated by nonlinear three dimensional finite elements. The numerical solution by the finite element method also includes dynamic analysis of shell foundation problem. The problem studies the effect of load frequency by taking a range of frequencies and dynamic load amplitudes into consideration through studying the response of shell machine foundation on sandy soil

A. Experimental Work Effect of Conical Shell Foundation

In this study, conical shell footings are prepared which are composed of reactive powder concrete. Specimen molds were cleaned thoroughly, tightened well and the internal surfaces were oiled with thin engine oil to prevent the hardened concrete adhesion with molds. Steel wires were fixed at their correct position inside the molds. Each layer was compacted by external table vibrator to minimize the air voids and to get well compacted concrete. Then, the top surface of the specimen was well finished using a steel trowel, so that the upper surface of the wooden block is kept level with the concrete surface.

Five values of steel fiber volume fractions of 0, 0.5%, 1.0%, 1.5%, and 2.0% were used in casting the shells, in order to study the effect of steel fiber content on the shear strength. Taking into consideration the aspect ratio of the fibers used and the type of concrete mix, a maximum of 2% fiber content was used in which the fibers were found to achieve a practical and uniform distribution within the fresh and hardened concrete. If greater than this percentage was used, mixing problems would rise as a result of the substantial immediate loss of workability of the mix and non- uniform distribution of fibers due to the effect of fiber balling so that great efforts and relatively long vibration time would be required in manufacturing the test shells (Al-Hamdani, 2013).

In this study, conical shell foundations are tested with ring beam with reactive powder cement and normal concrete to study the effect of steel fiber on the behavior of shell foundations. The shallow shell foundations details are presented in Figure (1) and Table (2).

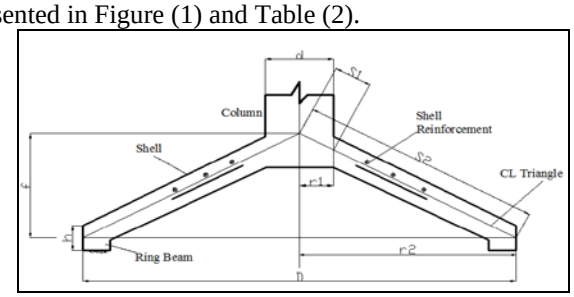

Fig. (1) Conical shell footings - general details.

Finite Element Analysis

The finite element method is a numerical procedure which can be applied to solve a numerous engineering problems, that has become a powerful and versatile tool for structural analysis in both linear and nonlinear formulations of reinforced concrete structures. In the study the finite element software ANSYS-Ver. 11 is used in the analysis. Some features of this program are discussed below.

Finite element idealization and material properties

Three dimensional brick element (Solid 65) is used to model the concrete with or without reinforcing bars (rebars). The element is capable of cracking in tension and crushing in compression. The steel reinforcing bars (tensile, compressive, and stirrups) are represented by using 2-node discrete representation (Link8 in ANSYS) and included within the properties of 8-node brick elements. The Solid 45 is used for the 3-D modeling of solid structures. The element is defined by eight nodes having three degrees of freedom at each node: translations in the nodal x, y, and z directions. By making use of symmetry of loading, geometry and reinforcement distribution, the RPC conical footings have been considered in the finite element analysis. The chosen segment was modeled by using the Solid 65 isoparametric hexahedral brick elements.

Figures (2) to (13) depict the frequency displacement curves for shell foundation under three amplitudes of vertical dynamic load and for three thicknesses. The vertical displacement was found to increase with increase of amplitudes of vertical dynamic load.

The vertical displacement decreases with the increase of shell foundation thickness by about (4, 5, 6)% for (15 mm) shell thickness and for the three amplitudes of dynamic load (30 kN, 40 kN, 50 kN) and then increases obviously in the case of (20 mm) thickness by about (6, 11, 15) more than the (10 mm) thickness; the reference case, for the three amplitudes of dynamic load due to increase of self-weight of the shell foundation as shown in Figures (2) to (4).

In shell foundation without ring beam, the vertical displacement decreases with the increase of shell foundation thickness by about (7, 10, 15) % for (15 mm) shell thickness under the effect of amplitude dynamic load (P= 30, 40, and 50 kN) and (11, 19, 25) % for (20 mm) shell thickness under the same amplitudes as shown in Figures (2) to (4).

The vertical displacement of shell foundation with ring beam decreases by about (20, 40, 56) % for shell foundation without ring beam of thickness (10 mm) for three amplitudes of dynamic load (30, 40, 50), respectively, while it decreases by about (18, 20, 19) % for shell foundation without ring beam of thickness (15 mm), and about (10, 40, 60) % for shell foundation without ring beam of thickness (20 mm) for the same amplitudes as shown in Figures (2) to (7).

The maximum displacement occurs for the (10 mm) shell foundation with ring beam thickness at frequency ratio of (1.11) for the three amplitudes applied, while for the (15 mm) thickness, it takes place at frequency ratio of (0.55), and for the (20 mm) at frequency ratio of (0.55) as shown in Figures (8) to (10). The foundation must be designed such that the frequency ratio is less than 0.5 or more than 2.

In Figures (11) to (13), the maximum displacement for the (10 mm) shell foundation without ring beam thickness occurs at frequency ratio of (0.66), for the (15 mm) thickness, it is noticed to taken place at frequency ratio of (1.11), while for the (20 mm) thickness foundation, it takes place at frequency ratio of (0.66) for the three amplitudes of load.

The maximum vertical displacement is reduced by about (11, 40) % of the beam size (20*20 mm) when the beam size is increased to (20*30 mm and 20*40 mm), respectively, This behavior is due to the ring beam importance in increasing the rigidity of the footing; therefore, the increase of the dimensions of the ring beam will reduce the vertical displacement as shown in Figure (14).

The maximum displacement occurs for the three sizes of ring beam at frequency ratio of (1.11, 1.11, and 0.77) for the beam size (20*20 mm, 20*30 mm, and 20*40 mm), respectively, as shown in Figure (15).

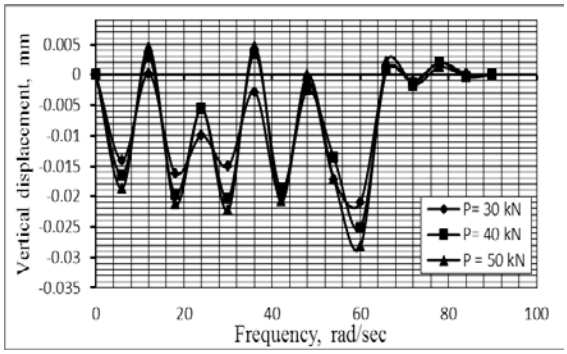

Fig. (2) Variation of vertical displacement with frequency of load for the conical foundation with ring beam, shell thickness = 10 mm due to vertical dynamic load.

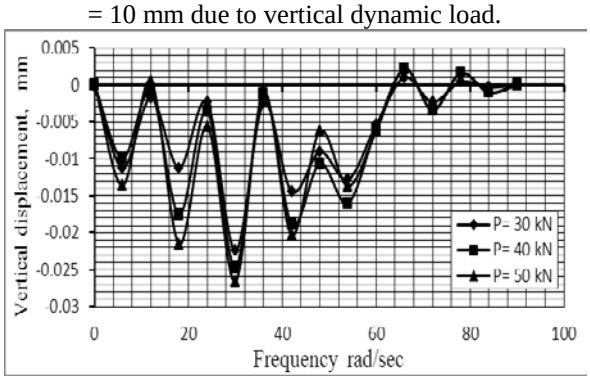

Fig. (3) Variation of vertical displacement with frequency of load for the conical foundation with ring beam, shell thickness = 15 mm due to vertical dynamic load.

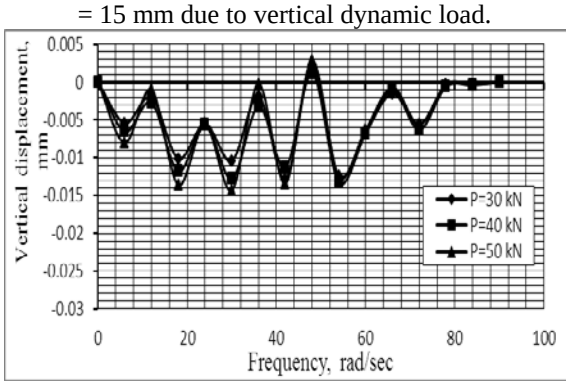

Fig. (4) Variation of vertical displacement with frequency of load for the conical foundation with ring beam, shell thickness = 20 mm due to vertical dynamic load.

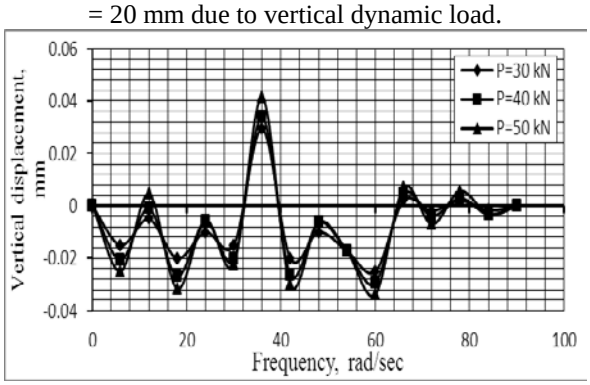

Fig. (5) Variation of vertical displacement with frequency of load for the conical foundation without ring beam, shell thickness = 10 mm due to vertical dynamic load.

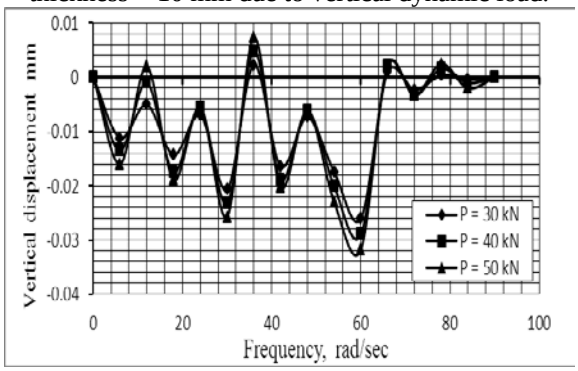

Fig. (6) Variation of vertical displacement with frequency of load for the conical foundation without ring beam, shell thickness = 15 mm due to vertical dynamic load.

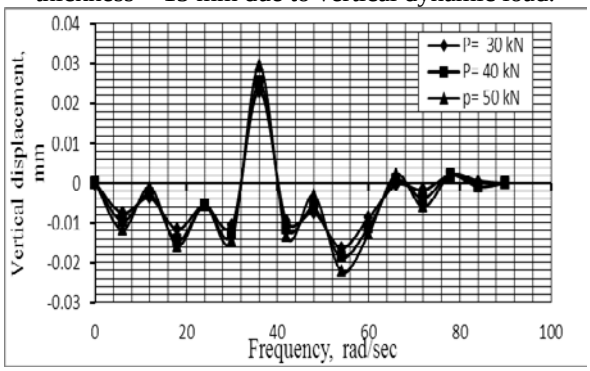

Fig. (7) Variation of vertical displacement with frequency of load for the conical foundation without ring beam, shell thickness = 20 mm due to vertical dynamic load.

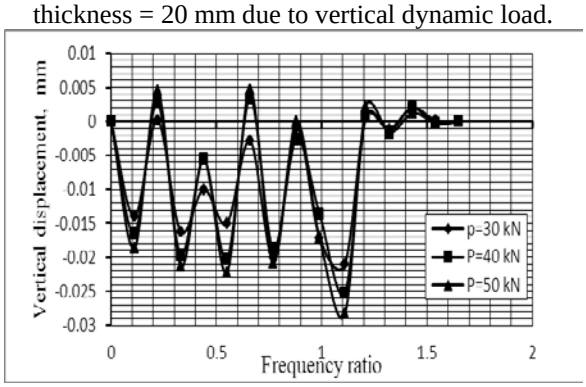

Fig. (8) Variation of vertical displacement with frequency ratio of load for the conical foundation with ring beam, shell thickness = 10 mm due to vertical dynamic load.

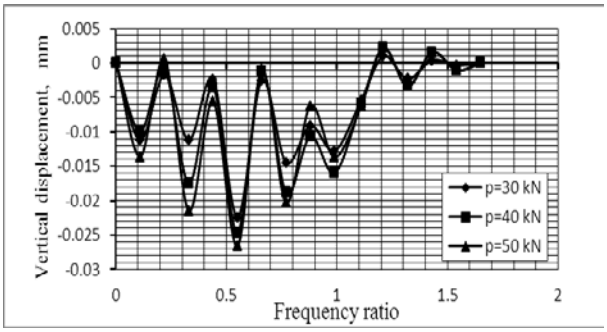

Fig. (9) Variation of vertical displacement with frequency ratio of load for the conical foundation with ring beam, shell thickness = 15 mm due to vertical dynamic load.

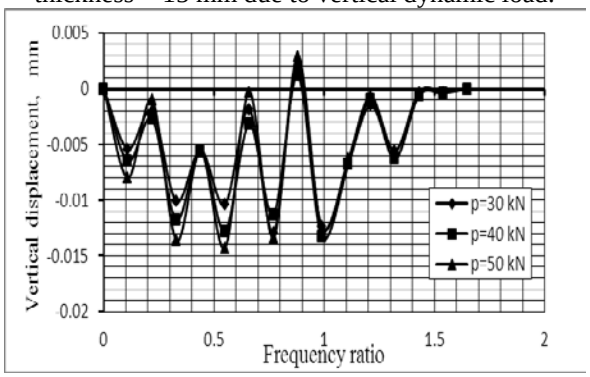

Fig. (10) Variation of vertical displacement with frequency ratio of load for the conical foundation with ring beam, shell thickness = 20 mm due to vertical dynamic load.

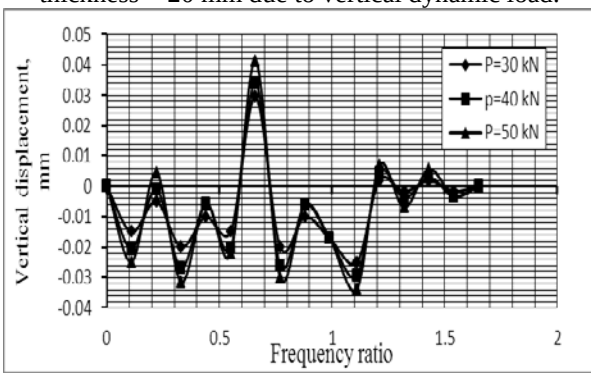

Fig. (11) Variation of vertical displacement with frequency ratio of load for the conical foundation without ring beam, shell thickness = 10 mm due to vertical dynamic load.

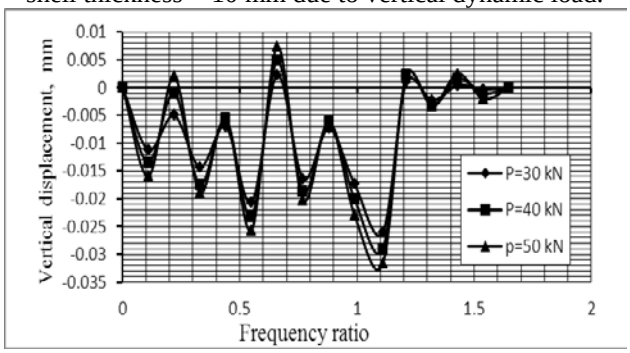

Fig. (12) Variation of vertical displacement with frequency ratio of load for the conical foundation without ring beam, shell thickness = 15 mm due to vertical dynamic load.

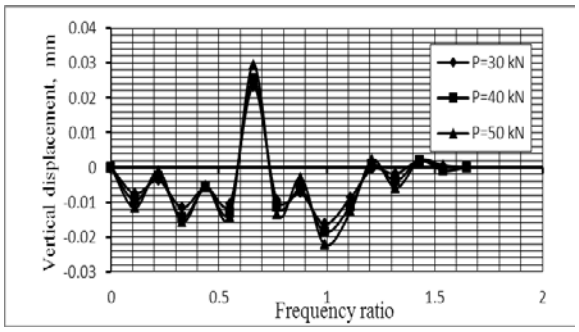

Fig. (13) Variation of vertical displacement with frequency ratio of load for the conical foundation without ring beam, shell thickness = 20 mm due to vertical dynamic load.

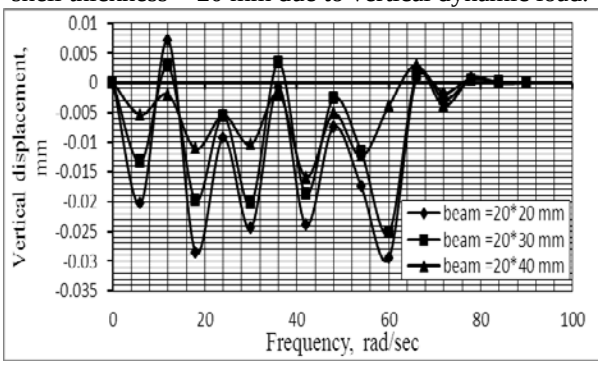

Fig. (14) Variation of vertical displacement with frequency of load for the conical foundation for different of sizes of ring beam, due to vertical dynamic load.

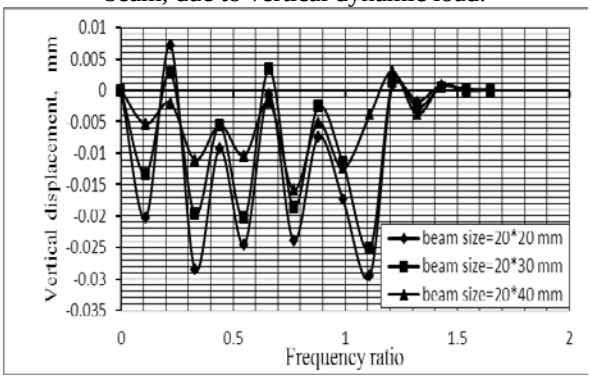

Fig. (15) Variation of vertical displacement with frequency ratio of load for the conical foundation for different of sizes of ring beam, due to vertical dynamic load.

B. Conclusions:

1. The increase of thickness of the conical footing with and without ring beam will reduce vertical displacement due to increase the rigidity of footing but the footing with ring beam has more rigidity than footing without ring beam.
2. The vertical displacement decreases with the increase of shell foundation thickness by about (4, 5, 6)% for (15 mm) shell thickness and for the three amplitudes of dynamic load (30 kN, 40 kN, 50 kN) and then

increases obviously in the case of (20 mm) thickness by about (6, 11, 15) more than the (10 mm) thickness; the reference case, for the three amplitudes of dynamic load due to increase of self-weight of the shell foundation.

3. The maximum vertical displacement is reduced when the size of the ring beam is increased, the reduction is about (11, 40) % of the beam size (20*20 mm) when beam size is increased to 20*30 mm and 20*40 mm, respectively.

References

1. **Al-Hamdani, M. A. E., (2013), " Analysis of Shell Foundations Constructed of Reactive Powder Concrete on Sandy Soil", Ph.D. thesis, Civil Engineering Department, College of Engineering, Al-Mustansiriyah University, Baghdad.**
2. **ASTM C109/C109M-2005, "Standard Test Method for Compressive Strength of Hydraulic Cement Mortars", Vol. 04.01, 2005, 6 p, American Society for Testing and Materials.**
3. **ASTM C1437-2001, "Standard Test Method for Flow of Hydraulic Cement Pastes and Mortars of Plastic Consistency", Vol. 04.01, 1999, 3 p, American Society for Testing and Materials.**
4. **Barkan, D. D., (1962), "Dynamics of Bases and Foundations" McGraw - Hill, New York.**
5. **Christian J. T., and Hall, J. R., (1982), " Soil-Structure Interaction Problems", Proceedings of the Fourth International Conference on Numerical Methods in Geotnechanics, Edmonton, Canada, May.**
6. **Chopra. A. K. (1995) "Dynamics of Structures: Theory and Applications to Earthquake Engineering," Prentice-Hall, Inc., Englewood Cliffs, New Jersey.**
7. **Collepardi, S., Coppola, R., Troli, R. and Zaffaroni, P.,(1999) "Influence of the Super plasticizer Type on the Compressive Strength of Reactive Powder Concrete for Precast Structures", Congress International BIBM, Venzia, Maggi o 25-28, pp. 25-30.**
8. **Colmenares, J. E., Kang, S. R., Shin, Y. J. and Shin, J. H., (2014), " Ultimate Bearing Capacity of Conical Shell Foundations", Structural Engineering and Mechanics, An International Journal, Vol. 52, No. 3, pp.507-523 , Techno press, Korea.**
9. **Hutton, D. V. (2004), "Fundamentals of Finite Element Analysis", 1st ed., New York, USA.**
10. **Philippot, S., Masse, S., Zanni, H., Nieto, P., Maret, V., and Cheyrezy, M., (1996) "Study of Hydration and Pozzolanic Reactions in Reactive Powder Concrete (RPC)" Magnetic Resonance Imaging, Vol. 114, No. 8, pp. 891-893.**
11. **Rao, K., N. S. V. (2011), "Foundation Design Theory and Practice", a book, university Malaysia Sabah, Malaysia.**
12. **Saderkarimi, A.,(2004) "Development of a Lightweight Reactive Powder Concrete", Journal of Advanced Concrete Technology, Vol.2, No.3, pp.409-417.**
13. **Vesic, A. S. (1975). "Bending Capacity of Shallow Foundations" Chapter Three in: Foundation Engineering Handbook, Van Nostrand Reinhold Co., New York.**
14. **Zienkiewicz, O.C. and Taylor, R.L. (2005), "The Finite Element Method", McGraw-Hill, London, UK.**

Determination of The Bearing Improvement Ratio For Clay Soil Improved With Stone Column Under Confined Condition

Asst. Prof. Dr. Maki Jafar Mohammed Al-Waily, Prof. Dr. Namir K. S. Al- Saoudi

Abstract - **The present work is focused towards the evaluation of bearing capacity improvement ratio q_r, determined trough the confined compression tests carried out on stone column penetrated in soft clay soil. The investigation was carried out using model tests of stone column performed inside cylindrical container of 300 mm in diameter and 350 mm in height. The undarined shear strength of the soil prepared in the containers ranged from 5.5 kPa to 13.5 kPa. The models ware tested immediately after preparation and some of the models were left to cure 10 days after preparation. It can be noticed from results that the treated soil loaded after 10 days shows an increase in bearing improvement ratio mare than that of treated soil loaded immediately.**

Index Terms: **Bearing Improvement, Stone column, Clay, Confined Condition**

I. INTRODUCTION

Soft soils require improvement of their properties if they have to be utilized as foundation .For this purpose, different soil improvement techniques such as preloading ,sand drains ,dynamic compaction and stone column have been used as economical alternative to deep foundations.

The most attractive appears to be the stabilization of soft soil by installation of stone column that have been widely used in many countries during the last three decades. This is related to feasibility and the suitability of stone column technique. Stone column were known in France in the 1830s they have recently been rediscovered and the mechanism of their behaviour under load is not well understood. This method consists in forming vertical holes in the ground that are filled with crushed rock to form columns or "piles" confined by the soil. They are ideally suited for improving soft clays and silts and also for loss sand. Stone columns have been used in the support of basic foundation types, such as small isolated footing, strip footing and very common for large raft foundation,, wide spread loads and embankments. Aboshi et al (1979) investigated the stress distribution in a loaded composite foundation. Juran & Guermazi (1986) conducted a series of triaxial compression tests by using a specially modified triaxial cell on a composite soil specimens. These test showed the significant influence of the group effect, the replacement factor, and the partial consolidation of the soft soil on the stress concentration factor (n) and the settlement reduction of the foundation .Terashi et al (1991) investigated the bearing capacity of the clay ground improved by sand compaction pile method (SCP). The influence of various factors specially of load inclination and intensity of preload are revealed by a series of centrifuge model tests. Stewart & Fahey (1994) discussed the stress -time and stress concentration ratio (n) relationships resulted from a confined compression test of a single stone column. Al-Khafagi(1996) used the centrifuge modeling technique in the examination of the use of the sand compacted pile (SCP) for reinforcing soft clay ground. Juran & Riccobono (1991) presented the main results of an experimental study of the feasibility of using artificially cemented ,compacted -sand columns in the reinforcements of soft cohesive soil. Rasheed (1992) used the finite element method in a parametric study on the behavior of soft soils reinforced by 5 columns .Both linear and nonlinear hyperbolic models for soil stone column were adopted. Different parameters were studied and presented . The most effective parameter was found to be the ratio of spacing to the diameter of the column. Goughnour & Bayuk (1979) studied the observation results of a long term field test on vertically loaded stone column in soft soil. Aboshi et al (1979) studied the distribution of stress between sand pile and ground in sites. Bergado et al (l987) conducted full scale plate load tests and full scale embankment load test on fully penetrating granular piles on the soft Bangkok clay. The variation of the stress concentration ratio (n) was measured by means of earth pressure cells .It found that the stress concentration ratio (n) increased with increasing the area replacement ratio a_s. The present paper investigate the behavior of stone columns under confined compression state oriented mainly towards the determination the bearing capacity improvement ratio q_r.

II. TESTING EQUIPMENT AND PROCEDURE

Fig. (1) shows details of the complete set up which consist mainly of steel container, loading frame and accessories . The ratio of container height to the diameter was chosen equal to one to avoid the side friction of walls (Garnier, 2001). These accessories include three dial gages (with accuracy of 0.0lmm) above of model to measure the settlement of composite material, (stone column and surrounding soil), and two proving rings at the top of the model to measure simultaneously the applied total stress and the stress supported by stone column .The model tests were carried out in a cylindrical steel container, 300mm in diameter and 300 mm in height made of steel plate (6 mm in thickness). The soil used brought from the vicinity of Al-

Musaib technical college in Babylon. The soil consists of 32% sand, 4l% silt, and 27% clay, with liquid limit equal to 33% plastic limit of 17%. The soil was classified as (CL) Symbol according to unified soil classification system. The tests were carried on a single stone column of 100 mm in diameter and 300mm in height. The natural calcium carbonate crushed stone was used as a backfill material. These sizes were chosen in accordance with the guidelines suggested by Nayak (1983),where the particle size (1/6 to 1/7) of the diameter of columns.

III. MODEL PREPARATION AND TESTING

A. Preparation of the Bed of Soil

Prior to the preparation of the bed of soil a relationship was obtained between the water content and the undrained shear strength of the soil, Fig. (2) illustrate this relationship. The undrained shear strength of the soil was measured by Swedish fall cone pentrometer. The conditional soil was mixed with enough quality of water to get the desired shear strength. The soil was placed in layers inside the steel container and each layer was tamped with a special tamping hammer of (50mmx50mm) in size. The final thickness of each layer was about 50 mm. The procedure continued until the final thickness of the bed of soil was 300 mm. After the completion of the preparation of the bed of soil, it was covered tightly with nylon sheets and left four days curing period.

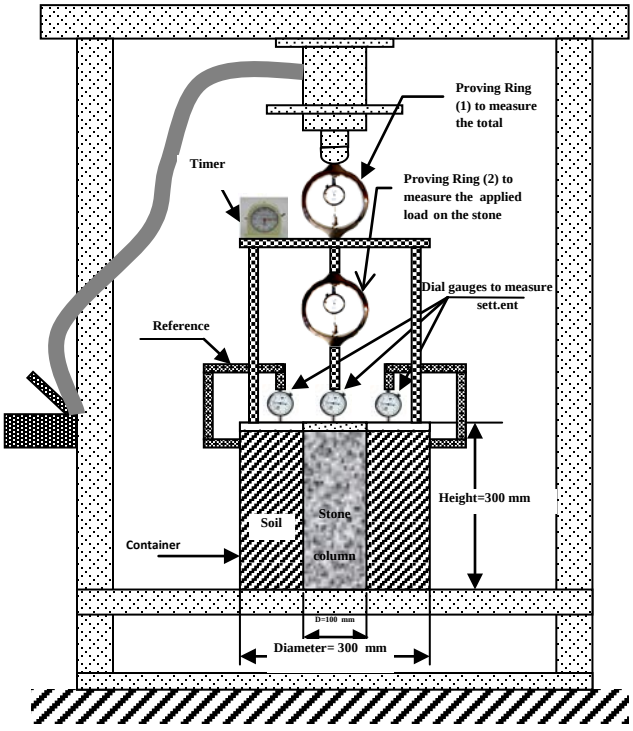

Fig. 1. Experimental set-up

B. Construction of Stone Columns

At the end of curing period, the top of the bed of soil was leveled. A hollow PVC tube, of external diameter (32 mm) and (2 mm) in thickness, coated with petroleum jelly was pushed vertically along the center of the soil to the required depth. The tube was then slowly withdrawn and twisted during the lifting process. The soil was removed from the tube and samples of the soil at different depths were taken for water content measurement. The crushed stone poured into the hole in layers and each layer was compacted gently using (30 mm) in diameter tamping rod. The unit weight of the compacted crushed stone was 16.3 kN/m^3 .The whole bed of clay was covered with a nylon sheet and protected from any lose of moisture and left for a period of 10 days .The temperature was measured daily along the period.

C. Model Testing Procedure

The surrounding soil was prepared at undrained shear strength of (cu=5.5 kPa, 8.5 kPa and 13.5 kPa) respectively. The models were tested immediately after preparation and some were left to cure for 10 days after preparation , the footing assembly was placed in position so that the center of the footing coincides with the center of the hydraulic jack. Loads were then applied through a loading disk in the form of load increments .Each load increment was left for (2.5 min). The dial gauge readings were recorded at the end of the period of each load. During each load increment, dial gauge of two proving rings measurements were recorded. The Load increments continued until total pressure reached 300 kPa. For comparison purposes. The loading tests were performed on container with untreated soil only.

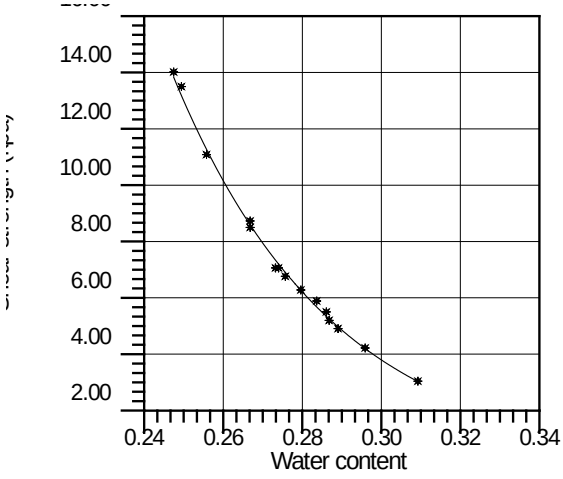

Fig. 2. Shear strength -water content relationship

IV. PRESENTATION AND DISCUSSION

Fig.(3)relates the bearing ratio (q/cu) versus deformation ratio(S/D) ratio for untreated soil and soil treated with stone only .The surrounding soil was prepared at undrained shear strength of (cu=5.5 kPa ,8.5 kap and 13.5 kPa)respectively. The models were tested immediately after preparation and some were left to cure for 10 days . This Fig. demonstrates that the stone column in all bearing ratio shows significant difference in the behavior corresponding to (S/D) ratio. This Fig. also indicates that when the shear strength of soil is decreased the effect of stone column became more visible and a clear increase in (q/cu) ratio is noticed . This behavior is attributed to the truth that the calculation of stresses is dependent on stress applied on replacement soil in zone of stone column only , disregarding stress applied on soil surrounding the column . Thus the affect of improvement seemed clearly in treated soil of low shear strength . It can be noticed also from Fig. (3) that the treated soil loaded after 10 days shows an increase in bearing capacity more than that of treated soil loaded immediately .This behavior is related to the drainage effect .

The bearing improvement ratio achieved by stone columns is presented by the ratio ($q_{treated}$ / $q_{untreated}$)versus (S/D) ratio (Fig. (4) ranges from 5.6 at S/D=5% to 6.3 at S/D=10% in an average of 6 and 2.9 at S/D=5% to 3.6 at S/D=10% in an average of 3.3 and 2 at S/D=5% to 2.6 in an average of 2.3 at shear strength of soil(cu=5.5 kPa ,cu=8.5 kPa and cu=13.5kPa) respectively for treated soil loaded after 10 days curing . Fig.(4) also shows the ($q_{treated}$ / $q_{untreated}$) ranges from 5 at S/D=5% to 5.3 at S/D=10% in an average of 5.2 and 2.8 at S/D=5% to 3.1 at S/D=10% in an average of 3 and 2 at S/D=5% to 2.6 at S/D=10% in an average of 2.3 at shear strength of soil(cu=5.3 kPa ,cu=8.5 kPa and cu=13.3kPa) respectively for treated soil loaded immediately .

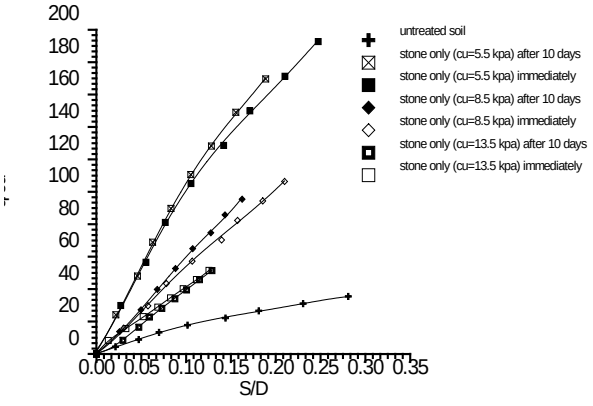

Fig. 3. Variation of (q/cu) ratio with (settlement/Dia.) (S/D) ratio

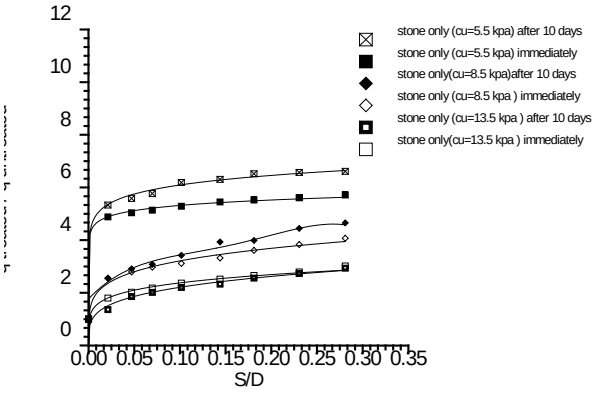

Fig. 4. Bearing improvement ratio with (settlement/Dia.) (S/D) ratio

V. REFERENCES

[1] Lambe, T. W., & Whitman, R. V., *Soil mechanic*, 1st edition, John, Wiley, New York, 1969.

[2] Aboshi, H., Ichimoto, E., Enoki, M. & Harada, K., "The compozer: a method to improve characteristics of soft clays by inclusion of large diameter sand columns", proceedings International Conference on soil reinforcement; Reinf. Earth and other techniques, Vol. 1, Paris, 1979, pp. 211 – 216.

[3] Goughnour, R. R., & Bayuk, A. A., "Afield study of long term settlement of louds supported by stone columns in soft ground', Proceedings International Conference on Soil Reinforcement; Reinf. Earth and other Techniques, Vol. 1, Paris, 1979,pp.279 - 285.

[4] ASTM, *American Society for Testing and Materials*, Part 14 & 19, Annual book of ASTM standards, 1981.

[5] Nayak, N. V., *Foundation design manual* , 3rd edition, Dhanpat Rai and Sons, Delhi, India, 1984.

[6] Juran, I., & Guermazi, A. , "Settlement response of soft soils reinforced by compacted sand columns", Journal of Geotechnical Engineering, ASCE, Vol. IL4, No. 8,1988, pp. 930 -943.

[7] Bergado, D .T., Huat, S .H& Kalvade,S .,"Improvement of soft Bangkok clay using piles in subsiding environment ", proceedings of the 5th international geotechnical seminar organised by Nanyang Technological institute , Singapore (2-4 December I 987) .

[8] Terashi, M., Kitazuma, M., & Okada, H., "Applicability of practical formula for bearing capacity of clay improved by SCP", Proceedings International Conference on Geotechnical Engineering for Coastal development, Vol. 3, September 1991, Yokohama, pp. 405 – 41013.

[9] Juran, I., & Riccobono, O., "Reinforcing soft soils with arterially cemented compacted-sand columns", Journal of Geotechnical engineering, ASCE, Vol. ll7, No. 7,1991, pp. 1042 - 1060.

[10] 1 Rasheed, A. H., "Efficiency of stone columns in improving the behaviour of footings resting on soft soil", M. Sc. Thesis, University of Technology, Baghdad, 1992.

[11] 12. Stewart , D.,& Fahey, M.,"An investigation of reinforcing effect of stone columns in soft clay", Vertical horizontal Deformations of foundation and embankments, proceeding of settlement 94, American Society of civil engineers ,New York , 1994, pp.513-524 .

[12] Al-Khafaji, Z. A., "Reinforcement of soft clay using granular columns", Ph. D. Thesis, University of Manchester, UK, 1996.

[13] Al-waily ,Maki Jafar M., *Confined compression behavior of stone columns*, M.Sc. Thesis , University of technology ,Baghdad, 2001.

[14] Granier, J. ," Physical Models in Geotechnics : State of the Art and Recent Advances", First Coulomb, lecture, Paris, 3 October 2001, CFMS(ed).

Contribution of Emulsified Asphalt in Strength and Permeability behavior of Gypseous Soil

S. I. Sarsam, and S. A. Hamza

***Abstract*—This paper deals with stabilizing Gypseous soil obtained from Husaibah with emulsified Asphalt. A laboratory-testing program was conducted through two phases.**

In the first phase, the optimum fluid content (emulsion and water) was determined using the unconfined compression test mold and testing procedure. 40- Asphalt stabilized soil samples have been constructed and tested using combinations of different percentages of emulsion and water content. The maximum dry density and optimum fluid content was selected for further testing in the next phase.

In the second phase, the effect of emulsion on the behavior of Gypseous soil in permeability was studied using constant head permeability technique. Stabilized soil samples were prepared, and divided into two groups; the first group was subjected to aeration before compaction while the second group was directly compacted in the permeability cell without aeration. The compaction was conducted using a tamping rod to the maximum dry density at optimum fluid content in three layers. The coefficient of permeability of both groups was determined and compared with that of pure soil.

It was concluded that emulsified asphalt has a positive effect on strength improvement, waterproofing and reduction of permeability potential of compacted Gypseous soil.

***Index Terms*— Asphalt emulsion, Gypseous soil, unconfined compression strength, permeability, stabilization**

I. Introduction

THE Gypseous soil which covers vast area in west, middle, east and south west regions of Iraq is considered as problematic soil for embankment construction, it possesses a type of cohesive forces when mixed with optimum amount of water and then compacted, but it loses its strength when flooded with water again, and exhibit collapsible behavior [1]. Stabilization of such soil with liquid asphalt may be considered as possible solution to retain its stability, strength. The addition of liquid asphalt may possess a waterproofing action to the soil when implemented in the construction of embankment1. The effect of emulsified asphalt on the Geotechnical, and Engineering properties of Gypseous soil was investigated. The results of compaction tests shows that the dry density increased with increasing asphalt emulsion content up to an optimum, then the dry density decreases [2]. Consolidation tests results showed that total volumetric strain, coefficient of consolidation, coefficient of permeability, and compression index of treated soil samples decreased upon increasing the percentage of emulsified asphalt. Unconfined compression tests results shows that the compressive strength of the treated Gypseous soil by different percentages of emulsified asphalt contents increased with increasing emulsified asphalt content up to an optimum content then decreased [3]. Another study [4] showed the effect of cyclic soaking – draining, on the compressibility characteristics of stabilized Gypseous soils with emulsified asphalt, and investigated the efficiency of emulsified asphalt to treat Gypseous soils of different collapse potential. Three Gypseous soil samples with different collapse potential and gypsum content were taken from Al – Najaf site, Al – Ramadi and Al – Dour site. It was concluded that using emulsified asphalt, as stabilized material should be limited to moderately trouble Gypseous soils. The shear strength and rebound consolidation of Gypseous soil stabilized with asphalt emulsion was investigated [5]. Soil asphalt specimen has been constructed using various percentages of asphalt emulsion. One dimensional confined compression test results under both dry and saturated test conditions indicated that the addition of emulsified asphalt had considerably reduced the void ratio and permeability.

Manuscript received June 28, 2015.

S. I. Sarsam, is with the department of Civil Engineering, College of Engineering, University of Baghdad, Baghdad, IRAQ (corresponding author phone: 00964-7901878167; e-mail: saadisasarsam@coeng.uobaghdad.edu.iq.

S. A. Hamza, was with the department of Civil Engineering, College of Engineering, University of Baghdad, Baghdad, IRAQ

II. Materials and Methods

The Gypseous soil used in this investigation was obtained from Husaibah city at Al-Anbar Governorate, west of Baghdad. A shovel was used to remove the top soil, and Gypseous soil was obtained from a depth of 0.5m to 1.0 m. The samples were stored in plastic bags, labeled and transported to the Laboratory.

The first phase of the testing program was conducted to find the chemical and physical properties of the Gypseous soil.

A. Chemical Test

The chemical tests were conducted, and the results are given in Table 1. The gypsum content was determined in the laboratory using the hydration method [6] as described in the following:

The soil sample is oven dried at (45°C) until it reaches a constant weight, then the weight of the soil sample is recorded. Then the same soil sample is oven dried at (110 °C) for 24 hours and the weight of soil sample is recorded again.

The gypsum content is calculated according to the following equation 1, [6].

$$x = [\,w45 - w110]\,\frac{4.778}{w45}\;100 \quad \text{---------- eq.1}$$

Where:
X = Gypsum content
W 45 = Weight of sample at 45° C Temperature
W 110 = Weight of sample at 110° C Temperature

Table 1.
Chemical composition of the Gypseous soil

Chemical composition	Value
Organic content (%)	0.05
Gypsum content (CaSO4) (%)	76.0
Carbonate content (CaCo3) (%)	31.97
Total soluble salts (T.S.S.) (%)	65.1
pH value	8.8

B. *Physical Test*

Classification tests were performed on the soil including particle size distribution, specific gravity, Atterberg limits, and compaction characteristics. Physical tests were conducted as described below:

The specific gravity of the Gypseous soil is determined according to the British standard, [7], but "Kerosene" was used instead of water, due to the dissolving action of gypsum in water, and a specific gravity of 2.22 was obtained.

The portion of soil passing sieve No.40 sieve was used in the determination of plastic and liquid limits. The plastic limit test is conducted following the (ASTM) [8] standard, while the liquid limit test was carried out in accordance to (B.S) [7] using cone penetrometer test. These tests showed that the soil is non-plastic. Table 2 presents the physical properties of soil.

Table 2.
Physical properties of soil

Physical property	Test result
Specific gravity	2.22
Plasticity index	Non plastic
Unified soil classification	SP
AASHTO Soil classification	A-3
Maximum dry density – standard proctor (gm/cm^3)	1.502
Optimum moisture content (%)	15

Grain size distribution of the Gypseous soil was determined by sieve analysis (dry method), according to (ASTM) [8]. However, for this test method, the reason of using this type of test is due to the solution of gypsum in water. The grain size distribution of the tested soil is shown in Fig.1. According to (ASTM) [8] (Unified Soil Classification System), the soil is classified as SP (poorly graded sand). Furthermore, the soil is designated as A-3 according to (ASTM D) [8] and (AASHTO Soil Classification System).

The compaction properties of natural soil are found using standard compaction test. Standard Proctor compaction test was performed following the procedure of (ASTM) [8]. Soil was compacted in three equal layers, 25 blows per layer using a rammer of 5.5 Lb. (2.5 kg) weight falling from a height of 12 in (304.8 mm) from the surface of the specimen. Soil was mixed thoroughly by hand with the different water and emulsified asphalt percentages, and the standard compaction tests was performed as per the procedure above. Fig.2. Shows the fluid content-dry unit weight relations of standard compaction tests. Table 3 shows the combination of water and emulsified asphalt used, the test was conducted using combinations of different percentages of emulsion and water content. The maximum dry density and optimum fluid content was selected for further testing in the next phase.

Table 3
Combination of water and emulsion content

Percent	Percentage				
Water content (%)	6	7	8	9	11
Emulsion content (%)	5	6	7	8	9
Total fluid content (%)	11	13	15	17	20
Unconfined compressive strength (kPa)	66	77	100	151	123

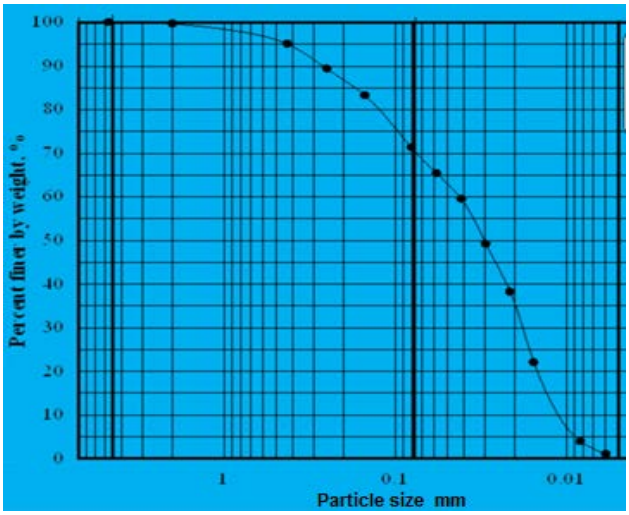

Fig.1. Grain size distribution of the soil

C. *Properties of emulsified asphalt*

Cationic Asphalt emulsion was implemented in this work. Al- Zahf Al- Kabeer Company manufactured it with low cost. The specifications as supplied by the manufactured are as given in table 4.

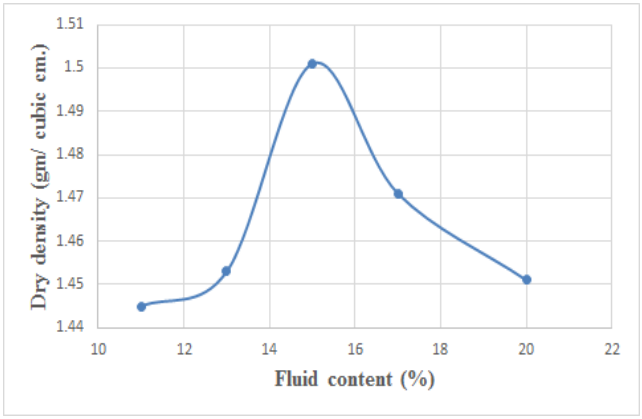

Fig.2 Dry density- fluid content relationship

Table 4.
Properties of asphalt emulsion (Al-Zahf Al-Kabeer Co. /Baghdad)

Property	Test result	Property	Test result
Particles charge	+ve	Settling Time (hour)	19
Viscosity CSt	45	Coating ability and water resistance	Good
Cement Mixing	1.2	Coating dry & wet aggregate	Fair

D. Preparation of Gypseous Soil-Asphalt Mixture

To prepare the soil- asphalt mixture, the pulverized and homogenous Gypseous soil (passing sieve No.4) was oven dried at a temperature of (45°C). The optimum moisture content and the maximum dry unit weight of the soil that were found through standard compaction test were 15% and 1.502gm/cm^3 respectively, and was selected as a target in compaction process. Such an issue is mostly considered as an acceptable relative compaction in most engineering requirements, it agrees well with [5] procedure. Then the required percentage of water as shown in Table 3, was thoroughly- mixed by hand until water dispersed throughout the mixture, the pertained amount of emulsion for the selected moisture content was added and then mixed by rubbing the mixture between palms, so that the mixture has a homogenous character.

E. Unconfined Compression Test

To prepare the specimen, the predetermined weight of the mix which gives the target dry unit weight for each fluid content was statically compacted in a cylindrical mold of a split type of 3.8 cm in diameter, and 7.6 cm in height in three equal layers according to the (ASTM) [8]. Specimens were prepared of soil samples mixed with moisture and emulsified asphalt contents as listed in Table 3. Each of the listed moisture contents was mixed with each of the listed emulsified asphalt contents; duplicate specimens having the same fluid content (emulsified asphalt and water) were prepared. Specimens were allowed to cure for seven days at room temperature of 25± 3º C according to [5], and the average value of the unconfined compressive strength for each duplicate specimens was calculated and considered for analysis. Fig.3 shows part of the prepared unconfined compression strength specimens.

Fig.3 Part of the prepared unconfined compression test specimens

The unconfined compression test was carried out according to the (ASTM) [8] standard, using a constant strain compression machine with a loading rate of 1.52 mm per minute. A calibrated proving ring of (3kN) capacity and (0.01mm) precision dial gauge for vertical deformation reading were implemented. Total of 40 of unconfined compressive strength test specimens were prepared and tested in the second Phase. After preparation of the unconfined compressive strength test specimens, the density was checked, and the specimens were subjected to curing at room temperature of 25± 3ºC for 7 day. Compressive strength was measured after curing. Fig. 4 demonstrates the variation of unconfined compressive strength with fluid content. On the other hand, Fig.5 shows the variation of unconfined compressive strength with Emulsified Asphalt content.

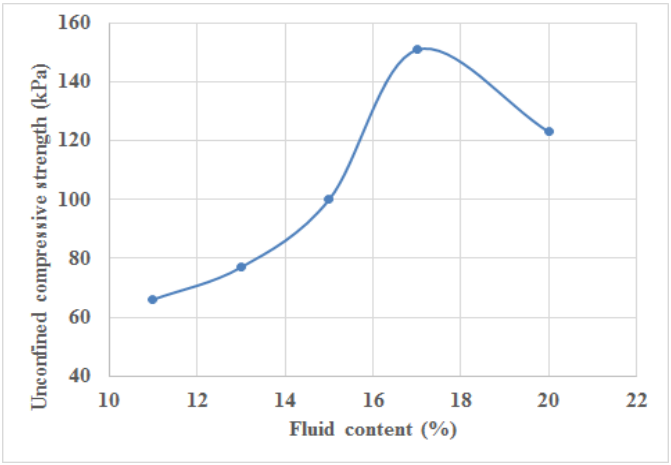

Fig.4 Unconfined compressive strength- fluid content relationship

F. Permeability test

For assessing the effectiveness of stabilization, Permeability test was conducted using the constant head permeameter on three types of specimens using both non-stabilized and asphalt stabilized soil specimens.

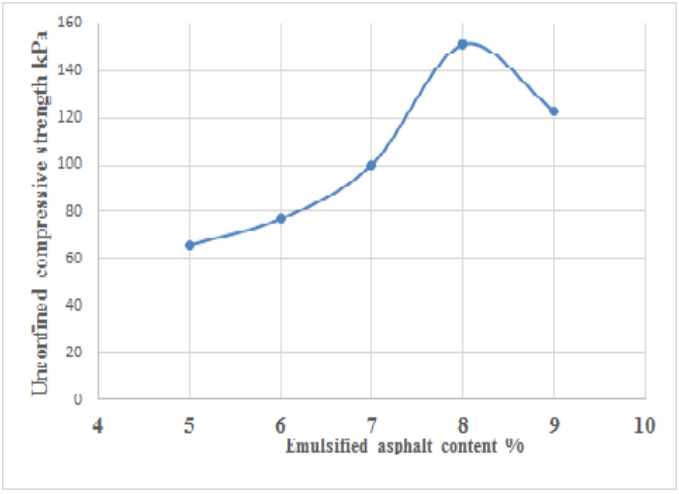

Fig.5 Unconfined compressive strength- Asphalt content relationship

First specimen was non-stabilized Gypseous soil, the

second was stabilized Gypseous soil with emulsified asphalt without aeration and the third specimen was stabilized Gypseous soil with emulsion after aeration. The predetermined weight of the soil, water and emulsion, that gives the maximum dry unit weight of 1.509 gm/cm^3, was mixed thoroughly by hand, and compacted in the permeameter cylinder in three equal layers; each layer was tamped with a 28 blows per layer using a tamping rod of 0.78 kg weight falling from a 15 cm height as the procedure described by [7]. The test was carried out using the constant head permeameter method according to the procedure of (ASTM D) [8]. Specimens were soaked for 48 hours before conducting the test as was done by [9]. Two specimens were prepared and tested for each case and the average value was considered. Fig.6 shows the prepared samples for permeability test.

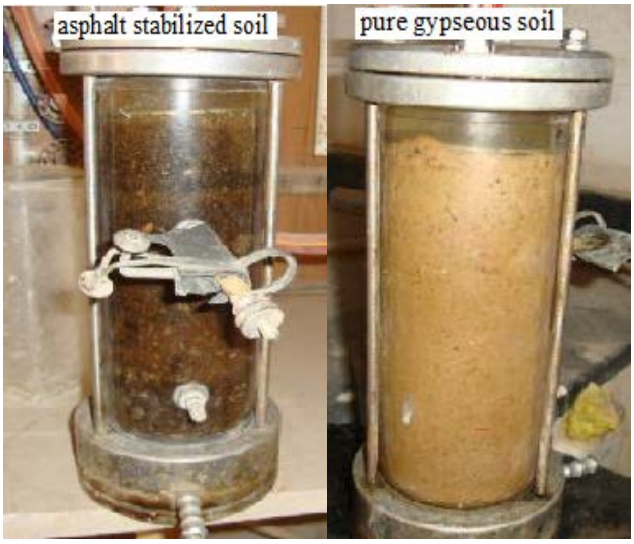

Fig. 6 Prepared samples for permeability test

III. Discussion of Test Results

A. Unconfined Compression Strength

The main objective of this test is to find the optimum fluid content (emulsified asphalt and water) that can achieve the maximum unconfined compressive strength. The stress-strain relationship of the unconfined compression strength shows that the stress increases until it reaches a peak value then it decreases as the strain increases. A brittle failure was observed in specimens of natural and stabilized Gypseous soil at lower asphalt content. When asphalt emulsion was introduced, typical shear failure could be observed. At higher asphalt content, plastic mode of failure was detected. Fig.7 demonstrated various mode of failure observed.

It can be concluded from the summary of test results shown in Fig.5 that the unconfined compressive strength increases with increasing emulsified asphalt content until it reaches an optimum asphalt of 8%, then it decreases with further increment in asphalt content. This behavior may be attributed to the gain in cohesion which is provided by continuous film of asphalt coating the soil particles.

Fig.7 Failure mode of specimens

The unconfined compressive strength reaches a maximum value at 17% fluid content (8% emulsified asphalt + 9% water), which may represent the optimum particle coating; but the unconfined compressive strength decreases as the emulsified asphalt content increases. This may be attributed to the increases in thickness of bitumen films surrounding the soil particles and the fluid content is such to fill the voids completely preventing the particle interlock, this causes a high reduction in friction, which in turn leads to a reduction in the compressive strength. Such results are in agreement with many researchers work, [9], [10], and [11].

B. Permeability Test

The first group of permeability test was conducted on the non-stabilized Gypseous soil specimen; the target dry unit weight used was 1.509 gm/cm^3. Soil was mixed with the water content of 17%. The second group was on asphalt-stabilized specimen. For the stabilized Gypseous soil specimen, the dry unit weight used was of the same value, but the fluid content to be added to the soil was 17%; 8% Emulsion and 9% water.

Two groups of asphalt-stabilized specimens were prepared for compaction in the permeability mold, the first group was mixed, and then subjected to aeration for two hours before compaction, while the second group was mixed, then compacted immediately. The adoption of aeration was to allow some of the fluid content to have a chance of evaporation. This may simulate the field conditions.

After finding the required weight for the target maximum dry density, soil then was compacted by three equal layers, each layer was compacted by 28 blows using a tamping rod weighing 0.78 kg in a free fall from a height of 15 cm above the layer surface. This procedure was in accordance with 7. The stabilized specimens were left (7) days in air for curing before the test.

The adopted permeability test was the constant head method in accordance with (ASTM D) [8]. The specimen was soaked in water until it was fully saturated and then the test was carried out. As noted from the results of permeability test, the value of coefficient of permeability (K) for the non-stabilized Gypseous soil specimen was (I.84 x 10-3 cm/sec) which is rated as low. Table 5 shows the permeability of various mixes. When using stabilized soil with emulsion. The specimen was left for possible fully saturation, then it was left

for (7) days under the test and no further recorded value for the coefficient of permeability could be obtained. It was found that the value of coefficient of permeability was almost negligible.

Table 5.
Permeability test results

Mix type	Coefficient of permeability (K), (Cm/sec.)	% change in (K)
Pure Gypseous soil	1.84×10^{-3}	-------
Emulsified asphalt stabilized soil- aeration not allowed	3.92×10^{-4}	78.7%
Emulsified asphalt stabilized soil- aeration allowed	4.0×10^{-5}	97.8%

This reduction in the coefficient of permeability could be attributed to the coating of the soil particles with asphalt films and plugging the air void space with asphalt, there by blocking the flow channels in the soil mass, thus the permeability of Gypseous soil will be reduced. Such behavior agrees well with work by [5], [11], and [12].

It can be noticed that the effect of emulsified asphalt on the coefficient of permeability of Gypseous soil presented in Table 5, that the coefficient of permeability of Gypseous soil has decreased by 78.7% when 8% emulsified asphalt was added. When the asphalt stabilized soil was subjected to aeration process, it shows further reduction in coefficient of permeability by 97.8%. This reduction in the coefficient of permeability could be attributed to possible reduction and plugging of the soil void spaces with asphalt.

IV. CONCLUSION

1. Poorly graded Soil with high gypsum content of 76.0% could successfully be stabilized by cationic emulsified asphalt.

2. The unconfined compressive strength of the soil-emulsified asphalt mixture increase with increasing fluid content up to an optimum of 160 kPa at 17% fluid content, then decreases with further increment of fluid content, while bulk density exhibit similar behavior.

3-The addition of 17% fluid content (8% emulsion + 9% water content) to Gypseous soil causes a high reduction in the coefficient of permeability by 78% without aeration, while the coefficient of permeability shows more reduction of 97.8% when the loose mix left 2 hours for aeration.

REFERENCES

[1] S. Sarsam, A. Al-Saidi, B. Al-Khayat, "Implementation of Gypseous soil-asphalt stabilization technique for base course construction," Journal of Engineering, Vol.17 No. 5. 2011, (pp1066-1076), Iraq.

[2] A. Olutaiwo, A. Adedimila, , and U. Sidiq, "An Examination of the Use of Liquid Asphalt Binders in Road Works in Nigeria," Journal of Engineering and Applied Sciences, Vol. 3, No. 1, 2008 (pp 134-142).

[3] A. H. Al- Deffaee, "The Effect of Cement and Asphalt Emulsion Mixture on the Engineering Properties of Gypseous Soils", M. Sc. Thesis, Civil Engineering Department, University of Al – Mustansiria, 2002.

[4] Z. K. Al-Qhralosy, "Effect of Cyclic Soaking and Drying on Compressibility Characteristics of Gypseous Soils Stabilized with Emulsified Asphalt", M. Sc. Thesis, Civil Engineering Department, University of Al-Mustansiria, 2003.

[5] S. I. Sarsam, and S. W. Ibrahim, "Contribution of Liquid Asphalt in Shear Strength and Rebound Consolidation of Gypseous Soil", Engineering and Technology, Vol. 26, No. 4, 2008.

[6] A. A. Al-Mufty, and I. H. Nashat, "Gypsum Content Determination in Gypseous Soils and Rocks", Third International Jordanian Conference on Mining, Amman, 2010, (pp.500-506).

[7] K. H. Head, "Manual of Soil Laboratory Testing", Volume 2, Prentice, Press, London, 1982.

[8] ASTM, "Annual Book of ASTM Standards", Volume 04.03, American Society for Testing and Materials, West Conshohocken, 2010, USA.

[9] N. A. Al-Kawaaz, "Characteristics of Soil Asphalt Mixture", M. Sc. Thesis, College of Engineering, University of Baghdad, 1990.

[10] A. I. Al-Mhaidib, "Sabkha Soil in the Kingdom of Saudi Arabia, Characteristics and Treatment", Journal of King Saud University, Volume 14, No. 2, 2002 (pp 29-80).

[11] M. G. Al-Safarani, "Improvement Ability of Gypseous Soil Characteristics Using Cutback Asphalt and Lime" M. Sc. Thesis, Civil Engineering Department, 2007, University of Al – Mustansiria.

[12] M. Taha, A. Al-Obaydi, and O. Taha, "The Use of Liquid Asphalt to Improve Gypseous Soils", Al-Rafidain Engineering, Vol. 16, No. 4, 2008 (p 38-48).W.-K. Chen, *Linear Networks and Systems* (Book style). Belmont, CA: Wadsworth, 1993, (pp. 123–135).

Supporting a Multi-Story Building Raft Foundation by Bored Piles to Prevent Collapse Failure

Mohammed Y. Fattah[1] Karim H. Ibrahim Al Helo[2] Ayad H. Mseer[3]

Abstract— **A geotechnical site investigation is the process of collecting information and evaluating the conditions of the site for the purpose of designing and constructing the foundation for a structure, such as a building, plant or bridge. Good planning and management of a geotechnical site investigation is the key to obtaining sufficient and correct site information for designing a structure in a timely manner and with minimum cost for the effort needed.**

In this paper, a case study of a multi-story building in Baghdad city is analyzed. The building was originally designed to be supported by a raft foundation. During construction, unexpected settlement was recorded before completion of the tenth floor. It was then decided to stop the work and make the required calculations to check the adequacy of the raft foundation.

The calculations based on the soil investigation report showed that the allowable bearing capacity of the shallow foundation does not exceed 50 kN/m^2 which makes the raft unable to sustain the load imposed by eight stories.

The decision was to increase the foundation load carrying capacity by introducing a piled-raft system through construction of a number of bored piles 400 mm in diameter and 15.0 m long beneath the raft distributed around the column locations at spacing of 2.5 pile diameters.

As a result, monitoring of the building settlement showed that the settlement ceased after construction of piles. Finishing works were then continued and constructed safely.

1 Professor, Building and Construction Engineering Department, University of Technology, Baghdad, Iraq.

2 Assistant Professor, Building and Construction Engineering Department, University of Technology, Baghdad, Iraq.

3Lecturer, Building and Construction Engineering Department, University of Technology, Baghdad, Iraq.

Keywords— **Bored pile, raft, support, settlement, collapse.**

I. INTRODUCTION

THE effort and detail of the geotechnical site investigation to obtain sufficient and correct site information to select and design a foundation for a building in permafrost is complex. It depends on (Holubec Consulting Inc, 2010):

a) design criteria of the proposed structure;

b) historic knowledge of general site conditions and building performance;

c) drilling equipment availability;

d) time of year the work needs to be done may determine the geotechnical site investigation method and finally;

e) the overall costs.

Good planning for and management of a geotechnical site investigation program is the key to obtain sufficient and correct site information for designing a building foundation in a timely manner and with minimum cost for the effort needed. The effort and detail of the geotechnical site investigation program in permafrost is complex.

Preliminary Site Characterization (Description)

It is important that before a field investigation program is developed a preliminary site characterization based on published literature and clients and consultants information be prepared. The site characterization should include climate and ground temperature at commissioning of the building and at the end of its service life. The extent and timing of the preliminary site characterization is a function of the size and settlement sensitivity of the building and the nature of the

frozen ground. It can be an office (desk) study based on available information and may include a site visit. For larger and settlement sensitive buildings, it is suggested that a site visit be made during late summer when the ground thaw is at its greatest, when surface drainage and groundwater can be observed and test pits can be excavated at the proposed building site, and at potential construction borrow materials. Test pits during the deepest thaw depth, during August and September, allow a detailed examination of the first 3 m depth that may consist of a stratigraphy of fill, organic and disturbed soil layers respectively and the summer groundwater. This upper zone is frequently a critical zone in the design of the foundation, its excavation and grading plan.

Although the technical achievements in terms of the observations are the necessary ingredients for a new level of applications, it is paramount that new models need to be developed to link the observations to parameters describing the driving forces behind the deformations. With increasing precision levels, more subtle movements of the earth become detectable. Moreover, in many cases there will be more than one mechanism responsible for the detected deformation. For this reason, geographic information systems become indispensable to systematically combine all possible sources of additional information that may contribute to the model formulation (Ferretti et al., 2000).

The objective of this paper is to make a trial to support a multi-story building by bored piles to prevent continuous settlement and expected collapse due to unsuitable foundation design.

II. PROBLEM DEFINITION

The building of Al Khafaji hotel is located close to Al Muheet Street in Al Khademyah in Baghdad city capital of Iraq. It consists of ten floors and one floor for basement. It was constructed on sandy clay soil of moderate bearing capacity, that the soil investigation report showed that the bearing capacity will not exceed 5 ton/m^2 at depth of 4 m below the natural ground level (N.G.L.). This means that the specifications of such soil do not ensure supporting a building of more than four stories without any treatment. In addition, the design was decided to be a raft foundation at a depth of 4 m below the N.G.L. and beneath the basement which was surrounded by concrete walls.

The building is located at intersection of two secondary streets and it is of rectangular area (44.25 X 15) m. The structure of the building was designed of concrete skeleton with cantilevers on both of the mentioned streets; one of about 2 m width along the short side and the other is of 3 m width along the long side as shown in Figure 1.

After completion of the skeleton for the ten floors and execution of most of finishing works, signals of differential settlements appeared. Hence committee of execution established observation of the building settlement by daily surveying for many points and they recorded such differential settlement of about 120 mm at the corner were the two cantilevers intersect (Point B).

Building Inspectors Association of Southeastern Wisconsin (2003) stated that signs of collapse of a building are as follows: One or more walls are bowed or leaning, with signs of current or recent movement. Wall cracks may be greater than 1/4" (6 mm) wide. The total amount of wall deflection is one inch (25 mm) or more from the original wall construction. Water seepage may present at the floor line. Previously repaired wall cracks show signs of continued cracking. Horizontal wall cracks are usually associated with bowing and may open and close with the seasons. Diagonal wall cracks or displacement at vertical cracks are usually associated with leaning walls or wall bowing adjacent to wall irregularities. Vertical cracks are usually associated with shrinkage of concrete. There is no indication of settlement of the wall footings.

These guidelines were followed to inspect the building under consideration.
(Building Inspectors Association of Southeastern Wisconsin, 2003).

Staff of consultants from the Scientific and Engineering Consultant Bureau of the University of Technology in

Baghdad advised the staff of construction to stop the works up to study this case and making evaluation for the structure and finding the suitable solutions.

Soil Investigation:

For the purpose of evaluation of the structural design for foundations and redesign, the soil investigation was repeated through two boreholes of 20 m depth for both at the long side of the building and the samples were tested in the laboratories of the University of Technology.

The investigation showed that the soil is medium to dense clayey silty sand or clayey soil with sand. The standard penetration test values were found to be (19 – 21) at the first six meters from the natural ground level and (22 – 23) down to a depth of 12 m and (35 – 46) between (12 – 20) m. The level of the ground water table was found at a depth of 1.5 m from the natural ground level. The report showed that the bearing capacity at a depth of 4 m (beneath the raft foundation) is about (5 – 6) ton/ m^2. This ascertains that the constructed raft foundation is not able to support the building when it will be loaded by the dead and live loads.

Monitoring of Settlement:

During this period, monitoring of the building settlement was continuous and the settlement at Points A, B, C and D located at the building corners were recorded (see Figure 1). Figure 2 traces the recorded settlement at these points.

Redesign of foundation:

At the site visit and observing of different concrete elements, it was found that the skeleton is not defected and all the concrete works were constructed per high specifications and there is no any traces of cracks and no any water seepage inside the basement and no any inclination of any of the structural members. The compressive strength for the concrete seems to be of about 30 MPa. These reasons indicate that the treatment will be directed to support the skeleton instead of releasing parts of the loading by release of some of the upper floors from the building.

The practical proposed solution is to strengthen the existing raft foundation by constructing bored piles of small diameters under the raft foundation and bored piled of relatively large diameters along the two sides parallel to the two intersected streets described above. Then, the raft will be connected with the pile cap by connecting the reinforcement of the existing raft foundation with the reinforcement of the new pile cap.

After long discussion with the constructer, there was an agreement to support the raft foundation by bored piles of 400 mm diameter after making an opening in the raft with large accuracy without damaging of the reinforcement.

This method means that the raft foundation will be converted to piled raft foundation to ensure such sharing of loads between the piles and raft. The piled raft foundation will be regarded as geotechnical structure which consists of three elements, the piles, raft and soil. In design of the pile raft foundation, the load will be shared between the piles and the raft and the piles will be designed to carry loads which may exceed the load supported by single pile or may be more. For that reason, the raft foundation is combined with piles which will decrease the settlement by economic way in comparison with the principals of traditional foundation design methods.

The previous studied showed that the ratio of load which can be carried by pile group may be 28 to 79% of the total load and this ratio will be increased with increasing of numbers of piles (Fattah et al., 2013, 2015).

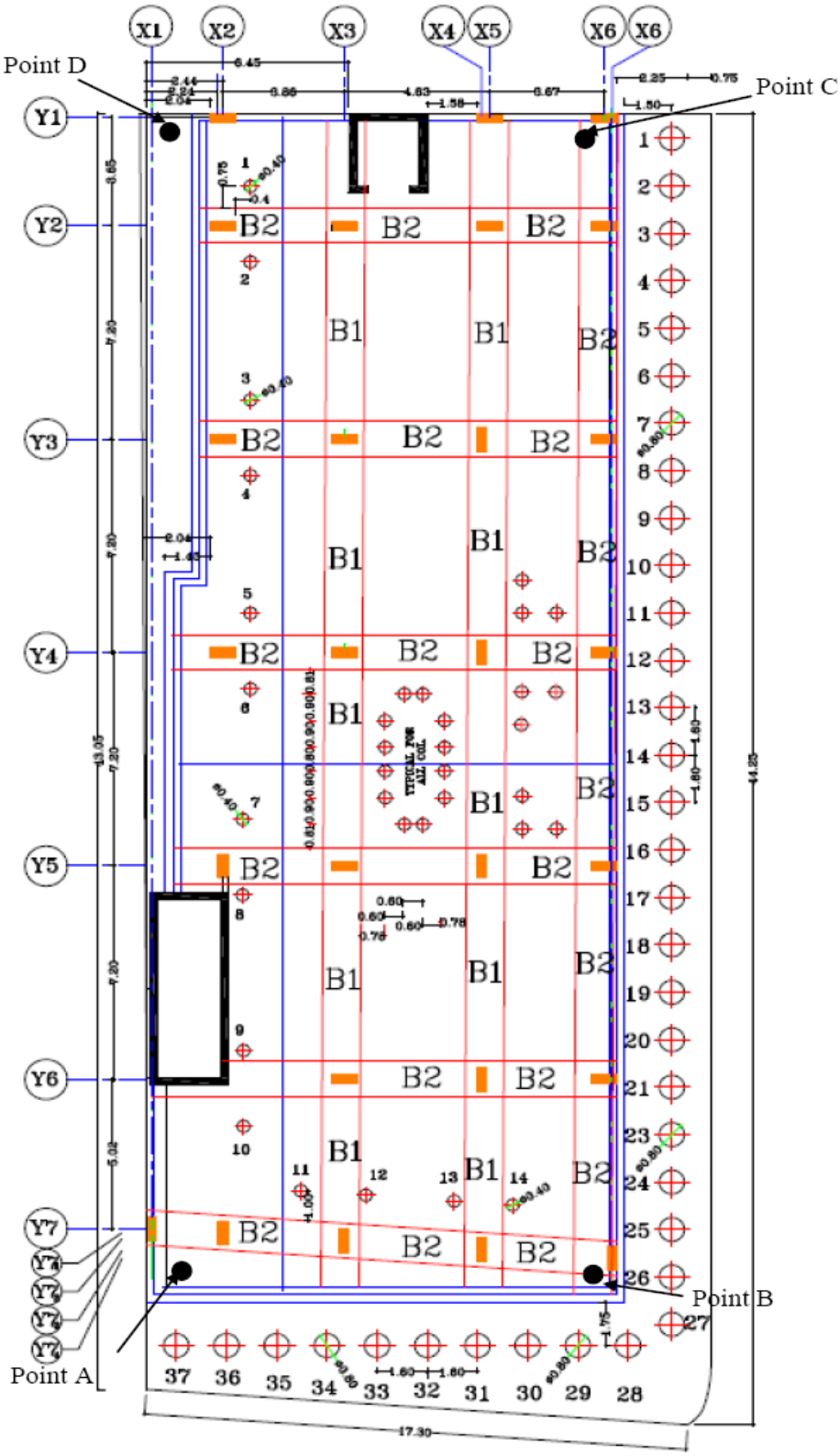

Fig. 1: Layout of the building showing observation points.

Calculation of piles capacity:

Statically method depending on the soil properties measured by laboratory tests.

Piles capacity can be calculated by many ways like:

From the field tests like standard penetration test and cone penetration test or others.

Laboratories tests:

The capacity of the pile to support the static load can be calculated through the following equation (Tomlinson and Woodward, 2008):

$$Qu = Q_b + Q_s \quad \text{---------- (1)}$$

where:

Qu: the load capacity of the pile,

Qb: end bearing of the pile, and

Qs: The total skin friction of pile.

For the purpose of determining Qs and Qb, many theories can be used like:

a. Nordlund Method:

According to this method, the pile capacity in sand soil can be calculated as follows:

$$Qu = \alpha_f .Nq.A_b.\sigma_L^{'} + \sum_{z=0}^{z=L} K.C_f .\sigma_z^{'}.\frac{\sin(\delta+\omega)}{\cos\omega} \quad \text{---------- (2)}$$

where:

α_f : non-dimensional factor for the relationship between the length of pile and its diameter,

Nq: factor of pile capacity,

A_b: cross sectional area of the pile,

σ_L' : the stress at the bottom of the pile,

K: factor of lateral soil pressure at depth z,

C_f : correction factor for k value when $\delta \# \phi$,

ϕ': effective angle of internal friction for soil,

δ: the angle of friction between the soil and the pile,

ω: angle of inclination of the pile with the vertical,

σ_z': effective overburden pressure acting at the centre of the pile length increment, ΔL ، $0 < z < L$, and

C_z: the perimeter of the pile at depth z.

It can be observed that the first term of the equation 2 is used to calculate the end bearing of the pile; and the second term is used to calculate the friction capacity. As the pile is supported by sandy soil; then the end bearing can be calculated from the first term of the equation. Then, the skin friction capacity cannot be calculated because the pile penetrates clay layers. The skin friction capacity in clayey soil can then be calculated using the α method according the following equation:

$$Q_s = \alpha_a .Cu.A_s \quad \text{---------- (3)}$$

where:

α_a : coefficient of adhesion,

Cu: undrained shear resistance, and

As: the surface area of the pile.

b. Tomlinson's Method

According to this method; the end bearing of the pile at sandy soil can be calculated as follow (Tomlinson and Woodward, 2008):

$$Q_b = \sigma_L'. Nq . A_b \quad \text{---------- (4)}$$

1. From the field tests:

Especially is by suing the standard penetration test (N).

a. Meyerhof Method:

The end bearing capacity can be calculated using the following equation:

$$Q_b = 0.8\ N \times L/B \quad < 8\ N \quad \text{---------- (5)}$$

Q_b will be in Ksf units. Q_b

Meyerhof suggested also the following equations for calculating the end capacity of piles using the magnitudes of standard penetration test (N) for driven piles:

$$Q_b = 0.45\ N \times L/B \quad (tsf) \quad \text{(for coarse sand)} \quad \text{------ (6)}$$

$$Q_b = 0.4\ N \times L/B \quad (tsf) \quad \text{(for medium sand)} \quad \text{------ (7)}$$

$$Q_b = 0.33\ N \times L/B \quad (tsf) \quad \text{(for fine sand)} \quad \text{----- (8)}$$

For the purpose of determination of the skin friction; Meyerhof suggested the following equation:

$$Q_s = N/50 \quad (tsf) \quad \text{---------- (9)}$$

where:

Q_s : the skin friction at ton / square foot, and

N: the ratio number of standard penetration test at all length of pile.

b. Martin et al. (1987):

The end bearing of pile can be determined by using the following equation:

$$q = C \cdot N \ (MN/m^2) \quad \text{---------- (10)}$$

C = 0.45 (for pure sand)

C = 0.35 (for silty sand)

Depending on the above equations; the load carrying capacity for the piles was calculated as follows:

1. For piles of 400 mm diameter; the load will be 30 tones.
2. For piles of 800 mm diameter; the load will be 80 tones.

Distribution of piles and signing up the sequence of construction:

After determination of the piles capacity according to the theoretical equations; the load exerted by the building was calculated to decide the number of needed piles.

Approximate weight of the building = 13,500 tones.

On assumption that the piles will support 50% of the building weight, then the load carried by the piles equals 6.750 tones.

Number of 800 mm diameter needed piles by assuming the distance between piles (centre to centre) will be two times the diameter of the pile:

27 piles are needed along the long side of the building, and

9 piles are needed along the short side of the building.

Total number of 800 mm diameter piles:

27 + 9 = 36 piles

Load can be carried by 36 piles is:

36 piles X 80 tones = 2,880 tones

The residual load is:

6,750 – 2,880 = 3,870 tones

The last mentioned load must be carried by internal 400 mm diameter piles and they are distributed according to the drawings (Figure 1) as follows:

10 internal piles (tension and compression piles) are needed along the long side of the building (the internal length opposite to the long side on the street).

4 internal piles (tension and compression piles) are needed along the short side of the building (the internal short side on the street).

3 piles x 4 bays = 12 piles will needed to surround each of the internal columns.

The number of internal columns is ten;

Then, 10 columns x 12 piles = 120 piles for surrounding the columns.

Total number of 400 mm diameter needed is:

10 + 4 + 120 = 134 piles

Total load that can be carried by 134 piles is:

134 x 30 tones = 4,020 tones

Total load carried by all the piles is:

2,880 + 4,020= 6,900 tones,

Thy last mentioned capacity is slightly higher than the load needed to be supported by all piles (6,750 tones).

For the purpose of stability of the building at the construction time and to prevent any defect in it, the procedure for construction of the piles was determined as follows:

1. Construction of the internal piles (400 mm diameter) which were numbered 1 to 10 as shown in Figure 1 in the beginning of the work. These piles will work as tension piles to prevent the overturning of the building outward when the external 800 mm diameter piles will be constructed.
2. The second stage is to construct the piles having the numbers 11 to 14.
3. The third step is to construct the internal piles (surrounding columns). The work will be started by demolishing an exacted area of the existing raft foundation for an area enough for execution three piles oriented in one corner of one column. The piles in the same bay will wait to another stage of time. In the same time, one can demolish the raft foundation in far corners related to other column to be

ready for casting and to execute piles away from that which had been just executed.

4. These procedures will ensure not to demolish a large area of the raft foundation in one bay to prevent any structural defect.
5. The last stage is to execute the external piles which are of 800 mm diameter at an spacing of 1.6 m (centre to centre). To prevent any failure of soil at construction time; it must be constructed by the sequence of constructing piles 1, 4, 7, 10 etc. and then 2, 5, 8 and the residual.
6. The construction of the external piles can be established after a reasonable time (one month) after execution of 1 to 14 piles and finishing the the raft foundation casting.

Figures 3 to 7 illustrate the stages of construction of bored piles.

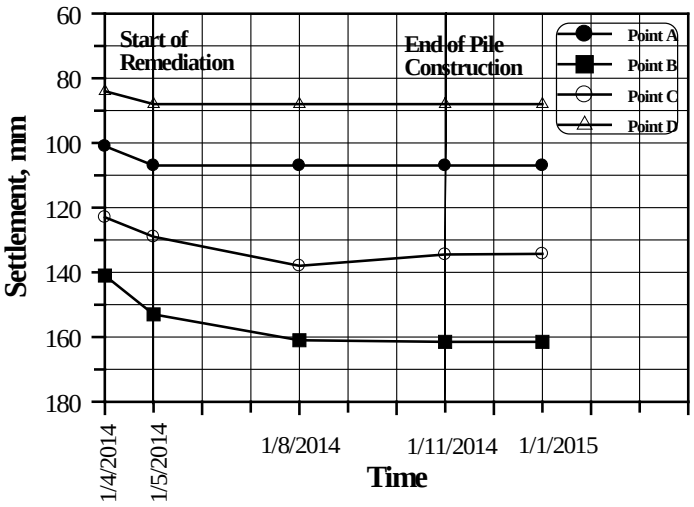

Fig. 2: Recorded settlement at selected points in the building.

a.

b.

Fig. 3: Boring of a pile.

a.

b.

Fig. 4: Inserting the cage of reinforcement through a pile.

Fig. 5: Pouring of concrete in a pile.

Fig. 6: Reconstruction of a raft (pile cap).

a.

b.

Fig. 7: Bonding of pile and raft reinforcement.

Conclusions:

1. The remediation work of the building which includes cantilevers from two sides started with construction of the internal piles in the beginning of the work. These piles worked as tension piles to prevent the overturning of the building outward when the external piles were constructed.
2. The construction of the internal piles (surrounding columns) required demolishing an exacted area of the existing raft foundation for an area enough for execution three piles oriented in one corner of one column. The piles in the same bay waited to another stage of time. In the same time, the raft foundation in far corners related to other column was demolished to be ready for casting and to execute piles away from that which had been just executed. These procedures ensured not to demolish a large area of the raft foundation in one bay to prevent any structural defect.
3. Good planning and management of a geotechnical site investigation program is the key to obtain sufficient and correct site information for designing a building foundation in a timely manner and with minimum cost and effort.

REFERENCES

1. **Fattah, A. Y., Yousif, M. A., Al-Tameemi, S. M., (2013), "Bearing Capacity of Pile Group and Piled Raft Foundations on Sandy Soil", Journal of Engineering and Development, University of Al-Mustansiriya, Vol. 17, No.2, pp. 64-96.**
2. **Fattah, A. Y., Yousif, M. A., Al-Tameemi, S. M., (2013), " Effect of Pile Group Geometry on Bearing Capacity of Piled Raft Foundations", Structural Engineering and Mechanics, Vol. 54, No. 5, Techno-Press Ltd., Korea, DOI: http://dx.doi.org/10.12989/sem.**
3. **Ferretti A., Ferrucci F. Prati C., Rocca F., (2002), "SAR Analysis of Building Collapse by Means of the Permanent Scatterers Technique" - Proceedings of the International Geoscience and Remote Sensing Symposium (IGARSS 2000).**
4. **Building Inspectors Association of Southeastern Wisconsin, (2003), "Best Management Standards for Foundation**

Repair", Wisconsin Association of Foundation Repair Professionals, www.WAFRP.com, USA, pp. 47.

5. **Holubec Consulting Inc., (2010), "Geotechnical Site Investigation Guidelines for Building Foundations in Permafrost", Prepared for: Department of Public Works and Services Government of the Northwest Territories, USA.**
6. **Tomlinson, M., Woodward, J., (2008), "Pile Design and Construction Practice", 5th edition, Taylor & Francis, New York, USA.**

Precious Experimental and Numerical Investigation of the Behavior of Strip Footing in Reinforced Sandy Soil with Geogrids under Different Loading Conditions

Aram M. Raheem, and Mohammed A. Abdulkarem

***Abstract*— For decades, the advantageous effects of using reinforcement to enhance the property of soil have been established. Lately, the use of geogrid reinforcement has increased enormously in geotechnical application. Soil reinforcement techniques have become constructive and economy to handle several complications in geotechnical engineering practice, such as improve the bearing capacity and settlement characteristics of the footing. A comparative large scale experimental and numerical study of the behavior of a strip footing under eccentric and inclined loading resting on a sandy soil reinforced with geogrid is presented. Several patterns of geogrid arrangement with number of geogrid layers, vertical spacing of layers, depth to the topmost layer of geogrid, distance between the layers and up to 280 experimental tests were investigated. A finite elements numerical study on a plane strain and fully 3-D conditions were performed. Test results specify that the footing performance could be appreciably enhanced by the presence of layers of geogrid. Nevertheless, the efficiency of the sand-geogrid system is dependent on the load eccentricity ratio and reinforcement parameters. Precious agreement between the experimental and 3-D numerical analysis is observed. Based on the numerical and experimental results, detailed values of the geogrid parameters for maximum reinforcing effect is created.**

***Index Terms*— strip footing, reinforced soil, geogrids, experimental study, FE analysis.**

I. Introduction

A strip footing is widely used in transferring loads from the superstructure to the supporting soils. Normally, theses footings might be under the impact of moments and shears in addition to vertical loads from different sources such as winds, earthquakes, earth pressure and water [1]-[3]. Consequently, an eccentric load or an eccentric-inclined load can replace such forces or moments where the bearing capacity of a foundation with such loading conditions can be considered one of the most fundamentals in geotechnical area. The footing eccentricity is possible to be canceled by moving the column from the center of the footing leading to uniform pressure distribution under the footing. Nevertheless, this solution is not possible always due to the interaction between the footings with the adjacent nearby footings leading to uneconomical design accompanied with structural problems. Eccentric loading could lead to differential settlement causing the footing to tilt. The amount of tilt and the pressure under the footing change based on the value of the eccentricity to the footing width ratio. When this ratio is less than 1/6, some tension zone will develop a way from the footing. Since the soil cannot sustain any tension, such situation cannot exist. Consequently, the contact area between the footing and the soil decreases with significant reduction in the bearing capacity and a great increase in the footing size making the design uneconomical.

Ramlot and Vandeperre [4] introduced the results of a model test with eccentrically loaded square and circular footings. Meyerhof [5] pointed out that the average bearing capacity of a footing decreases parabolically with an increase in eccentricity. Prakash and Saran [6] tried theoretical solution of the problem on the basis of the superposition technique. Purkayastha and Char [7] investigated stability analysis of a strip foundation on sandy soil with eccentric loading and suggested a reduction factor for quantifying the bearing capacity of eccentrically loaded footings. To reduce footing tilt, Mahiyar and Patel [8] examined an angle shaped footing exposed to eccentric loading.

Any forms of soil reinforcement is increasing the bearing capacity and decreasing the expected settlement of the soil. Different types of reinforcement layers have been used to reinforce the underneath soil such as galvanized steel strips, geotextiles, and geogrids [9]. The mechanism of mobilizing the frictional resistance in geogrids is different from that of geotextiles [10], [11]. In geogrid-reinforced soils, both the transverse members of the geogrid together with the longitudinal ribs frictionally interact with the soil, maintaining interfacial shear strength resisting the lateral flow. This mode of frictional interaction is not just interfacial but due to

Special thanks and appreciations to the civil engineering department at the University of Tikrit in Iraq for their help and support to the experimental work of this study.

Aram M. Raheem is a Ph.D. Student at Civil and Environmental Engineering Dept., University of Houston, Houston, TX 77004 USA (phone: 713-822-3838; e-mail: amraheem@uh.edu).

Mohammed A. Abdulkarem, Formerly M.Sc. Holder, Civil Engineering Dept., College of Engineering, Tikrit University, Tikrit, Iraq. (e-mail: En.muhammed@yahoo.com).

passive resistance mobilized by the bearing of soil particle as well. Mainly, it was concluded that geogrids generally offer a higher interfacial shearing resistance than geotextiles [12].

The response of footings loaded over a reinforced soil bed by metal strips has been investigated by Binquet and Lee [13] and Fragaszy and Lawton [14]. Binquet and Lee [13] pointed out that the bearing capacity of shallow foundations could increase by (2 to 4) times when the underneath soil is reinforced by galvanized steel strips. Additionally, Binquet and Lee [13] categorized three different types of failure mechanisms, specifically (1) the interface shear failure between steel strips and adjacent soil mass, (2) shear failure in top soil layer, and (3) tensile failure of the steel strips. Laboratory model tests on square footing to quantify the bearing capacity of foundations reinforced with geogrids and geotextiles have been conducted by Guido et al. [15]. Khing et al. [16] examined the bearing capacity of a strip foundation placed over reinforced sandy soil and concluded that the bearing-capacity ratio at limited levels of settlement is about 67% to 70% of the bearing-capacity ratio computed on the basis of the ultimate bearing capacity. Multiple layers of geogrids have been used through laboratory tests and it was determined that for the same soil, geogrid, and configuration, the ultimate bearing capacity increases with the increase in embedment ratio (D_f /B) [17]. In addition, it was found that the maximum depth of reinforcement measured from the bottom of the foundation, which contributes to the increase of the bearing capacity ratio, is about 1.8 times the foundation width [18]. Furthermore, for a maximum bearing-capacity ratio, the optimum width of the geogrid layers was about 8B in sand and 5B in clay [19]. It was pointed out that the bearing capacity ratio of sand-geogrid system decreases with an increase in the width of the foundation [20]. Test results indicate that the use of geosynthetic reinforced soil foundations may increase the ultimate bearing capacity of shallow spread footings by a factor of 2.5 [21]. The performance of different types of geosynthetics for strip foundations was compared [22]. Finite element method (FEM) with the use of elasto-plastic solution has been obtained to determine the bearing capacity of foundation without any reinforcements for various soils and loading conditions [23]-[25]. The stability of reinforced soil mass as a homogenous anisotropic material were analyzed through rigid plastic FEM [26], [27]. Numerical study was used through FLAC software to study the effect of geosynthetic reinforcement arrangement on two square footings on sandy soil [28], [29]. Yu and Sloan [30] modeled lower and upper bound limit analysis for a reinforced soil mass which were quite similar for solving the different bearing capacity problems without any reinforcement [31]-[34]. Limit equilibrium method was used to incorporate the effect of the reinforcement on the bearing capacity of foundations [35]. The upper bound theorem of limit analysis with the geometry assumption for collapse mechanism for calculating the bearing capacity of reinforced foundations was studied by Michalowski [36]. Fast Langrangian analysis was used to inspect the performance of a multilayered geosynthetic reinforced granular bed [37].

II. Objective

The overall objective of the study was to investigate the effectiveness of geogrid reinforcement on sandy soil of a strip footing under eccentric and inclined loading. The specific objectives were as follows:

A. Study the behavior of strip footing under eccentric and inclined loading on sandy soil reinforced with geogrid through large-scale experimental laboratory testing.

B. Explore the effectiveness of geogrid reinforcement using several arrangement patterns of different layers, vertical spacing of layers, depth to the topmost layer of geogrid and distance between the layers.

C. Perform numerical comparative study using plain strain and 3-D finite element analysis.

III. Materials and Methods

Laboratory Model Tests

Model Test Tank

The soil layers were prepared in a steel box with 900 mm × 900 mm and 550 mm dimensions made with a plate thickness of 6 mm supported by four steel channels as shown in Figure 1. The inner faces of the steel box were painted to minimize the slide friction between the soil and steel box that may develop during experimental testing. A mark lines were identified carefully to give preciously the required thickness of the soil layers and the location of the geogrid.

Footing

A strip steel channel of 80 mm in plan was used to represent the tested footing (Figure 2). The transferred load to the footing was measured with a proving ring of 5 kN capacity. Both horizontal and vertical displacements were measured using three dial gauges (0.01 mm/ division).The footing size was made based on the size of the steel model tank and the zone of the influence.

Test Material

A. Sand Properties

A poorly graded sand passing sieve No. 4 was used in this study. The sand was washed with running water to remove the dust as much as possible. Testing has been performed with dense and medium dense sand corresponding to approximately (16.9) kN/m^3 and (17.5) kN/m^3 consistent with relative densities of (60) % and (80) % respectively. The maximum and minimum dry unit weights of the sand were determined according to the ASTM (D 4253-00) and ASTM (D 4254-00), respectively.

Figure 1. Laboratory Testing Box.

Figure 2. Strip Footing Represented by Steel Channel.

The results have shown maximum and minimum dry unit weight of sand as 18 kN/m^3 and 15.6 kN/m^3 respectively. The specific gravity of the sand was 2.59 and the test has been done based on the ASTM D-854. The grain size distribution analysis of the sand was performed according to the ASTM D-421 and it can be seen in Figure 3. The sand was classified according to the unified classification system as poorly graded sand with coefficient of uniformity (C_u) = 3.0 and coefficient of curvature (C_C) = 1.0.

B. Geogrid

One type of commercially available geogrid type was used TriAx® TX140 Geogrid manufactured from a punched polypropylene sheet, which was oriented in three significantly equilateral directions so that the subsequent ribs shall have a high degree of molecular orientation. The properties influencing the performance of a mechanically stabilized layer are shown in Table 1.

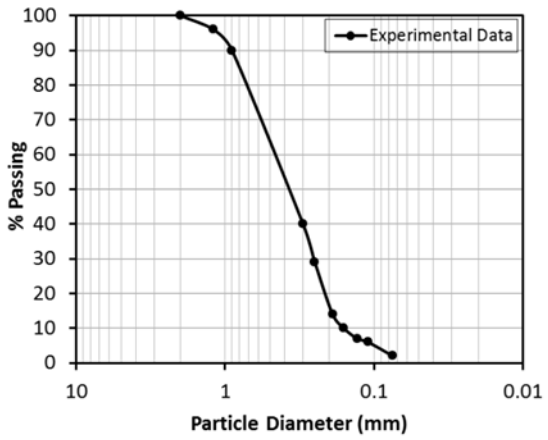

Figure 3. Particle Size Distribution of Tested Sand.

IV. Experimental Setup and Test Program

The footing was located in the centerlines of both length and width of the tank that already filled with sandy soil and the applied load on the footing was measured through the proving ring up to the failure. A series of experimental tests on the strip footing has been performed in order to study the overall behavior of reinforced soil by geogrid under inclined and eccentric loading.

Table 1. Engineering properties of Tenax TT Samp geogrid.

Index Properties	**Long.**	**Diag.**	**Trans.**	**General**
Rib pitch, mm(in)	40(1.6)	40(1.6)	-	
Mid-rib depth mm(in)	-	1.2(0.05)	1.2(0.05)	
Mid-rib width mm(in)	-	1.1(0.04)	1.1(0.04)	
Rib shape				Rectangle
Aperture shape				Triangle
Structural Integrity				
Junction efficiency				93
Aperture stability kg-cm/deg @ 5 kg-cm				3.0
Redial Stiffness at low strain, kN/m @ 0.5% strain (lb/ft @0.5% strain)				225 (15430)
Durability				
Resistance to chemical degradation				100%
Resistance to ultra-violent light and weathering				100%

V. The Studied Parameters

The bearing capacity of strip footing under inclined and eccentric loading resting on geogrid-reinforced sand has been studied under the impact of different parameters. In the

current study, these parameters have been varied within their acceptable ranges to investigate their effects on the bearing capacity and on each other. The effects of load inclination, load eccentricity, the number of geogrid layers and the depth of the topmost layer of the geogrid were studied. The load inclination (α) and eccentricity (e/B) were varied from 0^o to 15^o and from 0 to 0.15 respectively. Additionally, the number of geogrid layers (N) was varied from 1 to 5 while the depth of the topmost layer of geogrid (U/B) was ranged from 0.25 to 1.5. The distance between the consecutive layers (h/B) varied from 0.25 to 0.95. All above parameters were studied for two different relative densities (60% and 80%) to simulate medium and dense sand. The term bearing capacity ratio (BCR) is used to express the combined effect of soil reinforcement with load inclined and eccentricity on bearing capacity and it can be shown as follows:

$$\mathrm{BCR} = \frac{q_{ur}}{q_u} \quad (1)$$

where q_{ur} is the ultimate bearing capacity of inclined and eccentrically load strip footing on reinforced sand while q_u is the ultimate baring capacity of strip footing on unreinforced sand.

VI. Finite element analysis (FEA)

A series of two and three-dimensional nonlinear FEA on a prototype footing on reinforced sand was implemented to verify the laboratory model tests results and understand the deformation trends within the soil mass where plain strain condition was assumed for the two- dimensional case analysis. The analyses were performed using the finite element program Plaxis [38]. Plaxis is capable of modeling an extensive range of geotechnical problems such as piles, deep excavations, tunnels, and earth structures such as retaining walls and slopes. A strip footing rested on sandy soil with similar geometry to large-scale laboratory prototype was modeled. The same properties of sand and geogrid material were used in the FEA study.

A. Finite-element modeling

The nonlinear performance of sand was simulated using the hardening soil model, which is an elastoplastic hyperbolic stress-strain model, expressed in the framework of friction hardening plasticity. The foundation was modeled as elastic beam elements according to Mindlin's beam theory with significant flexural rigidity (EI) and normal stiffness (EA). The interaction between the geogrid and soil is demonstrated at both sides using interface elements, which allow for the condition of a reduced wall friction compared to the friction of the soil. An essential characteristic of the hyperbolic model is the stress dependency of soil stiffness.

The controlling state of stress are illustrated by means of the secant Young's modulus (E_{50}^{ref}), Poisson's ratio (μ), effective cohesion (c), angle of internal friction (ϕ) and interface reduction factor (R_{int}).

A refined mesh was created to minimize the influence of mesh reliance on the finite element modeling of cases including changes in the number, length, and the location of geogrid layers. An applied footing load was simulated in increments load control method through iterative analysis up to failure. The boundary conditions were selected such that the vertical boundaries are free vertically and constrained horizontally while the bottom horizontal boundary is fully fixed.

The analyzed prototype shape geometry, generated mesh, the boundary conditions, and deformed mesh for both 2-D plain strain and 3-D analyses are shown in Figures. 4 and 5 respectively. The effects of geogrid layer numbers, sand relative density, the load inclination, and the load eccentricity on the behavior of the footing have been examined.

An internal angle of friction and secant Young's modulus representing medium dense and dense sand conditions derived from a series of drained triaxial compression tests were used for the sand [1]. Table 2 includes the full details of the material properties that have been used in the FEA.

Table 2. Material properties used in FE analysis.

Parameter	Dense Sand	Medium Dense Sand	Footing	Geogrid
Secant Young modulus E_{50}^{ref} (kPa)	40000	30000	-	-
Cohesion (c) (kPa)	0	0	-	-
Friction angle ϕ	39	34	-	-
Soil unit weight (γ) (kN/m^3)	17.5	16.9	-	-
Poisson's ratio (ν)	0.3	0.28	-	-
Interface reduction factor (R_{int})	0.8	0.8	-	-
EA of the footing (kN/m)	-	-	5000000	-
EI of the footing (kN m^2/m)	-	-	8500	-
EA of the geogrid (kN/m)	-	-	-	2000

B. Mesh details

In two-dimensional modeling, plain strain condition of 15-noded triangular elements having total number of elements equal 211, total number of nodes equal 1759, total number of stress points equal 2532 and average element size of 48.5 mm for soil have been used. The footing was represented as an elastic beam with 5-noded line element having 4 Gauss point while the geogrid was identified as 5-node line element with 4-point Newton-Cotes. In three-dimensional modeling, three-dimensional parallel planes with 15-noded wedge elements

having total numbers of elements equal 728, total numbers of nodes equal 2365 and average element size of 782 mm have been used. Both the footing and the geogirds were represented as three- dimensional thin floor.

VII. Results and Analysis

A. Experimental results

1. Optimum Number of Geogrid Layers

In Figures 6 and 7, the relationship between the number of geogrid layers (N) and the bearing capacity ratio (BCR) for different values of load inclinations (α) for relative densities 60% and 80% are shown, respectively. It is clearly indicated that the (BCR) significantly increased with the increase of number of geogrid layers. Furthermore, there are an optimum number of geogrid layers where slightly increase in the (BCR) can be observed.

In Figures 8 and 9, the relationship between the number of geogrid layers (N) and the bearing capacity ratio (BCR) for different values of load eccentricity ratio (e/B) for relative densities 60% and 80% can be inspected, respectively. It is obviously shown that the BCR significantly increased with the increase of the number of geogrid layers. The optimum value for N is also obtained where almost no change in the BCR could be noticed.

The effect of the number of the geogrid layers (N) on the horizontal displacement of the footing due to load inclinations (α) in 60% and 80% relative density can be shown in Figures 10 and 11 respectively. Increasing the reinforcement layers (N) decreases the the horizontal displacements for different values of load inclination (α) for both tested relative densities 60% and 80% respectively.

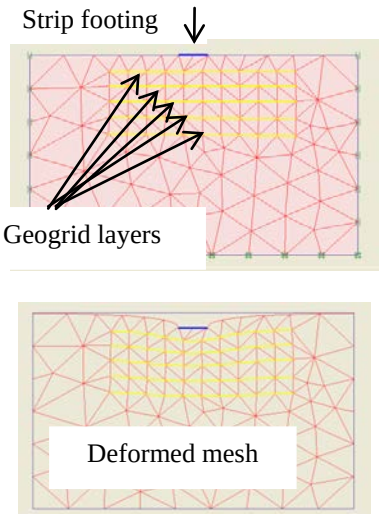

Figure 4. Finite element modeling with two-dimensional representation of strip footing in sandy soil reinforced with multiple geogrid layers.

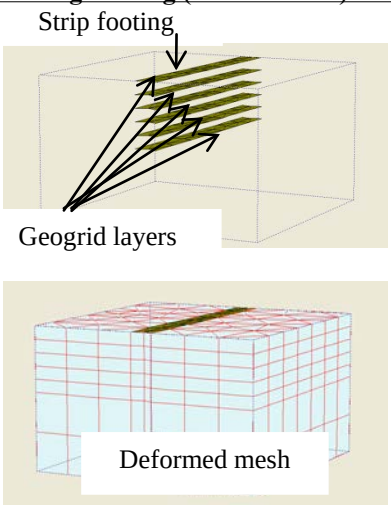

Figure 5. Finite element modeling with three-dimensional representation of strip footing in sandy soil reinforced with multiple geogrid layers.

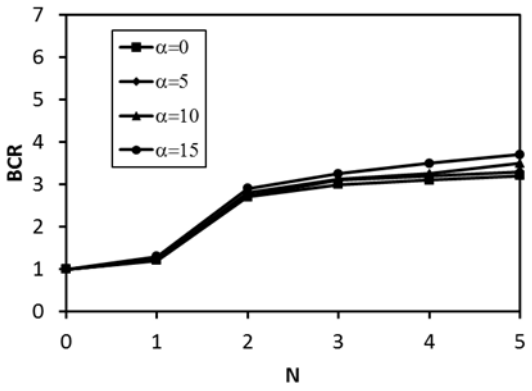

Figure 6. Bearing capacity ratio (BCR) versus Number of reinforcement layer (N) for (α = 0°, 5°, 10° and 15°) and (RD=60%).

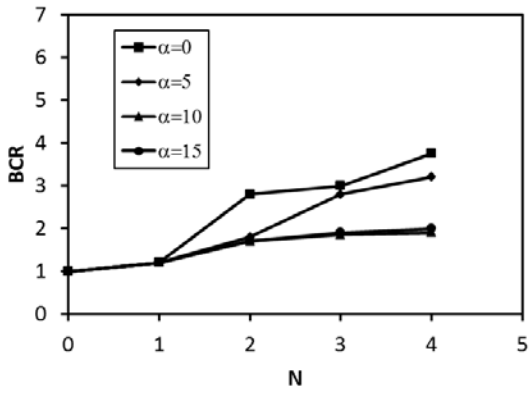

Figure 7. Bearing capacity ratio (BCR) versus Number of reinforcement layer (N) for (α = 0°, 5°, 10° and 15°) and (RD= 80%).

Footing tilting, which is the ratio of the difference between the settlements of the two edges of the footing to the footing width, of reinforced sandy soil with different number of geogrid layers (N) on 60% and 80% relative density has been shown in Figures 12 and 13 respectively. Footing titling increased with the increase of the reinforcement layers (N) for

different values of eccentricity ratio (e/B) for relative densities 60% and 80%, respectively.

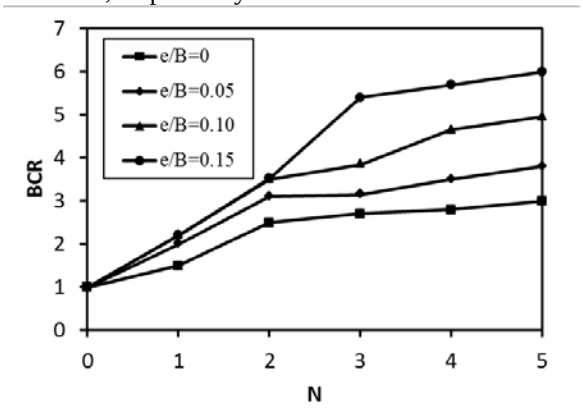

Figure 8. Bearing capacity ratio (BCR) versus number of reinforcement layer (N) for (e/B = 0, 0.05, 0.10 and 0.15) and (RD=60%).

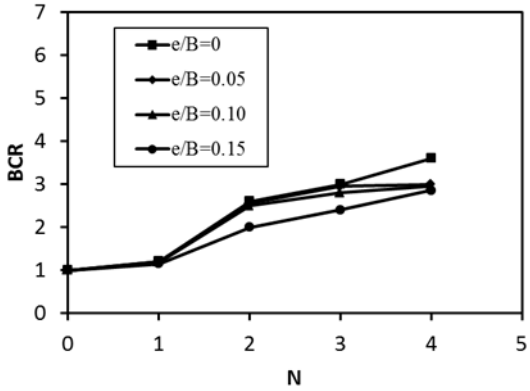

Figure 9. Bearing capacity ratio (BCR) versus number of reinforcement layer (N) for (e/B = 0, 0.05, 0.10 and 0.15) and (RD=80%).

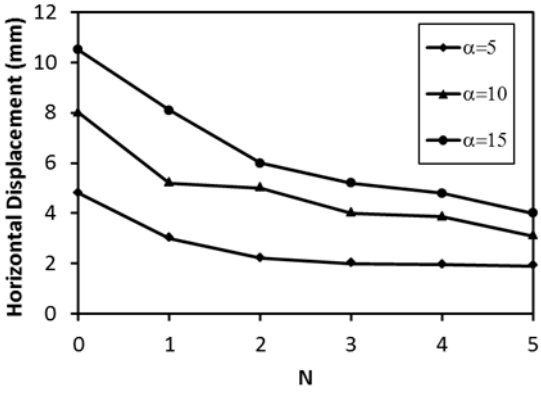

Figure 10. Horizontal displacement (mm) versus number of reinforcement layer (N) for different values of (α) and (RD= 60%).

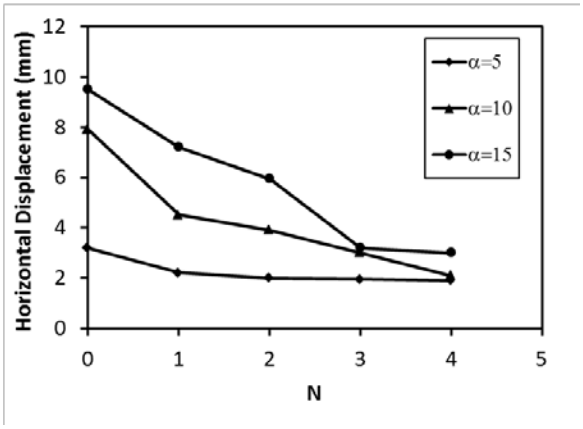

Figure 11. Horizontal displacement (mm) versus Number of reinforcement layer (N) for different values of (α) and (RD= 80%).

Figures 6 to 13 show the effect of the relative density (RD) on the bearing capacity ratio (BCR), horizontal displacements, the tilt for different values of load inclination (α), and load eccentricity ratio (e/B) for strip footing on sandy soil. Increasing the soil relative density has improved the strength of the soil that led to decrease all the studied parameters such as bearing capacity ratio (BCR), optimum number of reinforcement layers (N), horizontal displacement and footing tilting. Furthermore, it is observed that the bearing capacity ratio (BCR) for the medium sand is larger than that for the dense sand. The reinforcement is more adequate for medium sand than dense sand considering the unreinforced loaded case for each relative density as a reference, according to the definition of bearing capacity ratio (BCR). It should be mentioned that Figures 6 to 13 could be used as design charts to obtain the number of reinforcement layers required to cancel or to reduce the effect of load inclination and eccentricity or even to increase the factor of safety.

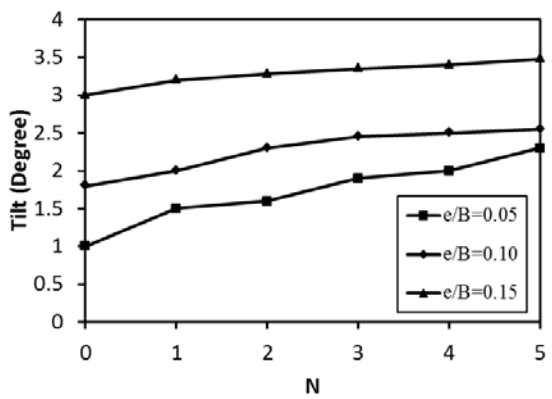

Figure 12. Tilt (Degree) versus number of reinforcement layer (N) for (e/B = 0, 0.05, 0.10 and 0.15) and (RD= 60%).

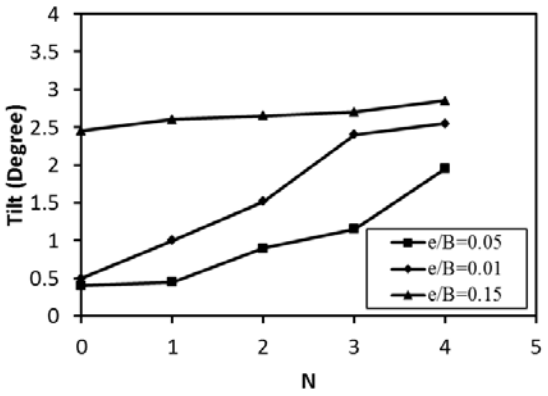

Figure 13. Tilt (Degree) versus number of reinforcement layer (N) for (e/B = 0, 0.05, 0.10 and 0.15) and (RD= 80%).

2. Optimum Depth of Topmost Layer

The optimum value of topmost layer of reinforcement (U/B) is obtained by changing the position of a single layer of reinforcement until no change in the bearing capacity ratio can be noticed. Figures 14 and 15 show the relationship between the topmost layer (U/B) and the bearing capacity ratio (BCR) for different load inclination (α) for two relative densities 60% and 80% respectively.

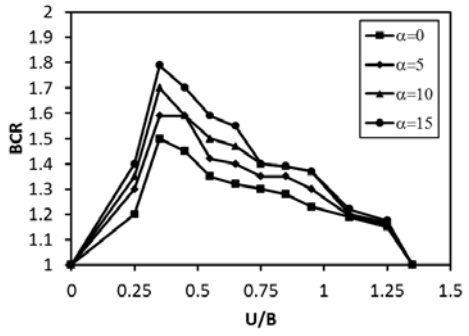

Figure 14. Bearing capacity ratio (BCR) versus the depth ratio of the topmost layer of reinforcement (U/B), for (α = 0°, 5°, 10° and 15°) and (RD = 60%).

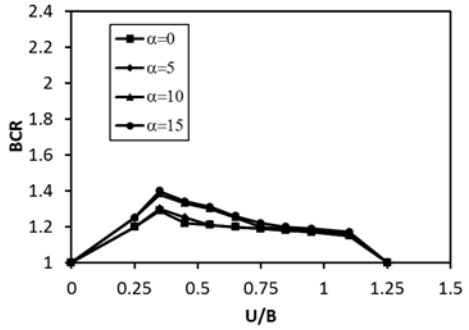

Figure 15. Bearing capacity ratio (BCR) versus the depth ratio of the topmost layer of reinforcement (U/B), for (α = 0°, 5°, 10° and 15°) and (RD = 80%).

Figures 16 and 17 show the relationship between the topmost layer (U/B) and the bearing capacity ratio (BCR) for different eccentricity ratio (e/B) for two relative densities 60% and 80% respectively.

It can be understood with increasing the depth of topmost layer (U/B), the bearing capacity ratio (BCR) enhances until achieve the maximum value when U/B=0.35, then after this point with increasing the depth of topmost layer (U/B) , the bearing capacity ratio (BCR) decreases. Figures 14 to 17 show the influence of the relative density (RD) on the value of topmost layer (U/B) for inclined and eccentrically loaded strip footing. It is obvious that the variation of relative density (RD) has no effect on the optimum value of topmost layer (U/B) but has a major effect on the value of bearing capacity ratio (BCR).

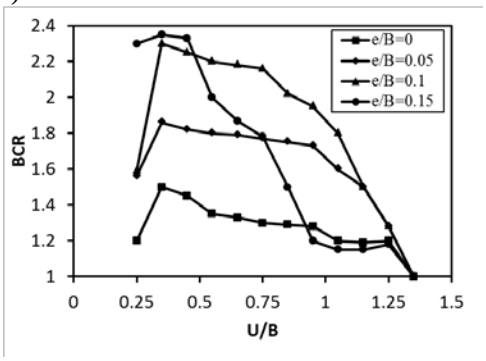

Figure 16. Bearing capacity ratio (BCR) versus the depth ratio of the topmost layer of reinforcement (U/B), for (e/B = 0, 0.05, 0.10 and 0.15) and (RD= 60%).

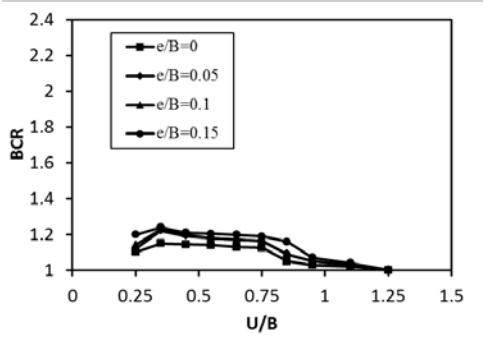

Figure 17. Bearing capacity ratio (BCR) versus the depth ratio of the topmost layer of reinforcement (U/B), for (e/B = 0, 0.05, 0.10 and 0.15) and (RD = 80%).

3. Optimum Vertical Distance between Geogrid Layers

For two layers of reinforcement, it has been maintained the first layer at (U/B=0.35) while the second layer location was changed with varying (h/B) (0.25, 0.35, 0.45, 0.55, 0.65, 0.75 and 0.85). Figures 18 and 19 show the relationship between the vertical distance ratio between consecutive layers of geogrid (h/B) and the bearing capacity ratio (BCR) for different load inclination (α) for two relative densities 60% and 80% respectively. Figures 20 and 21 show the relationship between the vertical distance ratio between consecutive layers of geogrid (h/B) and the bearing capacity ratio (BCR) for different eccentricity ratio (e/B) for two relative densities 60% and 80% respectively. It can be realized that maximum value of (h/B) is (0.25). Beyond this point, increasing the vertical distance (h/B) decreases the bearing capacity ratio (BCR).

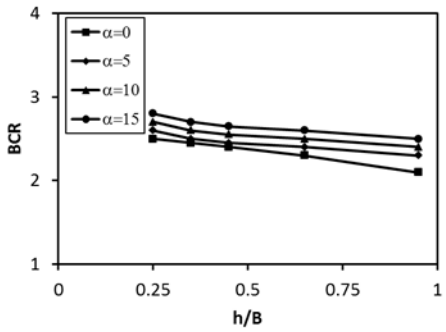

Figure 18. Bearing capacity ratio (BCR) versus the vertical distance ratio between consecutive layers of geogrid (h/B), for (α = 0°, 5°, 10° and 15°) and (RD= 60%).

Figures 18 to 21 show the effect of the relative density (RD) on the value of (h/B) for inclined and eccentrically loaded strip footing. It is obvious that the variation of (RD) has no effect on the optimum value of (h/B) but has a major effect on the value of (BCR).

For three and four layers of reinforcement, the first layer was kept at (U/B=0.35), also, the vertical distance (h/B) was kept constant (0.25).

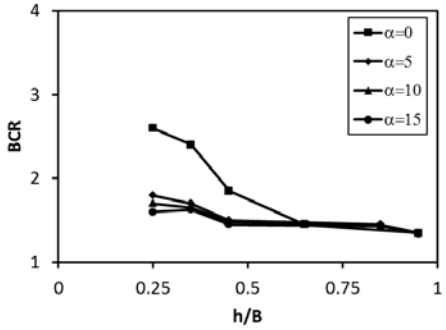

Figure 19. Bearing capacity ratio (BCR) versus the vertical distance ratio between consecutive layers of geogrid (h/B), for (α=0°, 5°, 10° and 15°) and (RD= 80%).

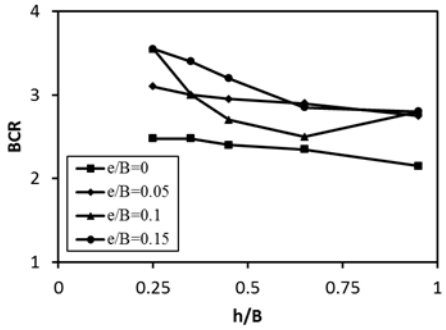

Figure 20. Bearing capacity ratio (BCR) versus the vertical distance ratio between consecutive layers of geogrid (h/B), for (e/B =0, 0.05, 0.10 and 0.15) and (RD= 60%).

B. Finite element analysis

Finite element analyses via 2-D and 3-D evaluation have been used in the study. The analyses included the verification of BCR quantification of different load inclination angle and different load eccentricity of sandy soil with both tested relative densities (60% and 80%) for up to four consecutive geogrid layers. Furthermore, the analyses included the verification of both horizontal displacement and tilting angle of the strip footing for up to four consecutive geogrid layers. In order to determine the accuracy of the FE predictions, the coefficient of determination (R^2) is used as a quantification parameter which is defined as follows (Eq. 2):

$$R^2 = \left(\frac{\sum_i \left(x_i - \bar{x}\right)\left(y_i - \bar{y}\right)}{\sqrt{\sum_i \left(x_i - \bar{x}\right)^2} \sqrt{\sum_i \left(y_i - \bar{y}\right)^2}} \right)^2 \quad (2)$$

where y_i is the actual value; x_i is the calculated value from the model; $\bar{y}$ is the mean of actual values; $\bar{x}$ is the mean of calculated values and N is the number of data points.

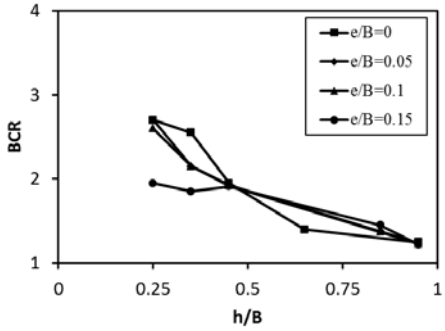

Figure 21. Bearing capacity ratio (BCR) versus the vertical distance ratio between consecutive layers of geogrid (h/B), for (e/B = 0, 0.05, 0.10 and 0.15) and (RD= 80%).

1. Load inclination angle (α)

The finite element verification of the bearing capacity ratio (BCR) of different geogrid layers under different load inclination angle (α) which varied from 0^o to 15^o for 60% and 80% relative density is shown in Figure 22 (a to d). For the studied cases, the 3-D prediction was more accurate than 2-D which was indicated through the coefficient of determination (R^2) due to the fact that 3-D representation is more realistic and closer to the real case scenario. As the sand relative density increased from 60% to 80%, the R^2 changed from 0.87 to 0.80 and 0.91 to 0.87 for 2-D and 3-D analyses under zero load inclination respectively. When the load inclination was 15^o and with the increase of sand relative density from 60% to 80%, the R^2 changed from 0.87 to 0.75 for 2-D analysis while it was constant for 3-D analysis (R^2=0.91).

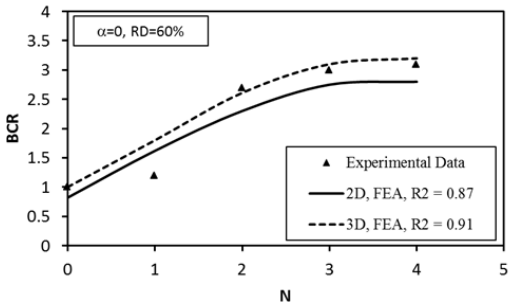

(a)

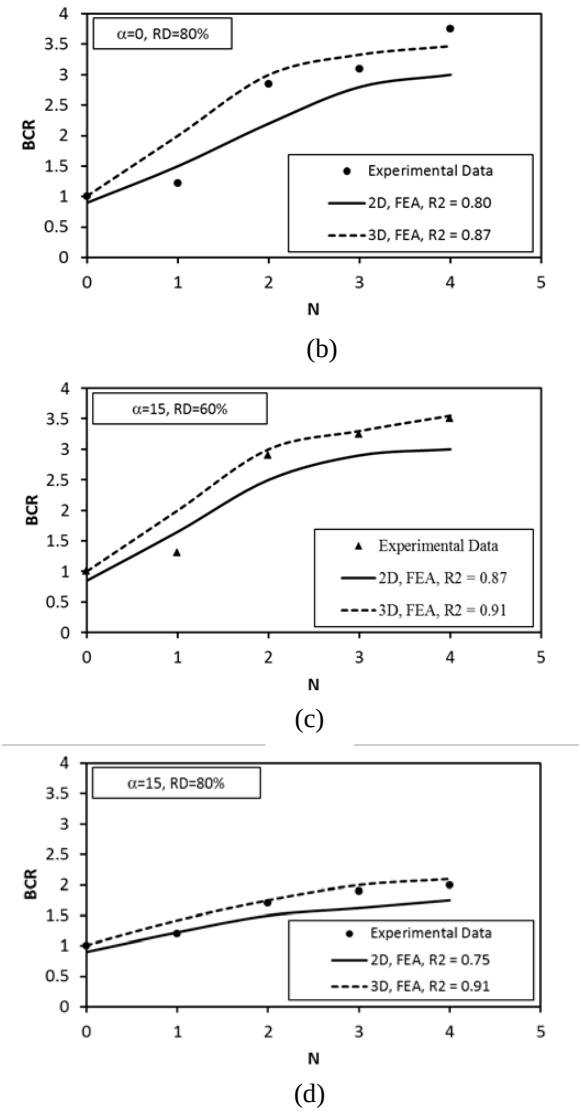

Figure 22. Finite element verification of bearing capacity ratio (BCR) versus number of geogrid layers of: (a) α=0, RD=60%, (b) α=0, RD=80%, (c) α=15, RD=60%, and (d) α=15, RD=80%.

2. Different load eccentricity (e/B)

The finite element verification of the bearing capacity ratio (BCR) of different geogrid layers under different load eccentricity (e/B) which varied from 0 to 0.15 for 60% and 80% relative density is shown in Figure 23 (a to d). For the studied cases, the 3-D prediction was more accurate than 2-D which was indicated through the coefficient of determination (R^2). As the sand relative density increased from 60% to 80%, the R^2 changed from 0.87 to 0.79 and 0.89 to 0.88 for 2-D and 3-D analyses under zero load eccentricity respectively. When the load eccentricity was 0.15 and with the increase of sand relative density from 60% to 80%, the R^2 changed from 0.91 to 0.72 and 0.97 to 0.93 for 2-D and 3-D analyses respectively.

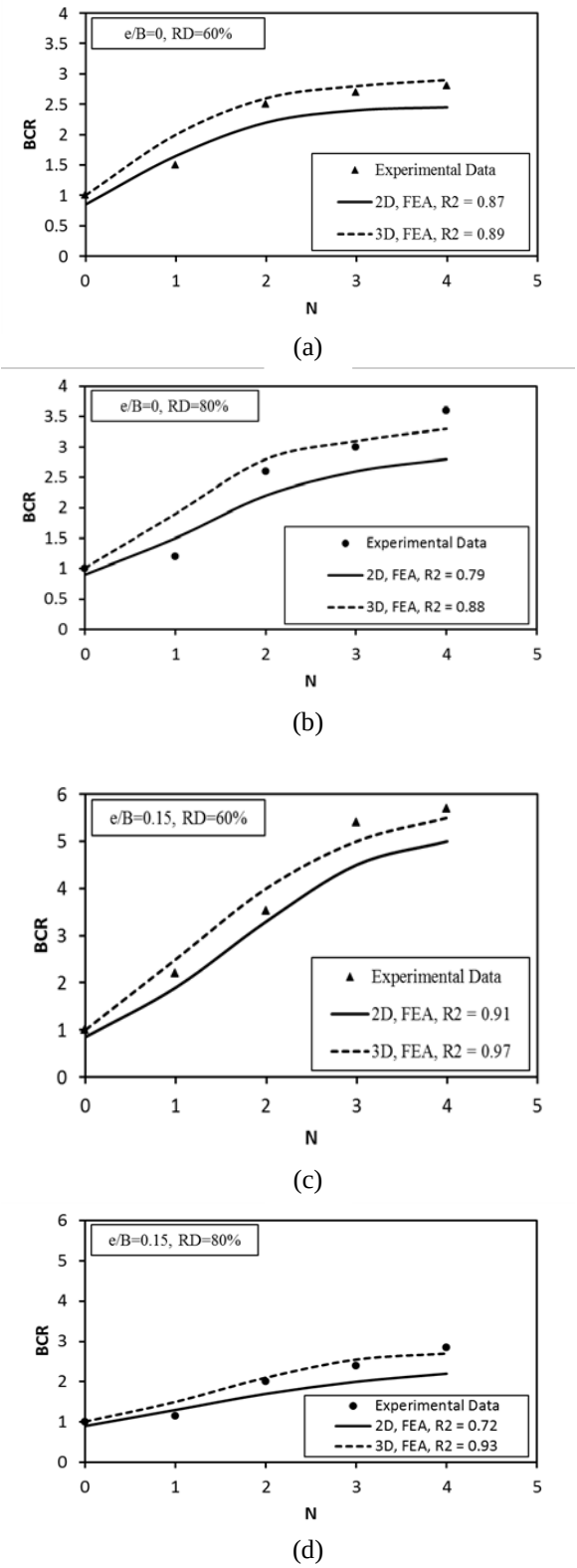

Figure 23. Finite element verification of bearing capacity ratio (BCR) versus number of geogrid layers of: (a) e/B=0, RD=60%, (b) e/B =0, RD=80%, (c) e/B =0.15, RD=60%, and (d) e/B =0.15, RD=80%.

3. *Horizontal displacement*

The finite element verification of the footing horizontal displacement for different geogrid layers under different load inclination angle (α) which varied from 0^o to 15^o for 60% and 80% relative density is shown in Figure 24 (a to d). For the studied cases, the 3-D prediction was more accurate than 2-D which was indicated through the coefficient of determination (R^2). As the sand relative density increased from 60% to 80%, the R^2 changed from 0.89 to 0.80 and 0.97 to 0.85 for 2-D and 3-D analyses under zero load inclination respectively. When the load inclination was 15^o and with the increase of sand relative density from 60% to 80%, the R^2 changed from 0.92 to 0.88 for 2-D analysis while it was constant for 3-D analysis (R^2=0.98).

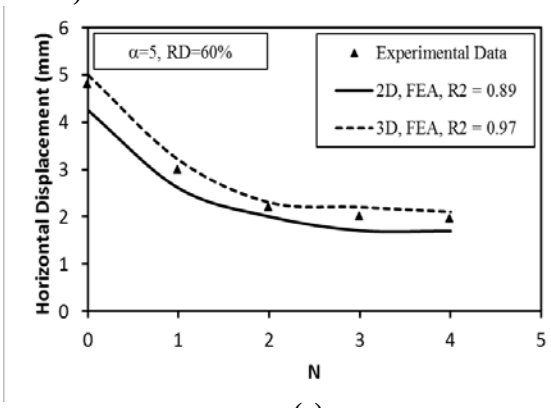

(a)

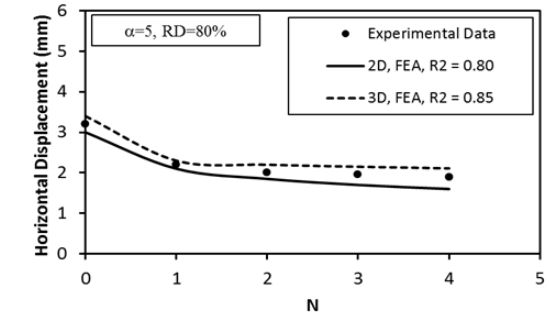

(b)

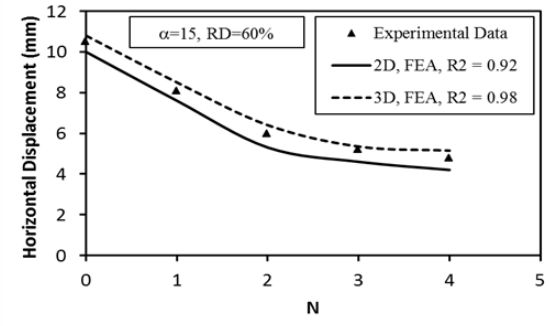

(c)

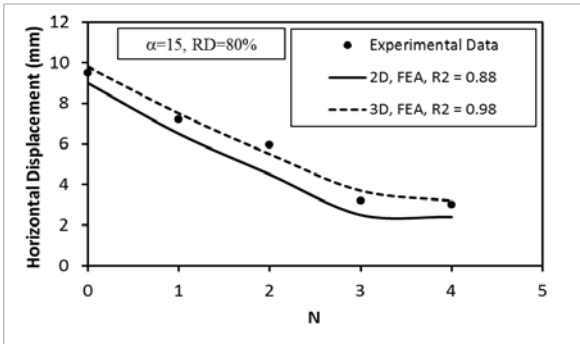

(d)

Figure 24. Finite element verification of horizontal displacement versus number of geogrid layers of: (a) α=0, RD=60%, (b) α=0, RD=80%, (c) α=15, RD=60%, and (d) α=15, RD=80%.

4. *Footing tilting*

The finite element verification of the footing tilting for different geogrid layers under different load eccentricity (e/B) which varied from 0.05 to 0.15 for 60% and 80% relative density is shown in Figure 25 (a to d). For the studied cases, the 3-D prediction was more accurate than 2-D which was indicated through the coefficient of determination (R^2). As the sand relative density increased from 60% to 80%, the R^2 changed from 0.71 to 0.62 and 0.83 to 0.80 for 2-D and 3-D analyses under 0.05 load eccentricity respectively. When the load eccentricity was 0.15 and with the increase of sand relative density from 60% to 80%, the R^2 was constant for 2-D (R^2=0.71) while it changed from 0.87 to 0.81 for 3-D analysis.

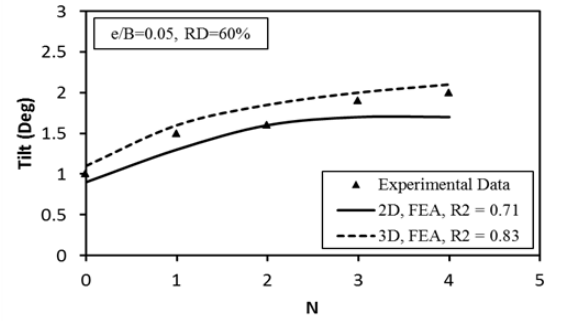

(a)

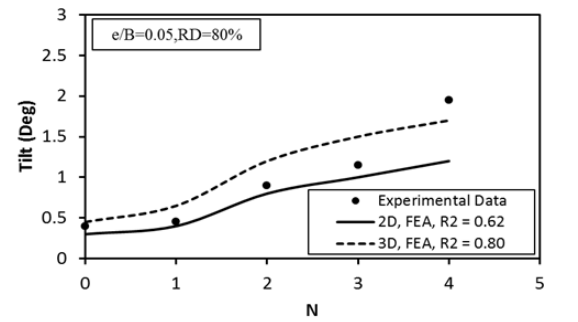

(b)

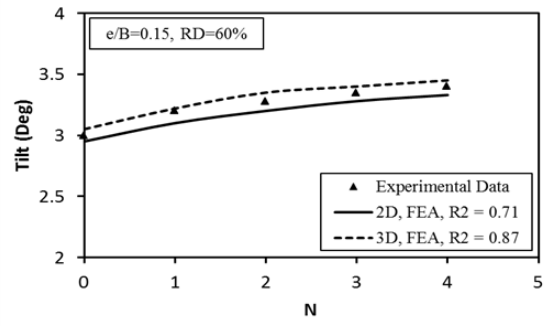

(c)

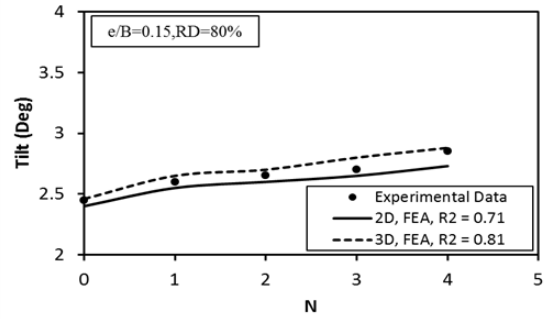

(d)

Figure 25. Finite element verification of footing tilting versus number of geogrid layers of: (a) e/B=0.05, RD=60%, (b) e/B =0.05, RD=80%, (c) e/B =0.15, RD=60%, and (d) e/B =0.15, RD=80%.

VIII. Conclusions

Based on the extensive experimental and numerical study, the following conclusions can be advanced:

1. Using geogrid as a reinforcement material has a significant impact in increasing the ultimate bearing capacity of cohesionless soil.
2. Increasing the number of geogrid layers (N) increases the ultimate bearing capacity notably with an optimum value of the geogrid layers. The optimum value for the geogrid layers (N) is varied from 4 to 5 depending on the soil relative density.
3. Having higher numbers of geogrid layers (N) decreased the horizontal displacement and increased the footing tilt.
4. The optimum value of (u/B) is (0.35) and it is independent on the load inclination (α), eccentricity ratio (e/B) and soil relative density (RD). 5. The optimum value of the vertical distance between the geogrid layers is (h/B=0.25) and it is independent on the load inclination (α), eccentricity ratio (e/B) and soil relative density (RD).
6. From extensive experimental investigation, the main factors affecting the ultimate bearing capacity of a strip footing under inclined and eccentric load on geogrid-reinforced sand can be addressed as follows:

a. The load inclination angle (α)

•Increasing (α) decreased the ultimate bearing capacity.
•Increasing (α) decreased the settlement due to failure pressure.
•Increasing (α) increased the horizontal displacement of the footing.

b. The load eccentricity (e)

•Increasing (e) decreased the ultimate bearing capacity.
•Increasing (e) decreased the settlement due to failure pressure.
•Increasing (e) increased the tilting of the footing.

c. The Relative density (RD)

•Increasing (RD) increased the ultimate bearing capacity.
•Increasing (RD) increased the settlement due to failure pressure.
•Increasing (RD) decreased the horizontal displacement of the footing.

7. Based on the coefficient of determination (R^2), finite element prediction for 3-D analysis was more accurate than 2-D analysis for all verified parameters such as BCR quantification of different load inclination angle and different load eccentricity, horizontal displacement and tilting angle of the strip footing.

IX. References

[1].El Sawwaf M. (2009). "Experimental and numerical study of eccentrically loaded strip footings resting on reinforced sand," Journal of Geotechnical and Geoenvironmental Engineering ASCE, 135(10), pp. 1509-1517.

[2].LU Liang, WANG Zong-Jian, and K. ARAI (2014). "Numerical and experimental analyses for bearing capacity of rigid strip footing subjected to eccentric load," J. Cent. South Univ., 21, pp. 3983−3992.

[3].Dewaikar D.M., Guptha K.G., and Chore H.S. (2011). "Behavior of eccentrically loaded model square footing on reinforced soil: an experimental investigation," Proceedings of Indian Geotechnical Conference, December 15-17, Kochi (Paper No. D-380).

[4].Ramlot C., and Vandeperre L. (1950). "Travaux de la commission d'Etude des Foundation de Pylones," Compt Rend Rech.

[5].Meyerhof G. G. (1953). "The bearing capacity of footings under eccentric and inclined loads," Proc., 3rd Int. Conf. on Soil Mech. And Found. Engrg., 1, pp. 440–445.

[6].Prakash S., and Saran S. 1971. "Bearing capacity of eccentrically loaded footings," J. Soil Mech. Found. Div., 971, pp. 95–118.

[7].Purkayastha R. D., and Char R. A. (1977). "Stability analysis for eccentrically loaded footings," J. Geotech. Engrg. Div., 1036, pp. 647–651.

[8].Mahiyar H., and Patel A. N. (2000). "Analysis of angle shaped footing under eccentric loading," J. Geotech. Geoenviron. Eng., 126(12), pp. 1151–1156.

[9]. Chakraborty D., and Kumar J. (2014). "Bearing capacity of strip foundations in reinforced soils," International Journal of Geomechanics, 14 (1), pp. 45-58.

[10].Jewell R. A., Milligan G. W. E., Sarsby R. W., and Dubois D. (1984). "Interaction between soil and Geogrids,"

Syrup. Polymer Grid Reinforcement in Cir. Engrg., London, England, pp. 18-30.
[11].Milligan G. W. E., and Palmeira E. (1987). "Prediction of bond between soil and reinforcement," Proc., Int. Conf. Prediction and Performance in Geotech. Engrg. ,Calgary, Alberta, pp. 147-153.
[12].Yetimoglu T., Jonathan T. H. Wu, and Ahmet S. (1994). "Bearing capacity of rectangular footings on geogrid-reinforced sand," Journal of Geotechnical Engineering, 120(12).
[13].Binquet J., and Lee K. L. (1975). "Bearing capacity tests on reinforced earth slabs," J. Geotech. Engrg. Div., 101(12), pp. 1241–1255.
[14].Fragaszy R., and Lawton E. (1984). "bearing capacity of reinforced sand subgrades," J. Geotech. Engrg., 10.1061/(ASCE)0733-9410110,10(1500), pp. 1500–1507.
[15].Guido V. A., Chang D. K., and Sweeney M. A. (1986). "Comparison of Geogrid and geotextile reinforced earth slabs," Can. Geotech. J., 23(4), pp. 435–440.
[16].Khing K., Das B. M., Puri V. K., Cook E. E., and Yen S. C. (1993). "The Bearing capacity of a strip foundation on geogrid-reinforced sand,"Geotext. Geomembr., 12(4), pp. 351–361.
[17].Omar M. T., Das B. M., Puri V. K., and Yen S. C. (1993). "Ultimate bearing capacity of shallow foundations on sand with geogrid reinforcement," Can. Geotech. J., 30(3), pp. 545–549.
[18].Shin E.C., Das B. M., Puri V. K., Yen S.-C., and Cook E. E. (1993). "Bearing capacity of strip foundation on geogrid-reinforced clay," J. ASTM Geotech Test., 16(4), pp. 534–541.
[19].Das B. M., Shin E. C., and Omar M. T. (1994). "The bearing capacity of surface strip foundation on geogrid-reinforced sand and clay—a comparative study," Geotech. Geol. Eng., 12(1), pp. 1–14.
[20].Das B. M., and Omar M. T. (1994). "The effects of foundation width on model tests for the bearing capacity of sand with geogrid reinforcement," Geotech. Geol. Eng., 12(2), pp. 133–141.
[21].Adams M. T., and Collin J. G. (1997). "Large model spread footing load tests on geosynthetic reinforced soil foundations," J. Geotech. Geoenviron. Eng., 10.1061/(ASCE)1090-0241(1997)123:1(66), pp. 66–72.
[22].Dash S. K., Rajagopal K., and Krishnaswamy N. R. (2004). "Performance of different geosynthetic reinforcement materials in sand foundations," Geosynth. Int., 11(1), pp. 35–42.
[23].Griffiths D. V., Fenton G. A., and Manoharan N. (2006). "Undrained bearing capacity of two-strip footings on spatially random soil," Int. J. Geomech.,10.1061/(ASCE)1532-3641, 6(421), pp. 421–427.
[24].Gourvenec S., Randolph M., and Kingsnorth O. (2006). "Undrained bearing capacity of square and rectangular footings," Int. J. Geomech.,10.1061/(ASCE)15323641, 3(147), pp. 147–157.
[25].Yamamoto N., Randolph M. F., and Einav I. (2008). "Simple formulas for the response of shallow foundations on compressible sands," Int. J. Geomech., 10.1061/(ASCE)1532-3641, 4(230), pp. 230–239.
[26].Asaoka A., Kodaka T., and Pokhaerl G. (1994). "Stability analysis of reinforced soil structures using rigid plastic finite element method," Soils Found., 34(1), pp. 107–118.
[27].Otani J., Ochiai H., and Yamamoto K. (1998). "Bearing capacity analysis of reinforced foundations on cohesive soil." Geotext. Geomembr., 16(4), pp. 195–206.
[28].Ghazavi M, and Lavasan A.A. (2008). "Interference effect of shallow foundations constructed on sand reinforced with geosynthetics," Geotext Geomembr, 26, pp. 404–415.
[29].Reza N., and Ebrahim M. (2014). "Bearing capacity of two close strip footings on soft clay reinforced with geotextile," Arab J Geosci, 7, pp. 623–639.
[30].Yu H. S., and Sloan S. W. (1997). "Finite element limit analysis of reinforced soils," Comput. Struct., 63(3), pp. 567–577.
[31].Terzaghi K. (1943). "Theoretical soil mechanics," Wiley, New York.
[32].Meyerhof G. G. (1963). "Some recent research on the bearing capacity of foundations," Can. Geotech. J., 1(1), pp. 16–26.
[33].Rodriguez-Gutierrez J. A., and Aristizabal-Ochoa J. D. (2012a). "Rigid spread footings resting on soil subjected to axial load and biaxial bending. i: simplified analytical method," Int. J. Geomech.,10.1061/(ASCE)GM., pp. 109–119.
[34].Rodriguez-Gutierrez J. A. ,and Aristizabal-Ochoa, J. D. (2012b). "Rigid spread footings resting on soil subjected to axial load and biaxial bending. ii: design aids," Int. J. Geomech., 10.1061/(ASCE)GM.1943-5622.0000210, pp. 120–131.
[35].Blatz J. A., and Bathurst R. J. (2003). "Limit equilibrium analysis of reinforced and unreinforced embankments loaded by a strip footing," Can. Geotech. J., 40(6), pp. 1084–1092.
[36].Michalowski R. L. (2004). "Limit loads on reinforced foundation soils," J. Geotech. Geoenviron.Eng.,10.1061/(ASCE)1090-0241, 4(381), pp. 381–390.
[37].Deb K., Sivakugan N., Chandra S., and Basudhar P. K. (2007). "Numerical analysis of multilayer geosynthetic-reinforced granular bed over soft fill," Geotech. Geol. Eng., 25(6), pp. 639–646.
[38].Bringkgreve, R., and Vermeer, P. (1998). "PLAXIS-finite element code for soil and rock analysis", version 7, Plaxis BV, The Netherlands.

The Laboratory Studies on Anisotropy of Gypseous Soil

A. A. Al-Obaidi and A. A. Al-Karawi

***Abstract*— an isotropic material is one in which the elastic properties are the same in all directions. Almost all naturally occurring soil deposits are anisotropic and non homogeneous. The anisotropy is produced from a combination of particle placement during deposition/formation and from overburden pressures.**

Gypseous soils occupy about 1.865 million Km^2 in the world; the percent of gypseous soils in Iraq is 6.7% of the total world gypsiferous area and about 28.6% of the total area of this country. The gypsum percent may be reached 70% in some Iraqi soils.

This property of anisotropy has been well known for soils but no attention has been made on the gypseous soils.

In this paper several laboratory tests were conducted in order to discover how anisotropy can qualitatively affect the engineering properties of Gypseous soils. The gypseous soil used was brought from Tikrit city, (Al-Qadissia district) which is located in Salah-Aldeen governorate, from depth ranging (2.5-3.0) m. The gypsum content was 27.8% - 31.45% and the soil classified as highly gypseous poorly graded sand with little or no fines (SP).

Series of laboratory tests on undisturbed samples including direct shear, collapsibility, and Permeability tests were conducted on samples, in both vertical and horizontal axes of the samples.

The main results indicate that the method of the gypsum accumulation in those soils was the major effect on the property of anisotropy, and the difference in the angle of internal friction may be reached 15%, whereas the difference in the coefficient of permeability was 50%. These results explained that the effect of soaking on gypseous soils is more dangerous than leaching.

***Index Terms*— Gypseous Soils, Anisotropy, Laboratory Tests, Gypseous Distribution.**

I. Introduction

THE good definition of soil anisotropy was given by [1]: "If at any point in the soil, the hydraulic conductivity is not the same in every direction, the soil is said to be anisotropic. Soil anisotropy is generally characterized by the numerical ratio of the horizontal permeability "k_H" to the vertical permeability "k_V" measured at the same location in the profile. On this basis an anisotropic soil has the ratio "k_H/k_V" either greater or less than unity, depending on whether the ease of horizontal movement of water is greater, or less than the ease of vertical movement. Reference [2] stated that an isotropic material is one in which the elastic properties are the same in all directions. The elastic properties for anisotropic materials are different in the different directions. Almost all naturally occurring soil deposits are anisotropic and non homogeneous. The anisotropy is produced from a combination of particle placement during deposition/formation (also called geometrical or inherent anisotropy) and from overburden pressures. In natural soils this commonly results in horizontal bedding planes that have both strength and elastic properties different for samples stressed perpendicular and parallel to the bedding planes. Some data up to 1957 has been reviewed by [1], it was found that for all soils, except for some sands, "k_H" exceeds "k_V" and the ratio "k_H/k_V" ranging from 2-40. Reference [3] measuring permeability of alluvial mineral soils, alluvial peat soils and alluvial clay soils, have observed that approximately half of the soils investigated proved to be anisotropic. Reference [4] reported that a Riverine Micaceous sandy clay loam to clay loam with little or no structural development was highly anisotropic in different locations of a relatively small area (less than 1 acre), moreover, that the anisotropy was highly variable from point to point. Reference [5] reported that artificially prepared kaolinite soil samples have "k_H" always greater than "k_V". Laboratory analyses of permeability from peat cores in northern Minnesota show that the ratio of "k_H" to "k_V" is highly variable throughout the peat column and reported that "k_H" was generally one to two orders of magnitude greater than "k_V" [6]. Reference [7] found from hydrological investigations carried out in the Lower Indus Plain of Pakistan by Hunting- Macdonald consulting engineers (1965 and 1971) that the typical values of anisotropy ratio "R" range from 7-25 for the upper and lower soils, respectively. Reference [8] observed from the results on four samples of clay soils investigated, a significant differences between vertical and horizontal saturated hydraulic conductivity in three of the four soils. Reference [9] found a significant difference between "k_H" and "k_V" in a St-Benoit soil of the Macdonald farm of McGill University. Reference [10] found that vertical k values that were three times the horizontal values for Oliver silt loam. On the other

Manuscript received Jun 29, 2015, Revised August 9, 2015 and accepted in the August 16, 2015.

A. A. Obaidi is Assist. Prof. in Civil Department, Engineering collage, Tikrit University (corresponding author to provide phone: +9647705357999; e-mail: consulting_tik@yahoo.com, Obaidi.a.h.@tu.edu.iq).

A. A. Al-Karawi was with M.Sc. in Civil Engineering (Soil Mechanics), (Phone: +9647903869919, e-mail: civileng88_2010@yahoo.com).

hand Reference [11] indicated that anisotropy is not a static quality, rather, it may change over time.

II. Gypseous Soils

Gypseous soils are those which contain appreciable amount of gypsum ($CaSO_4.2H_2O$) to change or affect construction adversely. They are present in dry arid to semi-arid regions where sources of Calcium Sulfate exist. Various authors have been described that gypsum accumulation occurs in two ways: by evaporation of mineralized ground water and by the precipitation within the ground water itself [12]. The gypsum origin varies in shape, size, form and distribution [13]-[14], thus, the mode of formation and observation in the field that the gypsum may be spots, elongated accumulations of 1 mm-2mm in diameter , pellicular layers, moss-like and covered with white powder on the surface must be considered. The classification of soils as gypseous soils depends on the gypsum content in these soils. Reference [15] used the value of 2% of gypsum content to define the gypsiferous soils. Reference [16] distinguished classes of gypsiferous soils based on the gypsum content as shown in Table I. Reference [17] defined the gypseous soil as that which contains more than 6% gypsum. In Iraq Reference [16] estimated that the gypseous soils covers 12.2% of the area of total Iraq area, whereas Reference [18] predicted that gypseous soils covers about 50% of the area of Iraq, this considered being high in comparison with other ones. On other hand, Reference [19] estimated that about 31.7% of the area of Iraq is covered with gypseous soil with gypsum percentage ranging between 10%-70%. These soils are concentrated in Samarah, Anna, Faluja, Najaf, Nassirya, Mosul, Baiji, Tikrit, Heet and Ramadi.

TABLE. I
CLASSIFICATION OF GYPSEOUS SOILS [16]

Gypsum content %	Classification
0-0.3	Non gypseous
0.3-3	Very slightly gypseous
3-10	Slightly gypseous
10-25	Moderately gypseous
25-50	Highly gypseous
>50	Gypseous soils to be described by the other fractions such as clayey or sandy gypseous soil

III. Experimental Work and Testing Program

In this study two samples of gypseous soils were examined; soil sample A where the gypsum randomly distributed in the soil (Plate (1.A)) and soil sample B where the gypsum appear as a layers in the soil(Plate(1.B)). These samples were taken from depth ranging (2.5-3.0) m below the natural ground level, after a power machine (shovel) excavation was used to remove the upper soil strata. This soil was brought from Tikrit city, (Al-Qadisiyah district) which is located in Salah-Aldeen Governorate, in the middle of Iraq and, then disturbed and undisturbed block samples were obtained and transported to the soil mechanics laboratory, Civil Eng. Dept., College of Engineering at the University of Tikrit. Approximately 100 Kg of soil were put in airtight plastic bags and prepare for the testing program. The samples used for testing were extruded carefully form these blocks, (Plate 1. C).

(A) (B) (C)

Plate. 1. Soil sample, (A) Randomly gypsum distribution, (B) Layered gypsum distribution and (C) tested sample

In this research, several laboratory standard tests (particle-size distribution, moisture content, specific gravity, Atterberg limits, and gypsum content), chemical tests, and engineering tests (Direct shear test, collapsibility test, and permeability test) were conducted in order to find how anisotropy can qualitatively affect the engineering properties of Gypseous soils.

IV. Results and Discussion

The results of all tests described in the testing program are presented as follows:

A. Soil Classification

According to (ASTM D422-02) [20] and from the sieve analysis Fig. 1. both (Sample A and Sample B) soils can be classified as poorly graded Sand (**SP**) with little or no fines according to Unified Soil Classification System. The other properties of the soils, specific gravity, liquid limit, plastic limit and water content were found according the specification as shown in Table II.

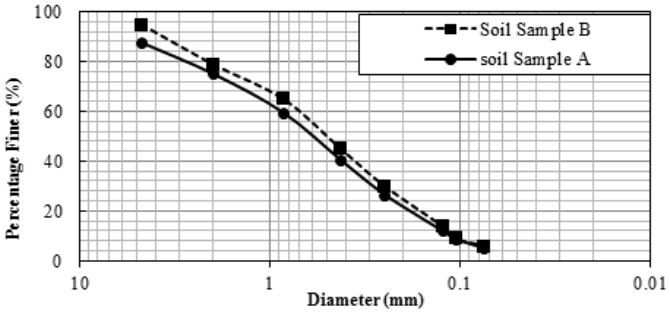

Fig. 1. Particle size distribution curve for soil sample A and sample B

TABLE.II
RESULTS OF PHYSICAL TESTS

Soil Properties	Value		Specifications
	sample A	sample B	
Moisture content, (ω) %	2.70	2.15	ASTM D2216-02 [21]
Specific gravity, (Gs)	2.58	2.60	ASTM D854-02 [22]
Liquid limit, (L.L)%	26	29	ASTM D4318-00 [23]
Plastic limit, (P.L)%	N.P	N.P	
Plasticity index, (P.I)%	---	---	
Dry density (gm/cm^3)	1.47	1.66	---

From the particle size distribution and results in Table II, it can be notice that the gypsum distribution manner in the sample has no effect the physical and classification test, where these results seems to convergent.

B. **Chemical Tests Results**:

The results of the chemical tests were tabulated in Table III, for soil sample A, the total soluble salts 32.4%, the pH was 7.61, and the organic matters was 1.68. For soil sample B the total soluble salts was 35.7%, the Hydrogen number "pH" was 7.53, and the organic matters was 1.98.The gypsum content in the two samples was determined using method of Reference [24].

TABLE. III
RESULTS OF CHEMICAL TESTS

Chemical Property	Value	
	Sample A	Sample B
Total soluble salts (T.S.S.)%	32.4	35.7
pH value	7.61	7.53
Gypsum content%	27.81	31.45
Organic matters(O.M)%	1.68	1.98

C. **The Engineering Properties**:

Several studies have been indicated that the engineering Properties affected if the soil was anisotropy. In these tests the two soil samples A and B were examined in two directions, vertical and horizontal direction. The first direction put in the test apparatus in the same direction as in field, whereas in the second group, i.e. horizontal direction, the soil samples rotate with 90° and then tested. The engineering tests in this group include direct shear tests, collapsibility tests and permeability tests.

a. The Strength Properties

The relationship between shear stress and normal stress from direct shear tests in vertical and horizontal direction were drawn for soil sample A and B and shown in Fig. (2a) and (2b) respectively. This test was conducted according to the ASTM D3080-03[25]. Table IV showed the apparent cohesion "c" and angle of internal friction "Ø", calculated from Fig. (2.a) and (2.b). From this table, it can be seen that the effect of gypsum distribution and direction of testing seems to be small.

b. The Permeability

The results of the permeability tests for the two soil samples A and B and for horizontal and vertical direction found according to ASTMD2434-68 [26], are shown in Table V. The values of the coefficient of permeability show that a little difference between the vertical and horizontal coefficient of permeability in sample A and the ratio "k_H/k_V" less than 1.0. For sample B; the coefficient increased due to increase of gypsum content and the ratio "k_H/k_V" also increased due to distribution of gypsum in the soil sample.

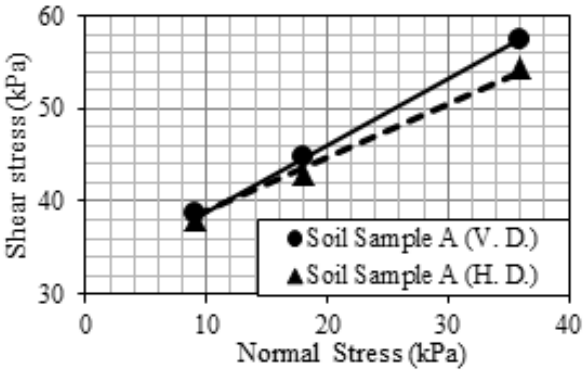

(a) Soil Sample A

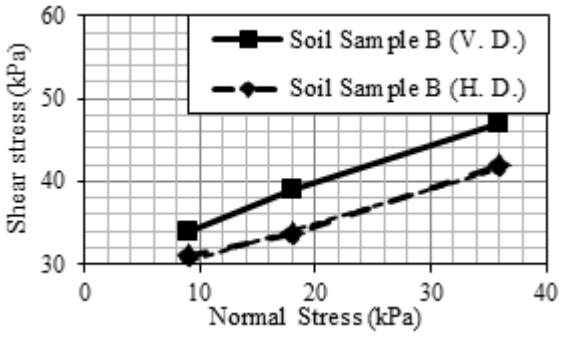

(b) Soil Sample B

Fig. 2. The relationship between shear stress and normal stress from direct shear test for vertical and horizontal direction for (soil sample A

TABLE. IV
THE STRENGTH PROPERTIES OF SAMPLES A AND B

Soil sample	Soil properties	Vertical direction	Horizontal direction	Ratio of horizontal to vertical
A	c (kN/m^2)	31.60	33.20	1.051
	Ø	35.83	30.10	0.840
B	c (kN/m^2)	29.73	26.80	0.901
	Ø	26.30	22.24	0.846

TABLE.V
PERMEABILITY OF SAMPLES A AND B

Soil Sample	Coefficient of permeability (cm/s)*10^{-3}		k_H/k_V
	Vertical direction	Horizontal direction	
A	1.867	1.317	0.705
B	1.630	2.610	1.601

c. The Collapsibility of Soils

This test was suggested by [27], and carried out on natural soil sample to determine collapse potential "Cp" value. The relationship between sample high reduction and pressure in collapsibility tests for vertical and horizontal direction for soil sample A and B were drawn and shown in Fig. (3.a) and (3.b) respectively. The collapse potential for these soils were shown in Table VI. The results indicate that the collapsible potential for sample A are closed in vertical and horizontal, but a high difference between vertical and horizontal collapsible potential were found for sample B, this due to dissolution of the layer of gypsum which is in horizontal manner due to its formation.

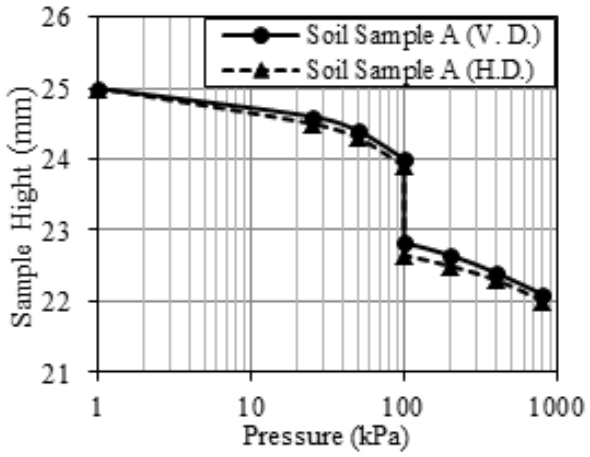

(a) Soil sample A

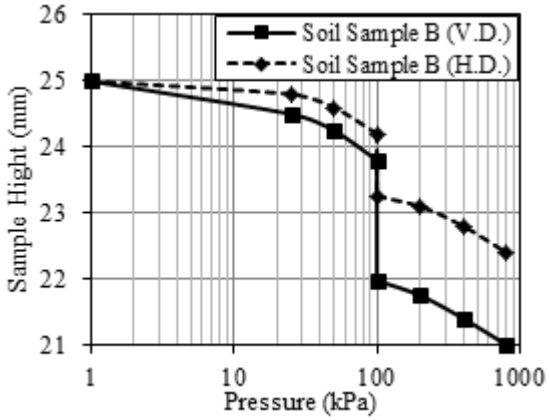

(b) Soil sample B

Fig. 3. Collapsibility test for soil samples (A and B) in vertical and horizontal direction

TABLE.VI
COLLAPSIBILITY OF SOIL SAMPLE A AND B

Soil sample	Collapsible Potential of samples A and B		Ratio of Cp_H/Cp_V
	Vertical direction	Horizontal direction	
A	4.7	5.0	1.06
B	7.3	3.8	0.52

CONCLUSIONS

From the results of tests described in this paper, a number of conclusions can be reached regarding the effects of gypsum distribution manner in the soil on the observed ratio of horizontal to vertical engineering properties. The main effect was found in collapsibility tests, where high collapsibility value was indicated for layered gypsum distribution in vertical direction and this may led to high values of settlement with "Cp_H/Cp_V" may reached 50% but no difference was found between "Cp_H" and "Cp_V", in randomly gypsum distribution. The value of anisotropy "k_H/k_V" may reach 1.6 in layered gypsum and 0.705 for randomly gypsum distribution. It's found that little or no differences in the shear strength parameters between the vertical and horizontal direction testing or between randomly distributed and layered formation of gypsum in the soil. Finally anisotropy needs to be accounted for in a variety of land use decisions, and more highlight must be considered in gypseous soil and upon its formation where the distribution of gypsum in the soil affects the anisotropy of the soil.

REFERENCES

[1] M. Maasland, "Soil Anisotropy and Land Drainage", In *Drainage of Agricultural Lands*, J.H. Luthin, Ed., Am. Soc. Agronomy, Monograph 7, Madison, WI, pp. 216-285, 1957.

[2] J. E. Bowles, *Foundation Analysis and Design*, 5th ed., New York: McGraw-Hill, 1996.

[3] E. C. Childs, Collis-George, N., and Holmes, J.W., "Permeability Measurements in the Field as Assessment of Anisotropy and Structure Development", *Soil Sci. J*. vol.8, no. 1, pp. 27-41, 1957.

[4] T. Talsma, "Measurement of Soil Anisotropy with Piezometer", *Soil Sci. J*. vol. 11, no.1, pp. 159-171, 1960.

[5] P. Basak, "Soil Structure and its Effects on Hydraulic Conductivity", *Soil Sci. J*., vol. 114, no. 6, pp. 417-422, 1972.

[6] D.B. Chason, and D.I. Siegel, "Hydraulic Conductivity and Related Physical Properties of Peat, Lost River Peatlands Northern Minnesota", *Soil Sci. J*., vol. 142, no. 2, pp. 91-99, 1986.

[7] J.H. Boumans, "Drainage Calculations in Stratified Soils Using the Anisotropic Soil Model to Simulate Hydraulic Conductivity Conditions", in *Proc*, Int. Drainage Workshop, Inst. for Land Reclamation. & Improvement (ILRI), Publ. 25, Wageningen. The Netherlands, p. 108-123, 1979.

[8] J. Bouma, and L.W. Dekker, "A Method for Measuring the Vertical and Horizontal ksat of Clay Soils with Macrospores", *Soil Sci. Soc. Am. J*., vol. 45, no.3, p. 662-663, 1981.

[9] A. B. Rashid-Noah, "Designing Subsurface Drainage System to Avoid Excessive Drainage of Sands", Ph. D. dissertation, Dept. Agricultural Engineering, McGill University, Montreal, Quebec, 1981.

[10] S. M. Dabney and H. M. Selim, "Anisotropy of a Fragipan Soil: Vertical vs. Horizontal Hydraulic Conductivity", *Soil Sci. Soc, Am. J*., vol.51, no.1, p. 3-6, 1987.

[11] J. Freeland, "Soil Anisotropy: Mechanisms and Hydrologic Consequences", Report submitted to terra central AGU Blogosphere, July, 2013.

[12] FAO, "Management of Gypsiferous Soils, Food and Agricultural Organization of United Nations", Rome, Internet, Http.//Fao.Org/Doc Rep/To 323e/Ro323e03.Htm, 1990.

[13] T. G. Boyadgiev, "Contribution to the knowledge of gypsiferous soils", AGON/SF/SYR/67/522, FAO, Rome.1974.

[14] T. G. Boyadgiev, "Les sols du Hodna, Etude des ressources naturelles et expérimentation et démonstration agricoles dans la région du Hodna", Algérie, FAO, Rome.1975.

[15] J. G. V. Alphen, and F. D. R. Romero, "Gypsiferous Soils Notes on their Characteristics and Management", International Institute for Land Reclamation and Improvement, Wageningen, Netherlands, 1971.

[16] A. F. Al-Barzanji, "Gypsiferous Soils of Iraq", Ph.D. dissertation, State University of Ghent, Belgium, 1973.
[17] K. Sirwan, R. R. Al-Omary, Y. N. Y. Nazhat, "Shear Behavior of Gypsiferous Soils", in *Proc*, 2ed Int. Symposium on Environmental Geotechnology, Shanghai, China,1989.
[18] A.D. Al-Mukhtar, "Mapping and Microscopic Investigation of Gypsiferous Soils in Al-Dour and Al-Jazira Area of Iraq", Ph.D. dissertation, State University of Ghent, Belgium. 1987.
[19] H. N. Ismael, "The Use of Gypseous Soils, Symposium on the Gypseous Soils and its Effect on Structures", N.C.C.L, Baghdad, 1997.
[20] ASTM D422-02, "Standard Test Method for Particle-Size Analysis of Soils", American Society for Testing and Materials, 2002.
[21] ASTM D2216-02, "Standard Test Methods for Laboratory Determination of Water (Moisture) Content of Soil and Rock by Mass", American Society for Testing and Materials, 2002.
[22] ASTM D854-02, "Standard Test Methods for Specific Gravity of Soil Solids by Water", American Society for Testing and Materials, 2002.
[23] ASTM D4318-00, "Standard Test Methods for Liquid Limit, Plastic Limit, and Plasticity Index of Soils", American Society for Testing and Materials, 2000.
[24] A. A. Al-Mufty and I. H. Nashat, "Gypsum Content Determination in Gypseous Soils and Rocks", 3rd International Jordanian Conference on Mining, pp. 500-506, 2000.
[25] ASTM D3080-03, "Standard Test Method for Direct Shear Test of Soils under Consolidated Drained Conditions", American Society for Testing and Materials, 2003.
[26] ASTM D2434-68, "Standard Test Method for Permeability of Granular Soils (Constant Head)", American Society for Testing and Materials, Reapproved 2000.
[27] K. Knight, "The Origin and Occurrence of collapsing Soils", in Proc., 3rd Regional Conference of Africa on Soil Mechanics and Foundation Engineering, vol.1, pp.127-130, 1963.

The Effectiveness of Fourier Analysis in Speckle Reduction for SAR Image with Two Polarisation before and after Applying Principal Components Transformation.

Amjed Naser Mohsin AL-HAMEEDAWI, University of Technology, Baghdad, Iraq.

***Abstract*— The contribution of digital image processing especially Fourier Analysis and Principal Components to SAR data in speckle reduction is significant because this technique offers specific features in frequency domain which spatial domain cannot attain. Generally, despeckling methods trade spatial details for noise reduction. The complexity of the speckle in Cosmo-SkyMed imagery with (HH and VV) polarisation where speckle is a real electromagnetic measurement, which is exploited in particular in SAR interferometry therefore the speckle elimination must be submit to the purpose of case study. The accuracy of the result strongly depends on the scattering mechanisms at the time of the data takes. This paper aims at linking the potential of Fourier Analysis with regard to speckle and at automatically reducing the noise intrinsic to such processing.**

Keywords: Synthetic Aperture Radar (SAR), Speckle, Fourier Analysis.

1. Introduction

The unavoidable occurrence of speckle noise in synthetic aperture radar (SAR) images seriously aggravates the edge and texture details and represents considerable effects on SAR image classification, segmentation and interpretation. Consequently, some essential procedures must be performed to minimize speckle before the images are extra processed for details retrieval. To reach this, various speckle reduction algorithms have been used recently (1). A modern procedure has been applied to diminish speckle noise in digital holography by altering the interference framework of hologram itself (2).

Remote sensing imagery usually includes noise owing to sensors malfunction, problems with data collection, compression, and image storage. Noise can be inconsistent with the data of interest. There are acceptable algorithms for reducing each degree of noise; hence, each image must be filtered with the most appropriate filter to eliminate or to reduce noise (3). The SAR data utilised in this study is Cosmo-SkyMed images with two polarisations HH and VV were provided free of charge from e-GEOS (an ASI/Telespazio company). Cosmo-SkyMed is the biggest Italian project for earth observation funded by the Italian Space Agency and the Italian Ministry of Defence and it is considered as a dual-use (Civilian and Defence) searching for building an international service supplying data for various purposes. The Cosmo-SkyMed image sensor works at X band (wavelength 3 cm, range 2.4 -3.8 cm) with a revisit time of less than 12 hours (4, 5). Cosmo-SkyMed as the SAR data also suffers from speckle noise which can be reduced using Principal Components Analysis (PCA) and Fourier analysis techniques together in addition to Gamma filtering. Principal Components Analysis (PCA) is a method of data compression. With it, data dimensions that are redundant can be decreased by reducing it into fewer layers. The result of applying PCA to data lead to improving data interpretation more than the source data itself in addition to reducing the noise in remote sensing data. The most common way of implementing neighbourhood enhancements is via a moving window convolution. However, as the size of the moving window become bigger, the amount of calculations becomes more. An enhancement that needs a convolution running in the spatial domain can be fulfilled simply in frequency domain with much faster calculations. Fourier analysis techniques can be used for eliminating noise in imagery (6, 7).The goal of the despeckling process is to minimize noise whereas most of the image's textural features will be kept. The most commonly employed despeckling filters are the Lee, Frost and Gamma filters (8).

2. Fundamentals

2.1 Speckle Noise

Coherent system frequently affected by the speckle such as

radar and laser. This speckle confuses the interpretation and classification of SAR images and has motivated much studied into methods of speckle reduction. Speckle refers to a noise generated by coherent systems which leads to influence the interpretation of the brightness of a pixel (9). Speckle can be attenuated by special filtering and averaging process. However, it cannot be fully eliminated (7, 10).

2.1.1 Speckle Filtering

Speckle noise elimination is an essential pre-processing phase in the analysis and interpretation of the microwave imagery to lessen the unusual variation present. To attenuate the speckle existing in the SAR image, a Gamma-Map (Maximum a Posteriori) filter is applied to it. The filter is relying on a multiplicative noise model with mean and variance in addition to considering Gamma distribution for the speckle noise (11). The Gamma filter not only provide perfect speckle diminishing but also keeps the spatial details .Additionally, texture of the SAR data were much better protected by applying the Gamma filter(5, 12). Here to, the best result is acquired when the Gamma filter is carried out comparing to other filters.

2.2 Principal Components Analysis

The aim of this transformation is to lessen the number of layers in the data. The resultant layers that come from this statistical procedure known as components. This process offers to amplify variance from the original data into the least number of new components. As an example of the use of Principal Components Analysis, seven bands Thematic Mapper (TM) data set may be transformed such that the first three principal components contain over 90 percent of the details in the original seven bands. Interpretation and analysis of these three bands of data, combining them either visually or digitally, is simpler and more advantageous than using all of the original seven bands. Principal Components Analysis, and other complex transforms, can be used either as an enhancement process to improve interpretation or to reduce the noise in data (5, 12).

2.3 Fourier Analysis

The Fourier Transform is a means or a tool that divides image into its spectral elements depending on its wavelength (i.e. frequency) content. This analysis was applied for enhancement purposes. Fourier Transform applied to convert an image from the spatial domain into a frequency domain image. The Fourier Transform measurements convert the image into a series of two-dimensional sine waves of dissimilar frequencies. The Fourier image itself cannot be simply observed, however the amplitude of the image can be computed. Analysts can modify the Fourier image to lessen noise or extract periodic features, such as striping. Once the Fourier image is corrected, it is then returned into the spatial domain by utilizing an Inverse Fourier Transform. The outcome is an enhanced form of the original image. Fourier Transformations are generally applied for the exclusion of noise such as striping, spots, or vibration in imagery by determining areas of high spatial frequency. Fourier operation might be used to extract regular errors in image such as those brought about by sensor anomalies (6).

The Fourier Transform calculation is as follows (13):

$$F(u,v) \leftarrow \sum_{x=0}^{M-1} \sum_{y=0}^{N-1} [f(x,y)e^{-j2\pi ux/M - j2\pi vy/N}] \qquad (1)$$

Where:

M : the number of pixels horizontally
N : the number of pixels vertically
u,v : spatial frequency variables
e : 2.71828, the natural logarithm base
j : the imaginary component of a complex number.

3. Data and Methods

The following lists specify an idea on data and software packages utilised within the study:

Data: Cosmo-SkyMed HH and VV acquired on 06.07.2011
Software: ENVI, ERDAS Imagine and SARscape.

3.1 Methods

The goal of image enhancement and speckle noise reduction are to improve the interpretability of an image. When Fourier transformation is applied to an image, the noise pattern which take place in horizontal orientation in Fourier spectrum tend to be in vertical orientation in original image. The lower frequencies in the image are plotted in centre of Fourier spectrum while higher frequencies are plotted outward (7). By using Fourier spectrum for transformed image the amount of noise can be estimated.

The subsequent paragraphs briefly explain the processing procedures, which have been applied to the input image:

1. SAR geocoding is typically known as the step of performing geometric transformation of SAR image with the aid of a digital elevation model (DEM) from the original radar azimuth/range coordinate system to map projection coordinate systems (14). Terrain geocoding and radiometric calibration was fulfilled applying SARscape software. The Cosmo-SkyMed Image was imported and transformed to single-look complex (SLC) SAR image products.

2. Cosmo-SkyMed images with two polarisations HH and VV were stacked.

3. Applying of Fourier Analysis to the stacked image after that Wedge Mask was used to enhance imagery in addition to removing the nearly radial line in the image. Thereafter, Inverse Fourier Transform was applied to get the filtered image.

4. Principal Components Analysis (PCA) was applied to Cosmo-SkyMed images with two polarisations HH and VV. The resultant of PCA transformation is two components (images PC1 and PC2). Subsequently, applying of Fourier

Transformation to the two images. Afterward, Wedge Mask was applied to filter them. Finally, Inverse Fourier Transform was applied to transforming back the two images. According to the less noise, either PC1 or PC2 was selected for comparison purposes.

5. Comparison of filtered images before and after applying Principal Components Analysis (PCA).

6. Finally, Applying Gamma filter to the resultant images in order to reduce speckle. Please see Figure 1.

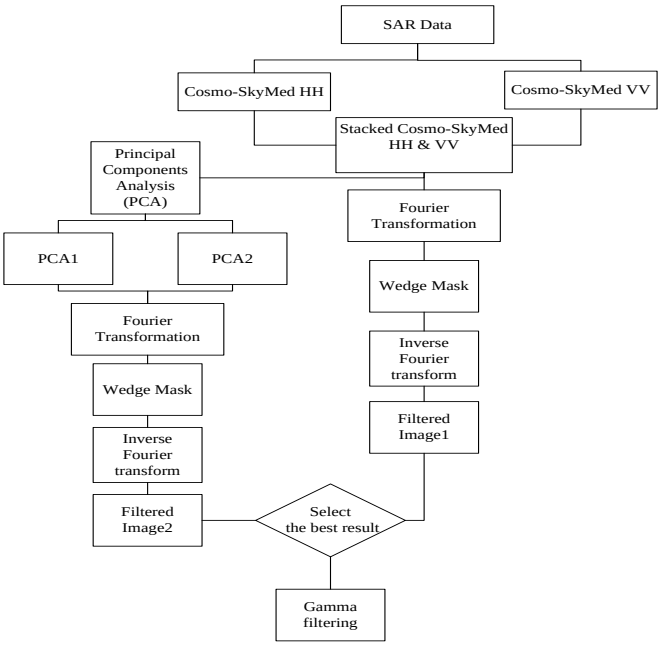

Fig. 1. Methodological Framework.

4 Results and Discussion

4.1 SAR Geocoding

SAR geocoding is commonly recognised as the process of applying geometric transformation of SAR imagery with the aid of a digital elevation model (DEM) from the original azimuth/range coordinate system to map projection coordinate systems (14). The bi-form SAR images were geocoded. Terrain geocoding and radiometric calibration was performed utilizing SARscape software. The Cosmo-SkyMed Image was imported and transformed to single-look complex (SLC)

SAR image products. After geocoding process Cosmo-SkyMed images with two polarisations were stacked.

4.2 Image Filtering for Stacked images

4.2.1 Fourier Analysis

Procedure that completed in the frequency domain can be viewed as the familiar convolution process. The algorithm of this interrelationship is the convolution theorem, which expresses that a convolution process in the spatial domain is equivalent to a multiplication process in the frequency domain (6). The stacked image was transformed to frequency domain using Fourier Transformation. Thus, the stacked image was plotted in 2D sketch which called Fourier spectrum. The low frequency is in the centre of Fourier spectrum while high frequency is drawn outward as shown in Fig 2.

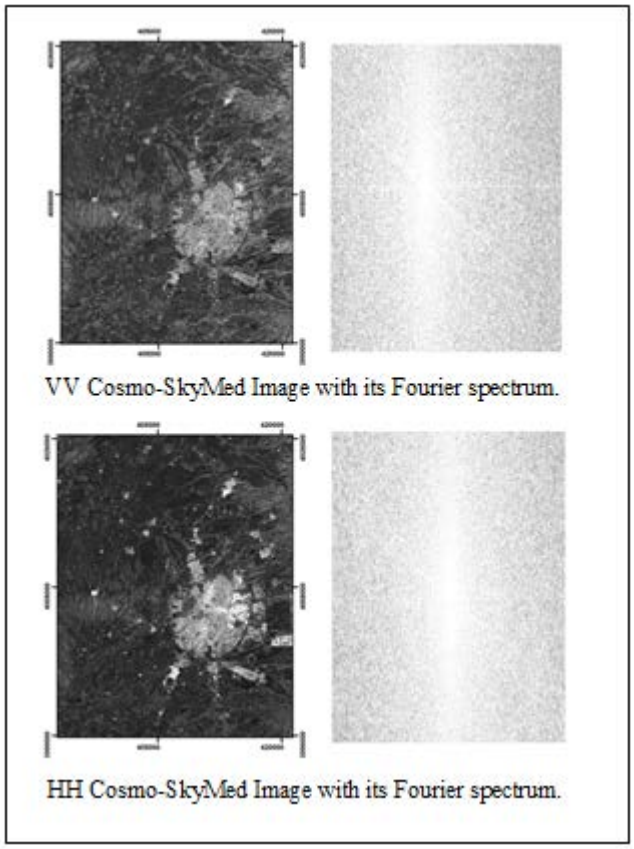

Fig. 2. HH & VV Stacked image with its Fourier Spectrum.

As shown in Figure2 the frequency domain (Fourier Spectrum) has been showed that the VV image of Cosmo-SkyMed imagery is suffered from noise more than HH image.

4.2.2 Appyling Wedge Mask

The wedge mask is applied to pass the low frequency component and block high frequency component in image that noticeable in the Fourier transformed image or layer as radial lines (6). Wedge Mask was used as enhancement techniques for the SAR image in the frequency domain (Fig.2).Subsequently, to the filtering process in frequency domain, Inverse Fourier Transform was applied to get the two filtered images (VV and HH). HH and VV images were stacked for display purposes as shown in Figure 3.

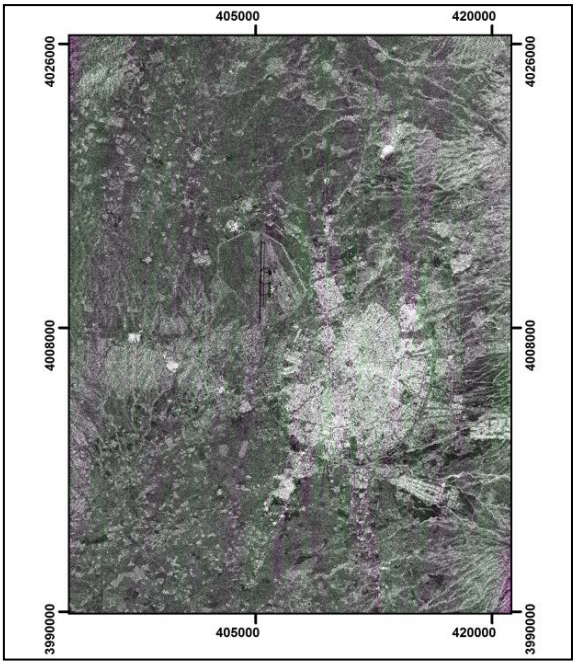

Fig. Filtered images (Stacked image VV & HH).

transformed images (e.g. PC1). It can be concluded that the second one is better in visual interpretation; in addition, it contains less noise where the values were compared according to Coefficient of Variation as illustrated in Table 1. The standard deviation of the noise can be mathematically defined as (6):

Standard Deviation of the noise => (Variance) 0.5 / (Mean) = Coefficient of Variation (Coef. Vari.). Moreover, it is less dimensionality. Therefore, Gamma filtering was applied to transformed image.

Table 1: Evaluation of speckle noise according to Coefficient of Variation. Hint : Best results are shown as italic values.

Images	Stacked image			Transformed image		
Evaluation Techniques	Mean	Std Dev.	Coef, Vari.	Mean	Std Dev.	Coef. Vari.
Layer 1 (HH)	236.54	237,424	*1.003*	356,494	372,705	1.045
Layer 2 (VV)	234,9	247,90	1.054	-100.132	206,05	*-0.00205*
AVG.	-	-	1.029	-	-	*0.521*

4.3 Image Filtering for Principal Components of Cosmo-SkyMed images

4.3.1 Principal Components Analysis

PCA was applied to Cosmo-SkyMed images with two polarisations HH and VV. Principal Components Analysis (PCA) is known as the most beneficial methods in applied linear mathematics. PCA is applied plentifully in all aspects of analysis because it is an easy to use, non-parametric method of finding related details from huge datasets. With less effort PCA paves the way for how to minimize a big data set to a lower dimension. The motivation of using PCA is to enhance SAR imagery before applying filtering process. PCA is re-organised the datasets in such way so that the SAR data is transformed to PC1 and PC2. The PC2 contain most of Speckle noise and redundant data. Therefore, PC1 was better for interpretation purposes.

4.3.2 Fourier Analysis

The PC1 and PC2 were transformed to the frequency domain using Fourier Transformation .

4.3.2.1 Appyling Wedge Mask

As in Section 4.2.2 Wedge Mask was applied to block high frequency details and pass low frequency details. Here to, the image will be enhanced. Then, Inverse Fourier Transform was applied to get the two filtered images (PC1 and PC2). PC1 and PC2 images were stacked for display purposes as shown in Figure 4. When, stacked image (Fig 3) is compared to

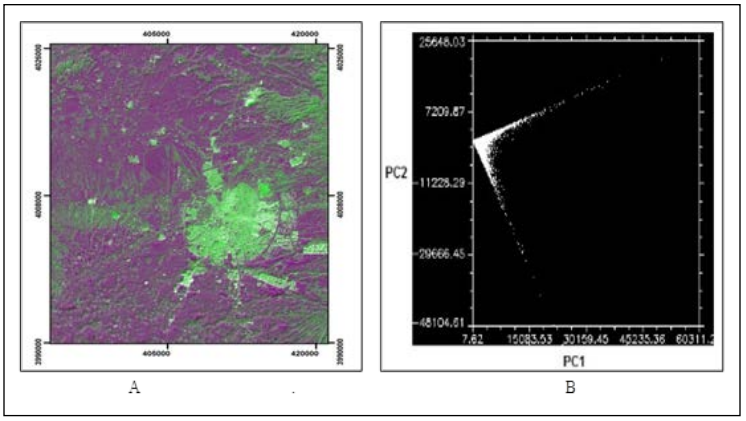

Fig. 4. A: Filtering of transformed images (Stacked image PC1 & PC2) & B: 2D plot PC1 vs. PC2.

4.3.3 Gamma Filtering

The Gamma filter with kernel size 7x7 was implemented on transformed noisy images (PC1 & PC2). Texture of the SAR imagery was much better well kept by applying the Gamma filter the best result is acquired when the Gamma filter is fulfilled comparing to other filters as illustrated in Section 2.

,

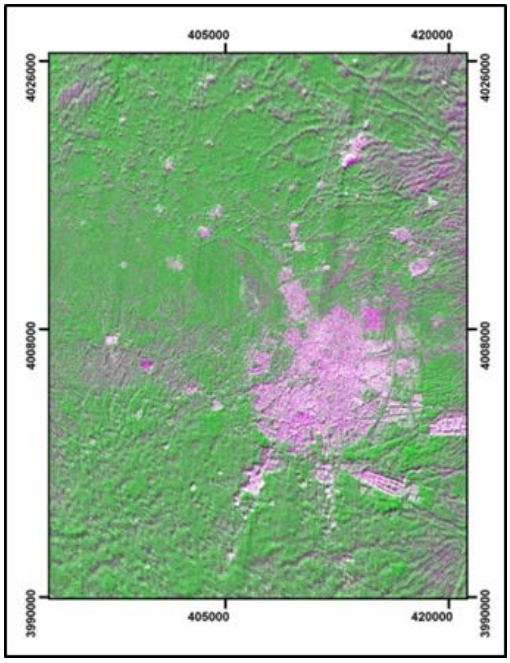

Fig. 5.Gamma filtering for transformed SAR images (Stacked image PC1 & PC2).

5 Conclusions

In this paper an approach was presented for speckle reduction in SAR data based on the Fourier Transform and Principal Components Analysis (PCA). Fourier Transformations are applied for the exclusion of noise by determining areas of high spatial frequency. PCA was applied not only to improve interpretation but also to reduce the noise in SAR data. In addition, a multifariousness of digital image processing was applied for SAR data .These processing procedures were very fruitful in amplifying features extracted from images, reducing errors in interpretation of images and sensing the spatial distribution characteristics of image.

The filtering procedure applied in this paper was to compute the coefficient of variation for SAR data. This coefficient presents us an index to perceive speckle. Afterwards, the speckle noise was decreased to a minimum value for SAR data (Cosmo-SkyMed image). It is motivational also to make the image more interpretable for diversified aims. For this purpose, a set of image enhancement approaches were applied. The resultant image could prove more favourable than original image in improving the accuracy regarding interpretation. The procedures and algorithms that were utilised in this paper can be extrapolated and applied to other datasets. Additionally,

these outputs meet the needs required for helping and guiding decision-makers.

Acknowledgements

I would like to thank e-GEOS, ASI/Telespazio Company for providing SAR data free of charge.

REFERENCES

[1] Jie C., Jing Z., Chunsheng L. & Yinqing Z. (2009). A Novel Speckle Filter for SAR Images Based on Information theoretic Heterogeneity Measurements. Chinese Journal of Aeronautics, 22: 528-534.

[2] Cai Xiao-ou (2014). Study on the reduction of speckle noise in the reconstructed image of digital hologram. Optik, 125: 4389-4393

[3] Santana Fabiana S. , Reali Costa Anna H., Truzzi Flavio S., Silva Felipe L., Santos Sheila L.,Francoy Tiago M., Saraiva Antonio M. (2014). A reference process for automating bee species identification based on wing images and digital image processing. Ecological Informatics, 24: 248-260.

[4] Fusilli L., Marzialetti P., Laneve G., & Santilli G. (2014). Urban growth assessment around Winam Gulf of Kenya based on satellite imagery. Acta Astronautica, 93: 279 - 290.

[5] Al-Hameedawi A. N. (2014). Integrative GI Technology Applied to Best-Site Selection for Industrial Areas in Erbil City, Iraq. PhD (Dissertation). Dresden University of Technology, Germany.

[6] ERDAS Field Guide™ (2010). ERDAS, Inc. United States of America.ERDAS Field Guide™, Volume One United States of America.

[7] Lillesand T., Kiefer R.W., Chipman J. (2008). Remote Sensing and Image Interpretation (6th ed.). JohnWiley, New York. Liu, J.G., Mason, P.J. 2009.

[8] Lua Y., Gao Q., Zhang D. & Sun D. (2011). Directionlet-based bayesian filter for SAR image despeckling: Procedia Engineering, 15 :2788 - 2792.

[9] Gnanadurai D., Sadasivam V., Nishandh J.P.T., Muthukumaran L., & Annamalai C. (2009). Undecimated double density wavelet transform based speckle reduction in SAR images. Computers and Electrical Engineering, 35: 209 - 217.

[10] Mahmoud A. (2012). Plot-based land-cover and soil-moisture mapping using X-/L-band SAR data: Case study Pirna-South, Saxony, Germany. Ph.D. thesis, Fakultät Forst-, Geo- und Hydrowissenschaften, Technische Universität Dresden.

[11] Foody Giles M. & Atkinson Peter M. (2002). Uncertainty in Remote Sensing and GIS. John Wiley & Sons Ltd, The Atrium, Southern Gate, Chichester,West Sussex PO19 8SQ, England.

[12] Biro T.K. (2011). Geovisualisation of Multi-Temporal Satellite data for landuse/landcover change analysis and its impacts on soil properties in Gadarif region, Sudan. PhD (Dissertation). Dresden University of Technology.

[13] Press, William H., et al. 1988. Numerical Recipes in C. New York, New York: Cambridge University Press.

[14] Zhang L., Balz T. & Liao M. (2012). Satellite SAR geocoding with refined RPC model. ISPRS Journal of Photogrammetry and Remote Sensing, 69:37 - 49.

Variation of pore water pressure under embankment on soft clay using finite element method

Dr. Nahla M. Noori M. Salim
Dr. Falah H. Rahil
Zahraa Qasim Mohammed

Abstract— Construction of embankments over soft clay is a great challenge because these soils may be too weak to support the entire load of an embankment. The analyses were carried out to review and estimate the excess pore water pressure, the total and rate of consolidation settlement. Methods of improving stability in these cases include constructing the embankment in stages. Furthermore, establishment of vertical drains is a standout amongst the most generally utilized methods for enhancing the characteristics of soft clays. All these Aspects of the study were carried out by using Soft ware computer program, Geo slope using Coupling Sigma-Seep to perform consolidation analysis.
. The analysis of the basic problem is conducted on the proposed embankment over soft clay in south of Iraq, specifically, in Basrah region. The main conclusions are as follows: the maximum settlement occurs under the center of the embankment, this settlement is reduced as moving towards the toe of the embankment. The vertical settlement increases by 38% using sand drain while the horizontal displacement decreases by 52%. The excess pore water pressure reduces by 83% via using sand drain. Toe berm causes increase in maximum vertical displacement to reach 25%while the horizontal displacement decreases by 10%.

Key words: Embankment, Soft clay, Stage construction, Sand drain, Toeberm, Finite Element (Sigma-Seep soft ware).

I. Introduction

In the field of geotechnical building emerges when embankments of moderate to extensive statures are to be built on exceptionally delicate soils with low shear strength and high compressibility in particular time. The full heights of the embankment can't be built at once and the staged construction must be carryout. To build the embankment in stages, the time of construction in every stage ought to be sufficient for the excess pore water pressure to dissipate and consolidation occurs. In the field, it is so difficult to control this process, so the finite element coupled Sigma-Seep program was used to give an indication of the time required for each stage for excess pore water pressure to dissipate and consolidation takes place. Vertical sand drains are generally used to enhance the characteristics of soft clays. The principle function of vertical drain application is to quicken soil consolidation by shortening the seepage way and enacting radial drainage. Using vertical sand drains increasing the shear strength of the soil while diminishing its post-construction settlement (Holtz et al. 1991).

Manuscript received June 28, 2015
Dr. Nahla M. Noori M. Salim
Asst. Prof. /Building and Construction Engineering Department, University of Technology/Baghdad.
Email-nahla_salim2007@yahoo.com
Dr. Falah H. Rahil
Asst. Prof./Building and Construction Engineering Department, University of Technology/Baghdad
Zahraa Qasim Mohammed.
Building and Construction Engineering Department, University of Technology/Baghdad

II. Geotechnical Characteristics of Soft Clays

Geotechnical Characteristics of Soft Clays**:**

Soft clays are profoundly plastic fine grained soils with moderate to high clay fraction. They are described by high compressibility and low shear strength (for the most part under 25 kPa).

Soft Clay in Iraq

Soft clays are concentrated in the centre and southern parts of Iraq. Basrah governorate (Figure 1) is one of the most important regions in the ancient and modern Iraq. Basrah is the socio-economic hub of southern Iraq and becomes an important commercial and industrial center, which demands construction of large engineering structures such as electrical power stations, port platforms, airport, bridges, railways, roads, embankments .The texture of these soils consists of fine silty clay loams, silty clay and clay fraction with up to 50-70% (Buringh 1960). These constituents with high water table throughout most of southerly section of the basins revealed a fair to poor soft deposits.

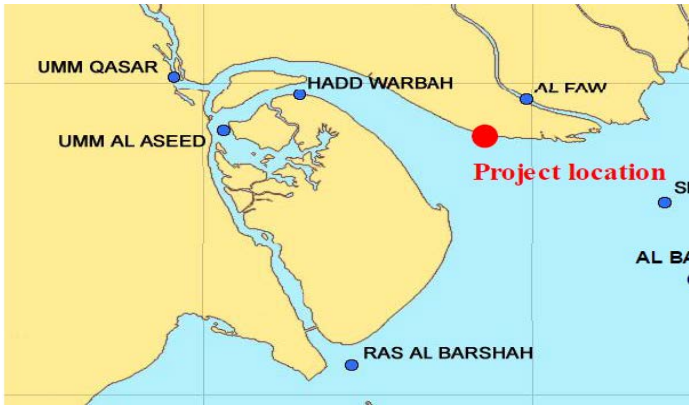

Figure (1): location of soft soil area in Iraq (Al-Razaq, 1990)

Hanzawa (1977) classified the clay sediments of a wide triangle area bounded by Basrah, Fao and Um-Qaser according to Bjerrum's classification (1973) into two types; normally consolidated young clay and normally consolidated aged clay.

Al - Qyssi (2001) studied 41 site investigation reports carried out by (National Center for Construction Laboratories and Research) in southern part of Iraq from 1970 to 2001. The reports demonstrated that most of the sites exhibited average undrained shear strength of less than 50 kPa and SPT value less than 5.

*Previous Studies on Embankments on Soft Clay***:**

Brown and King (1966) were the first analysts that used finite element in embankment problem. They analyzed built up and cut down embankments using an elastic model to represent the soil. The authors forecasted on possible failure mechanisms and compared the factors of safety calculated from the finite element predicted stress distributions with Taylor's (1948) stability parameters.

Clough and Woodward (1967) compared elastic embankments constructed in a single stage with those constructed in multi stages. The authors concluded that it is necessary to model the construction sequence to produce accurate embankment displacement predictions.

Wroth and Simpson (1972) investigated a test embankment constructed at King's Lynn, UK. The subsoil was modeled using Cam-clay model and the embankment loading by equivalent vertical loads applied over a number of increments. Undrained analyses were carried out representing the short term conditions. The predicted vertical and horizontal displacements were in good agreement with those observed. However, the predicted pore pressures were not in such good agreement.

Smith (1984) investigated some effects of stage constructed embankments. The embankment was constructed in 1 m lifts with partial dissipation of excess pore pressure specified after each increment. Smith observed large principle stress rotations during the first undrained loading stage and these rotations were greatest below the toe of the embankment.

Interestingly no rotations greater than 5° were observed during subsequent loading or consolidation stages.

Fattah and Salman (2006) reanalyzed the Streefkerk embankment which was constructed in 1984. The works of the embankment are performed in stages allowing for in between consolidation. The computer program SAGE-CRISP was used in the analysis.

The modified Cam-clay model was adopted for the clayey soil. A comparison has been made between the excess pore water pressures generated by loading and their decay due to consolidation with those measured using piezometers.

Fattahi et al., (2013) studied the behavior of the soft ground considering the modified Cam-Clay model including and excluding soil creep or secondary compression using finite element method (PLAXIS 2D). The analyzed data were verified with field measurements. The results indicate that the soft soil model based on the modified Cam-Clay model including soil creep can predict the ground settlement and the excess pore water pressure more precisely below the embankment crest.

Sand Drain

The consolidation settlement of soft clay subsoil creates a lot of problems in foundation and infrastructure engineering. Due to very low clay permeability, primary consolidation takes a long time to complete. To shorten this consolidation time, vertical drains are installed .The purpose of vertical drain installation is twofold. Firstly, to accelerate the consolidation process of the clay subsoil, and, secondly, to gain rapid strength increase to improve the stability of structures on weak clay foundation. Table 1 illustrated the methods of installation of vertical drain.

Table (1): Methods of installation of vertical drain.

Group Description	Particular methods	Remarks
Displacement methods	• Driving vibration • Pull down (static force) • Washing • Combination of above	A mandrel with or without a disposable shoe is used in each case
Drilling methods	• Rotary drill, with or without a casing • Rotary auger, including continuous standard and hollow flight augers • Percussive methods with or without casing • Hand auger	———
Washing methods	• Rotary wash jet • Washed open ended casing • Weighted wash jet head	Methods in which sand is washed in via the jet pipe, are not suitable for prefabricated drains

Balasubramaniam et al., (1997) investigated fully instrumented tests embankments and studied their role in the development of appropriate ground improvement techniques for highways, motorways and airfields. The ground condition along the route was considered to be very soft. Sand drains of

0.2m diameters were installed by the displacement method and in triangular pattern at 2m spacing.

Shen et.al (2005) analyzed the execution of two full-scale test embankments developed on soft clay store in the eastern beachfront district of China (Hangzhou –Ningbo or HN) , one embankment was built on regular subsoil and the other was developed on prefabricated vertical drain(PVD). The scientific results demonstrate that PVDs expanded the bulk vertical hydraulic conductivity of soft subsoil by around 30 times contrasted with the first.

The short comings in the information on the Iraqi soft clay directed the present work to study the variation of displacement and excess pore water pressure in soft clay due to embankment construction.

***Finite element computer programs*:**

In order to model accurately embankment over soft soils coupled finite element analysis SIGMA/W and SEEP/W has been shown to be capable of predicting the settlement and pore pressure response.

A fully coupled analysis requires both the stress – deformation and seepage dissipation equations be solved simultaneously. SIGMA/W computes displacements and stresses while SEEP/W computes the changes in pore-water pressure with time. Running these two software products in a coupled manner makes it possible to do a consolidation analysis. When coupled, both SIGMA/W and SEEP/W contribute to forming a common global characteristic (stiffness) matrix. Three equations are created for each node in the finite element mesh. Two are equilibrium (displacement) equations formed by SIGMA/W and the third is a continuity (flow) equation formed by SEEP/W. solving all the three equations simultaneously gives both displacement and pore-water pressure changes. When doing a coupled analysis, it is essential to recognize that all equilibrium (force and displacement) conditions are defined in SIGMA/W and all hydraulic (flow) conditions are specified in SEEP/W.

Description of the Basic Problem:

A trail embankment constructed on AL-Basrah city south of Iraq is suggested for analysis. The geological section is shown in Figure (2). Table (2) summarized some of the physical properties of Basrah area. (after Ministry of Transposition). The finite element mesh used in the numerical analysis is shown in Figure (3).

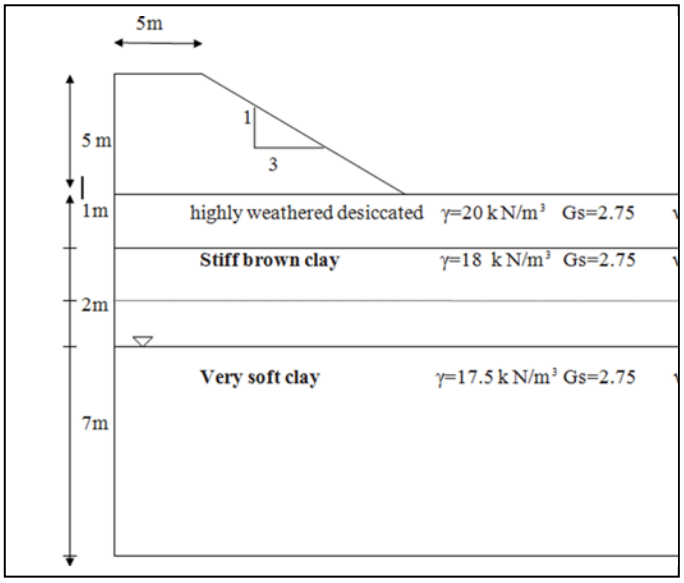

Figure (2): Geological profile along AL-Basrah region.

Table (2): Material parameter of Basrah soil (collected from reports of Ministry of Transportation in addition to (Al-Razaq, 1990).

TYPE OF SOIL	PARAMETER	VALUE	MODEL
CLAY	LIQUID LIMIT(LL) COMPRESSION INDEX (CC) SLOPE OF NORMAL CONSOLIDATION LINE ( ) SLOPE OF SWELLING LINE ( ) COEFFICIENT OF VOLUME COMPRESSIBILITY (MV) HYDRAULIC CONDUCTIVITY (K) EFFECTIVE FRICTION ANGLE ( ) COEFFICIENT OF EARTH PRESSURE AT REST (K0) POISSON, S RATIO ( ) OVER-CONSOLIDATION RATIO (OCR) UNIT WEIGHT ( )	38% 0.22 0.13 0.013 1 3×10^{-9} M/S 25 0.5 0.4 1 17KN/M^3	M CC
SAND	MODULUS OF ELASTICITY (E) POISSON, S RATIO ( ) HYDRAULIC CONDUCTIVITY (K) UNIT WEIGHT ( ) POISSON, S RATIO ( )	35 MPA 0.3 1×10^{-6} M/S 20KN/M^3 0.3	LINEAR ELASTIC

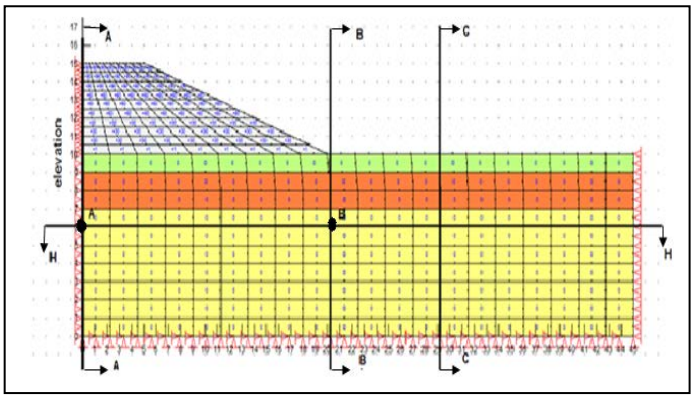

Figure (3): Typical finite element mesh of the embankment-soil system.

Loading Sequence:

In this study, the embankment fill is going to be placed in four stages as Loading sequence of construction of embankment. Figure (4) shows a graph of fill height versus time for staged construction.

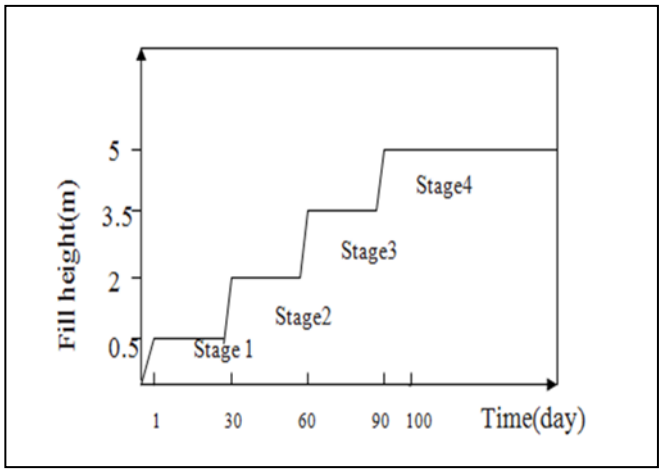

Figure (4): Fill height versus time (staged construction).

Staged construction is advantageous in that it requires no extra fill to consolidate the soil. It also increases the time needed to achieve the desired consolidation. In this work, two constitutive models are used to characterize the stress-strain behavior of the soil; linear elastic model is used for the embankment and the highly weathered desiccated layer, while modified cam clay model is used for modeling the soft clay soil.

*Results and Discussion of the Basic Problem***:**

The investigation focuses on influence of construction stages of embankment on vertical, horizontal displacement and the excess pore water pressure ,along section A-A (the centre of the embankment ,section B-B (the toe of embankment , section C-C (some distance from the toe of embankment) and section H-H .All these sections are clearly shown in Figure (3). Figures (5), a and b, shows the deformed mesh and displacement vectors respectively. In general, it can be seen that the movement of the soil is downward and reaches to maximum value under the center of the embankment and it reduces as we moved toward the toe of embankment .In addition, there is a horizontal movement, this horizontal movement reaches to maximum value as we move toward the toe of embankment.

The vertical, horizontal displacement and pore water pressure contour lines of the basic problem at the end of construction are shown in Figures (6) a, b, and c.

The contour values of vertical displacement concentrated with higher values under the center of the embankment and decreases as we move toward the toe of embankment while the contour values of horizontal displacement increased toward the toe of embankment .the excess pore water pressure increased with depth of the subsoil.

Figure (7) shows the progress of settlement with time at point A, B under the center and toe of embankment respectively. It can be seen that the settlement increases with time and reaches to the maximum value of (0.58 m) at point A and (0.3 m) at point B that agree with the results obtained by (Chin, 2005). Figure (8) illustrates the variation of excess pore water pressure with time at point A ,as predicted ,the pore water pressure increases with time until reach the maximum value of 80 (kPa) after 100 days(time for construction stages) ,then decreases. Figure (9) indicates the development of horizontal displacement with time and the maximum value is (0.092 m) after 1000 day.

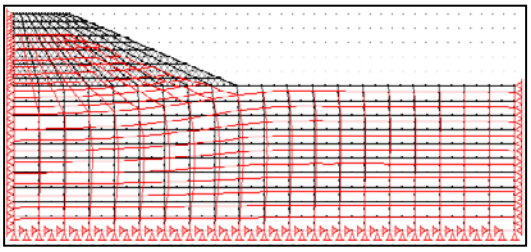

(a)Deformed mesh

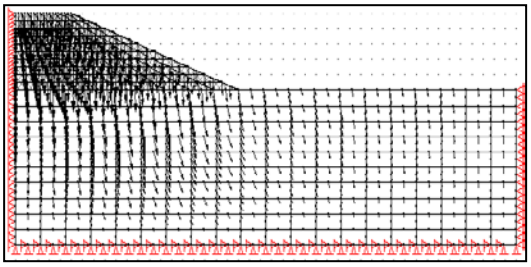

(b) Displacement vectors.

Figure (5): Deformed shape of mesh and displacement vectors due to filling.

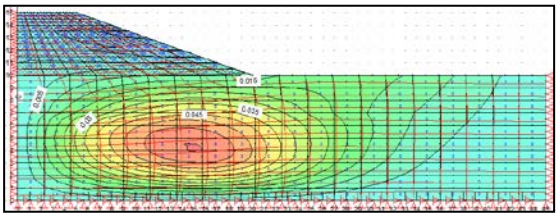

(a)

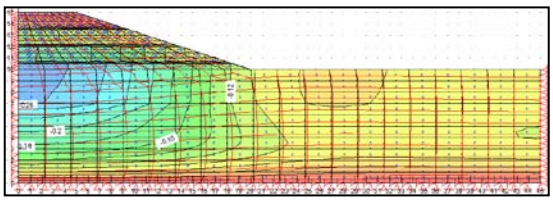

(b)

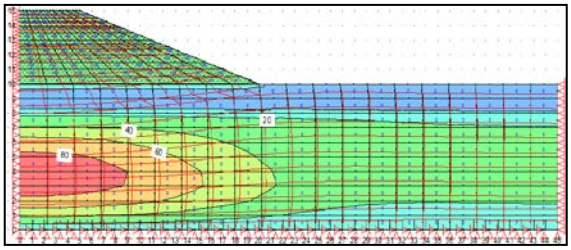

(c)

Figure (6): Contour lines of (a) horizontal displacement (b) vertical settlement (c) pore water pressure.

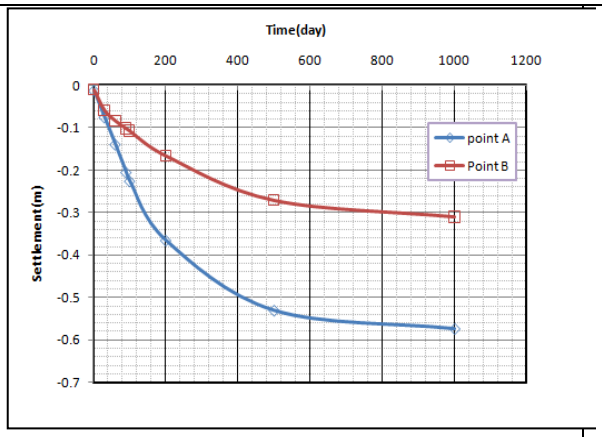

Figure (7):Variation of vertical displacement versus time at points A and B.

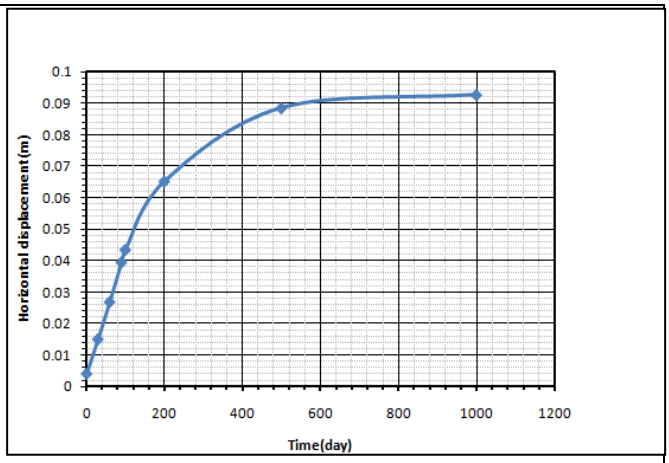

Figure (9): Horizontal displacement versus time at point B.

Vertical displacement:

The vertical displacement along section H-H at different times presented in Figure (10). It is clearly shown that the maximum displacement occurs under the center of embankment and reaches to (0.58 m). This displacement reduced as we moved away from the center and reaches to minimum value as (0.21 m) at the toe of the embankment after 1000 days.

Figures (11) and (12) show the variation of vertical displacement along sections (A-A) and (B-B). The results show the effect of construction time and the consolidation time on the vertical displacement.

Along section (A-A) the maximum vertical displacement approximates (0.64 m) occurs at the surface of soft clay and decreases with depth. These values reduced at section B-B and reaches to (0.34 m). The horizontal movement along two vertical sections (B-B) and (C-C) are presented in Figure (13) and (14). It can be seen that the maximum horizontal displacement occurs at the depth of 5m from the top of soft clay .The maximum horizontal displacement reaches approximately (0.05 m) at the end of construction and increases to (0.1 m) after 1000 days due to consolidation process. The lateral deformation along section C-C is approximately (0.038 m) from the centerline of the embankment as shown in Figure (14). It is clearly shown that lateral deformation seems to flow in different trend compared with section B-B.

Pore water pressure:

The distribution of excess pore water pressure during construction stages along section A-A are shown in Figures (15), (16), (17) and (18) while Figure (19) demonstrated the variation of pore water pressure after construction and till the end of consolidation. The maximum excess pore water pressure occurred during construction stages .The excess pore water pressure dissipated and reached to minimum value after approximately 800 days due to consolidation process. Figure (20) Comparing the excess pore water pressure at different section is done; the results are almost similar but the maximum values of excess pore water pressure extent to greater depth as we move away from the center of embankment. The maximum excess pore water pressure along section A-A (at the centerline of the embankment) occurred at

depth equals to 6m below the surface of soft clay layer and with the values of (105 kPa) while, the maximum values of excess pore water pressure along section (B-B) (at the toe of the embankment) occurred at depth 7 m from the surface with values equal to (40 kPa); these values of excess pore water pressure reduced to 25 kPa along section (C-C).

The effect of toe berm on vertical and horizontal displacement and pore water pressure is clearly demonstrated by using finite element analysis of the basic problem with toe berm is shown in Figure (20). Figure (21) shows the horizontal displacement at the toe of the embankment .The results reveal that there is a reduction in the maximum horizontal displacement; this reduction reaches approximately 10% via using berm. The maximum increasing in the excess pore water pressure reaches approximately 17% via using berm near the toe of embankment; this is clearly shown in Figure (22).

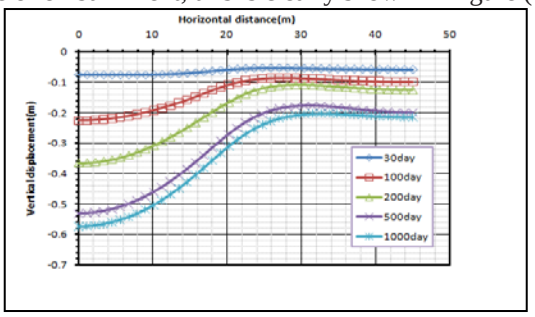

Figure (10): Vertical displacement along section (H-H)

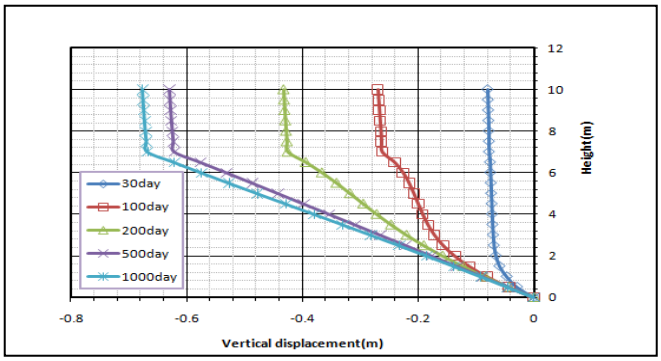

Figure (11): Vertical displacement along section (A-A)

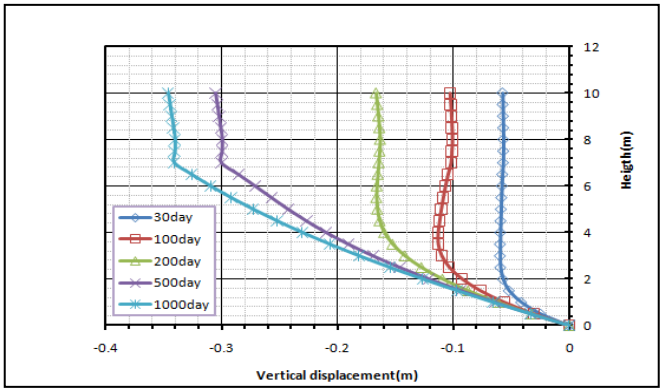

Figure (12): Vertical displacement along section (B-B).

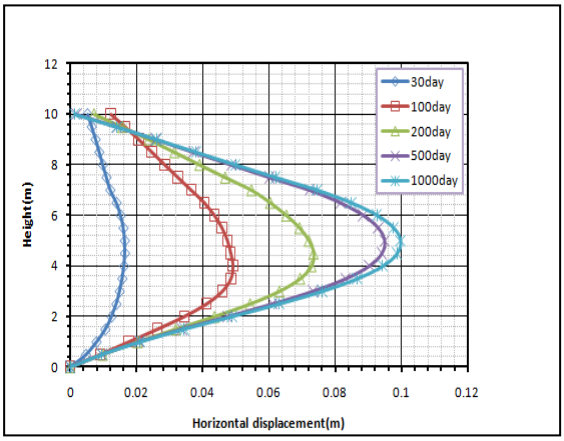

Figure (13): Horizontal displacement along section (B-B).

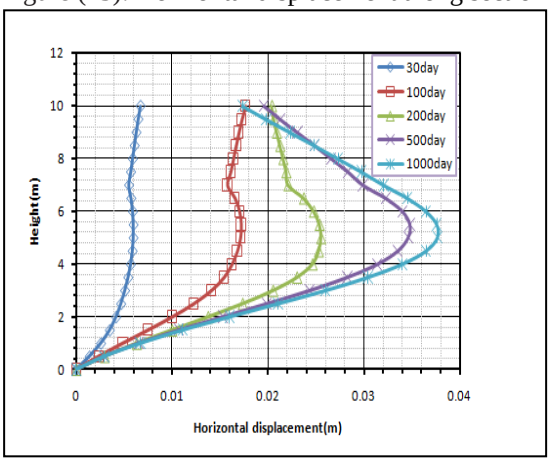

Figure (14): Horizontal displacement along section (C-C).

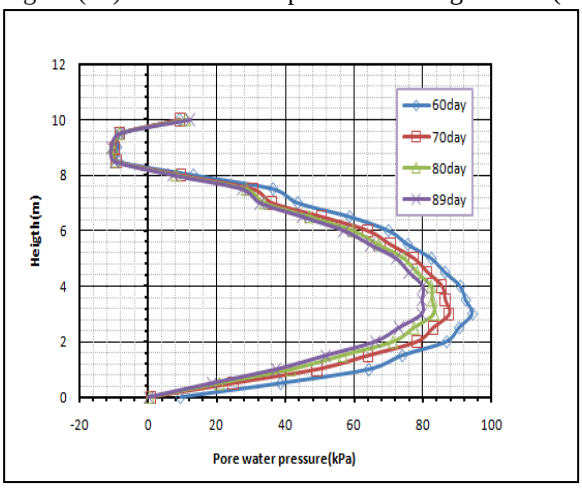

Figure (15): Variation of pore water pressure at stage 3 (60-89 day) along section (A-A) of basic problem embankment.

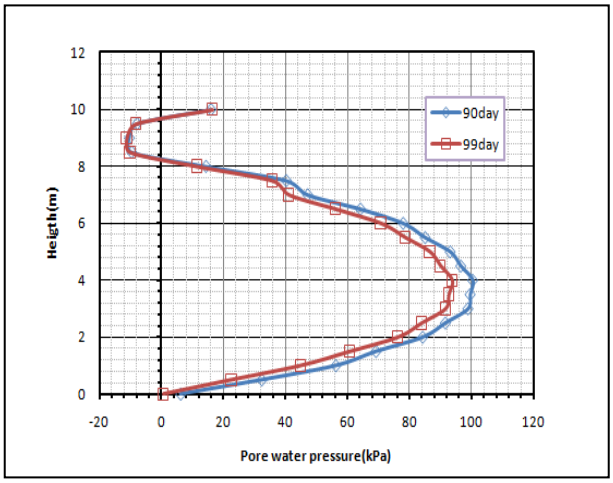

Figure (16): Variation of pore water pressure at stage 4 (90-99day) along section (A-A) of basic problem

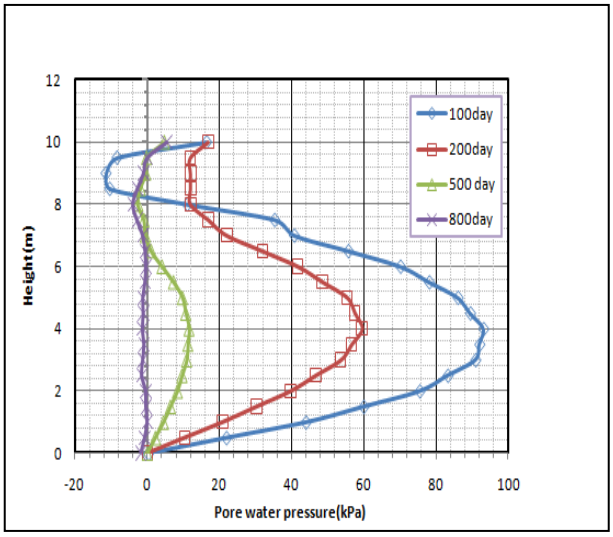

Figure (17): Variation of pore water pressure after construction along section (A-A) of basic problem embankment.

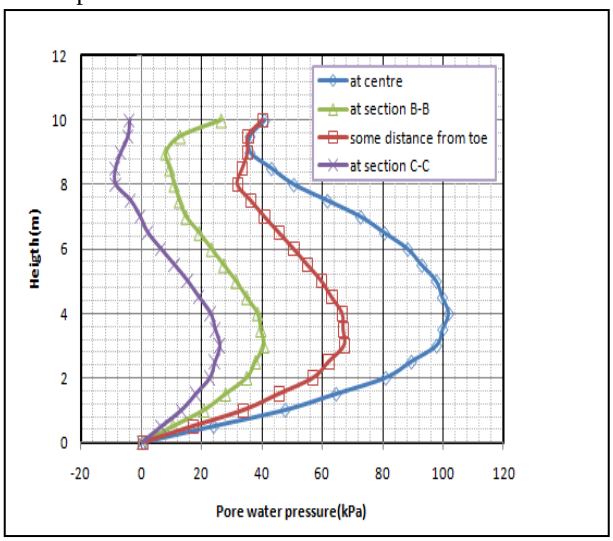

Figure (18): Variation of pore water pressure after construction along different sections of basic problem

embankment.

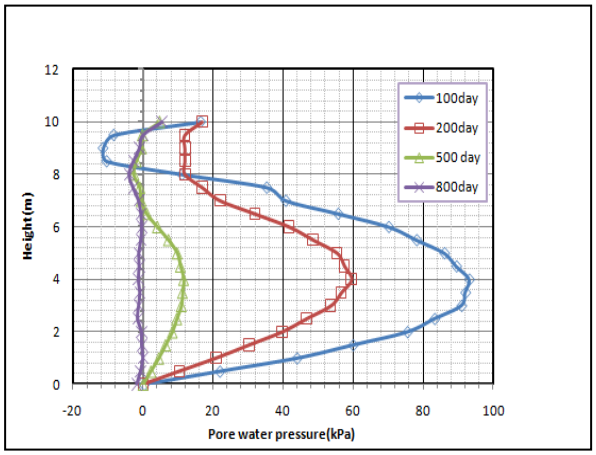

Figure (19): Variation of pore water pressure after construction along section (A-A) of basic problem embankment.

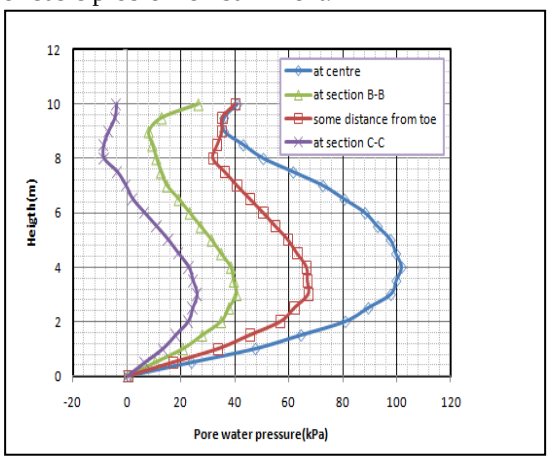

Figure (20): Variation of pore water pressure after construction along different sections of basic problem embankment

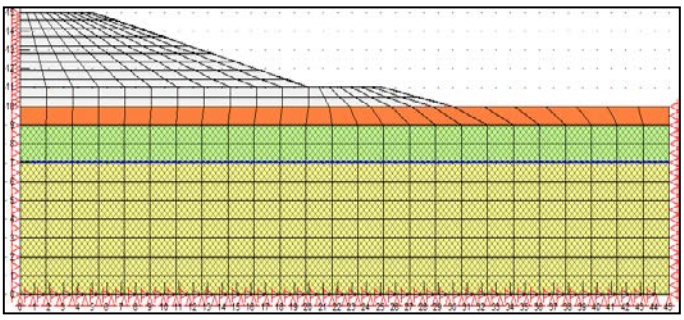

Figure (21): Finite element mesh for widened embankment using toe berm.

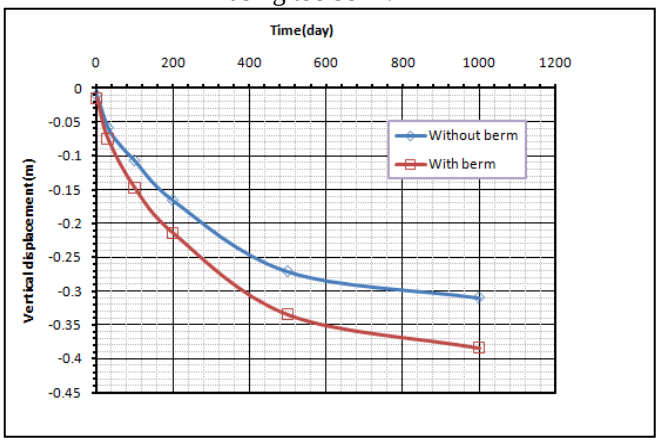

Figure (22): Effect of toe berm on vertical displacement at point B of basic problem.

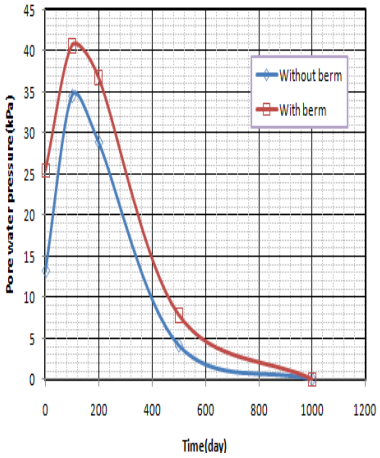

Figure (23): Effect of toe berm on horizontal displacement of basic problem**.**

Improvement of Soft Subsoil of the Basic Problem Using Vertical Sand Drain:

Sand drains are installed through soft clay soils to accelerate the speed of consolidation of the subsoil by reducing the drainage path length and utilizing the naturally higher horizontal permeability of clay deposits. In order to improve the deformation behavior of soft subsoil of basic problem in the present study, the vertical sand drains with 0.5m diameter and 3m spacing have been used. The finite element mesh of improved soil is shown in Figure (24). Figure (25) shows the deformed mesh using sand drain. It is clearly shown that the movement of the soil is downward and this movement increase as we move away from the toe . By comparing figures (5) and (25) ,It is clearly shown that using sand drain creates some confinement to the region and reduces the heave that occurs away from the toe.

Figure (26) illustrates the results of the progress of vertical displacement with time by using sand drain and without sand drain. The results show that the maximum settlement increases by 38% by using sand drain. The comparison of the results of excess pore water pressure with and without sand drain are shown in Figure (27). The results demonstrated that the maximum pore water pressure decreases by 83 % by using sand drain. Figure (28) shows the horizontal displacement versus time under the toe of embankment with and without sand drain .It can be seen that the maximum horizontal displacement decreased by 52% by using sand drain.

Conclusions:

The main conclusions which can be drawn from above studies are that:

1. Finite element analysis is powerful method in predicating vertical, horizontal settlement and excess pore water pressure.
2. In general, the maximum settlement occurs under the center of the embankment, this settlement is reduced as moving towards the toe of the embankment.
3. The modified-Cam clay model can mimic the soil conduct successfully. When the consequences of analysis are contrasted and the measured qualities, good agreement was obtained.
4. The vertical settlement increases by 38% via using sand drain while the horizontal displacement decreases by 52%. The excess pore water pressure reduces by 83% via using sand drain.
5. Toe berm causes increase in maximum vertical displacement to reach to 25%while the horizontal displacement decreases by 10%. The maximum increase in pore water pressure reaches 17%.

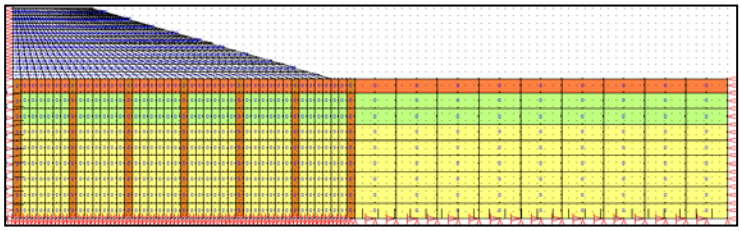

Figure (24): Finite element mesh of improved basic problem with sand drain.

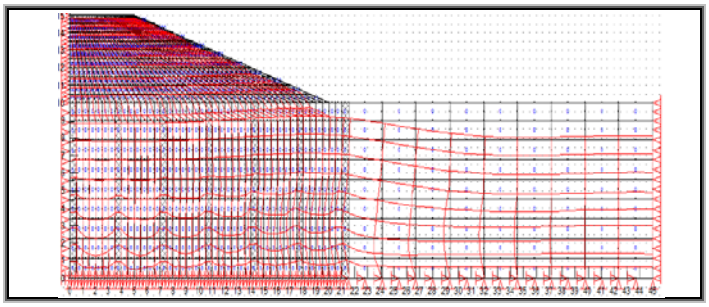

Figure (25): Deformed finite element mesh of improved subsoil of basic problem.

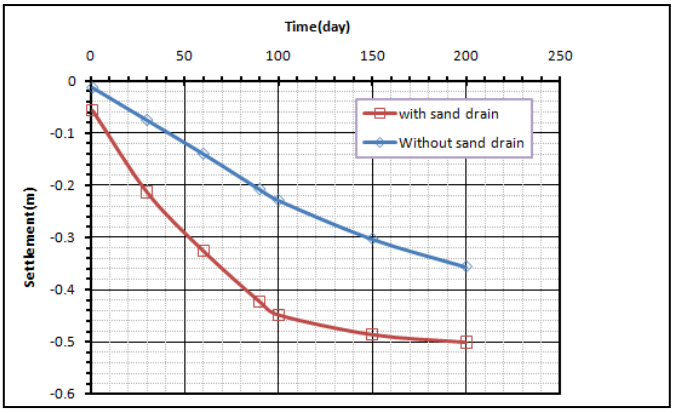

Figure (26): Vertical displacement versus time with and without sand drain.

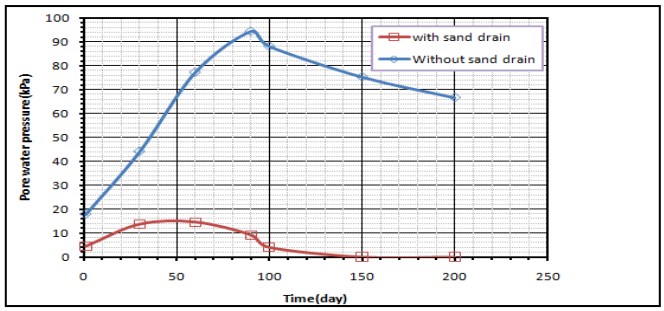

Figure (27): Variation of pore water pressure with time with and without sand drain.

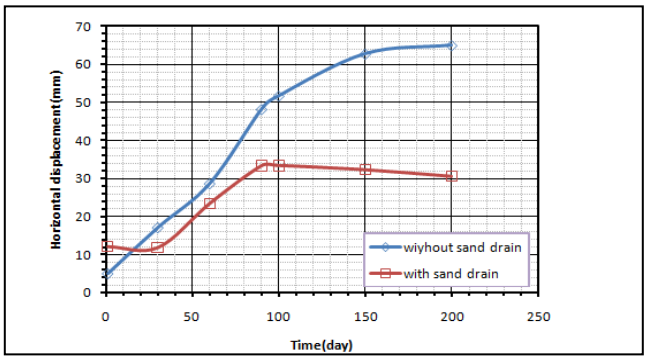

Figure (28): Horizontal displacement versus time with and without sand drain.

REFERENCES:

1-AL-Razaq,W.F., (1990): "Geotechnical properties of Fao soil", " M.sc. thesis, University of technology, Baghdad.

2-Al-Qysis M.R., (2001): "Unreinforced and reinforced behavior of single and groups of granular piles", Ph.D Thesis submitted to the civil engineering Faculty of the Military Collage of Engineering.

3-Balasubramaniam A.S., Phien-Wej N., Indraratna B., BergaDO D.T., (1989): "Predicted behaviour of a test embankment on Malaysian marine clay". Int. Symp. on Trial Embankments on Malaysian Marine Clays, Kuala Lumpur, pp. 1.1-1.8.

4-Brown, C.B. and King, I.P., (1966): "Automatic embankment analysis: equilibrium and instability conditions". Geotechnique, Vol. 16, No. 3, pp. 209-219.

5-Buringh. P., (1960): "Soils and soil conditions in Iraq", Netherlands by H. Veenman and Zonen N.V, Wageningen.

6-Clough, R.W. and Woodward, R.J., (1967): Analysis of embankment stresses and deformations Journal of Soil Mechanics and Foundations Division ASCE , Vol. 9, SM4, pp. 529-549.

7-Fatahi, B., Le, T.M, Le, M and Khabbaz, H., (2013): "Soil creep effects on ground lateral deformation and pore water pressure under embankments", School of Civil and Environmental Engineering, University of Technology Sydney (UTS), Sydney, Australia.

8-Fattah1, M.Y, .Salman1,F.A," Back Analysis of Staged Embankment on Very Soft Clay" Proceedings of the 4th Jordanian Civil Engineering Conference, 28-30 March 2006, 1Department of Building and Construction Engineering, University of Technology, Baghdad, Iraq Amman – Jordan.

9-Holtz, R.D. Jamiolkowski, M., Lancellotta, R. and Pedroni, S. 1991. Prefabricated vertical drains: design and performance, CIRIA ground engineering report: ground improvement. Butterworth-Heinemann Ltd. London, U.K.

10-Hanzawa H. (1977): "Geotechnical Properties of Normally Consolidated Fao Clay, Iraq"> Soils and Foundations, Vol. 17, No. 4, Dec. Japanese Socity of Soil Mechanics and Foundation Engineering.

11-Shen, S.L, Chai, J., Hong, Z., Cai,F., (2005): "Analysis of field performance of embankments on soft clay deposit with and without PVD-improvement", School of Naval Architecture, Ocean and Civil Engineering, Shanghai Jiao Tong University,1954 Hua Shan Road, Shanghai 200030, China bInstitute of Lowland Technology, Saga University, 1 Honjo, Saga 840-8502, Japan cInstitute of Geotechnical Engineering, Southeast University, Nanjing 210096, China.

12-Smith,P.R., (1984): "The constructiuon of multistage embankments on soft clay", MSc Dissertation, Imperial College, Londen..

13-Wroth, c.p. and Simpson, B., (1972). An induced failure at a trial embankment. Part. Finite element computations. Proc. Spec. Conf. on performance of Earth-Supported Structures, ASCE,Lafayette, pp. 65-79.

Analysis of Deep Supported Excavation in Elasto-Plastic Soil using Bounding Surface Model

Osamah M. Hussein, Assist. Prof. Dr. Qassun S. Mohammed Shafiqu,
Al-Nahrain University, Baghdad, Iraq

***Abstract*-The behavior of a three-dimensional deep-supported excavation system in saturated cohesive soils has been investigated in this study using the finite element method. The finite element analyses were carried out using the linear elastic model for the support material, while the elasto-plastic bounding surface model was used for representing the cohesive soil. Also, a sequential excavation has been rigorously modeled in the analysis, together with the transient effects through a fully coupled Biot formulation.**

The models and the excavation technique together with the consolidation process were implemented into the finite element program (MOD-3D-EXCON) modified for the purpose of these analyses. Then, the results of a finite element parametric study are conducted to define the effects of excavation geometry (i.e., length, width and depth of excavation), wall length, depth of embedment layer and bounding surface parameters, on the three-dimensional wall displacements and ground movements caused by excavation through a fully saturated Iraqi soil, within Baghdad city.

The result showed that the ratio of corner to center movements perpendicular to a wall is less than 1.0, and the ratio of the maximum horizontal displacement to the depth of excavation is ranged between 1 to 2 %. Also, the ratio of the maximum ground settlement to the depth of excavation is obtained to be in the range of 0.2 to 0.9 % with an average value of 0.5%. The results also indicated that λ and κ are the most effective bounding surface parameters on the values of displacements than others.

Keywords: Bounding surface model, Deep excavation, Finite element method.

I.INTRODUCTION

Excavation is usually employed in the construction of basement of buildings and underground space of the mass rapid transit and the subway system in urban areas. Braced excavation is a complicated soil-structure interaction problem, and it is a challenge to engineers to simultaneously ensure the safety of excavation system as well as the integrity of properties adjacent to the excavation site, including buildings, structures, and life pipes.

The finite element method (FEM) is often employed to model complex soil-structure interaction problems, such as braced excavations. Many investigators such as [12], [8] have verified the reliability of FEM applied to analyses of deep excavations, even though the uncertainty of soil models and parameters adopted is concerned. Although the deflection of the braced wall can generally be predicted well using FEM analysis with the conventional soil constitutive model, such as the Modified Cam-clay model, the prediction of surface settlement is usually not as accurate. And, the previous studies [13], [9] have shown that the accuracy of surface settlement predictions by FEM can significantly be improved if the soil behavior at small strain levels can properly modeled.

The complicated excavation system may be affected by a large number of factors, such as wall stiffness, wall length, ground conditions, groundwater, excavation geometry, construction sequences, strut stiffness, workmanship and so on [9]. Thus, it is essential to investigate the factors that may affect the excavation-induced wall deflection and ground movements when studying the deep supported excavation system using FEM.

In this study, a nonlinear three-dimensional finite element computer program (**MOD-3D-EXCON**) has been modified to investigate the influence of construction method (i.e, excavation), excavation geometry, wall length, depth of bearing stratum and soil model parameters on the behavior of deep supported excavation system using the elastoplastic bounding surface model as a constitutive model representing the cohesive soil which has the features that plastic deformation may occur for stress state within the surface, and the possibility to have a very flexible variation in the plastic modulus.

II. FINITE ELEMENT MESH AND EXCAVATION PROBLEM

The 3-D finite element mesh used in the analyses is shown in Figure (1). The mesh represents a sheet pile wall supporting a saturated cohesive soil. In the analyses, the undrained and drained conditions are carried out for the deposits of saturated clay soil and sand soil, respectively. The depth of stratum (C) is taken to be 40 to 50 m. A sheet pile wall of thickness 1cm and depth D taken to be 16 to 24 m is used to support the simulated excavation. The excavation length (primary wall) L is varied from 30 to 50 m, while the excavation width (complementary wall) B is varied from 25 m to 50 m. The rate of excavated volume is 300 m3/day, and the depth of excavation H is chosen to be 4, 8 and 12 m. The problem has been simplified as far as possible to reduce the number of variables and allow a meaningful study to be made.

The finite element mesh consists of 392 brick elements each of 20-nodes with a total number of 2096 nodes. The bottom face of the mesh is assumed to be fully fixed, whereas the vertical sides of the mesh are assumed to be fixed laterally and free to move vertically.

A typical excavation case with silty clay subsoil stratum of Al-Jadiriyah site is selected to investigate the characteristics of three-dimensional supported excavation behavior. The problem is analyzed assuming elastic model for sheet pile material with the parameters given in Table (1), and elasto-plastic bounding surface model for the silty clay soil with the parameters obtained experimentally by using the results of consolidated drained and undrained triaxial tests, as presented in Table (2).

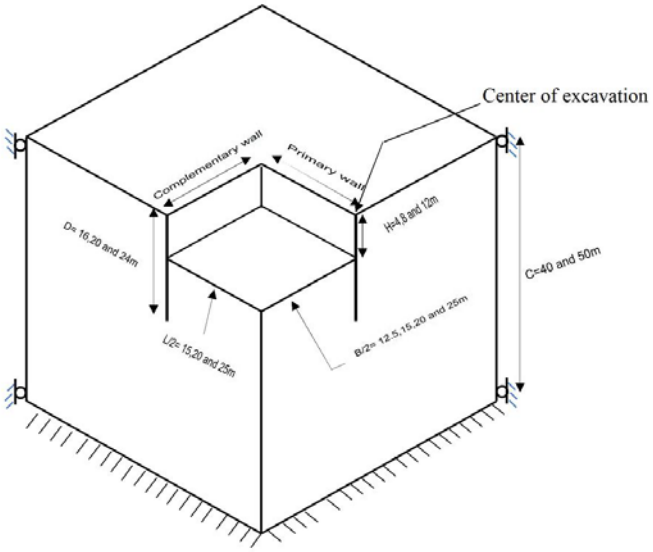

Figure (1) Problem Geometry

Table (1) Sheet pile wall parameters [1]

Parameters	Value
Modulus of elasticity, E (kPa)	2×10^8
Poisson's ratio, υ	0.2

Table (2) Bounding surface parameters for Al-Jadiriyah silty clay soil

λ	κ	ν	M_c	M_e	R_c	R_e	A_c
0.06	0.015	0.34	1.26	*	2.65	*	0.02
A_e	T	C	s_p	h_c	h_e	h_o	m
*	-0.1	0	1	2	1.5	1.75	0.02

* Material response in extension was not simulated.

III. PARAMETRIC STUDIES

1. Effect of Excavation Geometry

The length of sheet pile wall is assumed to be 20 m. Figure (1) shows a typical three-dimensional mesh, in which a quarter of the excavation is analyzed for L=30, 40 and 50 m , B= 25, 30, 40 and 50 m and H = 4,8 and 12 m:

In order to investigate the length effect of primary wall on the wall deflection for a section, excavations with various lengths of complementary and primary walls are analyzed.

Figure (2) shows the wall deflection profile with different excavation sizes at an excavation depth of 12 m, at end of excavation, as calculated by the program. Figure (3) shows the variation of maximum lateral wall deflection along the distance from the corner to the center section for various lengths of excavation primary and complementary walls. It can be seen from these figures that the increase in the length of primary wall results in increase of a section's wall deflection for a given length of complementary wall (B).

Also, the effect of width of excavation (B) shows that the wider the excavation, the larger is the magnitude of lateral wall displacement which indicates that the size of the yield zones being larger.

The behavior of the center section for the longer complementary walls is still affected by the existence of the corner, as shown in Figure (3). In all cases, the ratio of corner to center movements perpendicular to a wall, $\delta_{corner}/\delta_{center}$, is less than 1.0, indicating that the displacement decreases near the corners of the excavation due to the stiffening effects of the corners [5].

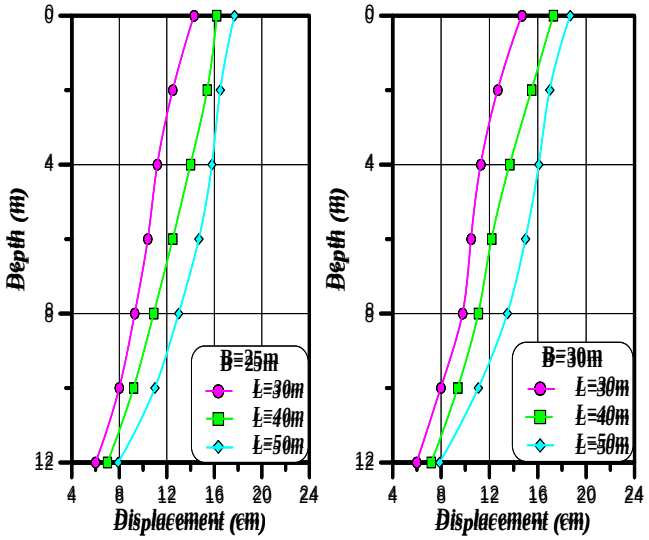

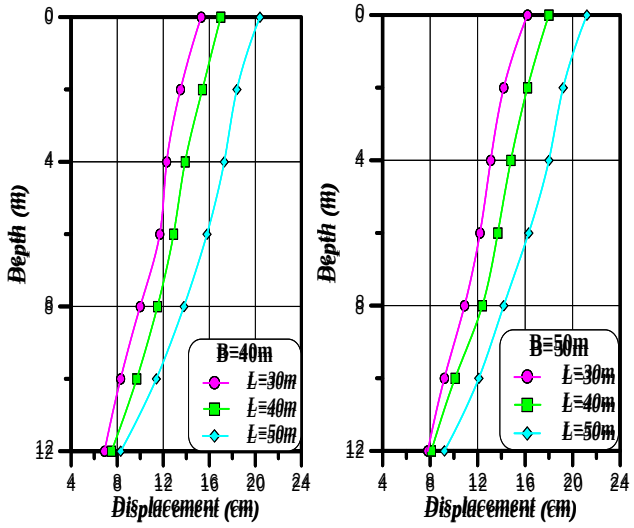

Figure (2) Wall displacement profile of different excavation widths at H= 12m

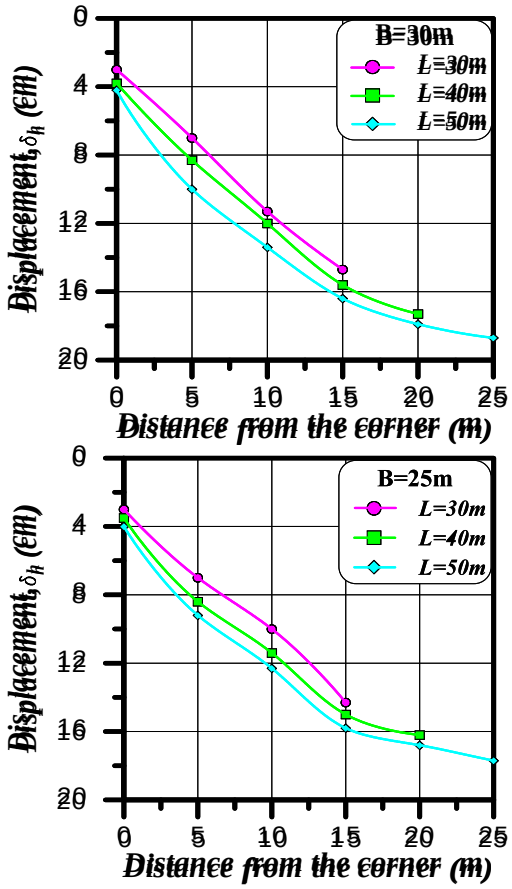

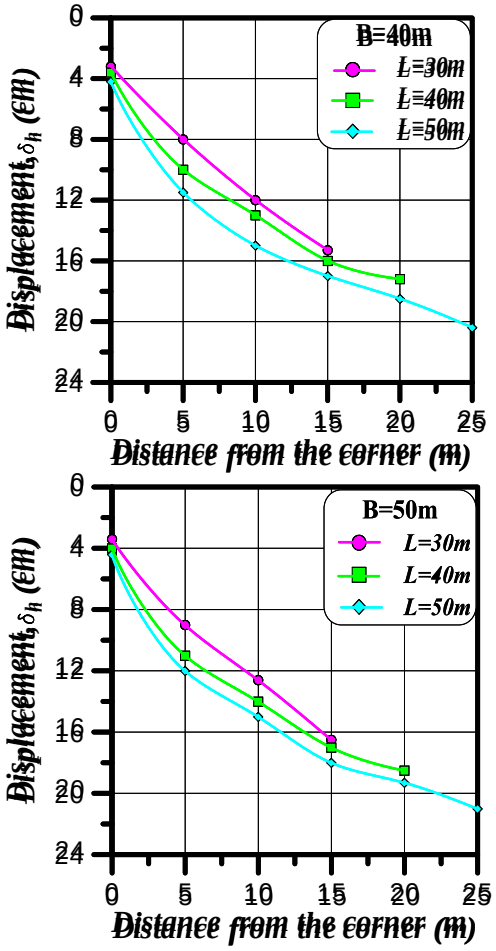

Figure (3), Variations of Maximum lateral Wall Displacement with the Distance from the corner.

Figure (4) summarizes the ground movements at the center of excavation (L/2) for depth of excavation 12 m. For each excavation geometry, the maximum settlement decreases with decreasing excavation size. The horizontal displacement of wall results in the settlement of the ground behind the wall. The magnitude of the surface settlement in fact depends on the type and stiffness of the support, position of the support, and on the stiffness of the wall [6]. From Figures (3) and (4), it has been seen that if the wall is permitted to deflect as a cantilever, the horizontal displacement can be greater than the settlements, and the maximum settlement usually takes place directly behind the wall.

The settlement profiles can be viewed as nearly parabolic curves joined by tangent lines or inflection points that can be divided into two categories: concave downward (hogging) and concave upward (sagging).The ground surface settlement takes the maximum value adjacent to the wall but decreases with increasing the distance behind the vertical cut. The magnitude of the settlement corresponds to

that of the horizontal displacement profile. The larger the horizontal displacement is, the larger is the settlement.

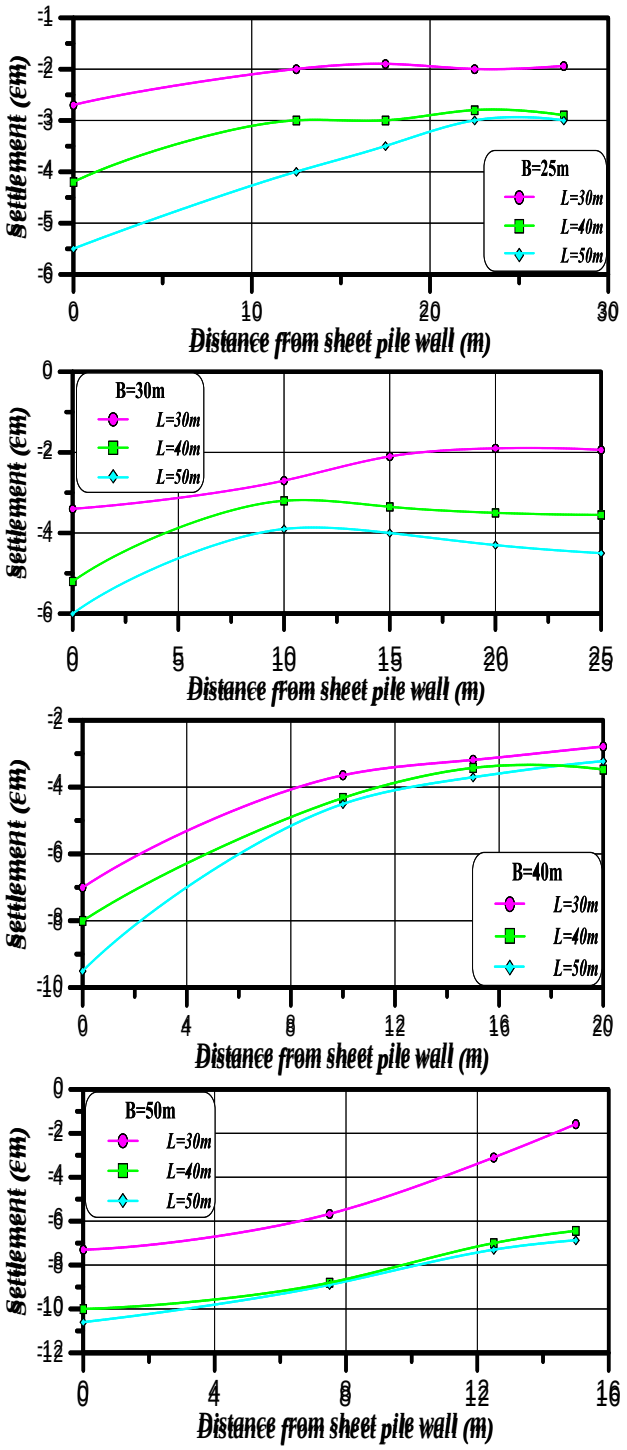

Figure (4) Ground surface settlement profile at different lengths of primary and complementary walls

Table (3) shows the ratio $\delta_{v\ max}$ / $\delta_{h\ max}$ at the center of excavations (L/2) with different excavation sizes. It is clear that the ratio ranges between 0.2 to 0.55, and according to [4], there is a wide variation in the ratio between the maximum vertical settlement δ_v max and the maximum horizontal displacement $\delta_{h\ max}$. The ratio $\delta_{v\ max}$ / $\delta_{h\ max}$ varies widely between 0.25 and 4.0.

Table (3) The ratio of δv max / δh max for variable excavation size for H=12m

(δ_v/δ_h) max	B=25			B=30		
	L=50	L=40	L=30	L=50	L=40	L=30
	0.3	0.264	0.2	0.32	0.3	0.233
(δv/δh) max	B=40			B=50		
	L=50	L=40	L=30	L=50	L=40	L=40
	0.46	0.48	0.45	0.5	0.55	0.45

Figure (5) shows the maximum ground settlement adjacent to the excavation for different excavation depths. From the results, δ_v max/H ratio is obtained to be in the range of 0.2 to 0.9 % with an average value of 0.5%. [3] showed that an average δ_v max/H value is about 0.15% during estimating the distribution of settlement adjacent to an excavation in soft to medium clays, while [4] summarized the performance of excavation in soft to stiff clays for the 1990-1998 time period and showed that the average value of δ_v max/H is about 0.4%.

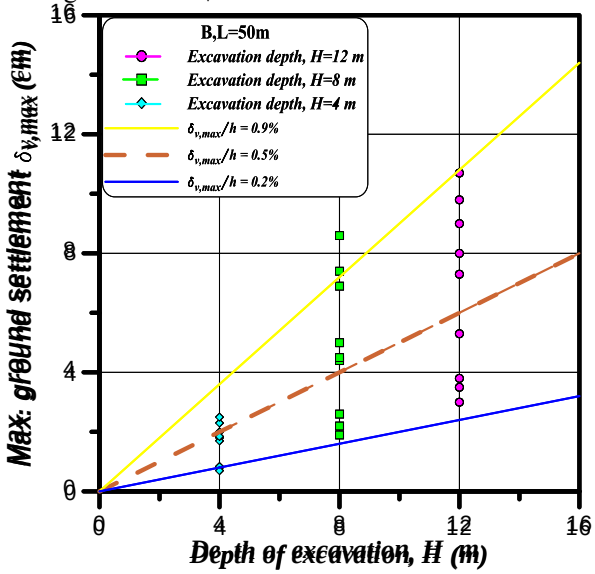

Figure (5) Maximum ground settlement with depth of excavation

2.Effect of Embedded Wall Length

Wall length is one of the geometric factors that affecting the behavior of a supported excavation. In this section, the effect of the embedded wall length D will be considered.

Excavations with an area (50×50m) supported with a varying length of sheet pile wall (D=16, 20, and 24m) are studied. Figure (6) shows the wall displacement against various depths of excavation (i.e, H=4, 8 and 12 m). It can be indicated that for a shallow excavation depth H=4m, the wall displacement shapes for all wall lengths are very similar, so the increase of the penetration depth will have a minimum influence on the performance of the shallow excavation.

In general, the results show that for shallow excavation depth ($\frac{H}{D} < 0.4$), insignificance influence of the length of wall on the values of displacement has been indicated, while for deeper excavations ($\frac{H}{D} \geq 0.4$), the influence of the length of sheet pile wall is appeared, clearly that as the penetration depth decreased the wall displacement increased, and the influence extended downward below the excavation level for ($\frac{H}{D} > 0.5$) as showed in figures below.

The horizontal deflection increases as the excavation size increases and the length of wall decreases, and it has been noticed that the rate of increasing will be lower if the ratio of length of wall to depth of excavation is higher than 1.6, being insignificant in case of the lowest complementary wall length (B=25 m).

The influence of the penetration depth on the ground surface settlement is shown in Figure (7). It can be seen that the ground settlement decreases with increasing penetration depth, that ground movement decreases significantly near the wall as the penetration depth increases, and that ground movement tends to decrease at a distance far from the wall as the penetration depth increases.

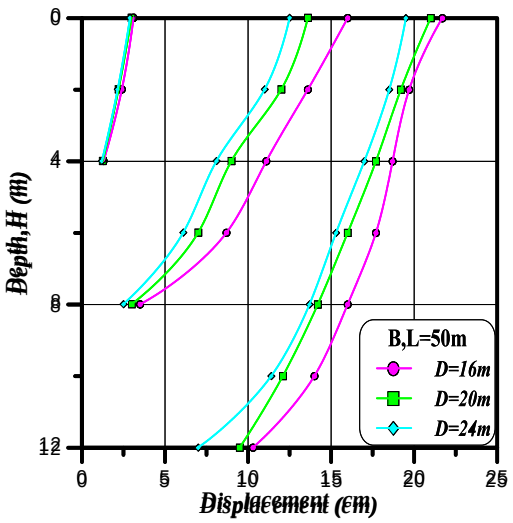

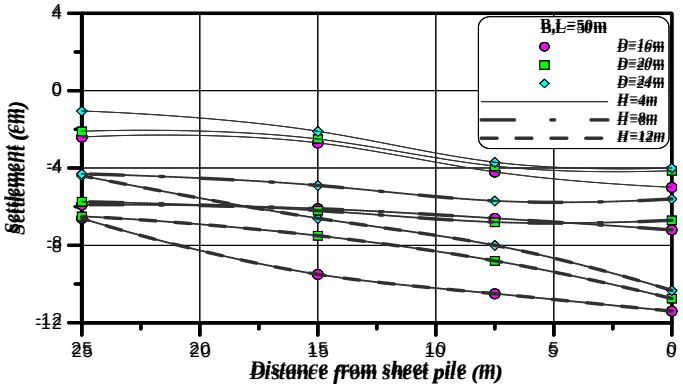

Figure (6) Displacement and ground settlement profiles with various length of sheet pile wall.

3.Effect of the Depth of Bearing Stratum

The depth of bearing stratum (C) is an important component of the excavation geometry. In practice, however, the clay layer is usually less than 100 m deep [10].

The wall deflection profiles for the excavations predicted by the program with two depths of the clay stratum (C = 40 m and 50 m) are compared in Figure (7). The depth of the firm stratum would only affect the wall displacement below the excavated level, hence the largest effects can be seen at the toe of the wall, particularly at a depth of excavation to the length of wall ratio ($\frac{H}{D} = 0.6$). The increase in incremental wall displacement decreases in a smaller excavation depth being insignificant for ($\frac{H}{D} = 0.2$).

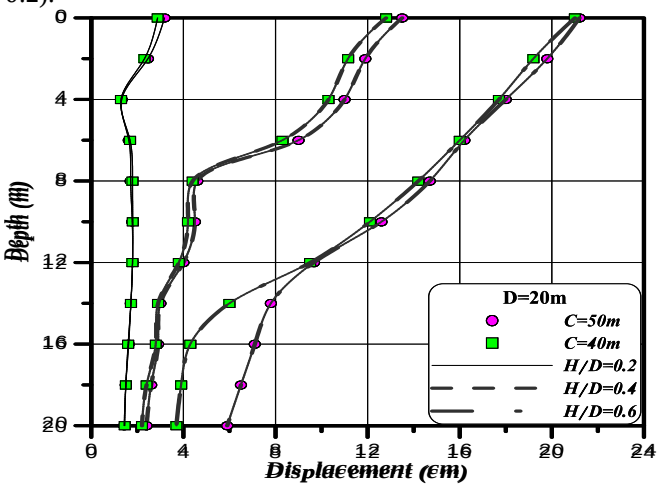

Figure (7) Wall displacement profile for excavation with different depths of firm stratum

4.Effect of Parameters of Bounding Surface Model

Due to the complexity of determining the parameters to be employed in the bounding surface model, it has been decided to adopt three soil conditions given in

[7], where the bounding surface parameters were already determined and are presently tabulated in Table (4).

Also, the bounding surface parameters for the cohesive soil of university of Technology site obtained by [2], will be used together with the bounding surface parameters for Al-Jadiriyah soil estimated in this study and as given in Table (4).

The results are related to excavation size of 50 m length, 50 m width and 12 m depth with a sheet pile wall of length 20 m. Figure (8) show the results for the wall displacement and ground settlement for all soil types at the end of excavation, respectively.

It can be observed that λ and κ are the most effective parameters on the values of displacements than others. Higher values for λ and κ will cause higher wall displacement for all types of soil except for Technology site soil, where the effect of the Poisson's ratio ν is found to be more pronounced.

Also, ground surface movements are the highest near the wall for Grenoble clay that has the highest values of λ and κ and lower value of ν. Higher displacements may be due to the fact that the excavation is completed over a considerably long period of time.

Table (4) Bounding surface parameters for the five cohesive soils

Soil type	Al-Jadiriyah Soil	Technology Soil	Kaolin Soil	Marine Soil	Grenoble Soil
λ	0.06	0.064	0.14	0.178	0.2
κ	0.015	0.017	0.05	0.052	0.1
ν	0.34	0.4	0.2	0.2	0.15
M_c	1.26	1.2	1.05	1.07	0.78
M_e	0.85	0.676	0.85	0.79	0.8
R_c	2.65	2.7	2.65	2.2	2.5
R_e	*	2.3	2.25	*	2
A_c	0.02	0.05	0.02	0.1	0.02
A_e	*	0.04	*	*	0.02
C	0	0	0.7	0.4	0.5
h_c	2	2	4	10	4.3
h_e	1.5	1	5.6	10	4.3

*Material response in extension was not simulated

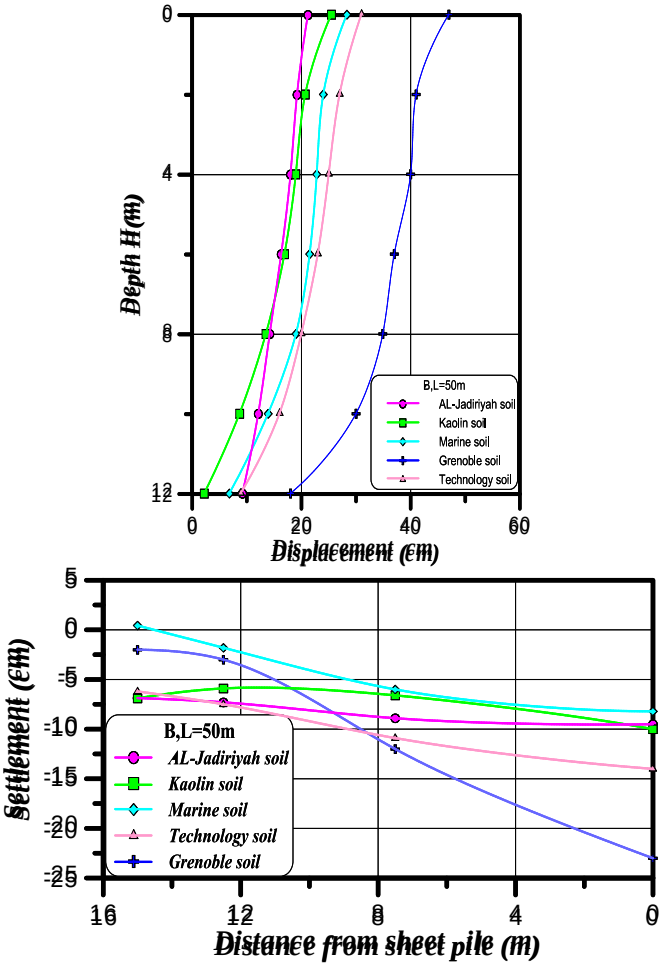

Figure (8) Wall displacement and ground settlement for all soil types at the end of excavation

The ratio of the maximum lateral wall displacement to the maximum ratio of surface settlement behind the wall for the five cohesive soils is shown in Figure (9). it has been shown that the ranges for the ratio is between 0.2 to 0.6, and this finding minimizes the range obtained by [11] which analyzed the field data from the excavations in soft clay and gave a range from 0.5 to 1.0 and also limited the range given by [4] which showed that this ratio varies widely between 0.25 and 4.0.

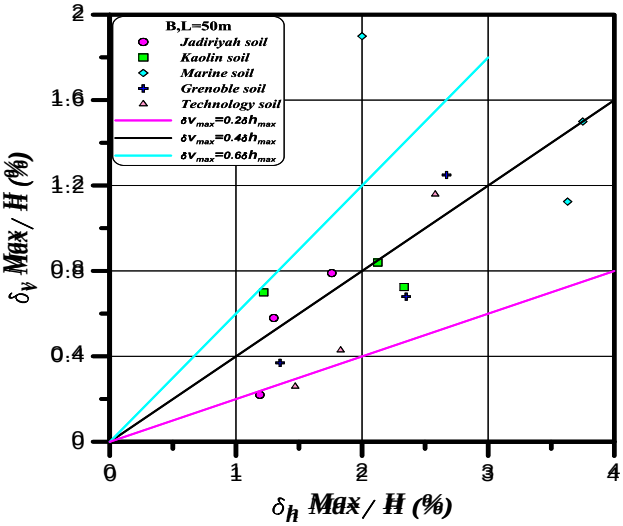

Figure. (9) Relationship between maximum ground settlement and maximum lateral wall displacement

IV. CONCLUSIONS

From the results the following conclusions can be drawn:

1. Wall displacements and ground surface movements for a deep supported excavation in saturated medium may be predicted using the finite element program **MOD-3D-EXCON**, and the elasto-plastic bounding surface model may provide a realistic stress distribution within the soil mass around the supported excavation.
2. Movements of the nodes along the corner edge of the excavation are insignificant compared with those along the vertical outline edge in the middle of excavation edge; the wall displacement is more prominent behind the outer edges and less pronounced behind the corner edge of the excavation.
3. Deformation behavior of a "short" primary wall can be heavily affected by the corners. And, the behavior of the center section for the longer complementary walls is still affected by the existence of the corner, the ratio of corner to center movements perpendicular to the wall (δ_{corner} /$\delta_{center)}$ is less than 1.0, indicating that the displacement decreases near the corners of the excavation due to the stiffening effects of the corners.
4. The ratio of the maximum horizontal displacement to the depth of excavation ($\delta_{h\ max}$/H) is ranged between 1 to 2 %. And, the ratio of the maximum ground settlement to the depth of excavation ($\delta_{v\ max}$/H) is obtained to be in the range of 0.2 to 0.9 % with an average value of 0.5%.
5. The results showed that the ground settlement profiles can be viewed as nearly parabolic curves joined by tangent lines or inflection points that can be divided into two categories: concave downward (hogging) and concave upward (sagging) with a maximum value usually takes place directly behind the wall being smaller than the horizontal displacement. The ratio $\delta_{v\ max}$ / $\delta_{h\ max}$ at the center of excavation (L/2) with different excavation sizes ranges between 0.2 to 0.55.
6. Insignificance influence of length of the wall on the values of displacement has been indicated for a shallow excavation depth ($\frac{H}{D} < 0.4$), while for deeper excavations ($\frac{H}{D} \geq 0.4$), the influence of the length of sheet pile wall is appeared clearly that as the penetration depth decreased, the wall displacement increased, and the influence extended downward below the excavation level for ($\frac{H}{D} > 0.5$).
7. The depth of the firm stratum would only affect the wall displacement below the excavated level, hence the largest effects can be seen at the toe of the wall particularly at a depth of excavation to the length of wall ratio ($\frac{H}{D} = 0.6$). The increase in incremental wall displacement decreases in smaller excavation depth being insignificant for ($\frac{H}{D} = 0.2$).
8. It can be observed that λ and κ are the most effective parameters on the values of displacements than others. Higher values for λ and κ will cause higher wall displacement for all types of soil except for Technology site soil, where the effect of the Poisson's ratio is found to be more pronounced.

NOTATIONS

κ	Slope of the swelling line
h_c, h_e	Slope-hardening factor in compression and extension, respectively.
A	shape parameter controls the shape of the hyperbola portion.
C	Cohesion
m	Hardening parameter of the bounding surface model
M	Slope of the critical state line (denoted by Mc and Me in the compression and extension, respectively)
R	A shape parameter determining the ratio of two major axes of ellipse 1 (it is denoted by Rc and Re in compression and extension, respectively)
T	A shape parameter controlling the size of ellipse 2
λ	Slope of the consolidation line
υ	Poisson's ratio for soil

REFERENCES

1. Abdulnaby, T.Y., Ghazi, Z., Abdullah, L.N., (2011) "Soil Investigation Report for Ansaam Al-Jadiriyah Restauran", National Center for Construction Laboratories and Research (NCCLR), No. 1/1/70/2011 – Baghdad.
2. Al-Busoda, B.S., (2004), "Static and Dynamic Non-Linear Soil Behaviour by the Bounding Surface Plasticity Model for an Iraqi Soil", Ph.D. Thesis, College of Engineering, University of Baghdad.
3. Clough, G.W., O'Rourke, T.D., (1990), "Construction Induced Movements of In-Situ Walls. Design And Performance of Earth Retaining Structures", Geotechnical special publication, ASCE, New York, pp. 439-470.
4. Duncan, J.M., Bentler, D.J., (1998), "Evolution of Deep Excavation Technology", International Conference on Soil-Structure Interaction in Urban Civil Engineering, Darmstadt, pp. 139-150.
5. Finno, R.J., and Blackburn, J.T.,(2007), "Three-Dimensional Responses Observed in an Internally Braced Excavation in Soft Clay", Journal of Geotechnical and Geoenvironmental Engineering, Vol.133,No.11,pp.1364–1373.
6. Hans, K., and Berhane, G., (2006), "Excavations and Foundations in Soft Soils", University of Kassel., Springer-verlag New York, LLC.
7. Kaliakin, V. N., and Dafalias, Y. F., (1991), "Details Regarding the Elastoplastic-Vescoplastic Bounding Surface Model for Isotropic Cohesive Soils", Civil Engineering Report No.91-1, University of Delaware, New York.
8. Kung, G. T. (2009), "Comparison of Excavation-Induced Wall Deflection Using Top-Down and Bottom-Up Construction Methods in Taipei Silty Clay" Computers and Geotechnics, Vol. 36, No. 3, pp. 373-385.
9. Kung, G.T.C., Juang, C.H., Hsiao, E.C.L., and Hashash, Y.M.A., (2007), "Simplified Model for Wall Deflection and Ground Surface Settlement Caused by Braced Excavation in Clays" Geotechnical and Geoenvironmental Engineering, Vol. 133, No. 6, pp. 731-747. IVSL.
10. Lam, S.S.Y., (2010), "Ground Movements Due to Excavation in Clay: Physical and Analytical Models",Ph.D. Thesis,University of Cambridge.
11. Mana, A. I., and Clough, G. W., (1981), "Prediction of movements for braced cuts in clay", Journal of Geotechnical Engineering, Vol. 107, No. 6, pp. 759–777.
12. Ng, C.W. and Yan, W.M., (2000), "A True Three-Dimensional Numerical Analysis of Diaphragm Walling", Geotechnical , Vol. 49, No. 6, pp. 825-834.
13. Stallebrass, S. E., and Taylor, R. N., (1997), "The Development and Evaluation of A Constitutive Model for the Prediction of ground Movements in Overconsolidation Clay" Geotechnical , Vol. 47, No. 2, pp.235–253.

Equivalent Pressure to Resist Swelling of Subgrade Soil under Flexible Pavement

Dr. Mahmood Rashid Mahmood Al-Qayssi

Abstract - **To prevent swelling pressure of subgrad soil under flexible road pavement, one of the following methods may be used (Replacement, Compaction, Pre wetting, Chemical Stabilization, Geosynthetics, and Moisture Barriers). Pavement thickness not taken into consideration to resist and prevent swelling pressure, this research focusing to the applied pressure due to increasing in pavement thickness to resist swelling pressure of sub grade soil. To conduct laboratory tests, two different tools were used (Oedometer cell and CBR mold) to predict directly swelling percent and swelling pressure of sub grade soil under flexible road pavement at different water contents. California bearing ratio tests (CBR test) were also used to determine the bearing ratio of soaked sub grade soil. Flexible pavement was designed by using C.B.R method as per IRC: 37-2001 to determine pavement thickness which used to prevent swelling pressure predicted from sub grade soil. The result shows that, using Oedometer test to predict swelling pressure more realized than that predicted from C.B.R molds and shows a marginal increase in pavement thickness can be used to prevent swelling pressure for highly swelling subgrade soils.**

Keywords: Expansive soil, swelling pressure, flexible pavement, Oedometer cell, CBR mold and subgrade soil.

. INTRODUCTION

During the last few years, with the rapid growth of traffic the pavement are required to be designed for heavy volume of traffic and to resist all the problems appear during it's useful life in an economic ways. The fast rate of construction with the lack knowledge in geotechnical engineering of the existing soils caused a structural defect that significantly affected the performance of flexible road pavements.

El-Baiati (2001) reported that one of the major causes of these defects is attributed to differential soil swell, and the contribution of moisture change that may occur in cycles of wetting and drying which lead to cycles of swelling and shrinkage of the soil.

Kumar and Prasada Raju (2009), show the stabilization process with model test of a heavy vehicle over expansive subgrade in flexible pavements. Cyclic plate load tests are carried out on the tracks with chemicals like lime and cement introduced in the fly ash subbase laid on sand and expansive subgrades.

Prasad et al. (2010), shows an evaluation studies on flexible pavements conducted by different reinforcement material in a subbase layer such as waste plastics and waste tire rubber reinforced stretch in the flexible pavement system laid on swelling sub grade soil and geogrid reinforced stretch followed by bitumen coated bamboo mesh, bitumen coated chicken mesh.

Catherine M.C. (2010), shows the best practice treatment of expansive subgrade soil and recommended to treat an expansive subgrade requires control of the variables that cause undesirable behavior, both short and long term.

Ali M.S. and Shubhada S.K. (2011), presents the results of an experimental program undertaken to investigate the effect of stone dust and fly ash combine at different percentage on expansive soil. The results observed that at optimum percentages, i.e., 20 to 30% of admixture, it is found that the swelling of expansive clay is almost controlled and also noticed that there is a marked improvement in the other properties of soil.

Harishkumar.K and K Muthukkumaran (2011), propose an alternative method to control the swelling behavior of expansive soil. The swelling properties were determined based on the swelling pressure and free swell index tests. Geotextile were used to stabilize the expansive soil.

Lakshmi K, and Mangaiarkarasi.V (2012), they studied the effect of fly ash on an expansive soil for flexible pavement design and to reduce the quantity of lime in lime fly ash by the effective use of fly ash it self.

Tank R. R. & Solanki U.J. (2012), studied the geotechnical properties of the swelling soil and the effect of stabilizers i.e by adding fly ash, lime and combination of both on the properties of expansive soil especially C.B.R behavior. They found that for economic of view the best option of stabilization is that the fly ash plus lime, combination of two stabilizers are the best option for the expansive subgrade soil stabilization with optimum lime.

Khushbu S. Gandhi (2013), show an experimental study in the stabilization of swelling soil in Surat, consisting of different geotechnical properties and mechanical capacities by the addition of by products and west materials of industrial origin such as marble dust and rise husk ash. This may achieve the double effect of reducing the sweeling of this type of soil.

Experimental Work

Physical and Chemical Properties of the Soil Used:

Brown to red of silty clayey soil brought from the earth dam around Baghdad city was used to carry out all the laboratory tests. The soil dried and crashed then sieved on sieve no.4, to conduct the laboratory tests. Standard tests according to ASTM specifications were carried out to determine physical and chemical soil properties.

Figure (1) shows particle size distribution of the soil sample used. Table (1), show results of physical and chemical soil properties which used as a subgrade material.

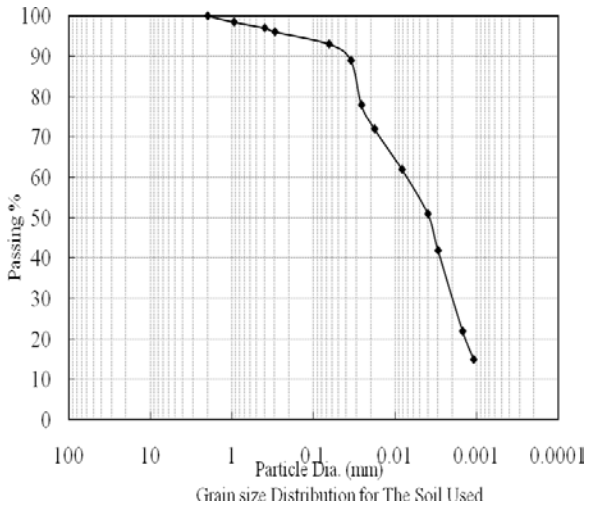

Fig.1. Grain Size Distribution of the Soil Used

Table (1): Values of Physical and Chemical Properties of the soil used According to Standard specifications.

The Property	Specific. No.	The value
Specific gravity	ASTM D_{854}	2.71
Gravel Cont.%	ASTM D_{422}	0.0
Sand Cont. %	ASTM D_{422}	7.0
Silt Cont.%	ASTM D_{422}	37.0
Clay Cont. %	ASTM D_{422}	56.0
Liqid Limit %	ASTM D_{4318}	55
Plastic Limit %	ASTM D_{4318}	33
Linear Shrinkage	ASTM D_{4318}	14
Plastic Index %		22
Tss %	BS(1377)	0.80
So_3 Cont. %	BS(1377)	0.35
Organic Matter %		0.38
PH value		7.75
Gypsum Cont. %	BS(1377)	0.57
CaCo3 Cont. %	BS(1377)	28.9
Soil Symbols (U.S.C.S)	ASTM $D_{2487-00}$	CH
AASHTO Classification	AASHTO M_{145-82}	A-7-5(25)

X - Ray Diffraction

X-ray diffraction is a technique that provides detailed information about the atomic structure of crystalline substances. It is a power full tool in the identification of minerals in soils.

Table (2) shows the composition of the soil sample minerals.

Table (2): Composition of The Soil Minerals

Soil Mineral	%
Montmorillonite + Chlorite	19
Plagoskite + Illite	16
Kaolinite	13
Feldspar	5
Quartz	17
Carbonate	30

X-ray diffraction shows that the main components of the soil sample minerals is Montmorilonite plus Chlorite with Palgoskite , Illite and Kaolinaite .While Quartz, Carbonate, Feldspar which are non-clay minerals.

Compaction Test

The moisture content and dry density relations for both standard and modified compaction tests were conducted according to (ASTM $D_{1557-02}$) for modified compaction test, and according to (ASTM D_{698-02}) for standard compaction test. Fig. 2 shows compaction specifications of the soil used.

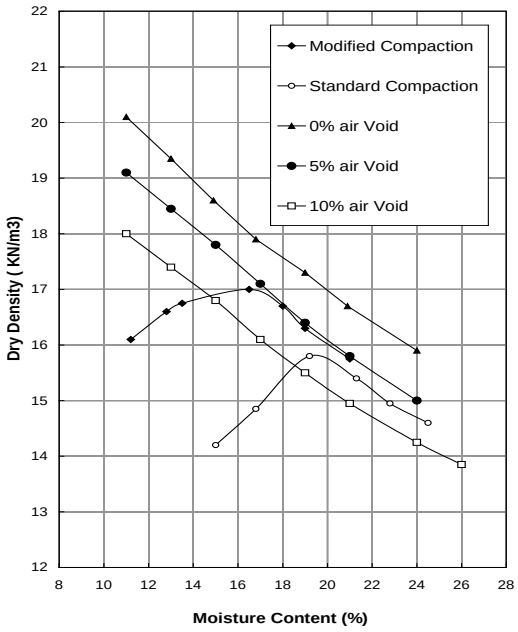

Fig(2) : Compaction Specifications of The Soil Used

Consolidation Tests:

Consolidation tests were conducted by using oedometer cell according to ASTM D_{2435} on remolded soil samples compacted in proctor mold, according to ASTM-$D_{1557-02}$ at optimum water content of 15.5%. The engineering soil properties of consolidation test for remolded soil samples are shown in table (3).

Table (3): Engineering Soil Properties of Consolidation test the for Remolded Soil sample.

Soil Property	The Value
Initial void ratio (e_o)	0.80
Compression Index (Cc)	0.14
Rebound Index (Sr)	0.02
Coeff. of Consolidation (C_v) (m^2/year)	0.75
Coefficient of Compressibility (m^2/kN)	$1.6 * 10^{-4}$
Coeff. of Permeability (k) (cm/min.)	$3.0*10^{-7}$
Initial molding moisture content % (m_i)	15.5
Saturated molding Unit weight (γ_{sat}) (gm/cm^3)	19.8
Dry molding Unit Weight (γ_{dry}) (gm/cm^3)	17.1

Swelling Tests:

-By Oedometer Cell

Swelling percent and swelling pressure were determined by using Oedometer cell. The tested soil samples were prepared by Modified Proctor compaction test. These samples compacted at different molding water contents (13, 14, 15, 16, 17, 18 and 19%) to predict swelling percent and swelling pressure. The soil samples soaked immediately at a seating pressure of (7kPa) and allow for free swelling until equilibrium condition is achieved. Then the samples were loaded by stress increments to back the swelling soil sample to its initial condition.

-By C.B.R Mold

C.B.R molds were also used to determine swelling pressure and swelling percent. The soil samples were compacted in C.B.R mold according to ASTM $D_{1883.87}$.

Different applied loads of (10, 20, 40 & 60 Ibs) were used to simulate the applied stresses used in consolidation test. The soil samples were compacted in C.B.R mold at the same different water contents that used at the consolidation test also. Swelling percent and swelling pressure were measured at each value of water content.

RESULTS AND DISCUSSION

Swelling Percent:

-By Using Oedometer Tests

Values of swelling percent by using odeometer cell under different applied surcharge loads and different water contents are shown in figure (3). It shows that at each increment of surcharge load, swelling percent decrease as water content increase.

-By CBR Mold

Values of swelling percent by using CBR molds under different applied surcharge loads and different water contents are shown in figure (4). It shows also, that for each increment of surcharge load, swelling percent decrease as water content increase.

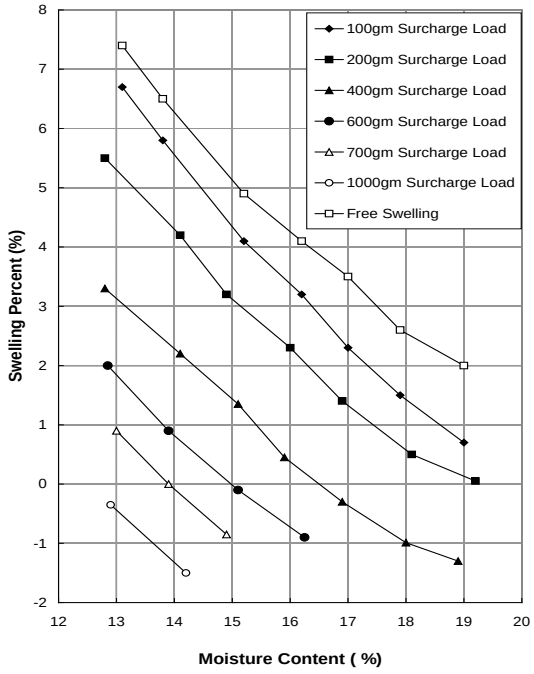

Fig (3): Swelling percent under different applied surcharge loads and different water Content by using oedometer Cell.

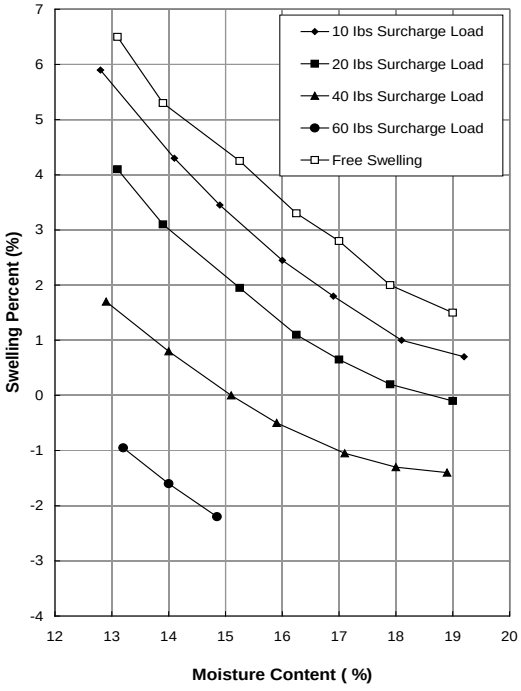

Fig (4): Swelling percent under different surcharge loads and different water content by using CBR molds.

Swelling Pressure:

Al-Asshou (1978) shows that the swelling pressure obtained from free swell procedure are approximately coincides with field. He also shows that the procedure used to determine free swell is usually used to obtain the swelling properties of subgrade soils because the applied stresses are very limited.

-By Oedometer Cell:

Figure (5) shows that swelling pressure under applied different stresses for different water contents.

Swelling pressure is obtained from the intersection of the swelling percent curve under applied pressure with zero swelling percent. Swelling pressure at different moisture content were determined and tabulated in table (4). Higher swelling pressure is occurred at lower water content and vies versa. Such behavior is in full agreements with the results obtained by Rasheed, K.A 1986. These values are used to design flexible pavement.

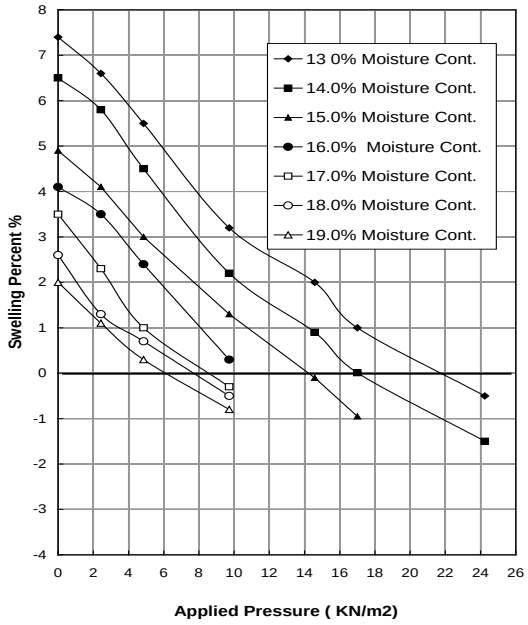

Fig. (5): Swelling pressure at different water contents
Obtained from oedometer cell

Table (4): Values of swelling pressure at different water content determined from oedometer cell.

Water Content (%)	Swelling Pressure kPa
13	22.0
14	17.0
15	14.2
16	10.0
17	8.5
18	7.8
19	6.2

- By C.B.R Mould

Figure (6) shows that swelling pressure under applied different stresses for different water contents.

The figure shows a significant reduction in swelling pressure with increasing water content under increment applied stress. The values of swelling pressure obtained from soil samples in C.B.R molds are tabulated in table (5).

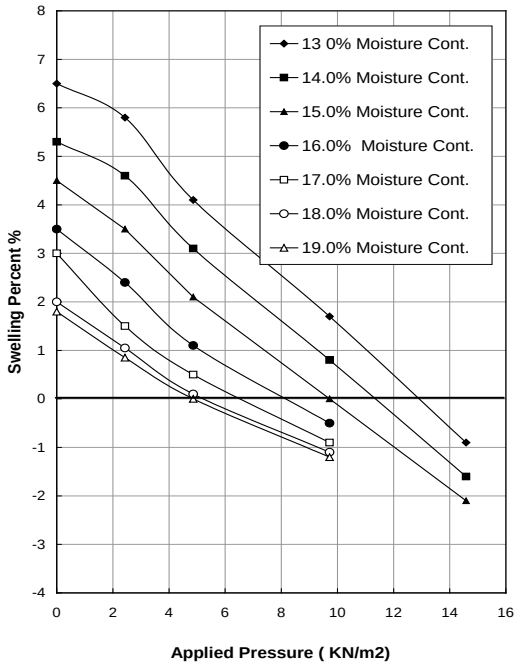

Fig. (6) Swelling pressure at different water contents Obtained from C.BR. mold.

Table (5): Swelling pressure values determined from CBR mould

Water Content (%)	Swelling Pressure kPa
13	13.0
14	11.5
15	9.7
16	8.2
17	6.8
18	5.1
19	4.8

BEARING TESTS

C.B.R tests were conducted to predict C.B.R values for the soil sample at different water contents.

Table (6) shows the values of C.B.R test using different applied loads with different water content. The effect of increasing moisture content on CBR values are shown in figure (7).

Table (6): Values of C.B.R test under differen surcharge loads

Water Cont. %	C.B.R Values (%) Surcharge Loads (Ibs)			
	10	20	40	
13	2.1	4.9	8.2	
14	2.3	5.2	9.1	
15	5.2	7.8	11.1	
16	8.0	9.9	Ng	
17	9.8	11.2	14.0	
18	7.8	9.1	12.5	
19	5.7	7.0	9.8	

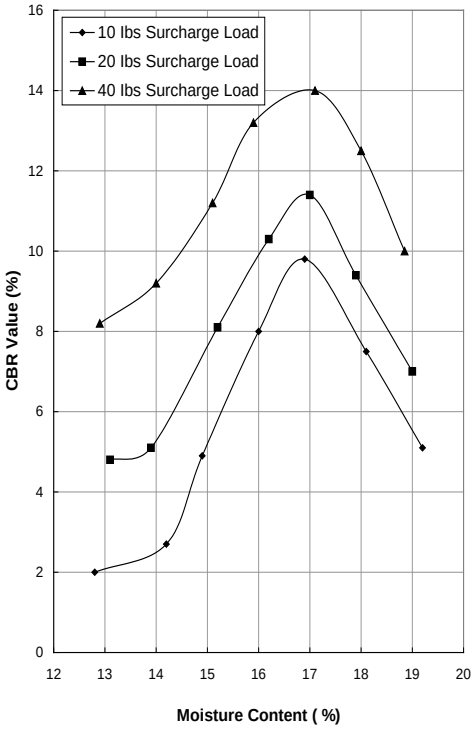

Fig.(7): Values of C.B.R with increasing water content under all the surcharge

The figure declared that the values of C.B.R at the dry side of compaction curve increase with increasing water content under all surcharge loads.

While it decreased with increasing water content at the wet side of compaction curve. The percent of 17% water content represent the optimum moisture content for maximum C.B.R values after which C.B.R values decreased with increasing moisture content.

FLEXIBLE PAVEMENT DESIGN

There are many methods used to design flexible pavement such as Group index method, C.B.R method, Triaxial method and California resistance value method. Saurabh Jain et al, (2013), show that the C.B.R method as per IRC;37-2001,is more convent and widely used in fields due to its relevant simplicity and the appropriate value of different component layers. Also it's suggested the minimum thickness of the pavement composition layers of sub base, base course and surfacing.

By adopting C.B.R method according to the Indian road congress IRC: 37-2001: "Code of guidelines for design of flexible pavements", which based on the concept of cumulative number of standard axle load .

The recommended method considers traffic in terms cumulative number of standard axles (18000Ib) 8160kg to be carried by the pavement during the design life in terms of million standard axles (msa). For estimating design traffic, the following information is needed:

(i) Initial traffic after construction (A) in term no. of commercial vehicle (cv/day), which assume as 4500 cv/day.

(ii) Traffic growth rate during the design life (r) If no data use 0.75%.

(iii) Design life in number of years (n), for flexible pavements it's assumes as 15 years.

(iv) Vehicle damage factor (F), based on axle load survey For no data use as 4.5.

(v) Distribution of commercial traffic over the carriageway (D), For two lane single carriage way use (0.75).

The cumulative number of standard axle (N) can be computed using the following equation:

$$N= 365 [(1+r)^n -1] \times A \times D \times F / r \quad \text{---- IRC: 37-2001}$$

By substituting the information values in the above question the cumulative number of standard axle (N) is about 150 msa.

The total pavement thicknesses for different design values of C.B.R. under surcharge load of 10Ib are shown in table (7).

Table (7): Total pavement thickness for different C.B.R values

Water Cont. (%)	C.B.R Values (%)	Total pavement thickness (mm)
13	2.1	967.0
14	2.3	950.0
15	5.2	760.0
16	8.0	660.0
17	9.8	651.0
18	7.8	667.0

19	5.7	735.0

El-Baiati (2001), declared that to eliminate or reduce the effect of swelling pressure on structures, loading the soil by enough resisting pressure.

So, to determine flexible pavement thickness, which resists swelling pressure, assume that the applied stress equate the swelling pressure.

Let, γ_1= unit weight of subbase material which is about (21.5kN/m^3), and h_1= thickness of the subbase layer (m).

Let, γ_2= unit weight of bituminous surfacing layer which is about (23.0kN/m^3), and h_2= thickness of this layer (m).

If the total thickness of the bituminous surfacing layers assumed as 200mm (Wearing course and Binder course), then thickness of the subbase layer (h_1) can be determine. The applied stresses of these layers can be used to resist the swelling pressure of subgrade soil.

For example the swelling pressure by oedometer test at water content of 13% is (22.0 kPa (table 4.0)), the thickness of subbase layer (h_1) will be 809mm and the total pavement thickness is to be 1009.0mm.

Table (8) shows values of total pavement thickness needed to resist swelling pressure predicted by C.B.R mold and oedometer cell.

Table (8): Pavement thickness determine to resist Swelling Pressure predicted by C.B.R mold and oedometer cell

Water Cont. (%)	Pavement Thickness (mm) equivalent to swelling pressure	
	From C.B.R test	From Odeometer Cell
13	590.6	1009.0
14	520.9	776.7
15	437.2	646.5
16	367.4	451.1
17	302.3	381.3
18	223.2	348.8
19	209.3	274.4

The table show that the values of total pavement thickness decreased with decreasing swelling pressure, and also shows that there is no large difference with the pavement thicknesses obtained from C.B.R method according to the Indian road congress IRC: 37-2001. It seems that for highly swelling pressure at moisture content of 13%, the designed pavement thickness is approximately equal to the pavement thickness determined to resist swelling pressure, and the other designed thicknesses more than that determined to resist swelling pressure at the other different moisture content.

CONCLUSIONS

1- At any surcharge load swelling percent and swelling pressure decreased as moisture content increase.

2- Swelling percent and swelling pressure predicted by Oedometer cell higher than that predicted by CBR molds at the same moisture content and the same applied pressure.

3- C.B.R values increases up to a certain limit of moisture content and then decreased. This limit is the optimum limit of moisture content gives maximum C.B.R values.

4- The resisting swelling pressure predicted from Oedometer test more realized than that predicted from C.B.R molds at the same moisture content.

5- The applied stresses due to the pavement thickness determined from swelling pressure can be used to resist swelling pressure of subgrade soil instead of the other methods of treatments in an economic way.

6- If the subgrade soil seems to be expansive, it's recommended to check the applied pressure due pavement thickness before choosing any treatment method.

REFERENCES

[1]. *Al-Ashou, M. O. 1978.* " Expansive Properties of the Clay in Mosil -Iraq. MSc Thesis ,Mosul University

[2] *Ali M.S. and Shubhada S.K. (2011)"* Performance Analysis of Expansive soil Treated With Stone Dust and fly Ash" EJEG vol. 16 (2011) Bund 1 pp.973-982.

[3] *Catherine M.C. 2010* " Effective Road Pavement Design for Expansive Soils in Ipswich" Bachelor of Engineering

[4] *El-Baiati, I.K.A. 2001."* The effect of Kcl on Swelling Potential of Clay " MSc Thesis Al- Nahreen University.

[5]. *Harishkumar.K and K Muthukkumaran (2011)* " Study on Swelling Soil behavior and its improvements" International Journal of earth Sciences and Engineering ISSN 0974-5904, Vol. 04,No. 06 SPL, Oct.2011 ,pp. 19-25.

[6]. *IRC: 37-2001"* Code of guideline for the design of flexible pavement" Indian Road Congress.New Delhi 2001.

[7]. *Khushbu S. Gandhi (2013)*" Stabilization of Expansive soil of Surat Region Using Rice Husk Ash & Marble Dust" International Journal of Current Engineering and Technology Vol.3 , No. 4, Oct.2013.

[8] . *Kumar and Prasada Raju (2009)*"Use of Lime Cement Stabilized Pavement Construction"
Indian Journal of Engineering & Materials Sciences, Vol. 16, Aug. 2009, pp. 269-276.

[9] *Lakshmi K, and Mangaiarkarasi.V (2012)*" Effect of Fly Ash on an Expansive Soil for Flexible pavement Design" International Journal of Engineering and Innovative Technology (IJEIT) Vol. 2, Issue3 . Sept. 2012.

[10] *Prasad D.S.V., M.A.Kumar & G.V.R.Raju 2010* :"Behavior of Reinforced Sub base on Expansive Soil Subgrade " Global Jornal of Researches in Engineering Vol.10 Issue 1 April.

[11] *Rashed K. A. 1986. "* Swelling Characteristics of Compacted Soil in Mosul Area " MSc. Thesis Mosul University.

[12] *Saurabh Jain et al, (2013)*" Design of Rigid and Flexible Pavements by Various Methods & Their Cost Analysis of Each Method" Int. Journal of Engineering Research and Applications Vol. 3, Issue 5, Sept-Oct 2013, pp.119-123.

[13] *Tank R. R. & Solanki, U. J. 2012."*Economic Evaluation of Flexible Pavement with Respect to Fly ash and Lime Stabilization of Expansive Sub-Grade Soil in Gujarat" IJDI- ERET Vol. 1 No.1 2012.

Effect of Particle Size Distribution on the Behavior of Single Model Pile Subjected to Static Lateral loads Embedded within Cohesionless Soils

Mahmood R. Mahmood Al-Qayssi,and Ahmmed Abed Al-Husain

Abstract— **The behavior of laterally loaded single pile under applied static lateral loads, studied in the laboratory on small scale model. The purpose of this research is to investigate the effects of grain size distribution of cohesionless soils with different densities on the behavior of single pile subject to static lateral loads. The experimental program consist of nine tests of single model pile of 15mm dia. and 450mm embedment length, within coarse , medium and fine sand, each type with three different densities (dense, medium and loose state). Lateral static load was achieved by special device designed to apply lateral loads at top of pile model in two directions with eccentricity of 5cm above soil surface. Eight strain gages of 5 mm length type FLA-5-23 were fixed on both sides along the model pile with equal distances to investigate the bending moment introduced from lateral loads along the pile model under applied lateral load. Lateral displacement of pile head was measured by a dial gage fixed laterally on both sides on the pile head. The results emphasized that the behavior of single pile was highly affected by the study parameters. It is found that the increasing static load level, produce an increase of pile head displacement and bending moment of the single pile. But these increments varied depending on the grain size distribution and the density state. The results show that the fine sand yielded higher displacement and bending moments than the other types with a lower resistance under the same lateral loads.**

Key Words: Model Pile, Lateral Pressure, Grain size Distribution

Dr. Mahmood R. Mahmood Al-Qayssi
Assist.Prof. Building and Construction Eng. Dept. University of Technology / Baghdad
M.Sc. Ahmmed Abed Al-Husain
Building and Construction Engineering Department, University of Technology/ Baghdad
E-mail : mahmoudal_qaissy@yahoo.com Mobile 00964 7901315445

INTRODUCTION

Piles are usually subjected to axial or lateral loading or a combination of lateral loads, axial loads and moments. Piles subjected to higher lateral loads are called laterally loaded piles. Understanding the behavior of laterally loaded piles is one of the major problems concerned with the soil structure interaction. The laterally loaded piles have a multi uses as a foundations of structures, such as high rise buildings subjected to wind and earthquake loadings and offshore structures (e.g., Platforms) (A1- Mandeel, 2000) [1].

It's clear that the most ideal procedure is to test a full scale pile model under actual lateral loading conditions to study the behavior of laterally-loaded single pile. However, conducting a full scale testing is rather expensive and requires a lot of time and great efforts, especially for single pile (A1-Mandeel, 2000)[1]. While small scale testing gives similar behavior to full scale model to some extent. Therefore, small scale testing model in the laboratory is still applicable and reliable within certain limit, by applying a similar field conditions as close as possible to those in the full scale testing model. In this research, tests were conducted on a small-scale single pile model embedded within different particles sizes and densities of cohesionless soils in the laboratory, which will reflect the behavior of full scale single pile.

There are several investigators who had studied the influence of the various parameters affecting the behavior of laterally loaded piles. **Matlock and Reese (1960),**[7] were one of the first studied the lateral load behavior of piles and presented solutions for lateral deflections following the approach of modulus of subgrade reaction. **Broms (1964),**[8] presented methods for the calculation of the lateral deflections at working loads, and the ultimate lateral resistance of laterally loaded piles driven into cohesive saturated soils. The lateral deflections at working loads were calculated utilizing the concept of a coefficient of subgrade reaction. Methods for the evaluation of the coefficient of subgrade reaction were considered and the results were presented in the form of graphs and tables. **Alizadeh and Davisson (1970)**,[9] carried

out a series of tests on piles of different sizes and cross sections in the Arkansas River project. They reported findings similar to those of Alizadeh's (1969) test, except that the lateral load test was carried out on different sized piles. **Reese et al. (1974)**,[21] performed tests on a fully instrumented pipe pile embedded in a submerged, heavily over consolidated clay deposit. The purpose of the tests was to develop criteria which could be used to predict the behavior of piles under short-term static and cyclic loading. **Richter et al. (1984)**,[12] developed an analytical solution for a laterally loaded pile based on the case of a rigid in homogeneous elastic half space. The results of photo elastic test cases modeling these conditions for both slip and no slip interface indicated that a significant portion (perhaps 40%) of the lateral load is transferred to the surrounding medium by horizontal normal shear stresses along the sides of the pile when there is adhesion. **Sumer et al. (1992)**,[14] obtained an expression for scour due to waves based on Kuelegan-Carpenter number (KC number) and estimated the lateral capacity of piles. **Gandhi and Selvan (1997)**,[15] studied the behavior of pile groups of different configurations under fixed head condition subjected to lateral load through laboratory experiments on aluminum pipe piles in a cohesionless soil. The effect of pile driving was studied by comparing the behavior of a single driven pile with that of a bored pile. **Ranjan and Jagannath (2001)**,[16]conducted model tests on pile groups of different configurations subjected to lateral loads, in dry Ennore sand. The load-displacement response, ultimate resistance, and group efficiency with spacing and number of piles in a group were investigated. **Briud et al (2005)**,[18] conducted a series of model tests on fine grained soils and developed an equation to predict the scour depth. **Sumer et al (2007)**,[20] conducted a series of experiments on wave scour around a pile in three kinds of soils and established that the scour depth was increased by a factor 16 when the soil bed changed from medium dense silt to dense silt, and the time scale of scour was influenced by density of the soil.

Material Used

Sand

The soil samples used in this research were brought from city of Alzubair at the south of Basra. To obtain the properties of the sand the following tests were carried out.

i. Sieve Analysis to determine the grain size distribution according to ASTM D421-58 & D422-63 as shown in Figure (1).
ii. Relative Dry Density of the sand was determined from maximum and minimum dry densities according to ASTM D4253, D4254, as shown in Table (1) .
iii. Direct Shear Test to determine the shear strength parameters namely: angle of internal friction (φ) and cohesion (C) according to ASTM D 3080-98, as shown in Table (1).

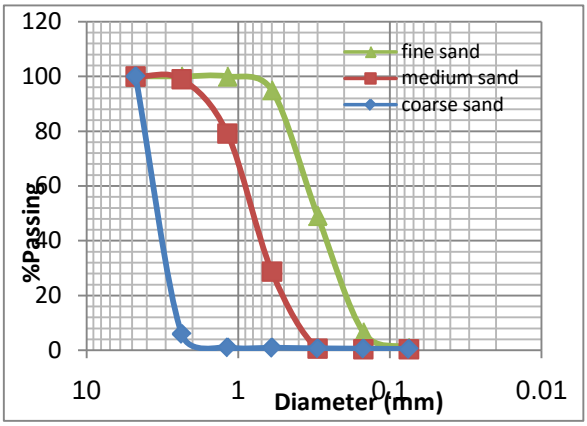

Figure 1: Grain size Distribution of the Sand Used

Table 1: Summary of test results for the sand

Type of Sand / Sand Properties	Fine sand	Medium sand	Coarse sand
Maximum Dry Density (kN/m^3)	17.87	18.70	18.53
Minimum Dry Density (kN/m^3)	13	14.8	13.85
Coefficient of Uniformity (Cu)	2.1	2.14	1.46
Coefficient of Curvature (Cc)	0.89	0.98	0.99
Maximum Dry Density (kN/m^3)	17.87	18.70	18.53

Pile model

Aluminum pipe was using to simulate single model pile. The nominal inside diameter of this pipe is 13 mm with a wall thickness of 1.5 mm and the length 450mm. Tensile tests were carried out on a sample of these model pile according to ASTM A370 to determine the modulus of elasticity (E). The mechanical properties of pile are: modulus of elasticity = 67100(N/mm^2), maximum ultimate yield strength =212(N/mm^2) and minimum yield strength = 186.5(N/mm^2).

EXPERIMENTAL WORK

Container for testing pile model

A cylindrical steel container having 600 mm internal diameter, 600 mm clear height and 5 mm wall and base thickness had been used for conducting the testing program. The container sits on four pulleys at the base of container to able moving on steel angle after filled with sand as shown Plate (1).

Sand raining technique

The apparatus consists of two pulleys fixed at the top of the main frame and a cable of (3mm) diameter that passes around the two pulleys carrying a sand hopper. The cable was pulled by revolving of a fixed pulley to ensure a constant height of fall. The sand hopper contain a hose at its lower base of (50mm) diameter and is provided with a screen of (10 mm) openings at its outlet which used to spread the falling sand during raining in order to obtain the same intensity and to distribute the sand particles uniformly. The sand flow was controlled by a valve at the exit of the hopper. The system can provide a required uniform density of the sand in the model tank through adjusting the height of the drop and intensity discharge of the sand as shown in Figure (2).

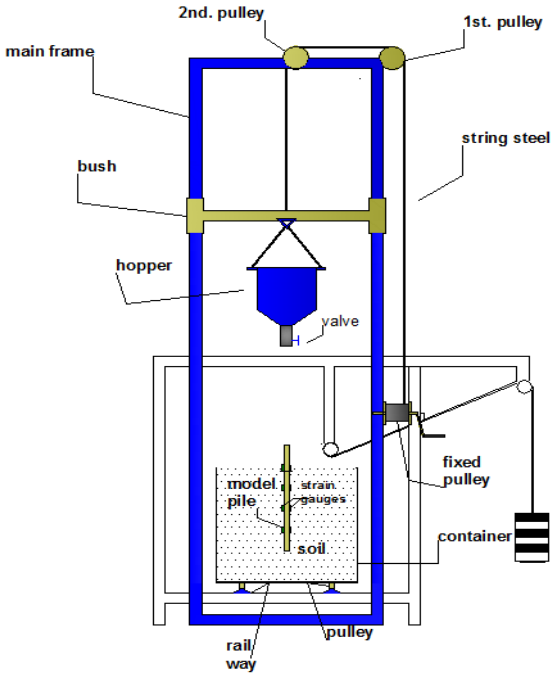

FIGURE 2:SKETCH SHOWN A SAND RAINING

Strain gauges

A model pile is instrumented with strain gauges of 5 mm length type FLA-5-23. In this test quarter bridge circuitry was used of the strain indicator. Which was product by (N.I.C., JAIPUR a sensors & Automation co.). Strain gauge indicator can be used to obtain extremely accurate, high resolution strain measurements in a variety of circumstances. Accuracy of ±1 με (micro strain), Sampling range max. ±19990 με. Type of Quarter Bridge with 120 Ω resistance of strain is used. Eight strain gages were fixed at equal spacing on both sides of pile model to measure compression and tension along the pile length during applied lateral loads as shown in Figure (3).

Static loading device

Static loading was applied through two pulleys with a high tension wire joined to the pile head at the soil surface by loading collar and the other end was attached to the loading disk. The wire passed through first pulley at the level of pile head and passes over the other pulley booth fixed to the main frame, which was freely rolling by ball bearing fixed on its center. After embedded the pile at its position, it was loaded vertically by its allowable capacity, then the lateral load was applied. The pile head displacement at the soil surface was measured using two dial gauges. It was recorded at pre-determined time intervals and strains readings were recorded at each load level as shown in Figure (3).

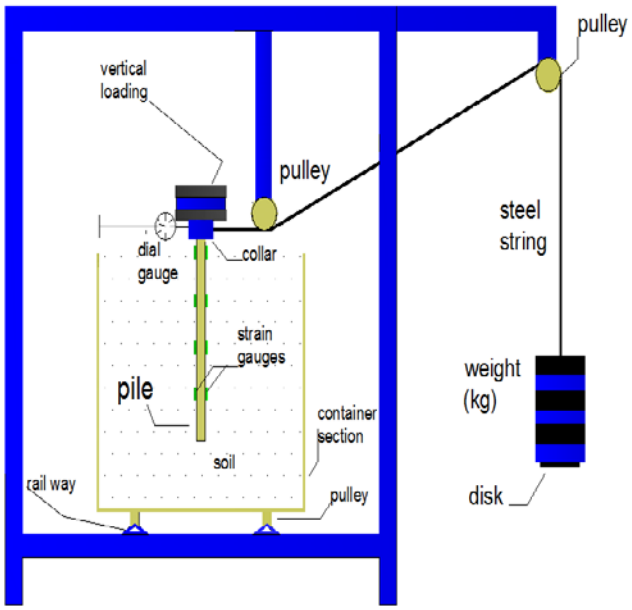

FIGURE 3: SKETCH SHOWN A STATIC LOADING DEVICE

CASES OF LOAD TESTING

Three cases were studied under applied lateral static loading:

Case one: single model pile embedded within loose state sand of different particle size distribution (fine, medium and coarse sand) with applying vertical allowable loading of (10 N) (Allowable pile load capacity).

Case two: single model pile embedded within medium dense sand of different particle size distribution (fine, medium and coarse sand) with applying vertical allowable loading of (20N).

Case three: single model pile embedded within dense state sand of different particle size distribution (fine, medium and coarse sand) with applying vertical allowable loading of (30 N).

The relative densities for each density sate for all the types of sand were the same to investigate the effect of grain size distribution on the behavior of single pile under lateral static load as shown in table (2).

Table (2): Properties of the sand used

Sand / Properties	Fine sand		
	loose	medium	dense
Used Measured Density (kN/m^3)	14.13	15.2	16.25
Used Relative Density (%)	29	53	73.4
Angle of Internal Friction (φ)	29^o	30^o	34^o
Cohesion (C) (kN/m^2)	0.0	0.0	0.0

Sand / Properties	Medium sand		
	loose	medium	dense
Used Measured Density (kN/m^3)	15.76	16.75	17.4
Used Relative Density (%)	29	53.3	73.14
Angle of Internal Friction (ϕ)	32^o	34^o	38^o
Cohesion (C) (kN/m^2)	0.0	0.0	0.0

Sand / Properties	Coarse sand		
	loose	medium	dense
Used Measured Density (kN/m^3)	14.94	16.01	17
Used Relative Density (%)	29	53.4	73.3
Angle of Internal Friction (ϕ)	31^o	35^o	40^o
Cohesion (C) (kN/m^2)	0.0	0.0	0.0

Results and discussion

Lateral loading levels

To discuss the results of laterally loaded single pile, first should be defined the adopted ultimate lateral loading which is a load required to produce horizontal displacement of 12 mm according to **Soneja, M. R., & Garg, K. G. (1980)** [4]. The incremental static lateral load was applied at a very slow rate allowing the pile to achieve equilibrium at each level of lateral loading and to have sufficient time to record the applied lateral load, pile head deflection and strains gages readings along the pile length. Tables (3 to 5) show the increment of lateral loading to load ultimate for each case.

Table(**2): Lateral load and max. deflection for fine sand with different densities**

Loose state		Medium state		Dense state	
loading (N)	deflection (mm)	loading (N)	deflection (mm)	Loading (N)	deflection (mm)
10	1	10	0.2	10	0
20	5.2	20	0.53	20	0.45
30	8.6	40	3.55	40	1.5
40	12	60	6.88	60	3.1
-	-	80	10.9	80	4.5
-	-	90	12	100	6
-	-	-	-	120	9
-	-	-	-	140	10.2
-	-	-	-	160	11.3
-	-	-	-	180	12

Table 3: Lateral load and max. deflection for medium sand with different densities

Loose state		Medium state		Dense state	
loading (N)	deflection (mm)	loading (N)	deflection (mm)	Loading (N)	deflection (mm)
10	0.15	10	0	10	0
20	0.26	20	0.23	20	0.2
40	2.7	40	1.85	40	1.4
60	6.41	60	3.45	60	2.16
80	12	80	5.5	80	3.48
-	-	100	7.5	100	5
-	-	120	9	120	8
-	-	130	12	140	9.1
-	-	-	-	160	10.7
-	-	-	-	180	11.4
-	-	-	-	200	12

Table 4: Lateral load and max. deflection for coarse sand with different densities

Loose state		Medium state		Dense state	
loading (N)	deflection (mm)	loading (N)	deflection (mm)	Loading (N)	deflection (mm)
10	0.24	10	0	10	0
20	0.4	20	0.19	20	0
40	3.85	40	1.2	40	0.5
50	6.41	60	3	60	1.45
60	9.6	100	5.3	100	3
70	12	140	7.5	140	6.8
-	-	180	12	180	9.4
-	-	-	-	200	11
-	-	-	-	240	12

Calculation of Bending Moments

From strain gages readings, bending moments along the pile length were calculated under static lateral loading using simple beam theory as cited by [1]&[2].

$$M = \varepsilon \frac{EI}{r} \qquad (1)$$

Where

M = Bending moment ($N.mm$)

ε = Measured strain (mm / mm)

E = Modulus of elasticity for aluminum pile (N/mm^2)

I = Moment of inertia of the pipe section (mm^4)

r = Outside radius of the pile (mm)

Lateral displacement of single model pile

Figures (3 to 5) shows the effect of the three different densities (loose, medium and dense state) for each type of sand on the horizontal displacement at the pile head under different levels of lateral loading. The displacement difference for the three densities of each type of sand, it increases as the load level increases. At low loading level, the difference is negligible, while at the high loading level, the difference is clearly noticeable. Also, it can be observed that the slopes of the curve are increasing with the loading level increases especially in dense state. This means when the load level increased, the soil resistance increased.

For the all cases, the figures show that the displacement decreases with the increase of grain size distribution in dense and medium state except for loose state of the medium sand which exerted a lower displacement, as shown in Figure (3). This is may be attributed to the angle of internal friction of medium sand in loose state is higher than that of the angle of internal friction for the other types.

Influence of sand relative density

Figures (6 to 9) shows the effect of the three types of sand (fine , medium and coarse) with three different densities (loose, medium and dense state) on the horizontal displacement at the pile head under different levels of lateral loading. It shows that the increase of sand relative densities resulted small increase in lateral resistance for loose condition while this increment is significant in medium and dense state. Generally, the lateral load capacity increases with increasing sand density due to increasing the shear strength parameters of the soil.

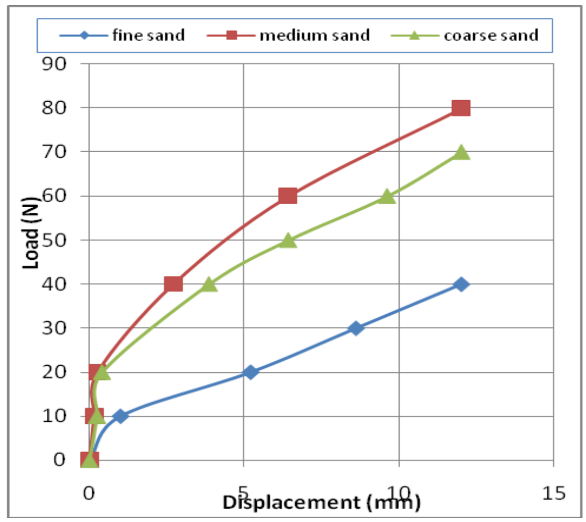

FIGURE 4: DEFLECTION VS. LOAD IN LOOSE STATE

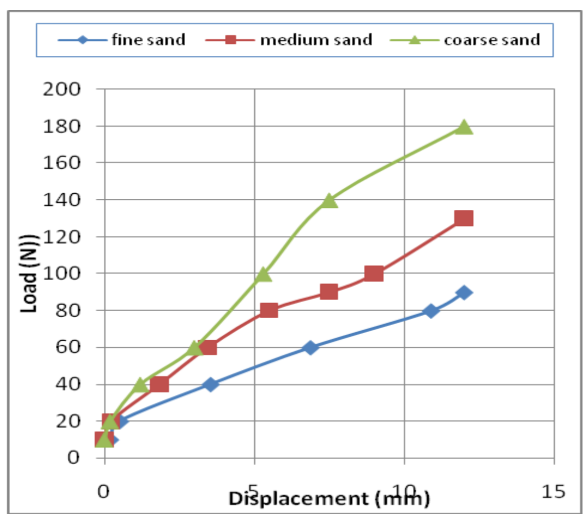

FIGURE 5 DEFLECTION VS. LOAD IN MEDIUM STATE

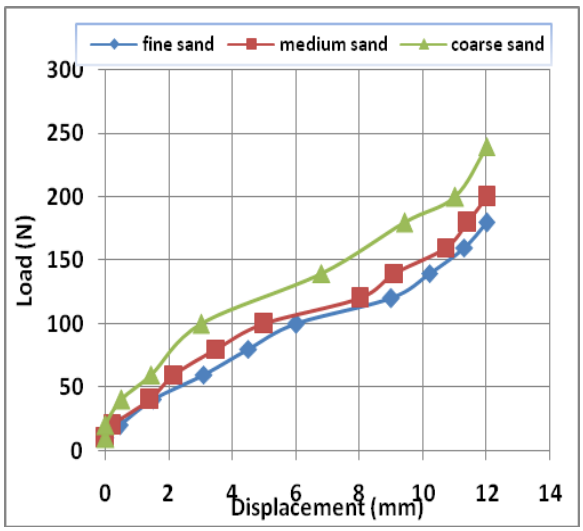

FIGURE 6: DEFLECTION VS. LOAD IN DENSE STATE

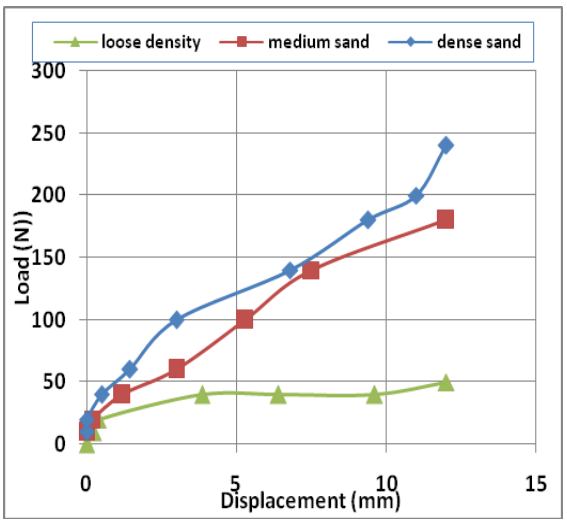

FIGURE 4: DEFLECTION VS. LOAD IN COARSE SAND

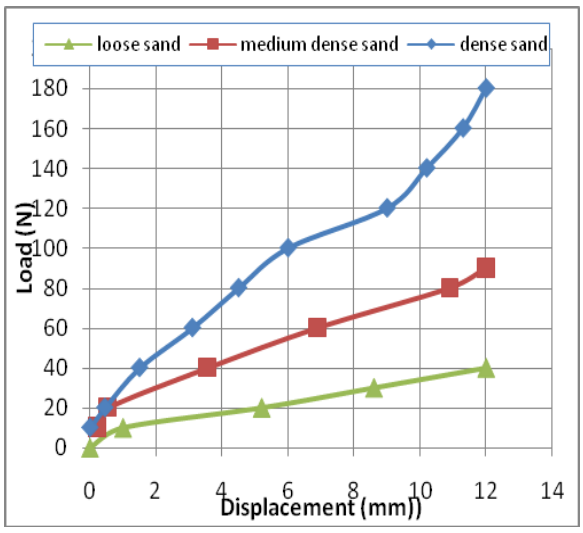

FIGURE 7: DEFLECTION VS. LOAD IN FINE SAND

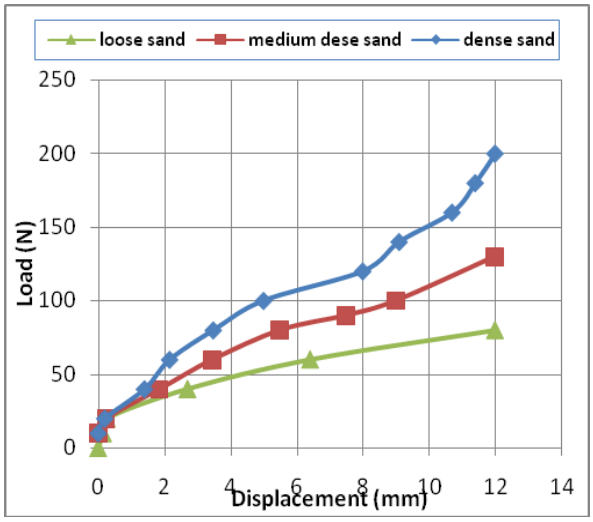

FIGURE 8: DEFLECTION VS. LOAD IN MEDIUM SAND

Bending moment of pile models

The bending moment profiles for both compressive and tensile were obtained from equation (1), depending on strain gages reading. Figures (10 to 18) shows the moment diagrams at different loading levels for a single pile subjected to static lateral loading embedded within three different particle size distribution of sand with three different densities for each type. The Figures clearly shows that the increase in loading levels causes an increase in moment and displacement along the pile. It also shows that the maximum bending moment location shifted down as the load level increases, which is a similar behavior of full scale testing conducting by Brown et al. (1988) [3]. The top portion of the moment diagram shows a cantilever beam behavior, with a straight line moment curve which is started from point of applied lateral load to the soil surface. After crossing the soil surface the soil starts to resist the movement of the pile and hence producing an opposite reaction since the soil behaves as Winkler springs foundation. Even-though the soil resisted the pile movement, the curvature and therefore the moment continue increasing but at a smaller increments. At this stage, the curvature of the moment diagram between the ground surface and the maximum moment increased. At the final stage of the moment diagram is falling between the maximum moment and the pile tip.The bending moment for all cases (fine, medium and coarse sand) for compression and tension have similar pattern and its symmetry in maximum bending moment except at the loose state where the difference of maximum bending moment for each type is different with depth where the compression side was shifting to a deeper depth. This is because of that the densification occurs during lateral loading appeared to be related to compaction of the sand when the pile is pushed forward as shown in Figures (10 to 13).

Generally, the bending moment decrease with increase the grain size particle for sand except at loose state for medium sand exerted lower bending moment as shown Figures (13 to18).

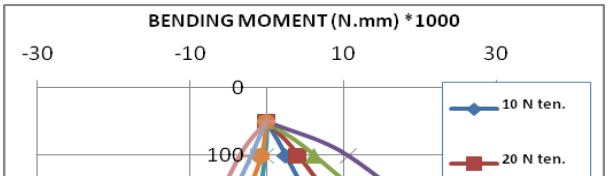

Figure 5: Bending moment distribution in single pile embedded within **fine sand in loose state**

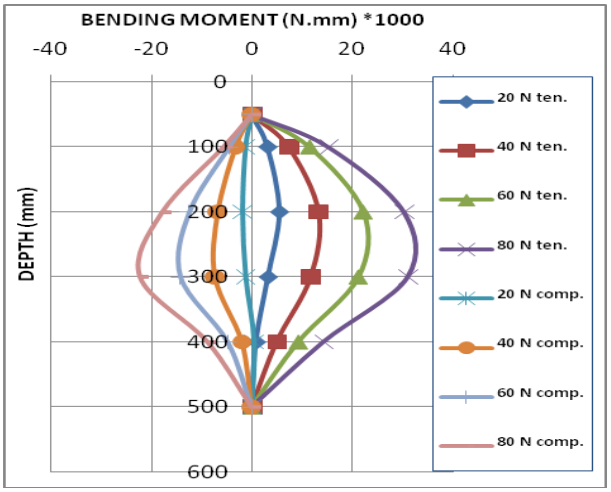

Figure 6: Bending moment distribution in single pile embedded within **medium sand in loose state**

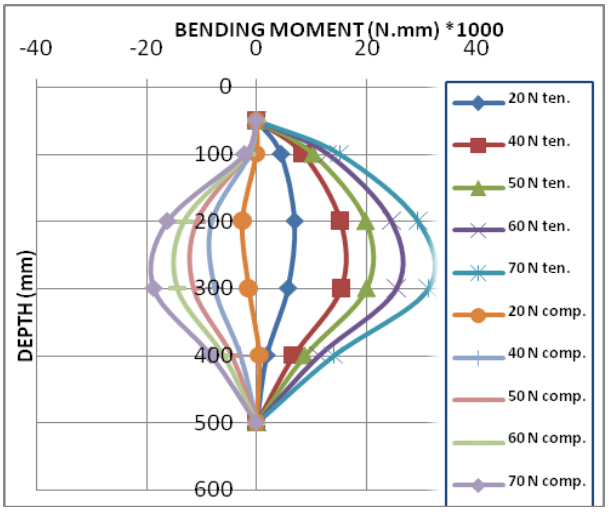

Figure 12: Bending moment distribution in single pile embedded within **coarse sand in loose state**

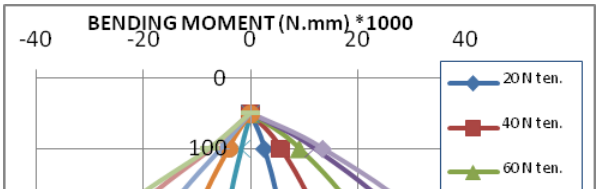

Figure 13: Bending moment distribution in single pile embedded within **fine sand in medium state**

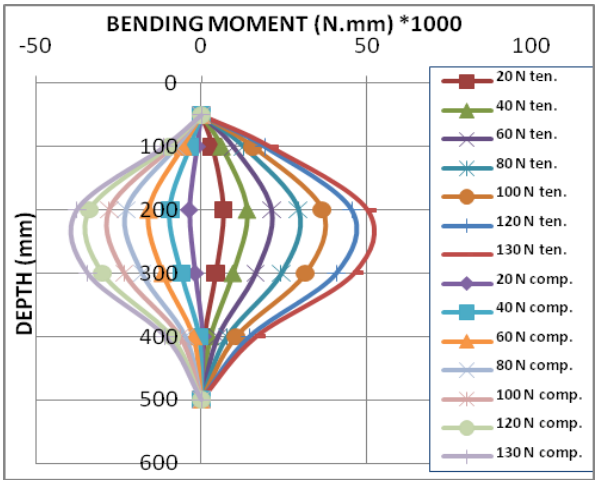

Figure 14: Bending moment distribution in single pile embedded within **medium sand in medium state**

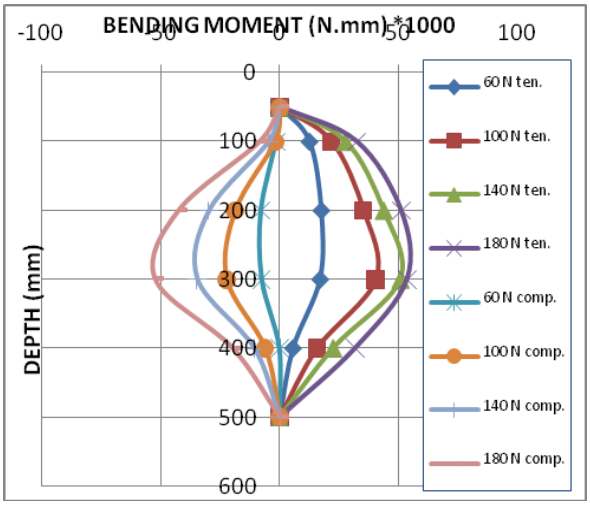

Figure 15: Bending moment distribution in single pile embedded within **coarse sand in medium state**

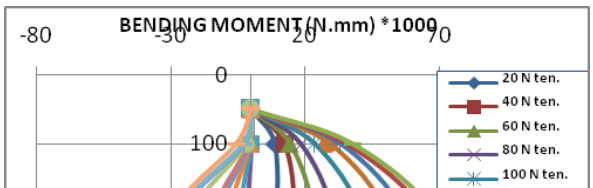

Figure 16: Bending moment distribution in single pile embedded within **fine sand in dense state**

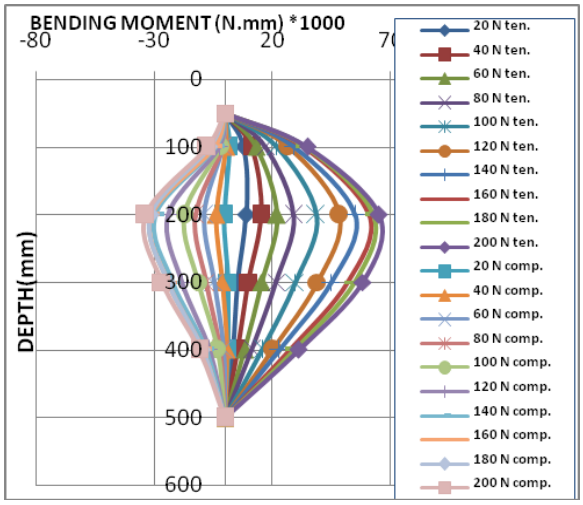

Figure 17: Bending moment distribution in single pile embedded within **medium sand in dense state**

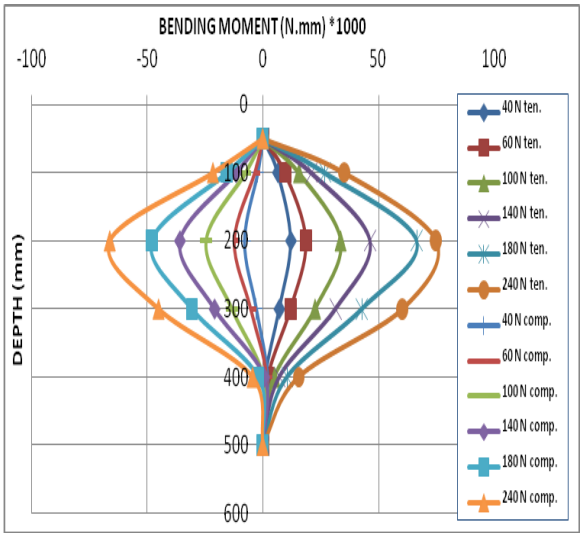

Figure 18: Bending moment distribution in single pile embedded within **coarse sand in dense state**

Location of maximum bending moment for tensile and compressive

Figures (19 to 21) show the effect of particle size distribution of sand with different densities on maximum bending moment profile for tensile and compressive with respect to (L/L_o) ratio, which defined as the ratio between maximum bending moment profiles from point of applied lateral load to the original length of the pile. In loose and medium state density the passive resistance increase to higher depth except for fine sand in loose state and medium sand in medium state density as shows in Figures (19 and 20). This is may attributed to the lower resistance of the soil which introduced due to densification during applied lateral load. This phenomenon was not appearing in dense sand due to lateral loading proportional to relative density, as shows in Figure (21).

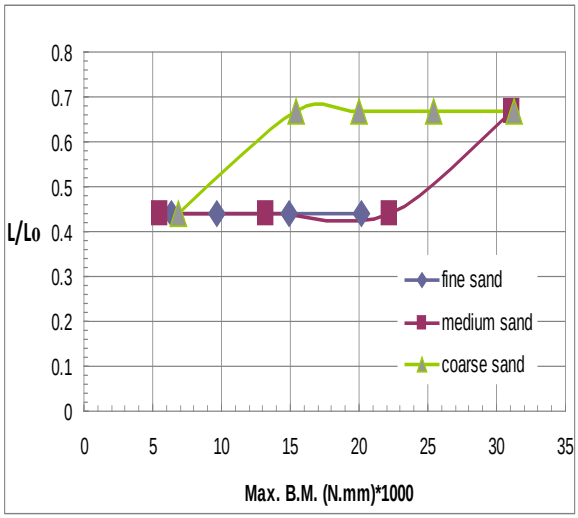

(A)

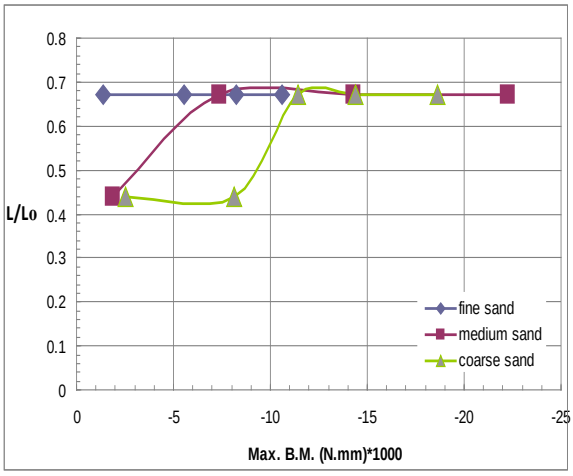

(B)

Figure 7: The variation max. moment with (L/L_o) for **loose state** (A) maximum bending for tension , (B) maximum bending for compression

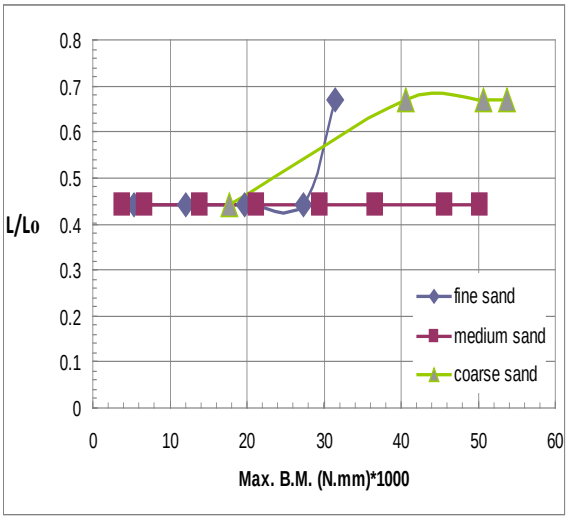

(A)

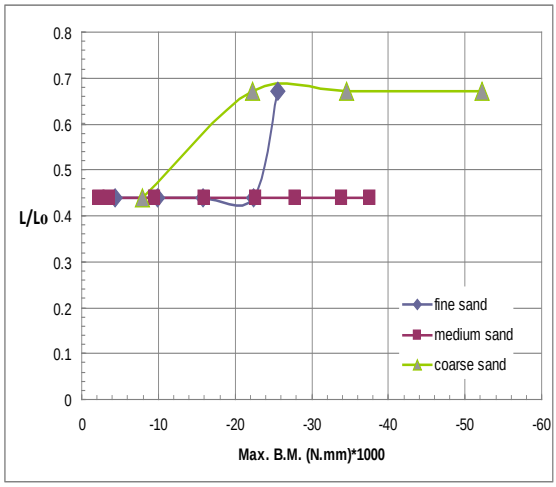

(B)

Figure 8: The variation max. moment with (L/L_o) for **medium state** (A) maximum bending for tension . (B) maximum bending for compression

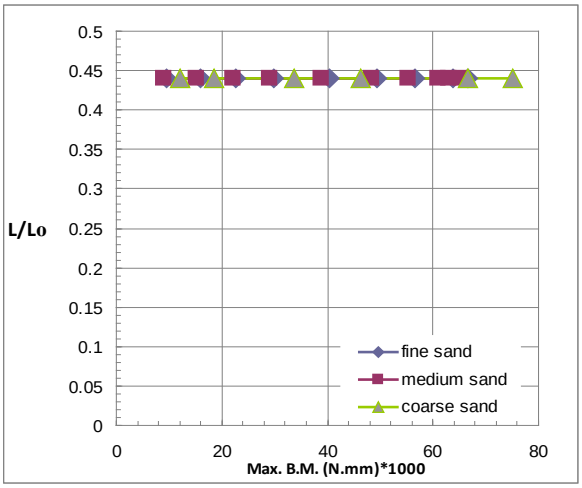

(A)

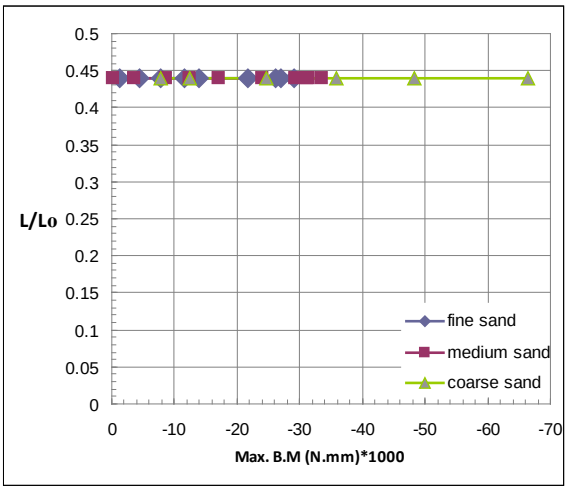

(B)

Figure 9: The variation max. moment with (L/L_o) for **dense state**(A) maximum bending for tension . (B) maximum bending for compression

p-y Curve for static lateral loading test

Figures (22 to 30) shows the curves for single model pile embedded within different grain size distribution and densities subjected to lateral static load. These curves present the soil pressure at three different depths (i.e. 200, 300 and 400 mm) below the soil surface. The figures show an increase in soil pressure due to an increase in both depth and pile deflection. The soil resistance increases with the depth since the confining stress increases with depth.

Generally, for all cases the figures show that the soil resistance increasing with larger grain size particles in dense and medium state except for loose state, the medium sand exerted higher soil resistance than that of coarse sand in loose state as shown in figure (23) this is may due to higher values of angle of internal friction for the medium sand in loose state.

Finally, for all types of sand in loose state the curves start with high soil pressure and deflection then decreased as shown in Figures (22 to 24). This is because of the initial modules of subgrade reaction k_1 of sand in loose state is lesser than that of the initial modules of subgrade reaction k_1 for the other states of sand.

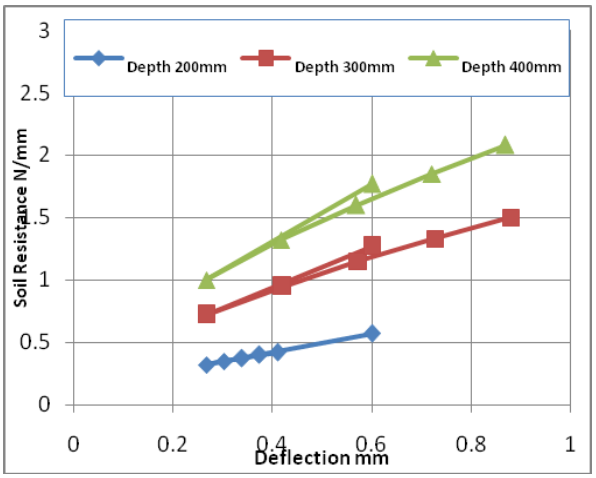

Figure 10: p-y Curves for single model pile within **fine sand at loose state**

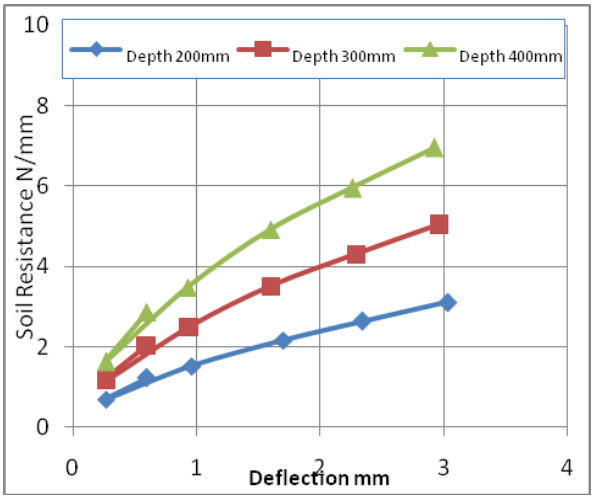

Figure 11: p-y Curves for single model pile within **medium sand at loose state**

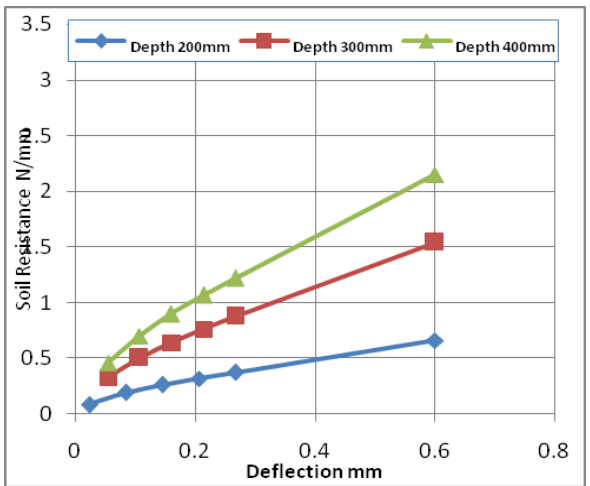

Figure 12: p-y Curves for single model pile within **coarse sand at loose state**

Figure 13: p-y Curves for single model pile within **fine sand at medium state**

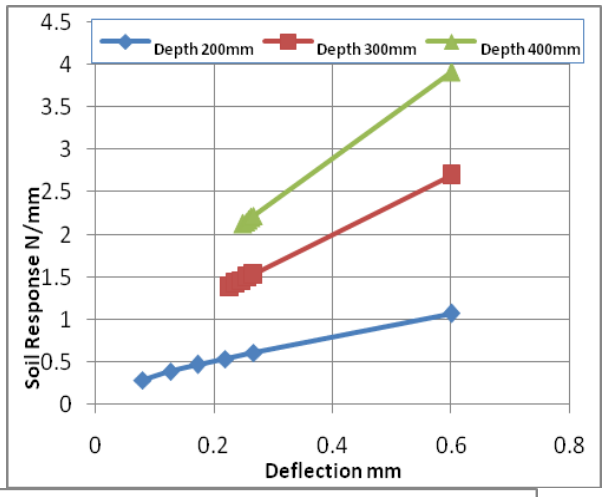

Figure14: p-y Curves for single model pile within **medium sand at medium state**

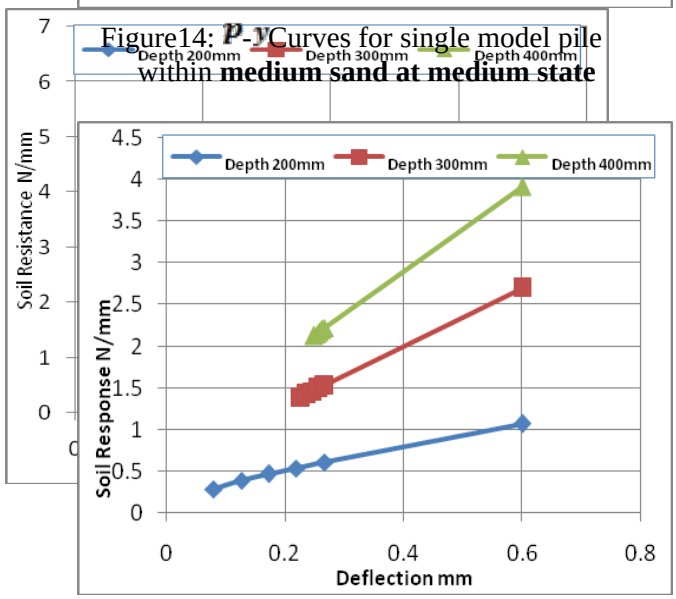

Figure 15: p-y Curves for single model pile within **coarse sand at medium state**

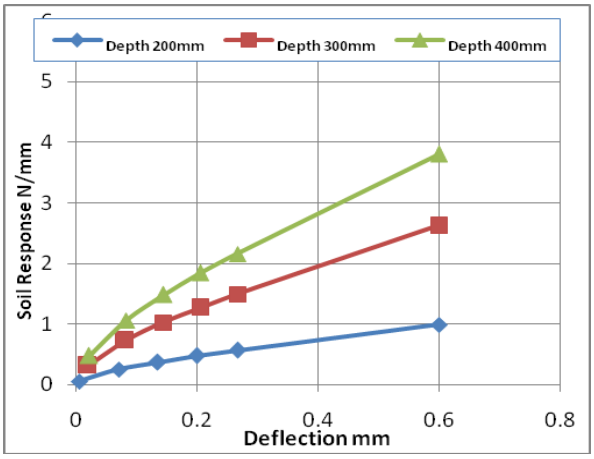

Figure 16: p-y Curves for single model pile within **fine sand at dense state**

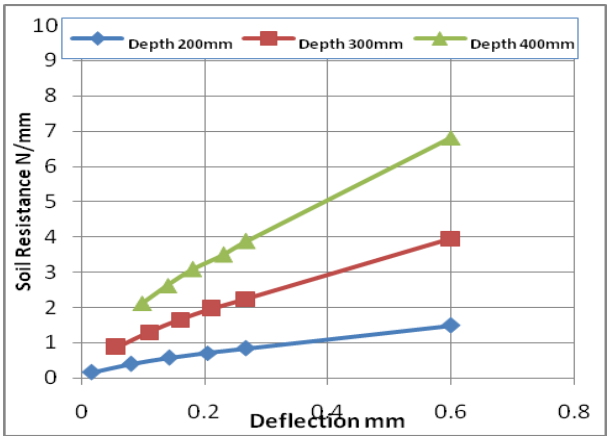

Figure 29: p-y Curves for single model pile within **medium sand at dense state**

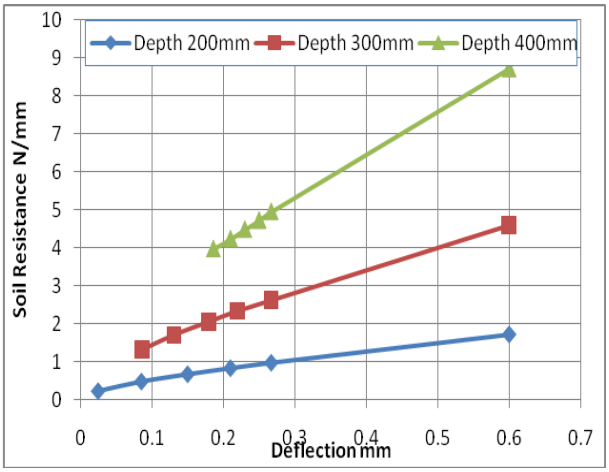

Figure 30: p-y Curves for single model pile within **coarse sand at dense state**

CONCLUSIONS

i. A small scale of model pile can be used to explain the behavior of piles when subjected to lateral static loading.

ii. In the static lateral loading under all different conditions, the lateral displacement of the pile head decreases with the increasing of grain size of cohesionless soils at dense and medium state, except when the sand in loose state, it is independent of grain size.

iii. Relative density of Sand has a significant effect on the lateral capacity of the pile. That's to say the higher the relative density of sand the higher the lateral capacity of the pile.

iv. The behavior of single pile embedded in coarse and medium grain size of sand was different to the single pile embedded within fine sand. However, due to the reduction in grain size where, fine sand was yielded higher displacement and bending moments.

v. The increasing in relative density is not much significant in maximum bending moment occurring depth, while in lower relative density in loose and medium state, it is much significant, especially in coarse sand.

vi. The results of p-y curves shows that the soil resistance increasing with larger grain size particles in dense and medium state except for loose state, the medium sand exerted higher soil resistance than that of coarse sand in loose state

REFERENCES

[1] A1 Mandeel, S. J. (MAY 2000): "Behavior of Laterally Loaded Pile Group Model in Sand". Dahran , Saudia Arabia: King Fahd University of Petroleum & Minerals.

[2] Arta, M. R. (January 1992): "The Behaviour of Laterally Loaded Two-Pile Groups". University of Durham.

[3] Brown et al. (1988):"Lateral Load Behavior of Pile Group in sand". Journal of Geotechnical Engineering, Vol. 114, No. 11, 1261-1276.

[4] Soneja, M. R., & Garg, K. G. (1980):"Under-ream Piles under Lateral Loads". Indian Geotechnical Jornal, Vol.10, No.3, p.p.232-244.

[5] Salgado, R. (2008),"The Engineering of Foundations", Inc.: The McGraw-Hill Companies.

[6] Huang, J. W. (2011), "Development of Modified p-y Curves for Winkler Analysis to characterize The Lateral Load Behavior of A Single Pile Embedded in Improved Soft Clay", Graduate Theses and Dissertations. Paper 12114: Iowa State University.

[7] Matlock, H and Reese, L.C. (1960), "Generalized Solution for Laterally Loaded Piles", Journal of Soil mechanics and Foundation Division, ASCE, Vol. 86, pp. 63-91.

[8] Broms, B. B. (March, 1964),"Lateral Resistance of Piles in Cohesive Soils", Journal of the Soil Mechanics and Foundations Division, Vol. 90, pp. 27-63.

[9] Alizadeh, M. & Davisson, M. T. (1970), "Lateral Load Tests on Piles-Arkansas River Project", J.S.M.F.D., ASCE, val. 96, SM5: pp 1583-1604.

[10] Meyer, B. J., and Reese, L. C. (December 1979), "Analysis of Single Piles Under Lateral Loading", Austin, Texas: The University of Texas at Austin.

[11] Price, C. and Wardle, I. F., (1979), " The Deformation of Vertical Piles in London Clay Under Static And Cyclic Horizontal Working Loads", Proc. of the Conf. at lEE. London pp. 87-94.

[12] Richter, J. A., Demars, K. R., and Jr, R. R. (April 1984),"Photoelastic Analysis of Laterally Loaded Rigid Piles", Journal of Geotechnical Engineering, Vol. 110 No. 4, pp. 548-551.

[13] Trochianis, A., Bielak, J., and Christiano,P (1988),"A Three-Dimensional Nonlinear Study of Piles Leading to the Development of a Simplified Model", Rpt. R-88-176, Dept. of Civil Eng., Carnegie Inst. of Technology.

[14] Sumer, B., Christiansen, N. and Fredsoe, J. (1992), "Time Scale of Scour around a Vertical Pile", Proc.2nd International Offshore and Polar Engineering Conference, ISOPE, San Francisco, Vol. 3. pp. 308-315.

[15] Gandhi, S. R., and Selvan, S. (1997), "Group Effect on Driven Piles Under Lateral Load", Journal of Geotechnical and Geoenvironmental Engineering, Vol. 123, No. 8, pp. 702 – 709.

[16] Ranjan,, N. P., and Jagannath, P. P. (2001), "Ultimate Lateral Resistance of Pile Groups in Sand", Journal of Geotechnical and Geoenvironmental Engineering, Vol.127, No.6, pp.481- 486.

[17] Kim, , B. T., Kim,, N. K., Lee,, W. J., and Kim, , Y. S. (2004),"Experimental Load–Transfer Curves of Laterally Loaded Piles in Nak-Dong River Sand", Journal of Geotechnical and Geoenvironmental Engineering,, Vol. 130, No. 4, pp 416 – 425.

[18] Briud J.-L, Chen H.-C, Y.Li, P.Nurtjahyo and J.Wang. (2005), "SRICOS-EFA Method for Contraction Scour in Fine Grained Soils" , Journal of Geotechnical and Geoenvironmental Engg, ASCE, Vol. 131, pp. 1283-1294.

[19] *Hansen, M., Wolf, T. K., Rasmussen, K. L., Roesen, H. R., and Ibsen, L. B. (June 2013)*,"Physical Modelling of Cyclic Laterally Loaded Pile in Cohesionless Soil", Denmark: Aalborg University Department of Civil Engineering Sohngaardsholmsvej 57, DK-9000 Aalborg, Denmark.

[20] *Sumer, B., Hatipoglu. F. and Fredsoe, J. (2007)*, "Wave Scour around a Pile in Sand, Medium Dense and Dense Silt", Journal of water way, port, coastal and ocean engineering, ASCE, Vol. 133, pp. 14-27.

[21] *Reese, L. C., Cox, W. R., and Koop, F. F. (1974), "Analysis of Laterally Loaded Piles in Sand"*, 6th Annual Offshore Technology Conference, Houston, Texas, pp. 473-483.

Effect of Crude Oil Contaminations on Some Geotechnical Properties of Al-Samawa-Depot site

Thaer Abedul-Rida Albaoey, Mahmood R. Mahmood. Al-Qayssi., and Falah H. Rahil

Abstract— **Most of the southern Iraqi areas are polluted by oil due to the multiple oil wells, oil exploration, damage storage tanks and pipelines. Therefore it is necessary to investigate the geotechnical properties of soil contaminated by crude oil for engineering purposes.**

An extensive laboratory testing program was performed on fine grained soil brought from Al-Samawa-Depot site. The program consist of laboratory tests to investigate physical and engineering properties carried out on clean and contaminated soil samples with crude oil at different percentages of 4, 8, 12, and 16 % by weight to the dry weight of the soil to determine, index properties, compaction, permeability and compressibility characteristics.

The results show that the moisture content required to achieve maximum dry density has decreased when oil content increased in contaminated soil. The crude oil contamination decreased the liquid limit and plastic limit values and indicated a lower of maximum dry density (MDD) and optimum moisture content (OMC).

Two groups of contaminated soil samples were tested for permeability and compressibility characteristics. The first group was compacted at its MDD and OMC for uncontaminated and contaminated soil samples with different crude oil content and the second group was compacted at the optimum water content for natural soil samples for all the uncontaminated and contaminated soil samples with the same different crude oil content at the compacted energy of the standard Procter test. The results show that the permeability for both groups are reduced as oil content increased. The initial void ratio for the first group of soil samples is less than that of the second group. The compression index slightly increases with increasing crude oil content for the first group while for the second group increases with the increase crude oil content. Swelling index values decreases for the first group, while it increases for soil samples of the second group with the increase crude oil content. Volume compressibility with respect to crude oil contents for the two groups increase with the increase crude oil content for the second group of specimens, but for first group of specimens the relation is not uniform. Coefficient of consolidation with respect to crude oil content for the two groups of specimens shows an increase up to 8% of crud oil content then decreased for the first group, while for the second group a decrease at 4% of crud oil content then slight increase for the other crud oil percents.

Key words: Fine grained soil, Contaminated Soil, crude oil, Compressibility Characteristics

Thaer Abedul-Rida Albaoey
M.Sc of Geotechnical Eng. Ministry of Oil
Dr. Mahmood R. Mahmood. Al-Qayssi
Assist. Prof. of Geotechnical Eng. Building & Construction Eng,. Dept. University of Technology
Dr. Falah H. Rahil
Assist. Prof. of Geotechnical Eng. Building & Construction Eng,. Dept. University of Technology
E-mail : mahmoudal_qaissy@yahoo.com Mobile 00964 7901315445

INTRODUCTION

Oil pollution has attracted a great deal of attention in the world for the past two decades and oil spillage has been found to be one of the major cause of environmental problem as they produce highly deleterious effects on the affected environment and their long term effects have become a very big source of concern study**,** (Nwagbara, 2006).

When an oil spill or leakage occurs, soils around the sources of leakage are contaminated. Some major tasks need to be performed for remediation and reclamation of the contaminated area.

Nigerian National petroleum Corporation official report estimates a total of approximately 2300 liters of spills in 300 separate incidents annually in the country especially in Niger Delta areas (Badom, 1995).

According to (Dejong, 1980) crude oil spills alters the soil structure, due to insufficient aeration of the soil due to displacement of air and entrainment of other substances into the soil.

Seleam (1988) studied the effect of some oil products on the characteristics of gypseous sandy soil. And the indication was both the kerosene and the gas oil affected the soil behavior in the same manner and no difference was observed between their effects. Furthermore both products caused swelling of the soil with low gypsum content up on contamination.

Meegoda and Ratnaweera (1994) studied the compressibility behavior of contaminated fine-grained soils of low plasticity and high plasticity clays (CL and CH). The results showed that the compressibility is controlled by the mechanical and physicochemical factors.

Izuakor (1997) pointed out that the presence of oil in soil increases the water holding capacity of soil and this affects the soil structure.

The extent of contamination depends on the chemical composition of the contaminant and the properties of the soil (Fine et al., 1997). Also, in connection with the cleanup works, and for any possible

applications of contaminated soils, acknowledge of the geotechnical properties and behavior of contaminated soil is required. This information is also required when oil leakage from storage tanks and processing plants cause oil contamination in the surrounding soils. In this case, it is necessary to determine the effect of oil contamination on existing structures.

Rasool (1999) studied the effects of kerosene contamination on some geotechnical properties of soil. The results of testing show that the contamination of soil by oil effects on physical properties as well as mechanical properties with in oil content. Liquid limit increases significantly while plastic limit increase slightly. Compaction tests indicate those contaminated specimens less than of uncontaminated.

Al-Mashhidani (1999) investigates the effects of some petroleum products (kerosene and gas oil) on the Atterberg limit and permeability of compacted clayey soil of different swelling potential and predicted its ability to store the products. The tests results show that the petrol caused a significant change in soil indices which may be related to the variation in permeability values, with a decrease in liquid limit and an increase in the sedimentation velocity. He also investigates the effects of some petroleum products (kerosene and gas oil) on the consolidation characteristics and permeability of compacted clayey soils .The petrol destroys the plasticity of the soil and affects the consolidation tests results through increasing the value of k, consequently c_v, and reducing the swelling pressure.

Rehman et. al., (2007) Study the geotechnical behavior of oil- contaminated fine-grained soils by conducting laboratory tests included all basic and advanced geotechnical tests. Crude oil was chosen as the contaminated; the addition of crude oil caused an increase in physical soil properties.

Habib and Sahel, (2007) one dimensional testing was used to study the volume change behavior of the uncontaminated as well as contaminated clay with crude oil. The compression index, Cc, increase in the contaminated soil, this depended on the crude oil content in the soil.

Zulfahmi et. al., (2010) investigated the effect of hydrocarbon contamination on the geotechnical properties of the studied soils. He showed that the oil would make earlier contact with clay particles, causing a removal of interaction between water and clay particles. In other hand, the plasticity index decreased with increase in oil for contaminated soil .Generally, the presence of oil has decreased the moisture contents of the liquid and plastic limits of the contaminated soils. The explanation for this condition is the presence of water around the charged clay particles lessen as non polarized liquid of oil occupies the soil. Oil would make earlier contact with clay particles, causing a removal of interaction between water and clay particles. Water acts as binding agent between clay particles that contributes to the plasticity characteristic.

Experimental Work

Material Used

-The Soil

A brown clayey soil was brought up from Al-Samawa Depot, 15 km south Al-Samawa city, 270 km south west of Baghdad city. A trial pit was excavated using mechanical shovel to a depth of 1m below N.G.L. Disturbed samples were collected from the bottom of the pit. The samples were put in air-tight plastic bags and transported to the soil laboratory. Standard tests were performed on air dried soil samples to determine physical and chemical properties of the soil. Details of physical properties are shown in Table (1). The particle size distribution of the soil used is shown in Figure (1). Analysis of mineral compositions of the soil conducted by (X-Ray Florescence) is shown in Table (2).

Table (1) : Physical properties of the soil use

Index Property	Index Value
Liquid limit (W_L) %	40.5
Plastic limit (W_P) %	19.8
Plasticity index (P_I) %	20.7
Shrinkage limit (W_S) %	14.1
Specific Gravity (GS)	2.69
Sand (0.075 to 2 mm) %	15
Silt (0.005 to 0.075 mm) %	60
Clay (less than 0.005 mm) %	25
O.M.C (%)	18
Dry Unit weight (kN/m³)	17.2
USCS	CL

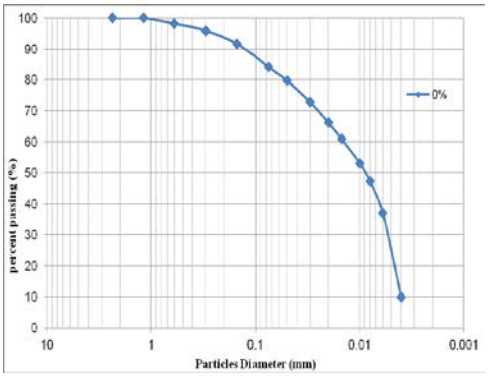

Figure (1): Particle size distribution of the soil usde

The Crude Oil

The agent used in this study was the crude oil. This product was brought up from Al-Samawa Depot also. The physical properties were conducted by Iraqi Ministry of Oil. The results are shown in Table (3). This product was chosen in this study because it is the product stored in Al-Samawa Depot.

Table (2) Mineral composition of the soil

Name of Mineral	Mineral formula	% By Weight
Sodium Aluminum Silicate	$NaAl(Si_2O_6)$	11.1
Sulfur Oxide	SO_3	4.2
Selenium Oxide	SeO2	13.9
Calcium Carbonate	$CaCO_3$	14.7
Calcium Magnesium	$CaMg(CO_3)^2$	11.3
Aluminum Oxide	Al_2O_3	33.0
Chlorine Oxide	ClO_2	2.0
Magnesium Oxide	MgO	9.3

Table (3) : Crude oil properties (strategy line- Basra).

Index Property	Index Value
API @ 60°F	28-32.4
Density @ 15°C kg/ cm^3	0.879-0.859
Density @ 50°C kg/ cm^3	0.868
Water & Sediment Vol %	0.1-0.05
RVP kg/cm^2	0.4-0.34
Specific Gravity @ 60°F and 15.6°C	0.832
Viscosity @ 10°C	24.1
Viscosity @ 21°C	18.2
Viscosity @ 50°C	7.8

Preparation of Soil Samples

The soil sample was air dried and pulverized so as to pass through the sieve no.(10), then divided into five portions.

The crude oil was used in this study to represent one of the hydrocarbon components. Each portion of soil sample was mixed thoroughly with crude oil at different percentages of 4, 8, 12, and 16 % by weight to the dry weight of the soil. The samples were kept into airtight plastic containers for 10 days to attain a homogeneous mixture.

Control Test

To determine the actual water content of the contaminated samples, the percentage losses of crude oil at 105°C must be determined. To do this, samples were taken from the homogeneous mixture for the four contaminated samples (4, 8, 12, and 16%).These samples were put in the oven (105°-110°C) and the percentages of losses were daily checked. The process was continued until the weight of samples became constant. The relationship between drying time and percentage of losses of crude oil for the fine grained samples contaminated with different crude content is shown in Figure (2).

According to the curves, the drying time required for a constant weight is 7 to14 days. When a wet contaminated sample put in an oven (105°-110°C) for 14 days, the evaporation material represents the water and the losses of crude oil (C_L). The content of this materials represent the fluid content.

$$W_f = \frac{W_1 - W_2}{W_2} \times 100$$

Where:

W_f = fluid content

W_1= wet weight of contaminated soil (soil +water +crude oil).

W_2= dry weight of contaminated soil (soil+ remained of crude oil). Therefore, the water content can be determined as following:-

$$W_C\ \% = W_f\ \% - C_L\ \%$$

Where C_L = losses content of crude oil.

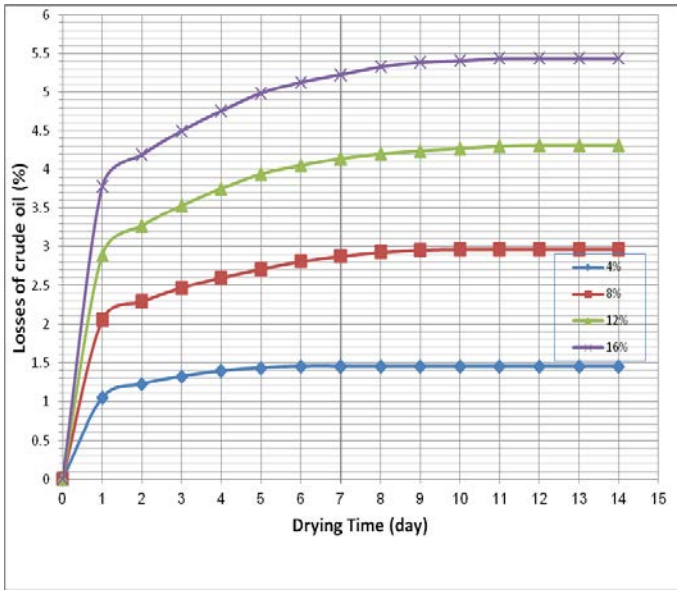

Figure (2) Relationship between drying time and losses of crude oil for fine grained contaminated soil with different percent of crude oil content

Effect of the Contamination on Compaction Characteristics

The compaction characteristics were presented in graphical plots as shown in figure (3). The compaction curves of contaminated soils are clearly located to the left of the uncontaminated soil as crude oil content. The results from the compaction tests performed from the standard compaction effort are shown in Table (4). The effect of crude oil contamination on the maximum dry density and optimum moisture contents illustrate in Figures (4) and (5) respectively.

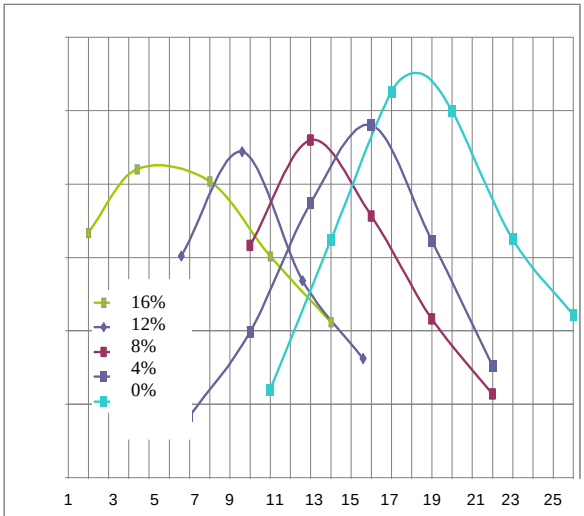

Figure (3) Relationship between Dry unit weight and water content for fine grained contaminated soil for different crude oil content.

Table (4) : Compaction test results of contaminated soils

Crude oil cont.%	OMC %	Max Dry DensitykN/m^3
0	18	17.25
4	16	16.93
8	13	16.8
12	9.6	16.72
16	5.4	16.70

The maximum dry density values in figure (4) show a slight steady drop with crude oil content increased. Figure (5), indicated that the drawdown trend of optimum moisture content with increasing crud oil content.

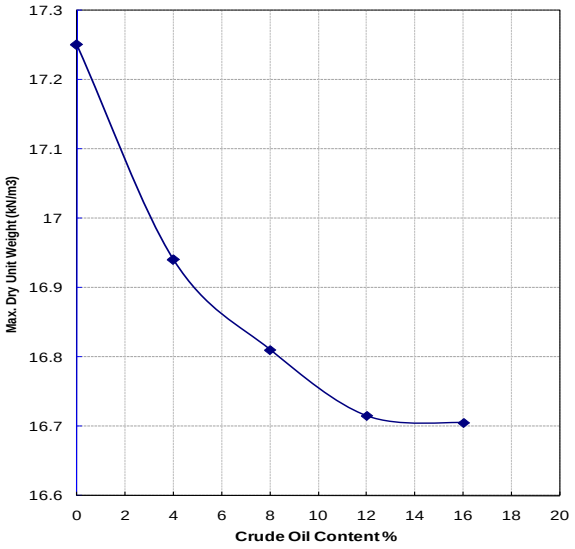

Figure (4): Relationship between crude oil content and maximum unit weight

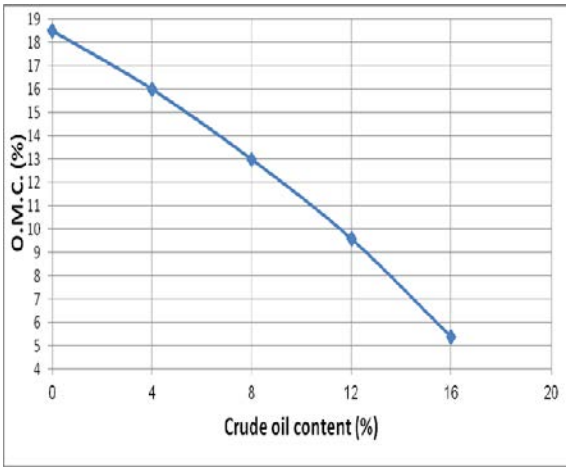

Figure (5): Relationship between crude oil content and the O.M.C

It is clearly suggests that the moisture content required to achieve maximum dry density has decreased when oil content increased in contaminated soil. This probably due to the fact that the oil has partially occupied the inter-particles spaces and the occurrence of oil has changed the soil to a state of loosing material then an uncontaminated soil.

Effect of Contamination on Permeability Characteristics

Permeability-odometer cell (direct method) & consolidation tests (indirect method) were used to perform permeability tests .The soil permeability was investigated from the results of falling head in the direct method in order to establish the capacity of contaminated soil to permit water flow and oil flow within the soil media.

Two groups of contaminated soil samples were tested. The first group was compacted at its MDD and OMC for uncontaminated and contaminated samples with different crude oil content and the second group was compacted at 18 % of Wc (which is the optimum water content for natural soil sample) also for all the uncontaminated and contaminated soil samples with different crude oil content at the compacted energy of the standard Procter test.

Figure (6) shows the variation of the coefficient of permeability with respect to crude oil content for the two groups of the contaminated soil samples permeated with water by using permeability Oedometer cell (direct method). As expected that the permeability for both groups are reduced as oil content increased. The decrease in permeability of the contaminated soil has likely associated with the clogging of some inter-particles spaces by oil. Therefore, an increase in oil content in contaminated soil will reduce the available inter-particles spaces for water seepage. The result also showed that the permeability for the second group of samples has a higher value than samples of the first type. This can be explained from the difference in water content. The dry density of the first group is greater than that of the second group. It can

be expected that the permeability of both types would not change further if the oil contaminated level is increased.

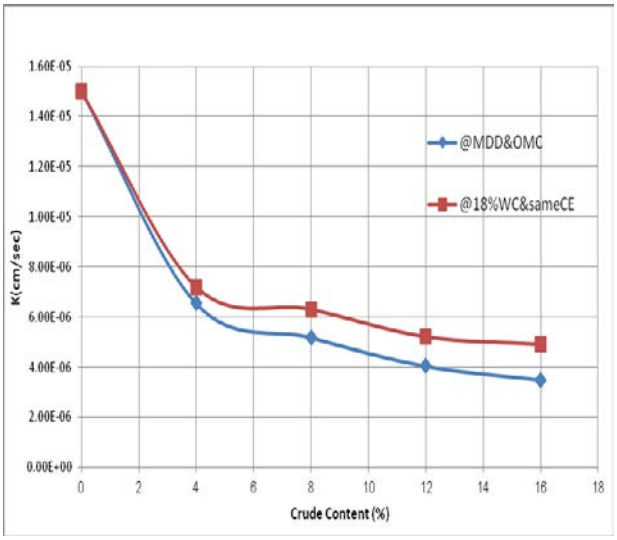

Figure (6) : Effect of crude oil content on permeability for uncontaminated and contaminated samples with different crude oil content with different Wc using permeability Oedometer cell .

Effect of the Contamination on the Compressibility Characteristics:

One dimensional consolidation test was used to study the consolidation behavior of uncontaminated as well as contaminated soil samples. A consolidation ring of 7.5cm diameter and 1.90 cm height was used in testing the two groups of soil samples which tested at the permeability test. All specimens were soaked in water except one specimen (uncontaminated) was soaked in crude oil. The test was performed in accordance with (ASTM D2435).

The results of consolidation tests are presented as void-ratio versus logarithm of effective consolidation stress and are shown in figures (7) to (14) for all the tested specimens with different crud oil content socked in for the two groups. Figures (7and 8) shows that the natural void ratio for soil samples socked in water is less than that socked in crud oil, which is may be attributed to the soil suction property. Figures (9 to 12) shows that the e-log p curves individually for the two groups of soil contaminated samples with different crud oil content. The figures showed that the initial void ratio for the first group of soil samples which compacted at its MDD and OMC is less than that of the second group which compacted at 18 % of Wc. Figures (13 and 14) show the behavior of initial void ratio and void ratio under consolidated pressure of 214 kPa with crude oil content for the two groups of specimen. Figure (13) shows that slightly increase in void ratio for soil samples contaminated with 4% crude oil content then decreased for the other percents of crude oil content for initial void ratio and void ratio under consolidated pressure of 214 kPa for the first groups.

Figure (14) shows an increase in void ratio for soil samples contaminated with all the different percents of crud oil content for the second group .While the void ratio of the soil samples under consolidated pressure of 214 kPa shows marginal changes for the same group. It was noticed that during the test the crude oil expelled and increased the percent of expelled with increasing crude oil content so that the change in void ratio may be attributed to this reason.

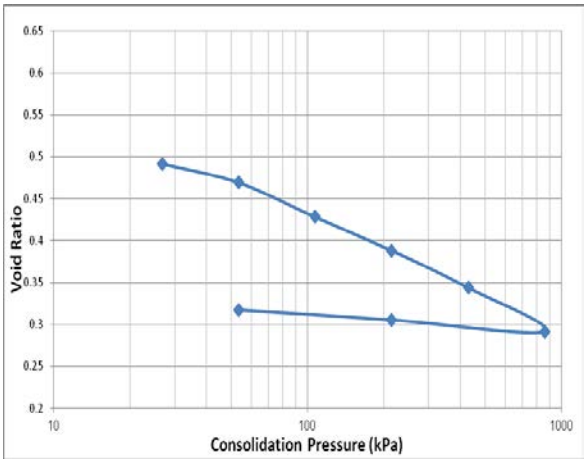

Fig. (7): e – log p curve for natural soil **soaked in crude oil** for specimen compacted at its MDD and OMC

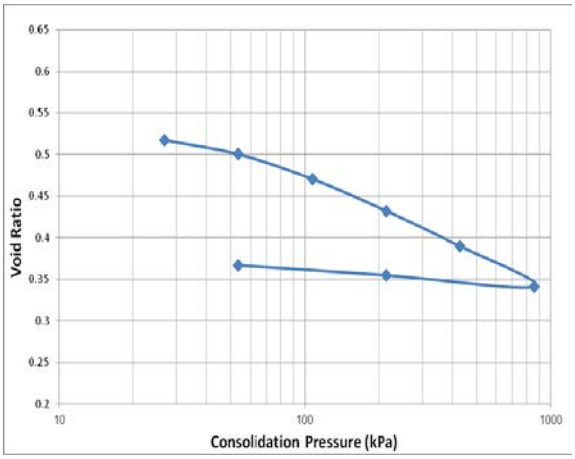

Fig. (8): e – log p curve for natural soil **soaked in water** for specimen compacted at its MDD and OMC.

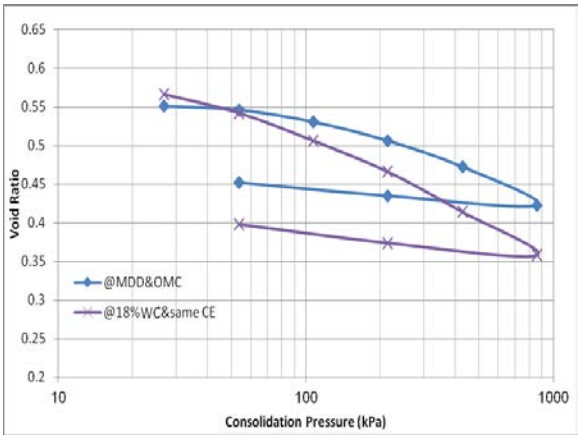

Fig.(9): e–log p curve for **4% crude** oil soaked in water

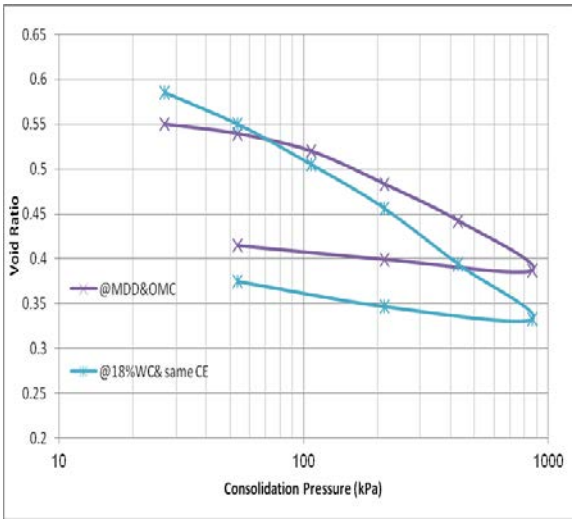

Fig. (10): e – log p curve for **8 % crude** oil soaked in water.

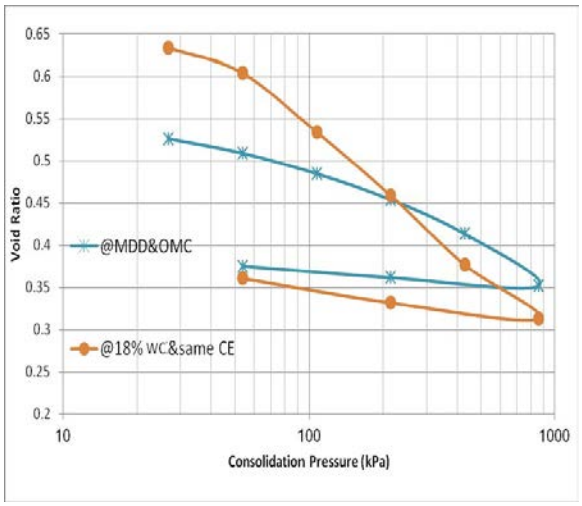

Fig.(11): e–log p curve for **12% crude** oil soaked in water.

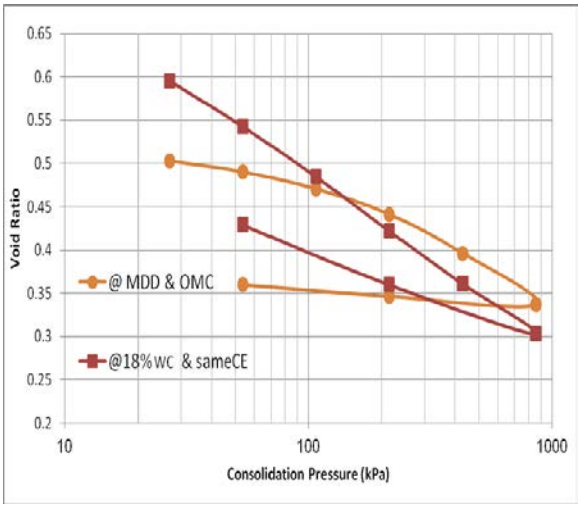

Fig.(12): e–log p curve for **16% crude** oil soaked in water.

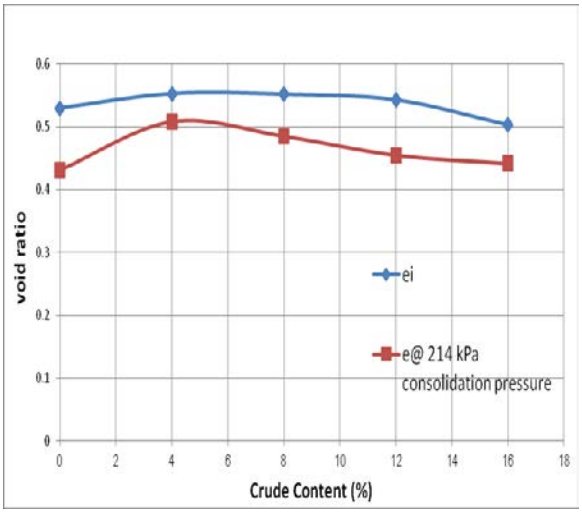

Fig. (13) Relationship between void ratio and crude oil content for specimens compacted at its MDD & OMC

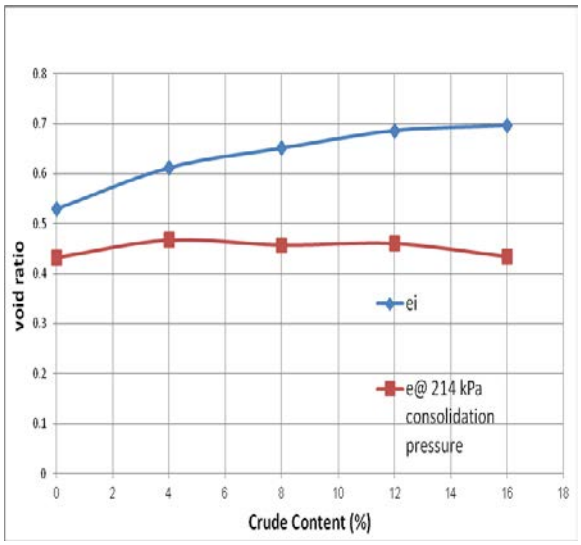

Fig.(14):Relationship between void ratio and crude oil content for specimens compacted at 18 % WC & at the same compaction energy

Figure (15) shows the variation of compression index (Cc) with respect to crude oil content for the two groups of specimens. For soil samples of the first group the compression index slightly increases with increasing crude oil content except at 4 % crude oil content.

The increase in compression index can be attributed to the presence of organic matter in the crude oil. While Cc for soil samples of the second group increases with the increase crude oil content.

Figure (16) shows the variation of swelling index (Cr) with respect to crude oil content for the two groups of specimens. The values of Cr increase at 4% of crude oil content and then decreases after that value for the first group. While the values of Cr for soil samples of the second group increases with the increase crude oil content .

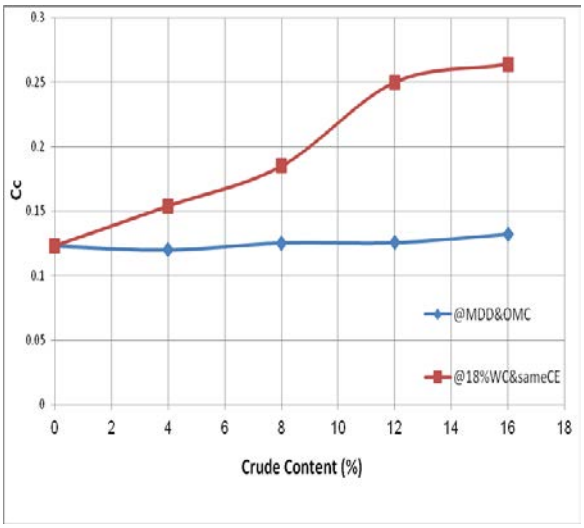

Figure (15): Relationship between Cc and crude oil content for the two types of specimens

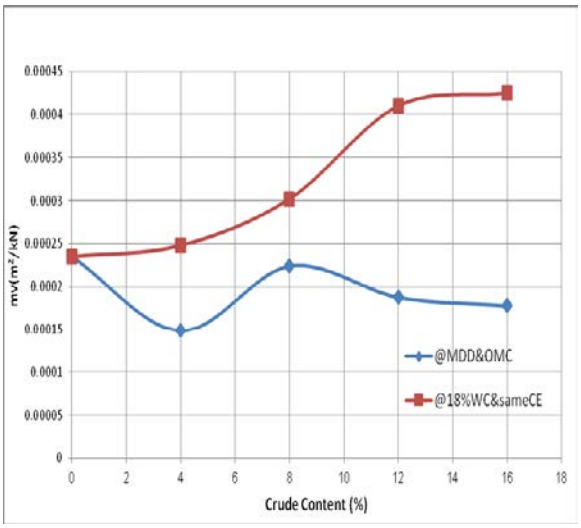

Fig. (17): Relationship between the coefficient of volume compressibility (m_v) and crude oil content for the two types of specimens.

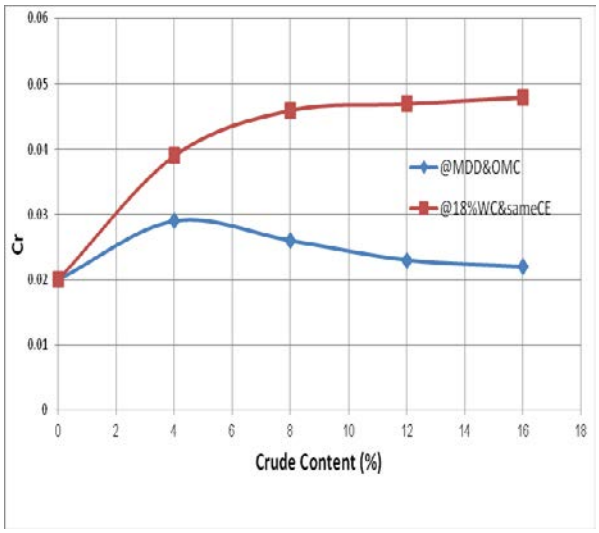

Figure (16): Relationship between Cr and crude oil content for the two types of specimens

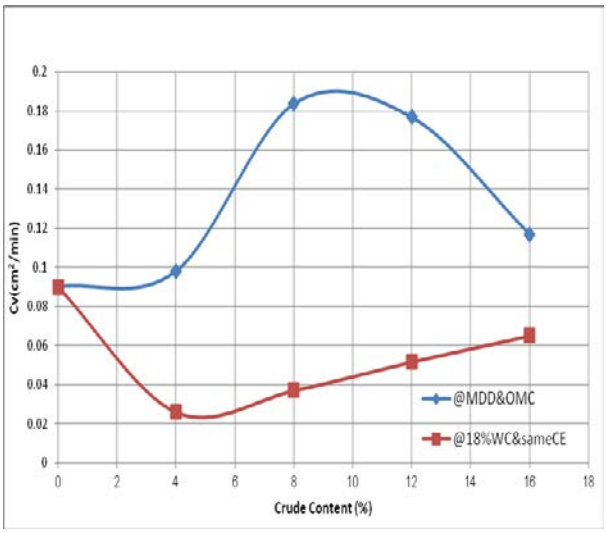

Fig. (18): Relationship between the coefficient of consolidation (C_V) and crude oil content for the two types of specimens.

Figurer (17) shows the variation of the coefficient of volume compressibility with respect to crude oil contents for the two groups of specimens. It can be noticed that from the figure, m_V increase with the increase crude oil content for the second group of specimens, but for first group of specimens the relation is not uniform.

Figure (18) shows the variation of the coefficient of consolidation with respect to crude oil content for the two groups of specimens. The figure shows an increase of Cv up to 8% crud oil content then decreased for the first group, While for the second group a decrease for 4% crud oil content then slight increase for the other crud oil percents.

Values of compression index, swelling index, and initial void ratio, coefficient of consolidation and coefficient of volume of compressibility, void ratio under consolidation pressure of 200kPa and coefficient of permeability of the tested soil are tabulated in Table (5).

Table (5) Result of consolidation tests
(C_V, m_V, and **e** determined at 200 kPa).

Type of Tested Soil	Crude oil %	C_C	C_r	e_0	C_V (cm^2/min)
Soaked in Water	0	0.123	0.02	0.53	0.09
At MDD & OMC	4	0.120	0.029	0.553	0.098
	8	0.125	0.026	0.552	0.1839
	12	0.125	0.023	0.543	0.177
	16	0.132	0.022	0.503	0.117
At18% Wc &Same CE	4	0.154	0.039	0.612	0.026
	8	0.185	0.046	0.651	0.037
	12	0.250	0.047	0.686	0.0517
	16	0.264	0.048	0.696	0.065
Soaked in crud oil	0	0.14	0.020	0.53	0.106

Type of Tested Soil	Crude oil %	m_V (m^2/kN)	$e_{@200\ kpa}$	K (cm/sec)
Soaked in Water	0	2.35E-04	0.432	3.45E-08
At MDD & OMC	4	1.49E-04	0.508	2.38E-08
	8	2.24E-04	0.485	6.73E-08
	12	1.88E-04	0.455	5.44E-08
	16	1.78E-04	0.442	3.40E-08
At18% Wc &Same CE	4	2.48E-04	0.467	1.05E-08
	8	3.02E-04	0.457	1.83E-08
	12	4.10E-04	0.46	3.46E-08
	16	4.25E-04	0.434	4.51E-08
Soaked in crud oil	0	2.45E-04	0.388	4.24E-08

Conclusions:

As a result of the testing program conducted in this study and the discussion presented above, the following conclusions could be drawn:-

1- Crude oil has a complex composition and volatiles even under room temperature but some parts remain as a solid material, therefore the usual procedure cannot be used to determine the water content of crude oil contaminated soils. A proposed procedure, considering the amount of remained crude oil after drying, was used to determine water content of crude oil contaminated soils.

2- Contamination of soil by crude oil effects the gradation of particles, as they become coarser than the uncontaminated soil.

3- Increasing of crude oil content in soil causes a slight reduction in maximum dry density and a significant reduction in optimum water content. The dry density decreases with increasing crude oil content for the samples compacted at the same water content of natural soil and compacted energy.

4- The crude oil contamination induces a reduction in permeability of the soil samples, permeated with water or crude oil. The values of coefficient of permeability for soil samples permeated with water are larger than that for the crude oil. The coefficient of permeability (k) determined from consolidation test of contaminated soil have irregular values with different percents of crud oil contamination.

5- The compression index (Cc) of the crude oil contaminated soil increase slightly with increasing crude oil content. While swelling index (Cr) increase at 4% of crude oil content and then decreases after that.

6- Coefficient of volume compressibility (m_v) increase with the increase crude oil content and coefficient of consolidation (C_V) of contaminated soil shows an increase of up to 8% crud oil content then decreased

REFERENCES

[1].AL-Mashhidani, Hadeel A.A., 1999. "Effect of petroleum products on permeability of clayey soils of normal and high swelling potential", M.Sc. Thesis Submitted to the College of Engineering University of Baghdad W.-K. Chen, *Linear Networks and Systems* (Book style). Belmont, CA: Wadsworth, 1993, pp. 123–135.

[2].*Badom, C.J 1995.* "Land degradation", Cambridge university press: New York.

[3].*Dejong, F.O., 1980.* "Reclamation of soils contaminated with oils, Journal Inst", Petroleum..

[4]. *Fine, P., Graber, E.R., and Yaron, B., 1997.* "Soil interactions with Petroleum hydrocarbons", a biotic processes. Soil Technology 10, 133-153.

[5]. *Habib-ur-Rahman, S.N. Abduljauwad, and T.Akram, 2007.* "Geotechnical behavior of oil-contaminated fine grained soils", Elect. Geol. Eng., 12.

[6]. *Izuakor, F.C. 1997.* "The effect of oil spillage on soil of Nigeria delta area of Nigeria ", SNAP press: Enugu.

[7]. *Khamehchiyan, Hossein, Tajik, 2007.* "Effects of crude oil contamination on geotechnical properties of clayey and sandy soils", Engineering Geology 89, 220-229.

[8]. *Meegoda, N.J. and Ratnaweera, P., 1994.* "Compressibility of contaminated fine grained soils", Geotechnical Testing J., 17: 101-112.

[9]. *Nwagbara, Augustin, okey, 2006.* "Effects of crude oil pollution on shear strength of soil", M.Sc. Thesis, Department of Civil Engineering Faculty of Engineering, University of Nigeria NSUKKa.

[10]. *Rasool, Haifaa Abdul, 1999.* "Some Geotechnical properties of oil contaminated soil", M.Sc. Thesis Submitted to the College of Engineering University of Baghdad.

[11]. *Rahman, Z.A. Umar, H. and Ahmed, N., 20l0.* "Geotechnical characteristics of oil-contaminated granitic and metasedimentary soils", Asian J. Applied Sci, 3: 237-249

[12]. *Seleam, Shewnim N.M., 1988.* "Geotechnical Characteristics of a Gypseous Sandy Soil Including the Effect of Contamination with Some Oil Products", M.Sc. Thesis Submitted to the Building and Construction Department University of Technology.

[13]. *Zulfahmi, A.R., Umar, H., and Mohd, R.T, 2010.* "Influency of oil contamination on Geotechnical properties of Basaltic Residual soil", American J. of Applied Sce., 7:954-961

Microstructural Characterization of Iraqi Gypseous Soils

Hussein H. Karim[1], Tom Schanz[2], and Ali N. Ibrahim[3]

***Abstract*—As large areas of Iraq are covered with gypseous soils causing serious damages to foundation built on, three site locations (Baiji, Tikrit and Samarra) in northern Iraq characterized by their high gypsum content were chosen. In this research, the direct shear test was used to obtain shear parameters (cohesion and internal friction angle) for the soils in both natural and water soaked conditions. The laboratory test results showed a decrease in soil shear parameters when soaked in water particularly in its cohesion value. Soaking of soils reduced cohesion by approximately (12-17) folds, while the internal friction angle exhibited a slight reduction. A microstructural study of such soils was also performed using Scanning Electron Microscope (SEM) technique carried out on selected soil thin sections in their natural state and after soaking and/or loading. SEM micrographs reflect appreciable microstructural changes which were observed and identified such as voids, solid domains (gypsum fibers as binding materials). The micrographs of soils subjected to short term soaking showed the occurrence of large voids which are responsible for the higher collapsibility in such soils due to high solubility of gypsum in water.**

***Index* Terms—Microstructure of gypseous soil, Soaking Effects, Shear Parameters and Collapsibility, Scanning Electron Microscopy (SEM)**

I. Introduction

THE presence of gypsum in soil affects its engineering properties and behavior in a degree, which is greatly dependent on the amount of gypsum in the soil. Gypseous soils are characterized by decreasing strength upon wetting, increasing primary and secondary compression and dissolution in continuously seeping water. In general, gypseous soils are reliable for construction under dry and even under short term flow, but become problematic, collapsible and undergo large settlement under long term flooding with water [1] [2].

Manuscript received April 20, 2015; accepted August 16, 2015.

[1] Professor, Building and Construction Engineering Department, University of Technology, Baghdad, Iraq. (corresponding author: e-mail: husn_irq@yahoo.com).

[2] Professor Chair for Foundation Engineering Soil and Rock Mechanics, Ruhr Universität Bochum, Bochum-Germany. (e-mail: tom.schanz@rub.de).

[3] Lecturer (Ph.D), College of Engineering, Al-Iraqia University, Baghdad, Iraq. (e-mail:ali_nasir_79@yahoo.com).

The dissolution of gypsum within the soil mass under wetting and loading conditions leads to one or a combination of the following three processes: a collapse in the soil structure as a result of the immediate softening and bonding destruction of gypsum particles from inundation, consolidation after rearrangement of the soil structure at the end of the collapse process and the leaching process due to a continuous flow of water through the soil mass [3] [4]. In general, the settlement of gypseous soils is mainly due to the dissolution of the cementing gypsum which is a companied by the collapse of the soil structure especially in sandy gypseous soils.

Gypseous soils are distributed in many locations in Iraq forming more than 20% of Iraq total surface area [5]. As the engineering properties of such soils are changed upon wetting causing danger on the structure built on. In the last years, many damages were recorded in some strategic projects in Iraq due to presence of gypseous soils underneath the base of foundation. Investigations proved that most of these projects were constructed on gypsum stratum or soil containing an amount of gypsum.

The fabric of a soil is the geometric arrangement of particles and associated voids has a profound effect on the properties of soils and characterization of the deformation behavior [6]. “Reference [7] studied the structure (fabric plus bridges) of collapsible soils who observed that the chemical cementing material can generate bridges between the solid grains in metastable open fabrics of such soils and water can weaken any bond strength.”

The present work concentrates on evaluating the microfabric of gypseous soil using scanning electron microscopy (SEM) analysis and to elucidate the changes in soils microstructure after soaking or/and loading conditions.

II. MATERIALS AND SAMPLING TECHNIQUES

The present investigation was carried out on gypseous soils obtained from Baiji, Tikrit and Samarra sites in northern Baghdad, Iraq (Fig. 1). Physical tests conducted on these soil samples include liquid and plastic limits which were determined according to [8] [9] respectively. Water content was determined according to [10]. The specific gravity (Gs) test was conducted according to [11] but kerosene was used instead of water due to the dissolution of gypsum in water. The grain size distributions were made according to

specification in [12], while the soil classifications were done according to the unified soil classification system USCS. Grain size distribution of soils and classification together with their soil physical properties are listed in Table 1.

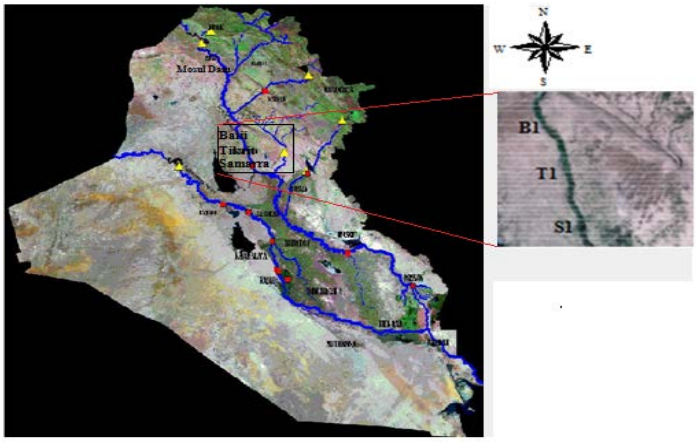

Fig. 1. Study area sites with satellite image.

Direct shear tests were conducted to find the effective shear strength parameters (cohesion, c, and angle of internal friction, ϕ) on dry and soaked soil samples. The time of specimens soaking in water was 6 and 24 hrs. In order to study the effect of soaking period on shear strength parameters of gypseous soil, two tests were conducted on 12 samples for Tikrit site; 4 of them in dry condition, while the other 8 samples were tested in short and long term soaking condition after 6 and 24 hrs respectively (4 samples for each case). The normal stresses were 50, 100, 200 and 400 kPa. The tests were conducted according to [13]. The pneumatic shear device was used for this test. The results of direct shear test of Tikrit soil for conditions of dry and after short term soaking are presented in Table 1 and Fig. 2.

X-Ray diffraction analyses were carried out for the three soil samples at the same Department of Bauhaus-University Weimar, Germany. The qualitative and quantitative XRD results are shown in Figs. 3 and 4 respectively. It is obvious from Table 2 that Tikrit soil sample contains the highest gypsum content (73.9 %), an intermediate for Samarra soil sample with gypsum content (65.7%) and the lowest for Baiji soil sample with gypsum content (51.2%). For Scanning Electronic Microscope (SEM) technique, thin section samples of gypseous soil were prepared using Environmental Scannining Electronic Microscope (ESEM), of F. A. Finger-Institute for Building Science at Bauhaus- Universität Weimar in Germany. This microscope is combined with an EDX for chemical analysis. The tested soil samples are observed, stored and analyzed at different magnifications.

III. RESULTS AND DISCUSSION

Microstructural Characterization

SEM examinations were achieved on different gypseous soil samples, i.e. on natural soil samples and after short term soaking and/or loading. The soil thin sections have been examined using Scanning Electron microscope analysis with high brightness and resolution allowing for the delineation between solid particles (gypsum crystals) and voids. Scanning Electron micrographs were obtained and digitally recorded at different magnifications from 200x to 32000x.

SEM Micrographs

As dissolution has severe economic ramification on civil engineering projects in areas of gypseous soils, microstructural analysis by SEM is essential to understand deformation behavior of soils for economical design of infrastructure. The SEM analysis performs morphological correlation and microstructural assessment with gypsum crystals dissolution or softening and gives a full elemental description. The different magnifications allowed the delineation of solids, voids and the change of interparticle bonds in these micrographs showing the effect of flooding or/and loading on microstrutural changes which could have a significant impact on soil stress deformation.

As described in the previous section, the variation in microstructure was examined in different conditions to understand the effect of both soaking and/or loading on microstructural changes. From SEM results, the appreciable

Table 1. Soil properties, grain size distribution and soil classification (USCS).

Soil Name & No.	W.C (%)	G.C (%)	Sp. Gr. (Gs)	Atterberg's Limits			Grain Size Distribution %						Class. USCS	Shear Strength Parameters					
				L.L (%)	P.L (%)	P.I (%)	C_u	C_c	Gravel (%)	Sand (%)	Fines (%)			*c* (kPa)			ø (°)		
														Dry	Soaked		Dry	Soaked	
											Silt	Clay			6 hrs	24 hrs		6 hrs	24 hrs
Baiji	1.3	51.2	2.5	37	19	18	3.4	1.1	6	78	16	-	SC	-	-	-	-	-	-
Tikrit	0	73.9	2.4	26	21	5	3.0	0.1	8	74	18	-	SM-SC	330	19	28	49	44.5	42
Samarra	6.5	65.7	2.5	32	25	7	1. 6	0.3	22	61	17	-	SM	-	-	-	-	-	-

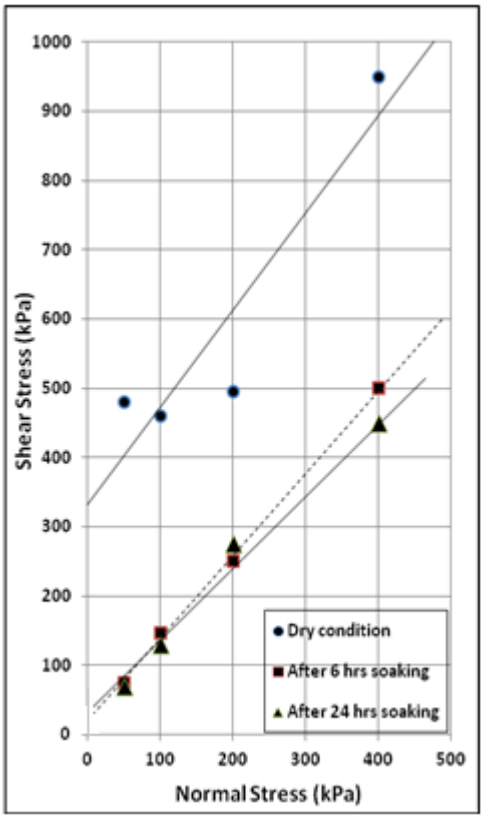

Fig. 2. Direct shear test results for Tikrit soil sample for the dry and water soaked conditions.

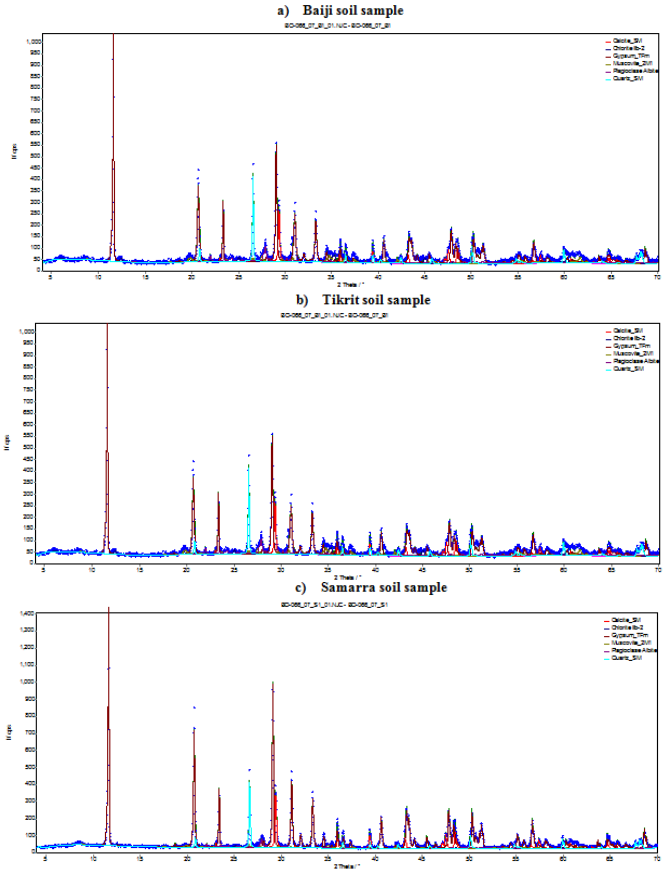

Fig. 3. Qualitative XR-Diffraction test result for (a) Baiji (b) Tikrit and (c) Samarra soil samples.

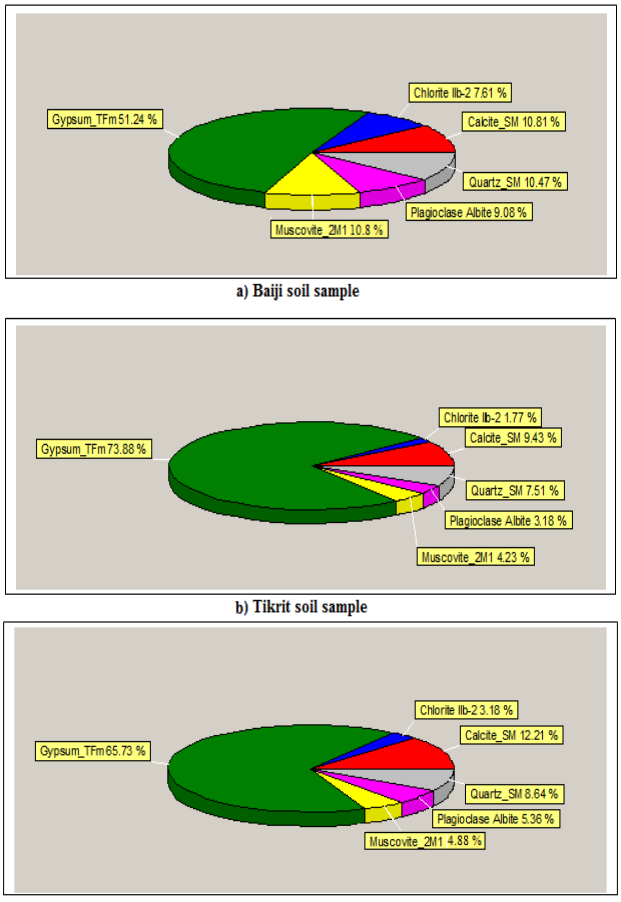

Fig.4. Quantitative XR-Diffraction test results: (a) Baiji, (b) Tikrit and (c) Samara soil samples.

Table 2. XRD test results for the three sites.

Mineral Type (%)	Site		
	Baiji	Tikrit	Samarra
Gypsum	51.2	73.9	65.7
Calcite	10.8	9.4	12.2
Quartz	10.5	7.5	8.6
Muscovite	10.8	4.2	4.9
Plagioclase (Albite)	9.1	3.2	5.4
Chlorite	7.6	1.8	3.2

shape. In these initial natural soil sections, it is clearly shown the high proportion of gypsum and its crystals appeared with very clear edges within soil samples. It is also shown how these gypsum crystals act as bridges (binding material) for soil filling voids between these crystals. With low magnification 200x, gypsum crystals were also identified. With 1000x enlargement, the gypsum crystals as well as voids within soil were well defined. At high magnification, 4000x to 32000x, the gypsum fibers were very clearly appeared as binding materials (Figs. 5, and 7).

Besides, SEM for the same soil samples, after subjecting to short term soaking at different magnifications, are presented in Figs. 8, 9, and 10. At low magnifications 200x and 400x, these Figures show clearly the regions of dissolved gypsum particles which become smaller and the formation of large voids due to soaking. Besides, these Figures show the partial dissolution due to short soaking of gypsum particles forming

large voids between soil particles which may lead to collapsibility. It is worth to mention that gypsum mineral with intermediate solubility (0.2% or 4000 ppm ≈2.6 g/l at 25℃) [14] [15]. So, when the soil sample is subjected to constant water content, some amount of gypsum particles will be dissolved until the water reach fully saturation, then no more gypsum dissolves. It is also shown the large gypsum particles are partially dissolved due to fully water saturation which becomes small particles acting as a binding material which can be easily destroyed when soil subjected to slight loading. In addition, at higher magnification, some organic materials are well defined as circular shapes as shown in Fig. 10.

Table 1 and Fig. 2 present the results of direct shear test of Tikrit soil for conditions of dry and after soaking. It can be seen that the percentage of reduction due to soaking in the angle of internal friction (ϕ) and cohesion (c) due to soaking after short term soaking were 9 % and 94% respectively. It can be stated that a loss of strength by soaking, basically in cohesion is mainly due to bonds destruction and softening of soil interparticle bridges. The SEM for Tikrit soil sample subjected to flooding and loading (after single collapse test) condition at different magnifications is presented in Fig. 11. At low magnification 200x and 400x, the soil sample showed that parts of gypsum particles are dissolved and broke down due to soaking and loading application leading to high collapsibility under loading. This finding is in agreement with [16] who pointed out that the collapse in cemented soil structure with relatively large voids commonly occurs when the soil grains are weakened by adding water and/or an additional load, allowing particles to slide over one other, which results in collapse. At higher magnifications, the fibers of gypsum are well defined.

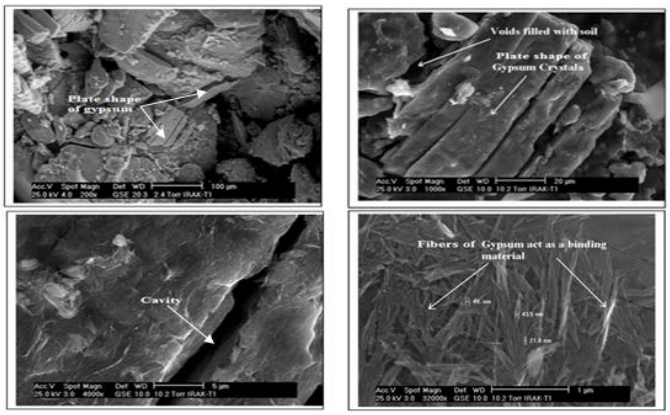

Fig. 5. SEM for Tikrit soil sample in its natural state (undisturbed) in different enlargements.

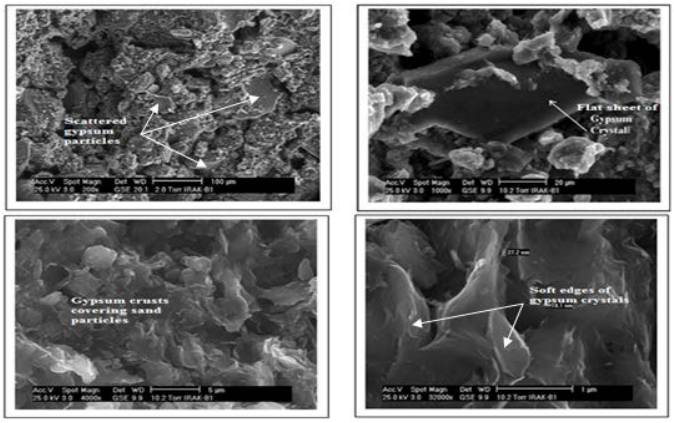

Fig. 6. SEM for Baiji soil sample in its natural state (undisturbed).

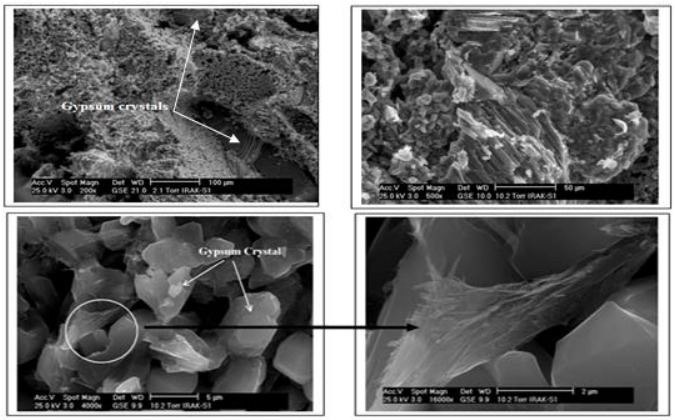

Fig. 7. SEM for Samarra soil sample in its natural state (undisturbed).

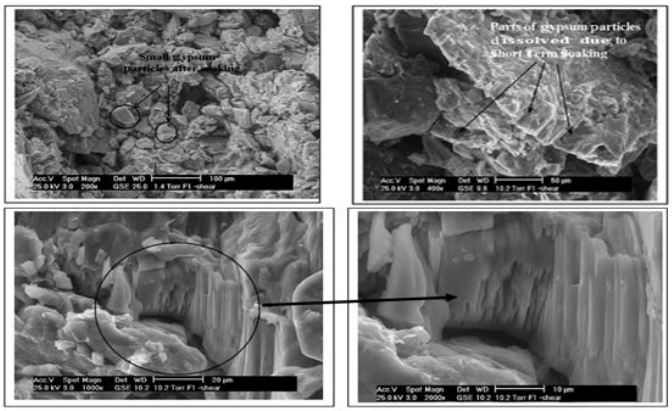

Fig. 8. SEM for Tikrit soil sample subjected to short term soaking.

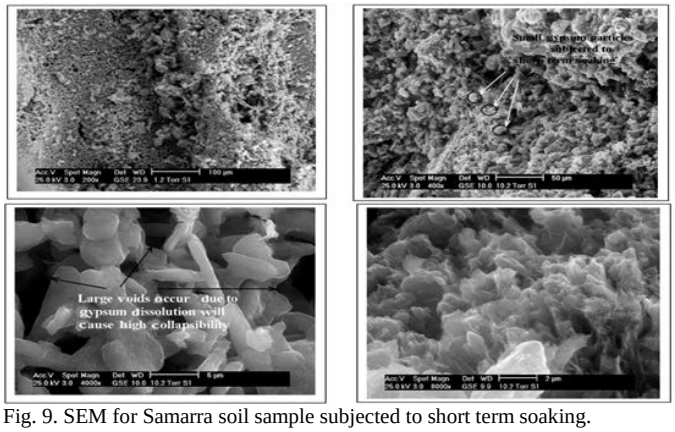

Fig. 9. SEM for Samarra soil sample subjected to short term soaking.

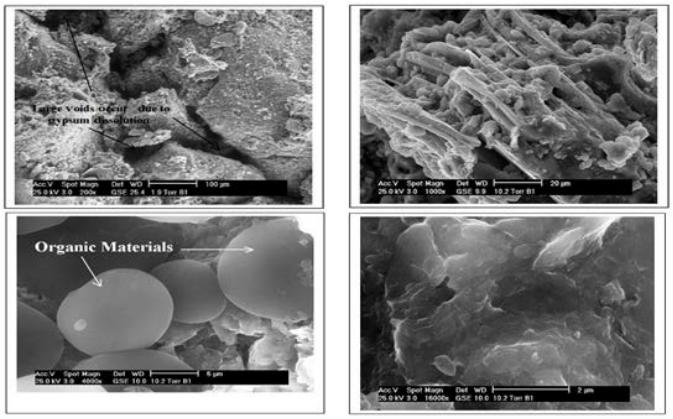

Fig.10. SEM for Baiji soil sample subjected to short term soaking.

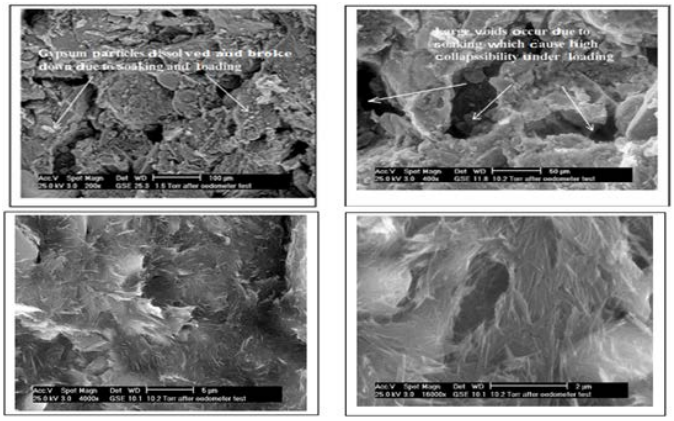

Fig. 11. SEM for Tikrit soil sample subjected to single collapse test.

IV. CONCLUSION

In this work, a microstructure study of Iraqi gypseous soil samples in their natural state and after short term soaking was made for three site locations with different gypsum contents. In the light of experimental tests, the following conclusions can be drawn:

1. The tested gypseous soils exhibit very high shear strength when dry, but a loss of strength basically in cohesion is well observed for soaked specimens with a reduction of about 94% with slight reduction in the internal friction angle. This behavior may be due to bonds destruction in the soil after soaking.
2. From SEM results, appreciable microstructural changes are observed and identified such as voids and solid regions in the micrographs. Also gypsum fibers are very clearly appeared as binding materials.
3. The micrographs of soils subjected to short term soaking showed the occurrence of large voids which are responsible for the higher collapsibility in such soils due to high solubility of gypsum in water.

ACKNOWLEDEMENT

This work was supported by Iraqi Ministry of Higher Education and Scientific Research for the 3rd author. Sincere thanks are expressed to the staff of the Soil Mechanics Laboratory at Bauhaus-Universität Weimar in Germany for their assistance in carrying out the laboratory tests. Deep thanks are also expressed to F.A. Finger-Institute and to the Chemical Laboratories at Bauhaus-Universität Weimar for ESEM, X-Ray and chemical tests.

REFERENCES

[1] A. A. Al-Mufty, "Effect of gypsum dissolution on the mechanical behaviour of gypseous soils", Ph.D thesis, Civil Eng. Dep., University of Baghdad, Baghdad, Iraq, 1997.

[2] N. K. S. Al-Saoudi, I. M. A. Al-Nouri, and A. A. H. Sheikha, "The collapsible behavior of gypseous soils," *Jordanian Geologists Association, the 7th Jordanian Geological Conference*, 2011.

[3] M. M. Al-Ani, and S. N. Seleam, "Effect of initial water content and soaking pressure on the geotechnical properties of gypseous soils," *J. of Al-Muhandis*, No.116, 1993.

[4] O. Al-Farouk, S. Al-Damluji, A. Al-Obaidi, R. Al-Omari, M. Al-Ani, and M. Fattah,"Experimental and numerical investigations of dissolution of gypsum in gypsiferrous Iraqi soils", in M. Hamza et al., Ed., *Proc. of the 17th Inter. Conf. on Soil Mechanics and Geotechnical Engineering*, IOS Press, 2009, pp. 820-824.

[5] I. H. Nashat, "Engineering characteristics of some gypseous soils in Iraq", Ph.D thesis, Civil Eng. Dep., University of Baghdad, Baghdad, Iraq, 1990.

[6] J. K. Mitchell, "*Fundamentals of soil behavior*," 2nd ed., John Wiley and Sons Inc, 1993.

[7] G. Lefebvre, "Collapse mechanisms and design considerations for some partly saturated and saturated soils," in E. Derbyshire et al., Ed., Genesis and properties of collapsible soils, Kluwer Acad. Pub., 1995, pp. 361-374.

[8] *BS 1377: 2A (British Standard Institution)*, Method of test for soils for civil engineering purposes, British Standard Institution, London, UK, 1990.

[9] *BS 1377:3 (British Standard Institution)*, Method of test for soils for civil engineering purposes, Chemical and electro-chemical tests, British Standard Institution, London, UK, 1990.

[10] *ASTM D2216*, Standard test method for laboratory determination of water (moisture) content of soil and rock by mass, Annual book of ASTM standards, vol. 04.08, West Conshohocken, PA, 1998, pp. 1-5.

[11] *BS 1377:6B*, Method of test for soils for civil engineering purposes, Chemical and electro-chemical tests, British Standard Institution, London, UK, 1990.

[12] *ASTM D422*, Standard test method for particle size analysis of soils, Annual book of ASTM standards, vol. 04.08, ASTM International, West Conshohocken, PA, 2002, pp. 1-8.

[13] *ASTM D3080*, Standard test method for direct shear test of soils under consolidated drained conditions, Annual book of ASTM standards, Vol. 04.08, ASTM international, West Conshohocken, PA, 1998, pp.1- 6.

[14] J. Herrero, and J. Porta, "The terminology and concepts of gypsum-rich soils," *Geoderma*, vol. 96, 2000, pp. 47-61.

[15] Z. M. Mansour, Z. Chik, and M. R. Taha, "On the Procedures of soil collapse potential evaluation," *J. of Applied Sciences*, vol. 8, 2008, pp. 4434-4439.

[16] I. Jefferson, and C. Rogers, "ICE manual of geotechnical engineering," vol. 1 of ICE manuals, ICE Publishing, London, UK, 2012.

Prof. Dr. Hussein Hameed Karim received the B.S. and M.S. degrees in Earth Science/ Geophysics from the University of Baghdad, in 1978 and 1982 respectively, and the Ph.D. degree in Engineering Geophysics from University of Baghdad in 1996, Iraq.

From 1983 to 1997 he was within the academic staff of University of Basrah and graduated from Asst. lecturer to Asst. Professor. Since 1997 he is within the academic staff of University of

Technology. Since 2000, he has been a Professor with the Building & Construction Engineering Department/ University of Technology. He is the supervisor of more than 45 post graduate (M.Sc. and Ph.D) students, the author of 5 books, and one under preparation, more than 100 scientific researches, more than 100 scientific articles, and two patents. His research interests include Engineering Geophysics, Soil & Rock Mechanics, Site Investigation, and Geomatics Engineering.

Prof. Karim was chosen by the Committee of University of Technology as the 1st Professor in the University of Technology for the academic year (2010-2011). Prof. Karim's awards and honors include training session to Bordeaux University- France (4 months, 1984); Visiting Professor to University of Hodeidah University- Yemen (3 months, 2002); Visiting Professor (one month, 2010) to Malaya University- Kuala Lumpur, Malaysia; and 3 Professor Visits sponsored by DAAD (Germany), Bauhaus University- Weimar 2006, Rhur University – Bochum 2010 and 2014 (3-months for each).

Implementation of Electrical Resistivity Imaging (ERI) Technique For Near Surface Investigation

Hussein H. Karim*

***Abstract*—The present study deals with field implementation of 1D and 2D Electrical Resistivity Imaging (ERI) survey to investigate the subsurface resistivity distribution related to near surface features. The three common arrays (Wenner, Wenner-Schlumberger and dipole-dipole) were used for 2D survey, while Schlumberger array was used for 1D vertical electrical sounding (VES). The length of each spread was 40 m with depth of penetration of was 5-8m. The study stated that the pseudosections are useful to present the measured apparent resistivity, while the inversion sections represent the final picture of the true subsurface resistivity. The two-dimensional inversion was used to invert the apparent resistivities to their corresponding true values. Different arrays strength and also different depth of investigation have been obtained according to their resolving power and ability for detecting lateral and vertical variations which is clearly represented by different contour shapes in the pseudosections that map the same region. The resistivity distribution of the inversion models for the study site reflects the highly inhomogeneous subsurface soil with a wide variation of soil resistivity at different depths. Three main geoelectric layers have been distinguished with resistivity range values <1- >50 ohm.m representing silty clay with some sand and gravel with relatively higher resistivity values; silty clay with some amount of sand with a value of about 5 ohm.m; and saturated silty clay-clayey soil with low resistivity (< 1 ohm.m). In addition to the presence of pockets of some anomalous areas related to the existing organic materials (date palm roots).**

***Index Terms*—1-D VES, 2D Electrical Resistivity Imaging, Soil, Near Surface Investigation**

I. Introduction

THE resistivity method is an efficient tool and also one of the most commonly applied technique for geophysical investigation in geotechnical site investigations. This is due to the ability of detecting cavities, sinkholes, karsts, voids, walls and other man-made structures and because of the low cost of the investigation and the fact that there is resistivity contrast between these structures and the surrounding soil. Furthermore, the high technological development of computer controlled multi-electrode survey systems and the development of 2- and 3-dimensional resistivity inversion software packages, resulted to more effective surveys and reliable resistivity high resolution images [1] [2]. During the last few decades, several electrical resistivity procedures have been used. Among these procedures were the implementations of 2 and 3D Electrical Resistivity Imaging (or Tomography) (ERI or ERT). In many geological conditions, the 2D electrical imaging surveys can produce results that are complimentary to the information obtained from other geophysical methods. The most commonly used arrays in the 2D electrical imaging surveys are conventional arrays such as Wenner, Schlumberger or dipole-dipole arrays. These arrays are often well understood in terms of their depths of investigations, lateral and vertical resolution and signal- to-noise ratios. At the present time, the 2D surveys are the most practically economic compromise both in achieving accurate results and in limiting the survey cost [1].

These surveys are considered to be the most applicable for geotechnical investigation. Besides, the ground resistivity is related to various geological parameters such as the detecting minerals and sub-surface ground water, fluids content, porosity and degree of water saturation in soils/rocks. Electrical resistivity surveys have been used for many decades in hydrogeological, geothermal and environmental and archeological investigations [3] - [5].

The present study is aimed to show the efficiency of 2-D Electrical Resistivity Imaging (ERI) in probing the subsurface soil for site investigation, in addition to highlight the characteristics of pseudo and inversion sections with different arrays and their resolving power.

II. Electrical Resistivity- Basic Theory

The ground resistivity is related to various geological parameters such as the minerals and fluids content, porosity and degree of water saturation in soils/rocks. Electrical resistivity surveys have been used for many decades in geotechnical, hydrogeological, mining, geothermal and environmental investigations. The purpose of electrical surveys is to determine the subsurface resistivity distribution by making measurements on the ground surface by means of four electrodes (two current electrodes A and B and two potential electrodes M and N) which can be placed at arbitrary locations on the surface. Electric currents are introduced into the ground and the resulting potential differences are

Manuscript received April 20, 2015; accepted August 23, 2015.

*Professor, Building and Construction Engineering Department, University of Technology, Baghdad, Iraq. (e-mail: husn_irq@yahoo.com).

measured at the surface. Deviations from the pattern of potential differences expected from homogeneous ground provide information on the form and electrical properties of subsurface inhomogeneities [6]. From these measurements, the true resistivity of the subsurface can be estimated.

The surveys, depending on the areas heterogeneities can be performed in three different models (1-, 2-, and 3-D) and also at different scales resolution (Fig. 1). 1D resistivity sounding method is preferable for aquifers but its greatest limitation is that it does not take into account horizontal changes in the subsurface resistivity. A more accurate model of the subsurface is the 2 and 3D imaging models where the resistivity changes in the vertical direction, as well as in the horizontal direction along the survey line, and are now practical commercial techniques with the relatively recent development of multi-electrode resistivity surveying instruments [7] and fast computer inversion software [8].

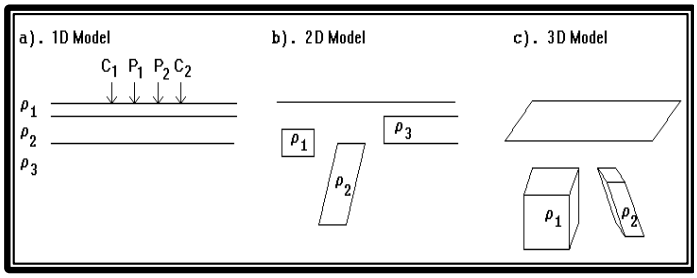

Fig. 1. Three different models used in the interpretation of resistivity measurements.

At the present time, the 2D surveys are the most practically economic compromise both in achieving accurate results and in limiting the survey cost [1]. In many geological conditions, the 2D electrical imaging surveys can produce results that are complimentary to the information obtained from other geophysical methods. There are numerous configurations or arrangements for placing the current and potential electrodes for surveying. In practice, the conventional arrays that are most commonly used in resistivity surveys are (a) Wenner (b) dipole-dipole, and (c) Wenner- Schlumberger (Fig. 2).

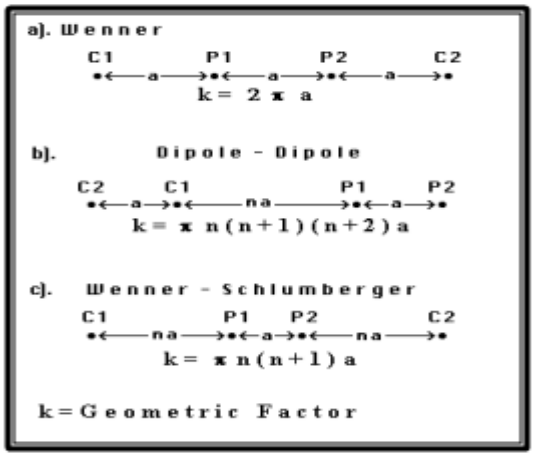

Fig. 2. Common arrays used in resistivity surveys and their geometric factors.

III. FIELD WORK AND DATA ACQUISITION

The current research is based on the 2-D field work and data carried out by [9] in the University of Technology site. As a complementary study, the present author made a new 1-D survey in the same site to compare results with more analysis and interpretation. Boreholes data (Table 1) and soil profile (Fig. 3) show three major subsoil stratifications that are distinguished at the site [10]. The top layer consists of silty clay with less amounts of sand and more less of gravel extending from ground surface to about 4.5 m in depth with water table <1m. The second layer (4.5-10.5 m) consists of silty clay with fine sand, at about 5.5 m within this layer perched unclean water exists; The third layer (10.5- E.O.B 15 m) consists of clean sandy layer with some amounts of silt. Clean water exits at about 12 m.

Table 1. Boreholes data near the site [10].

Depth (m)	**B.H.1**				**B.H.2**				**B.H.3**			
	Clay (%)	Silt (%	Sand (%)	Gravel (%)	Clay (%)	Silt (%)	Sand (%)	Gravel (%)	Clay (%)	Silt (%)	Sand (%)	Gravel (%)
1.5	47	28	15	10	43	32	14	11	41	31	18	10
3	51	29	12	8	40	33	17	10	52	46	2	0
4.5	-	-	-	-	-	-	-	-	48	47	5	0
6	51	46	3	0	57	41	2	0	57	40	3	0
7.5	52	42	6	0	56	41	3	0	55	41	4	0
9	-	-	-	-	-	-	-	-	56	40	4	0
10.5	59	36	5	0	55	41	4	0	63	35	2	0
12	-	-	-	-	0	4	94	2	-	-	-	-
15	-	-	-	-	0	3	95	2	-	-	-	-

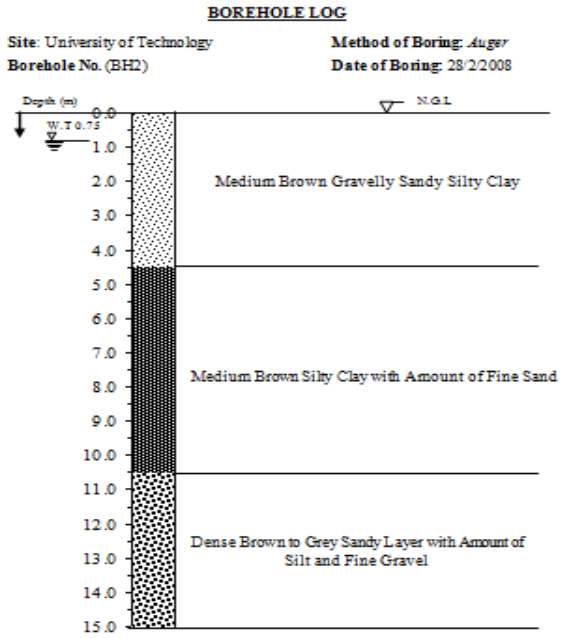

Fig. 3. Stratigraphic column for the existed borehole in the site [11].

The method adopted in the field investigation is the 2-D electrical resistivity imaging technique. The ERI investigations were carried out along a profile lane in the site using three arrays. Terrameter SAS 4000 of the Building and Construction Engineering Department–University of Technology was used in this study (Fig. 4).

Fig. 4. Terrameter SAS 4000with 2D electrical imaging spread at the site.

2-D Survey Design

Multiple surveys can be planned in order to image the vertical as well as horizontal extent of subsurface variations. For two-dimensional field work, the multi-core cable is attached to an electronic switching unit which is connected to a laptop computer. In a typical survey, most of the fieldwork is in laying out the cable and electrode and most of the survey time is spent waiting for the resistivity meter to complete the set of measurements. After selecting the appropriate array and electrodes spacing for each measurement, the measurements are taken automatically and stored in the computer.

A variety of specific electrode arrangements are commonly employed. Each layout offers advantages in equipment handling or in measurement instrumentation. Taking into account both existing geotechnical and geological information about the site and the advantages of the ERI technique, several arrays must be initially applied. Then one can decide the most suitable arrays to be considered and used for such investigation according to their suitability for field conditions, providing high signal strength and having adequate penetration depth. Three common arrays have been used in the present survey; these are Wenner, dipole-dipole, and Wenner-Schlumberger [12] [13]. 41 steel electrodes were placed in a line with 1 m separation, connected to the ABEM ES464 with a LUND cable. The spread length of 40 m was used in the site (Fig. 4). The measurements of these arrays consist of many sequences and each sequence has many subsequences with different steps. Each array combines the advantages and disadvantages.

IV. DATA INTERPRETATION

After the field survey, the resistance measurements are reduced to apparent resistivity values. Practically, the SAS system is provided with the computer software to carry out this conversion. In this section, a general look is given at the steps involved in converting the apparent resistivity values into true resistivity (for 1-D) and into resistivity model section (for 2-D) that can be used for interpretation.

1-D Resistivity Survey

The classical Schlumberger array is one of the most commonly used array for resistivity sounding surveys. Verical electrical sounding (VES) using Schlumberger array was made with electrode spacing (AB = 40 m) and (MN = 10m). Thirteen measurements were made along the spread. The relation of apparent resistivity versus AB/2 and its interpretation is shown in Figure 5. It is shown that the resistivity decreases with depth and its interpretation shows three geoelectric layers with resistivities about 8, 5 and 3 ohm.m respectively with thicknesses of the first and second layers are around 3 and 4 m respectively. Correlating the 1-D survey with borehole log (Fig. 5), it is clearly shown the agreement between both results. The first geoelectric layer represents medium gravelly sandy and silty clay assigned to the relatively higher resistivity value (8 ohm. m) and 3 m thick. While the second electric layer corresponds to silty clay with some amount of sand, with 5 ohm.m and around 4 m

thick. While the third layer with resistivity of <1 ohm.m which is assigned to saturated silty clay soil. Clayey soil is known to be relatively impermeable, but sandy soil which is relatively permeable, thus the clayey soils, which have a relatively lower resistivity, can be easily distinguished from the sandy soils. The interpretation model from this survey was confirmed by the existed borehole along the survey line.

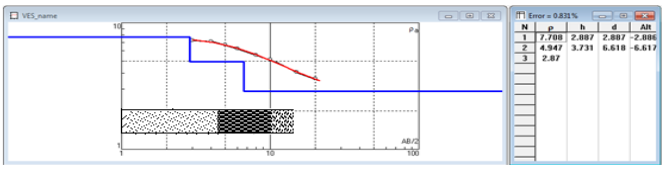

Fig. 5. 1-D VES using Schlumberger array showing apparent resistivity versus AB/2 with its interpretation.

2–D Resistivity Surveys

Pseudosection data

The program, RES2DMOD.EXE, is a 2-D forward modeling program which calculates the apparent resistivity pseudosection for a user defined 2-D subsurface model. With this program, the user can choose the finite-difference or finite-element [14] method to calculate the apparent resistivity values. In the program, the subsurface is divided into a large number of small rectangular cells. The program might also assist the user in choosing the appropriate array for different geological situations or surveys. Applying this program, one can get a feel of the effects of array type over the size and shape of the contours in the pseudosection.

To plot the data from a 2-D imaging survey, the pseudosection contouring method is normally used. In this case, the horizontal location of the point is placed at the mid-point of the set of electrodes used to make that measurement. The vertical location of the plotting point is placed at a distance which is proportional to the separation between the electrodes. The final step is to plot the data from a 2-D imaging survey using RES2DINV software which will give three sections: measured and calculated apparent resistivity pseudosections and inverse model resistivity section.

Fig. 6 shows the 2-D imaging resistivity survey for the selected arrays. The pseudosection gives a very approximate picture of the true subsurface resistivity distribution. However the pseudosection gives a distorted picture of the subsurface because the shape of the contours depends on the type of array used as well as the true subsurface resistivity. The pseudosection is useful as a means to present the measured apparent resistivity values in a pictorial form, and as an initial guide for further quantitative interpretation. One common mistake made is to try to use the pseudosection as a final picture of the true subsurface resistivity. Besides, different arrays used to map the same region can give rise to very different contour shapes in the pseudosection plot. Also these sections give an idea of the data coverage that can be obtained with different arrays. One useful practical application of the pseudosection plot is for picking out bad apparent resistivity measurements. Such bad measurements usually stand out as points with unusually high or low values.

(a) Wenner

(b) Dipole-Dipole

(c) Wenner-Schlumberger

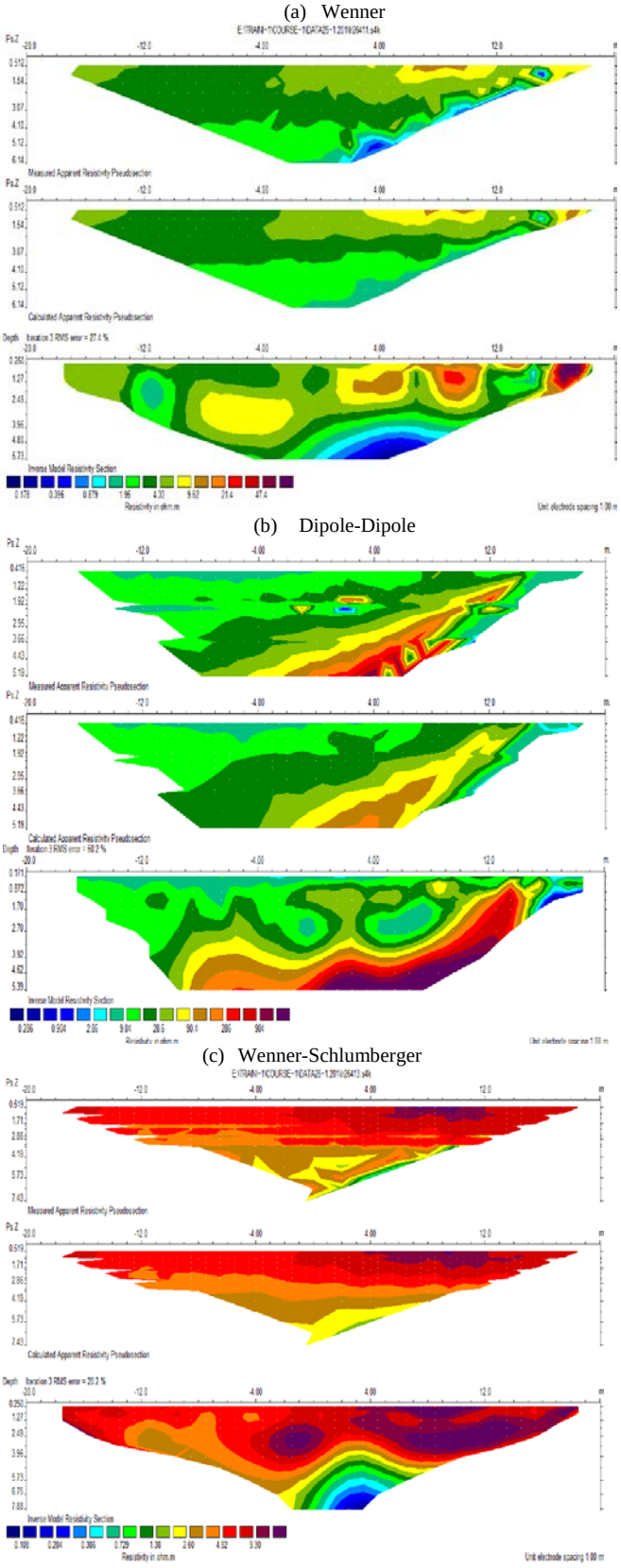

Fig. 6. 2-D imaging resistivity survey for the selected arrays.

Resolving power of the used arrays

The RES2DMOD.EXE program shows that the shape of the contours in the pseudosection produced by the different arrays over the same structure can be very different. The choice of the "best" array for a field survey depends on the type of structure to be mapped, the sensitivity of the resistivity meter and the background noise level. Among the characteristics of an array that should be considered are: the sensitivity of the array to vertical and horizontal changes in the subsurface resistivity; the depth of investigation; the horizontal data coverage; and the signal strength.

Fig. 6 (a to c) shows the results of the resistivity surveys using Wenner, dipole-dipole and Wenner-Schlumberger arrays respectively. The different arrays used to map the same region give rise to very different contour shapes in the pseudosection plot as indicated by dipole-dipole array which might be due to its high root mean square (RMS) of around 60% or more obtained using 3 to 10 iterations compared to around 20% obtained in the Wenner and Wenner-Schlumberger arrays using 5 iterations remaining with this value till 10 iterations. The sensitivity pattern for the Wenner-Schlumberger array is slightly different from the Wenner and dipole-dipole arrays with a slight increase in resistivity values below the centre of the array, and slightly lower sensitivity values in the regions between the C1 and P1 (and also C2 and P2) electrodes. The difference in the contour pattern in the sensitivity function plot helps to explain the response of the different arrays to different types of structures as shown in the inverted resistivity sections for the three arrays are shown in Fig. 6 (a to c).

It is worthy to note that as the electrode spacing increases, the number of measurements decreases. The number of measurements that can be obtained for each electrode spacing, for a given number of electrodes along the survey line, depends on the type of array used. The Wenner array gives the smallest number of possible measurements compared to the other common arrays that are used in the present 2-D surveys. The number of readings, observed and theoretical maximum depth, total number of data level and the spent time of measurement for each type of array are shown in Table 2. The median depth of investigation gives an idea of the depth to which we can map with a particular array. The median depth values are determined by integrating the sensitivity function with depth. If there are large resistivity contrasts near the surface, the actual depth of investigation could be somewhat different. The spent time gives an idea about the number of readings. Note that the dipole-dipole array gives the widest horizontal coverage, while the coverage obtained by the Wenner and Wenner-Schlumberger arrays decreases much more rapidly with increasing electrode spacing.

Array Type	No. of Readings	Observed Max. Depth (m)	Calculated Max. Depth (m)	Total No. of Data Levels	Spent Time of Measurement (min)	RMS (%)
Wenner	177	5.73	5.56	8	30	20-22
Dipole-Dipole	321	5.39	4.81	14	45	57-60
Wenner-Schlumberger	312	7.88	7.6	17	40	19-20

Table 2. The median depth of investigation for the different arrays.

The 2-D survey carried out with Wenner array (Fig. 6a) reflects the sensitivity plot for this array which has almost horizontal contours beneath the centre of the array. Because of this property, Wenner array is relatively sensitive to vertical changes in the subsurface resistivity below the centre of the array. However, it is less sensitive to horizontal changes in the subsurface resistivity. In general, Wenner is good in resolving vertical changes (i.e. horizontal structures), but relatively poor in detecting horizontal changes (i.e. narrow vertical structures). It can be seen that for Wenner array, the median depth of investigation is approximately 0.5 times the "a" spacing used (Table 3) [15]. Compared to other arrays, Wenner array has a moderate depth of investigation. The signal strength is inversely proportional to the geometric factor used to calculate the apparent resistivity value for the array (Fig. 2). For Wenner array, the geometric factor is $2\pi a$, which is smaller than the geometric factor for other arrays. Among the common arrays, Wenner array has the strongest signal strength. This can be an important factor if the survey is carried in areas with high background noise. One disadvantage of this array for 2-D surveys is the relatively poor horizontal coverage as the electrode spacing is increased (Fig. 6a). This could be a problem when a relatively small number of electrodes is used.

Table 3. The median depth of investigation (z_e) for the different arrays. L is the total length of the array. Where a is the maximum electrode "a" spacing, or maximum array length "L" [15].

Array type		z_e/a	z_e/L
Wenner		0.519	0.173
Dipole-dipole	n = 1	0.416	0.139
	n = 2	0.697	0.174
	n = 3	0.962	0.192
	n = 4	1.220	0.203
	n = 5	1.476	0.211
	n = 6	1.730	0.216
Wenner - Schlumberger			
	n = 1	0.52	0.173
	n = 2	0.93	0.186
	n = 3	1.32	0.189
	n = 4	1.71	0.190
	n = 5	2.09	0.190
	n = 6	2.48	0.190

For dipole-dipole array, the sensitivity function plot in Fig. 6b shows that the largest sensitivity values are located between the C2- C1 dipole pair, as well as between the P1-P2 pair. This means that this array is most sensitive to resistivity changes between the electrodes in each dipole pair. Note that the sensitivity contour pattern is almost vertical. Thus, the dipole-dipole array is very sensitive to horizontal changes in

resistivity, but relatively insensitive to vertical changes in the resistivity. That means it is good in mapping vertical structures, such as cavities, but relatively poor in mapping horizontal structures such as sedimentary layers. The median depth of investigation of this array also depends on the "n" factor, as well as the "a" factor (Table 3). In general, this array has a shallower depth of investigation compared to Wenner array. However, for 2-D surveys, this array has better horizontal data coverage than Wenner (Fig. 6b). One possible disadvantage of this array is the very small signal strength for large values of the "n" factor.

Regarding Wenner-Schlumberger arrays which is the new hybrid between Wenner and Schlumberger arrays [16] arising out of relatively recent work with electrical imaging surveys. The sensitivity pattern for Wenner-Schlumberger array (Fig. 6c) is slightly different from the Wenner array with a slight vertical curvature below the centre of the array, and slightly lower sensitivity values in the regions between the C1 and P1 (and also C2 and P2) electrodes. There is a slightly greater concentration of high sensitivity values below the P1-P2 electrodes. This means that this array is moderately sensitive to both horizontal and vertical structures. In areas where both types of geological structures are expected, this array might be a good compromise between Wenner and dipole-dipole array. The median depth of investigation for this array is about 10% larger than that for Wenner array for the same distance between the outer (C1 and C2) electrodes. The signal strength for this array is smaller than that for the Wenner array, but it is higher than the dipole-dipole array.

Wenner-Schlumberger array has a slightly better horizontal coverage compared with Wenner array. The horizontal data coverage is slightly wider than Wenner array (Figs. 6a and 5c), but narrower than that obtained with the dipole-dipole array (Fig. 6b).

Soil electrical resistivity and its spatial variability

To assess the quantitative relationships between soil electrical resistivity and its spatial variability for some anomalous areas, Figure 7 shows this relation based on the results of the resistivity surveys. The range of resistivity values for Wenner array is ranging from <1 to 50 ohm. m; for dipole-dipole are <1 to >500 ohm. m; and for Wenner-Schlumberger <1 to about 15 ohm. m. Clayey soil is known to be relatively impermeable, but sandy soil which is relatively permeable can provide an infiltration path for the pollutants to enter the aquifers.

The top layer of the profile is characterized by relatively low resistivity layer with thickness of about 5 m in the left half to < 4m in its right half. This layer represents the clayey soils, which have a relatively lower resistivity, can be easily distinguished from the sandy soils. In addition, this layer consists pockets of lower and higher resistivity values, so it is highly inhomogeneous (e.g. electrode locations 9, 17, 24, 28, 33 and 36 m). This layer shows that the subsurface consists of clay and silt with amounts of sand and sometime gravel. In addition the existence of organic materials (e.g. the roots of three adjacent date palms along the profile) could probably cause some anomalies with low or high resistivity depending whether in dry or wet conditions (e.g. electrode locations 9-10, 17-18 and 24-25 m). Very low resistivity (<1 ohm.m) is identified near water well at electrode positions 33-34 m. While a high to very high resistivity materials at electrode positions 28 and 36 m near the surface could be as a result of concrete boulder materials, which could be now buried in the sediment (Fig. 7a). At the intermediate depth (2.5-5m), three elongated anomalies with high resistivity are appeared which represent the inhomogeneity of the site and could refer to the amounts of sand and sometime gravel. At greater depth below the top soil (> 5m), in both arrays Wenner and Wenner-Schlumberger (on the contrary, dipole-dipole gives the reverse for its high RMS), the sharp decrease in resistivity (<1 ohm.m) indicates the presence of saturated soil interpreted as an perched aquifer which is confirmed by water well in the site which could be silty clayey soil. All other areas are marked by relatively low resistivity (<1 ohm.m) (blue colour), indicating the presence of fine soil material and increase in the percentage of clay in soil matrix.

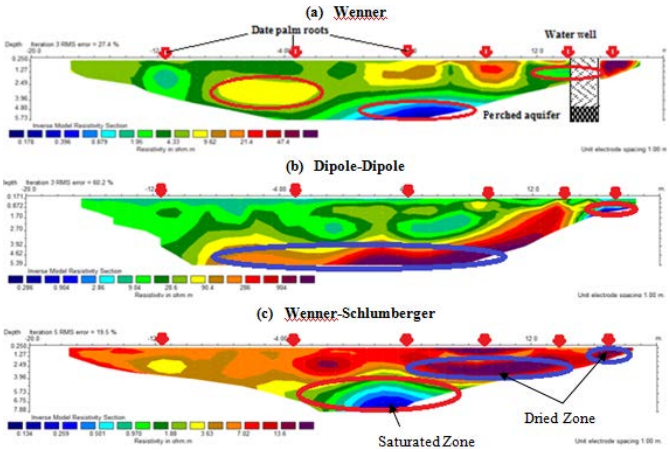

Fig. 7. 2-D imaging soil resistivity survey for the selected arrays and its spatial variability.

V. CONCLUSION

Conclusion remarks may be summarized as follows:

1. The pseudosections are useful to present the measured apparent resistivity. While, Inversion sections represent the final picture of the true subsurface resistivity.
2. The different arrays strength and depth of investigation are due to their resolving power which is clearly represented by different contour shapes that map the same region as indicated by dipole-dipole array which might be due to its high root mean square (RMS).
3. Wenner array gives the smallest number of possible measurements has a moderate depth of investigation compared to other arrays with relatively poor 2-D horizontal coverage as the electrode spacing is increased.
4. Generally, dipole-dipole array gives the highest number of possible measurements and has shallower depth of investigation compared to Wenner and Wenner-

Schlumberger arrays. However, for 2-D surveys, this array gives the widest horizontal coverage with increase in the number of measurements.

5. Wenner-Schlumberger gives moderate number of possible measurements and has a median depth of investigation of about 10% larger than that for Wenner array and its coverage decreases much more rapidly with increasing electrode spacing compared to dipole-dipole array.
6. The studied site is highly inhomogeneous represented by its clayey soil with lower resistivity compared to sandy soils. Good correlation is obtained between 1-D survey and borehole log. Three main geoelectric layers have been distinguished with resistivity range values <1- >50 ohm.m representing silty clay with some sand and gravel with relatively higher resistivity values; silty clay with some amount of sand with a value of about 5 ohm.m and saturated silty clay-clayey soil with low resistivity (<1 ohm.m). In addition to the presence of some anomalies related to existing organic materials (the roots of adjacent date palms).

REFERENCES

[1] T. Dahlin, "2D resistivity surveying for environmental and engineering applications," *First Break*, vol. 14, 1996 pp. 275-284.

[2] D. S. Parasnis, *Principles of Applied Geophysics*, 5th ed., Chapman & Hall, 1997.

[3] L. Heather, S. Reccelli, A. S. Berth, L. Jeffery, P. G. Leberfinger, and J. W. Jeffery, "Electrical Imaging: A method for identifying potential collapse and other karst features near roadways," Science Applications international cooperation Middletown Pennsylvania, *50th Annual Highway geology symposium*, 1999.

[4] M. H. Loke, and R. D. Barker, "Rapid least-squares inversion of apparent resistivity pseudosections using a quasi-Newton method", *Geophysical Prospecting*, vol. 44, 1996, pp. 131-152.

[5] T. Günther, "Inversion Methods and Resolution Analysis for the 2D/3D Reconstruction of Resistivity Structures from DC Measurements," Ph.D. thesis, University of Mining and Technology, Freiberg, Germany, 2005. www.ivsl.org.

[6] P. Kearey, M. Brooks, and I. Hill, *An introduction to geophysical exploration*, Blackwell Science, 2002.

[7] D. H. Griffiths, J. Turnbull, and A. I. Olayinka, "Two dimensional resistivity mapping with a computer controlled array," *First Break*, vol. 8, 1990, pp.121-129.

[8] M. H. Loke, "The inversion of two-dimensional resistivity data," Ph.D thesis, Un. of Birmingham, 1994.

[9] H. H. Karim, I. A. K. Alwan, and M. A. Al-Neami, "Characteristics of 2-D electrical resistivity imaging survey for soil," *Eng. & Tech J.*, vol. 31, Part A, No. 19, 2013, pp.70-89.

[10] *Consulting Engineering Bureau- University of Technology*, "Site exploration report at the University of Technology", 2008.

[11] A. Samouelian, I. Cousin, A. Tabbagh., A. Bruand, and G. Richard, "Electrical resistivity survey in soil science: a review," *Soil Tillage Research*, 2005, pp.1-28.

[12] M. H. Loke, "Tutorial: 2D – 3D electrical imaging surveys," 2004, 128 P.

[13] A. Dey, and H. F. Morrison, "Resistivity modelling for arbitrary shaped two-dimensional structures," *Geophysical Prospecting*, vol. 27, 1979, pp. 1020-1036.

[14] P. P. Silvester, and R. L. Ferrari, *Finite elements for electrical engineers*, 2nd ed., Cambridge University Press, 1990.

[15] M. H. Loke, "Electrical imaging surveys for environmental and engineering studies: A practical guide to 2-D and 3-D surveys," 1999, 61 P.

[16] O. Pazdirek, and V. Blaha, "Examples of resistivity imagine using ME-100 resistivity field acquisition system," *EAGE 58th conference and technical exhibition extended abstract*, Amsterdam, 1996.

Prof. Dr. Hussein Hameed Karim received the B.S. and M.S. degrees in Earth Science/ Geophysics from the University of Baghdad, in 1978 and 1982 respectively, and the Ph.D. degree in Engineering Geophysics from University of Baghdad in 1996, Iraq.

From 1983 to 1997 he was within the academic staff of University of Basrah and graduated from Asst. lecturer to Asst. Professor. Since 1997 he is within the academic staff of University of Technology. Since 2000, he has been a Professor with the Building & Construction Engineering Department/ University of Technology. He is the supervisor of more than 45 post graduate (M.Sc. and Ph.D) students, the author of 5 books, and one under preparation, more than 100 scientific researches, more than 100 scientific articles, and two patents. His research interests include Engineering Geophysics, Soil & Rock Mechanics, Site Investigation, and Geomatics Engineering.

Prof. Karim was chosen by the Committee of University of Technology as the 1st Professor in the University of Technology for the academic year (2010-2011). Prof. Karim's awards and honors include training session to Bordeaux University- France (4 months, 1984); Visiting Professor to University of Hodeidah University- Yemen (3 months, 2002); Visiting Professor (one month, 2010) to Malaya University- Kuala Lumpur, Malaysia; and 3 Professor Visits sponsored by DAAD (Germany), Bauhaus University- Weimar 2006, Rhur University – Bochum 2010 and 2014 (3-months for each).

Impact of Gradation and Modifier on Moisture Susceptibility of Iraqi Hot-Mix Asphalt

Dr. Alaa Hussein Abed * and Dr. Zaynab I. Qassim**
*Assistant. Professor / Civil Engineering Department /University of AL-Nahrain, Baghdad -Iraq
Call Phone: 00964- 7706911226
Email: Alaah29@yahoo.com
** Lecturer / Building and Construction Department/ University of Technology, Baghdad -Iraq
Call Phone: 00964-7722661262
Email: zaynab.2010@yahoo.com

***Abstract*— Moisture damage in asphalt mixtures refers to loss in strength and durability due to the presence of water. Iraqi road network is showing severe deterioration such as raveling and stripping because the bond between aggregates and asphalt film is broken due to water intrusion.**

The primary objectives of this research are evaluating the factors influencing on susceptibility of pavements to moisture damage and assessing the effect of additives on asphalt concrete mixtures which has been assessed through moisture damage resistance. To meet the objective of this research, available local materials were used including asphalt binder (40-50) grade or PG (64-16), aggregate with nominal maximum size of 12.5 mm, and mineral filler, two anti-stripping additives are used (Portland cement and Styrene Butadiene Styrene polymer SBS) in this research. The Superpave mix design system was adopted with varying volumetric composition. The Superpave Gyratory Compactor was used to compact 24 asphalt concrete cylindrical specimens. The impact of moisture damage was evaluated by indirect tensile strength test.

From the results it can be concluded that using cement as filler, tensile strength ratio TSR is increased by 5 and 3.5 percent for coarse and fine gradation at opt. design asphalt binder content, while TSR increases by 2.07 and 2.5 percent for coarse and fine gradation at modified opt. design asphalt binder content.

Also it can be concluded that TSR is increased by 6.1 and 4.5 percent when using the SBS polymer modifier for coarse and fine gradation at modified opt. design asphalt binder content for lime filler respectively, while TSR increases by 3.2 and 3.4 percent for coarse and fine gradation at modified opt. design asphalt binder content for cement filler respectively. Based on laboratory results that are judged to be simulative of field loading conditions, models were developed to predict the resistance to moisture sensitivity of compacted local asphalt concrete mixtures after considering the local material properties, stress level and environmental impacts variables. In general, laboratory results were analyzed using statistical analyses by the aid of (SPSS V22) software. Moisture sensitivity model for superpave asphalt concrete wearing course mixtures was developed.

***Index Terms*— Moisture sensitivity; Stripping; Superpave; anti-stripping additives; and SPSS software**

Manuscript received October 1, 2015. This work was supported in part by the Civil Engineering. Department of Baghdad University.

I. Introduction

THE Moisture damage of asphalt concrete is defined as the loss of strength and stability caused by the active presence of moisture, the propagation of moisture damage generally occurs through two main mechanisms: the loss of adhesion (stripping) and loss of cohesion (softening), [1]. The loss of adhesion occurs between the aggregate and surrounding asphalt binder film, while the loss of cohesion occurs within the asphalt binder itself. Although moisture damage is not a failure mode, it leads to and accelerates several pavement distresses such as rutting, raveling, shoving, and bleeding, [2].

For many years, moisture damage has been a major concern for asphalt technologists. Researchers have been searching for a test that differentiates between good and poor performing asphalt concrete mixtures from stripping potential since the 1920s, [3].

The use of various additives and modifiers in an asphalt mixture is one of the most popular, cost-effective measures adopted by transportation agencies to mitigate moisture damage as polyamines, fatty amidoamines and hydrated lime, are mostly recommended as anti-stripping additives. These additives can be found naturally or are chemically processed, these additives and modifiers are either added to asphalt binder or aggregate, additives and modifiers are added to asphalt binder, while Portland cement and hydrated lime are added to the aggregate, [4].

Al-Qadi et al, [5] concluded that the mix is greatly affected by moisture damage, as expected; the SBS addition provided the highest mix strength and was equal to the mix with hydrated lime wet. This indicates that SBS partially fulfills the intended purpose, but when used in certain climatic/environmental conditions, the increased susceptibility to moisture damage could overshadow the intended improvements.

II. Problem Statement

Maintenance of roads in Iraq costs annually high percentage of the total road construction costs or in other words, in the futures, the maintenance cost will have equaled the construction cost of new roads. Roads in Iraq usually show

excessive failures of an early stage of pavement life, as shown in Figure (1). Some factors contributing to the early failures are excessively high temperature and humidity. On highways and urban roads, damaged spots can be seen after the seasonal rains, which may cause stripping due to the properties of local aggregates. Moreover, the severe water damage problems in Iraq are due to the high water table. Therefore, the road network is facing a lot of durability problems including stripping, raveling and pothole formation.

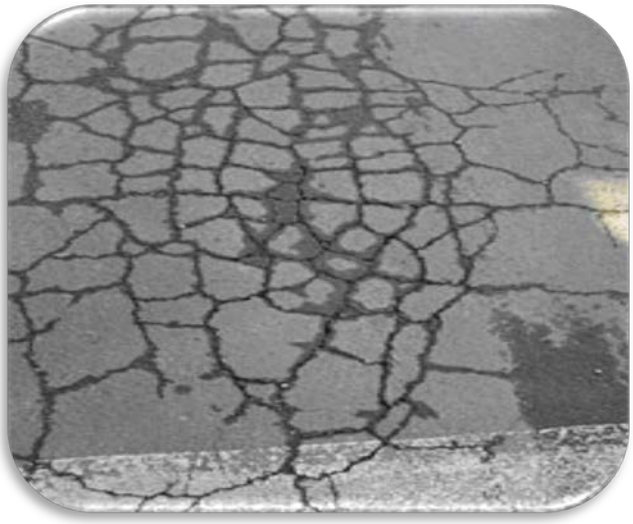

Fig. 1. : Severe Water Damage in Pavements

III. Research Objectives

The main objectives of this study are to evaluate the durability of asphalt concrete mixture prepared from locally available materials by using Superpave mix design system through assessing resistance to moisture damage of asphaltic mixtures using indirect tensile strength test. In addition to study the effect of additive on the improvement of asphalt concrete mixes against the moisture damage.

IV. Laboratory Testing

1. Material

To meet the objectives of this research, available local materials were used including asphalt binder, aggregates and mineral filler. Asphalt binders (40-50) grade or PG (64-16) was obtained from Al-Daurah refinery in Baghdad and the aggregate from Al-Nibaie quarry in north of Baghdad whereas the mineral filler was brought from lime factory in Karbala province and Portland cement is from Kubbesa factory which obtained from market. The aggregates are sieved and recombined in the proper proportions to meet the wearing course gradation as required by SCRB specifications R9, [6]. A 19 mm aggregate maximum size gradation is used in this research.

The fractions of aggregate are separated into 9 sizes, as retained on each of the following sieves, 3/4", 1/2", 3/8", No.4, No.8, No.16, No.30, No.50, and No.200) using dry sieve analysis. Mineral filler (Limestone, Portland cement) has been added according to the desired gradations requirements. The gradation curve for the aggregate is shown in Figure (2); four lines are presented: the upper, the lower curves of the Iraqi specifications of SCRB in addition to the controls points of Superpave system. In this research the Superpave mix design system was adopted with varying volumetric composition. The Superpave Gyratory Compactor was used at the National Center for Constructions Laboratories and Researches NCCLR laboratories to prepare 24 asphalt concrete cylindrical specimens for carrying out volumetric design according to Superpave system as presented in AASHTO Designation T 312 [7].

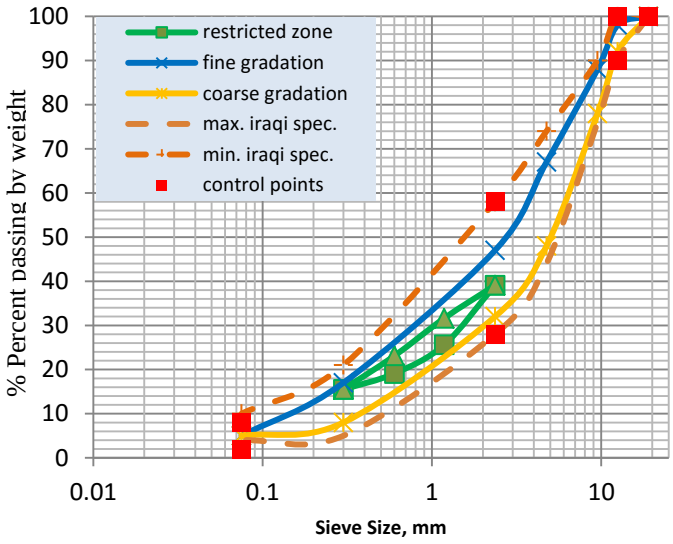

Fig. 2 : Gradation Blends with Iraqi and Superpave Requirements

2. Sample Preparation

The Superpave Gyratory Compactor can compact asphalt cylinders to a target density using loads, which are consistent to those of pavements rollers used in the highway construction. The roller compactor provides a pneumatically powered means of compacting cylinders of asphaltic material in the laboratory under conditions, which simulate in-situ compaction.

In this research, compacted asphaltic samples for indirect tensile testing are prepared at air voids equal to (7%) according to AASHTO T -283 [7].

Proportion of aggregate and asphalt binder are used for mixing, curing, and compacting. The fractions of aggregate are separated into 9 sizes, as retained on each of the following sieves, 3/4", 1/2", 3/8", No.4, No.8, No.16, No.30, No.50, and No.200) using dry sieve analysis. The aggregate retained on the 3/4" sieve is discarded. Mineral filler (Limestone) and cement have been added according to the desired gradations

requirements. The aggregate is combined on the mixing bowl and heated to the mixing temperatures prior to mixing with asphalt binder which heated to the mixing temperatures corresponding to each binder, as shown in Figure (3).

For the modified binder preparation, the asphalt cement for convention mixture is heated in the factory oven to the temperature of mixing prior to adding the specific 3 and 6 percent amount of SBS additive which is preheated in an external oven until liquid at 180 ºC, the desired weight of additive which is determined by multiplying its percent by the required weight of asphalt content which added gradually and mixed until getting homogenous binder.

The aggregate and asphalt are mixed in mixing bowel by hand on hot plate for three minutes until asphalt had sufficiently coated the surface of the aggregates or until a homogeneous mixture is achieved. The asphalt mixture was then aged in short term oven for 2 hrs at 135°C for the determination of the maximum specific gravity and 4 hrs at the same temperature for compaction in according with Asphalt institute, [8].This aging represents the aging that occurs in the field between mixing and placement and allows for absorption of the asphalt binder into the aggregate pores. The mix is stirred every 30 minutes during the short-term aging process to ensure uniform aging throughout the mix.

Compaction is then performed using the Superpave Gyratory Compactor in accordance with AASHTO Designation T 312, [7], the mold and the plates are heated in the oven at the specified compaction temperature to ensure that the mix temperature is not reduced. The load is 600 kPa which applied on the specimens to achieve proper compaction and sufficient air voids.

3. Indirect tensile strength Ratio Test

The test was performed to evaluate the moisture damage resistance of mixtures, and the procedure followed by AASHTO T -283 [7]. A set of six specimens were prepared, three specimens were tested for indirect tensile strength by storing them in a water bath at 25º C for 30 minutes, and an average value of ITS for these specimens was computed as SI (ITS for unconditioned specimens). The other three specimens were subjected to vacuum saturation followed by a freeze cycle followed by a 24 hour thaw cycle, then they were placed in a water bath at 25º C for 1 hour, and they were tested for indirect tensile strength, the average value was computed as S II (ITS for moisture-conditioned specimens). The indirect tensile strength ratio could be calculated from the following equation:

$$TSR=S_{II}/S_{I} *100 \quad \ldots\ldots\ldots\ldots\ldots\ldots\ldots\ldots (1)$$

Where:
TSR = Indirect tensile strength ratio, %
S_{I} = Average ITS for unconditioned (dry) specimens, kPa
S_{II} = Average ITS for moisture-conditioned specimens, kPa

V. Results and analysis

In this research the results of indirect tensile tests conducted on different asphaltic mixtures are analyzed and discussed through studying the impact of moisture damage on the properties of superpave asphalt concrete mixtures, the specimens were tested for indirect tensile strength ratio. Six specimens for each mixture type were tested, and the average value was obtained for each three specimens, The results of these specimens are compared, to clarify the effect of unconditioned and conditioned mixes on mixture performance, Table I shows the results of moisture sensitivity test for example, whereas eight superpave asphaltic mixtures are conducted, consisting of coarse and fine gradation, SBS modified asphalt binder and unmodified, and lime and cement filler. The indirect tensile strength (ITS) property of hot mix asphalt HMA gives an indication on the overall strength of the mix. Figures (3) and (4) depict the effect of unconditioned and conditioned mixes on indirect tensile strength for coarse and fine gradation mixtures.

Results indicate that tensile strength at 60º C for conditioned has lower resistance than unconditioned mixtures by 20.5 %, 16.6%, 18.6%, 15.7%, 15.6%, 13.8%, 14.9% and 12.7% for asphaltic mixtures numbered in Table II. Tensile Strength Ratio (TSR) has been used for predicting moisture susceptibility of mixtures. The recommended limit of (80%) for indirect tensile strength ratio (TSR) is used to distinguish between moisture susceptible mixture and moisture resistance mixtures, AASHTO T-283, [7]. Figure (5) shows the tensile strength ratio (TSR) for different mixtures, the results show that higher value of TSR for unconditioned SBS modified asphalt mixtures with cement filler, while the lowest value of TSR for conditioned conventional asphalt mixtures with limestone filler. Figures (6) and (7) show the effect of SBS modifier and cement filler on asphaltic mixtures for moisture conditioned and unconditioned samples. The results show that the modified mixtures have resistance to the action of water at optimum asphalt content mixtures, Table II shows that the SBS modified binders have higher tensile strength for conditioned mixtures in comparison to the neat binder for both cement and limestone filler aggregates.

It can be concluded that asphalts modified with SBS polymer shows less susceptibility to moisture conditioning in comparison to neat asphalts. In addition, the effect of SBS polymer is better with cement than in limestone filler due to increase in the bond between the binder and aggregate.

From the results it can be concluded that using cement as filler TSR is increased by 5 and 3.5 percent for coarse and fine gradation at opt. design asphalt binder content, while TSR increases by 2.07 and 2.5 percent for coarse and fine gradation at modified opt. design asphalt binder content.

Also it can be concluded that TSR is increased by 6.1 and 4.5 percent when using the SBS polymer modifier for coarse and fine gradation at modified opt. design asphalt binder content for lime filler respectively, while TSR increases by 3.2 and 3.4 percent for coarse and fine gradation at modified opt. design asphalt binder content for cement filler respectively.

TABLE I: MOISTURE SENSITIVITY DATA FOR COARSE GRADATION AT 4.6% DESIGN ASPHALT BINDER CONTENT AND LIME FILLER

Sample		1	2	3	4	5	6
		Conditioned			Dried		
Diameter, mm	D	150	150	150	150	150	150
Thickness, mm	t	95	105	96	102	100	95
Dry mass, g	A	3835.3	4255	3954.3	4160.1	4027.5	3864.1
SSD mass, g	B	3806.9	4226.67	3925.9	4131.7	3999.1	3835.7
Mass in Water, g	C	2147.6	2377.3	2196.6	2312.4	2229.8	2136.4
Volume, cc (B-C)	E	1659.3	1849.37	1729.3	1819.3	1769.3	1699.3
Bulk Sp Gravity	F	2.311	2.3007	2.286	2.2865	2.2762	2.273
Max Sp Gravity	G	2.45	2.45	2.45	2.45	2.45	2.45
%Air Voids (100(G-F)/G)	H	5.6617	6.0909	6.671	6.671	7.092	7.190
Vol. Air Voids (HE/100)	I	93.950	112.644	115.37	121.37	125.50	122.19
Load, N	P	-	-	-	20010	20980	20460
Saturated							
SSD mass, g	B'	3910.1	4333.2	4039	–	–	–
Mass in Water, g	C'	2420.1	2634.7	2453.2	–	–	–
Volume, cc (B'-C')	E'	1490	1698.5	1585.8	–	–	–
Vol.Abs.Water,cc (B'-A')	J'	74.8	78.2	84.7	–	–	–
% Saturation (100J'-I)	-	79.616	69.422	73.41	–	–	–
% Swell (100(E-E')/E)	-	10.207	8.1583	8.302	–	–	–
Conditioned							
Thickness, mm	t"	95	105	96	–	–	–
SSD mass, g	B"	3923.5	4346.6	4052.4	–	–	–
Mass in Water, g	C"	2117.7	2242.3	2170.5	–	–	–
Volume, cc (B"-C")	E"	1805.8	2104.3	1881.9	–	–	–
Vol. Abs.Water,cc (B"-A")	J"	88.2	91.6	98.1	–	–	–
% Saturation (100J"-I)	-	93.87	81.317	85.024	–	–	–
% Swell (100(E"-E)/E)	-	8.823	13.784	8.819	–	–	–
Load, N	P"	16650	16100	15840	–	–	–
Dry Strength(2000P/(tDp))	S_{td}	–	–	–	832.47	890.28	913.91
Wet Strength(2000P"/t"Dp))	S_{tm}	700.17	650.672	743.73	–	–	–
Average Dry Strength (KPa)		–			878.8953		
Average Wet Strength (KPa)		698.1945			–		
%TSR, tensile strength ratio		0.7944% (80%min)					

TABLE II: TENSILE STRENGTH RATIO FOR CONDITIONED AND UNCONDITIONED MIX.

Mix No.	Type of mix.	Average Tensile Strength for unconditioned mixtures, kPa	Average Tensile Strength for conditioned mixtures, kPa	Change in Tensile Strength,%	Tensile Strength Ratio TSR %
1	Coarse gradation at 4.6% Design Asphalt Binder Content and lime filler	878.8953	698.1945	-20.56	79.44
2	Coarse gradation at 4.6% Design Asphalt Binder Content and cement filler	1001.483	834.9946	-16.6242	83.37
3	Fine gradation at 4.9% Design Asphalt Binder Content and lime filler	987.5302	803.8497	-18.6	81.4
4	fine gradation at 4.9% Design Asphalt Binder Content and cement filler	1050.696	885.7133	-15.7022	84.29
5	coarse gradation at 4.8% Design modified Asphalt Binder Content and lime filler	1089.622	919.2508	-15.6358	84.36
6	coarse gradation at 5.0% Design modified Asphalt Binder Content and cement filler	1370.703	1180.413	-13.8827	86.11
7	fine gradation at 5.0% Design modified Asphalt Binder Content and lime filler	1146.329	975.4684	-14.905	85.09
8	fine gradation at 5.0% Design modified Asphalt Binder Content and cement filler	1350.931	1178.392	-12.7719	87.22

Fig. 3 : Indirect Tensile Strength for Unconditioned and Conditioned Coarse Gradation Mixture at 60° C

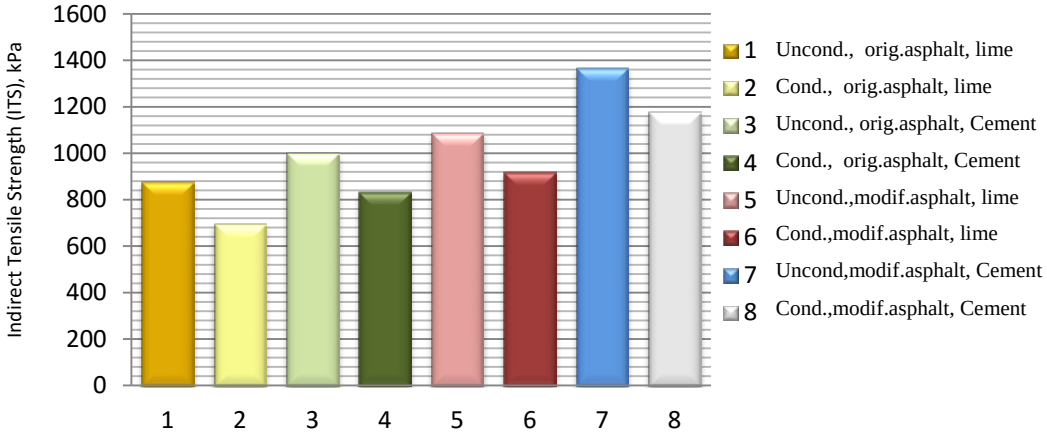

Fig. 4 : Indirect Tensile Strength for Unconditioned and Conditioned Fine Gradation Mixture at 60° C

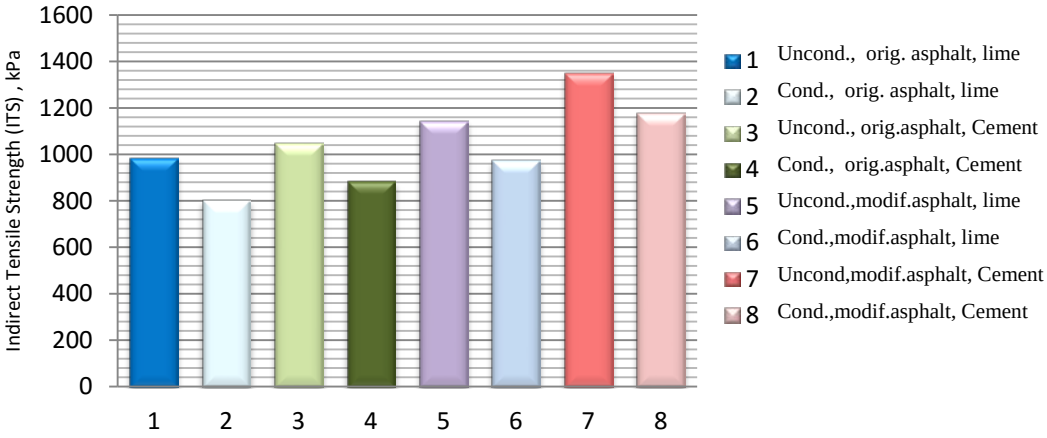

Fig. 5 : Indirect Tensile Strength Ratio for Different Asphaltic Mixtures

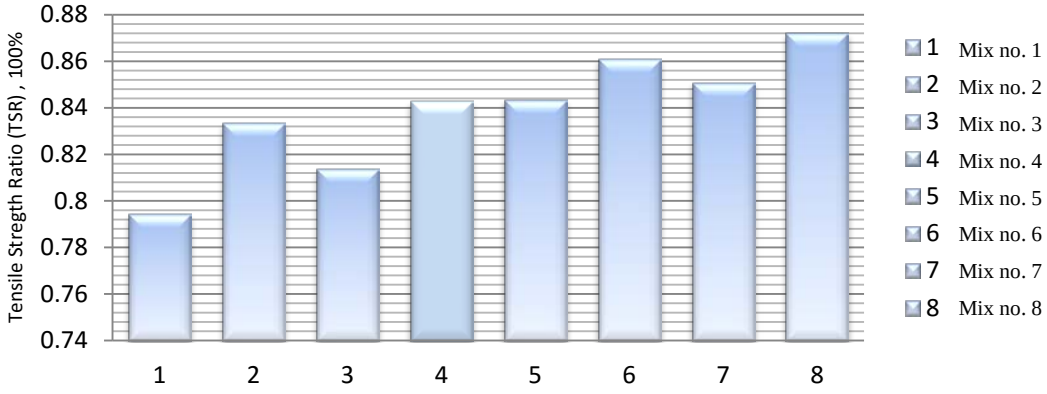

Fig.6 : Effect of SBS Additive on Moisture Sensitivity of Asphalt Mixtures

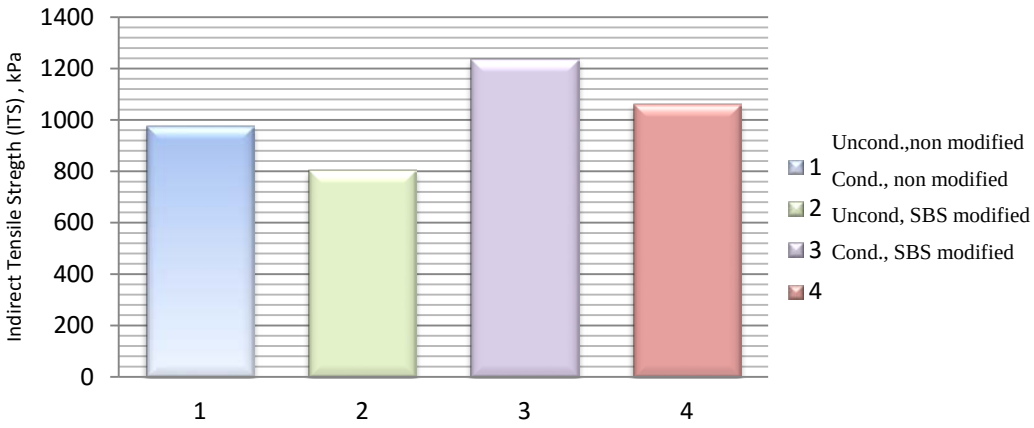

Fig.7 : Effect of Type of Filler on Moisture Sensitivity of Asphalt Mixtures

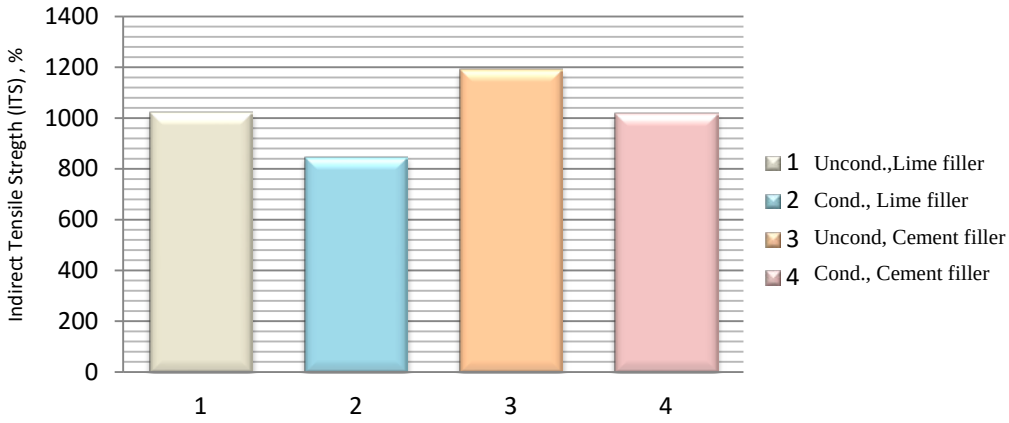

VI. Building Statistical Model

The overall objective in statistical modeling is to develop a predictive equation which correlates the moisture susceptibility in the form of indirect tensile strength with the independent variables which include: aggregate gradation, environmental condition, type of filler, and SBS additive content. Laboratory results were analyzed using statistical analyses by the aid of (SPSS V22) software. Table III shows the bivariate correlation coefficients are determined to identify the underlying form of the relationship between the dependent variable and each of the predictor variables for Moisture Susceptibility (Ms) values.

Table III: Correlation Coefficient Matrix (R) for Moisture Susceptibility (Ms)

Variable	C	G_a	V_b	F_t	Ms
C	1	.007	.074	-.021	-.44**
G_a	.007	1	-.126	-.049	-.008
V_b	.074	-.126	1	.142	.639**
F_t	-.021	-.049	.142	1	.585**
Ms	-.44**	-.008	.639**	.585**	1

* Correlation is significant at the 0.05 level (2-tailed)
** Correlation is significant at the 0.01 level (2-tailed)

Multiple regression analysis was used to find out the effect of the independent variables (aggregate gradation, filler type, modified asphalt and conditions) on the dependant variable (Ms). SPSS program was used to predict the model of (Ms) .The model's coefficients and detailed analysis can be seen in Table IV.

Table IV: Coefficients of Moisture Susceptibility Model

Model	Unstandardized Coefficients		Standardized Coefficients	t	Sig.
	B	Std. Error	Beta		
(Constant)	2.041	0.133		15.289	.000
Log C	-0.255	0.030	-.496	-8.490	.000
Log G_a	0.129	0.062	0.121	2.060	.048
LogV_b	0.445	0.042	0.622	10.474	.000
Log Ft	1.207	0.148	0.480	8.154	.000

It can be noticed that standardized coefficient (Beta) for the first independent variable: susceptible conditions to asphalt mixtures is slightly affectedly the prediction of the dependent variable (Ms) because the value of Beta is (-0.255). The second independent variable is the aggregate gradation; Beta value is (0.129) which has the lowest effect on the prediction

of the (Ms). The third variable is the effective of modified asphalt in terms of asphalt viscosity; Beta value is (0.445). The fourth variable is the filler type in asphalt mixtures, its Beta value is (1.207) which has the highest effect on the prediction of the (Ms). As presented in Table IV all of the independent variables have a significant level less than 5%.

Analysis of results, calculation of standard error, and coefficient of variation for moisture sensitivity in term of indirect tensile strength (Ms) model are presented in equation (2).

$$Ms = 109.9 * C^{-0.255} * Ga^{0.129} * Vb^{0.445} * F^{1.207} \ldots\ldots\ldots\ldots(2)$$

Where:

Ms= Moisture susceptibility of asphaltic mixtures, in terms of indirect tensile strength for asphaltic mixtures (kPa),

Ga = Gradation of aggregate in asphaltic mixtures in terms of percentage of aggregate passing on sieve No. 4, (%),

Vb= Viscosity of the asphalt binder (Pa.sec),

Ft = Filler type in the asphaltic mixtures (lime and Portland cement), and,

C = Conditions susceptible to asphaltic mixtures in moisture sensitivity test (Dry and wet conditions).

Coefficient of determination values are found to be (0.88) for the moisture susceptibility (Ms) model, seem to be good correlation between observed and estimated results, with the standard error of regression of (0.026) , and only 12.0 percent of observed variation is unexplained by the developed models. This indicates that the measured moisture suitability can be explained with high degree of accuracy in terms of test conditions and mix parameters.

VII. Conclusion

Considering all results of laboratory tests and analysis, the following conclusions are presented:

1-Based on indirect tensile test results, a model was developed to predict moisture susceptibility of local asphalt concrete wearing course after mixtures for different test conditions and mix properties using statistical technique. The following forms were found:

$$Ms = 109.9 * C^{-0.255} * G_a^{0.129} * V_b^{0.445} * F_t^{1.207} \ldots\ldots\ldots\ldots(2)$$

2- The influence of variables on tensile strength ratio TSR and moisture susceptibility is evaluated. It is found that that using cement as filler, TSR is increased by 5 and 3.5 percent for coarse and fine gradations at opt. design asphalt binder content, while TSR increases by 2.07 and 2.5 percent for coarse and fine gradations at modified opt. design asphalt binder content.

3-Also it can be concluded that TSR is increased by 6.1 and 4.5 percent when using the SBS polymer modifier for coarse and fine gradations at opt. design asphalt binder content for lime filler respectively, while TSR increases by 3.2 and 3.4 percent for coarse and fine gradations at modified opt. design asphalt binder content for cement filler respectively.

Acknowledgment

The authors would like to acknowledge the National Centre for Construction Researches and Laboratories (NCCRL) in Iraq for their support during the preparation of this research.

References

[1] Sebaaly, P. E., D. Little, E. Y. Hajj, and A. Bhasin, "Impact of Lime and Liquid Antistrip Agents on Properties of Idaho Hot-Mix Asphalt Mixture,"Transportation Research Record: Journal of the Transportation Research Board, No. 1998, Transportation Research Board of the National Academies, Washington, D.C., 2007.

[2] Wasiuddin, N. M., C. M. Fogel, M. M. Zaman, and E. A. O'Rear, "Effect of Anti-Strip Additives on Surface Free Energy Characteristics of Asphalt Binders for Moisture-Induced Damage Potential," Journal of Testing and Evaluation.Vol. 35, No. 1, 2007.

[3] Solaimanian, M. J., Harvey, M., Tahmoressi, and Tandon, V., " Test Methods to Predict Moisture Sensitivity of Hot-Mix Asphalt Pavements,"Moisture Sensitivity of Asphalt Pavements CD-ROM, Transportation Research Board, National Research Council, Washington, D.C., 2004.

[4] Huang, B.; Xiang S.; and Xinwei, C., "Effects of mineral fillers on hot-mix asphalt laboratory measured properties,"International Journal of Pavement Engineering 8:1, 2009.

[5] Al- QadiImad L., Ibrahim M. Abuawad, HeenaDhasmana, and R. Coenen, "Effects of Various Asphalt Binder Additives/ Modifiers on Moisture Susceptible Asphaltic Mixtures," University of Illinois at Urbana Champaign, 2014.

[6] SCRB, *Standard Specification for Roads and Bridges.* Republic of Iraq, Ministry of Housing and Construction, 2007.

[7] *AASHTO Guide for Design of Pavement Structures*,. The American Association of State Highway and Transportation Officials, Washington, D. C., USA. (2010).

[8] Asphalt Institute, *Asphalt Hand Book*. Manual series No. 04, Six Edition, Kentucky, USA., 2007.

Geotechnical Properties of Soft Clay Soil Stabilized by Reed Ashes

Hussein H. Karim[1], Zeena W. Samueel[2], and Salsabeel F. Ahmed[3]

***Abstract*—Problematic soil, particularly soft clay, is wide spread in southern Iraq which is characterized by its low bearing capacity and strength besides its low California bearing ratio (CBR). The aim of this research is to investigate the suitability of some local natural material to be used as a stabilizer for soft soil such as reed ash (RA), which is available in Iraq with low cost. The immediate effect of the addition of such organic material ashes (biomass ashes) to the soil much like Portland cement is to cause flocculation and agglomeration of the clay particles. This study is carried out on soft soil brought from Maysan Governorate, southern Iraq. Different percentages of reed ash (RA) in incremental order of 3% up to 12% by dry weight of soil were added to natural soil sample. Physical and mechanical properties that have been studied before and after addition are specific gravity, consistency limit, unconfined compressive strength, compaction, California bearing ratio (CBR), consolidation, in addition to scanning electron microscope (SEM) and mineralogical analysis by X-ray diffraction (XRD). Testing results show that RA improved the consistency, strength, and deformation characteristics. It was found that the plasticity index of the natural soil has been decreased by about 22% with the addition of 12% RA. Treatment with RA showed a general reduction in the maximum dry unit weight with increase in the RA content to minimum values at 12% RA content. The optimum moisture content generally increased with increase in the RA content. There was colossal increase in the unconfined compressive strength value by about 86% and in the CBR value by about 227% with increase in RA content to 12%. A reduction in the compressibility index C_c from 0.196 to 0.073 was observed with increasing RA up to 12%. The angle of internal friction for soil-RA mix increased from 4° to 19° with 12% RA addition. Thus, it can be concluded that reed ash was an effective stabilizer for improving the geotechnical properties of soft soil samples and this will encourage the use of such matter as stabilizer in road building and obtaining a cheaper and effective replacement for the conventional soil stabilizers.**

***Index* Terms— Soil Stabilization, Soft Clay, Reed Ash**

Manuscript received July 16, 2015; accepted August 23, 2015.

[1] Professor, Building and Construction Engineering Department, University of Technology, Baghdad, Iraq. (corresponding author: e-mail: husn_irq@yahoo.com).

[2] Lecturer (Ph.D), Building and Construction Engineering Department, University of Technology, Baghdad, Iraq. (e- mail: zinawaleed2004@yahoo.com

[3] M.Sc. in Geotechnical Engineering. (e-mail: sall.f.mashhadany@gmail.com).

I. Introduction

SOFT clay soils are recent alluvial deposits presumably formed through the most recent 10,000 years described by their featureless and flat ground surface. “References [1] and [2] identified such clays by their low undrained shear strength (C_u< 40 kPa) and high compressibility (C_c between 0.19 to 0.44)”. These soils are found at high natural moisture content (typically ranging from 40-60%) with plasticity index ranging from 45-65% [3]. Soils with such characteristics create serious problems to geotechnical engineering associated with stability and settlements problems [4]. A soft sub grade in construction of roadways is one of the most frequent problems for highway construction in many parts of the world [5].

This research focuses on studying the feasibility of improving geotechnical properties of soft clay soil with chemical admixtures obtained from the burning of reeds. As a matter of fact, reeds ash has never been used before as useful materials in Iraq. So, an attempt has been made to manufacture and examine this organic material ash for the first time in Iraq. The effort was made for several reasons: first to utilize a natural resource self-renewable, reed, which grown over a wide range of mid and southern parts of Iraq. Second, this material, reed, has been used in this product were very cheap, very popular and easily available.

II. MATERIALS USED

Soil

Soil samples used in this study were obtained from a location in Maymouna site (Latitude 31°54′ N and Longitude 47° 2′ E) about 393 km south of Baghdad near Al-Amarah City in Maysan Governorate, southern Iraq. This soil is collected by disturbed sampling from borrow pits at a depth of 1.5 m. The properties of the soft soil used in this investigation are given in Table 1. According to the USCS classification system [6], the soil is classified as CL soil. The plasticity chart showing the location of the soil is shown in Fig. 1.

Table 1. Physical and chemical properties of natural soil used.

Index Property	Index Value
Initial water content (WC) %	42
Depth (m)	1.5
Liquid Limit (L.L) (%)	45
Plastic Limit (P.L) (%)	25
Linear Shrinkage (SL) (%)	11
Plasticity Index (P.I) (%)	20
Activity (At)	0.50
Specific Gravity (Gs)	2.72
Gravel (larger than 2mm) (G) %	0
Sand (0.06 to 2mm) % (S)	0.5
Silt (0.005 to 0.06) (M)%	37.5
Clay (less than 0.005mm) (C)%	62
Classification (USCS)	CL
Organic Material (O.M) (%)	0.925
Calcium Oxide (CaO) (%)	14.616
SO_3 Content (%)	1.108
Total Dissolved Salt (TDS) (%)	4.91
pH Value (%)	8.16

Note: All tests were performed according to the ASTM (2002).

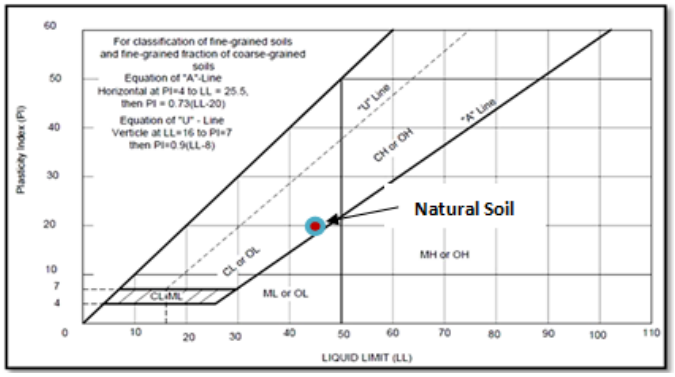

Fig. 1. Plasticity chart for the natural soil.

Organic Material Ash

The main ground improvement admixture used in this work was reed plants, which have been collected from Al-Amarah marshland area. At the beginning, the plants are spread on the ground and air dried to facilitate their burning.

Then, reed plants are burnt to be ash and then sieved through a sieve of 75μm to remove any tarnishes and get very fine reed ashes (RA). Then the sieved ashes were put in oven at 500°C for two hours. Physical properties and chemical composition of this ash are given in Table 2.

Water

Ordinary drinking water was used in the experimental work.

Table 2. Physical properties and chemical composition of reed ash.

Description	Abbreviation	Value (Index)
Specific gravity	G.S	2.44
Silica (%)	SiO_2	65.2
Iron (%)	Fe_2O_3	2.6
Alumina (%)	Al_2O_3	12.3
Calcium (%)	Cao	6.4
Magnesium (%)	MgO	N.R
Sodium (%)	Na_2O	N.R
Potassium (%)	K_2O**	2.5
Sulfur trioxide (%)	SO_3***	1.52
Phosphorus (%)	P_2O_5	0.03
Chloride (%)	Cl	N.R
Titanium (%)	TiO_2	0.19
Manganese (%)	MnO	0.08
Moisture Content (%)	*w*	0
Loss on Ignition (%)	L.O.I	1.47

*Chemical composition values are calculated using EDX-7000 instrument.
**K_2O value is calculated using XRD-6000 instrument.
***SO_3 value is calculated using MXF-2400 instrument.

III. SAMPLING AND PREPARATION OF SOIL MIXTURES

Disturbed soil samples were used in this work. These samples were packed in nylon bags and they were transported to the Soil Mechanics Laboratory of the University of Technology. First, the soil is oven dried and then pulverized. The prepared samples are then mixed with the predetermined amount of stabilizer (RA), while the dosage rates can be determined in various ways. In this study, the best approach to characterize the measurements rate is taking into account the dry weight of soil to be dealt with. Accordingly, the amount of stabilizer to be used was found from the following formula:

$$\text{Amount of stabilizer} = \frac{(ps * Wtot)}{(1+w)} \quad (1)$$

where:

ps = Percent by dry weight of stabilizer to be used,

Wtot = Wet weight of soil prior to addition of stabilizer, and

w = Moisture content of soil prior to addition of stabilizer, expressed as a decimal.

The selected percents of ash are (3, 6, 9 and 12%) of the dry weight of the untreated soil. The soil-additive mixtures were prepared by thoroughly mixing of dry quantities of soil and ash in a mixing tray to obtain a uniform color for a minimum of 5 minutes, and the required amount of distilled water was added to the dry mixtures. After that, the soil –ash mixture is mixed carefully until a homogeneous color was obtained.

IV. EXPERIMENTAL TESTS

Several tests are made to investigate the soil behavior after adding the RA. These tests are as presented in Table 3. All samples for UCS, CBR and compressibility tests were at the optimum moisture content (OMC) and maximum dry unit weight (MDD) values of the natural soil.

Table 3. Tests with their standards.

1. Specific Gravity [7].	2. Atterberg's Limits [8].
3. Modified compaction [9].	4. q_u (UCS) [10].
5. Unsoaked CBR & Soaked CBR [11].	6. Compressibility [12].
7. SEM (Scanning Electron Microscope).	8. XRD (X-Ray Powder Diffraction, (XRD).

V. TEST RESULTS AND DISCUSSION

The specific gravity of the treated soil decreased with increasing of reed ash (RA) content due to the its low values of the specific gravity (2.44) compared to that of the soil (2.72). The effect of RA on specific gravity of the soil is presented in Fig. 2. There was an increase in liquid limit and plastic limit, and a decrease in the plasticity index with increasing in RA content. The addition of RA at a maximum value of 12% result in an increase in liquid limit from 45 to 50.5%, plastic limit increased from 25 to 34.8%. Hence, plasticity index decreased from 20 to 15.7%. The reduction in the plasticity is attributed to the transformation in soil nature (granular nature after flocculation and agglomeration) and the resulted soil is as crumbly as silt soil.

The optimum moisture content (OMC) and the maximum dry unit weight (MDD) of the untreated natural soil were 17% and 18.62 kN/m^3 respectively. The addition of RA led to increase in OMC values and a reduction in the maximum dry unit weight values with the increasing in RA content from 0 to 12% as shown in Fig. 3. The effect of RA on unconfined compressive strength of the soil is presented in Fig. 4. When the RA content was increased from 0 to 12%, the unconfined compressive strength increased from 164 to 304.9 kPa. The chemical reactions that occur when RA is mixed with clay include pozzolanic reactions. These result in agglomeration in large size particles. CBR values increased from 4.9 to 16%, in RA stabilized samples with the addition of RA. This increase is due to pozzolanic reactions (the silica, SiO_2) from RA interacts with the Ca^{++} from the soil to form cementitious components (CSH), within the ash-soil mixture and resulting in strength gain over time. The effect of RA on unsoaked and soaked CBR of the soil is presented in Figs. 5 and 6. The addition of RA improved the compressibility of soft clay soil by reducing the compressibility index C_c from 0.196 to 0.073. And the reloading index C_r decreased from 0.0394 to 0.005. The effect of the RA addition on soil compressibility is presented in Fig. 7. The micrograph of the natural soil (Fig. 8) showed the sheet-like structure and flaky arrangement of the clay particles which is a closed fabric. While, Fig. 9a and b illustrates the micrographs of the treated soil and stabilized with 12% reed ash. Both micrographs of the treated soils with RA show crumbs of floccules with a porous nature and cementitious compounds (calcium silicate hydrate) coating the clay particles. Additionally, the reaction of reed ash with clay led to the formation of aggregates of various sizes and rod-like crystals (as a result of pozzolanic reaction). Mineralogical compositions (from XRD analysis) of the natural soil and reed ash (RA) are illustrated in Table 4. XRD patterns for natural soil and RA are shown in Figs. 10 and 11 while Fig. 12 illustrates the treated soil with 12% RA. XRD scan for RA showed a long amorphous hump from 20° to 34° (2θ). This hump pattern is most likely entirely a silica gel. From Fig. 12, one can notice a considerable increasing in calcite ($CaCO_3$) and CSH. There was a considerable increasing in quartz (SiO_2), anhydrite ($CaSO_4$), feldspar, halite (NaCl) and dolomite (Ca $(MgCO_3)_2$) content. The increase contents of feldspar and dolomite made the CBR and q_u of treated soil to gain up. The increasing of quartz (SiO_2) crystals content led to increase in sand-sized particles as well as increasing the pore voids size. Hence, reduction in plasticity index and swelling potential and increasing the CBR and q_u values of the stabilized soils are observed.

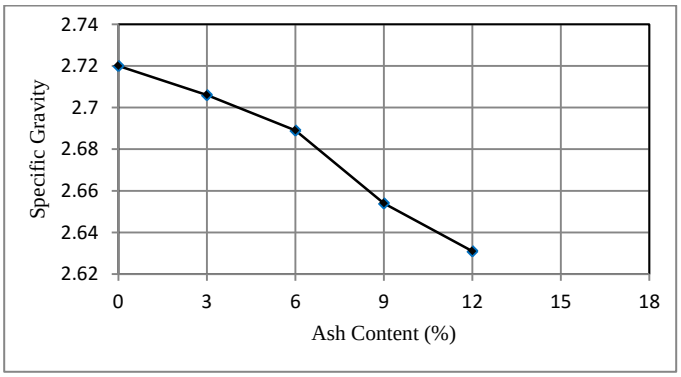

Fig. 2. Specific gravity for treated soil with RA content.

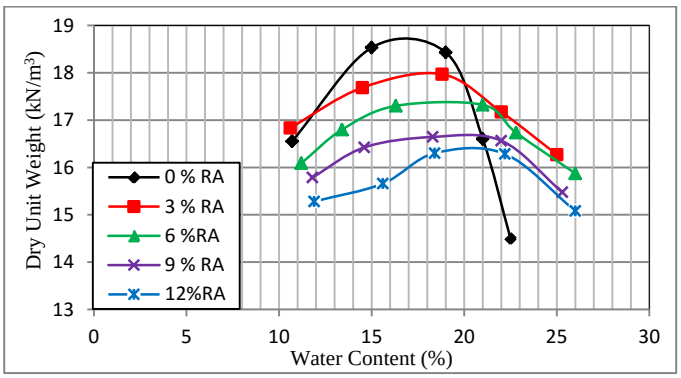

Fig. 3. Dry unit weight – water content curve for soil–RA mix.

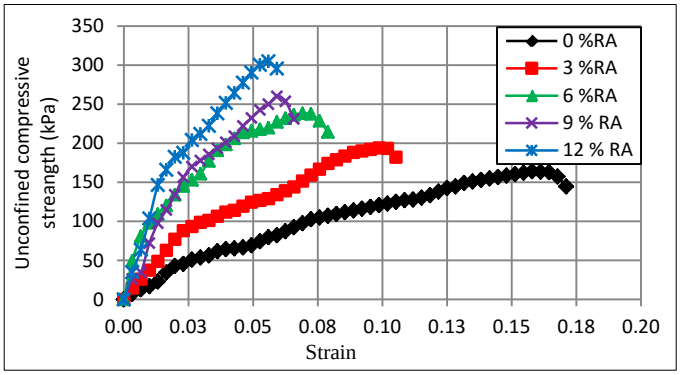

Fig. 4. Stress-Strain relationship from unconfined compression test for treated soil with RA.

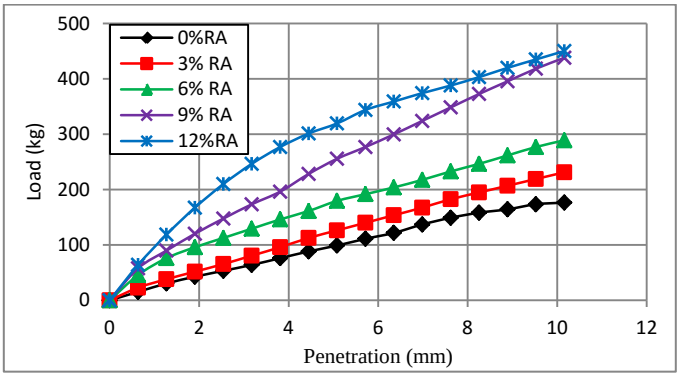

Fig. 5. Load-penetration relationship for unsoaked stabilized soil with RA.

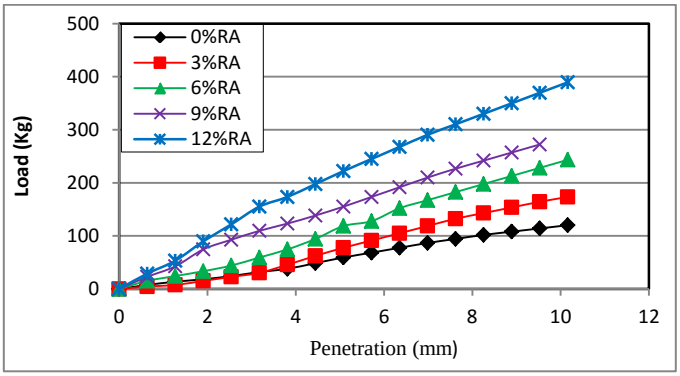

Fig. 6. Stress-penetration relationship for 4-days soaked stabilized soil with RA.

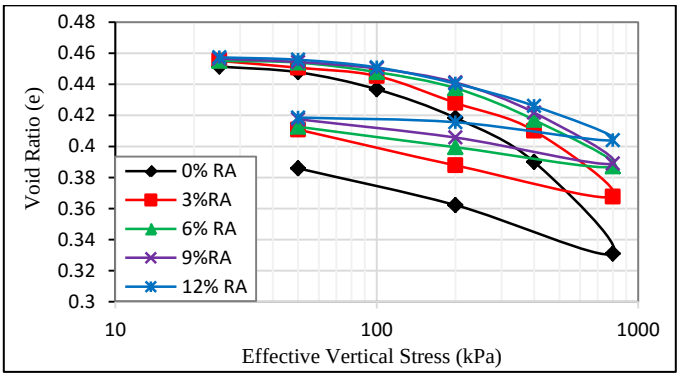

Fig. 7. Void ratio versus effective stress curves from the consolidation test on soil stabilized with different RA percents.

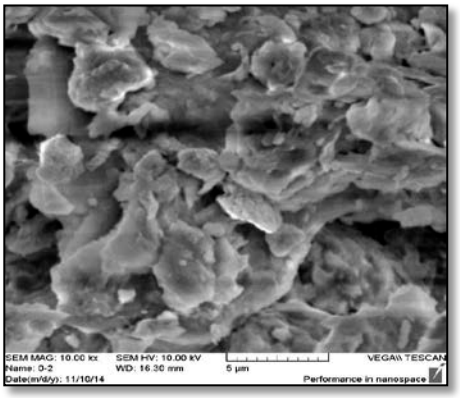

Fig. 8. SEM micrograph of natural soil.

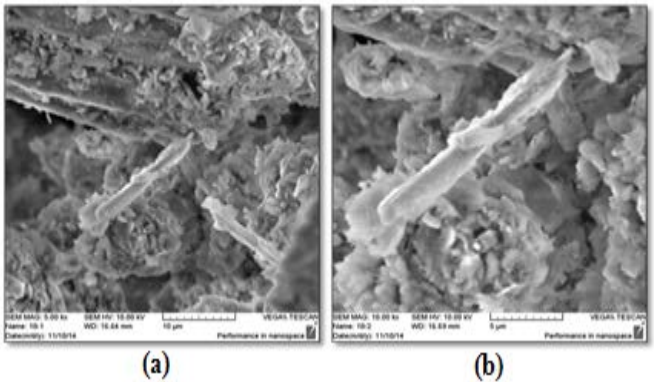

Fig. 9. SEM micrographs of (a) treated soil with 12% RA (b) magnified micrograph for the same specimen.

Table 4. Mineralogical composition (from XRD analysis) of the natural soil and reed ash (RA).

Material type	Arrangement of the minerals according to the majority (from primary to secondary components)
Natural Soil	Calcite ($CaCO_3$), Quartz (SiO_2), Muscovite, Halloysite, Dolomite ($Ca(MgCO_3)_2$), Illite, Feldspar, Montmorillonite and Kaolinite.
RA	Quartz (SiO_2), Anhydrite ($CaSO_4$), Feldspar, Calcite ($CaCO_3$), Potassium chlorite (KCl) and Halite (NaCl).

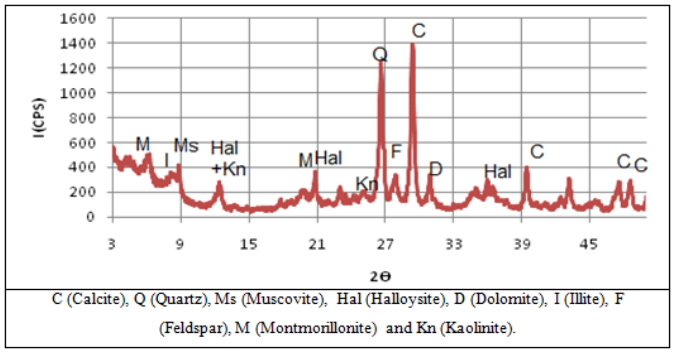

Fig. 10. XRD of the natural soil.

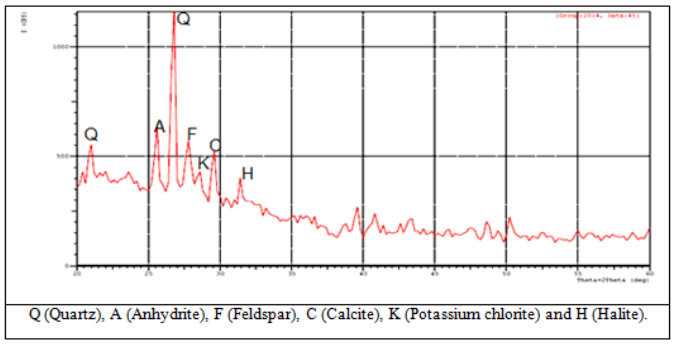

Fig. 11. XRD of reeds ash (RA).

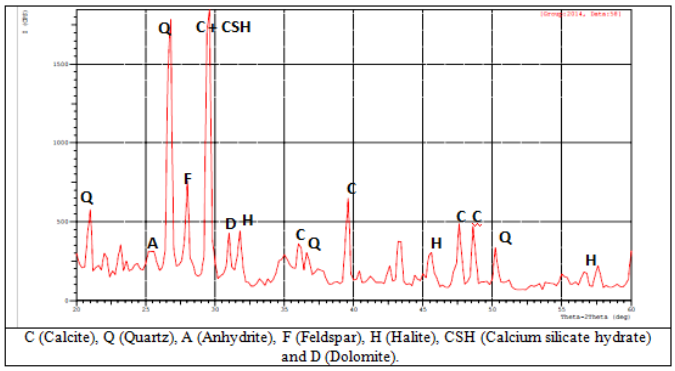

Fig. 12. Treated soil with 12% RA.

VI. CONCLUSION

In the light of experimental tests, the following conclusions can be drawn:

1. There is a decrease in specific gravity of soil with increasing reed ash (RA) content. MDD is decreased too with increasing RA content resulting in large particles with larger voids and hence less density due to the relatively lower specific gravity of RA compared to soils. While OMC is increased as RA content increases up to 12%.
2. For soft soil-RA mix, there is an increase in liquid and plastic limits, a reduction in the plasticity index of treated soil.
3. It is noticed that UCS and CBR increase by about 86 and 227% respectively with increasing the addition of RA which is due to pozzolanic reactions.
4. It can be noted that RA addition can improve the compressibility of soft clay soils by reducing the compressibility index C_c due to the flocculation and cementitious phenomenal effects by the pozzolanic reactions that forms the secondary minerals.
5. For microstructural analysis of natural soils**,** the SEM-micrographs for 12% RA treated soils show crumbs of floccules with a porous nature and cementitious compounds coating the clay particles.
6. From UCS and CBR tests, it can be concluded that 6 to 9% are the optimum dosage of RA in which it can be added to improve the geotechnical properties such problematic soft soil. Accordingly, the general relationship between q_u and CBR-values with the quality of the subgrade soils used in pavement applications for RA addition consider treated soil as a good subgrade material and it also can be used as highway sub-base material.

REFERENCES

[1] E. W. Brand and R. P. Brenner, *Soft Clay Engineering*, Elsevier Scientific Published Company, Amsterdam, 1981.

[2] *British Standard B.S*: C.P. 8004, "Code of Practice for Foundations," British Standard Institution, London, 1986.

[3] B. B. Broms, "Stabilization of soft clay in Southeast Asia," *Proc. 5th International Geotechnical Seminar*, 2- 4 Dec., 1987.

[4] Z .W. Abbawi, "Proposed techniques for improving soft soil underneath a ballasted track," Ph.D. thesis, Building and Construction Engineering Department University of Technology, Baghdad, Iraq, 2010.

[5] A. Fauzi, W. M. Nazmi, and U. J. Fauzi, "Sub grade stabilization of Kuantan clay by using fly ashes and bottom ash," *Proc. 8th International conference on Geotechnical and Highway Engineering (Geotropika 2010)*, UTM, Sabah, 2010.

[6] *ASTM D 2487*: "Standard practice for classification of soils for engineering purposes (Unified Soil Classification System)," American Society of Testing and Materials, 2000.

[7] *ASTM D 854*: "Standard test methods for specific gravity of soil solids by water Pycnometer, "Annual Book of ASTM Standards, ASTM International, West Conshohocken, PA, United States, 2002.

[8] *ASTM D 4318*: "Standard test methods for liquid limit, plastic limit, and plasticity index of soils," West Conshohocken, PA, United States, 2000.

[9] *ASTM D 1557*: "Standard test methods for laboratory compaction characteristics of soil using modified effort (56,000 ft-lbf/ft^3 (2,700 kN-m/m^3))," Annual Book of ASTM Standards, ASTM International, West Conshohocken, PA, United States, 2000.

[10] *ASTM D 2166*: "Standard test method for unconfined compressive strength of cohesive soil," West Conshohocken, PA, United States, 2000.

[11] *ASTM D 1883*: "Standard test method for CBR (California Bearing Ratio) of laboratory-compacted soils," Annual Book of ASTM Standards, ASTM International, West Conshohocken, PA, United States, 2002.

[12] *ASTM D 2435*:"Standard test method for one-dimensional consolidation properties of soils," Annual Book of ASTM Standards, ASTM International, West Conshohocken, PA, vol. 04.08, 1996, pp. 1–10.

Prof. Dr. Hussein Hameed Karim received the B.S. and M.S. degrees in Earth Science/ Geophysics from the University of Baghdad, in 1978 and 1982 respectively, and the Ph.D. degree in Engineering Geophysics from University of Baghdad in 1996, Iraq.

From 1983 to 1997 he was within the academic staff of University of Basrah and graduated from Asst. lecturer to Asst. Professor. Since 1997 he is within the academic staff of University of Technology. Since 2000, he has been a Professor with the Building & Construction Engineering Department/ University of Technology. He is the supervisor of more than 45 post graduate (M.Sc. and Ph.D) students, the author of 5 books, and one under preparation, more than 100 scientific researches, more than 100 scientific articles, and two patents. His research interests include Engineering Geophysics, Soil & Rock Mechanics, Site Investigation, and Geomatics Engineering.

Prof. Karim was chosen by the Committee of University of Technology as the 1st Professor in the University of Technology for the academic year (2010-2011). Prof. Karim's awards and honors include training session to Bordeaux University- France (4 months, 1984); Visiting Professor to University of Hodeidah University- Yemen (3 months, 2002); Visiting Professor (one month, 2010) to Malaya University- Kuala Lumpur, Malaysia; and 3 Professor Visits sponsored by DAAD (Germany), Bauhaus University- Weimar 2006, Rhur University – Bochum 2010 and 2014 (3-months for each).

Using Rice Husk in Improving Soil

Dr.Anwar Luay M. al-Obaidi Aya Abd Al-Kareem Sabah

***Abstract*—Rice husks ash having high potential and suitability in so many well established papers but uses of rice husk has been limited. In north of Iraq, they transform this agricultural waste material made from rice paddy replacement into an economic use of it after being mixed into the soil in the construction of economic houses This study concerns with using cheap materials (rice husks) to improve soil properties and produce soil stabilization. The effect of Rice Husks on some geotechnical properties of soil brought from Al- Jadiriya site with three different percentage of Rice Husks (4%,8% and12%)by weight of dry soil was studied. The study included evaluation of their properties such as compaction, consistency limit, consolidation and unconfined compressive strength. It was found that the liquid limit of soil has been increased with the addition of Rice Husks as well as the plasticity index while, the plastic limit decreased. Treatments with Rice Husks show a general reduction in the maximum dry unit weight with increase in the Rice Husk content. The optimum moisture content generally increased with increase in Rice Husk content. The increases in the unconfined compressive strength with increase in Rice Husk content for the soil to its maximum at rice husk less than 4%. The relationships between void ratio and logarithm pressure for different percentage of rice husk are the same such as without rice husk except at 12% which deviated from traditional one.**

***Index Terms*— Improving, Rice husk, Soil**

I. Introduction

RICE Husk (RH) is one of the most widely available agricultural wastes in many rice producing countries around the world. Globally, approximately 600 million tons of rice paddies are produced each year. On average, 20% of the rice paddy is husk, giving an annual total production of 120 million tones. In majority of rice producing countries much of the husk produced from processing of rice is either burnt or dumped as waste. In many occasion, RH is used as a heat isolators in primitive stores. RH can be considered as durable isolator materials because it cannot be eaten by Termites.

Rice Husk removal during rice refining, creates disposal problem due to less commercial interest. Also, handling and transportation of RH is problematic due to its low density. Therefore, commercial use of rice husk and its ash is the alternative solution to disposal problem. It has been used directly or in the form of ash either as a value added material for manufacturing and synthesizing new materials or as a low cost substitute material for modifying the properties of existing products. Easy availability and low price of rice husk in rice producing countries is an extra benefit towards the use of this material. Despite having high potential and suitability in so many well established uses, the use of rice husk has been limited.

Anwar Luay M. al-Obaidi is with the Building Research Directorate / Ministry of Const. and Housing, Iraq; e-mail: alobeydi_63@yahoo.com.
Aya Abd al-Kareem Sabah; e-mail: aya_alazaawi77@yahoo.com.

II. Literature Review

This experimental study planned to make benefit using rice husks as an agricultural waste material to improve soil properties by providing laboratory test results for different percentages of rice husks. The test results are used to investigate the behavior of the soil after mixing with these percentages. Cement and lime are the two main materials used for soil stabilization. These materials have rapidly increased in price due to the sharp increase in the cost of energy. The over dependent on the utilization of industrially manufactured soil improving additives (cement, lime etc), have kept the cost of construction of stabilized road financially high. Thus the use of agricultural waste (such as Rice Husk ash - RHA) will considerably reduce the cost of construction and as RHA on the geotechnical properties of cohesive soil. Fidelis and Ugochukwu (2009), studied the effect of RHA on some geotechnical properties of a lateritic soil classified as A-2-6 (0) or SW for sub-grade purposes. well reducing the environmental hazards they causes. Fattah et al.(2013) presented the results of experimental study carried out on three different soils improved with different percent of rice husk ash. Samples were brought from different sites of Iraq. Grytan et al. (2012) also studied the effect of RHA on the geotechnical properties of cohesive soil. Fidelis and Ugochukwu (2009), studied the effect of RHA on some geotechnical properties of a lateritic soil classified as A-2-6 (0) or SW for sub-grade purposes.

.

III. Experimental Work and Materials Specification

Material Used

a) Soil used

Samples of soils were brought from Al-Jadiriya site at depth of 0.5m from the ground surface. Standard tests were performed to determine the physical properties of the soil. Grain size distribution of this soil (taken from building research center) is shown in Fig. (1).The geotechnical index properties of al-Jadiriya soil before addition of stabilizer are shown in TABLE (1).

TABLE 1
PROPERTIES of NATURAL SOIL before STABILIZATION

Characteristics	Description
Liquid limit (%)	17
Plastic limit (%)	12
Plasticity index (%)	5
Maximum dry density (kN/m^3)	16.2
Optimum moisture content (%)	13

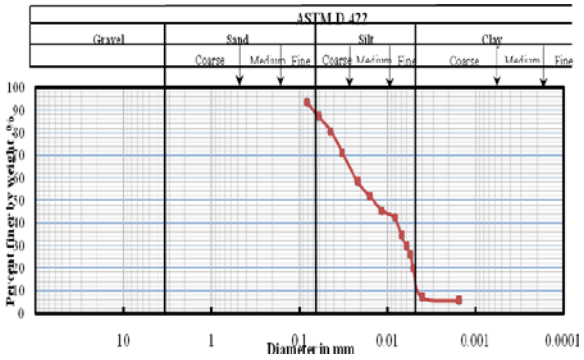

Fig. 1. Grain size distribution of the soil

b) Rice husk

In this study, the Rice Husk was collected from rice farms west of Baghdad city as shown in plate 1. The chemical properties of rice husk are illustrated in Table 2.

PLATE 1 RICE HUSK

TABLE 2
TYPICAL ANALYSIS OF RICE HUSK (KUMAR ET AL.,2010)

Property	Range
Bulk density (kg/m3)	96-160
Hardness(Moh's Scale)	5-6
Ash,%	22-29
Carbon, %	˜ 35
Hydrogen,%	4-5
Oxygen,%	31-37
Nitrogen,%	0.23-0.32
Sulphur,%	0.04-0.08
Moisture	8-9

IV. Laboratory Testing Programmer

The testing program conducted on the soil samples was included determination of the physical and chemical properties of soils at their natural state. On the other hand, the testing program conducted on the soil samples mixed with rice husk materials included Atterberg limits, specific gravity, compaction, unconfined compression test and consolidation tests.

a) Atterbergs Limits

The liquid limit test was conducted on samples passing 0.425 mm (no. 40) sieve; clayey soils and soil mixed with (4, 8 and 12%) Rice Husk, using Casagrande liquid limit apparatus as per the procedures laid down in ASTM D 431 8-00. The plastic limit test was conducted as per the specifications laid down in ASTM D 431 8-00.

b) Compaction

The standard compaction tests were performed in accordance with ASTM D 1557. The specimens were of 102 mm diameter and 116 mm height. The degree of compaction of soil influences several of its engineering properties such as compressive strength, permeability, shrinkage, and swelling potential. Therefore, it is important to achieve the desired degree of relative compaction necessary to meet the required soil characteristics.

c) Unconfined compression tes:

This test was performed in accordance with ASTM D 2166-00. The sample sizes were 38 mm diameter and 76 mm length. Samples were at optimum moisture content (OMC) and maximum dry unit weight. Test was applied using Harvard compaction apparatus as shown in Plate (2) with mould and collar clamped to base. The desired amount of loose soil was placed in the mold for five layers.

PLATE 2 HARVARD COMPACTION APPARATUS

d) Consolidation test

This test were performed in accordance with ASTM D 2435-02 setup and was used for determining the compressibility behavior of the soil. The sample was 60 mm high and 50 mm diameter. The sample was prepared at dry density of the standard compaction curve.

V. RESULTS AND CONCLUSIONS

a)Effect on Atterberg limits

Liquid limit results for soil and rice husk combination at different percentages are shown in Fig. 2a. Similar trend was observed for plasticity index as shown in Fig. 2c. This trend may be attributed to the replacement of the finer soil particles by Rice Husk with consequent reduction in the clay content and ability of Rice Husk to absorb water since it is an organic material. Plastic limit decreased with increase in Rice Husk content as shown in the Fig. 2b. the plastic limit decreases with increasing in Rice Husk content. The increased in the values implies that rice husk in treated soil required more water to change its plastic state to semisolid state.

b)Compaction characteristics

The variation of maximum dry unit weight and optimum moisture content with stabilizer contents are shown in Fig. 3. and Fig. 4. which indicates that the maximum dry unit weight decreased with increasing Rice Husk Content. It observed that maximum dry unit weight decreased with increasing in the stabilizer. Fig. 4. indicates that optimum moisture content increases within increasing Rice Husk content. The decrease in the maximum dry unit weight can be attributed to the replacement of soil by the rice husk in the mixture which has relatively lower specific gravity compared to that of the soil which is (2.65) it may also be attributed to consider the rice husk as filler with low specific gravity in the soil voids.

c) Effect on unconfined compressive strength :

Unconfined compressive strength is the most common and adaptable method of evaluating the strength of stabilized soil. It is the main test recommended for the determination of the required amount of addition to be used in the stabilization of soil. Variation of strength with increase in rice husk from 0% to 12% are shown in Figures (5) and (6).The results show that the unconfined compressive strength is increased with increasing Rice Husk content from 0% to 4% and subsequently reduced with further addition but still higher than untreated soil. The general increase may be attributed to the formation of bonds with Rice Husk. The 4% Rice Husk content gave the highest improvement of the unconfined compressive strength of the soil and hence would appear to be the optimum Rice Husk content.

d)Effect on compressibility characteristics

All samples were compacted at the maximum dry unit weight and optimum moisture content using the same compaction energy of the standard proctor test. All specimens were soaked in water. The results of consolidation tests are presented as void -ratio versus logarithm of effective stress as shown in fig. 7. for all percentages of rice husk except for 12% which was deviated from traditional curves.

It was noticed that the addition of Rice Husk leads to decrease the initial void- ratio up to 4% Rice Husk content, while (8% and 12%) percentages increase the void- ratio. Fig. 8. a, b, and c indicated that the addition of Rice Husk leads to increase in modulus of volume compressibility this may be due to increase in the initial void-ratio at 8% and 12%.

CONCLUSIONS

1- An increase in the rice husk content results in increasing in liquid limit as well as in plasticity index but reduced in plastic limit
2- The results obtained show that the more rice husk percentage is used in the mix, the lighter the soil stabilization results which leads to decrease in the maximum dry density
3- Since the rice husk is an organic matter which have the ability to absorb water, an increasing in rice husk content leads to increase in optimum moisture content
4- The addition of rice husk increased in the unconfined compressive strength of the soil comparing with untreated soil. It can be optimized with the addition of less than 4% and subsequently reduced with further addition of rice husk.
5- Initial void ratio increased with increasing in rice husk content this lead to increase in compression index and modulus of volume compressibility up to 4% percentages while the rice husk (8%to12%) leads to decrease in void ratio.
6- The relationships between void ratio and pressure for different percentages of rice husk were the same such as without rice husk except at 12% which deviated from traditional one.
7- From above, it would appear that rice husk with small percentages (less than 8%) has been used directly as a low cost material for modifying the properties of existing soil.

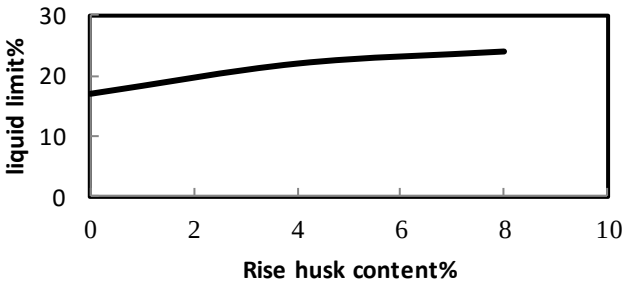

(a)

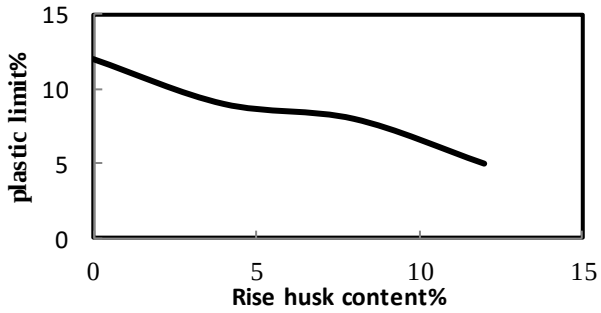

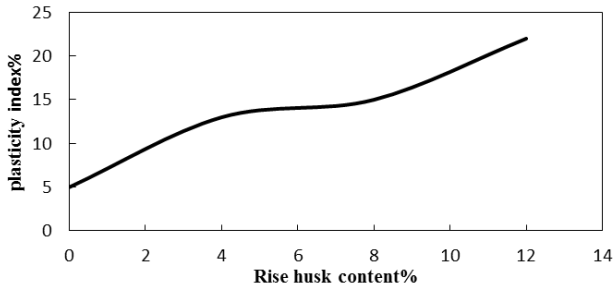

(b)

(c)

Fig. 2. Effect of rise husk on (a) Liquid Limit, (b) Plastic Limit, and (c) plasticity index of soil

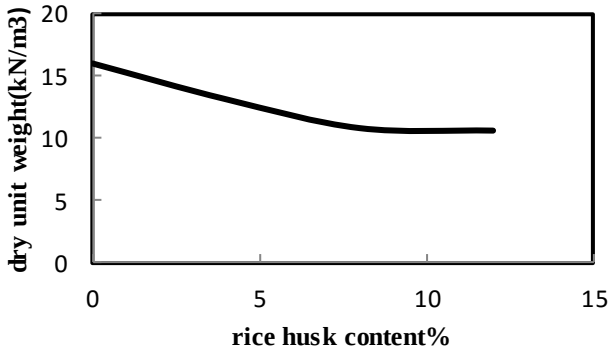

Fig. 3. Effect of Rice Husk percentages on maximum dry unit weight

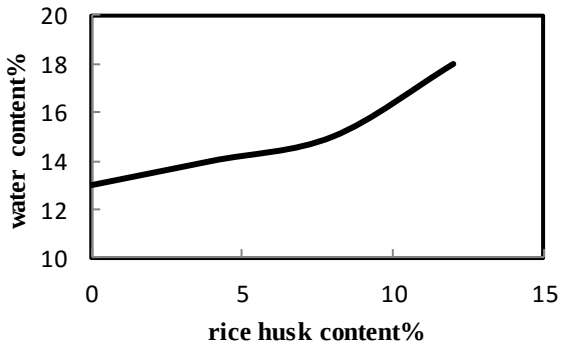

Fig. 4. Effect of Rice Husk percentages on optimum moisture content

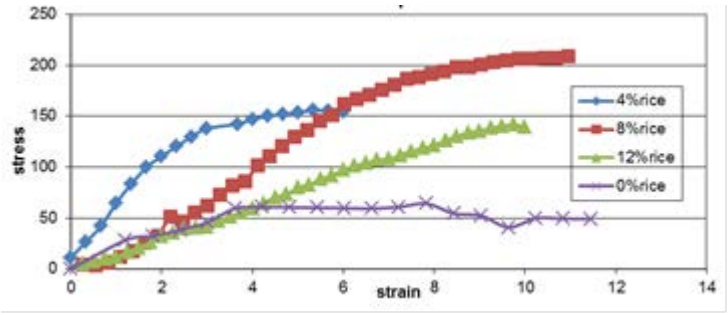

Fig. 5. Stress-strain relationships from unconfined compression tests for different percentages of rice husk

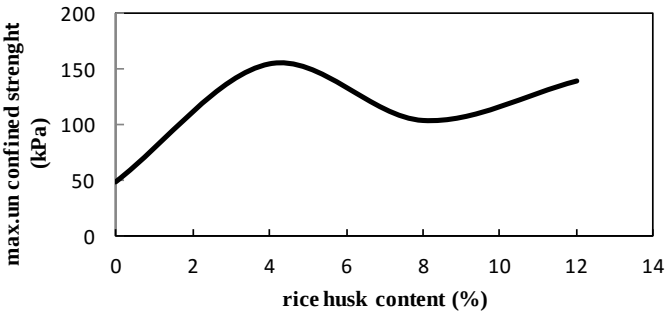

Fig. 6. The relationship between maximum unconfined compressive strength and Rice Husk percentages.

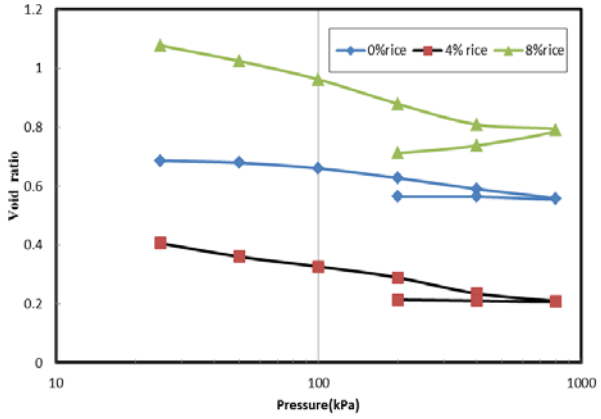

Fig. 7. Pressure-void ratio for different percentages of rice husks

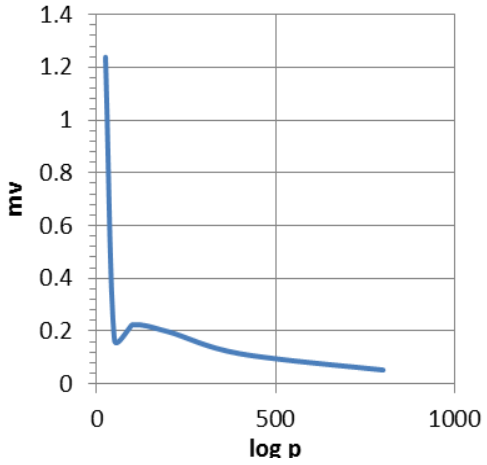

(a) Rice Husk percentage 0%

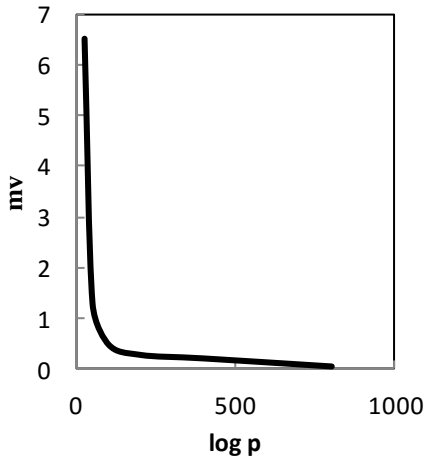

(b) Rice Husk percentage 4%

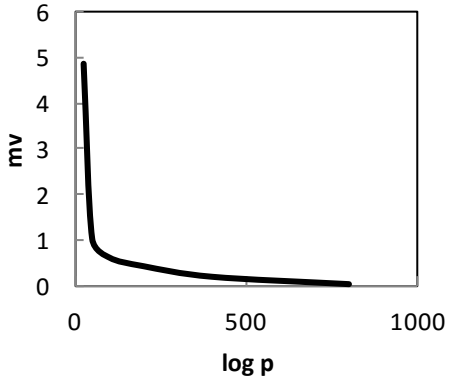

(c)Rice Husk percentage (8%)

Figs. 8a, b and c. Effect of rice husk percentages on modulus of volume compressibility

REFERENCES

[1] **Ajay kumar, Kalyani Mohanta, Devendra Kumar and Om Parkash, "Properties and Industrial Applications of Rice husk", International Journal of Emerging Technology and Advanced Engineering Website: www.ijetae.com (ISSN 2250 -2459, Volume 2, Issue 10,October 2012).**

[2] **ASTM D1557, (2002), "Standard Test Methods for Laboratory Compaction Characteristics of Soil Using Standard Effort", Annual Book of ASTM Standards,Vol. 04.08, ASTM International, West Conshohocken, PA, p. 1–10.**

[3] **ASTM D 2166, (2000), "Standard Test Method for Unconfined Compressive Strength of Cohesive Soil", Annual Book of ASTM Standards, Vol. 04.08, ASTM International, West Conshohocken, PA, p. 1–6.**

[4] **ASTM D 2435,(2002),"Standard Test Methods for One-Dimensional Consolidation Properties of Soils," Annual Book of ASTM Standards, Vol.04.08,ASTM International ,West Conshohocken, PA,pp.1-10**

[5] **ASTM D 4318,(2000)," Standard Test Method for Liquid Limit ,Plastic Limit, and Plasticity Index of Soils," Annual Book of ASTM Standard ,Vol. 04.08,ASTM International ,West Conshohocken, PA, p 1_14.**

[6] **Mohammed Y. Fattah, Falah H. Rahil, Kawther Y. H. Al-Soudany,(2013), "Improvement of Clayey Soil Characteristics Using Rice Husk Ash", Journal of civil engineering and urbanism ,volume 3,Issue1.**

[7] **Alhassan Musa,(2008), "Potentials of Rice Husk Ash for Soil Stabilization", Australian Journal of Technology, Volume 11,Issue 4,April,pp.246-250.**

[8] **Vgohukwu,(2009),"Effect of Rice Husk Ash on Some Geotechnical Properties of Lateral on Soil", Lenoardo electronic Journal of practies and Technologies, Issn 1583_1078,P 67-74.**

[9] **Grytan Sarkar, Md.Rafiqul Islam, Dr. Muhammed Alamgir, Dr. Md Rokonuzzaman, (2012),"Interpert Action of Rice Husk Ash on Geotechnical Properties of Cohesive Soil", Global Journal of researches in engineering civil and structural engineering, online Issn:1249-4596 and print:0975-5861.**

Evaluation of Statistical Derived Equation for Calculating Driven Pile Capacity in Sand

Ali, A.M., Shlash, K.T., and Al-Neami M.A

Abstract— until now days, the challenge in scale model tests is how these results can be translated to the behavior of prototype structure. In geotechnical applications, (i.e. pile load test) the model tests may present a more economical option than corresponding to full scale test, and the ability to quantitatively recognize the mechanism of these systems. The objective of this study is, to derive a statistical equation which may be utilized to expect as possible as the actual behavior of structure. In this research, different parameters have been considered as the model pile dimensions and others related to the driving process as the driving energy and pile to hammer weight ratio (P/W).

The statistical data of the model tests are grouped using (STATISTICA) program. It was employed as a beneficial tool to predict the ultimate capacity of driven piles based on model test results, and to correlate them to the full scale tests. Thus, to check the reliability of the statistical analysis, a comparison has been made between the results obtained from the derived equation and field load tests results taken from (Al-Russafa water treatment plant). The analysis of experimental work showed that the number of blows is affected by diameter more than with pile length when two piles have same total areas are driven by the same constant driving energy

Statistical analysis demonstrated a good agreement between the models and actual results. Also, the results indicated that, the observed capacities obtained from the statistical equation are slightly more than the capacities computed from the field tests. Moreover, the coefficient of determination (R^2) for driven pile equation is about (93.3%) which may give a remarkable visualization about the quality of the output data represented with pile capacity.

Keywords: statistical analysis, driven pile, scale model, driving energy, pile capacity.

I. Introduction

Design of foundations usually is based on special theories for satisfying the requirements of design such as, calculating the bearing capacity of foundation. These theories represented with the mathematical equations are almost has a conservative property due to the neglect of number of cases under the pretext of making the problem to be solved is more easy and simplified.

Manuscript received May 23, 2015.

Ahmed Majeed Ali author is with the building and construction engineering department, university of technology, Baghdad, Iraq (e-mail: ama.civil85@gmail.com).

Kais Taha Shlash was with University of Technology, Baghdad, Iraq. He is now with the Department of Civil Engineering, Al- Israa University, Iraq (e-mail: ktishlash1@yahoo.com).

Mohammed Abdullattef Al- Neami author is with the building and construction engineering department, university of technology, Baghdad, Iraq (e-mail: Al_Neami74@yahoo.com).

Physical modeling has significantly contributed to facilitate the expected behavior of the actual structure therefore, it can

be used as a qualitative estimation to that real conditions. However, resorting to the physical models in the geotechnical applications should be taken into the account, the influences of soil particle sizes and stress level as well as, the boundaries where the model is being installed to get as possible a quantitative interpretation for model test results.

II. Behavior of Driven Piles in Sandy Soils

Driving of pile is associated with moving large amounts of sand in vertical and radial direction. The vibrations resulting from driving a pile in sand have two effects involve condensing the sand and increasing the value of lateral earth pressure around the pile. Meyerhof (1959) showed that the amount of compaction near the tip is greater and becomes less near the top of the shaft.

Horn in 1966, presented test results of sand prior and after pile driving, a significant densification of the sand was noticed for distance as large as eight diameters away from the center of the pile.

Kishida (1967) stated that in very loose sand (relative density, "R.D" = 17%), soil movement extended 3 to 4 pile diameters from the side of the pile and 2.5 to 3.5 diameters below the pile tip, In medium sand (R.D = 35%), the extent of movement was larger, extending 4.5 to 5.5 diameters from the side and 3 to 4.5 diameters below the tip.

Salgado, (2006) pointed out that, the increase of driven pile capacity in dense sand may be attributed to the generation of large normal stress on the pile shaft due to dilation effect throughout driving process.

III. Testing Program

A total number of 12 model driven pile tests were performed in laboratory. Hiley formula was implemented in all tests of model driven piles to calculate the predicted loads and compare these values with the observed loads obtained from the laboratory tests.

The piles are embedded in sandy layer with different lengths and diameters/widths. Piles with square and circular cross-sections under the effect of vertical static compression loads are tested. Table (1) shows the model pile dimensions and embedded length (L_P) tested during this study.

The study focuses on the small scale models behavior with controlled conditions and how this behavior used to obtain a

link which may be utilized to expect the actual prototype behavior with assistance of statistical derived equations.

Prior to the testing, bed of soil is prepared with a dry unit weight of 16.5 kN/m^3 which is corresponding to relative density R.D = 31% (loose sand) using raining technique. All piles are loaded to the double working load.

TABLE 1
DIMENSIONS AND SHAPES OF THE MODEL DRIVEN PILES TESTED

Test No.	Diameter/ width (cm)	Length (cm)	Embedded length (L_P) (cm)	Cross sectional area
1	2.1	50	41	Square
2	2.1	40	31	Square
3	2.1	30	21	Square
4	2.1	50	41	Circular
5	2.1	40	31	Circular
6	2.1	30	21	Circular
7	1.6	50	41	Square
8	1.6	40	31	Circular
9	1.6	50	41	Square
10	1.6	40	31	Circular
11	1.1	50	41	Square
12	1.1	50	41	Circular

To decide how much energy is required to drive every single model pile, a simple equation which can be called as (state equation) has been derived. The mathematical formula for the state equation used for driving model piles can be written as: -

$$E_{model} = E_{refrence\ pile} \times \frac{(A_{s_o} + A_{b_o})_{model}}{(A_s + A_b)_{prototype}} \times \frac{\sigma_{V\,model}}{\sigma_{V\,prototype}} \quad \dots (1)$$

Where:

$E_{reference\ pile}$: Energy corresponding to 3 (Ton. m) which was considered as a field energy to simulate the models energy.

$(A_{s_o}, A_{b_o})_{model}$: Surface and bearing areas of model pile respectively.

$(A_s, A_b)_{prototype}$: Surface and bearing areas of actual pile (B = 30cm and L =12m) respectively and,

$(\sigma_{v\,model}, \sigma_{v\,prototype})$: Overburden pressure for model and actual size pile respectively.

When the pile is driven into the soil, it will be influenced by the stress level and the area of pile subjected to shearing (surface and bearing areas) where the embedded length of pile can be considered as a major parameter in specifying the efficiency of driving energy.

Also, a preferable range of pile to hammer ratio (P/W) about (1- 1.5) were chosen depending on the concluded findings of (Shlash, 1986) who stated within which the tension stresses generated during driving are limited and not dangerous.

The whole model pile lengths are divided into equidistance equal of 25mm to count the number of blows needed to penetrate this distance which simulates 25cm in the field.

IV. EXPERIMENTAL WORK

Karbala sand was used in present study. Standard tests were performed to determine the physical properties of the sand. The details of these properties are listed in Table (2).

TABLE 2
PHYSICAL PROPERTIES OF THE SAND USED IN PRESENT TESTS

No.	Index property	value
1	Specific gravity (G_s)	2.66
2	D_{10} (mm)	0.148
3	D_{30} (mm)	0.35
4	D_{60} (mm)	0.58
5	Coefficient of uniformity (C_u)	3.92
6	Coefficient of curvature (C_c)	1.43
7	Maximum dry unit weight (kN/m^3)	19.0
8	Minimum dry unit weight (kN/m^3)	15.6
9	Dry unit weight (kN/m^3) at R.D = 31%	16.5
10	Maximum void ratio	0.67
11	Minimum void ratio	0.37
12	Relative density (R.D %)	31.0
13	Angle of internal friction (ϕ) at R.D =31%	35°
14	Soil classification (USCS)	SP

A- Model piles details

Steel solid piles covered with cement mortar with specific weight of (7.75gm/cm3) and modulus of elasticity of (1.85×108 kPa) (Murphy, 1950) are used.

B- Model setup formulation

To simulate the pile load test in the field, a new apparatus was manufactured and described as the following:

C- Description of setup

Steel container is used to host the bed of soil. It was made from five separated parts. The internal dimensions of the container are (75×75×75) cm. Each part from the container is made of (6 mm) thick steel plate. A steel base was made to support the container and the loading frame weight. The axial load is applied through a hydraulic jack system.

The maximum load that can be applied is about (10 ton) according to hydraulic jack catalogue. The bed of soil is prepared with a dry unit weight of (16.5 kN/m^3) at a height of drop equal to 20 cm using raining technique.

The driving system consists of a base plate with (86 × 20) cm and 20mm in thickness. This plate involves three holes manufactured to be considered as focus place to penetrate the piles in the box.

The steel helmet was manufactured with different grooves that are suitable for all model piles sizes that are used in the tests. These grooves are designed to make sure the fixity of piles and as possible to reserve the vertical direction for pile penetration without tilting during the driving process. Details of setup and pile driving hammer device are shown in Plates (1 and 2).

V. PRESENTATION AND ANALYSIS OF TEST RESULTS

A series of 12 model tests were carried out as driven piles and installed in dry sand with a relative density of 31%. Many factors are considered which includes variation of driving energy used to penetrate pile, (P/W) ratio which significantly influences the tension and compression stresses generated in the pile body, effect of driving extension within the boundary, and the use of different diameters/widths and lengths for square and circular pile shapes. All details are listed in Table (3).

Plate 1. General view of the apparatus used with details

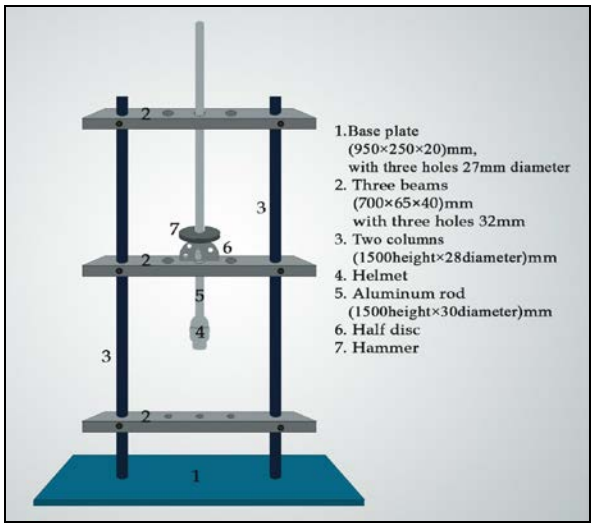

Plate 2. Details of the pile driving hammer device

TABLE 3
THE PARAMETERS EMPLOYED TO PERFORM MODEL DRIVEN PILES AND OUTPUT DATA

D (cm)	2.1	2.1	2.1	1.6	1.6	1.1
L (cm)	50	40	30	50	40	50
shape	Cir. Sq.	Cir. Sq.	Cir. Sq.	Cir. Sq.	Cir. Sq.	Cir. Sq.
E_{LAB} (kg.cm)	20.2 25.6*η	12.5 15.9	5.9 7.6	16.3 20.7*η	9.5 12.05	12.2*η 14.2*η
H (cm)	9.3 11.7	5.73 7.3	2.8 3.5	7.5 9.5	5.5 6.7	7.9 10
W (kg)	2.18	2.18	2.18	1.42	2.18	1.42
Set mm/blow	4.55 1.65	3.57 3.13	2.78 2.78	6.52 3.57	4.17 5.66	6.25 6.25
P/w	1.23 1.39	1.12 1.25	1 1.1	1 1.08	1.42 1	1.25 1.3
$(q_o)_{lab}$ (kg)	26.2 32	19 23.4	13.2 20	14.1 17.2	10.3 11.7	6.1 6.4
$(q_o)_{eq.}$ (kg)	21.1 28.2	17.8 23.1	9.4 17.2	14 16.4	8 9.1	3.6 5.2

*η is efficiency of hammer blow.

These factors are used to obtain the best representation of field conditions as to achieve the reasonable results. Figures (1 to 6) illustrate the test results of model driven piles presented as load–settlement curves.

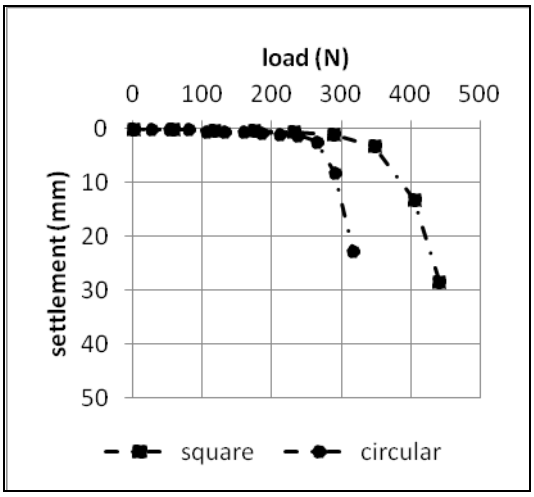

Fig.1. Load-settlement curves for model driven pile (L=50cm, L_D=41cm, B/D=2.1cm)

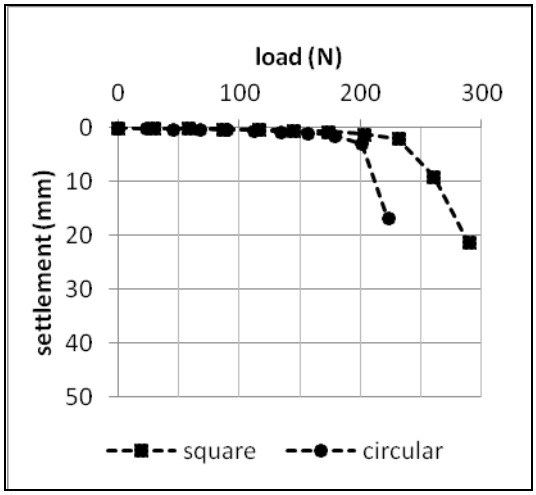

Fig.2. Load-settlement curves for model driven pile (L=40cm, L_D=31cm, B/D=2.1cm)

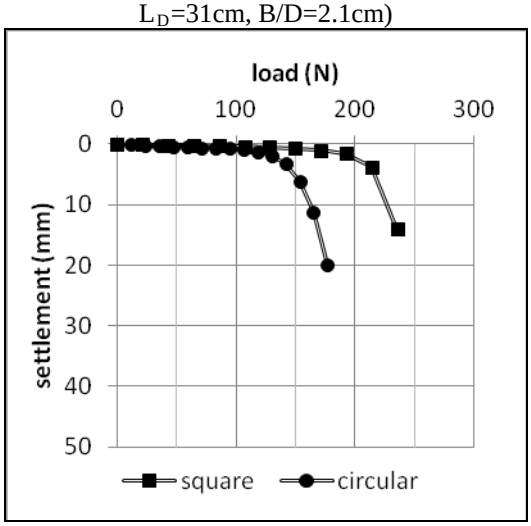

Fig.3. Load-settlement curves for model driven pile (L=30cm, L_D=21cm, B/D=2.1cm)

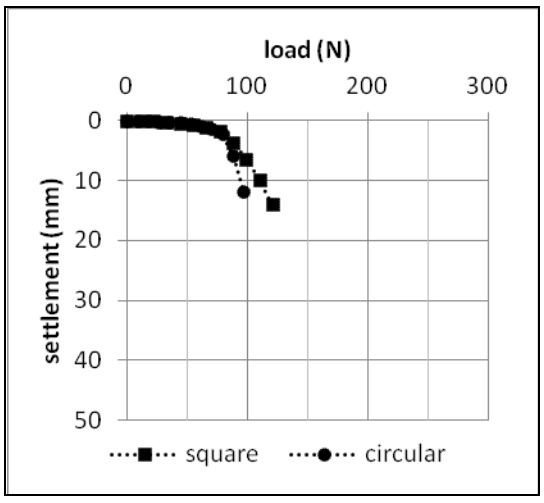

Fig.4. Load-settlement curves for model driven pile (L=50cm, L_D=41cm, B/D=1.1cm)

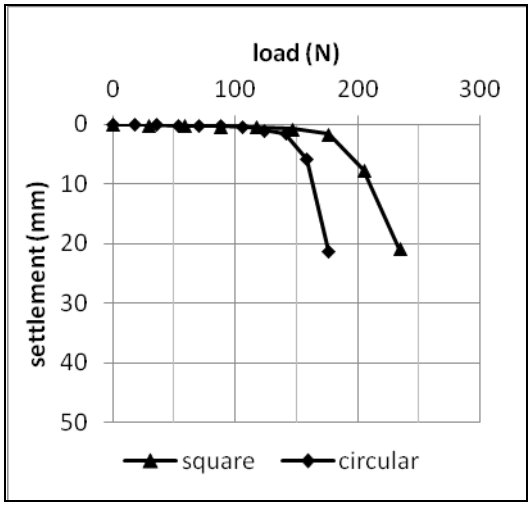

Fig.5. Load-settlement curves for model driven pile (L=50cm, L_D=41cm, B/D=1.6cm)

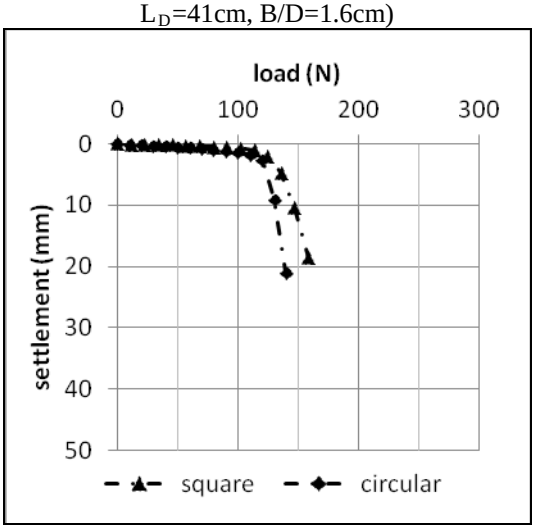

Fig.6. Load-settlement curves for model driven pile (L=40cm, L_D=31cm, B/D=1.6cm)

To study the effect of pile diameter/width on model driven pile tests, three values of (diameter/width) ratio of 1.1, 1.6 and 2.1cm for a pile length of 50cm are selected for both pile shapes (square or circular). From the mathematical calculation related with state equation (1), it is discerned that, the model piles contribute with same energy that is resisted by each cm^2 of pile area. Therefore, the results definitely reveal that the pile with larger diameter/width is the higher bearing capacity. This state is justified practically to decrease the penetration value (set) with increase in pile diameter/width.

For the effect of model pile length, one diameter of 2.1cm is used at three values of length of 30, 40 and 50cm. Depending on Table 3, the results exhibit that, the rate of pile capacity increases with the increase in pile length, which may be referred to the increase of displaced soil volume due to the increase in surface area of pile, in addition to the nonlinear increase of lateral pressure exerted on the pile.

VI. MATHEMATICAL MODELING OF RESULTS

In this section, the results obtained from the laboratory model pile tests which relate the ultimate pile capacity for model driven piles are grouped as a statistical data.

The computer package (STATISTICA) was used to represent relationships between the model piles capacity and hammer weight, falling height, penetration value (set), and pile to hammer weight ratio (P/W), besides diameter/width. Three dimensional contour areas for the variation of ultimate bearing capacity with the variables related to pile diving process are shown in Figures (7 to 8).

The computer package presents the results of experimental data as a mathematical model of ultimate pile capacity as a function of different parameters concerning the driven piles. Accordingly, the statistical model for pile capacity is derived to be: -

$$Log\ Q_{(ult)} = 0.0062D - 2.7\times10^{-6}\ H^{P/W} + (set/W)^{-0.19} - 0.186. \quad (2)$$

Where:-

$Q_{(ult)}$: Ultimate capacity of model driven piles in statistical model in kg.

D: Pile diameter/width in cm.

H: Hammer stroke in cm.

W: Weight of ram in kg.

Set: Number of blows corresponding to a penetration 25mm and 25cm of model and prototype pile length respectively in (mm/blow), and

P/W: Pile to hammer weight ratio.

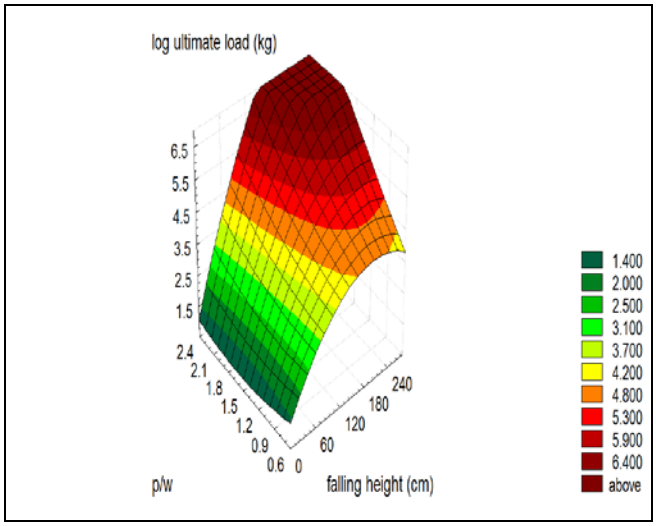

Fig. 7. Three dimensional contour plot of variation of ultimate capacity of driven piles with P/W ratio and falling height (H).

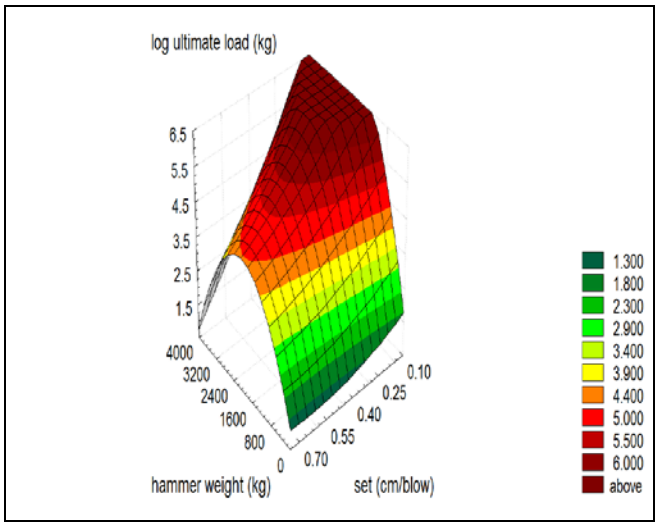

Fig. 8. Three dimensional contour plot of variation of ultimate capacity of drive piles with hammer weight (W) and penetration value (set).

The above mathematical formula was derived based on the assumption that a relationship between parameters is nonlinear. Due to the high difference between the prototype and small scale model values, it is necessarily required to use a logarithmic function for the statistical derived equation to reduce the magnitude of the standard deviation for the input data used in analysis

It can be concluded that the ultimate capacity of driven piles increases with hammer weight and falling height and moreover, pile diameter/width and inversely proportionate with P/W ratio and penetration value (set). To determine the adequacy of the derived equation, an expression of "coefficient of determination" (regression) that has denoted (R^2) is usually used to clarify the quality of output results. In this study, the value of R^2 was found to be (93.3 %) which gives an excellent indication for the power of output.

VII. VERIFICATION BETWEEN THEORETICAL DYNAMIC AND STATISTICAL EQUATIONS FOR MODEL DRIVEN PILES

Results of pile capacities calculated by dynamic (Hiley) formula and by the statistical equation (2) for driven piles are also compared with actual results of pile tests carried out at (Al-Russafa water treatment plant). The results of comparison are tabulated in Table 4.

It can be noticed that the dynamic statistical equation demonstrates slightly higher results compared with theoretical equation and this may be attributed to the fact that the model piles capacities obtained from the experimental tests are larger than the model piles capacities predicted using theoretical dynamic equation which deals with Briaud and Tucker (1988).

TABLE 4
COMPARISON OF RESULTS BETWEEN STATISTICAL AND DYNAMIC EQUATIONS

B (cm)	28.5

L (m)	12				
L_D (m)	11	9.5	7.75	9	8
Rated energy E (kg. m)	5500	3125	5500	3125	3125
Set (mm/blow)	5.84	2.97	7.3	3.28	2.4
Pile capacity calculated by statistical equation (2) in (Ton)	112	141	115	103	63
Pile capacity calculated by Hiley formula in (Ton)	114	105	99	102	93
Pile capacity calculated from field test in (Ton)	80	101	89	84	76

However, this analysis displayed a reasonable compatible between the models and actual results. It is to be expected that, the driving process leads to significant densification of the sand for the surrounding area where the model pile is being tested, which in turn increase the relative density. This increase in the sand density makes the tendency of the model pile to dilate more than the full scale model.

This condition is compatible with (So, 1991) who found out that, the shaft resistance of small model will be greater than of large- diameter pile. To justify the mechanism of this state the shear zone generated near the pile wall is affected with the area subjected to shearing. Therefore, the smaller area is the less room for soil particles to rearrange and less space for shear zone to fully develop to a critical state.

For this, the interlocking between the particles would be increased and hence increase the friction resistance which makes the dilation of sand is occurred more probably. This behavior is effectively reflected on the results of small model tests which revealed that, the bearing capacity obtained from the statistical derived equation is larger than that computed from load test in field.

VIII. CONCLUSIONS

Based on analysis of the 12 pile model tests performed as driven piles, the following conclusions can be raised:

1. The number of blows is affected by diameter more than with pile length when two piles have same total areas are driven by the same constant driving energy.
2. The statistical equation manifests bearing capacity results slightly higher than those values obtained by dynamic formula, which may be referred to particle size effect.
3. The coefficient of determination (R^2) for driven pile equation is about (93.3%) which may give a remarkable conception about the solidity of the derived equation.
4. A reasonable convergence between the models and actual results can be obtained when the scale effects related to stress level and boundary conditions are taken into the consideration.

REFERENCES

[1] Briaud, J.L. and Tucker, L.M. (1988): "Measured and Predicted Axial Response of 98 Piles", Journal of Geotechnical Engineering, ASCE, 114(9), pp. 984-1001.

[2] Horn, H. M. (1966): "Influence of Pile Driving and Pile Characteristics on Pile Foundations Performances," Notes for Lectures to New York Metropolitan Section, ASCE, Soil Mechanics and Foundation Group.

[3] Kishida, H. (1967):"Ultimate Bearing Capacity of Piles Driven into Loose Sand", Journal of Soil Mechanics and Foundations Division, ASCE, Vol.7, No.3, pp. 20-29.

[4] Meyerhof, G.G. (1959): "Compactions of Sands and Bearing Capacity of Piles", Journal of Soil Mechanics and Foundations, ASCE, Vol.85: SM6, pp. 1-29.

[5] Murphy, G.C (1950): "Similitude in Engineering", the Ronald Press Company, New York.

[6] Salgado, R. (2006):"The Engineering of Foundations", 1st ed. Mc Graw-Hill book company, New York.

[7] Shlash, K.T. and Abdul Razzak, M.M. (1986): "An Approach for Evaluating Hammer Used for Pile Driving", Journal of the Technology and Engineering, Vol.4, No.3, pp.67-80.

[8] So, C.W. (1991):"Large-Section Excavated Piles in Hong Kong", M.Sc. Dissertation, University of London, 163 p.

Improvement of Expansive Soil Properties Using Metakaolin and Rice husk Ash

Mahmoud D. Ahmed[1], Haifaa A. Ali[2] . and Nisreen A. Hamza[3]

Abstract— **Expansive soil spreads in Iraq and some countries of the world. But there many problems can be occurred to the structures that built on, so we must study the characteristics of these soils due to the problems that may be caused to these structures which built on these kinds of soil and then study the methods of treatment. The present study focuses on improving the geotechnical properties of expansive soils by treating it with mix of Rice Husk Ash and Metakaolin. The soil used in the present study can be classified according to the Unified Soil Classification System as clay with high plasticity (CH). Rice Husk Ash (R) is well-known material for stabilizing the expansive soils. In this study Rice Husk Ash was prepared by simply burning rice husk, collected from the locally available mill. In this arrangement, rice husk has been burned in control oven for two hours at 600°C. The produced R contains more than 80% silica which is a key factor for improving the properties of soil. Metakaolin is a pozzolanic material. It's obtained by calcination of kaolinite clay at temperatures from 700°C to 800°C. Kaolin chemical composition is basically aluminous silicates hydrates associated with Mn, Fe, Ca, K, Na. Its crystal has a lattice structure of tetrahedral and octahedral layers with interplanar distance of 7.2 Å. The soil sample R11M4 gives the maximum reduction in swelling and swelling pressure about 97% and also increase the shear strength parameters about 155% for the soil therefor, it can be considered the best percentage of the combined replacement materials in improving the properties of expansive soil.**

Index Terms— **expansive soil; improvement; Metakaolin; Rice Husk Ash**

I. Introduction

The Expansive soil is one of the problematic soils that face many geotechnical engineers in the field (others include collapsible soil, quick clays, etc.). The expansive soil is known to cause severe damage structures that are founded on it. In Iraq, there is no confirmed information about the economic losses due to structures founded on expansive soils. However, there are several well-documented cases of studying the behavior of expansive soil in Iraq. Expansive soils are very sensitive to variations in water content and show excessive volume changes because of an increase in their water contents. Expansive soils have the tendency to swell when they become in contact with moisture and to shrink if moisture is removed from them. Expansive soils are a worldwide problem (Seed et al., 1962, Kormonik and David, 1969) this highly plastic soil may create cracks and damage on the pavements, railways, highway embankments, roadways, building foundations, channel and reservoir, water lines, sewer lines etc.(Gromko, 1974). Swell response of expansive soils has been investigated by researchers since the 1950s based on Atterberg limits, index properties, and other soil tests carried out in the laboratory (Seed et al., 1962). These studies were a major success but they have failed to determine the associated engineering properties. This is mainly because soils with the same atterberg limits and index properties show different engineering properties. In order to control the volume change in expansive soils, many admixtures are adequately used in the researches (Kehew,1995). Metakaolin has never been studied its effect on the expansive soils. Metakaolin is a dehydroxylated form of the clay mineral kaolinite. Rocks that are rich in kaolinite are known as kaolin, traditionally used in the manufacture of porcelain. The particle size of metakaolin is smaller than cement particles, but not as fine as silica fume. Metakaolin is a pozzolanic material and has never been used before as an additive to improve the expansive soil therefore studying its effect will give us the way to use it as pozzolanic material to reduce the swelling potential. The standard chemical requirements of ASTM C618-03 include the sum of SiO2 , Al2O3 and Fe2O3 content (≥ 70%) for class F and (≥ 50%) for class C to define the material as pozzolanic.

Manuscript received July 4, 2015. This work was supported in part by the University of Technology/ Construction and Building Department.

[1] Mahmoud D. Ahmed Asst. Prof., Civil Engineering Department, University of Baghdad ,Baghdad, Iraq. (e-mail: Mahmoud_baghdad@yahoo.com)

[2] Haifaa A. Ali Leacture., Civil Engineering Department, University of Baghdad ,Baghdad, Iraq. (e-mail: Haifaaali2013.@yahoo.com)

[3] MSc in geotechnical engineering ,Civil Engineering Department, University of Baghdad ,Baghdad, Iraq. . (email: heart_owen1077@yahoo.com)

II. MECHANISM OF SWELL

Mitchell, 1993 showed that soil swelling happens due to several factors:

1-Capillary Imbibition: The surface tension caused by air in the unsaturated soil and the soil suction caused water adsorption to the soil system.

2-Osmotic Imbibition: The double layer acts as semi permeable membrane with difference in the ion's concentration inside and outside of it causing the flow of water and increase in the soil volume.

3- Hydration of Exchangeable Cations: as described previously the cations attracted to the negatively charged soil surface causing an increase in the volume of the double layer. Then these cations will be hydrated causing an increase in the ion's volume and as a result an increase in the soil volume.

4-Van Der Waals forces: these forces are secondary in-directional forces and less strong than the hydrogen bonding and they connect the montmorillonite sheets, when adsorption of water happens a repulsion between these forces will happen leading to an increase in the volume of soil.

The objectives of this study are

1- Improve the properties of expansive soil to be used as construction material in the pavements, railways, highway embankments, roadways, building foundations, channel and reservoir linings, irrigation systems, water lines, sewer lines etc.

2- Reduce the industrial wastes, this reduction is considered one of the concept used in contamination control.

3- Use local materials in soil treatment which reduces the costs.

III. EXPERIMENTAL WORKS AND MATERIALS

1- Materials used

The materials used during the experiments were bentonite, sand, and metakaolin. Table (1) shows the physical properties of the materials that have been used in the study.

1-prepared soil: mixture of bentonite (Ca-based bentonite manufactured by Al-Fallujah Cement Factory is used as the expansive soil) with sand (from Ali Al-Gharbi city south of Baghdad) were tested till getting the mixture of 85% of bentonite to 15% of sand (Bentonite-Sand) by dry weight depending on the required plasticity indices.

2- Rice husk ash (R): Rice milling generates a by-product known as husk. This surrounds the paddy grain. During milling of paddy about 78% of weight is received as rice, broken rice and bran. Rest 22% of the weight of paddy is received as husk. This husk is used as fuel in the rice mills to generate steam for the boiling process. This husk contains about 75% organic volatile matter and the remaining 25% of the weight of this husk is converted into ash during the firing process, known as Rice Husk Ash (R). This R in turn contains around 85% - 90% amorphous silica. So for every 1000 kg of paddy milled, about 220 kg (22%) of husk is produced, and when this husk is burnt in the boilers, about 55 kg (25%) of R is generated. The rice husk ash in this study was prepared by simply burning rice husk, collected from the locally available mill. In this arrangement, rice husk has been burned in control oven for two hours at 600°C. The produced rice husk ash contains more than 80% silica which is a key factor for improving the properties of soil.(Rao et al., 2012).

2- metakaolin (M) is a pozzolanic material. It's obtained by calcination of kaolinite clay at temperatures from 700°C to 800°C as shown in Eq.(1).Kaolin chemical composition is basically aluminous silicates hydrates associated with Mn, Fe, Ca, K, Na. Its crystal has a lattice structure of tetrahedral and octahedral layers with interplanar distance of 7.2 Å (Cited in Clovis, et al., 2004).

$$Al_2Si_2O_5(OH4) \xrightarrow{700°C} Al2O3.2SiO2+2H2O \quad (1)$$

Kaolin → Metakaolin

The chemical properties of these materials are presented in Table (2).

Table (3) shows the list of percentages of replacement materials into the soil.

Table (1). The physical properties of materials used.

Physical properties	Index properties	Prepared soil	Bentonite	Sand	M	specification
Atterberg limits	Liquid limit,L.L(%)	112	150	NP	39	ASTM D-4318
	Plastic limit,L.L(%)	45	45	NP	22	
	Plasticity index,P.I(%)	67	105	NP	17	
Grain size analysis	% sand (0.06-2)mm	4	0	97.68	0	BS 1377-1975
	% silt (0.002-0.06)mm	24	5	2.32	0	
	% clay (<=0.002)mm	72	95		100	
Specific gravity,Gs		2.78	2.89	2.63	2.57	ASTM D-854
Compaction test	Max dry density,(KN/m³)	13.4	12.64	15.15	-	ASTM D-1557
	Optimum moisture content,%	36	37	12.5	-	
USCS*		CH	CH	SP	-	ASTM D-2487

*Unified soil classification system.

Table (2). Chemical properties of materials used.

Materials / Chemical prop.	Bentonite	Sand	Rice husk ash	Metakaolin
SiO_2 %	51.92	55.55	87.67	59.62
Fe_2O_3 %	5.45	0.08	0.298	1.629
Al_2O_3 %	14.23	0.5	0.40	26.63
CaO %	8.24	11.25	1.40	0.74
MgO %	2.86	3.9	0.37	0.0034
Na_2O %	0.96	1.73	1.15	0.43
K_2O %	0.69		3.84	
TiO_2 %	0.8	-	0.031	1.875
PH	7.7	7.6	-	-
SO_3 %	1.3	1.33	1.54	-
Gypsum %	2.64	2.86	-	-
T.S.S %	5.25	0.7	-	-
O.M %	0.7	1.3	-	-

Table (3). List of percentages of replacement materials into the soil and their abbreviations.

Percentage of the replacement material	Abbreviation
5% of rice husk ash	R5
8% of rice husk ash	R8
11% of rice husk ash	R11
14% of rice husk ash	R14
10% metakaolin with 5% rice husk ash	M10R5
10% metakaolin with 8% rice husk ash	M10R8
10% metakaolin with 11% rice husk ash	M10R11
11% rice husk ash with 4% metakaolin	R11M4
11% rice husk ash with 6% metakaolin	R11M6
11% rice husk ash with 8% metakaolin	R11M8

2- SOIL PREPARATION

The physical tests was carried according to (BS 1377: 1975) and the prepared soil is composed of 72% of clay , 24% of silt ,and 4% of sand.

3- Shear Strength Tests:

1. Sample Preparation

Remolded specimens were prepared in the laboratory depending on the proctors data at the required molding water content according to (ASTM D 2850 – 03a) .

2. Unconfined Compression Tests

The specimens were compacted statically for the maximum dry density and optimum moisture content values then sealed and allowed to cure for one day. The test has been carried according to (ASTM D-2166).

4- The swelling test

Three types of swelling tests have been made (free swell test, constant volume test, and consolidation test). The tests were done according to Head 1984 and ASTM D 4829-03. In these tests, the oven dried soil passing 2mm sieve was mixed with the required amount of water and were remolded at the oedometer ring (75 mm in diameter and 19 mm in height) but the sample was prepared by a height equal to 14 mm to insure that the specimen will be laterally confined (Al-Omari, et al., 2010). A load of about 7 KPa was applied as seating pressure, left for ten minutes then an initial reading was recorded. The soil sample was submerged with distilled water for 24 hours then the final reading was recorded. To measure the swelling pressure, weights will be added in increments to the soil sample to get the dial gage reading zero again.

IV. RESULTS OF TESTS

1. Results of grain size distribution

Fig. 1 shows the effect of metakaolin on the grain size analysis of the prepared soil. It can be noticed one can notice that the improvement with RM (11% of R and different percentages of M) decreases the percentages of fines in the soil and shifted the grain size distribution curve of soil A to coarser size due to the coarser size of R , but we can noticed that increasing M while R remains constant causes an increment in the clay content , for example Soil R11M4 causes 50% reduction in the clay content , 50% increment in the silt content and 600% increment in the sand content, whereas soil R11M6 causes 36% reduction in the clay content , 75% increment in the silt content and 200% increment in the sand content, this behavior could be related to the finer size of M causes the best results for the grain size distribution for the previous replacement.

Soil R11M8 gives 68% reduction in the clay content , 79% increment in the silt content and 750% increment in the sand content and show the same previous behavior but in different direction within the replacement process and that could be explained that the chemical reaction caused high temperature and hence the reason for high hydration which could be noticed later at the compaction test results.

It is worth mentioning that the last replace (R11M8) gave the best results to the sieve analysis and hydrometer tests as compared with the optimum ratios for each replacement. material as pozzolanic).Table 4 shows the results of the grain size distribution test.

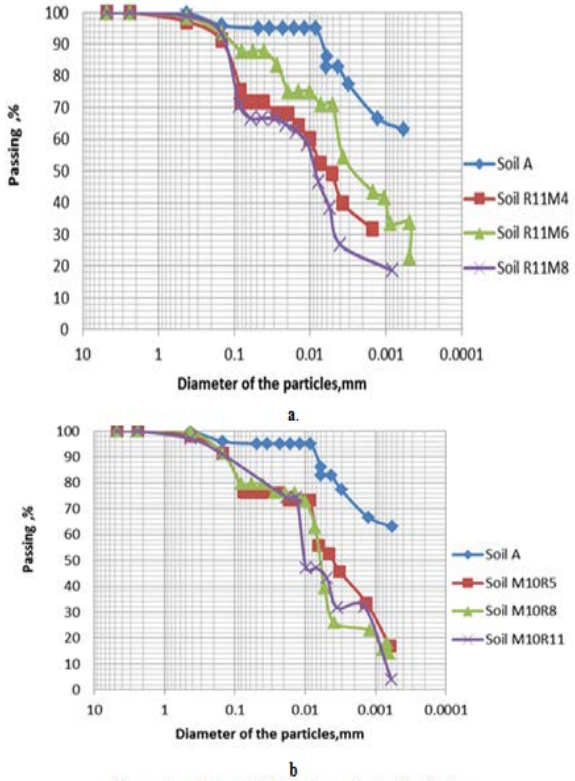

Figure 1. a. Effect of RM on the grain size distribution.
b. Effect of MR on the grain size distribution.

Table (4). Results of the grain size distribution tests.

Soil Sample	% Sand	% Silt	%Clay
A	4	24	72
R5	4	34	62
R8	4	36	60
R11	12	32	56
R14	28	46	26
M10R5	24	36	40
M10R8	20	56	24
M10R11	14	52	34
R11M4	28	36	36
R11M6	12	42	46
R11M8	34	43	23

2. Results of specific gravity tests

the effect of metakaolin on the specific gravity results. it can be noticed that the combination of two replacement materials causes a reduction in the specific gravity from 2.78 to 2.5 for RM replacement and from 2.78 to 2.58 for MR replacement due to lower specific gravity of R and M that have been used as shown in **Table (5).**

3. Results of the compaction tests

1- The replacement materials MR decrease the max dry unit weight and decrease the optimum moisture content for soil samples M10R5 and M10R8. The decrease in the maximum dry unit weight may be explained by considering the MR as filler (with lower specific gravity) in the soil voids **(Cited in Fattah et al., 2013)** whereas soil M10R11 shows an increment in the optimum moisture content due to the excess water needed by R for hydration .

2- The replacement materials RM decrease the max dry density and increase the optimum moisture content for soil samples R11M4 and R11M8. This is due to the light weight of RM and more water holding capacity of the rearranged particles. Except for soil sample R11M6 which shows different behavior and can be noticed when the specific gravity increasing which causes increasing in max dry unit weight and a reduction in water content.

Table (5) shows the results of the compaction and specific gravity tests results.

4. Results of unconfined compression test

Figure (2) shows effect of the replacement materials on the unconfined compression strength of the expansive soil. This Figure illustrate the stress-strain behavior of prepared and treated soil under vertical load. Initially the stress gradually increases with the increase in strain. After attaining the peak stress, it decreases with the increase in strain for all the combinations of replacement materials and soil. Approximately all the specimens show shear failure after the failure of plane of specimens. **Figure (5)** shows the effect of M on the cu and Table (6) shows the results of the unconfined compression tests .it can be noticed that the replacement material M causes a linear increment in cu from (160.73 to 315.00) KPa for soil samples from (M4 to M10). This increment was due to the reactive silica which reacts and produce cementations material and binds soil particles together to increase strength (Kumar, 2012). The reduction in cu at M12 to 258.90 KPa may be due to the excess M introduced to the soil and therefore forming weak bonds between the soil and the cementations compounds formed.

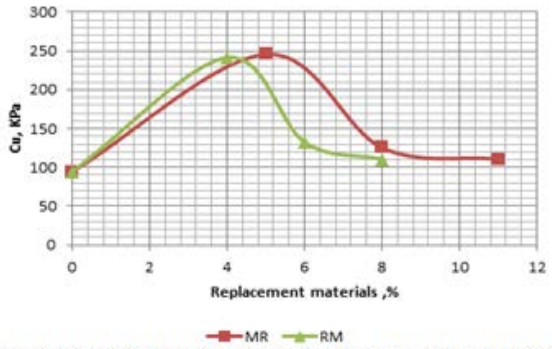

Figure (2). effect of the replacement materials on the undrained cohesion

Table 6. Results of the unconfined compression tests.

Soil Samples	Cu(kpa)				Φ UU Test	
	Unconfined Compression Test	Increasing in Cu,%	UU Test	Increasing or reduction in Cu,%		Increasing in Φ,%
A	94.75813	0.00	111.1	0.00	10.4	0.00
M10R5	245.5942	159.18	252.0607	126.88	19.91986	91.54
M10R8	125.2963	32.23	249.8768	124.91	18.17047	74.72
M10R11	110.5982	16.72	146.9012	32.22	31.11551	199.19
R11M4	241.4092	154.76	327.2839	194.58	22.80524	119.28
R11M6	132.3311	39.65	149.8275	34.86	36.80705	253.91
R11M8	110.5982	16.72	194.8019	75.34	26.3484	153.35

5. Results of unconsolidated undrained triaxial test

The replacement materials MR or RM in **Figure (3)** cause various increment in the cu due to the different pozzolanic reaction that occur between rice husk ask, metakaolin and the prepared soil. **Figure (4)** illustrates that the slope of the of curve increases linearly with the increase of the replacement materials R and MR. The improvement of angle of internal friction(φu) implies that the silica content in the replacement materials act as a binder which agglomerate the particles into a larger one.

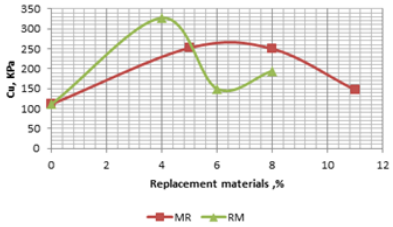

Figure (3). Effect of Different Replacement material Percentages on the Cohesion of the Soil from UU tests.

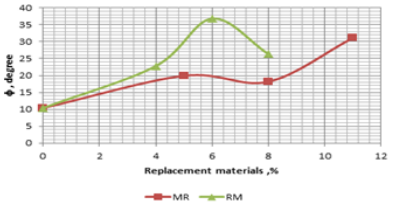

Figure (4). Effect of Different Replacement material Percentages on the Angle of Internal Friction of the Soil.

6. Results of swelling tests

Figure (5) shows the effect of the replacement materials on the Time – Percent Swell The prepared soil shows a high rate of swell within the 11 days and then reaches a fix point ,whereas the treated soil reaches its point with less than that. It is due to the electrical equilibrium when the double layer

arrives to its full required thickness to balance the net negative charges at the faces of clay particles. The swell percent decreases due to the effect of pozzolanic reaction for the replacement materials that have been used which take place during the process.

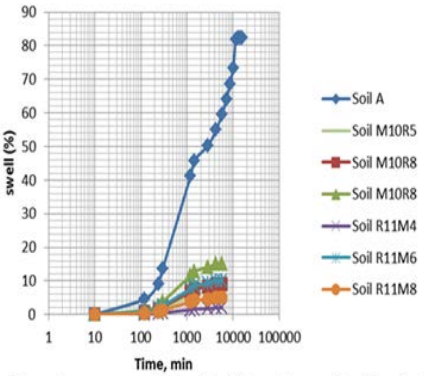

Figure(5) .Effect of the replacement materials on the Time – Percent Swell for the Prepared Soil and Soil .

Figure (6) shows e- logσ_v for the prepared soil and **Figure (7)** shows e- logσ_v for the effect of the replacement materials **.**

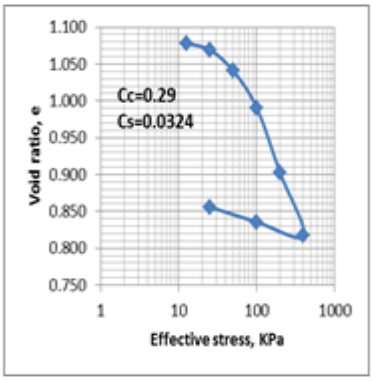

Figure (6). e- logσ_v for prepared soil sample A.

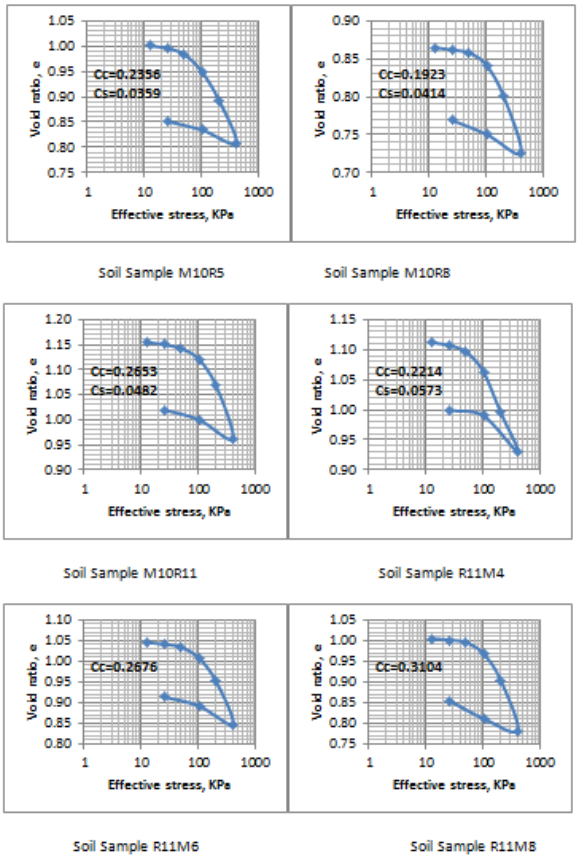

Figure (7). e- logσ_v for Soils Treated with R and M.

Table (7) shows the results of the free swell and constant volume tests. The potential expansion has been classified according to **ASTM- D (4829 – 03)** as shown in **Table (8).**

Table (7). The results of the free swell and constant volume tests.

Soil Samples	Free Swell Test			Constant Volume Test			Reduction in the Swelling Potential,%	Potential Expansion for Constant Volume Test
	Free Swell, %	Expansion Index	Swelling pressure, kpa	Free Swell, %	Expansion Index	Swelling Pressure, KPa		
A	83	825	882	46	458	588	0	very high
M10R5	7	73	113	6	61	75	87	medium
M10R8	9	90	120	8	76	80	83	medium
M10R11	15	150	183	13	128	122	72	high
R11M4	2	20	9	2	16	6	97	very low
R11M6	10	100	150	9	85	100	81	medium
R11M8	5	50	38	4	42	25	91	low

Table (8). The classification of a potentially expansive soil (ASTM- D 4829 – 03).

Expansion Index, EI	*Potential Expansion*
0–20	Very Low
21–50	Low
51–90	Medium
91–130	High
>130	Very High

The soils samples turned from very high expansive to moderate and even very low expansion potential due to the effect of pozzolanic materials which could be due to the pozzolanic and cation exchange reactions which occurred between the soil and replacement materials. Eq.(2) shows the calculation of the expansion index according to ASTM- D (4829-0).

EI=(ΔH/H)*1000 (2)

Where:

EI: Expansion Index,

ΔH = change in height, D2 − D1, mm,

H1 = initial height, mm,

D1 = initial dial reading, mm, and

D2 = final dial reading, mm.

Based on the results of consolidation as shown in Table (9) ,the coefficient of permeability of the soil can be calculated from Eq. 3:

$$K = C_v \, m_v \, \gamma_w \quad (3)$$

where:
C_v = Coefficient of consolidation,
m_v = Coefficient of volume change, and
γ_w = Unit weight of water.

Table (9). Results of Consolidation Tests.

Soil Group	e_o	C_c	Cs	$m_{v\ x10^{-4}}$ m^2/KN	$C_{v\ x10^{-8}}$ m^2 / sec	$K_{x\ 10^{-8}}$ m/sec
A	1.106	0.290	0.032	2.030	1.949	0.004
R5	1.110	0.255	0.031	2.192	1.970	0.004
R8	1.239	0.286	0.032	1.602	4.161	0.007
R11	1.226	0.213	0.025	5.607	6.562	0.036
R14	1.198	0.262	0.024	1.851	30.579	0.056
M10R5	1.014	0.236	0.036	2.355	12.468	0.029
M10R8	0.870	0.192	0.041	2.163	10.948	0.023
M10R11	1.158	0.265	0.048	2.736	9.203	0.025
R11M4	1.115	0.221	0.057	1.707	21.814	0.037
R11M6	1.046	0.268	0.055	6.464	5.300	0.032
R11M8	1.005	0.310	0.060	3.450	5.204	0.018

V. CONCLUSIONS

Based on the experimental results of the experimental work, the following conclusions may be obtained

• The compaction curves shows that the behavior of the combined additives shows that if there is an increase in R up to 11% and a decrease in M down to 4%, this would cause a reduction in the maximum dry density and an increase in the optimum moisture content.

• The results of swelling pressure test using constant volume method show that the addition of admixture combination of (R-M) to expansive soils significantly reduces the swelling pressure, as follows: the addition of (11%) R causes a reduction of about (79%), and the reduction increases to about (99%, 83% and 96%) after the addition of (4, 6 ,and 8%) of M respectively. The addition of (10%) M causes a reduction of about (87%) whereas the reduction various to about (87%, 86%, 79%) after the addition of (5, 8 ,and 11%) of R respectively.

• From the consolidation test results, it can be concluded that the values of compression index decreases for all soils samples and the initial void ratio shows a positive relation with all soil samples except soils samples M10R5, R11M6, and R11M8 which show decrease in the initial void ratio to about (21, 9, and 5)% respectively.

• From the unconfined compression tests results show that the prepared soil A has (Cu=94.76 KPa) whereas, soils samples (M10R5, and R11M4) have Cu equal to (246, and 241) KPa respectively.

• The strength parameters obtained from unconsolidated undrained triaxial tests results show that the prepared soil A has (Cu=110 KPa and φu=10.4°) whereas, soil sample M10R8 has (Cu=249.88 KPa and φu =18.17°), soil sample R11M8 has (Cu=194.80 KPa and φu =26.35°).

• The soil sample R11M4 gives the maximum reduction in swelling and swelling pressure about 97% and also increase the shear strength parameters about 155% for the soil therefor, it can be considered the best percentage of the combined replacement materials in improving the properties of expansive

First A. Author (M'76–SM'81–F'87) and the other authors may include biographies at the end of regular papers. Biographies are often not included in conference-related papers. This author became a Member (M) of IEEE in 1976, a Senior Member (SM) in 1981, and a Fellow (F) in 1987. The first paragraph may contain a place and/or date of birth (list place, then date). Next, the author's educational background is listed. The degrees should be listed with type of degree in what field, which institution, city, state, and country, and year degree was earned. The author's major field of study should be lower-cased.

The second paragraph uses the pronoun of the person (he or she) and not the author's last name. It lists military and work experience, including summer and fellowship jobs. Job titles are capitalized. The current job must have a location; previous positions may be listed without one. Information concerning previous publications may be included. Try not to list more than three books or published articles. The format for listing publishers of a book within the biography is: title of book (city, state: publisher name, year) similar to a reference. Current and previous research interests end the paragraph.

The third paragraph begins with the author's title and last name (e.g., Dr. Smith, Prof. Jones, Mr. Kajor, Ms. Hunter). List any memberships in professional societies other than the IEEE. Finally, list any awards and work for IEEE committees and publications. If a photograph is provided, the biography will be indented around it. The photograph is placed at the top left of the biography. Personal hobbies will be deleted from the biography.

REFERENCE

Al-Omari, R. R., Ibrahim, S. F. and Al-Bayati, I. K., (2010) "Effect of Potassium Chloride on Cyclic Behavior of Expansive Clays", International Journal of Geotechnical Engineering, Vol. 4, No.2, pp. 231-239.

ASTM C 618(2003), "Standard Specification for Coal Fly ash and Raw or Calcined Natural Pozzolan for Use in Concrete", Reprinted from the Annual Book of ASTM Standards. Copyright ASTM, Vol.4, No.2.

ASTM D 2166 (2000), "Standard Test Method for Unconfined Compressive Strength of Cohesive Soil", Reprinted from the Annual Book of ASTM Standards. Copyright ASTM, Vol.4, No.8.

ASTM D 2487 (2000), "Standard Practice for Classification of Soils for Engineering Purposes (Unified Soil Classification System)", Reprinted from the Annual Book of ASTM Standards. Copyright ASTM, Vol.4, No.8.

ASTM D 4318 (2000), "Standard Test Methods for Liquid Limit, Plastic Limit and Plasticity Index of Soils", Reprinted from the Annual Book of ASTM Standards. Copyright ASTM, Vol.4, No.8.

ASTM D 4829 (2003), “Standard Test Method for Expansion Index of Soils”, Reprinted from the Annual Book of ASTM Standards. Copyright ASTM, Vol.4, No.8.

ASTM D 854 (2000), “Standard Test Methods for Specific Gravity of Soil Solids by Water Pycnometer”, Reprinted from the Annual Book of ASTM Standards. Copyright ASTM, Vol.4, No.8.

ASTM D1557, (2002), “Standard Test Methods for Laboratory Compaction Characteristics of Soil Using Standard Effort”, Annual Book of ASTM Standards, Vol. 04.08

ASTM D2850, (2003a), “Standard Test Method for Unconsolidated-Undrained Triaxial Compression Test on Cohesive Soils”, Annual Book of ASTM Standards, Vol. 04.08

B.S.1377 , (1975) “Methods of test for soils for civil engineering purposes” , British Standard

Clovis N. , Vanderley M. J. , Cleber M. R. D., Holmer S. Jr. , Mario S. T. , (2004): "Effect of Metakaolin on the Performance of Pva and Cellulose Fiber Reinforced Cement.

D. Koteswara Rao, G. V. V. Rameswara Rao, P. R. T. Pranav,(2012) “A Laboratory Study on the effect of Rice Husk Ash & Lime on the Properties of Marine Clay”. International Journal of Engineering and Innovative Technology (IJEIT), Volume 2, Issue 1, pp.345-353.

Fattah, M.Y. Rahil,F.H.Al-Soudany ,K.Y.H., (2013) "Improvement of Clayey Soil Characteristics Using Rice Husk Ash", Journal of Civil Engineering and Urbanism Vol. 3, No. 1,pp.12-18 .

Gromko, G. J., (1974): "Review of Expansive Soils," Journal of the Geotechnical Engineering Division, ASCE, Vol. 100, No. GT6, pp. 667-687.

Head, K. H., (1984): "Manual of Soil Laboratory Testing", Pentech Press, London, Vol. 1.

Kehew, E.A., (1995):"Geology for Engineers and Environmental Scientists", 2nd ed. Prentice Hall Englewood Cliffs, New Jersey, pp. 295-302.

Kormonik, A., and David, D., (1969):"Prediction Of Swelling Pressure of Clays", Journal of Soil Mechanics and Foundation Division ASCE, Vol. 95 (SM1), pp. 209–225.

Kumar S. M. P. , (2012): "Silica and Calcium effect on Geo-Technical Properties of Expansive soil Extracted from Rice Husk Ash and Lime", International Conference on Environment Science and Engineering, Singapore , Vol. 32 , pp. 119-123.

Mitchell, J. K. (1993), “Fundamentals of Soil Behavior”, 3rd edition, John Wiley and Sons, New York, USA.

Seed, H. B., Mitchell, J. K., and Chan, C. K., (1962): "Studies of Swell and Swell Pressure Characteristics of Compacted Clays," Highway Research Board, Bulletin No. 313 (1962), pp. 12-39.

The Characteristics of Collapsibility and Compressibility of Gypseous Soils in Iraq

Mr. Alaa Dawood Salman
Engineering College,University of Baghdad
dawood.alaa2000@yahoo.com

Abstract-
The gypseous soils are distributed in many regions in Iraq and other countries. Therefore, it is necessary to study the geotechnical properties of such soils upon wetting due to the large damages that affect the structures founded and constructed on it. In this study, Compressibility and shear strength Characteristics are studied for three soils used in this work, were brought from three different areas in Iraq (Karblaa, Kirkuk and Al-Ramadi) and taken at depth ranging from (1-1.5) m below ground level after excavating the upper soil strata. All fundamental tests were performed on these soils.

Laboratory tests results showed that these soils have high collapsibility and that shear strength parameters of (C, ϕ) decrease when soaked in water but the main decrease was in (C) value. Also the study includes the influence of the initial void ratio and the water content on the modules of the collapsibility. The value of Collapse Potential seems to depend mainly on the natural water content and initial void ratio. The Collapse Potential increase with the increase of void ratio and decrease with increase of water content.

Key word : gypseous soils, Collapsibility, Compressibility, Shear Strength,

Introduction

Collapsible soil is defined as soil that is susceptible to a large and sudden reduction in volume upon wetting [13]. Collapsible soil deposits share two main features, they are loose, cemented deposits; and they are naturally quite dry. Gypseous soils are disturbed in many regions in world especially in arid and semi-arid regions, where the annual quantity of rainwater is insufficient for leaching the gypsum form these soils, [4]. Gypseous soil are soils which has enough gypsum content to change or affect its engineering properties.

Gypsum is a mineral salt commonly known as Hydrated Calcium Sulphate (CaSO4.2H2O), [2]. The soil is strong when it was dry but loses its strength when exposed to water causing collapse and distortions. Many attempts (laboratory and field investigations) have been made to understand the behavior and the characteristics of these soils cause problem observed when construction on it [1], [5], [17]. Collapsible soil is defined as any unsaturated soil that goes through a radical rearrangement of particles associated with great loss of volume upon wetting with or without additional loading, [9], [19]..The main objective of this study is to investigate the collapsibility and compressibility characteristics of gypseous soil.

Distribution of gypseous soil in Iraq

Gypseous soils exist mainly in arid and semi-arid regions, concentrates in continents like Africa, central and southern Asia. Iraq is among the countries of south Asia where gypsum covers about 12 % of its total area. [13], [14] The first map demonstrating the distribution of gypsum in Iraq was presented by (Buringh 1960) [10], indicating five zones as shown in figure (1A) . The primary gypsum is located in the extreme north area between Tigris and Euphrates rivers. The second zone where primary gypsum mixed with limestone located below and parallel to the Euphrates river extending from the west desert to the south. The secondary gypsum is

identified in two areas, one in the north below the first zone and one in the south – west. The fourth zone is gypsiferous alluvium extends from the north in a narrow band and gradually widened towards the south. The fifth zone representing the non gypsiferous soil, mainly limestone is identified in two areas one in the north east and the other in the west desert. A more refined map exhibiting the distribution of gypsum in Iraq was presented by (Al-Barrazanji 1973) [3]. He investigated thoroughly the type and gypsum content in different parts of Iraq and proposed the map shown in figure (1B) .Six zones are distinguished according to their origin and gypsum content. In Iraq, Reference [3] classified the soils for agricultural purposes according to gypsum content, as Table 1.

Figure (1) A : First map of distribution of gypsum in Iraq.[10] B: Distribution of gypsum in Iraq.[3]

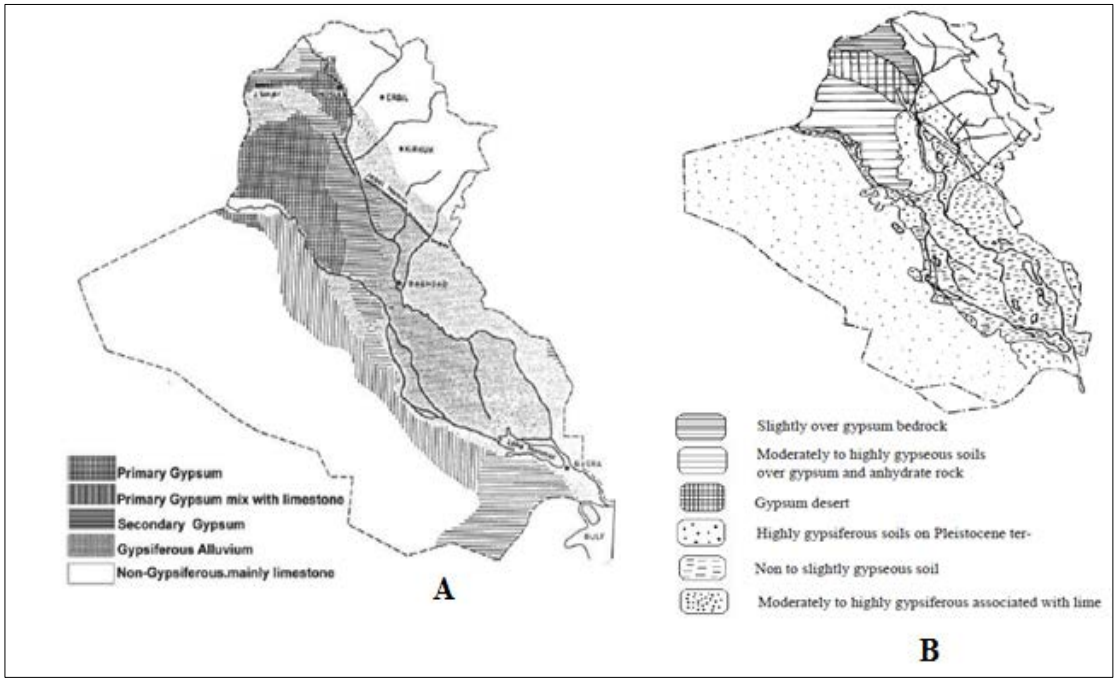

Table (1): Classification of gypseous soil.

Classification	Non gypsiferous	Very slightly gypsiferous	Slightly gypsiferous	Moderately gypsiferous	Highly gypsiferous	Gypsiferous soil to be described by other fractions such as clayey or sandy gypsiferous soil.
G.C.%	0-0.3	0.3-3	3-10	10-25	25-50	>50

Testing program

Classification tests were performed first including physical and chemical tests. The physical tests included specific gravity, Atterberg limits, and dry density . [12]The chemical test were carried out on the samples include total soluble salts, PH value, gypsum content, organic content and total sulphate content. The results are shown in table (2) and table (3)

Geotechnical properties

The geotechnical properties of gypseous soils cover, compressibility, collapsibility, and shear strength parameters (C and Ø).

Compressibility Characteristics:

Lots of researchers have investigated the influence of gypsum on the compressibility characteristics. It is hard to judge about the contradicting results as many parameters such as the placement conditions, degree of disturbance, and testing methodology. Similar contradicting results were reported for the recompression index. Most of the researchers demonstrated an increase in the secondary compression index with increasing gypsum content. This phenomenon is attributed to the continuous dissolution process of gypsum with time. [6],[7] [19],[20]

Type of Soil	L.L %	P.L %	P.I	Gs	γd kN/m³	O.M.C %	Clay %	Silt %	Sand %	Gravel %	U.C.S
S1	34	15	19	2.48	17	18	48	32	20	0	CH
S2	33	19	12	2.61	16	14	16	26	58	0	SM
S3	36	25	11	2.63	16.87	16	0	20.5	73	6.5	SM with gravel
Standard	ASTM (D2216-80)			BS-1377:1975 test No.6,B	BS -1377:1975 test No.1, A		USCS				

Table (2): Physical properties of the soils used

Table (3): Chemical properties of the soils used

Property / Soils	T.S.S %	SO3 %	PH	O.C %	$CaCo_3$ %	G.C %
S1	30	15.2	8	2.45	4,1	31
S2	33	24.6	8.4	0.089	4.56	52
S3	71	32.3	7.85	0.078	5.06	69.5
Standard	Earth manual E8 (1975)	B.S (1377-1975) [12]				Improvement soil-saline and Al-Kali soil

Collapsibility

A collapsible soil is defined as any saturated soil that goes through a radical rearrangement of particles and great loss of volume upon wetting with or without additional loading. [16] According to (ASTMD 5333, 2003)[8] collapse is defined as the decrease in height of

confined soil following wetting at a constant applied vertical stress as shown in table (4). A collapsible soil may withstand relatively large applied vertical stress with small settlement while at low water content, but this soil will exhibit settlement after wetting with no additional increase in stress. Large applied vertical stress is not necessary for collapse. Table (5) shows some values of collapse potential to describe the degree of severity of problem.

Table (4) Classification of Collapse Index (Ie) According to (ASTMD 5333, 2003)[8]

Degree of Specimen Collapse	None	Slight	Moderate	Moderate Severe	Severe
Collapse Index (Ie)%	0	0.1 -2.0	2.1-6.0	6.1-10	>10

Table (5): The Severity of Collapse Potential. [16]

Severity of Problem	No Problem	Moderately Trouble	Trouble	Severe Trouble	Very Severe Trouble
C P %	0-1	1-5	5-10	10-20	>20

The void ratio – log P results and

The typical **e - logP** results are shown in figure (2), when the soil samples are flooded with water under constant stress, a sudden decrease in void ratio will occur to structural collapse of the soil skeleton .The coefficient of specific collapse (Ic) could be determined from the figure (2) as Eq.(1)

$$Ic = \frac{e_2 - e_1}{1 + e_1} \text{.....1}$$

Where e_1: void ratio before adding water.
e_2: void ratio after adding water.

Specific collapse - Stress relationship

As the samples are flooded at different stress levels and different values of specific collapse could be obtained at each effective stress .This implies that specific collapse is a function of the void ratio and other factors .The results are presented graphically in figure (3) .It can be noticed that the values of coefficient of specific collapse (Ic) are extremely high reaching 18% and these values will cause severe trouble to foundations and engineering structures according to table (4).

Effect of time on collapse ratio

The typical relationships between the collapse ratio and time are shown in figures (4),(5) and (6)

$$Rc = \frac{R_t}{R_\infty} \times 100 \text{ ... ... 2}$$

Where R_t: compression of the sample at any time after adding water.
R_∞ : final compression of the sample when it comes to equilibrium.
It can be noticed that the compression occurs very quickly, this behavior may be related to the gradation of soils which effects its permeability, the higher the permeability the quicker the collapse occurs.

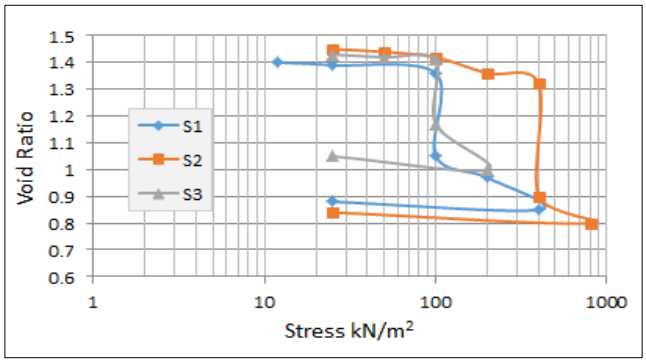

Figure (2) : Void ratio – log Pressure results.

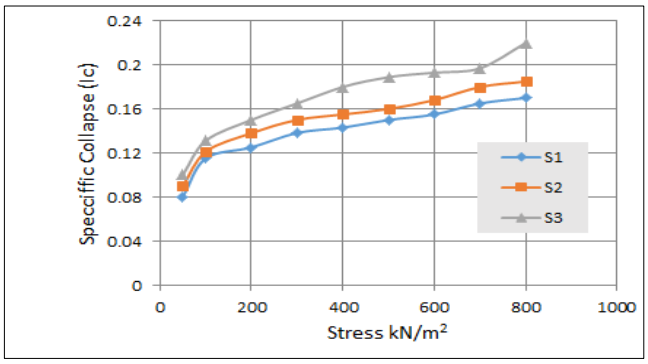

Figure (3) : Specific collapse - Stress relationship.

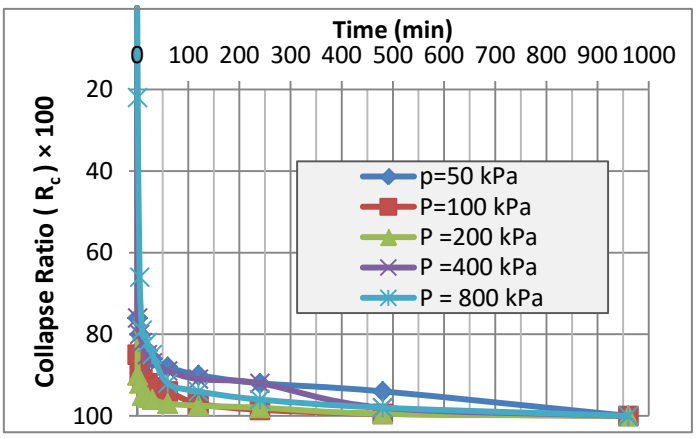

Figure (4): Collapse ratio with time for Karblaa soil .

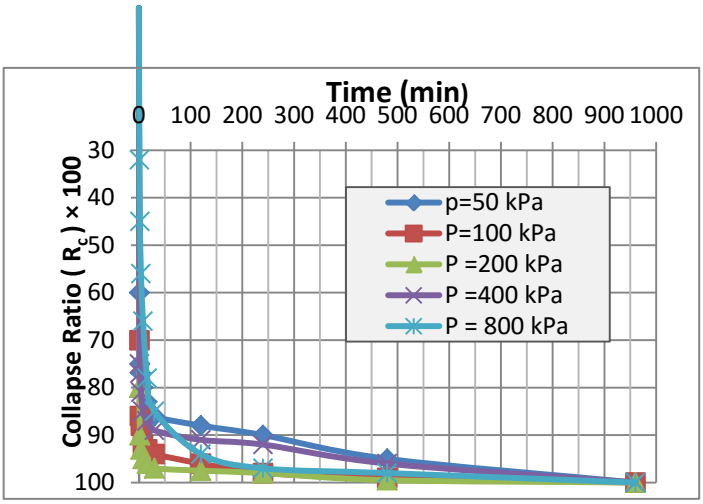

Figure (5) : Collapse ratio with time for Kirkuk soil .

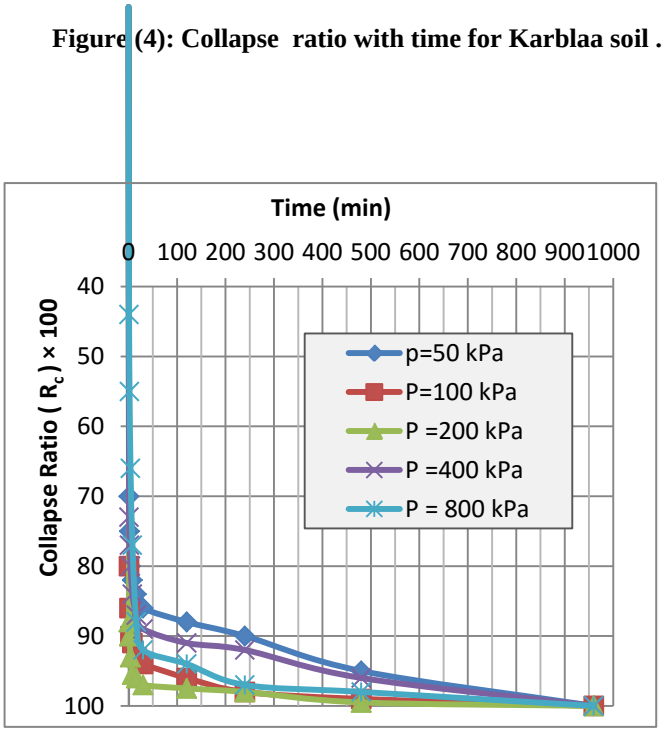

Figure (6) : Collapse ratio with time for Al-Ramadi soil

Shear Strength Test

The shear strength of gypseous soil were evaluated through standard strength test using triaxial compression test. [15], [17] To predict the shear strength parameters (C, ϕ), two types of tests were conducted on (6) samples which obtained from three soils samples, (3) samples of them are tested in natural state, while the other (3) samples were tested after soaked in water. The summary of the results of triaxial compression test conducted on the three soils (S1,S2, ana S3) for both before and after soaked state is given in figures (7)and (8) show the

relationship between axial strain and shear stress. It is clear that the stress – strain relationship of soaked soils and unsoaked soils are similar.

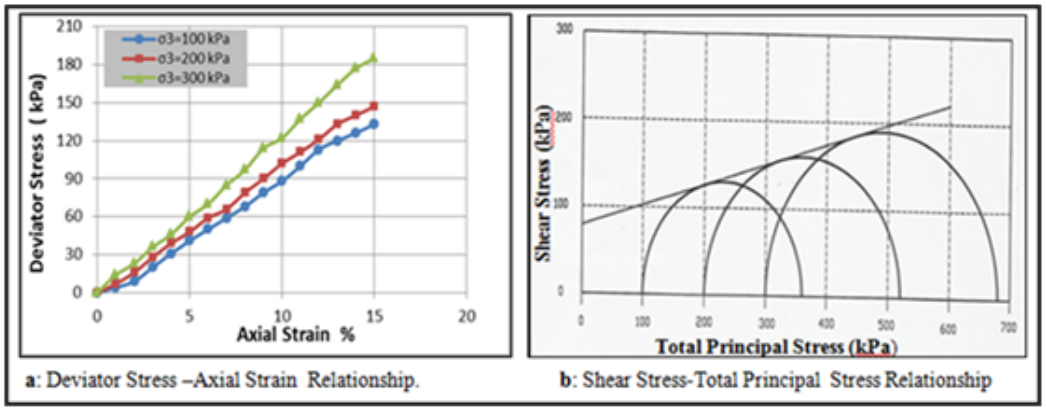

a: Deviator Stress –Axial Strain Relationship. b: Shear Stress-Total Principal Stress Relationship

Figure (7): Results of triaxial compression test of Unsoaked for Kirkuk soil

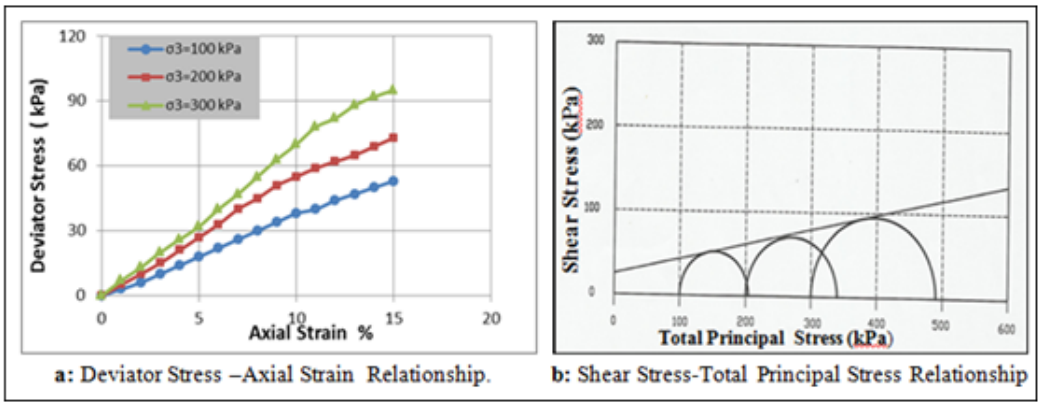

a: Deviator Stress –Axial Strain Relationship. b: Shear Stress-Total Principal Stress Relationship

Figure (8): Results of triaxial compression test of soaked for Kirkuk soil

Table (5): Variation of cohesion and angle of internal friction of soaked and unsoaked

Type of Test	Natural computed samples		Soaking computed samples	
	C (kPa)	**Φ deg**	**C (kPa)**	**Φ deg**
S1	**25**	**33**	**8**	**27**
S2	**66**	**20**	**21**	**14**
S3	**80**	**12**	**25**	**9**

Effect of Initial Void Ratio and Natural Water Content on the Collapse Potential:

The relation between the initial void ratio on the collapse potential and the relative collapse potential is presented in figures (9),(10) and (11) , for the water content between (12,18and24)% and under loads (50,100 and 200) kN in general collapse potential increase with increasing initial void ratio. Figures (12),(13)and(14) shows the relation between the natural water content and the collapse potential under stress (50,100 and 200) kN and for different initial void ratio, when natural water content increase in general collapse potential**.**

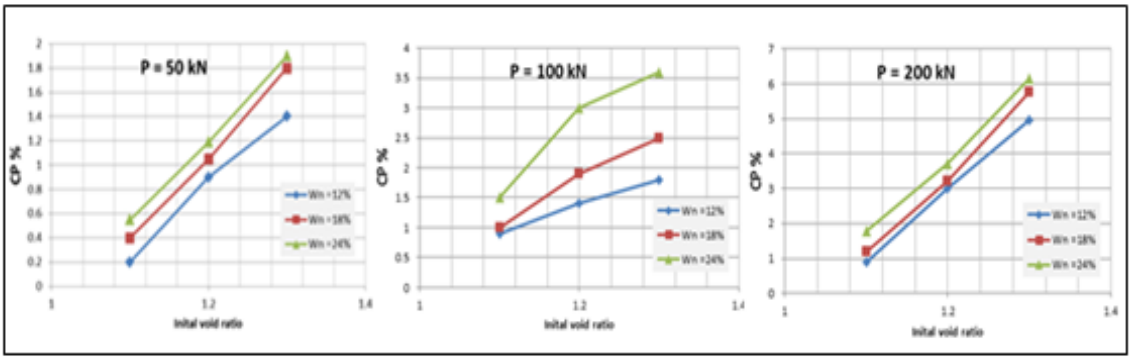

Figure (9): Initial void ratio and the collapse potential for Karblaa soil.

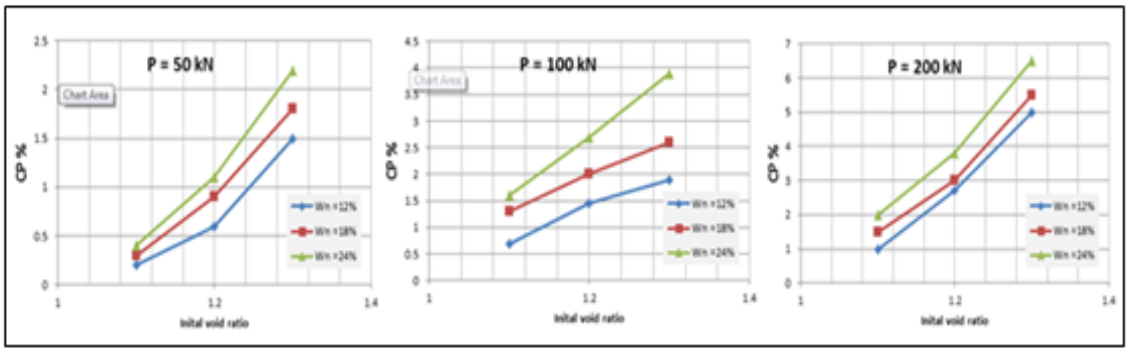

Figure (10): Initial void ratio and the collapse potential for Kirkuk soil.

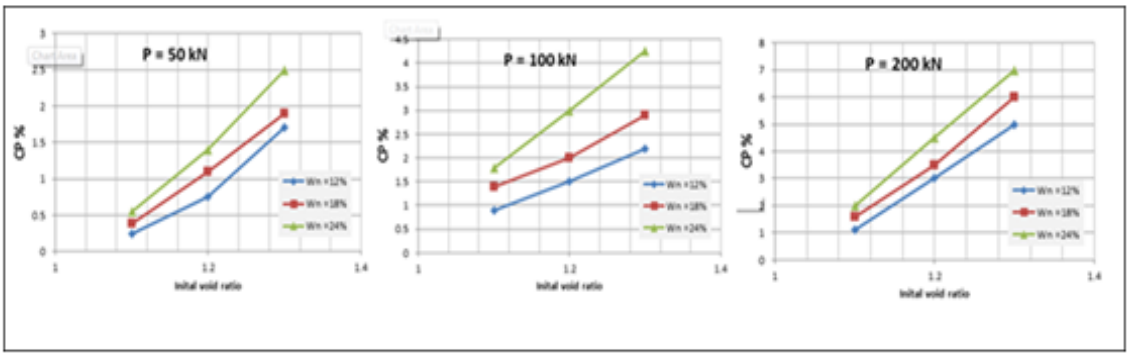

Figure (11): Initial void ratio and the collapse potential for Al-Ramadi soil.

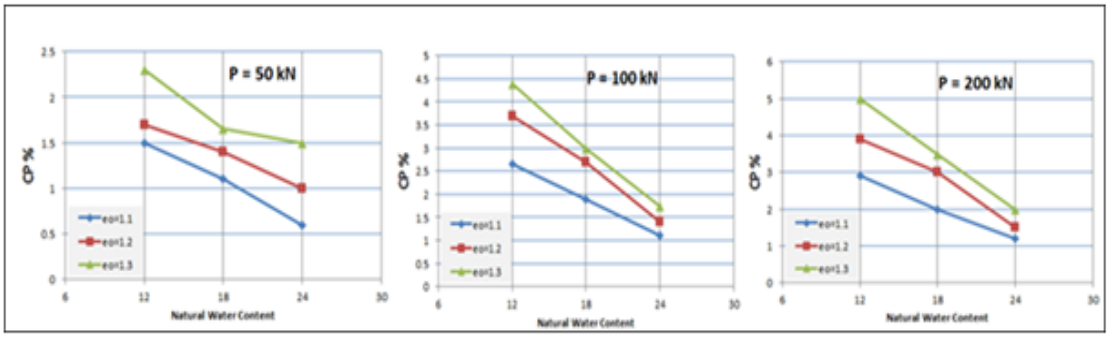

Figure (12): Natural water content and the collapse potential for Karblaa soil.

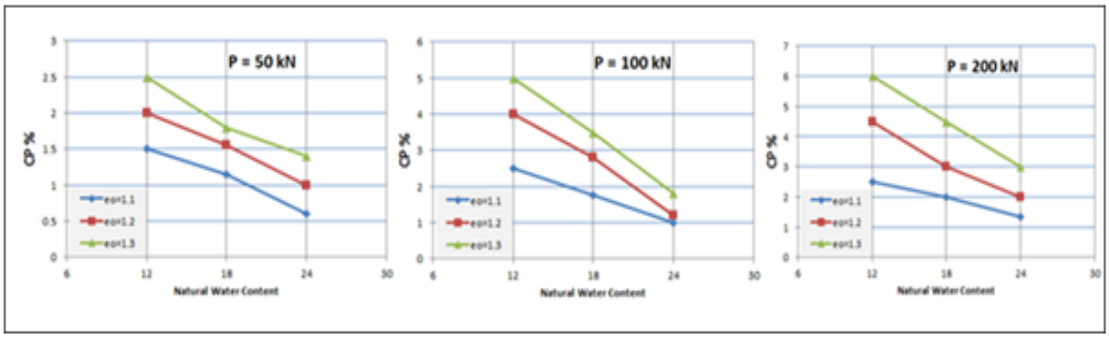

Figure (13): Natural water content and the collapse potential for Kirkuk soil.

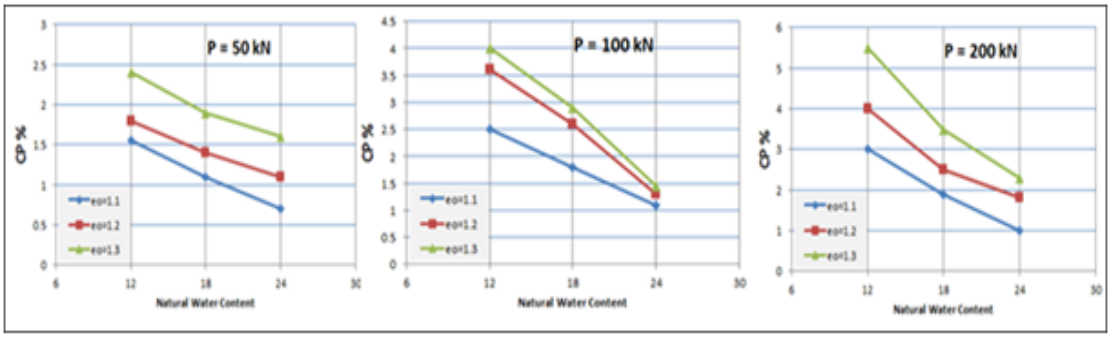

Figure (14): Natural water content and the collapse potential for Al-Ramadi soil.

Conclusion:

The main conclusions obtained from the experimental work of this study are.

1. The gypseous soils have high collapsibility because the collapse or compression occurs very quickly when the soil is soaked with water which may endanger the engineering structures.
2. The specific collapse of the test soil for the three soils ranges between (0.1-0.25) indicating that the soil has a high collapse potential which cause very server troubles for structures constructed on these soils.
3. Soaking of soils reduced cohesion by approximately (3) folds, while the angle of internal friction exhibited marginal reduction.
4. The value of collapse potential seems to depend mainly on the natural water content and initial void ratio. The collapse potential increase with the increase of void ratio and decrease with increase of water content.

References

[1] **Abid Awn, S.H.(2010),** *"A Modified Collapse Test For Gypseous Soils."* Proc., 1st Eng. Sci. Conf., Diyala Univ. Iraq, pp: 299-309.

[2] **Ahmad, F., M.A. Said and L. Najah, (2012),** "Effect Of Leaching And Gypsum Content On Properties Of Gypseous Soil." IJSRP, 2(9): pp:1-5.

[3] **Al-Barazanji A.F. (1973)** " *Gypsiferous soils in Iraq*" Dissertation.*Ghent University. Belgium.*

[4] **Al-Emami, O.H.,(2007),**"Collapsibility Of Gypseous Soil Under Fluctuation Of Ground Water Table". M. Sc. thesis, Univ. of technology, Iraq.

[5] **AlNouri, I. and Sh. Saleam, (1994),**"Compressibility Characteristics of Gypseous Sandy Soils." Geo. Testing J., 17(4): 465-474.

[6] **Al-Morshedy A.D. (2001),** "The use of cutback MC-30 for controlling the collapsibility of gypseous soils".MSc. thesis University of Technology. Baghdad.Iraq.

[7] **Al- Mufty A.A. (1997),** "Effect of gypsum dissolution on the mechanical behaviour of gypseous soils" PhD. Thesis . University of Baghdad.Iraq.

[8] **ASTMD Standards 5333 (2003),** "Soil Mechanics and Foundation Engineering, Building, Stone; Peats", Part 3.

[9] **AYadat, T. and A.M. Hanna,(2005**) "Encapsulated Stone Column As A Soil Improvement Technique For Collapsible Soil." Proc., ICE - Ground Improvement, 9(4): pp137-147.

[10] **Buringh P. (1960**), "Soils and soil conditions in Iraq. Ministry of Agriculture. *Baghdad.*

[12] **British Standard Institution, (1990)** "Methods of test for soils for civil engineering purposes

[13] **Day,R.W. (2001**) "Soil testing manual" (2001) *McGraw- Hill.*

[14] **FAO. (1990**) "Management of gypsiferous soils. Food and Agricultural Organization of United Nations Rome" Internet http//fao.org/docrep/to323e/ro323e03.htm

[15] **Head, K.H.(1986),** "Manual of Soil Lab. Testing", Vol.2,Prench Press, London.

[16] **Jennings,T.E.,Knight,K., (1975)**,"The Additional Settlement of Foundation due to Collapse of Structure of Sandy Soil on Wetting ". Proc.4th Int.Con. on Soil Mech. and Found.Eng. Vol. 3a/12, pp. 316–319.

[17] **Lumbe, T.W., (1967),**"Soil Testing for Engineering", Standard Publishers ,John Wiley and Sons, New York

[18] **Mansour, Z., Z. Chik and M.R. Taha, (2008),** "On Soil Collapse Potential Evaluation" Int. Conf. on Construction and Building Techology. E, (03): 21-32.

[19] **Nashat I.H. (1990)**, " Engineering characteristics of some gypseous soils in Iraq" PhD. Thesis . University of Baghdad. Iraq

[20] **Saleam S.N.,(1988**) "Geotechnical characteristics of gypseois soil including the effect of c contamination with some oil products", MSc. Thesis . Univ. of Technology. Baghdad.Iraq.

List of Symbols:

Symbol	Definition	Symbol	Definition
C	Cohesion Strength (kPa).	G. C.	Gypsum Content (%).
C.P	Potential Collapse	γd	Dry Unit Weight (k N/m^3)
Gs	Specific Gravity.	T.S.S	Total Soluble Salts.
L.L	Liquid Limit (%).	S1	Karblaa Soil
P.L.	Plastic Limit (%).	S2	Kirkuk Soil.
P.I	Plastic Limit (%).	S3	Al-Ramadi Soil
O.C	Organic Content (%).	T.S.S	Total Sulphate Content (%).
O.M.C	Optimum Moisture Content	Φ	Angle of Internal Friction (degree)

Stabilization of Dune Sand Using Fly Ash and Cement Dust

Assist.Prof. Dr. Bushra Suhale Al-Busoda and Asst. Lecturer Hadeel Majid

***Abstract*— Accumulation of sand grains shaped into a mound or ridge by the wind under the influence of gravity is called Sand dune. Dunes are found wherever loose sand is windblown, in deserts, on beaches, and even on some eroded and abandoned farm fields in semiarid regions, such as south of Iraq. In this paper, dune sand stabilization was studied. Two materials which are industrial byproducts (fly ash and cement dust) were used as stabilizers. The geotechnical properties of dune sand before and after stabilization were investigated. Good results were obtained in stabilization process**

***Index Terms*— dune sand, stabilization, fly ash, cement dust**

I. Introduction

In desert regions wind scouring causes sand to move and poses either erosional or depositional hazards on urban areas, civil structures and utilities.

Under arid condition, wind scouring is much more severe than rainwater or stream water erosion. Wind scouring causes the sand to drift from an erosional surface to a depositional surface causing erosional or depositional hazards. These two surfaces could be separated by a distance or could exist in one dune body and causing the dune to move forward. Several types of dunes can be formed depending on the different environmental conditions including original topography, wind regime, sand supply and presence of vegetation.[1],[2]

II. Aeolian Sand Transport and Types of Dunes

The aeolian process is divided into three stages, erosion, transportation and deposition, starting when the wind moves a particle from rest and carries it for some distance. When the aerodynamic forces applied to the particle becomes less than the gravitational force, the particle finally settles back to ground [1]. In general, sand grains move in three different modes based on their grain sizes. Coarse grains move slowly down-wind by creeping while fine grains move in suspension where sand particles remain for long distances suspended in the air. The third and most important mode of movement is the saltation where sand grains are unable to remain in suspension and fall to the ground. In their fall they bombard other particles to move in definite trajectories to hit other grains to move.

These modes of movements results in moving the sand in two basic dynamic forms, the natural sand drifting which takes place over open terrain and the migration in the form of individual dunes in the direction of sand transport.

The formation of a dune generally depends on three main factors, sand supply, wind velocity, and Presence of vegetation.

III. Sand Dunes Hazards

Sand dunes have harsh effect on the human's health, especially skin, eyes and respiratory system diseases, besides the corrosion ability of the windblown sand on the nearby constructed structures. In addition it represents an effective source for desertification. Different types of hazards were recorded in different parts of Iraq, few examples are given below: -

A military air base was abandoned west of Tikrit, central part of Iraq, due to the presence of sand dunes; nearby the base. Large parts between Baiji and Samarra area; on both sides of the Tigris River, were considered as unfavorable areas and excluded from site selection of a Nuclear Power Plant (C.E.S.A., 1992). Large parts of the Highway No.1 between Diwaniyah and Hilla were not completed since 1985, due to the presence of a main field of sand dunes along and the nearby path of the highway; their presence was an obstacle for the construction. - Many other main roads, like Nu'maniyah – Hashimaiyah, Samawa Najaf and others, suffer from blockage due to accumulation of the sand dunes. - Recently, south and west of Samawa city suffer from the creep of sand dunes. They are covering (continuously) agricultural fields, roads and even some mapped out crops[3].

IV. Stabilization of Dune Sand

Stabilizing a dune to control the sand movement could be accomplished chemically, mechanically or biologically. Most literature presents six different methods that can be employed singly or in combination to control aeolian sand. These are: a) transposing, b) planting, c) paving, d) paneling, e) fencing, and f) oiling.

The chemical industries produce a variety of chemicals that can be used as stabilizers to control erosion until a permanent control system is applied. Bitumins, polyelectrolytes, latexes, cement dust, fly ash and other compounds have been used for

Manuscript received May 30, 2015. Stabilization Of Dune Sand Using Fly Ash And Cement Dust.

Asst.Prof.Dr. Bushra Suhale Albusoda. Author is with the University of Baghdad,Civil Engineering Departement, Baghdad, Iraq (corresponding author to provide phone: +964 7903 253 683; e-mail: albusoda@yahoo.com)

Asst.Lecturer Hadeel Majid, Al-Esra'a University College, Baghdad, Iraq. (e-mail: hadeel_mh_84@yahoo.com).

stabilizing sand in the desert environment. The nature of the bonding by chemical stabilizers in sand is adhesive bonding in which the chemical is the binder and the sand grains are the substrates. Some other chemicals form a film on the sand grains that increases its specific gravity and consequently decrease the rate of erosion. In order to determine the effectiveness of a chemical as a stabilizer and its economic status, it is important to know the optimum application rate, bonding strength, and effective life of the chemical under field conditions (heat, and humidity).

V. Objectives of Research

The main objectives of this paper are to present the geotechnical properties of Al-Diwaniya dune sand and investigate the possibility of stabilization using byproducts materials obtained from industrial factories.

VI. Material Properties

A. *Dune Sand*

Dune sand from Al-Diwaniya Governorate (282 Km south of Baghdad) was brought to use in this study. Plate1 shows the site that the dune sand brought from Final Stage

Plate 1. The site of Dune Sand

B. *Stabilizers (fly ash and cement dust)*

Two byproducts materials that produced from industrial factories were used as stabilizers materials. These materials are the fly ash that produced as byproduct of Al-Doura station for electric power production in Baghdad, and the cement dust which is byproducts of Al-Sulaimaniya cement factory.

It is important to note here that, the use of byproducts materials are not work as stabilizer material only, it serve to get a clean environment of the country in addition to its availability and its minimum cost (the cost of transportation only).

VII. Experimental Work, Results and Discussions

An extensive testing program were performed to investigate the geotechnical properties of Al-Diwaniya dune sand and to studying the efficiency of using fly ash and cement dust in stabilizing the dune sand. It is worthy to note that all the standard tests were conducted according to ASTM standards.

A. *Tests on Dune Sand before Stabilization*

According to the Unified Soil Classification System, the soil is classified as **SP.** when dry sieving is performed as shown in figure (1). This classification is coincide with that found by Al-Taie et.al[4],for Baji dune sand, while the results is different when wet sieving is conducted as shown in figure (2).

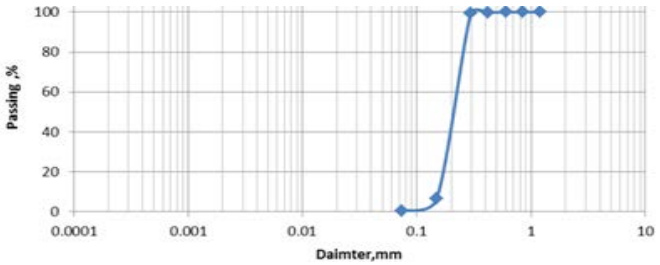

Fig. 1. Results of Dry Sieving

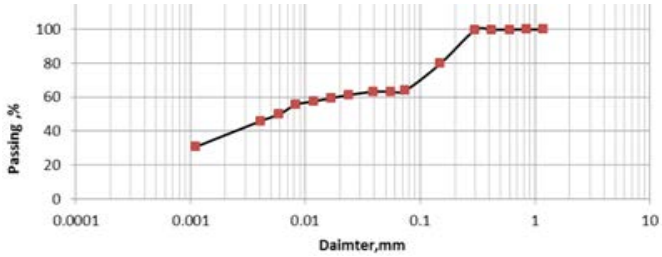

Fig, 2. Results of Wet Sieving

It is obvious from the above figures that the soil contains fines more than 40%. This means that Al-Diwaniya dune sand is classified as SM-SC.

Compaction tests (Standard and modified) were conducted. The results obtained could be shown in figures (3) and (4).

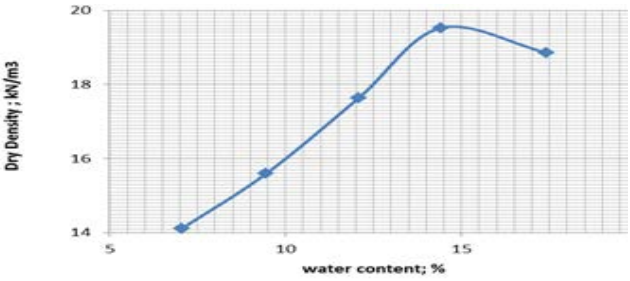

Fig. 3. Results of Standard Compaction Test

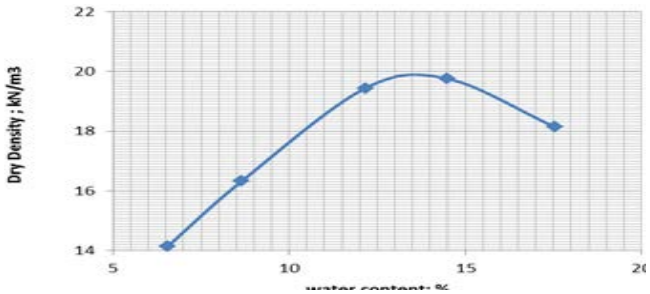

Fig. 4. Results of Modified Compaction Test

The collapsibility of the soil and its compressibility were investigated using the double oedometer test. The results could be shown in figures (5), (6), (7), and (8). It is important to note that the compressibility and collapsibility were studied on samples compacted (standard and modified) at optimum and 5% at the dry side of optimum. It is observed that the collapse potential of samples compacted at the optimum water content were not noticeable. Conversely, there was noticeable collapse in the samples that compacted at 5% of the dry side of optimum. Generally, the collapse for samples compacted by standard proctor is greater than those compacted by modified proctor.

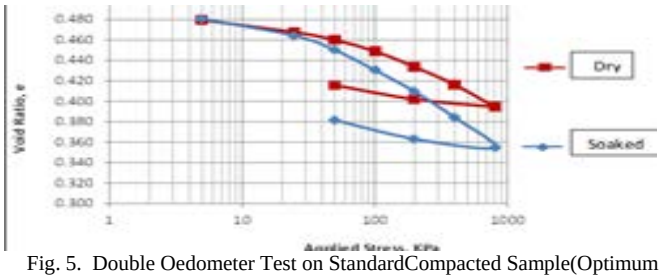

Fig. 5. Double Oedometer Test on StandardCompacted Sample(Optimum moisture content)

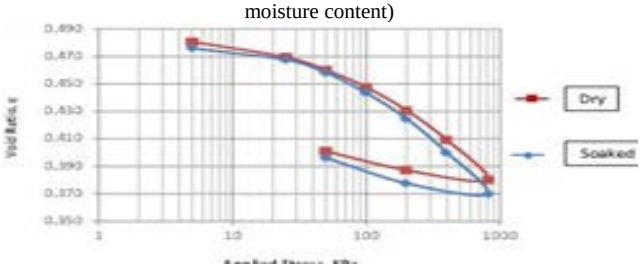

Fig. 6. Double Oedometer Test on Modified Compacted Sample (Optimum moisture content)

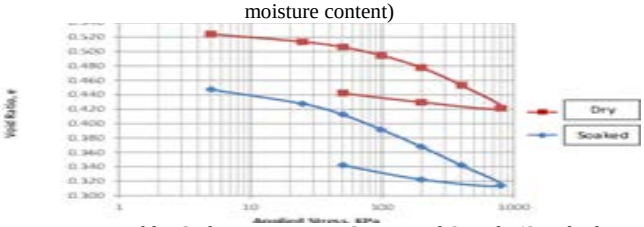

Fig. 7. Double Oedometer Test on Compacted Sample (Standard

\Fig. 7. Double Oedometer Test on Compacted Sample (Standard compaction, 5% Dry of Optimum moisture content)

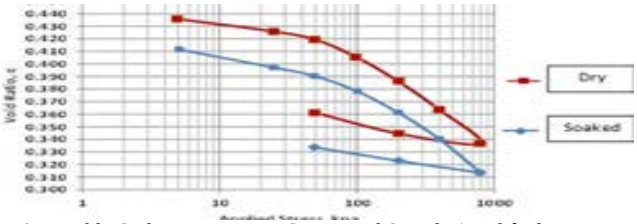

\Fig. 8. Double Oedometer Test on Compacted Sample (Modified compaction, 5% Dry of Optimum moisture content)

The Shear Strength of compacted (Standard proctor) samples at 5% dry side of optimum tested with and without soaking using direct shear device. The results obtained could be shown in figures (9a and 9b).

From examining the results of direct shear tests, it is noticed that the soil has small value of cohesion. This behavior seems logical, since the soil contains small portions of clays (SM-SC). It is obvious that slight reduction in cohesion were observed due to soaking, while the angle of internal friction remains without change.

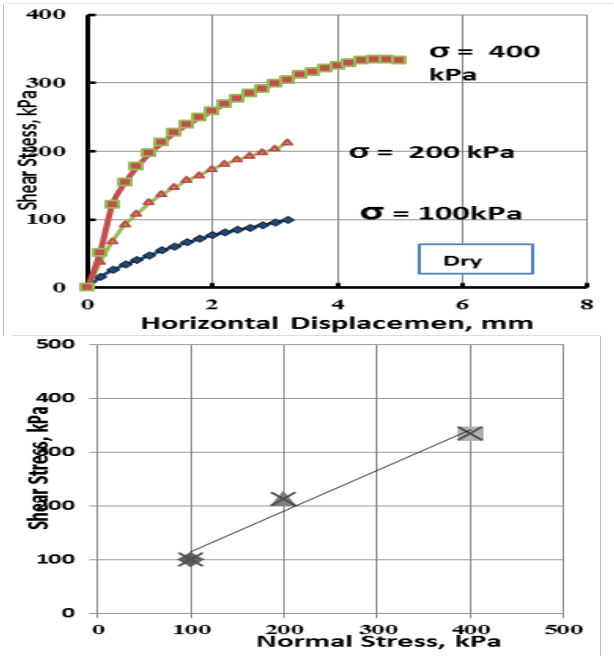

a. Dry Samples

Fig. 9a. Results of Direct Shear Test (Standard Compacted,5% Dry side) for Dry Samples

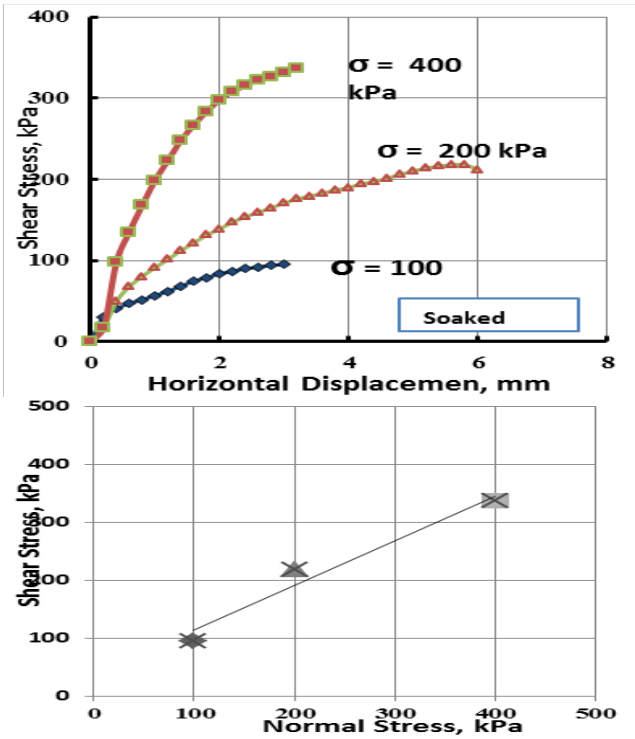

b. Soaked Samples

Fig. 9b. Results of Direct Shear Test (Standard Compacted,5% Dry side) for Soaked Samples.

B. *Tests on Stabilized Soil*

The compaction characteristics of stabilized soil by mixing different percentages of fly ash and cement dust were studied. The results could be shown in figures (10) and (11).

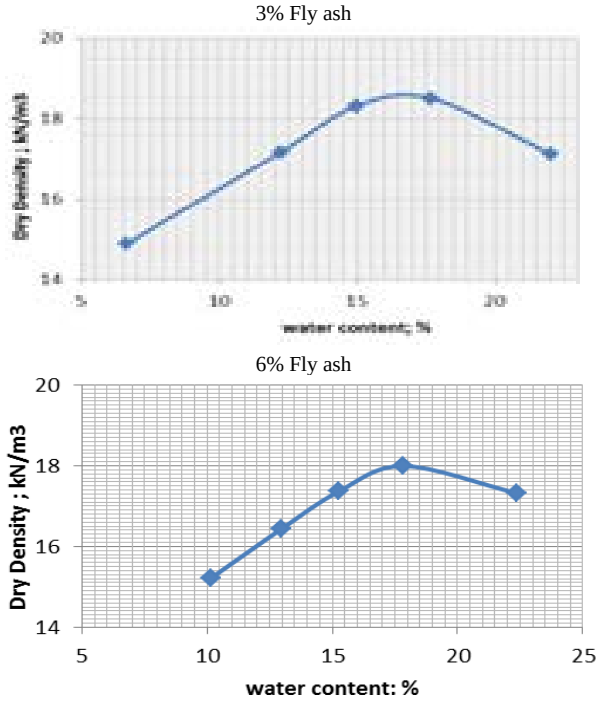

Fig. 10. Results of Standard Compaction Tests of Stabilized Soil with Different Percentages of Fly Ash

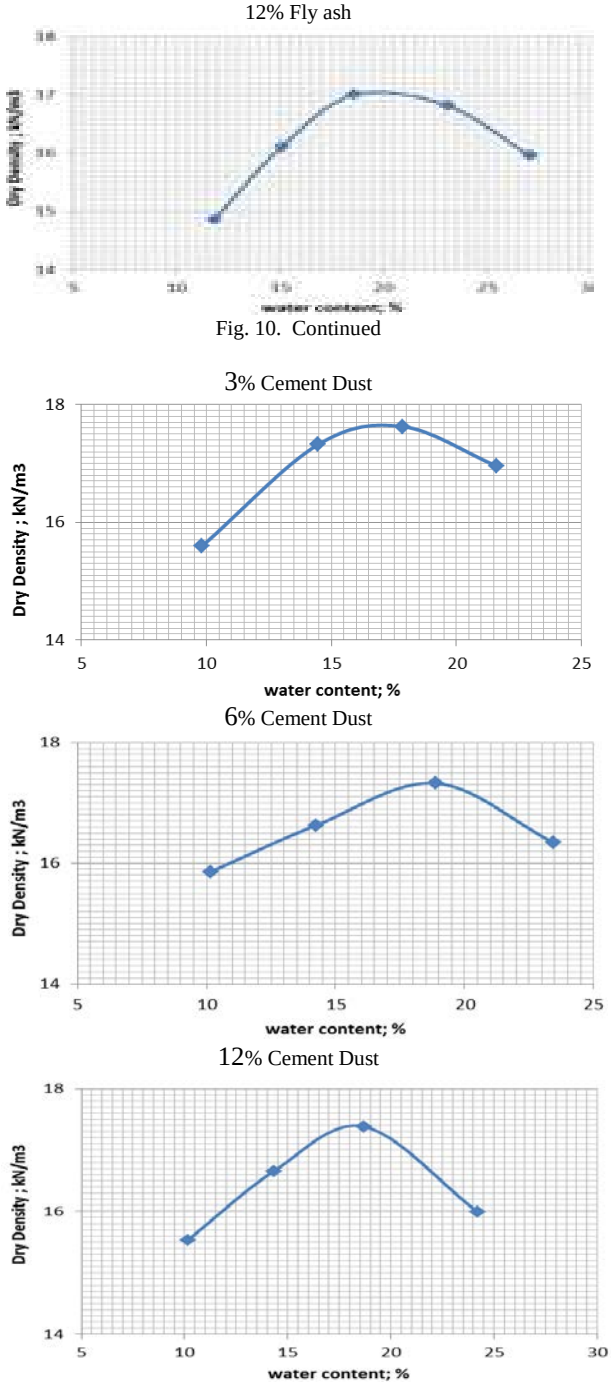

Fig. 10. Continued

Fig. 11. Results of Standard Compaction Tests of Stabilized Soil with Different Percentages of Cement Dust

The maximum dry density of the stabilized soil is decreased when adding cement dust or fly ash as shown in figure (12). This behavior may be attributed to the low specific gravity of both materials. Similar behavior was observed by Al-Busoda and Salem[5], when studied the stabilization of dune sand by cement Kiln dust.

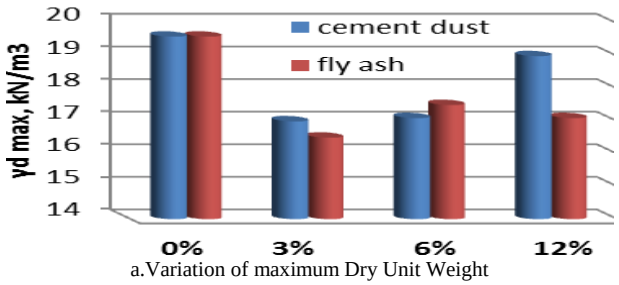

a.Variation of maximum Dry Unit Weight

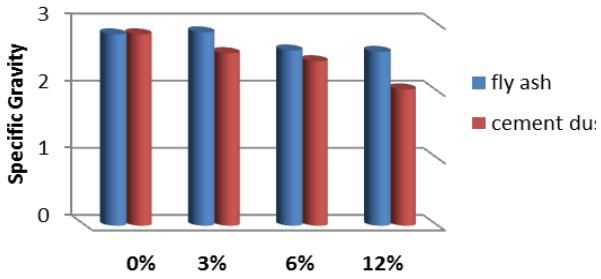

b.Variation of Specific Gravity

Fig. 12. Variation of Maximum Dry Density and Specific Gravity with Different Percentages of Additives

The collapse and compressibility of stabilized soil by adding different percentages of fly ash and cement dust were investigated. The results of double oedometer tests could be seen in figures (13).

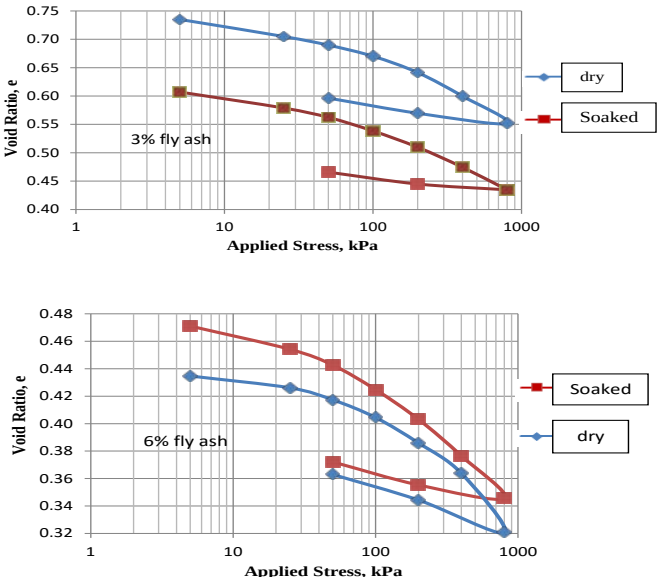

Fig. 13. Double Oedometer Tests on Compacted Samples (Stabilized with different percentages of fly ash and cement dust)

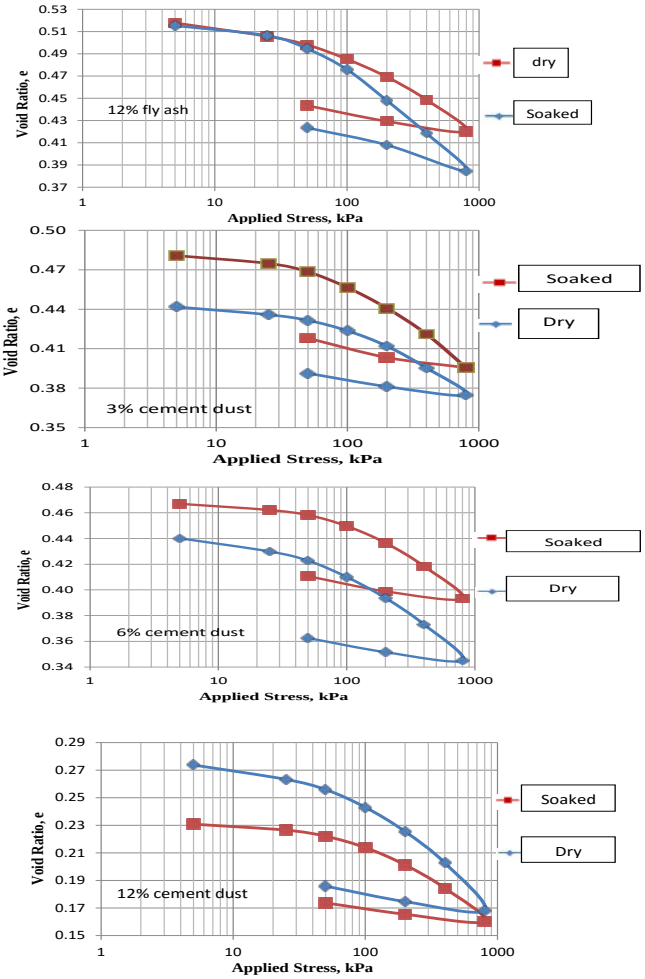

Fig. 13. Continued

It is clear that the additives, in general, decreasing the collapse potential as shown in figure (14). Similar behavior was observed by Al-Busoda and Salem [5].

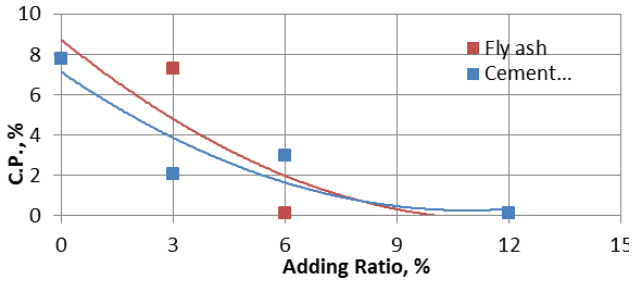

Fig. 14. Variation Of Collapse Potential With Different Percentages Of Additives

Series of direct shear tests on compacted stabilized samples by adding different percentages of fly ash and cement dust. The stabilized samples were tested with and without soaking. The results of direct shear tests could be shown in figures (15) and (16).

Through the examining of figures (15) and (16), it was found that stabilizing soil with fly ash made the soil gets cohesion and increasing the angle of internal friction, especially with 6% fly ash. While, when stabilizing soil with cement dust, it is

found that the adding of 3% increased the shear strength noticeably.

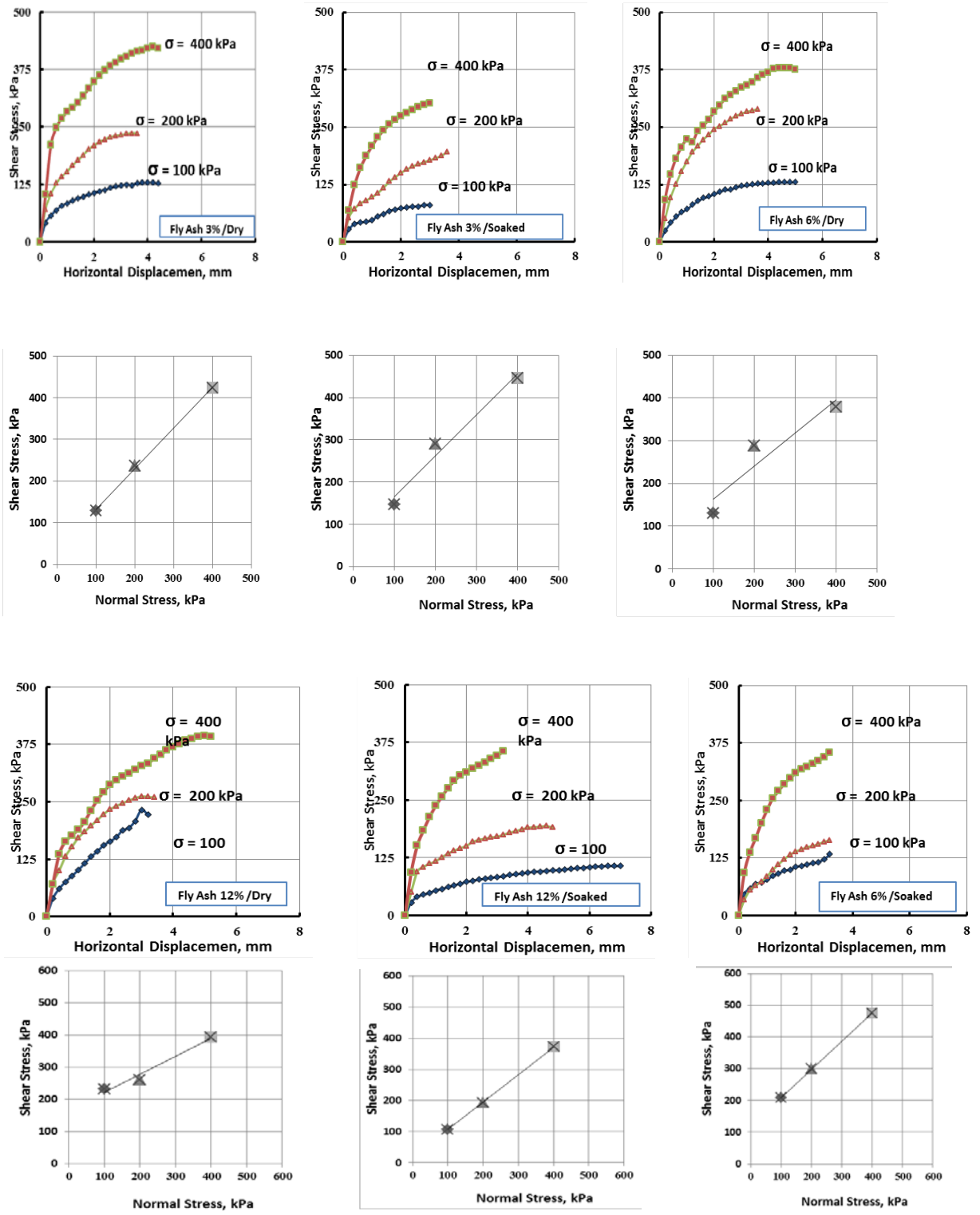

Fig. 15. Results of Direct Shear Test (Standard Compacted,5% Dry side) for Dry and Soaked Samples Stabilized by Different Percentages of Fly Ash (3%, 6%, 12%)

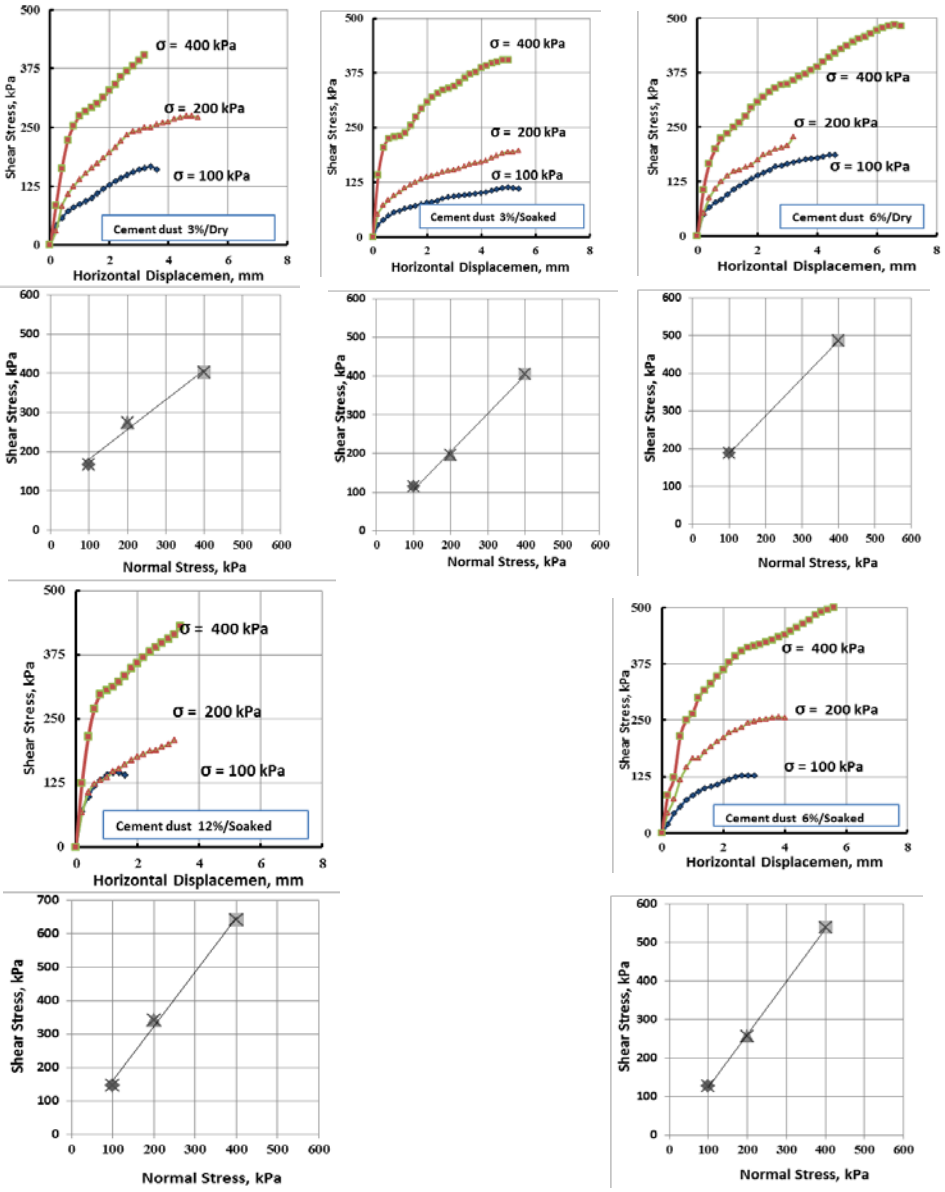

Fig. 16. Results of Direct Shear Test (Standard Compacted,5% Dry side) for Dry and Soaked Samples Stabilized by Different Percentages of Cement Dust (3%, 6%, 12%)

VIII. Conclusion

The dune sand of Al-Diywania is classified as SM-SC soil. The soil shows severe collapse potential.

Stabilization of dune sand by adding 6% fly ash decreasing clearly the collapse potential while increasing shear strength. Stabilization of dune sand by adding 3% fly ash decreasing clearly the collapse potential and increasing shear strength, while adding 3% cement dust decreasing the collapse potential in less efficiency of that of fly ash and increased the shear strength noticeably.

References

[1] Bagnold, R. A., 1953, The physics of blown sand and desert dunes: Chapman & Hall, p. 265

[2] Bader, T., Shehata, W., Lotfi, H., Ali, A. and Abdallah, M., Engineering and mineralogical properties of dune sand: Proc. 2nd Geotech. Engng. Conf., Cairo University, 1994, p. 14-27.

[3] Sissakian Varoujan K., Ayda D. Abdul Ahad and Amal T. Hamid,: Geological Hazards In Iraq, Classification And Geographical Distribution, Iraqi Bulletin of Geology and Mining, 2011, Vol.7, No.1, p 1- 28.

[4] Al-Taie Abbas J., Yousif J. Al-Shakarchi And Ali A. Mohammed,: Investigation Of Geotechnical Specifications Of Sand Dune Soil: A Case Study Around Baiji In Iraq. IIUM Engineering Journal, 2013, Vol. 14, No. 2

[5] Al-Busoda and Salem ,: Stabilization of Dune Sand by Using Cement Kiln Dust (CKD), Journal of Earth Sciences and Geotechnical Engineering, vol. 2, no. 1, 2012, pp.131-143.

Numerical Analysis for the Effect of Container Size on Model Bored Pile Capacity in Sand

Ali, A.M

Abstract-Scaling process for the small model piles essentially is forced by the influences of stress levels and soil particles size. So, carrying out a series of model pile tests must be taken into account the effect of container size. Since, the shear mechanism at the pile- soil interface is approximated by means of direct shear test; different boundary conditions have been investigated on the test results. However, a pronounced link was seen between the base boundary and the formation of plastic zone below the pile tip. This research aims to quantitatively evaluate the appropriate container dimensions at which there no further boundary effects are appeared by the assistance of statistically derived equations. Numerical simulation using (Plaxis 3D Foundation) program was employed to model vertically loaded piles positioned in sand. The test results demonstrate that the container size has a predominant effect in dense and medium states of sand in the contrast with loose state. However, a container size effect approaches to be non-existent for loose sand, and as the size of container increases, the pile capacity decreases. The coefficient of determination (R^2) for the derived equation is (95.4%) which indicates the accuracy of output results in specifying the required target of this analysis.

Keywords: Model piles, container size, Numerical simulation and loose sand.

I. INTRODUCTION

Generally, Scale effect topics focus on how to simulate the actual prototype behavior by identifying the distortions of small scale models anticipated due to stress levels and particles size effects. Therefore, the complexities and difficulties associated to these effects require investigating another factor that largely affects the results of small scale models which is a container boundary. From 1948 to 1968, the model tests were conducted in large tanks generally filled with sand, aimed to establish the forces on retaining walls and piles. These models were not intended to replicate any particular field scale; they were aimed at understanding general modes of the behavior **Muir Wood, (2004**). So, to make a quantitative prediction of prototype response, the effect of container boundary must be taken into the consideration to obtain as possible as a real field condition.

II. MATERIAL DATA SETS FOR SOIL AND INTERFACES

The well-known Mohr-Coulomb model was adopted to represent soil behavior, and its five parameters values (Modulus of elasticity, Poisson's ratio, cohesion, angle of internal friction and angle of dilatancy) are defined separately according to the state of sand being tested.

Manuscript received May 30, 2015.

Ahmed Majeed Ali author is with the building and construction engineering department, university of technology, Baghdad, Iraq (e-mail: ama.civil85@gmail.com).

The type of soil element used is 15 nodes- wedge element, composed of 6- nodes triangular in horizontal direction; and 8- nodes quadrilateral in vertical direction. All details are listed in the Table (1).

Table 1
Sand characterization used in the numerical analysis

Property index	Loose	Medium	Dense
Modulus of elasticity, E_s (kN/m^2)	10000	24000	31000
Poisson's ratio, ν	0.3	0.35	0.35
Angle of internal friction, φ	29°	37°	40°
Cohesion, c (kN/m^2)	0	0	0
Angle of Dilation, ψ	0	0	5°
Dry unit weight, γ (kN/m^3)	15.3	16.3	17.1
Relative density (R.D %)	31	58	80

To simulate the dry state of sand, the type of material is considered as drained. The main soil-pile interface parameter is the strength reduction factor R_{inter} and assumed to be a rigid which correspond to R_{inter} =1. Non porous behavior is considered to mimic the model pile structure. The type and the parameters of pile used in this analysis is lised in Table (2). Soil properties at loose and medium states of sand used as input data in the numerical modeling was taken from **(Jawad 2012)** and with respect to the dense state, the characterizations of soil was adopted by **(Das 2006)**.

Table 2
Model pile properties used in the present study

Identification	Value
Material Type	Non porous- concrete
Material density (kN/m^3)	24
Material Model	Linear elastic
Modulus of elasticity, E_p (kN/m^2)	26000000
Poisson's ratio, ν	0.15

III. TESTING PROGRAM

Theses (74) tests were analyzed numerically. Dry sand was used and prepared in three different states of sand loose, medium and dense respectively (Relative density R.D = 31, 58 and 80%) which are corresponding to dry densities of (15.3, 16.3 and 17.1kN/m^3). The dimensions of model piles involve using diameters of (2, 3 and 4cm) with lengths ranging from (20 -70cm). All model pile dimensions used in the tests and their related details are listed in Table (3). Embedment ratio (L/D) was specified from (10) to (23) according to the dimensions adapted in tests in order to cover a wide range of pile types (short and long piles). For dense sand, the angle of dilation ψ was considered in the calculations due to the higher value of friction angle (φ=40) where most researchers have been seen the effect of dilation is more pronounced about this range. All model piles were loaded at different mesh boundaries for identifying a relationship between model pile capacity and container boundary (mesh dimension in numerical simulation).

Table 3
Details of pile dimensions used in the numerical analysis

Model pile diameter (cm)	Model pile length (cm)	Relative density %	Box dimensions (cm)
2	20	31	30,40,50 and 60
3	30		40,50,60,70 and 80
4	40		50,60,70,80,85 and 90
2	20	58	30,40,50,60 and 70
3	30		40,50,60,70,80 and 90
4	40		50,60,70,80,90 and 100
2	20	80	30,40 and 50
3	30		40,50,60,70 and 80
4	40		50,60,70,80,85 and 90
3	50	31	60,70,80 and 90
3	50	58	60,70,80 and 90
3	50	80	60,70,80,90,100 and 110
3	70	31	80,90,100 and 110
3	70	58	80,90,100 and 110
3	70	80	80,90,100,110 and 120

IV. PREVIOUS LITERATURES

Overview of the previous work of laboratory tests can be summarized as the following:

Puech (1975) stated that, the end effects of piles can be minimized with a minimum spacing of 5D between the inclusion tip and the bottom of the boundary.

Parkin and Lunne (1982) suggested that for their chamber tests, boundary effects were negligible for loose sand. However, they showed that the effect of the container walls becomes more pronounced as the relative density of the sand increases. They suggested that a chamber to pile diameter ratio of 50 was desirable in order to eliminate boundary effects. The boundary effect is particularly evident for dense soils at low confining pressures.

Gui (1995) suggested that for centrifuge tests on silica sand, the boundary effects should be negligible if the diameter of the container is greater than that of pile by a factor of 40 or more. The test results reveal that a ratio of 20 should be acceptable at a relative density of 76%. Also, he concluded the use of 190mm diameter plastic cylindrical container with a 10mm diameter pile was deemed acceptable for the dense samples.

Lunne et al. (1997) suggested the sphere of influence over which the cone penetrometer can sense an interface is about 2 to 3 cone diameters for soft materials and up to 10 to 20 cone diameters for stiff materials.

The work of **Garnier and Konig (1998)** showed that the measured side friction is not influenced by the scale effect related to the size of grains if the D/d_{50} =100.

Gui et.al (1998) studied the effect of the container/cone diameter ratio (B/D) by performing the tests in containers with various diameters. The test results revealed that for dense sand, there is no apparent increase in cone resistance ($\mathbf{q_p}$) for a test done with B/D=85 and 44. However, ($\mathbf{q_p}$) is larger for B/D=21 and significantly effect for B/D=8.85.

Bolton et. al. (1999) showed that, the ratio of the diameter of container to diameter of the model pile embedded in sand should be larger than 30 to avoid the effect of tip resistance on the container boundary.

Lee and Salgado (1999) found that, the bottom boundaries of the meshes were located at a depth larger than two times the corresponding pile lengths measured from the ground surface. The width of the mesh was equal to or larger than the pile length. Finite-element analyses performed separately with infinite elements at the lateral boundary showed that the mesh dimensions used in this study are large enough to eliminate geometric boundary effects.

Al-Mhaidib (2006) supposed the dimension of the test tank (50 cm) used in the present study is about 20 pile diameter in the lateral direction and there is about 8 pile diameter clearance in the vertical direction beneath the base of the model pile. Therefore, it is expected that there will be a minor boundary effect in this study.

Yang (2006) pointed out to the influence zone surrounding the pile in sand is properly linked with the angle of shearing, soil stiffness and mean effective stress. For piles in clean sand, the mean range of the influence zone above the pile tip is between 1.5 and 2.5D and the zone below the tip ranges from 3.5 to 5.5D, where D is pile diameter.

A. Container Size Theory

Initially, during erection the pile in the container an expansion or cavity is generated. After expansion, a

plastic zone is created in the immediate vicinity of the cavity. The plastic zone radius mainly depends on the relative density, the angle of internal friction, model pile diameter and stress level effect. A plastic zone is bounded by a nonlinear elastic zone, and this region is surrounded by a linear elastic zone. The shear strains in the linear elastic zone are small, and the material in this zone has a shear modulus G_o and Poisson's ratio ν_o. In the linear elastic zone the elastic parameters change continuously from the interface between the linear and nonlinear elastic zones to the elastic – plastic interface. Also, there is nonlinearity in the plastic zone, where the friction angle varies from a value equal to the critical state friction angle at the cavity wall to a value equal to the peak friction angle at the nonlinear elastic – plastic interface **(Salgado, et.al, 1998**).

V. RELATIONSHIP BETWEEN MODEL PILE CAPACITY AND CONTAINER SIZE

Numerical model tests (74) were implemented to get a link between the capacities of model piles and container size at different states of sand (Relative density =31, 58 and 80%). It can be noticed that, the model pile capacity trends to decrease as the box size (container) increases until a certain size of box then, it reaches to the steady state and no effect of container size is beyond this range. Figures (1) to (5) present relations between pile capacity and box dimensions (BD).

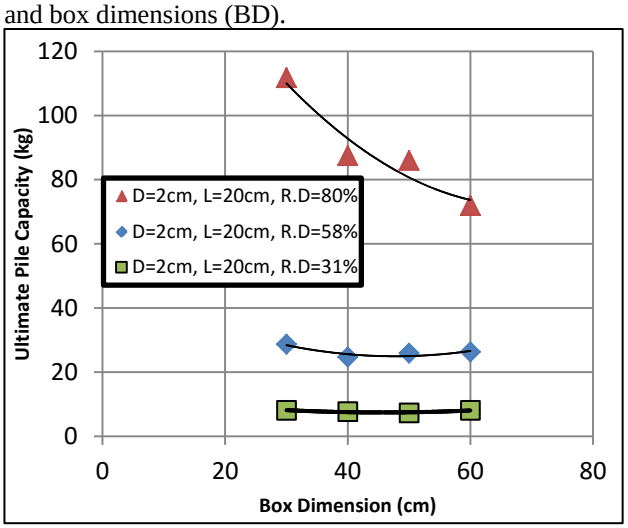

Fig. 1. Relationship between pile capacity and container size for pile with D=2cm and L=20cm

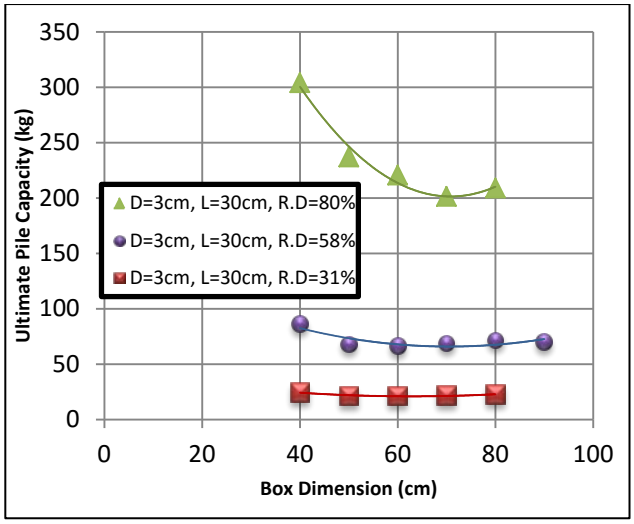

Fig. 2. Relationship between pile capacity and container size for pile with D=3cm and L=30cm

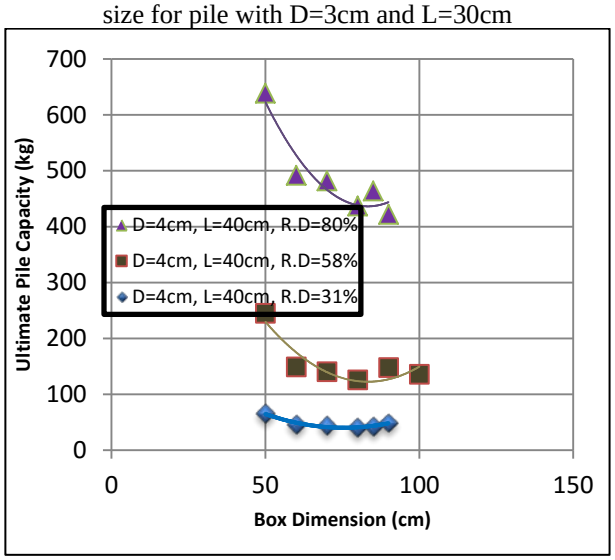

Fig. 3. Relationship between pile capacity and container size for pile with D=4cm and L=40cm

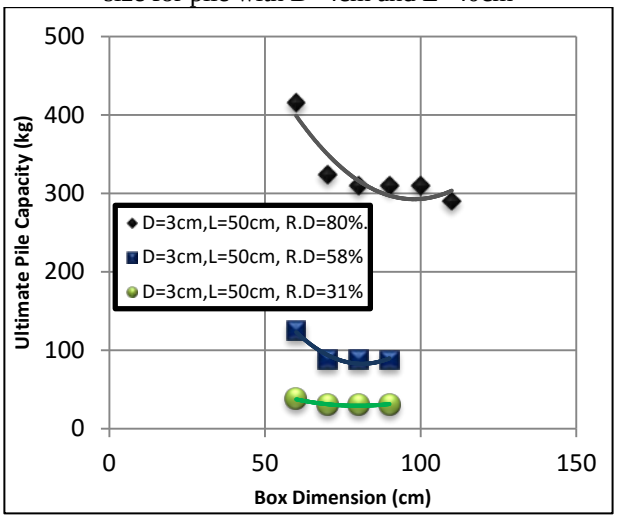

Fig. 4. Relationship between pile capacity and container size for pile with D=3cm and L=50cm

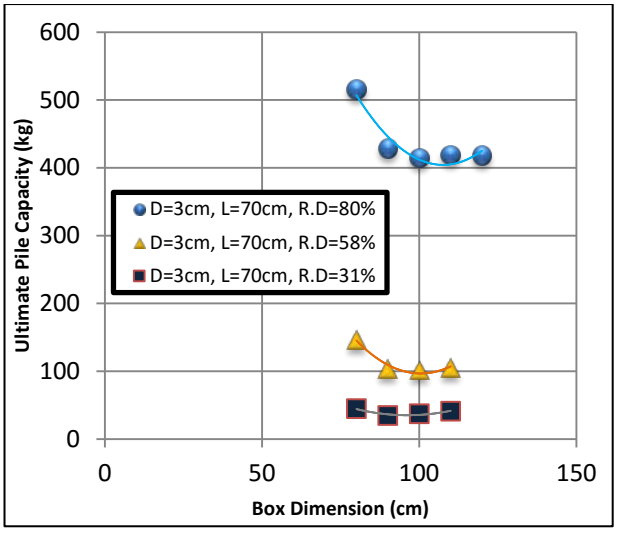

Fig. 5. Relationship between pile capacity and container size for pile with D=3cm and L=70cm

The test results demonstrate that, the box size required for eliminating the boundary effect increases as the relative density increases when the pile dimensions are constant. So, it may be concluded that the scale effect due to container size is more significant in dense sand.

A. Influence of Pile Dimensions

The relative dimensions of model piles with respect to the container width also affect the magnitude of increase in the bearing capacity of piles. This is because the size of the tank containing the soil is constant, and as the pile size increases, the size of pressure bulb increases, leading to larger mobilization of frictional forces within the container. This may in turn increase the variation occurring in the bearing-capacity measurement. Hence, the influence of dimensions of piles was analyzed in this study by varying the container dimensions starting with a value of (**L**+10) where **L** is a pile length and then the increasing in container width keep in equidistance of 10cm until the test results of pile capacities reach to steady state beyond which no boundary effects are displayed. To investigate the effect of diameter of model piles on the boundary conditions of container, a series of 46 model pile tests were carried out using a constant embedment ratio (**L/D**) equal to 10 but for different pile diameters of (2, 3 and 4cm) and corresponding pile lengths of (20, 30 and 40cm). As a general trend, it is noticed that, when the model pile diameter increases the plastic zone formed increases and this condition is more prominent in dense sand. This behavior has been found by **Kumar and Khatri (2008)** that have also reported the size of the plastic zone in relation to the footing width becomes gradually larger for greater values of friction resistance which in other words at larger relative density. But, the important thing seen here is, the region below the pile tip containing the plastic zone which is calculated as the subtraction the pile length from the container width increases as the pile diameter decreases as listed in Table (4). This state may be justified to the reduction of the angle of internal friction with pile diameter which is consistent with the conclusions of **(Ali 2012, Awad 2003,** and **Meyerhof 1983).**

Table 4
Effect of model pile dimensions on the distance between pile and the boundary

Pile diameter (cm)	Pile length (cm)	Distance from pile tip to rigid bottom boundary		
		Loose	Medium	Dense
2	20	15D	15D	20D
3	30	10D	10D	13.3D
4	40	10D	10D	11.25D

B. Effect of Container Size on the Side Friction of Pile

In the first approximation, the mechanism of the mobilization of the skin friction along the pile shaft can be considered to be similar to a direct shear interface test with constant normal stress corresponding to the lateral stresses of the surrounding soil. Volumetric changes of the soil within interface induce a normal displacement in the surrounding soil and the changes in the normal stress imposed on the shaft.

The localization of deformations in the interface is occurred in narrow regions of intensely sheared material "shear bands" in which significant decreases in density occur. The overall mechanism of localization is much larger than individual shear bands; therefore the term "shear zone" is used instead of "shear band" in describing the area where localization happens.

Boulon and Foray (1986) have shown that a significant scale effect in the shaft friction measured on model piles can be expected due to formation of shear bands along the pile shaft. It is thought that the shear zone formed during shearing mainly depends on an average diameter of grains; but in the real the scale effect of container boundaries also affects the test results.

Analysis

Practically, all model piles to be tested in the container are subjected to stresses from all directions. As a result, the container size plays a significant role in the state of lateral stresses affected on model piles which in some way has the largest impact being affected in scaling process of container modeling than the vertical stresses.

If may be said that, the model piles which are constructed as bored piles, the situation of soil surrounded piles approaches to active state due to installation effects.

When a model pile is positioned in a distance near to the container boundary wall, the pile would be much supported by surrounding soil and consequently, more capable to bear the external loads and at which the soil stresses in the container are at maximum values as being close to the boundary.

In the contrast way, increase the distance between model pile face and container boundary will reduce the ability of pile to be supported by surrounding soil and as a result this will make to decrease the bonds between soil particles and to increase the contracted interface zone

leading the soil to arch around the pile and decrease the side friction due to decreasing the effective length of pile embedded into the sand as shown in Figure (6).

Principles of direct shear test may be implemented in modeling the shaft friction of model pile because the studies concerning the scale effect on lateral friction due to shear bands in the soil pile interface based on direct shear test. So, the modeling of side friction of model pile with direct shear test was not intended to obtain quantitative test results; but the objective is to utilize the mechanism of direct shear test in identifying the pile friction behavior. It was shown that the disadvantages in simulation the direct shear interface of lateral friction of the pile shaft are the circumferential stress influence and its evolution during the shearing of model pile shaft cannot be reflected in the direct shear interface test in addition to the Arching phenomenon can appear in the soil-pile interface in the loose soil therefore; the contact between the interface and the surrounded soil may be lost.

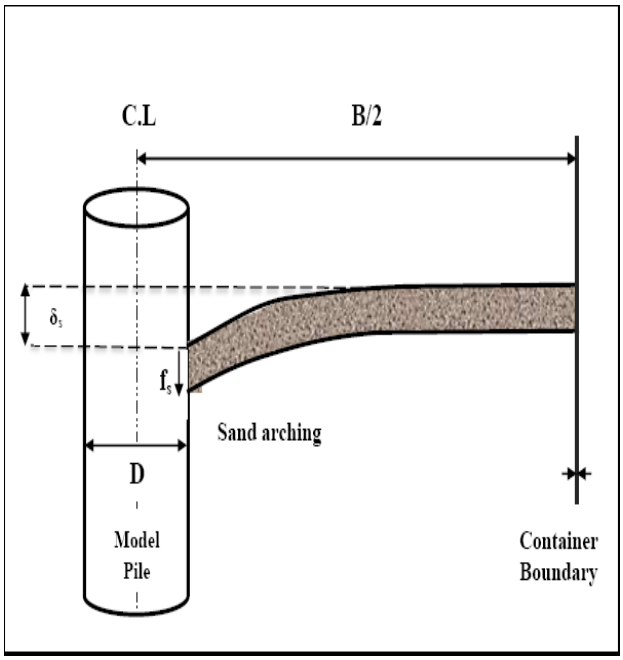

Fig. 6. Arching effect around a model pile constructed into a container boundary

As mentioned before, the thin layer of sand that is involved in the shearing process (shear zone) has been affected by the scaling of tests. Shear zone thickness is significantly influenced by the size of shear box and it has a direct proportion to the size of box. This property can be possibly considered as an inception key in making the interpretation of test results of model piles acceptable and more easily.

Therefore, as the container size increases the contraction in the interface increase due to the increasing in shear zone thickness which is expanded and developed to the sides of piles at which the soil is in active state. To clarify the effect container size on the state of soil and what will be associated to the scaling of tests. The mechanism of model bored pile loaded in different box sizes are shown in Figure (7). It can be noted that, in stage (A): plastic zone in alignment to the bottom boundary and active zone is small and the distance from (A to 0) is less than the actual length of pile. Stage (B): plastic zone moved away from the boundary and the active zone started to increase due to the increase in the container size, and the distance from (B to 0) became less than in stage (A). In Stage (C): plastic zone is further than the previous stages and the active zone is larger due to ability of sand to arch. So, the line (C0) is much less than the actual pile length consequently, pile side friction will decrease as the container size increase

VI. MATHIMATICAL MODEL OF RESULTS

In this section, the results obtained from the numerical analyses which relate the model container size required for carrying out the model bored are grouped as a statistical data. The computer package (*STATISTICA*) was used to represent relationships between the model container size, pile diameter and pile length at different

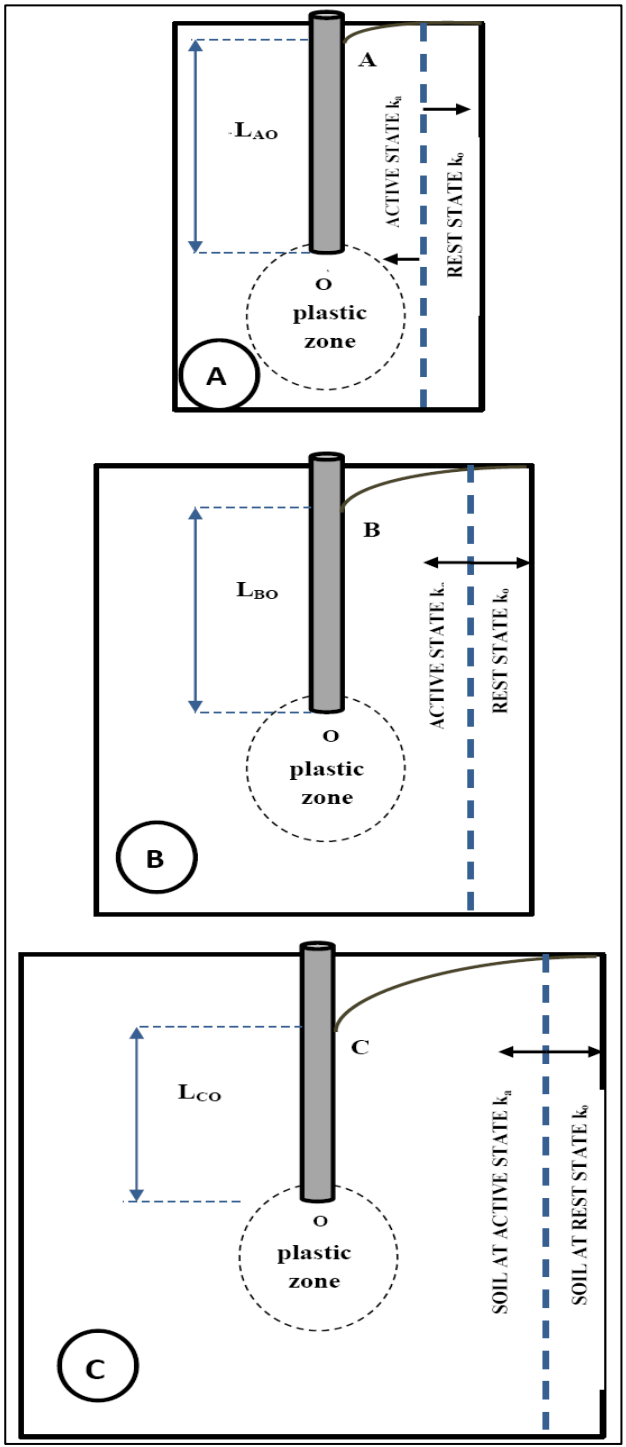

values of relative densities (loose, medium and dense) for model bored piles. Three dimensional contour areas for the variation of model container size with diameters and lengths of piles and relative density are shown in Figures (8) to (9). The assumption used to represent these relationships is nonlinear.

Fig. 7. Evolution of plastic and active zones at different box dimensions

The computer package presents the results of numerical analysis as a mathematical model of model container width (the shape of container is a cube) as a function of pile dimensions in addition to the soil friction and relative density for sand. Accordingly, the statistical model for pile capacity is derived to be: -

$$\mathbf{C.W} = 9.5\mathbf{D}^{\tan\varphi} - 133/\mathbf{R.D} + 0.96\mathbf{L} + 16.8\ldots \quad (1)$$

Where

C.W: Container width in cm.

D and L: Model pile diameter and length respectively in cm.

R.D: Relative density as integer value, and

φ: Angle of internal friction.

The coefficient of determination (R^2) for the derived equation is (95.37 %)

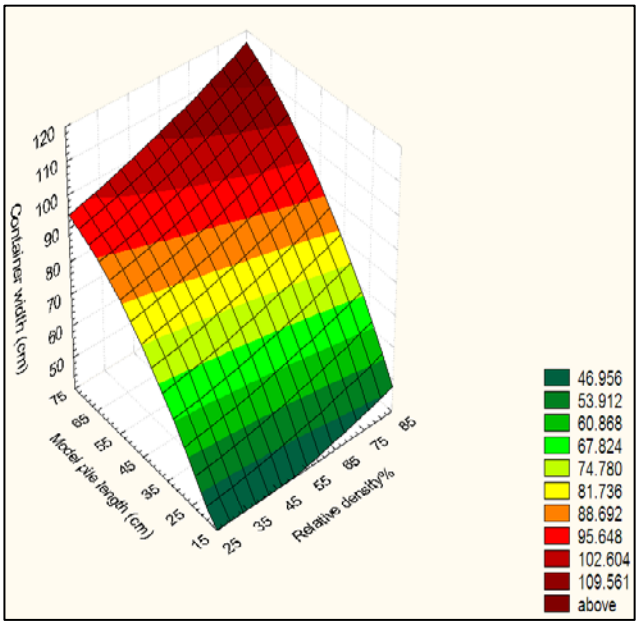

Fig. 8. Three dimensional contour plot of variation of container width model pile length

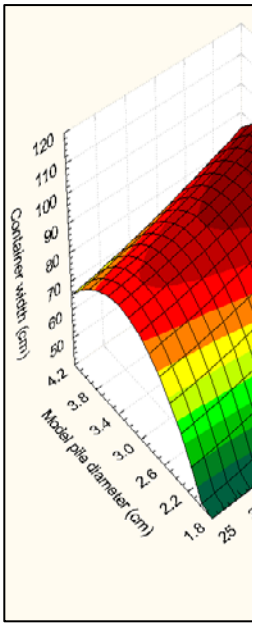

Fig. 9. Three dimensional contour plot of variation of container width and model pile diameter

It can be observed that the model container size increases with the increase in both diameter and pile length. Also, a direct proportion was seen for the container size with the angle of internal friction and the relative density of sand. However, it is noticed that, the most influence parameters in the derived statistical equation are the pile dimensions in the contrast to the relative density and angle of internal friction which exhibit a less effect than the others. This may be attributed to the test results at which no scale effect appears where the boundaries of container are out of the influence regions (plastic and nonlinear elastic zones) and all stresses exerted on the model piles and soil friction are in steady state within the elastic zone.

Stage (A): plastic zone in alignment to the bottom boundary and active zone is small and the distance from (A to 0) is less than the actual length of pile.

Stage (B): plastic zone moved away from the boundary and the active zone started to increase due to the increase in the container size, and the distance from (B to 0) became less than in stage (A)

Stage (C): plastic zone is further than the previous stages and the active zone is larger due to ability of sand to arch. So, the line (C0) is much less than the actual pile length consequently, pile side friction will decrease as the container size increase.

VII. CONCLUSIONS

Based on the numerical analysis performed during this study, the following main conclusions can be listed as:

1. Generally, as the size of container increases, the model pile capacity decreases at all states of relative densities.
2. A pronounced influence of container boundary was noticed, when a model pile is erected in dense and medium sand, and a marginal effect was shown at the loose state of sand.
3. The distance below pile tip to the bottom boundary at which, no further boundary effect increase with the decrease in the model pile diameter.
4. A statistical derived equation can be employed to get quantitative values of model pile capacities at different dimensions and relative densities.
5. As the container size increases, the contraction in the interface due to the increase in the shear zone thickness will be expanded and developed to the sides of pile.

VII. REFERENCES

[1]. Ali, A.M. (2012): "Effect of Scaling Factor on Model Pile Test Results", M.Sc. Thesis, Department of Building and Constructions, University of Technology, Baghdad.

[2]. Al-Mhaidib, A.I, (2006): "Loading Rate Effect on Piles in Clay from Laboratory Model Tests", P.O. Box 800, Saudi Arabia.

[3]. Awad, M.A. (2003):"The Dependence of Bearing Value on Diameter of Driven Steel Piles in Sand", Journal of the Islamic University of Gaza, Vol.11 (1), pp. 26-42.

[4]. Bolton, M. D., Gui, M. W., Garnier, J., Corte, J. F., Bagge, G., Laue, J.and Renzi, R. (1999): "Centrifuge Cone Penetration Test in Sand",Geotechnique, Vol. 49, No. 4, pp. 543-552.

[5]. Boulon, M. and Foray, P., (1986): "Physical and Numerical Simulation of Lateral Shaft Friction along Offshore Piles in Sand," 3rd International Conference on Numerical Methods in Offshore Piling, Nantes, France, pp. 127–147.

[6]. Das, B.M. (2007): "Principles of Foundation Engineering", 6th Edition, Thomson Learning Academic Resource Center.

[7]. Garnier, J. & Ko¨nig, D. (1998): "Scale effects in piles and nails loading tests in sand", Centrifuge 98 (Kimura, Kusakabe & Takemura, eds), 205–210. Rotterdam: Balkema.

[8]. Gui, M.W, M.D. Bolton, Garnier, J., Corte, J.F, Bagge, G., Laue, J. and Renzi, R. (1998): "Guidelines For Cone Penetration Tests in Sand", Centrifuge 1998, Kimura, Kusakabe and Takemura (eds), Balkema, Rotterdam.

[9]. Gui, M.W., (1995): "Centrifuge and Numerical Modeling of Pile and Penetrometer in Sand", Ph.D. dissertation, University of Cambridge, England.

[10]. Jawad, F.W, (2012): "A Numerical and Experimental Investigation for Piled Raft Foundation under Static and Impact Loads" Ph.D. Thesis, University of Baghdad, Iraq.

[11]. Kumar, J., and Khatri, V. N. (2008): "Effect of Footing Roughness on Lower Bound Nγ Values" Int. J. Geomech., Vol. 8, No.3, pp. 176–187.

[12]. Lee, J. H., & Salgado, R., (1999): "Determination of Pile Base Resistance in Sands", Journal of Geotechnical and Geoenvironmental Engineering, ASCE, Vol. 125, No.8, pp. 673-683.

[13]. Lunne, T., Robertson, P.K., & Powell, J.J.M., (1997): "Cone penetration testing in geotechnical practice", Blackie Academic & Professional, London.

[14]. Meyerhof, G.G. (1983): "Scale Effect of Ultimate Pile Capacity", Journal of Geotechnical Engineering, ASCE, Vol. 109, No.6, pp. 797-806.

[15]. Muir Wood, D. (2004): "Geotechnical Modeling", 2nd, Cambridge University Press, Cambridge.

[16]. Parkin, A.K., & Lunne, T., (1982): "Boundary effects in the laboratory calibration of a cone penetrometer for sand", Proceedings of the Second European Symposium on Penetration Testing, Amsterdam, pp.761-768.

[17]. Puech. (1975): "De l'influence de la compressibilite sur la force portante limite des fondations profondes", These Doctorate de specialite, unversite de Grenoble, France, (cited by Weinstein, 2008).

[18]. Salgado, R., Mitchell, J.K., and Jamiolkowski, M. (1998): "Calibration Chamber Size Effects on Penetration Resistance of Sand", ASCE, Journal of Geotechnical and Geoenvironmental Engineering, Vol. 124, No. 9, pp. 878-888.

[19]. Yang, J. (2006): "Influence Zone for End Bearing of Piles in Sand", ASCE, Journal of Geotechnical and Geoenvironmental Engineering, Vol. 132, No. 9, pp. 1229-1237.

AUTHOR'S PHOTO

Performance of Sand-Cement Dust Mixture Reinforced by Natural Fiber

Athraa Mohammed Jawad Al-hassani

Athraa M. J. Structures & *Water Resources Dep. College of Engineering, Kufa University, AL-Najaf city, AL- Najaf province, Iraq. Tel: +964-7802510211, E-mail: Athraa_alhassani@yahoo.com*

***Abstract*— This study investigates the effect of including randomly spaced palm fibers in a soil matrix and soil-cement dust mixture. Cemented specimens were prepared with cement kiln dust (CKD) contents of 5% by weight of dry sand and cured for seven days. The length of fiber used is 12 mm, with contents of 0%, 0.5%, 1%, and 1.5% by weight. Direct shear and CBR tests were carried out for samples at maximum dry density and optimum moisture content obtained from standard Procter test. The shear strength test results indicated that the inclusion of fiber within the soil increase the shear strength significantly, while it is decreasing for cemented reinforced soil. Palm fiber changes the soil and soil-CKD mixture to be more ductile. The CBR tests show that the value increase with palm fiber reinforcement of the sand and the optimum fiber content is 1% while, the CBR value of soil-CKD mixture decrease with palm fiber reinforcement.**

***Index Terms*— palm fiber, cement kiln dust, CBR test, and direct shear**

INTRODUCTION

AT the present time, there is a greater awareness that landfills are filling up, resources are being used up, the planet is being polluted and that non-renewable resources will not last forever. So, there is a need to more environmentally friendly materials to be in agreement with the sustainability requirements. Sustainability requires resources to be conserved, the environment to be protected, and a healthy environment to be maintained. The World Commission on the Environment and Development has suggested the following definition for sustainable development: ‘‘sustainable development is the development that responds to the needs of the present, without abandoning the ability of future generations to supply their own needs". It has been observed that tree roots and vegetation effectively increase the shear strength of soil. Early attempts to increase soil strength by mixing it with other materials (such as palm fibers or wicker) date back 3000 years to the construction of ziggurats (Iraqi ancient). Cement kiln dust is a significant by-product material of the cement manufacturing process, which poses an environmental threat. To deal with this problem, researches are being carried out in different parts of the world to find out efficient ways of using cement dust in various applications such as soil stabilization.

In the case of sandy soils, which are commonly selected in the pavement layers, the usage of CKD may provide cementitious materials when it is mixed with water in a similar way to the mechanism by which Portland cements provide their binding characteristics.

Any potential application of CKD, including sand and clay stabilization, is governed by the physical and chemical composition of the dust. In practical terms, the dust varies markedly from plant to plant in chemical, mineralogical, and physical composition, depending upon the feed raw materials properties, type of kiln operation, dust collection facility, and the type of used fuel [1]. However, the addition of cement to soil results in a brittle behavior that can be reduced and controlled by the application of fibers.

The compressive strength of artificially cemented sandy soil has been studied in the past by several investigators (e.g., [2]; [3]; [4]; [5], [6]; [7]). In addition, studies of the reinforcement of sand by the inclusion of fiber have also been reported (e.g., [8]; [9]; [10]; [11]; [12]; [13];[14]; [15]; [16]). Compared to uncemented soil, the addition of small amounts of cement significantly increases the peak strength and initial stiffness. In general, reports in the literature show that the shear strength of naturally and artificially cemented soil, especially that of cemented sand, can be adequately represented by a straight Mohr–Coulomb envelope defined by a cohesive intercept (c'), which is a function mostly of the cement content, and internal friction angle (ϕ') that seems to be hardly at all affected by cementation. In addition, the marked brittle behavior observed for low confining stress changes to ductile behavior as the stress increases. The general characteristics of granular soils reinforced with discrete fiber reported in previous studies were reviewed by [10] and [17]. Their reviews show that the inclusion of fiber definitely provides an increase in material strength and ductility.

The palm fibers in date production have filament textures with special properties such as low costs, plenitude in the region, durability, lightweight, tension capacity and relative strength against deterioration [18]. Fibers extracted from decomposed

palm trees are found to be brittle, having low tensile strength and modulus of elasticity and very high water absorption [19]. Unconfined compression strength (UCS), California Bearing Ratio (CBR) and compaction tests were performed on neat and palm fiber reinforced soil samples by Marandi et al [20]. It was reported that at a constant palm fiber length, with increase in fiber inclusion (from 0% to 1%), the maximum and residual strengths were increased, while the difference between the residual and maximum strengths was decreased. A similar trend was observed for constant palm fiber inclusion and increase in palm fiber length (from 20 mm to 40 mm) [20]. Ahmad et al. mixed palm fibers with silty sand soil to investigate the increase of shear strength during triaxial compression. The specimens were tested with 0.25% and 0.5% content of palm fibers of different lengths (i.e. 15 mm, 30 mm and 45 mm). Reinforced silty sand containing 0.5% coated fibers of 30 mm length exhibited approximately 25% increase in friction angle and 35% in cohesion compared to those of unreinforced silty sand. In addition, palm fibers coated with acrylic butadiene styrene thermoplastic increased the shear strength of silty sand much more compared to uncoated fibers [21].

Date palm fibers are available in the Middle East in huge amounts as well as the cement kiln dust all over the world, and there are a few studies about the mechanical properties of such additives. This motivates the current work to be on the influence of the date palm fiber on the mechanical properties of soil and soil-cement kiln dust mixture.

EXPERIMENTAL WORK

Materials and Test Methods

Properties of Soil

Clean and uniform quartz river sand with sub rounded to sub angular particles was used as the base material in the tests. The soil used in the investigation was classified as SP according to Unified Soil Classification System. The engineering properties of this soil are shown in table (1). The grain size distribution curve of the soil shown in Figure (1) which indicates that the soil is composed of 92.9% sand, and 7.11% silt.

Properties of Cement Kiln Dust (CKD)

The cement kiln dust used in this study was obtained from Al-Kufa cement factory. The physical properties and the chemical composition of the dust are reported in Table 2. The cement kiln dust content 5% (by dry weight of the soil) was selected as consistent with a previous study [22].

Palm Fiber

Raw mesh surrounding the date palm tree stems was collected from a date palm farm in Kufa. The fibres were separated from the meshes manually then, cleaned and cut to a specified length. The moisture absorption characteristics of the palm fibers were examined by soaking the fiber samples and weighing two hours intervals. The average results are shown in Figure 2. The results indicate that the maximum water absorption of 240% was achieved after a period of 28 hours (after this period the rate of water absorption was very low). The fiber strength characteristics were obtained through tensile strength test performed according to ASTM D 638. To prepare the tested sample, 10 individual randomly selected fibers were taken and twisted together by hand. Then the fibers glued to plastic squares using Epoxy glue, the plastic squares had dimensions of 2.5 cm x 5 cm. The results show that; the maximum tensile strength of 57.81 MPa was achieved at a strain of 10.17%. The average diameter is 0.38mm, in determining the fiber diameter three measurements were taken at different cross-sections in each fiber and average diameter was calculated.

Preparation of samples

The compacted soil, soil-cement kiln dust mixture, and fiber-reinforced specimens used in the direct shear and CBR tests were prepared by hand-mixing the dry sand, cement kiln dust, water and palm fibers. During the mixing process, it was found to be important to add the water prior to adding the fibers, to prevent floating of the fibers with making sure all the fibers were mixed thoroughly to achieve a uniform mixture. Specimens were compacted in three layers, to a maximum dry density (MDD) and optimum moisture content (OMC) obtained from Standard Procter Test. Finally, the specimen moulds which contain cement dust were wrapped in moisture-proof bags and stored in a humid room (at a temperature of 21$\pm$ 2 ˚ C and a relative humidity of 90%) to cure for 7 days before testing.

TABLE 1
SOIL CHARACTERISTICS

Characteristics	*Value*
Sand content (0.075 – 2 mm)	*92.89%*
Silt content (0.002 – 0.075 mm)	*7.11%*
D_{10}	*0.09*
D_{30}	*0.17*
D_{60}	*0.22*
C_u	*2.44*
C_c	*1.46*
Soil classification	*SP*
Maximum unit weight	*17.66 kN/m^3*
Optimum moisture content	*12%*
Plasticity	*NP*
Specific gravity of solids (G_s)	*2.67*

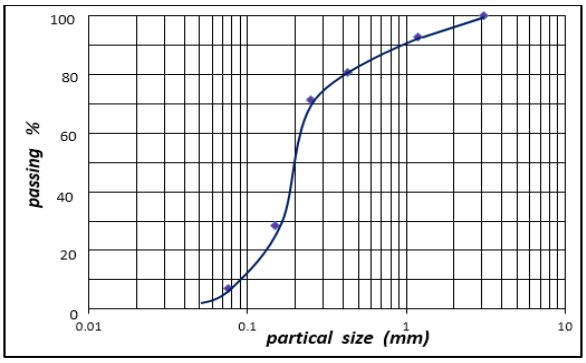

Fig. 1: Grain size distribution curve of the soil

TABLE 2
PROPERRIES OF CEMENT KILN DUST

Color	*Light brown*
Surface texture	*Fine*
Surface shape	*Semi-circle particles*
Specific gravity	*2.85*
Chemical Analysis (% by weight)	
Sio_2	*14.1*
Al_2O_3	*4.7*
Al_2O_3	*4.7*
Fe_2O_3	*1.97*
CaO	*40.17*
Mg0	*2.79*
So_3	*5.85*
K_2O	*3.13*
Na_2O	*1.55*
Cl	*1.83*
Loss of ignition (L.O.I)	*24.25*

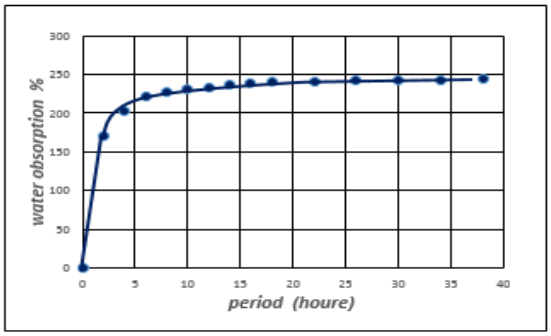

Fig. 2: Results of water absorption of palm fiber

Compaction Tests

Standard compaction tests were conducted with according to ASTM D 558-76. The relationship between the dry unit w mens, s ı, and r were s e was a %. In a ensity i isture a nsity. I m dry u isture c able 3 a

California Bearing Ratio (CBR) Test

California Bearing Ratio tests were conducted for base sand soil specimens, soil-cement dust mixture, reinforced soil, and reinforced soil-cement dust mixture specimens with fiber contents of 0.0%, 0.5%, 1% and 1.5% (according to ASTM D 698). All specimens were prepared at maximum dry densities and optimum moisture contents. The results for specimens of sand soil and soil-cement dust with various fiber contents are shown in Table 4 and Figures 6, and 7.

Direct Shear Test

The experimental study involved performing a series of direct shear tests according to ASTM D 3080. Soil-fiber mixes with and without CKD were compacted in the shear box of 60 × 60 mm in plan and 20 mm in thickness. The speciemens were prepared to standard Proctor's maximum density and optimum moisture content. The specimens were prepared at 0%; 0.5%, 1%, and 1.5% palm fiber content by dry weight. Three specimens were prepared for each test. The specimens were tested at normal stresses of 100, 200 and 400 kPa with loading rate 1 mm/minute. Shear stresses were recorded as a function of horizontal displacement. The results of direct shear tests were shown in Table 4 and Figures 8 to 13.

RESULTS AND DISCUSSIONS

Table 3 and Figure (3) show the compaction curves of soil, fiber reinforced soil, treated soil with cement kiln dust, and reinforced-treated soil. It is clearly shown from the table that the optimum moisture content and maximum dry density of base soil are 12% and 17.66kN/m^3, respectively. From Figures 4 and 5, it is clear that the increasing of fiber content causes increase of optimum moisture content and decrease the maximum dry density. The same results are obtained for reinforced specimens of soil-cement dust mixture. Increase in optimum moisture percentage is due to the fact that the palm fibers absorb water more than soil. The decrease in maximum dry density is because of replacing heavy soil particles or soil-CKD mixture with light palm fibers. Khedari et al. (2001) found similar results [23]. The compaction behavior of the reinforced specimens at each fiber content exhibits similar compaction behavior to unreinforced specimens.

The results of CBR tests for specimens of base soil and soil-cement dust mixture with various fiber contents of 0%, 0.5%, 1%, and 1.5% are shown in Table 4 and Figures 6 and 7. It was observed that adding of 0.5–1% fibers enhances the CBR strength significantly up to 83% compared with base soil specimens. However, this effect gradually diminishes at higher fiber contents. For example the strength at 1.5% fiber content decreases slightly. Figures also, show the effect of fiber inclusion on the stabilized soil by cement kiln dust. It is clear from figures that the CBR value of soil-cement dust mixture decreased with increasing the palm fiber content compared with unreinforced soil-cement kiln dust mixture.

Shear stress-displacement curves (for normal stress of 400 kPa) of sandy soil, and soil-cement dust mixture with 5% CKD by dry weight of sand are given in Figures 8 and 9 respectively for 0%, 0.5%, 1% and 1.5% palm fiber content. Data for other normal stresses (100 and 200 kPa) have been found to show similar tendencies, but are not shown here for the sake of conciseness. The common features for the non-

reinforced soil and non-reinforced soil-cement kiln dust of direct shear test results shown in Figures 8 and 9 are that a marked brittle failure behavior, whereas the fiber-reinforced soil and reinforced cemented specimens demonstrate a ductile behavior.

The peak strength envelopes for both fiber-reinforced and non-reinforced soil and sand-cement dust mixture are presented in Figures 10 and 11. The peak strength parameters for non-reinforced and fiber-reinforced cemented and uncemented sand are presented in Table 4. The data show that the peak friction angle changes from 36 ° for uncemented non-reinforced sand to 40-48 ° by fiber inclusion (depending on the fiber percentage added) and 43 ° by treating the soil by CKD as shown in Figure 13. Including both cement dust and fiber in the sand gives a peak friction angle ranging from 33.5-36 °. Cohesion intercept increases with increasing fiber content for uncemented sand and decreases with increasing fiber content for soil-cement dust mixture as shown in Figure 12 . However, the unreinforced soil-CKD mixture gives a higher cohesion intercept of 40 kPa. It is clearly observed that reinforcement is more effective for uncemented sand. For the cemented sand, the proportional gain in strength in comparison with uncemented sand due to fiber inclusion decreases, that is, the fiber reinforcement becomes less effective.

TABLE 3
Results of Standard Procter tests

Soil identification	***MDD kN/m^3***	***OMC %***
Base soil only	*17.66*	*12*
Soil + 5% CKD	*18.25*	*14.5*
Soil + 0.5% fiber	*17.17*	*15.8*
Soil + 1.0% fiber	*17.04*	*16.5*
Soil + 1.5% fiber	*16.95*	*18.0*
Soil + 5% CKD + 0.5% fiber	*17.58*	*13.7*
Soil + 5% CKD + 1.0% fiber	*17.51*	*14.0*
Soil + 5% CKD + 1.5% fiber	*17.36*	*15.0*

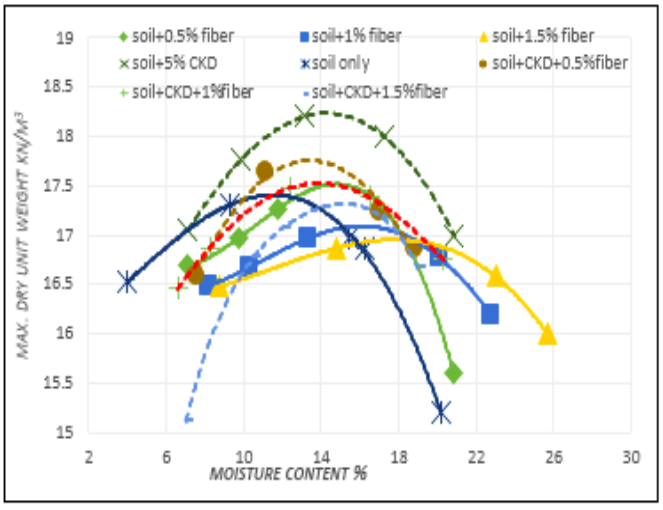

Fig.3: Compaction curves for reinforced and unreinforced soil and soil – cement dust mixture

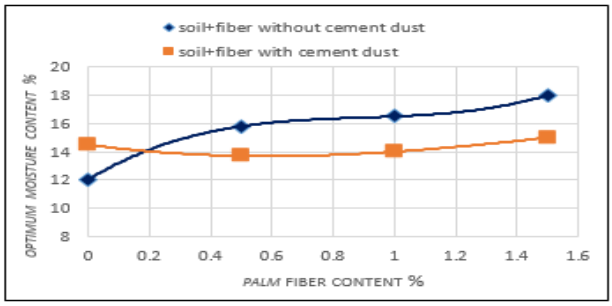

Fig.4: Variation of optimum moisture contents with palm fiber content

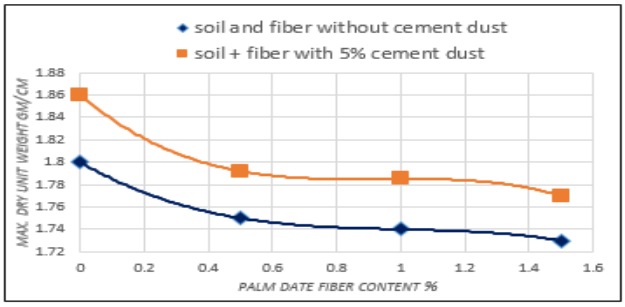

Fig.5: Variation of maximum dry unit weight with palm fiber content

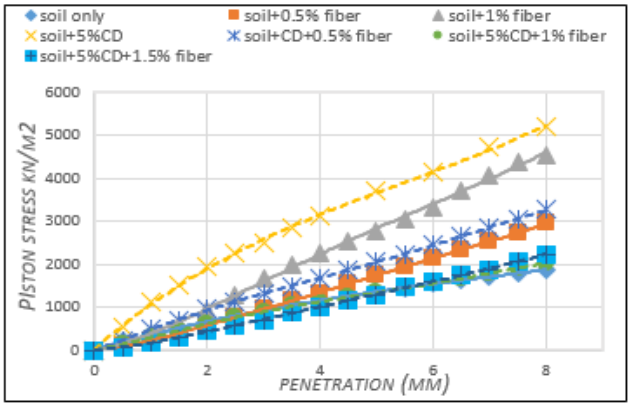

Fig.7: Effect of fiber content on CBR value for soil, and soil-CKD speciemens

TABLE 4
Results of direct shear. CBR tests for reinforced and

Soil identification	***C, kPa***	***ϕ °***	***CBR %***
Base soil only	*0*	*36*	13.3
Soil + 5% CKD	*40*	*43*	30.45
Soil + 0.5% fiber	*10*	*40*	16.85
Soil + 1.0% fiber	*30*	*48*	24.34
Soil + 1.5% fiber	*32*	*40*	15.55
Soil + 5% CKD + 0.5% fiber	*30*	*36*	20.0
Soil + 5% CKD + 1.0% fiber	*22*	*35*	13.0
Soil + 5% CKD + 1.5% fiber	*18*	*33.5*	12.5

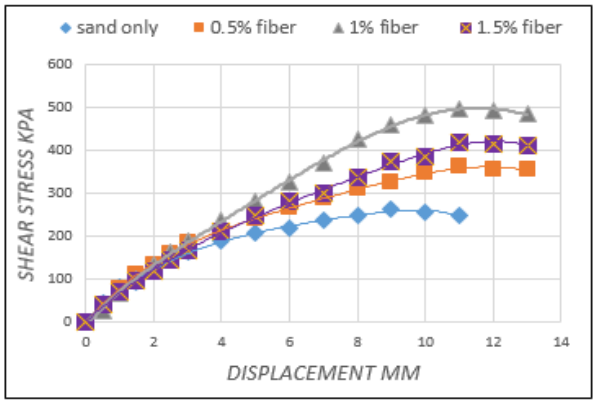

Fig. 8: Shear stress-displacement from direct shear test results for fiber reinforced and unreinforced soil speciemens

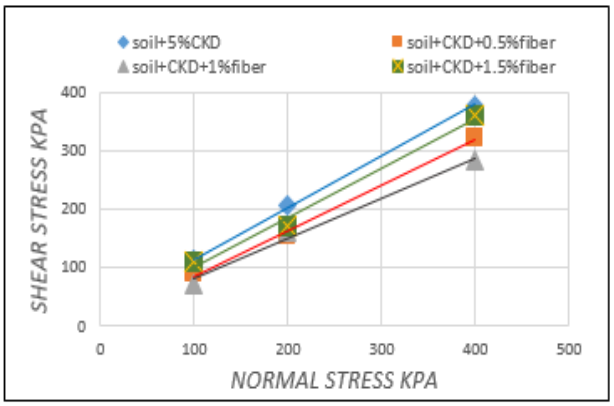

Fig. 11: Mohr-Coulomb failure envelopes for fiber reinforced and unreinforced soil- CKD

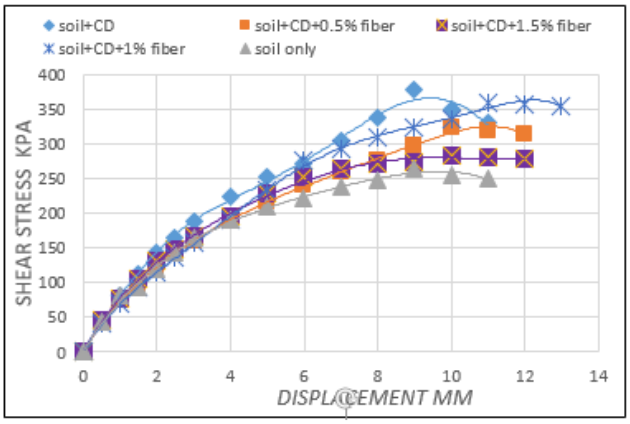

Fig. 9: Shear stress-displacement from direct shear test for fiber reinforced and unreinforced soil-cement kiln dust specimens

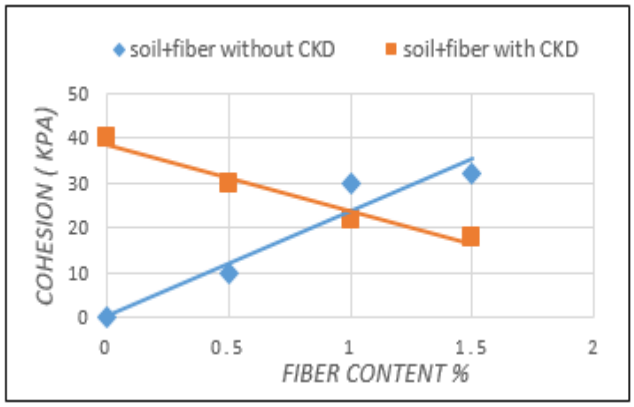

Fig. 12: Effect of fiber inclusion on the Cohesion for soil and soil-CKD specimens

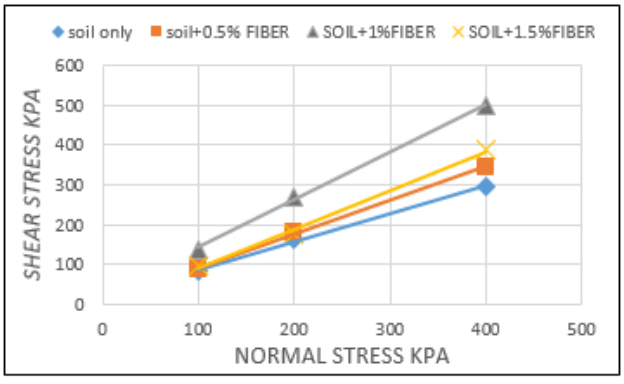

Fig. 10: Mohr-Coulomb failure envelopes for reinforced and unreinforced soil-CKD

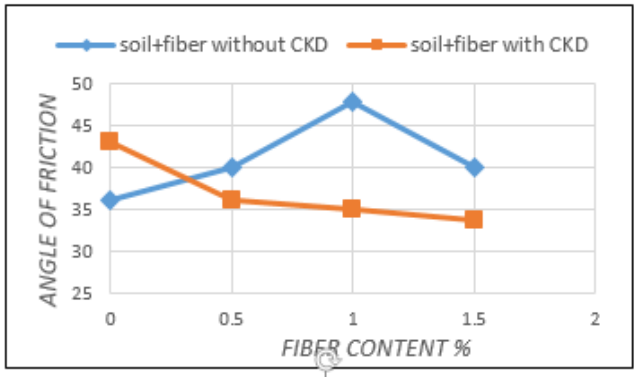

Fig. 13: Effect of fiber inclusion on the angle of friction for soil and soil-CKD specimens

CONCLUSION

On the basis of the above experimental investigations the following conclusions are drawn.

1. The shear strength of soil increases with inclusion of date palm fiber up to 1%, and it decreases beyond this ratio.
2. The fiber reinforcement is more effective for uncemented sand. For the cemented sand, the proportional gain in strength in comparison with uncemented sand due to fiber inclusion decreases, that is, the fiber reinforcement becomes less effective.
3. Palm fiber changes the soil sand and soil-cement kiln dust mixture to be more ductile.
4. The CBR tests show that its value increase with palm fiber reinforcement of the sand and the optimum fiber content of studied range is 1%, while the CBR values of soil-CKD mixture decrease with palm fiber reinforcement.

REFERENCES

[1] *Klemm, W. A.*: Kiln Dust Utilization, *Martin Marietta Laboratories Report MML TR 80-12*, Baltimore, Maryland, U.S.A (1980).

[2] *Saxena, S.K., Lastrico, R.M.*: Static properties of lightly cemented sand. Journal of Geotechnical Engineering, 1978; ASCE 104 (12), 1449-1465.

[3] *Coop, M.R., Atkinson, J.H.*: The mechanics of cemented carbonate sands. Geotechnique 1993; 43 (1), 53–67.

[4] *Huang, J.T., Airey, D.*: Properties of artificially cemented carbonate sand. Journal of Geotechnical and Geoenvironmental Engineering 1998; 124 (6), 492–499.

[5] *Consoli, N.C., Rotta, G.V., Prietto, P.D.M.*: The influence of curing under stress on the triaxial response of cemented soils. Geotechnique 2000; 50 (1), 99–105.

[6] *Consoli, N.C., Rotta, G.V., Prietto, P.D.M.*: Yielding-compressibility-strength relationship for an artificially cemented soil cured under stress. Geotechnique 2006; 56 (1), 69–72.

[7] *Consoli, N.C., Foppa, D., Festugato, L., Heineck, K.S.*: Key parameters for strength control of artificially cemented soils. Journal of Geotechnical and Geoenvironmental Engineering, ASCE 2007a; 133 (2), 197–205.

[8] *Gray, D.H., Al-Refaei, T.:* Behavior of fabric versus fiber-reinforced sand. Journal of Geotechnical Engineering, ASCE 1986; 112 (8), 804–820.

[9] *Maher, M.H., Gray, D.H.:* Static response of sands reinforced with randomly distributed fibers. Journal of Geotechnical Engineering, ASCE 1990; 116 (11), 1661–1677.

[10] *Morel, J.C., Gourc, J.P.:* Mechanical behavior of sand reinforced with mesh elements. Geosynthetics International 1997; 4 (5), 481–508.

[11] *Consoli, N.C., Casagrande, M.D.T., Prietto, P.D.M., Thome, A.:* Plate load test on fiber-reinforced soil. Journal of Geotechnical and Geoenvironmental Engineering 2003b; 129 (10), 951–955.

[12] *Consoli, N.C., Casagrande, M.D.T., Coop, M.R.:* Performance of fiber reinforced sand at large shear strains. Geotechnique 2007b; 57 (9), 751–756.

[13] *Consoli, N.C., Heineck, K.S., Casagrande, M.D.T., Coop, M.R.:* Shear strength behavior of fiber-reinforced sand considering triaxial tests under distinct stress paths. Journal of Geotechnical and Geoenvironmental Engineering 2007c; 133 (11), 1466–1469.

[14] *Park, T., Tan, S.A.* Enhanced performance of reinforced soil walls by the inclusion of short fiber. Geotextiles and Geomembranes 2005; 23 (4), 348–361.

[15] *Latha, G.M., Murthy, V.S.* Effect of reinforcement form on the behaviour of geosynthetic reinforced sand. Geotextiles and Geomembranes 2007; 25 (1), 23–32.

[16] *Chauhan, M.S., Mittal, S., Mohanty, B.* Performance evaluation of silty sand subgrade reinforced with fly ash and fiber. Geotextiles and Geomembranes 2008; 26(5), 429–435.

[17] *Heineck, K.S., Coop, M.R., Consoli, N.C.* Effect of micro-reinforcement of soils from very small to large shear strains. Journal of Geotechnical and Geoenvironmental Engineering 2005; 131 (8), 1024–1033.

[18] *Yusoff M, Salit M, Ismail N, Wirawan R.* Mechanical properties of short random oil palm fiber reinforced epoxy composites. Sains Malay 2010; 39:87–92.

[19] *Swamy N.* New reinforced concretes. Surry University Press; 1984.

[20] *Marandi M, Bagheripour H, Rahgozar R, Zare H.* Strength and ductility of randomly distributed palm fibers reinforced silty-sand soils. Am J Appl Sci. 2008; 5:209–20.

[21] *Ahmad F, Bateni F, Azmi M.* Performance evaluation of silty sand reinforced with fibers. Geotext Geomembr 2010; 28:93–9.

[22] *S.M.Kadhim, Athraa M.* Effect of cement dust content on soil properties of river sand soil. Journal of Al-buhooth Al-tachaniya 1994; vol.7, No.20, pp. (28-49).

[23] *Khedari, J., et al.* New lightweight composite construction materials with low thermal conductivity. Cement and Concrete Composites, 2001; 23, 65–70.

Cement – Lime Additives to Stabilize Iraqi Soils

Dr. Nahla M.Salim
Husam Hikmat Baqir
Kawther Y.H.AL-Soudany

***Abstract*—** Chemical stabilization has been used for the soft clayey soils in order to enhance the shear strength and limiting deformaion behavior. Cement is widely used as a stabilizing material for soils, but increasing cost causing economic concerns among practitioners. In this paper two types of materials were used as soil stabilizer such cement and lime. Cement was used in (3, 5, 7 and 10) %. Lime also used as stabilizer in four percent representing (3, 5, 7 and 10) %. Combination of 50% of cement and 50% of lime used as stabilizer in four percent representing (3, 5, 7, and 10) %. The clay specimens were taken from Baladroz East –North of Iraq.

The experiments were carried out in University of Technology /soil mechanics Lab. The physical properties were measured by conducting standard laboratory test such as Atterberg limits (L.L., P.L.) and specific gravity. A standard compaction on natural and improved soils were carried out, the maximum dry density and optimum moisture content were measured for different % of lime and cement content. The results revealed that as the cement content increases, the maximum dry density increases too. While as the lime content increases, the maximum dry density decreases. The results of unconfined compressive strength test for natural and improved soil reveal, that the shear strength increases as lime and cement content increase with increasing the curing period (3, 7, 14 and 28) days.

Keywords: Soil Stabilization, Cement Stabilization, Lime Stabilization, Unconfined Compression Test, Curing Period, Soil Strength

I. INTRODUCTION

Unstable soils can create significant problems for pavements and structures, therefore soil stabilization techniques are necessary to ensure the good stability of soil so that it can successfully sustain the load of the superstructure especially in case of soil which are highly active, also it reduce cost when compared to soil replacement method. Additives like lime, cement, fly ash and asphalt are known as chemical admixture. These methods have been used to improve the inherent properties of the soil such as increase in strength, a reduction in compressibility, an improvement in swelling or squeezing characteristics and increasing the durability of soil, [Bergado et al. 1996(3)]. Lime or cement has commonly been used as chemical admixtures for soil stabilization and extensively used in both shallow and deep stabilization methods these methods have been used to improve the properties of soil since old time. The application of deep stabilization method of in situ started in the late 1970's in Japan. [Terashi et al.1979(13); Kawasaki et al. 1981(6); Suzuki 1982(12)]. Shallow stabilization of soft soil with Lime and / or cement has been extensively used for road construction purpose in order to improve mechanical properties of the bearing layers. Recently, Lime or cement stabilization has been extended to greater depth in which acts as reinforcement. Additional application of these additives as columns to improve the stability of slops and deep excavation; to increase the bearing capacity and reduce the total and differential settlement under lightly loaded structures.

[Fonseca et al. 2009(5)] studied the characteristics of two soils, Osorio sand and Botucatu residual sand stone. Stabilization with cement after the untreated soil to acceptable materials for the construction of roads, railways and etc. the study of soil stabilization with cement relies on the quantification of the influence of percentage of cement and porosity adopted in the mixing process for different state and stress conditions. The results by assuming that the voids/ cement ratio (Vv/Vce) a very consistent framework can be obtained for the engineer to select the amount of cement and the appropriate compaction to provide a soil-cement admixture with the strength and stiffness required by the project at an optimum cost. Single equation derived for the unconfined compression strength used for all materials. qu = A {Vv/(Vce)c}-B this request conducting a few unconfined compression tests to determine the coefficients A,B and C which range according to the soil and cement type.

[Sariosseiri, F. and Muhunthan, B. 2009(11)] conducted an experimental study on using of the Portland cement in the modification and stabilization of soils in Washington state. Cement was added in percentages of 2.5, 5, 7.5 and 10% by dry weight of the soils. Laboratory tests to determine the drying rate of soils, Atterberg's limits, compaction characteristics, unconfined compressive strength and consolidated-undrained triaxial behavior were performed. Results of investigation showed significant improvement in drying state, workability, unconfined compressive strength and shear strength. This improvement is dependent on type of soil. Results of undrained triaxial tests showed that while

Dr. Nahla M.Salim
Assistant Professor, Building and Construction Engineering Department, University of Technology/ Baghdad, Iraq
Email: nahla_salim2007@yahoo.com
Husam Hikmat Baqir
Assistant Professor, Building and Construction Engineering Department, University of Technology/ Baghdad, Iraq
Email: hasamb65@yahoo.com
Kawther Y.H.AL-Soudany
Lecturer, Building and Construction Engineering Department, University of Technology/ Baghdad, Iraq
Email: k.y.alsoudany@gmail.com

cement treatment improved shear strength significantly the type of failure behavior varied. Non-treated, 5%and 10% cement treated soils displayed ductile planar and splitting type of failure, respectively. Therefore, while increased strength is achieved by cement treatment, high percentages of cement should be used with caution in field applications.

[Okonta and Govender 2011(10)] studied the effect of wetting and drying cycles on the unconfined compressive strength (UCS) and California bearing ratio(CBR) of compacted and cured sample mix with (4% and 8% of lime) and (0%, 6%, 12% and18% of flyash) and tested after 4,8 and 12 cycles of wetting and drying. Changes in mass of stabilized sands were measured to facilitate the interpretation changes in strength properties. The results showed a reduction in UCS and CBR with increases in the number of wetting and drying cycles that is dependent on the amount of lime and flyash and the ratio of lime to flyash.

[Abbasi et al. 2013(1)] investigated the improvement of silty sand desert soil from Iran using pozzolan from a cement factory in four levels (0, 5, 10 and 15)% and lime in five levels (0, 1, 3, 5 and 7)% for cured period including 7,14 and 28 days. Their results showed that adding lime to the soil improves the compressive strength while using both of lime and pozzolan, cause substantial increase in compressive strength up to 16 times in comparison of natural soil, and that curing time plays an important role in increasing the compressive strength of treated silty sand soil with lime and pozzolan . The optimum binder for the stabilization of this silty sand was found to be a combination of 15% natural pozzolan and 3% lime.

[Ajayi 2012(2)] studied the effect of lime variation on moisture content and dry density of Lateritic soil in Ilorin, Nigeria. The lime concentrations used were 0%, 2.5%, 5% and7.5% respectively. The results analysis showed that there is a significant variation at 5% level of significance in moisture content and dry density with lime concentration. The increase in the moisture content due to the addition of lime results lower amount of compaction or less compactive effort and this could be achieved by addition of small amounts of lime to laterite soil.

[Dash and Hussain 2012(4)] stabilized soft soil with different percentages of lime (1, 3, 5, 9 and13%) and cured for period (3, 7, 21 and 28 day). They studied the effect of additives on liquid limit, plastic limit, swell compressive strength, mineralogy and microstructure. They found that the liquid limit of soils initially decreases with an increase in lime content while plastic limit increased because the viscosity of the pore water increased and refers to higher resistance, the swell potential of soils decreases with increased percentages of lime to a practically negligible value.

Materials AND METHODS

1- Soil:

The soil used in this work was obtained from located at Baladroz city East –North of Iraq. Standard tests were performed to determine the physical and chemical properties of the soil. Details are given in Table 1.

Figure (1) shows the particle - size distribution of the soil. According to the unified soil classification system (USCS), the soil is classified as CL.

Table 1: Physical and chemical properties of natural soil.

No.	Index property	Index value
1	Natural water content %(wc)	2.1
2	Liquid limit %(LL)	46
3	Plastic limit %(PL)	18
4	Shrinkage limit %(SL)	14.2
5	Plasticity index %(PI)	28
6	Activity (A_t)	0.45
7	Specific gravity (Gs)	2.69
8	Gravel (larger than 4.75mm)%	0
9	Sand (0.075 to 4.75mm)%	3
10	silt (0.002 to 0.075mm)%	50
11	Clay (less than 0.002mm)%	47
12	Gypsum content %	2.92
13	Total dissolved salt TDS %	4.7
14	SO_3 content %	1.36
15	Organic matter O.M %	0.44
16	pH value	8.9
17	Soil classification symbols (USCS)	CL

Note: all tests were performed according to the ASTM (2002).

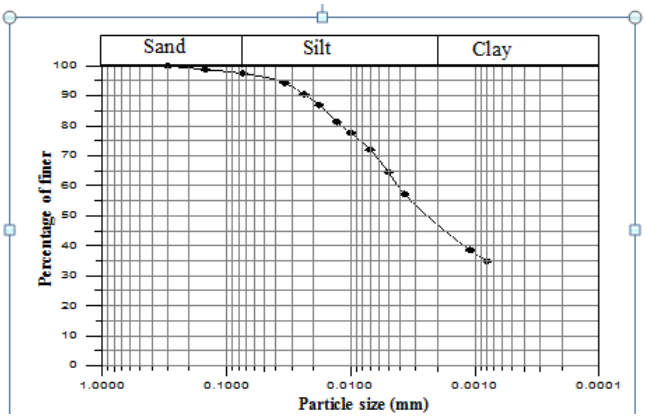

Figure 1: Particle - size distribution curve of soil

2- Lime:

Unhydrated lime was used in this investigation. The physical and chemical properties of lime and the ASTM specifications are given in Table 2.

Table2: Physical and chemical properties of lime.

Index Property	Index Value	ASTM specifications
Retained on Sieve#30(% by weight)	0	3% (max.)
Retained on Sieve#200(% by weight)	10	25% (max.)
CaO Content (%)	93.34	90% (min.)
Free Water Content (%)	0.08	2% (max.)
IR (%)	2	
SO_3 Content (%)	0.07	
L.O.I (%)	25.24	

3-Cement:

Sulfate resistance cement was used in this investigation. Physical and chemical properties of the cement and Iraqi specification No.5 (1984) are shown in Table 3.

Table3: Physical and chemical properties of cement.

Index Property	Index Value	Iraq specifications No. 5/1984
Compressive strength after 3 days (MPa)	17	15 (min.)
Compressive strength after 7 days (MPa)	26	23 (min.)
Time of initial setting (minute)	93	45 (min.)
Time of final setting (hour)	4.28	10 (max.)
SiO_2%	19.79	----------
CaO%	63.8	----------
MgO%	3.19	5 (max.)
SO_3%	2.15	2.5 (max.)
C_3A%	3.27	≤ 3.5
L.O.I (%)	0.89	4.0 (max.)

Laboratory Work

The testing program conducted on the clayey soil samples including determination of the physical and chemical properties of soils at their natural state. On the other hand, the testing program conducted on the clayey soil samples mixed with different percentages of lime, cement material, including Atterberg limits, specific gravity, compressibility, and unconfined compression test.

Liquid limit: The liquid limit test was conducted on samples passing 0.425 mm (No. 40) sieve; clayey soils and soil mixed with (0, 3, 5, 7 and 10%) lime, cement and lime- cement mixture 50% percent each using Casagrande's liquid limit apparatus as per the procedures laid down in ASTM D 4318-00.

Plastic limit: The plastic limit test was conducted on samples passing 0.425 mm (No. 40) sieve; clayey soils and soil mixed with (0, 3, 5, 7 and 10%) lime, cement and lime-cement mixture 50% each, as per the specifications ASTM D 4318-00.

Specific gravity: The specific gravity test was conducted on the soil in accordance with ASTM D 854- 02.

Compaction: The standard compaction tests were performed in accordance with ASTM D 1557. The specimens were of 102 mm diameter and 116 mm height. The degree of compaction of soil influences of its engineering properties such as CBR value, compressibility, stiffness, compressive strength, permeability, shrink, and swell potential. It is, therefore, important to achieve the desired degree of relative compaction necessary to meet the required soil characteristics.

Unconfined compression test: This test was performed in accordance with ASTM D 2166-00. The sample sizes were of 38 mm diameter and 76 mm length. , the specimens were prepared by static compaction at a dry density of (14.8 kN/m3) and moisture content of (26%).

Results and Discussions

Effect of Cement, Lime and Cement –Lime Mixture on the Atterberg's Limit, Specific Gravity and Compaction Characteristics

Effect of adding cement, lime and cement-lime combination 50% of lime and 50% of cement to the soft soil on its Atterberg limits is shown in Figure (2), (3) and (4). It can be noticed that the liquid limit increase with increasing cement content and it reaches to the maximum value approximately 59%. While it can be noticed that there is a decrease in liquid limit due to the addition of lime and cement-lime mixture at different percent of additive, there is a general decrease in plasticity index with increasing cement, lime and cement – lime mixture (50% percent each). This reduction occurs by decreasing the thickness of the double layer of the clay particles, as a result of action exchange reaction, which causes an increase in the attraction force leading to flocculation of the particles [Nalbantoglu & Gucbilmez, 2001(8)]. Unlike the pozzolanic reaction, flocculation tends to modify the soil without producing new secondary minerals [Marks & Haliburton, 1972(7)].

The addition of lime, cement-lime to the studied soils contributed to an increase in the optimum moisture content and a decrease in the maximum dry density. The moisture-density curves of the stabilized soils have a typical flattened form. This typical flattening of the compaction curves makes it easier to achieve the required density over a wider range of possible moisture contents. This change in the shape and characteristics of the peak of the compaction curves can allow for significant savings in time, effort, and energy [Nicholson et al., 1994(9)]. The addition of cement to the studied soils contributed to a decrease in the optimum moisture content and increase in the maximum dry density. Figure (2), (3) and (4) shows the specific gravity values of the soil mixed with different percentages of cement and lime. Figure (2) shows the increase in specific gravity of the soil with increasing of cement due to the high value of specific gravity of cement. While figure (3) shows the decrease in specific gravity of soil with increasing of lime content due to the low value of specific gravity of lime.

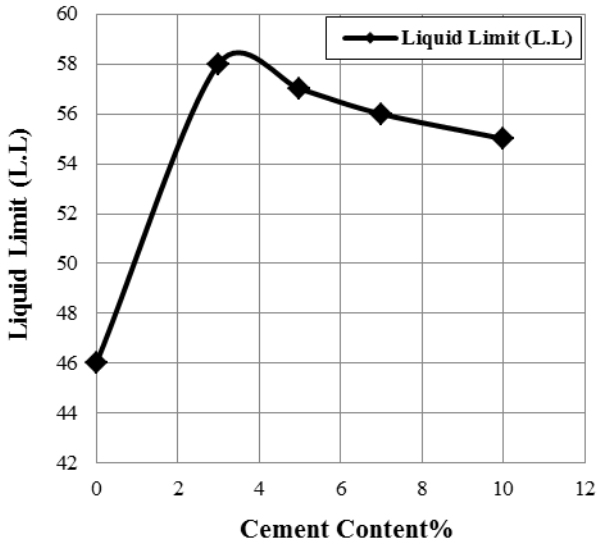

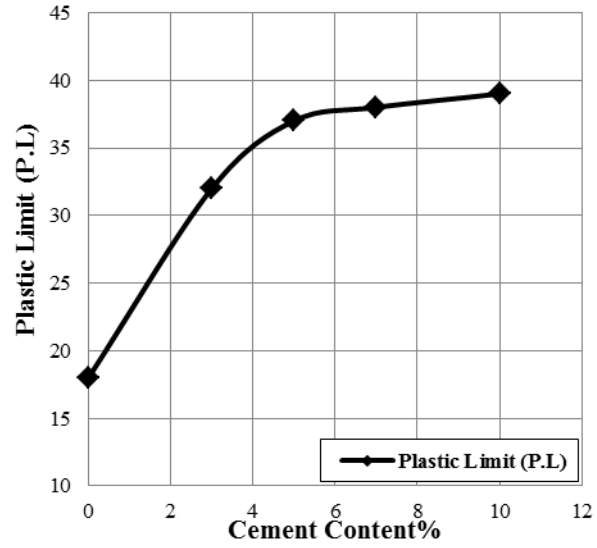

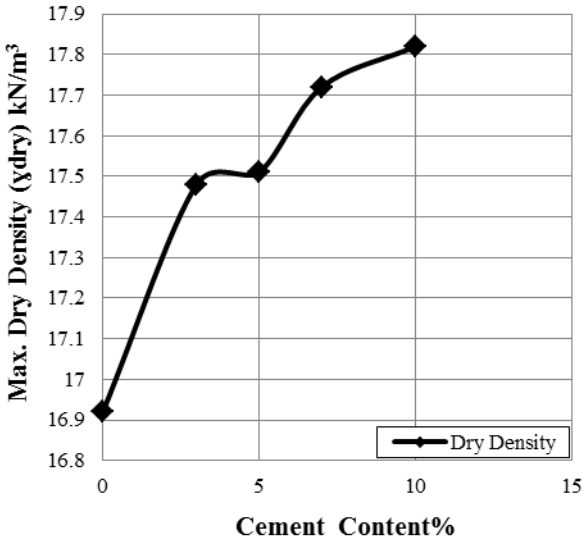

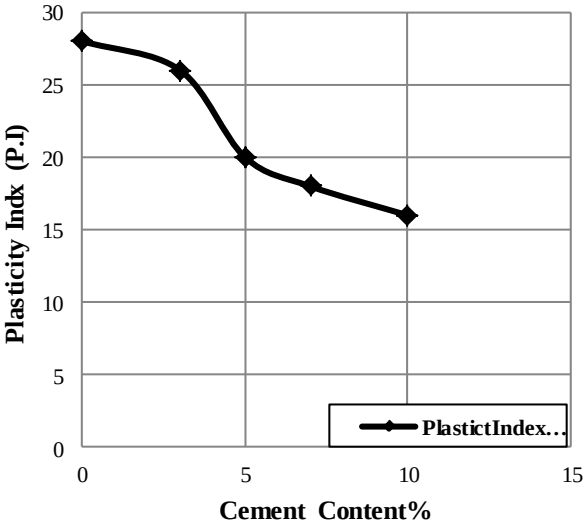

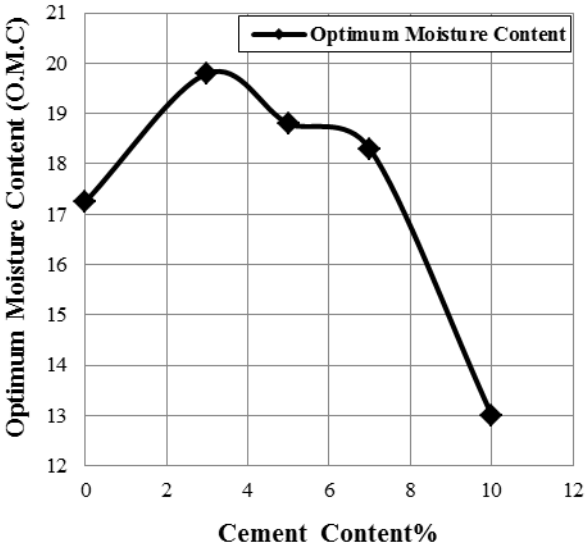

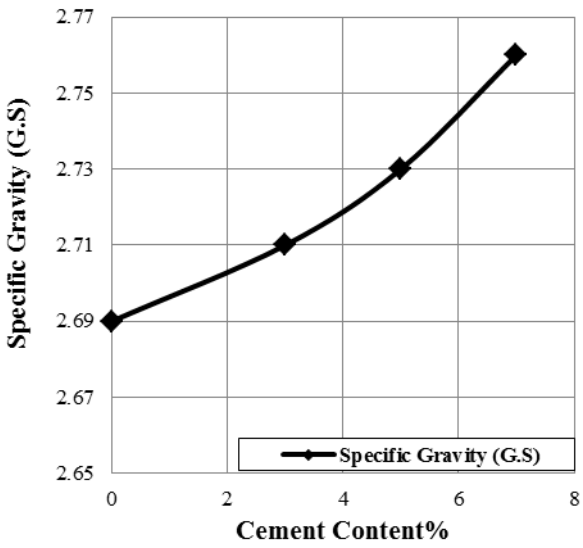

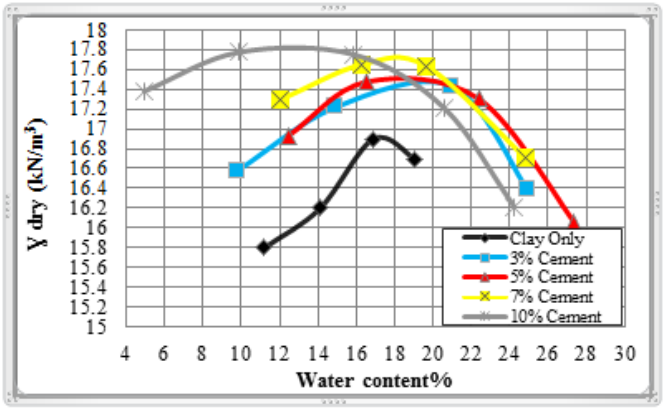

Figure 2. The Effect of Cement on the Atterberg's Limit, Specific Gravity and Compaction Characteristics.

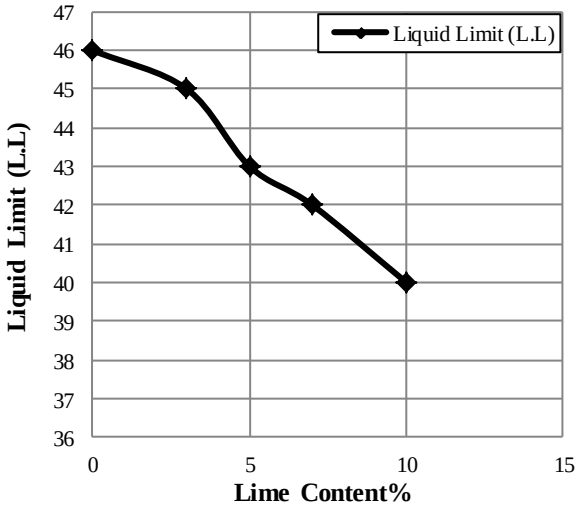
Liquid Limit (L.L)
Liquid Limit (L.L)
Lime Content%

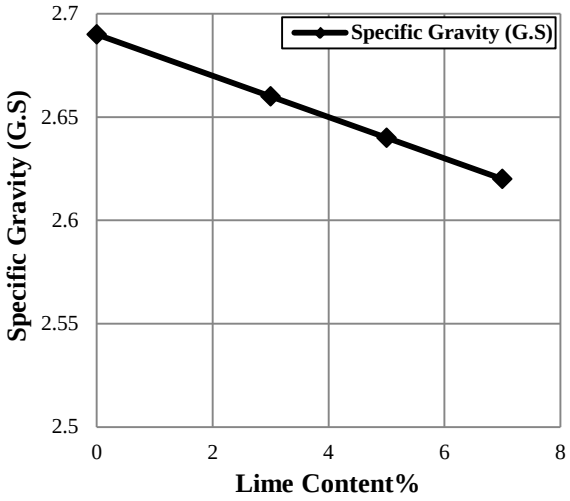
Specific Gravity (G.S)
Specific Gravity (G.S)
Lime Content%

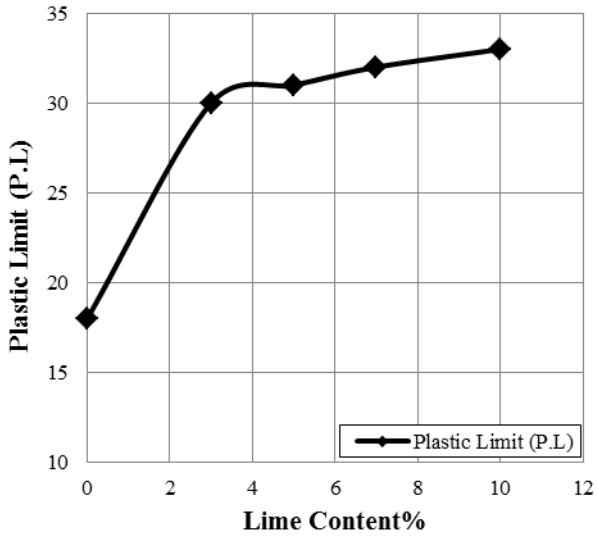
Plastic Limit (P.L)
Plastic Limit (P.L)
Lime Content%

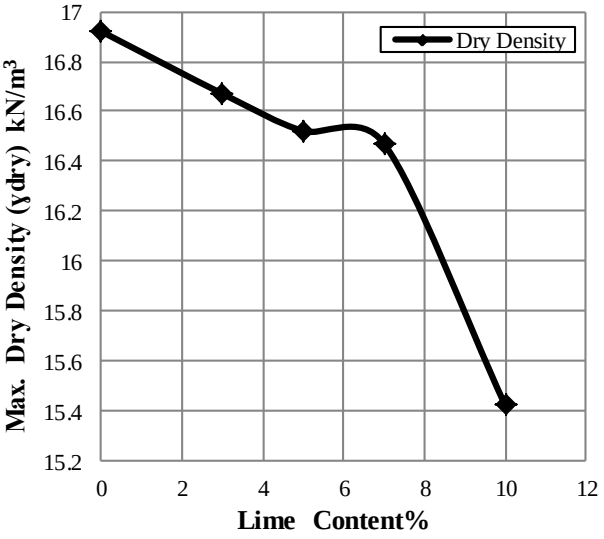
Dry Density
Max. Dry Density (ydry) kN/m3
Lime Content%

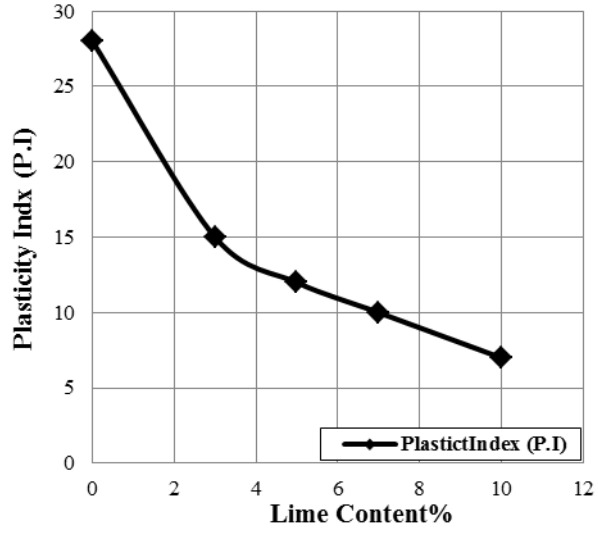
PlastictIndex (P.I)
Plasticity Indx (P.I)
Lime Content%

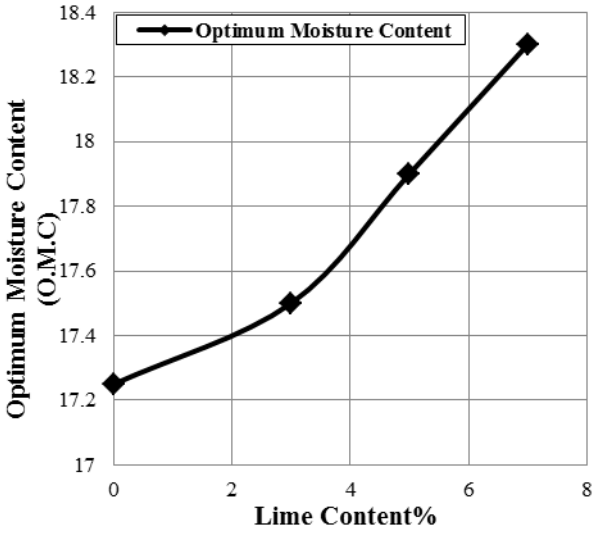
Optimum Moisture Content
Optimum Moisture Content (O.M.C)
Lime Content%

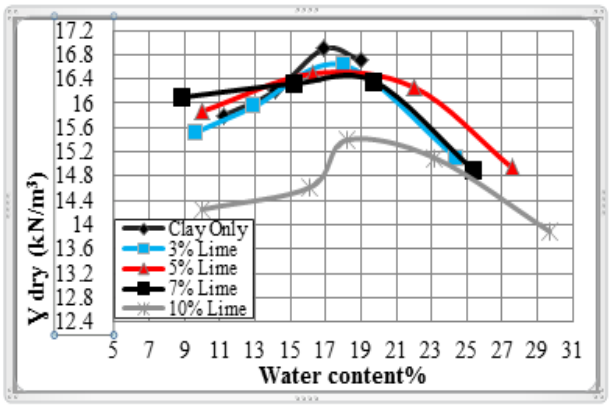

Figure 3. The Effect of Lime on the Atterberg's Limit, Specific Gravity and Compaction Characteristics.

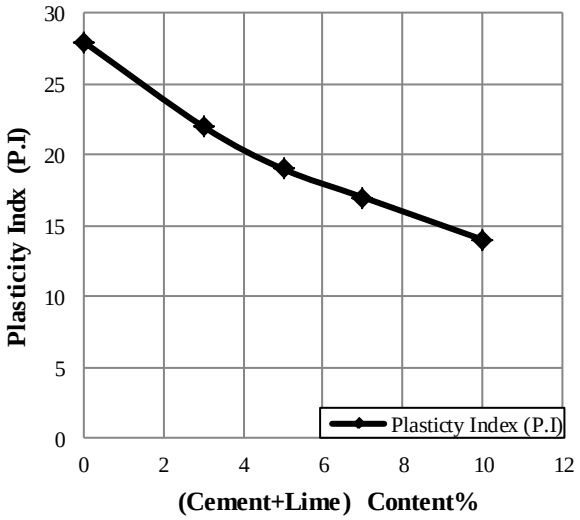

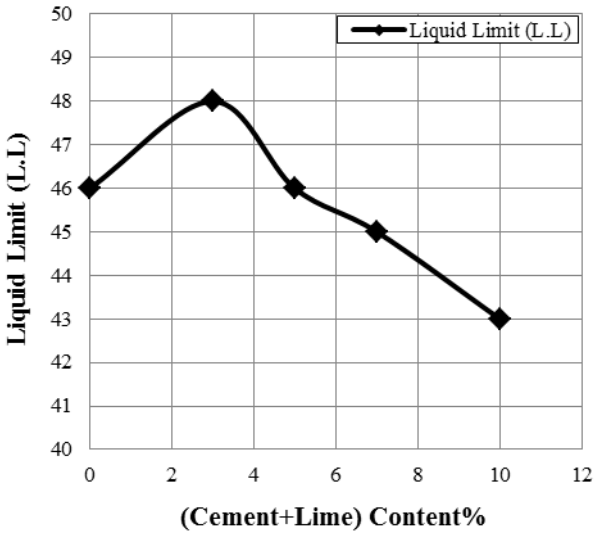

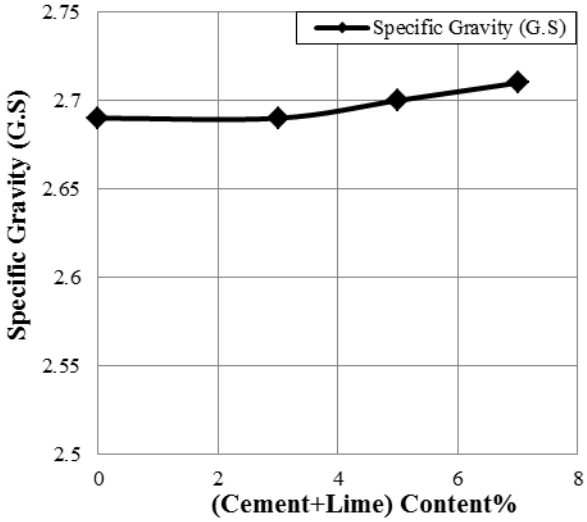

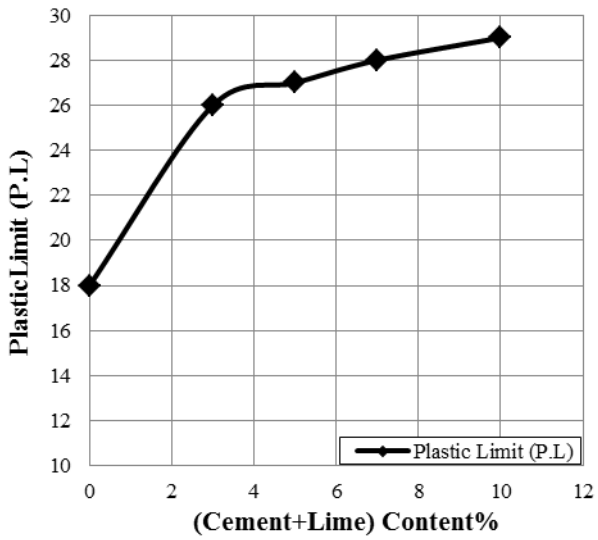

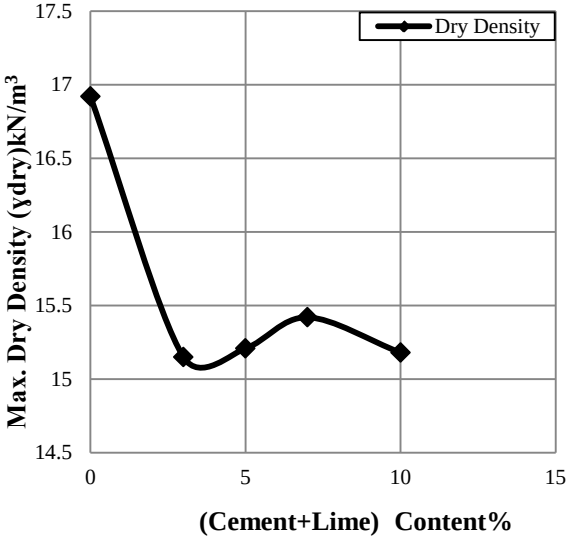

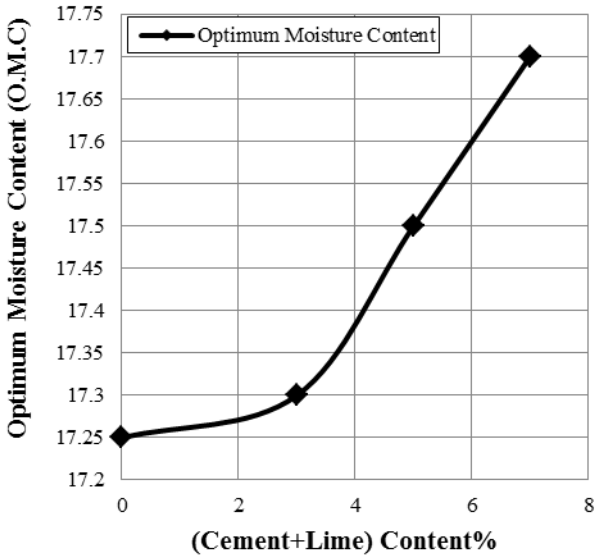

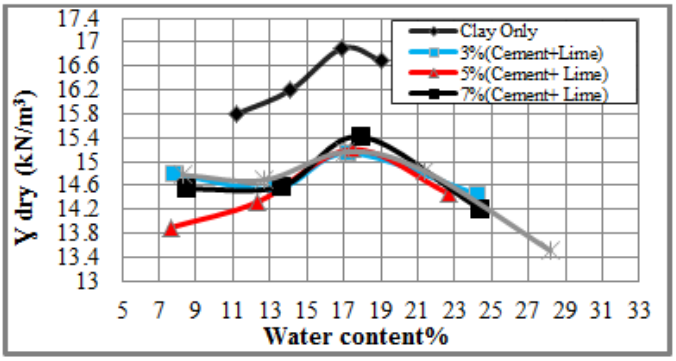

Figure 4. The Effect of Cement- Lime Mixture on the Atterberg's Limit, Specific Gravity And Compaction Characteristics.

Effect of Cement, Lime and Cement –Lime Mixture on the Unconfined Compression Strength

The effect of cement, lime content and curing time on unconfined compressive strength is shown in Figures 5, 6 and 7. Figure 5 shows that unconfined compressive strength for soils increases with increasing cement content. It is clear that there is a continuous strength progress with respect to time due to cement hydration and pozzolanic reaction between soil particles and chemical stabilizer as well as the complicated reactions causing cementation of soil particles. The immediate increase in strength results from flocculation-agglomeration reaction and leads to better workability, whereas long-term strength gain is due to pozzolanic reactions [Thompson, 1966(14)]. Figure 6 shows that, as lime content increases unconfined compressive strength increases. Figure 7 shows the strength increase with lime and cement increase due to the interaction that occurs between lime and soil particles which produces a gel of calcium silicate, which do not dissolve in water and act as a buffer and a binder. The strength increase with cement content increase because of hydration of cement which work as a link between the soil particles to increase the resistance.

In the case of lime stabilization process, the optimum lime content of clay weathered soil is 0, 3,5and 7%. Clay is strongly reactive with lime. Unconfined compressive strength of the lime-stabilized tertiary clay increased continuously with the increase in lime content, because it contains a high amount of the clay particles including kaolinite, montmorillonite, and halloysite where montmorillonite reacts strongly and fast with additional lime values of untreated compacted specimens, the continual increase in lime resulted in the increase in the values.

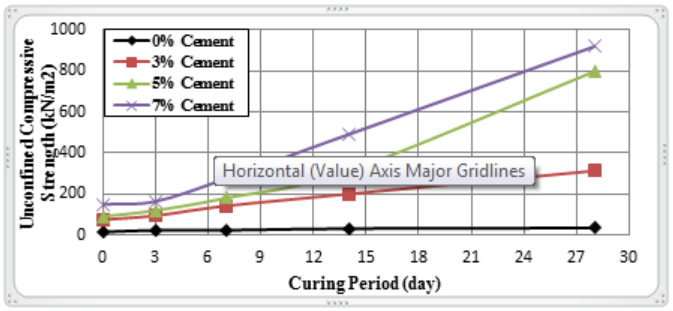

Figure 5. Effect of Cement on the Unconfined Compressive Strength of Soils.

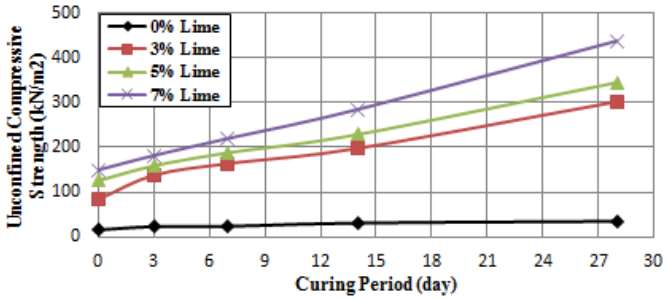

Figure 6. Effect of Lime on the Unconfined Compressive Strength of Soils.

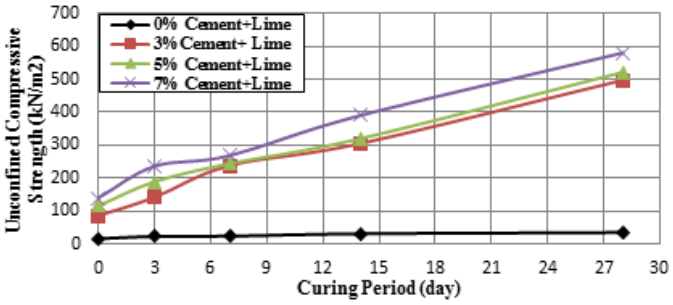

Figure7. Effect of Cement-Lime on the Unconfined Compressive Strength of Soils.

References:

1. Abbasi, N., Mahdieh, M. and Davoudi,M.H.,(2013), "Application of Lime and Pozzolan for Stabilization of Silty Sand Soils in Irrigation and Drainage Networks" Journal of

Science & Technology of Agriculture & Natural Resources,Vol.16, No.62, pp.245- 257.

2. Ajayi,E.S.,(2012),"Effect of Lime Variation on The Moisture Content and Dry Density of Lateritic in Lorin, Nigeria" International Journal of Forest Soil & Erosion, Vol.2, No.4, pp.165- 168.

3. Bergado,D.T., Anderson,L.R., Miura,N. and Balasubrsmaniam, A.S., (1996), " Soft Ground Improvement in Lowland and Other Environments" ASCE Press, NewYork, USA, PP.427.

4. Dash, S.k. and Hussain,M., (2012), "Lime Stabilization of Soils" Journal of Materials in Civil Engineering, ASCE, Vol.24, No.6.

5. Fonseca, A.V., Cruz, R.C. and Conso, N.C.,(2009)," Strength of Sandy Soil_ Cement admixtures" Journal of Geotechnical & Geology Engineering, Vol.27, pp.681-686.

6. Kawasaki, T., Niina, A., Saitoh,S., Suzuk,Y. and Honjo,Y.,(1981), "Deep Mixing Method Using Cement Harding Agent" Proc. 10th Int. Conf. Soil Mechanics and Foundation Eng., Stockholm, pp.721-724.

7. Marks, B. D, and Haliburton, T. A. (1972). "Acceleration of lime Clay reactions with Salt". J. Soil Mech. Found Div 98(41), 327-339.

8. Nalbantoglu Z, Gucbilmez E (2001) Improvement of calcareous expansive soils in semi-arid environments. J Arid Environ 47:453–463.

9. Nicholson. R.Barnard.G., Robbins, L.&.Hankins, G.(1994) Predicting treatment outcome for incompetent defendants Bulletin of the American Academy of Psychiatry and the Law. 22, 367-377.

10. Okonta, F.N. and Govender, E.,(2011), "Effect of Desiccation on the geotechnical Properties of Lime_Flyash Stabilized Collapsible Residual sand" Journal of Engineering &Applied Sciences, Vol.6, No.6.

11. Sariosseiri, F. and Muhunthan, B.,(2009), "Effect of Cement Treatment on Geotechnical Properties of Some Washington State Soils" Journal of Engineering Geology Vol.104, pp.119-125.

12. Suzuki,Y., (1982), "Deep Chemical Mixing Method Using Cement Harding Agent" Proc. Symposium on Soil & Rock Improvement Techniques Including Geotextiels, Reinforced Earth & Modern Piling Method, AIT, Bangkok, Thailand.

13. Terashi, M., Tanka, H. and Okumura, T., (1979), "Engineering Properties of Lime_ Treated Marine Soil and Deep Mixing Method" Proc. 6th Asian Regional Conf. on Soil Mechanics and Foundation Eng., Vol.1, pp.191-194.

14. Thompson, M.R. 1966: Shear Strength and Elastic Properties of Lime-Soil Mixtures.

Highway Research Record, Washington, D.C., 139: 1–14.

Comparison of High Speed Railway Bridge Foundation Design

Hussein Yousif Aziz
University of Muthanna, College of Engineering, email: husseinyousif3@hotmail.com, Tel. 07723747384

***Abstract*—This project scussed the design and analysis of bridge foundation subjected to load of train using three codes, namely AASHTO code, British Standard BS Code 8004 (1986), and Chinese code (TB10002.5-2005). The study focused on the design and analysis of bridge's foundation manually with the three codes and which code is better for design and controls the problem of high settlement due to the applied loads. The results showed the Chinese codes are costly that the number of reinforcement bars in the pile cap and piles is more than those with AASHTO code and BS code using the same dimensions. Settlement of the bridge was calculated depending on the data collected from the project site. The ultimate bearing capacity of single pile for three codes was also discussed. Furthermore analysis by using two-dimensional Plaxis program, SAP2000 14 and PROKON and many parameters were calculated. The maximum values of the vertical displacement were close to the calculated ones. The results indicate that the AASHTO code was economics and safer in the bearing capacity of single pile. The purpose of this project is to study out the pier on the basis of the design of the pile foundation. There is a 32m simply supported beam of box section on top of the structure. The pier of bridge is round-type. The main component of the design is to calculate pile foundation and the settlement. According to the related data, we choose 1.0m in diameter bored pile of 48m.**

The pile is lain out in the rectangular pile cap. The dimension of the cap is 12m×9 m. Because of the interaction factors of pile groups, we must check the load-bearing capacity of simple pile, the punching resistance of pile cap, the shearing strength of pile cap, and the part in bending of pile cap, all of these are very important to the structure stability. Also, checking soft sub-bearing capacity is necessary under the pile foundation. This project provides a deeper analysis and comparison about pile foundation design schemes. Firstly, here are brief instructions of the construction situation about the Bridge. With the actual construction geological features and the upper load on the Bridge, this project analyzes the bearing capacity and settlement of single pile. In the paper the Equivalent Pier Method is used to calculate and analyze settlements of the piles .

***Keywords*—About four key words or phrases in alphabetical order, separated by commas.**

I. INTRODUCTION

IN Iraq we have very limited data and information in design of bridge subjected to earthquake. Currently in our code of practice BS 5400, it did not have allocation or rules in earthquake design consideration for bridge structure.
Therefore we must take into consideration when we start to design bridge so that the effect of earthquake damage can be minimized to our structures especially bridge. This situation might cause cracking and collapse to our bridge [1]. So ,in solving this problem we need a code of practice that considered earthquake loading in design process.

II. METHODS

In this research , two codes of practice AASHTO-ACI and BS 5400 for bridge design resist of seismic loading were compared. The design of a highway bridge, like most other civil engineering project, is dependent on certain standards and criteria [1]. Naturally, the critical importance of highway bridges in a modern transportation system would imply a set of rigorous design specification to ensure the safety and overall quality of the constructed project.
Most bridge engineers in many countries such as Malaysia are using BS 5400 code for guideline in design bridge project [2]. This is because bridge engineers in that countries got their basic knowledge or tertiary education from European countries like United Kingdom , New Zealand , and others countries that practices BS 5400 as a code of practice. Therefore , a need to review our practice design code and also our construction method especially in design of bridge is much needed so as to protect bridge structure from the undesired damaging effect due to this natural disaster. The aim of this research is to compare our currently code of practice (BS5400) with AASHTO-Seismic Design Code in term of efficiency in design a bridge [3]. It also investigate which two code much applicable are to be applied in our country. The way to compare these two codes is by trying to redesign our existing bridge structure by using the different code of practices. In our case , we analyze and determine which code is much better for our country in design [4].

III. RESULTS AND DISCUSSIONS

The results of the design bending moment resistance of the pile cap for the AASHTO code, BS code using SAP 2000 program and Plaxis 2D program are shown in Table 1. The calculation details of AASHTO code are shown in Appendix A, in the same manner the details of BS code are shown in Appendix B.

TABLE. I. THE DESIGN BENDING MOMENT RESISTANCE IN PILE CAP

The codes	**AASHTO**		**BS**
The value (kN.m/m)	**M_{ux}**	**M_{uy}**	**M_u**
	2125.045	**1336.745**	**36200**

The results of the design shear resistance of the pile cap for the AASHTO code, BS code are shown in Table. (2).

TABLE. II. THE DESIGN SHEAR STRENGTH IN PILE CAP

The codes	**AASHTO**		**BS**
The value (kN)	**Vux**	**Vuy**	**Vu**
	525.705	**547.83**	**9778.8**

The results of The Design Shear Resistance Analysis in the pile for the AASHTO code, BS code are shown in Table. (3).

TABLE . III. THE DESIGN SHEAR RESISTANCE ANALYSIS IN THE PILE

The codes	AASHTO		
The shear resistance (Vr)	One way shear		Two way shear
	Longitudinal Face(x)	Transverse face(y)	
	3467.08	3477.216	207751.3

The results of The settlement in the pile for the AASHTO code, BS code are shown in Table. (4) and the calculations are done using the following equation.

$$S_{ci}=(C_{ci}.H_i)/(1+e_0)Log(\sigma_{0i}+\Delta\sigma_i/\sigma_{0i})$$

TABLE . IV

S_{ci}(mm)	σ_{0i}(kN/m)	$\Delta\sigma_i$ kN/m^2	Z_i(m)	σ_i (kN/m^2)
17.6	**639**	**110**	**0.65**	**17.7**
25.6	**632**	**78.1**	**2.68**	**54.6**
15.3	**738**	**51.6**	**5.68**	**93**
8.6	**817**	**33.5**	**9.55**	**271**
7.09	**905**	**22.7**	**13.8**	**444**
3.49	**986**	**16.8**	**17.8**	**519**
1.89	**1087**	**12.1**	**22.8**	**595**
1.39	**1177**	**9.37**	**27.3**	**632**
1.02	**1224**	**8.26**	**29.8**	**679**
0.19	**1249**	**7.77**	**31**	**738**
1.8	**1297**	**6.94**	**33.4**	**817**

The results of Flexural resistance of AASHTO code, BS code, Pile cap reinforcement due to BS code, Results of stress that founded by using SAP program and Bending and displacement that founded by using PLAXIS program are shown in Tables from 5 to 8.

TABLE. V. PILE CAP REINFORCEMENT USING AASHTO CODE

Due to	Flexural resistance	
At the	Longitudinal face	Transversal face
NO.bars	90#9	61#9

TABLE . (6) PILE CAP REINFORCEMENT DUE TO BS CODE

Due to	Flexural resistance	
At the	Bottom face	Top face
NO.bars	28#9	28#9

TABLE . (7) RESULTS OF STRESS USING SAP PROGRAM

Stress	Bending moment (kN.m)	Shear stress(kN)	Deflection of pile(m)	
Maximum value	506.957	922.011	Edge pile value	0.0052
Minimum value	124.824	4.133	Mid. pile value	0.0058
			Edge mid. pile value	0.0057

TABLE .(8) RESULTS OF BENDING AND DISPLACEMENT USING PLAXIS PROGRAM

Displacement (m)	Vertical displacement	0.1082
	Total displacement	0.0076
Bending moment (kN.m/m)	Exterior pile	40.83
	Interior pile	3.78

The results of the SAP 2000 program are shown in Figures from Figure 1 to Figure 6.

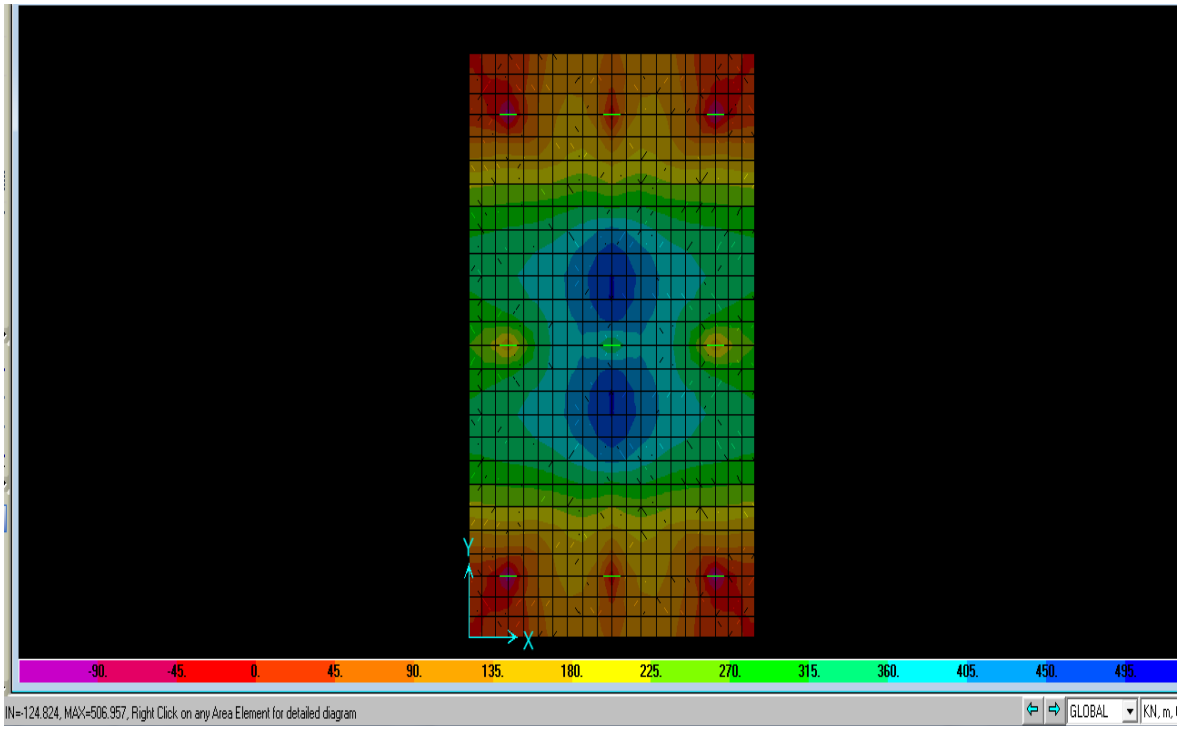

Fig. 1 Max. moment (506.957 kN.m), Min. moment (124.824KN.m)

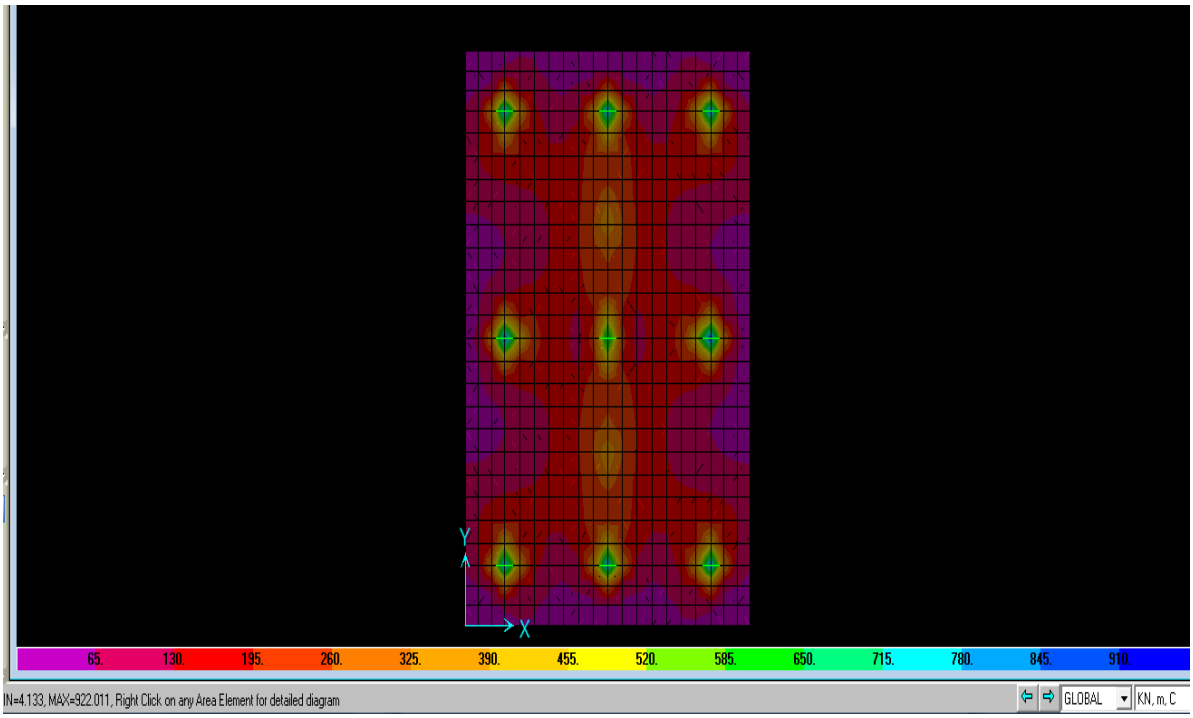

Fig. 2 Max. shear (922.011kN), Min. shear (4.133kN)

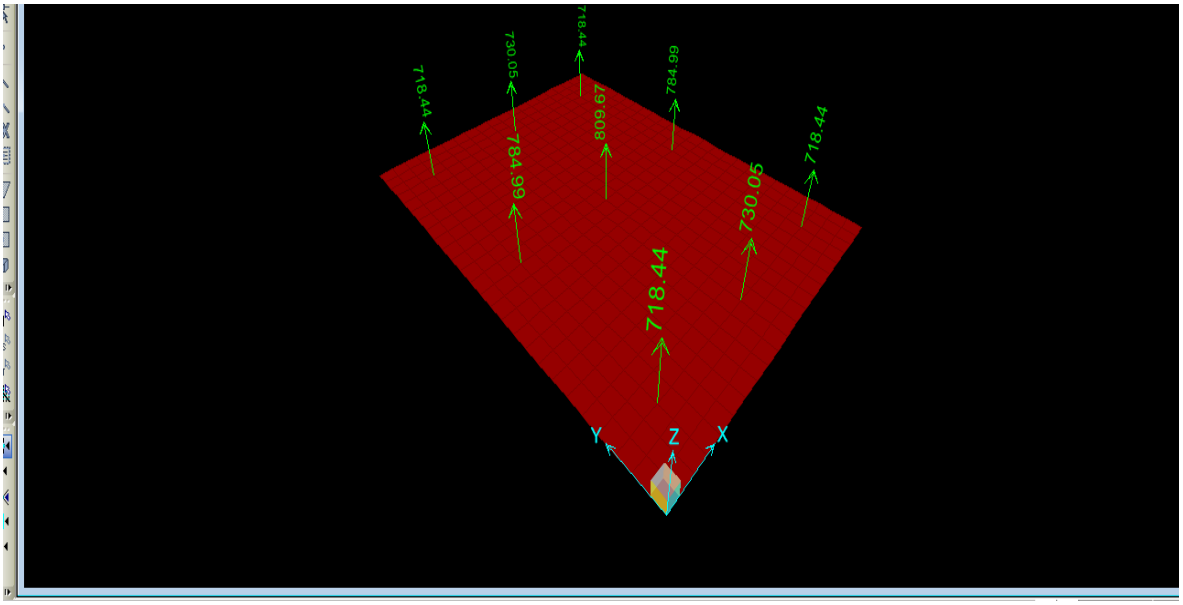

Fig. 3 Reaction of pile due to applied load

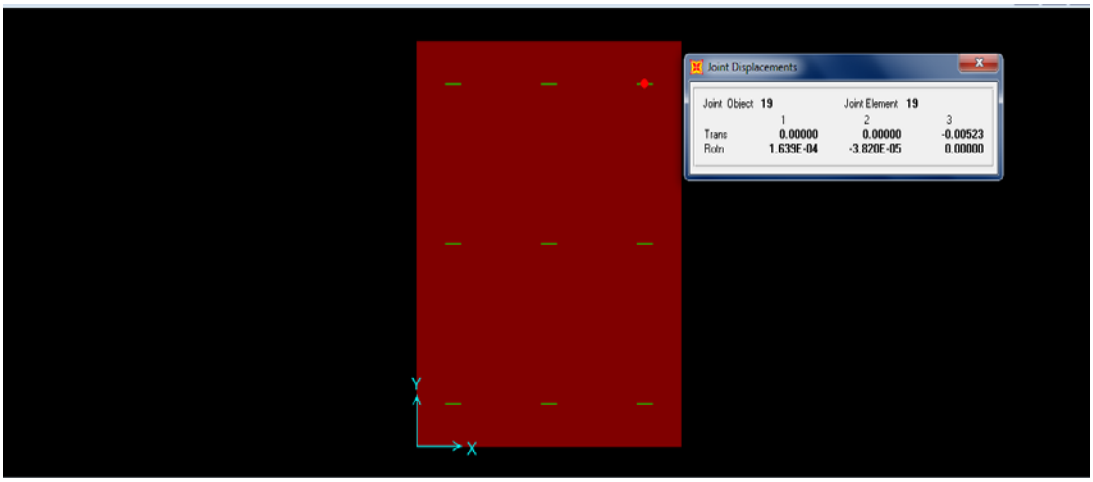

Fig. 4 Deflection at edge pile (0.0052 m)

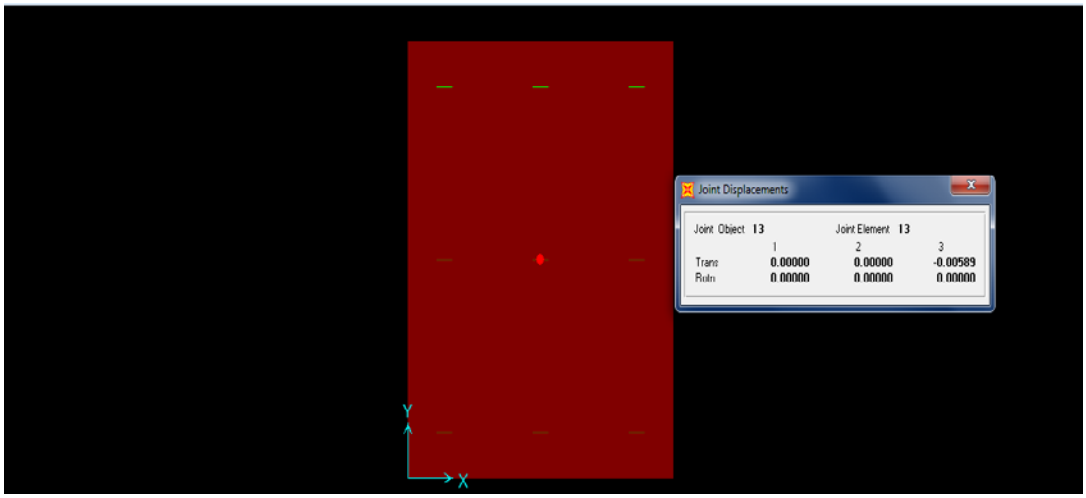

Fig. 5 Deflection at mid. pile (0.0058 m)

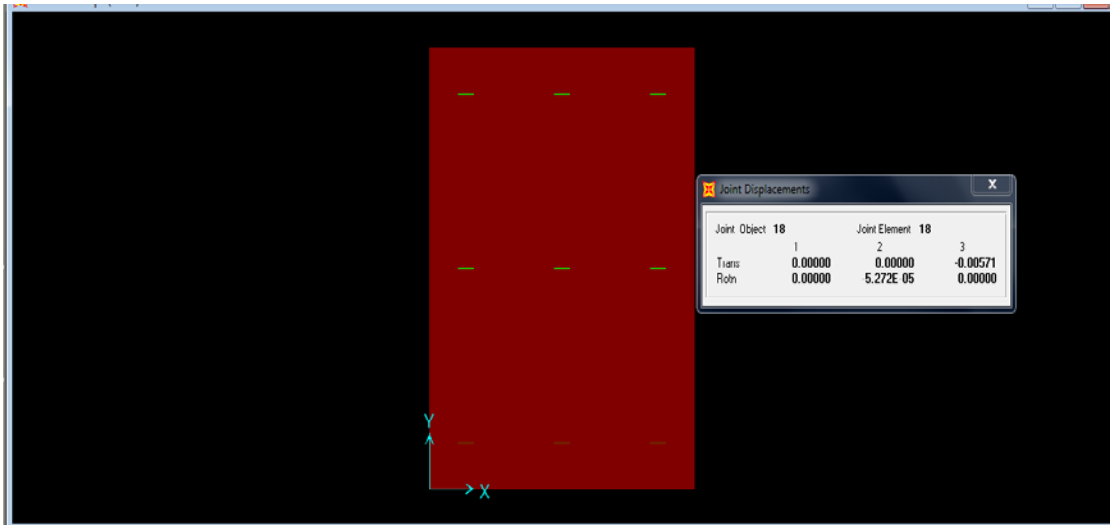

Fig. 6 Deflection at mid. edge pile (0.0057 m)

The results of the Plaxis program are shown in Figures from Figure 7 to 11.

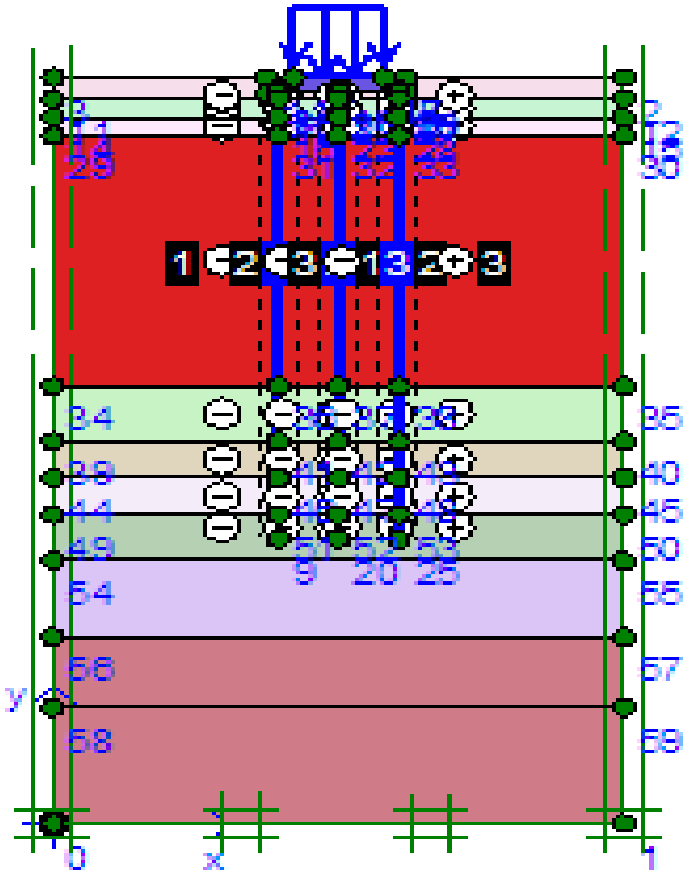

Fig.7 The model of pile cap analyzed by using PLAXIS program

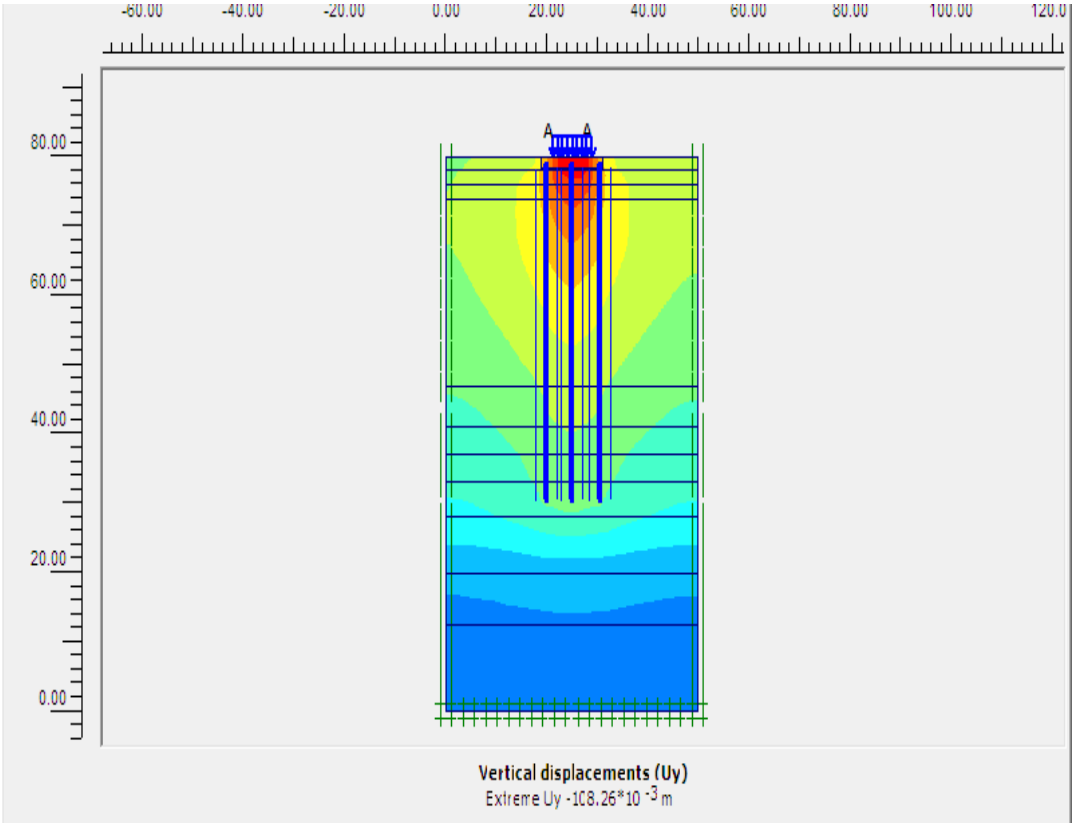

Fig. 8 Vertical displacement of the model.

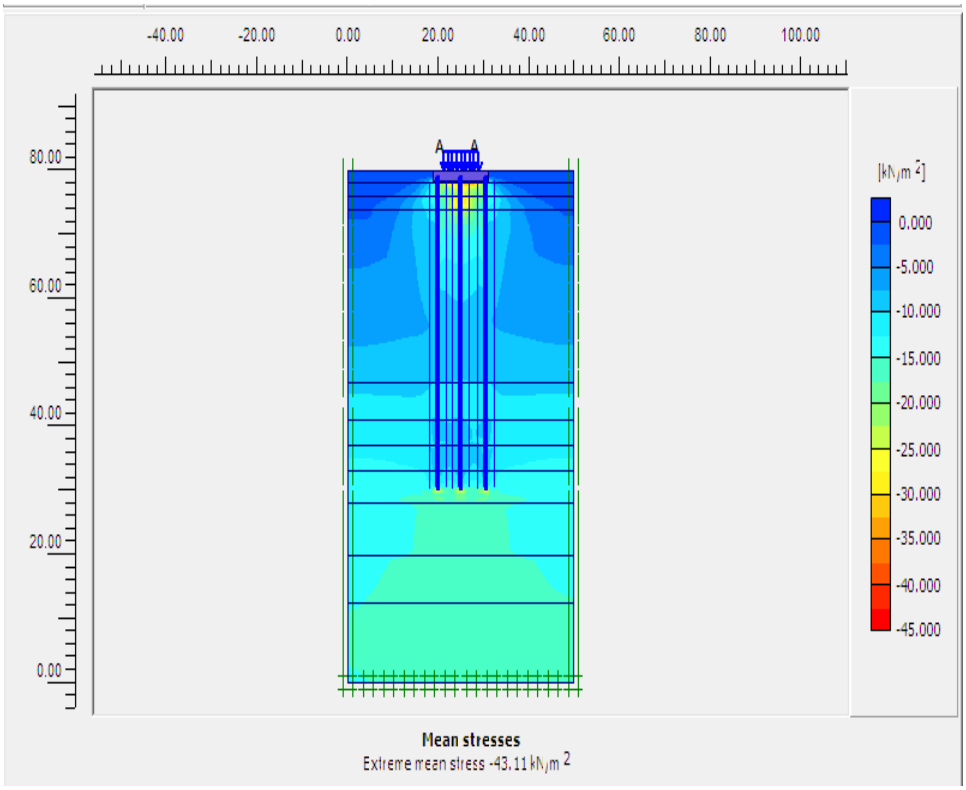

Fig. 9 Mean stress

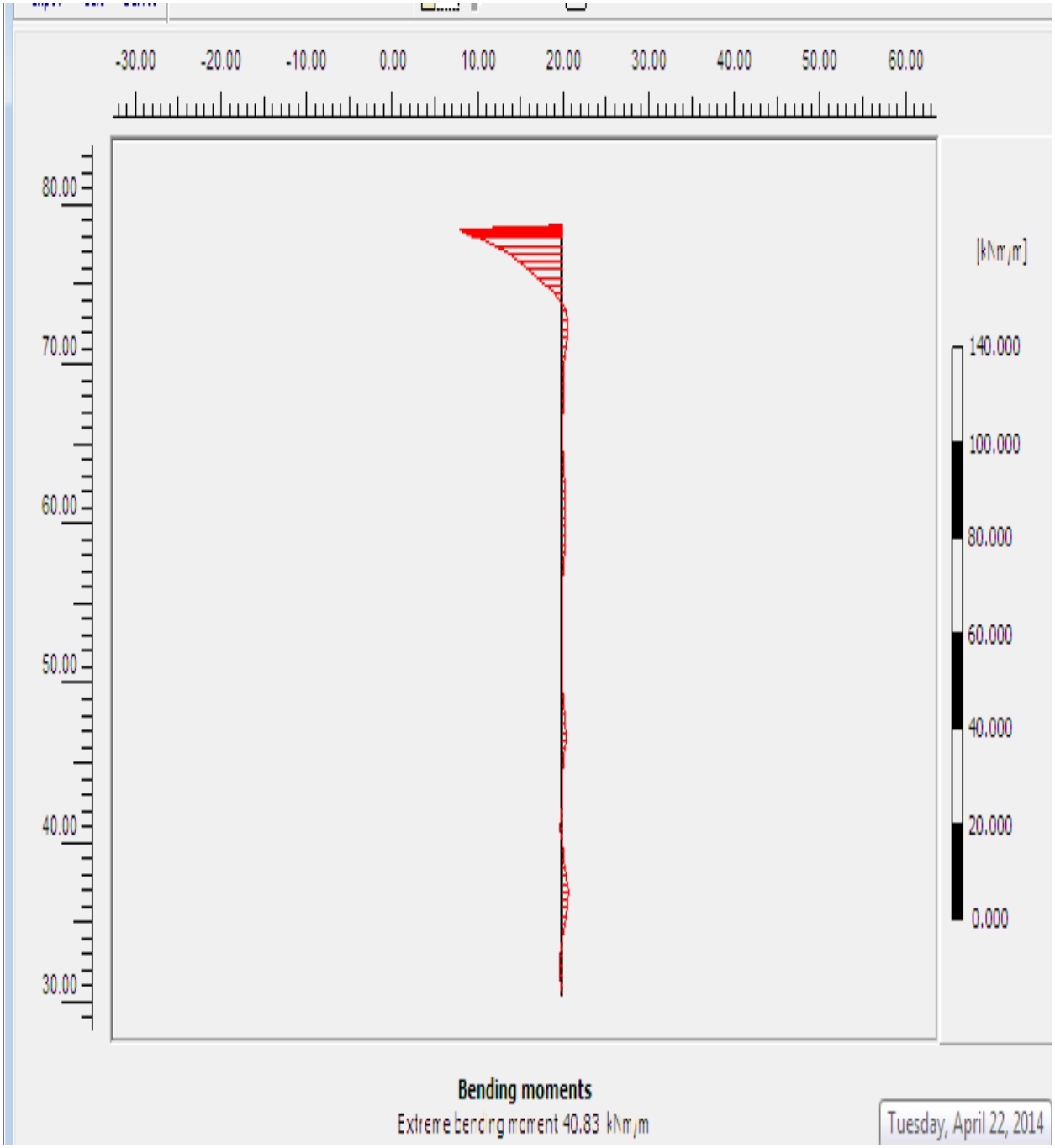

Fig. 10 The exterior moment at exterior pile

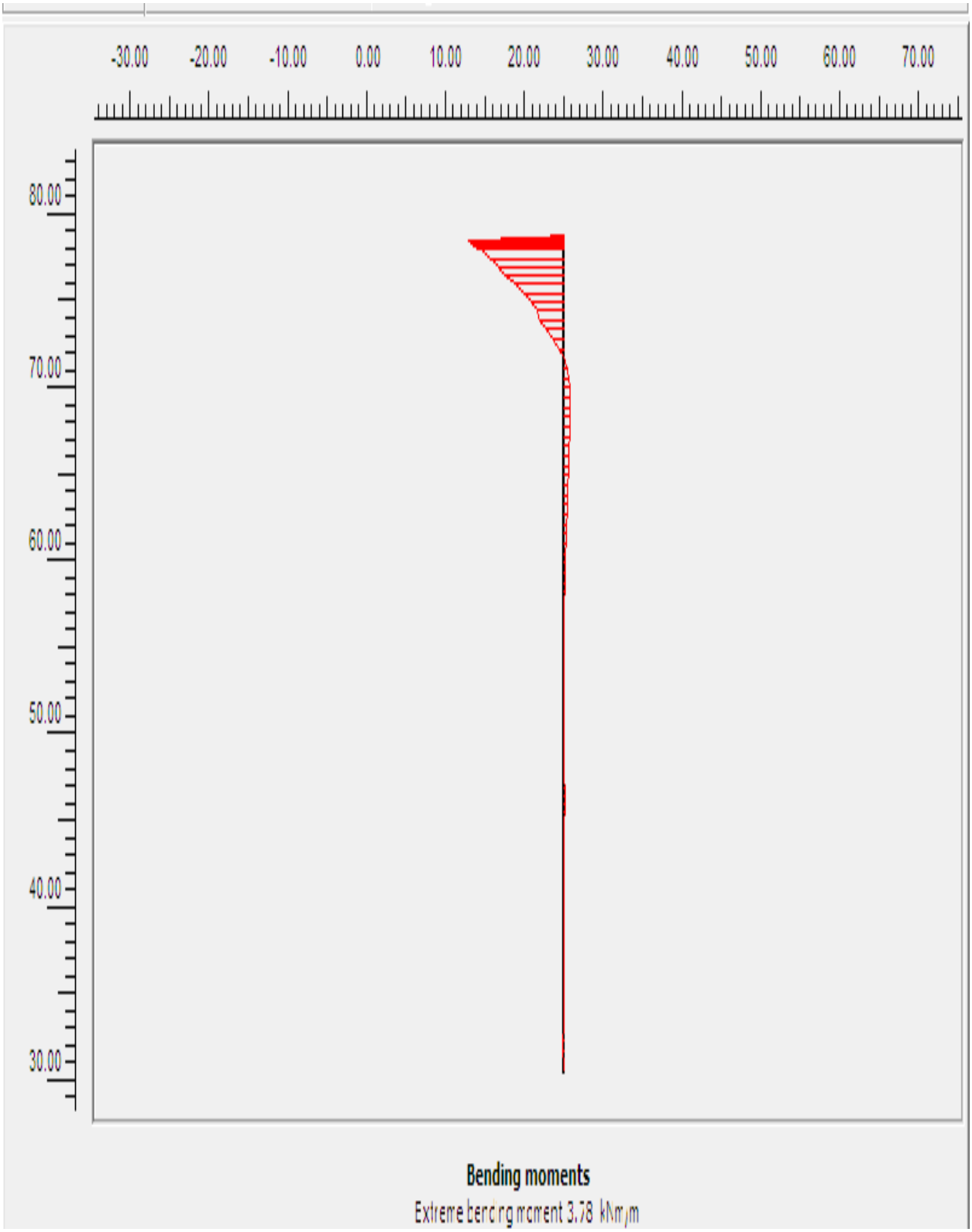

Fig. 11 Interior bending moment of piles

This figure shows the interior moment in interior pile because the high value of shear

IV. CONCLUSIONS

The bridge has unchanging cross section with similar support s and a uniform mass and stiffness and it is essential bridge.
The beam weight is equal to 364.215(kN/m) .
The AASHTO code take the live load =84.158 (kN/m) .
The BS code take the live load = 83.6 (kN/ m) .

A. Pier cap

1. Seismic Effect

In the AASHTO code it take for effect of seismic load y that including all of the dead , buoyancy load , stream flow force , earth pressure , and earth quake effect in its calculation, while this code take 30% as longitudinal motion and 100% as transversal motion effect for this purpose. But in BS code we don't have any calculation for seismic load.

2. Dynamic Action

In BS code, dynamic action for both shear and bending moment stress but because the dynamic effect for the shear was equal to (1) and the dynamic effect of bending moment was equaled to(1.1) their effect can be neglected. But in the AASHTO code.

3. Temperature Effect

In the AASHTO code we have the calculation of the minimum temperature and shrinkage steel reinforcement . it founded to be 10#7 near the surfaces of the concrete . but there is no calculation in BS code for this purpose.

B. pier column

1. Slenderness Effect

In the AASHTO code we can studied the slenderness effect in pier column .this column is un-braced and effecting by the motion of pier cap so this column founded that is slender and it must to be regarded the moment that produced from the slenderness effect. but in BS code we doesn't have this calculation for this effect.

2. Seismic Effect

In AASHTO code we have the calculation for this effect for both of longitudinal and transversal motion due to earth quake we found that the pier column need for 60#18@10 cm, but do not have this consideration in BS code .

3. Temperature Effect

Both AASHTO and BS codes studies the temperature effect on pier column but due to symmetry of bridge superstructure no force is developed at intermediate bent due to temperature expansion/shrinkage of the superstructure.

4. Skin Reinforcement

The AASHTO code include the skin reinforcement that needed in the pier column that must to be distributed at (d/2) from the flexural tension reinforcement but in BS code.

C. Pile cap

1. Traction and Breaking Load

The BS code have the studies for this effect on the pile cap and suggested the required steel reinforcement that needed for resistance this applied load but in AASHTO code there no consideration for this applied load .

2. Shear Effect Analysis

Both codes studied this effect on the footing and founded the maximum design shear resistance as shown in Table (2) .

3. Flexural Effect Analysis

Both codes studied the maximum flexural resistance in pile cap design . and we note that the AASHTO code suggested more amount of steel reinforcement than
BS code suggestion as shown in Tables (5) and (6) .

4. Soil Bearing Capacity

The soil bearing capacity using Terzaghi equation equal to (288.36 kN) which less than the applied load on the soil so it is not safe and need to use pile in addition to footing .
In BS code it founded to use 4 piles but in AASHTO code it found to use 9 piles

5. Settlement

By using the AASHTO code equation we found the structure is to more than 80 mm settlement that non logical but by using the Plaxis program 2D we obtained the settlement equal to 108 mm as shown in Table (8) is also un-logical and far from the standard limitations because in the actual state we have the same value for the settlement of the structure. But by using the SAP program we obtained the deflection under each pile not exceed the (5) mm as shown in Table (7). In the same manner we found the total displacement is 29.9mm by the Chinese Code [5] which is considered as reasonable value compared with other results maintained from the codes and programs but can conclude that the Chinese code is giving good indication in calculating the settlement for pile foundation. The limitations of settlement in the high speed rail way according to the Chinese code is 10mm, TB-5001 code limit the settlement for a range between 50-80mm, and CNS code (China National Standards, 2002) limit the settlement about 50mm. So the result of settlement from the CNS code which is about 30mm is accepted according to the above limitations and can be considered in the design of pile foundations.

REFERENCES

[1]. Hussein Yousif Aziz and Jianlin Ma, 2012: Experimental and Theoretical Static Analysis of High-speed Railway Bridge Settlement for deep soft soil, construction and building Technology Journal, P.P (17-31)

[2] Ascalew Abebe & Dr Ian Gn Smith,1987 : Pile Foundation Design.

[3]. Shri Ajay Goyal & Shri R.K.Yadav, 2007 : Design Parameters Of High Speed Corridor.

[4]. Coenraad Esveld, 2006 :Developments In High-Speed Track Design.

[5] China National Standards, 2002.

Evaluation of Geotechnical and Collapsible Characteristics of Different Types of Iraqi Soils during the Leaching Process

Dr. Saad F. Ibrahim* and Dr. Zaynab I. Qassim**
* Professor / Highways and Transportation Engineering Department/ University of AL-Mustansiriya, Baghdad -Iraq
Call Phone: 00964- 7901303569
Email: drsaadfarhan@yahoo.com
** Lecturer / Building and Construction Department/ University of Technology, Baghdad -Iraq
Call Phone: 00964-7722661262
Email: zaynab.2010@yahoo.com

***Abstract*— Gypseous soils are distributed in many regions in Iraq. The dissolution and leaching of gypsum by the action of water flow through soil masses cause several problems. Such problems are observed in soils underneath foundations of many buildings and engineering structures due to continuous changes in engineering properties of soils with time. The main purpose of this study is to evaluate the behavior of three types of gypseous soils 59.5, 41 and 2.3 % Gypsum Content brought from different sites in Iraq during leaching under variable hydraulic gradients. From the interpretation of test results, it is found that conventional testing is inapplicable to gypseous soils due to the effect of gypsum dissolution and leaching due to soaking or/and flowing of water through porous media.**

Therefore, a new special large diameter modified Soil Leaching Apparatus was adopted to study the effect of leaching on the behavior of gypseous soils under different leaching stresses with two flow directions. These are upward flow (UWF) and downward flow (DWF) conducted under different hydraulic gradients, as well as to study values of the permeability coefficient of such soils under leaching. Results show that the leaching strain and accumulative dissolved gypsum increase with time, while a gradual decrease can be observed in permeability coefficient (k) with time and with the increase in the leaching stress. Moreover, permeability obtained by upward flow direction (UWF) is less than that obtained by downward flow one (DWF). In addition, the leached samples show an increase in the collapse potential (Cp) especially for soils that contain high percentages of gypsum. Results also show that the collapse potential (Cp) decreases as diameter to height ratio (D:H) increases. Finally, direct shear tests are carried out on the soils before and after leaching and results show that shear strength parameters (c & Ø) decrease after leaching them.

***Index Terms*— Gypseous soils, Leaching process, Permeability, Collapsibility, and Direct shear test.**

Manuscript received October 1, 2015. This work was supported in part by the Civil Engineering Department of Al-Mustansiriya University.

I. Introduction

Dissolution of soluble salts is one of the processes which leads to the change in the engineering properties of the soil. This phenomenon must be well understood. A deteriorating effect generates due to the dissolution of many chemical compounds known as soluble salts. Therefore, the term "soluble salt" is restricted to those minerals which dissolve and recrystallise within the range of moisture and temperature variation which occurs during the atmospheric conditions, [1].

These kinds of salts may include gypsum, sodium chloride, potassium chloride, carbonates, etc. They may be uniformly scattered in the soil or in the form of lenses, they may be also carried in the ground water.

In gypseous soils, collapse or compression occurs very quickly when the site is flooded with water during heavy rainfall, irrigation or breaking of sewerage and water pipes. This may damage the engineering structures because the element of the structure cannot follow the sudden deformation by rearrangement of the inside forces or stresses, [2].

Al-Abdullah [3] described leaching as a process which removes material in solution (e.g. salts) and cementation agents from a section in the soil profile. The process takes place under hydraulic gradient or by diffusion. Al-Banna [4] stated that leaching of soil, especially of those containing soluble salts causes changes in the engineering properties. These changes may create adverse problems for the structures founded on such soils.

The continuous flow through gypseous soils causes removing soluble salts and hard particles from these soils, Al-Kaisi [5]. Gypseous soils undergo several changes in their characteristics due to the continuous loss in their mass and due to alternation in properties of materials constituents during leaching.

In Iraq gypseous soils are mostly found in the "basin of Iraq". Ismael [6] estimated that about 31.7% of the area of Iraq is covered with gypseous soil with gypsum percentage ranging between 10-70%. This percentage can be considered as

problematic for both agriculture and engineering purposes. The problems encountered in Iraqi soils containing significant amounts of gypsum are summarized as great losses in strength upon wetting, sudden increase in compressibility upon wetting, continuation of deformation and collapse upon leaching due to water movement, existence of cracks due to seasonal changes in addition to existence of sink holes in the soil due to local dissolution of salts such as gypsum, Al-Mufty [7]. The main purpose of this research is to investigate the effect of leaching on the characteristics of different types of soils with various soluble salts contents, by adopting a new special leaching apparatus designed and manufactured especially to test large soil samples under different conditions. The soil samples are brought from three different regions in Iraq namely, Abu-Ghraib district, Al-Karma village, and Al-Baladiyat district within Al-Rasafa side in Baghdad containing (59.5, 41 and 2.3) % Gypsum Content respectively.

From the interpretation of test results, it is found that conventional testing is inapplicable to gypseous soils due to the effect of gypsum dissolution and leaching due to soaking or/and flowing of water through porous media. Therefore, a new special large diameter modified Soil Leaching Apparatus was adopted to study the effect of leaching on the behavior of gypseous soils under different leaching stresses with two flow directions. These are upward flow (UWF) and downward flow (DWF) conducted under different hydraulic gradients, as well as to study values of the permeability coefficient of such soils under leaching. Results show that the leaching strain and accumulative dissolved gypsum increase with time, while a gradual decrease can be observed in permeability coefficient (k) with time and with the increase in the leaching stress. Moreover, permeability obtained by upward flow direction (UWF) is less than that obtained by downward flow one (DWF). Finally, direct shear tests are carried out on the soils before and after leaching and results show that shear strength parameters (c & Ø) decrease after leaching them.

II. Soil Leaching Apparatus tests

In particular, to meet the objectives of this research, Soil Leaching Apparatus as shown in Figure 1 has been locally manufactured to test soil cylindrical specimens of 15 cm diameter and 30 cm height to study the effect of leaching on the engineering properties of salty soil. This apparatus has the following properties:

1. The ability to study the effect of leaching on the large block soil sample for thickness ranging between (4 cm to 30 cm).
2. High stresses of more than (400 kPa) are applied to soil sample.
3. The ability to conduct different types of tests such as consolidation, collapse and leaching tests.
4. The ability of water to flow in different directions during leaching process i.e. upward flow direction (UWF) and downward flow direction (DWF) .
5. The simplicity in combining and separating the apparatus parts.

Generally, the apparatus consists of a cylindrical steel pipe divided into lower part of (I.D= 15 cm, O.D= 17 cm, H=35 cm) dimensions and upper part of dimensions (inner dimension I.D= 15 cm, outer dimension O.D= 17 cm, height H=25 cm).

The two parts are connected together by two circular flanges of (I.D= 17 cm, O.D=27.5 cm, t= 0.8 cm) dimensions by (8) bolts. Circular rapper washer is positioned between the two circular flanges to prevent any leakage of water from the apparatus. The lower part is connected with supported steel frame by the third circular flange using (4) bolts. Bolt dimensions are equal to (D= 1.25 cm, H= 5.25 cm). Due to the difficulty in obtaining the undisturbed soil sample from the site, compacted sample is prepared at moisture content equal to the optimum moisture content according to ASTM D698 [8] inside the lower part between the upper and the lower filters to permit water to flow through the soil sample without permitting any washing out of soil particles and to ensure uniform distribution of the applied load on the soil sample. To satisfy the above mentioned criteria properly, two perforated steel plates of (D= 14.8 cm, t = 1cm) dimensions are provided and placed immediately above and below the soil sample. A proper gravel filter is placed above upper perforated plate and below the lower perforated plate. Filter paper and metal screen are placed above and below the soil sample. The lower perforated plate is supported by four short steel rods as a supporter from the bottom to ensure that any settlement of gravel filter does not confuse the measurements of volume change in the soil sample.

Loading system of soil leaching apparatus consists of loading arm and details are shown in Figure 2. This arm is extended horizontally and hinged in the front end with the weight hanger at point (a), then it vertically meets the loading shift at point (b). Dial gauge of (0.002 mm) accuracy is fixed at point (b) to record the volume change in soil sample. The loading arm is extended to the back to meet the rotation axis. This axis consists of rigid shift welded at the perpendicular state with the loading arm and connected with rigid supported steel frame by using ball bearing bracket which permits the arm to rotate freely. Sliding counter of balanced weight is supplied at the back end of loading arm to balance the weight of the loading arm during the test. Loading shift of stainless steel and dimensions (D= 5 cm, L= 45 cm) is used to transport the load from the arm to soil sample. The leaching system of apparatus consists of four control water pipes, which work as inlet and outlet of the water through the soil leaching apparatus. The main function of these pipes is to control the direction of flow through the soil sample and to permit water go into and out of the apparatus. The inlet pipe is connected to an elevated cylindrical vessel of three lines, one for supplying water to the vessel and the second works as an over flow to keep the level of water constant. The third line leads to leaching apparatus.

Fig. 1. A photograph of the Soil Leaching Apparatus

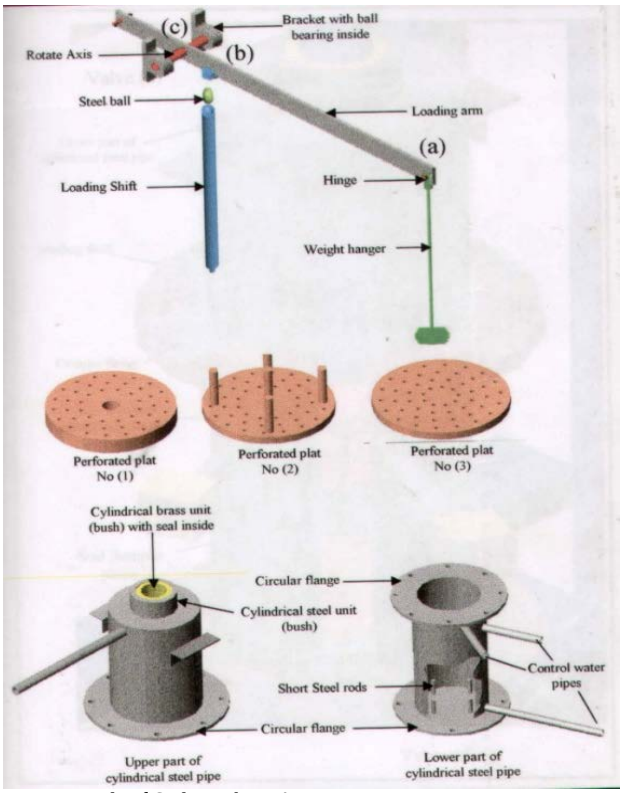

Fig. 2. Details of Soil Leaching Apparatus Parts

III. Results and Analysis

In this research the results of physical tests, chemical tests, compressibility and direct shear tests conducted on different soils are analyzed and discussed. For physical properties as the gypsum content decreases by leaching, the plasticity characteristics also decrease especially if the clay content is not very high as soil no.3, as shown in Table I. The decrease in gypsum content (by leaching) below the initial value of gypsum content will cause a decreases in the initial void when the initial gypsum content is low as in soil no.3, and at higher initial gypsum content, the effect becomes less.

Leaching process decreases the number and amount of contact area between soil particles, destroys some of or all the gypsum cementation and increases the voids as some of the solids volume is gone due to dissolution, which makes the structure of the soil particles less stable. The results of compaction tests are presented in Figure (3). The relationship between dry density and water content for the tested soils for compactive efforts are associated with the modified and standard Proctor tests. Atterberg limits tend to increase with the increase in gypsum content .This behavior may be related to the small particles of gypsum, which cause an increase in the surface area of the soil. So, the requirement of water increases until these limits.

For compressibility tests the results of standard consolidation test of compacted (unleached) and leached soils are presented as volumetric strain versus logarithm of effective stress curves as shown in Figure (4). The respective value of the total volumetric strain (εv)800 , compression index (Cc), swelling index (Cs) of standard consolidation test are presented in Figures (5) to (7). It can be noticed that the total volumetric strain (εv)800 at an effective stress equal to (800 kPa) increases for the same soil type during the leaching process. At some points, this behavior is due to the dissolution of gypsum and the destruction of its bonds between the soil particles which cause an enlargement in voids among them, causing reorientation of particles which increases the total volumetric strain. The increase in compression index (Cc) could be attributed to the same reason. On the other hand, the swelling index (Cs) has decreased after leaching process due to the removal of swelling salts like (SO3) and other soluble salts. The other properties of the soil such as coefficient of volume compressibility (mv), coefficient of consolidation (Cv) and permeability coefficient (k) are presented in Figures (8) to (10). It can be seen that the soil sample tested in Soil Leaching Apparatus is less compressible than the sample tested in Oedometer device. This behavior may be due to the increase of (H:D) ratio which leads to increase the effect of side friction between the sample and inner face of apparatus.

TABLE I
UNITS FOR MAGNETIC PROPERTIES

Soil Property	Type of Soil		
	Soil No.1	Soil No.2	Soil No.3
Depth (m)	0.5	1.5	2
Gypsum Content (%)	59.5%	41.0%	2.03%
Specific Gravity (Gs)	2.34	2.41	2.66
Initial Void Ratio (e_o)	0.85	0.842	0.833
Liquid Limit (L.L) %	33	28	26
Plastic Limit (P.L)%	-	18	23
Plasticity Index (P.I)%	-	10	3
Coefficient of Curvature (C_Z)	0.802	0.73	1.01
Fine soil Percent (%)	4.8	11	80
Uniformly Coefficient (C_u)	4.50	5.17	9.17
Soil Classification According to (USCS)	SP	SP-SM	CL

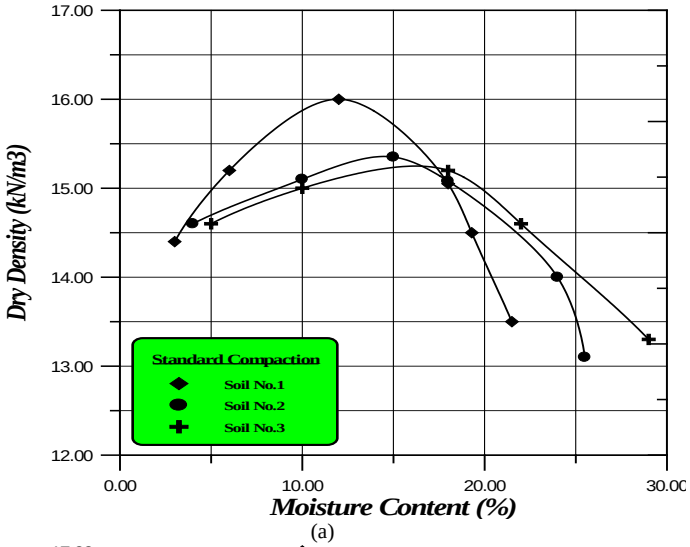

(a)

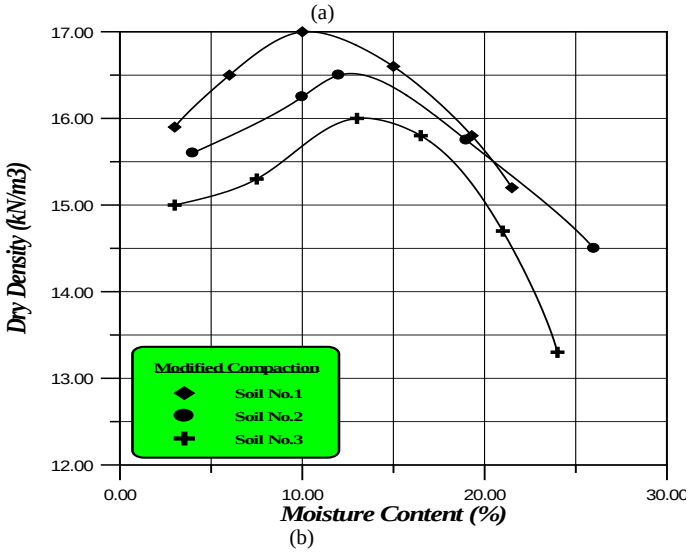

(b)

Fig. 3. Compaction Curves for Soils, (a) Standard Compaction test, (b) Modified Compaction test

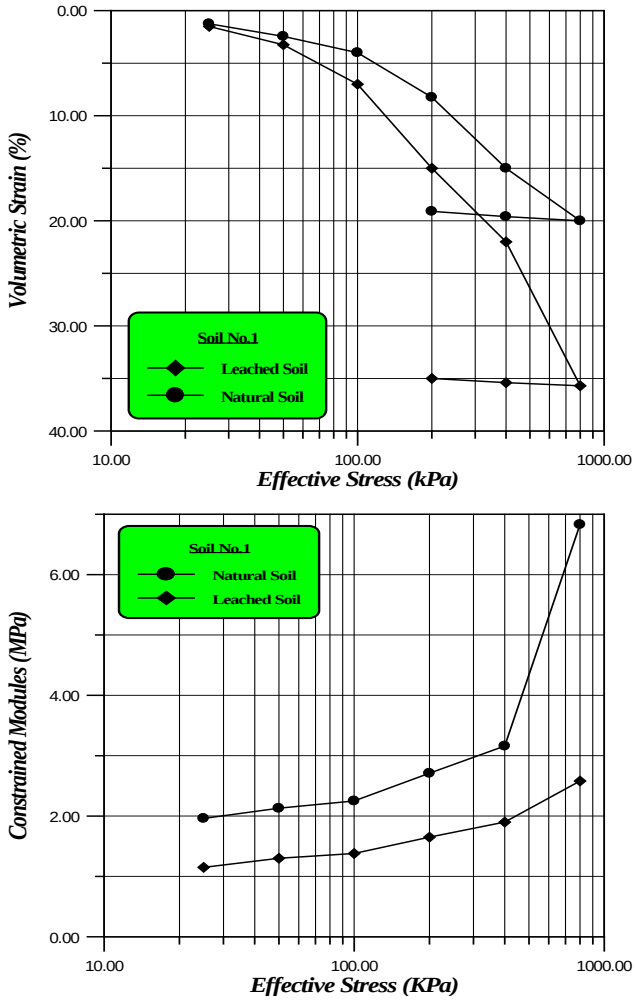

Fig. 4. Results of standard consolidation test of natural and leached soil, for Soil No.1

For Collapse Test (CT) the collapse potential for the three types of natural soils are shown in Table II. It can be found that of the first soil of Abu-Ghraib district is 8.0%. Therefore, this soil is classified as (Trouble) according to the classification suggested by Clemence and Finbarr [9], and the collapse potential for the second soil of al-Karma village is 4.7%, so it is classified as (Moderate Trouble), while the collapse potential for the third soil from Baghdad is 0.32%, so it is classified as (No problems). The sudden increase in strain explained by vertical line is attributed to the sudden collapse of soil structure when water is added at stress level 200 kPa because the dissolution of salts in water leads to increase the volume of voids due to bonds breaking between soil particles. Therefore, rearrangement of soil particles takes place and the settlement of soil samples occurs under constant load. It can be seen that the collapse potential (CP) for soils after leaching is greater than that in natural state because of leaching decreases the number and the amount of the contact areas between soil particles and destroys some or all the gypsum cementations which leads to increase the void volume due to the dissolution and collapse to form a more stable one, as shown in Figure (11).

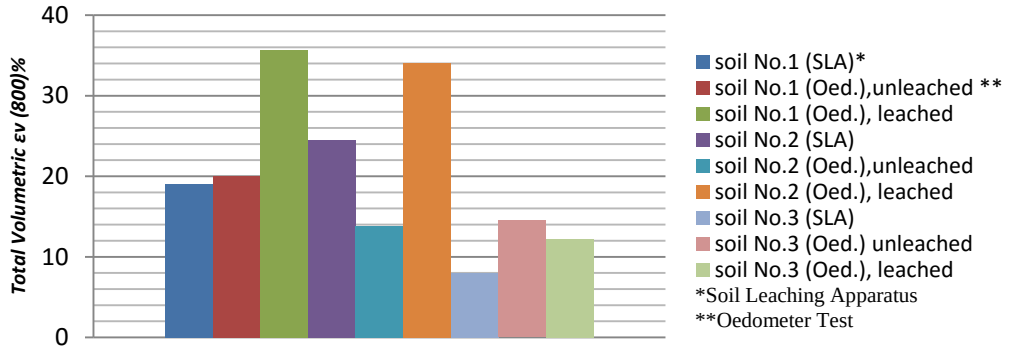

Fig. 5: Results of Standard Consolidation test for total (εv) 800% Volumetric Strain

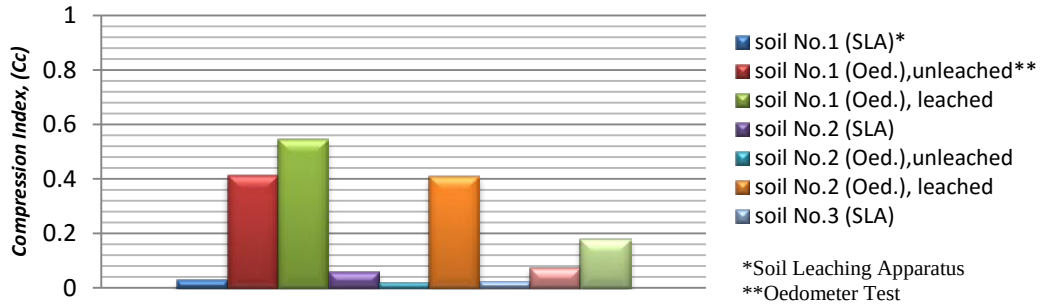

Fig.6 : Results of standard consolidation test for compression index, Cc

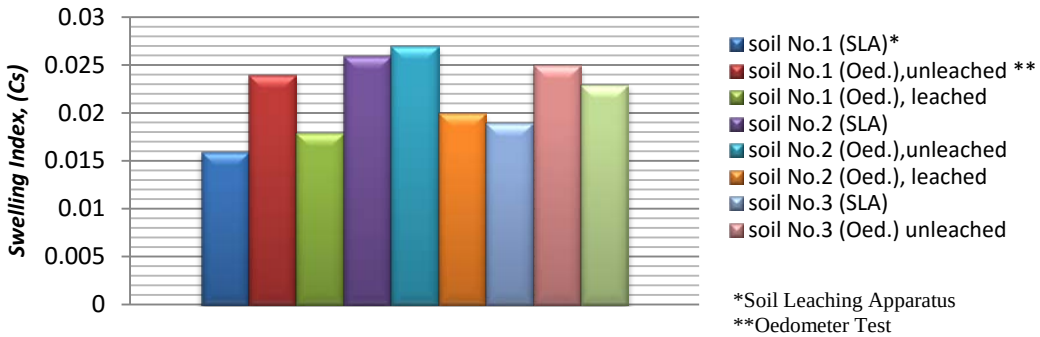

Fig.7 : Results of standard consolidation test for swelling index, Cs

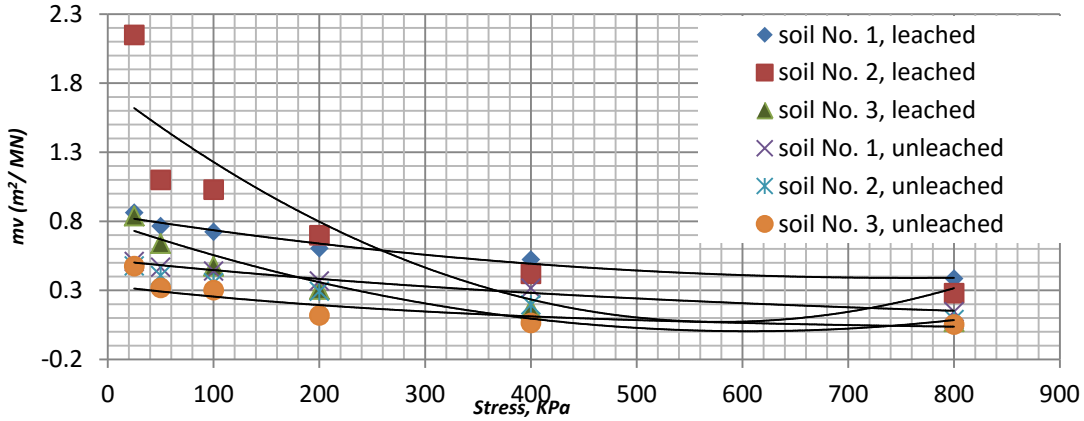

Fig.8: Results of standard consolidation test for volume compressibility (mv)

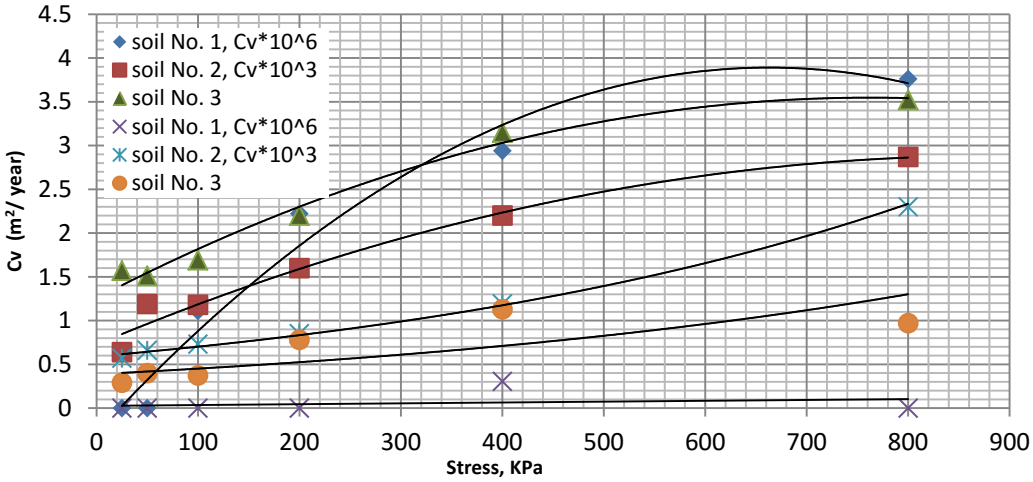

Fig. 9 : Results of standard consolidation test for coefficient of consolidation (cv)

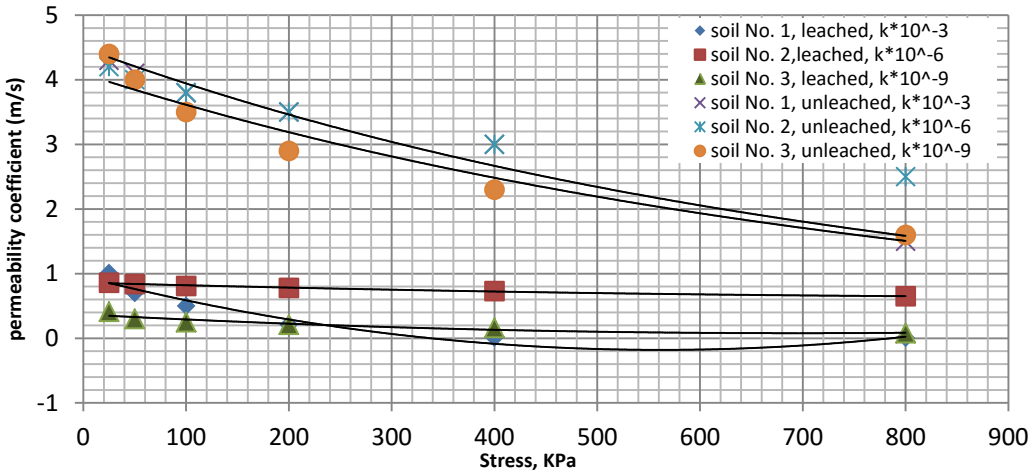

Fig. 10 : Results of standard consolidation test for permeability coefficient (k)

The collapse behavior of leached soil by Soil Leaching Apparatus with two directions of flow upward flow (UWF) and downward flow (DWF) at leaching stress equal to (200 kPa) is investigated as shown in Figures (12). Relationship between the effective stress and volumetric strain for (UWF), and (DWF) were investigated. From results, it can be observed that the collapse potential (CP) during leaching process at two directions of flow is less than that of natural (unleached) soil .This behavior could be attributed to the leaching process which reduces the amount of salts i.e., gypsum between soil particles thus soil fabric becomes free from gypsum bonds by leaching process. These results give a clear picture about the effect of salts mainly gypsum content on the collapsible potential of soil samples.

To investigate the effect of sample thickness and (H:D) ratio on collapse potential (Cp) of gypseous soil, collapse test is conducted by using Soil Leaching Apparatus at different (D:H) ratios such as (D:H =1:1, 1:2 and 1:3.75) . It can be found that collapse potential of gypseous soils decreases as the sample thickness increases (i.e. D:H increases) . This behavior may be attributed firstly to the effect of side friction between the sample and inner face of apparatus. Secondly, the soil sample becomes less compressible with the increase of its thickness especially at dry condition, as shown in Figures (13) to (15). Also, an increase of sample thickness with constant diameter leads to make water paths through the samples Skelton longer; therefore, collapse potential decreases due to the reduction in the amount of dissolved salts.

The permeability-leaching test is carried out under a stress equal to (200 kPa) with two flow directions, upward flow (UWF) and downward flow (DWF). The leaching process is conducted using hydraulic gradient (i) equal to (28) . The Permeability coefficients (k) obtained from Apparatus of Permeability-Leaching test is listed in Table III. To give a clear picture for understanding of behavior of soils during leaching process, many relations are obtained from several tests on these three soils. These relations are as follows:

a- Leaching strain vs. time relation: The relations between leaching strain and time for upward flow direction (UWF) of apparatus of permeability-leaching test and for downward flow direction (DWF) are investigated for a stress level equal

to (200 kPa). In general, it is found that the leaching strain increases with time increasing as the leaching process continues. This behavior is attributed to the continuous dissolution of salts (i.e.,gypsum) that causes a continuous correspond settlement as shown in Figure (16). It can be observed from that, the leaching strain obtained by applying downward flow (DWF) to soil samples is greater than that of upward flow (UWF). This behavior explains the effect of flow direction through the soil sample where soil particles settle largely when water percolates through the soil mass by the same direction of the applied stress i.e. (DWF). This is due to piping phenomenon that leads to speed up the soil particles collapse, while at upward flow of water (UWF) through the soil mass, water needs long period to penetrate and dissolute gypsum particles especially in the opposite direction of the applied stress. Moreover, it is observed that the total leaching strain increases. This behavior could be related to the soil particles more susceptible to collapse at high stress level.

b- Dissolved gypsum vs. time relation: The relations between the accumulative dissolved gypsum with time for Apparatus of permeability-leaching test (APLT) for upward flow direction (UWF) and for downward flow direction (DWF) are shown in Figure (17). From this figure, it can be seen that the accumulative dissolved gypsum increases with time. This behavior is due to the continuous dissolution of gypsum bonds as a result of leaching process.

Also, it can be observed that the total dissolved gypsum of Apparatus of permeability-leaching test of (APLT, UWF) is more than of (APLT, DWF). This behavior may be attributed to the uniform distribution of water through the soil mass where no piping occurs. Also, this leads to the dissolution of large amounts of gypsum bonds due delaying of water to percolate through the soil mass.

c- Permeability coefficient vs. time relation: Typical curves that show the permeability coefficient (k) with time relationship are shown in Figure (18) for Apparatus of Permeability-Leaching test (APLT, UWF) and for (APLT, DWF).

In this test, it can be generally observed that, the permeability coefficient (k) decreases sharply with time and with the increase of leaching stress due to the reduction in void ratio at high stress level. These lead to eliminate and close the links between water paths which cause reduction in the value of (k) obtained by upward flow.

TABLE II
RESULTS OF COLLAPSE TEST

Cp (%) / Soil Type	Oedometer Device		Soil Leaching Apparatus	
			Leached	
	Unleached	Leached	UWF	DWF
Soil No.1 (SP)	8.0	9.5	6.0	7.41
Soil No.2 (SP-SM)	4.7	5.0	1.67	4.5
Soil No.3 (CL)	0.32	0.37	0.17	0.26

TABLE III
RESULTS OF PERMEABILITY-LEACHING TEST OF SOIL LEACHING APPARATUS

Soil Type	Test Type	σ_v, (kPa)	ε_{VLT} (%)	Total Dissolved gypsum (gm/l)	K_{av}.(m/sec)
Soil No.1	UWF	200	3.5	28	$0.53*10^{-3}$
	DWF		3.7	30.3	$0.38*10^{-4}$
Soil No.2	UWF	200	2.5	19	$0.55*10^{-6}$
	DWF		3	21	$0.30*10^{-6}$
Soil No.3	UWF	200	2.2	2.4	$0.51*10^{-10}$
	DWF		2.4	2.6	$0.40*10^{-10}$

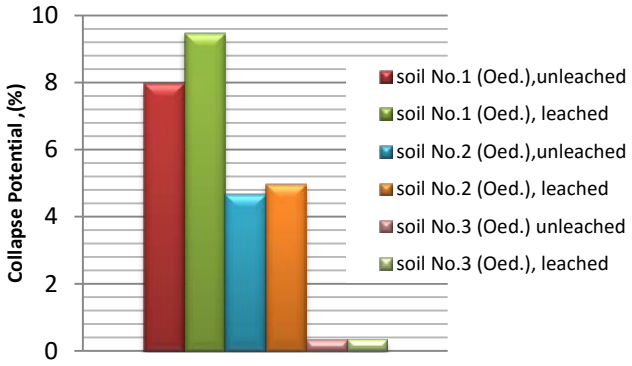

Fig.11: Results of Collapse Test on Natural (unleached) and Leached Soils by Oedometer Device

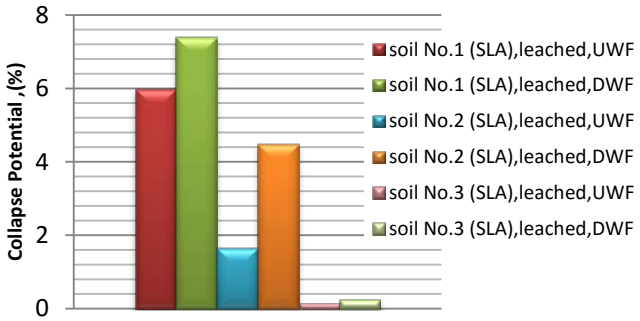

Fig.12.: Results of Collapse Test for UWF and DWF direction by Soil Leaching Apparatus

Direct shear tests are conducted on unleached and leached samples for the three types of soils to predict the shear strength parameters (c and Ø) .This test is conducted on two samples for each soil at three normal stresses (40, 67.4, 95) kPa. The first sample is tested dry (at natural state), while the other is tested after leaching. The results of direct shear tests carried out on the three soils before and after leaching are shown in Tables IV to VI .The shear stress versus horizontal displacement is investigated for each test .In addition to maximum shear stress versus normal stress is drawn for each test , as shown in Figure (19).

1. Unleached (Natural) Soils: The typical results of direct shear test of natural (unleached) soils are shown in Tables IV

to (6), it can be observed that the maximum shear strength increases with the increase in normal stress. This may be due to the percent of angle of internal friction (Ø), cohesion (c) generated by the cementation action of gypsum and fine particles of soils.

2. Leached Soils: Direct shear tests is carried out on two samples of each soil leached by using Soil Leaching Apparatus, soils are leached by applied upward flow (UWF) and downward flow (DWF) at two leaching stresses (100 and 200) kPa .

Generally, from results, it can be observed that the shear strength parameter C increases for Soil No.1 during the leaching process, mainly due to the decrease in the void ratio (e) and the elimination of gypsum content (%) and sulphat (SO3), while the angle of internal friction Ø decreases because of friction between gypsum particles or between gypsum and soil particles which is greater than that between minerals components of the soil. Therefore, the reduction in gypsum - content due to leaching leads to a decrease in (Ø) value . On the other hand, and for Soil No.2 & No.3 the shear strength parameters decrease upon leaching process mainly due to the loss of cementation action (gypsum) bonds as a result of leaching process. This phenomenon leads to sharp reduction in apparent cohesion (c) and a decrease in angle of internal friction (Ø). This behavior, related to gypsum, is uniformly distributed over the entire volume of soil in the form of fine and coarse crystals and leaching causes decreases over the area of interaction between particles, and their contact.

Also, a reduction in shear strength due to leaching by applied downward flow (DWF) is more than the reduction in upward flow (UWF). These results mean that the leaching process by applying (DWF) is more effective than leaching by applying (UWF) due to the ability of water to percolate through the soil samples and leaching up salts, (i.e., gypsum bonds) between soil particles .

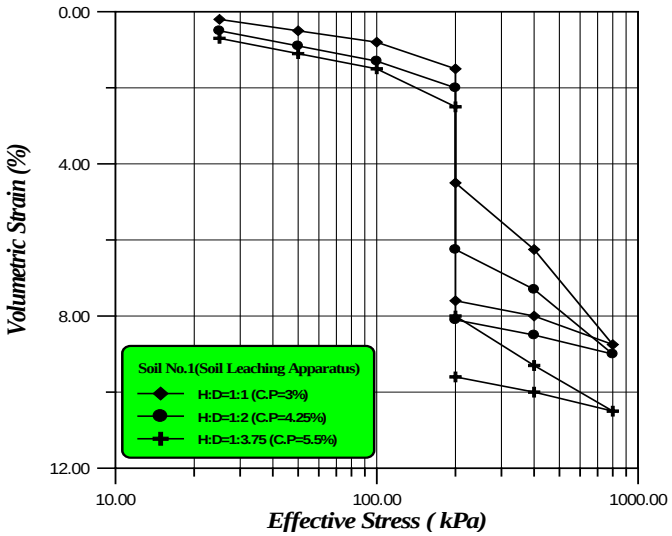

Fig. 13: Results of Collapse Test Conducted by Soil Leaching Apparatus for Soil No.1

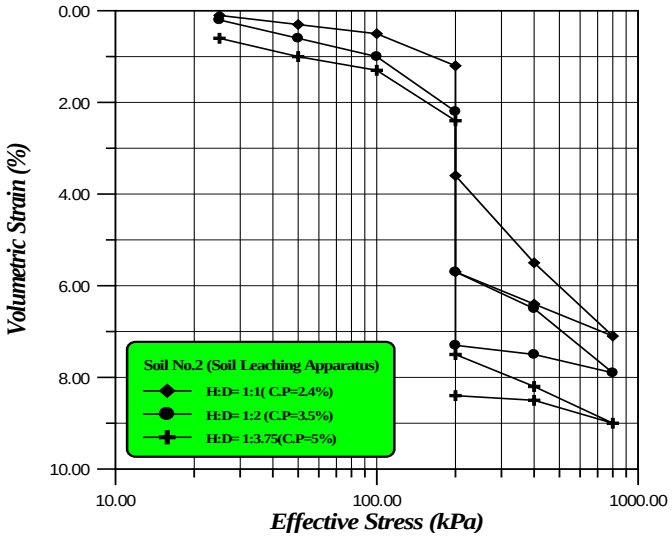

Fig. 14: Results of Collapse Test Conducted by Soil Leaching Apparatus for Soil No.2

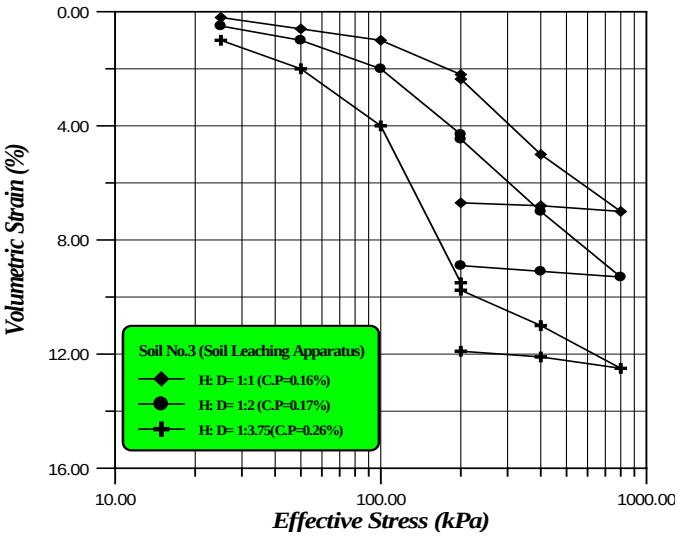

Fig. 15: Results of Collapse Test Conducted by Soil Leaching Apparatus for Soil No.3

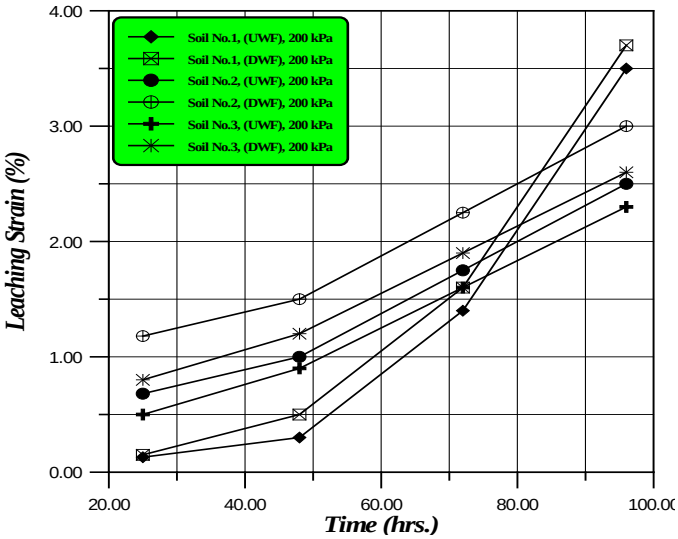

Fig. 16: Variation of leaching strain vs. Time relations

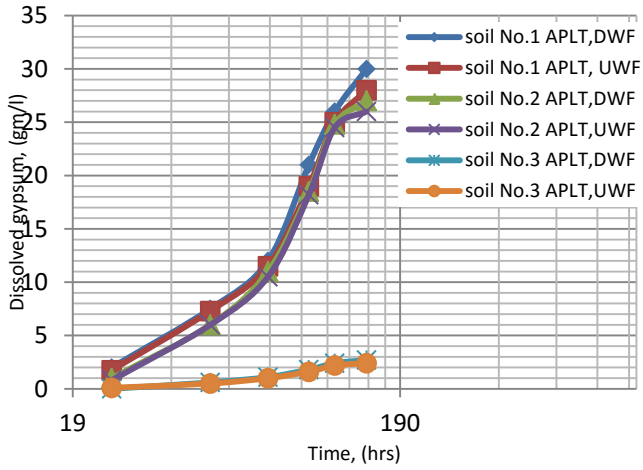

Fig. 17: Variation of Dissolved gypsum vs. Time relations

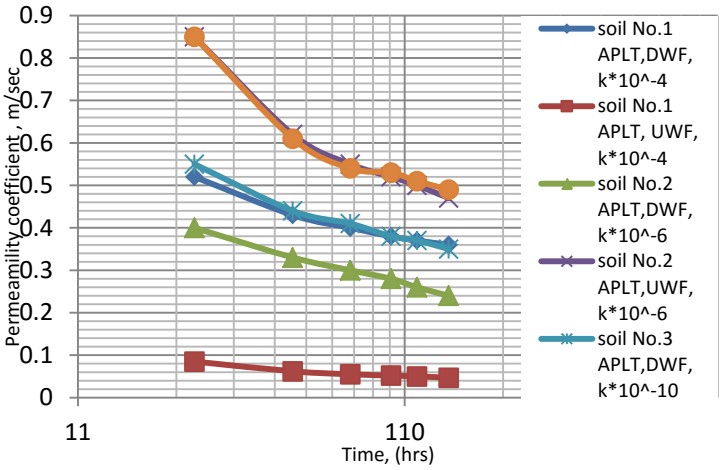

Fig. 18: Variation of Permeability coefficient vs. Time relations

TABLE IV
RESULTS OF DIRECT SHEAR TEST FOR SOIL NO.1 (SP)

Soil Properties	Normal Stress (kPa)	Un-leached	Leached			
			UWF		DWF	
			100 kPa	200 kPa	100 kPa	200 kPa
Cohesion, c (kPa)	39.9	1.1	22	14.1	47.1	29
	67.4					
	94.9					
Angle of internal friction, Φ (Deg.)	39.9	43	8	25.3	5.14	17.2
	67.4					
	94.9					
Max. Shear stress, τ_{max}(kPa)	39.9	36	23.3	31	52	40
	67.4	68	31.4	50	53	52.5
	94.9	88	34.3	57	57	56
Max. Horizontal Dis.,Δx(mm)	39.9	21	12.5	15	22	14
	67.4	22.25	14.5	18	25	15.5
	94.9	22.3	16	19.5	27	16.5

TABLE V
RESULTS OF DIRECT SHEAR TEST FOR SOIL NO.2 (SP-SM)

Soil Properties	Normal Stress (kPa)	Un-leached	Leached			
			UWF		DWF	
			100 kPa	200 kPa	100 kPa	200 kPa
Cohesion, c (kPa)	39.9	39.9	13.26	27.4	10.3	17.9
	67.4					
	94.9					
Angle of internal friction, Φ (Deg.)	39.9	46.6	22.24	20.3	6.22	1.34
	67.4					
	94.9					
Max. Shear stress, τ_{max}(kPa)	39.9	84	27	46	17	18
	67.4	105	45	50	13	55
	94.9	144	50	70	23	48
Max. Horizontal Dis.,Δx(mm)	39.9	10.5	16.5	21	15	15
	67.4	13.5	18	22	17.5	16
	94.9	15	21.5	23.5	19	11.5

TABLE VI
RESULTS OF DIRECT SHEAR TEST FOR SOIL NO.3 (CL)

Soil Properties	Normal Stress (kPa)	Un-leached	Leached			
			UWF		DWF	
			100 kPa	200 kPa	100 kPa	200 kPa
Cohesion, c (kPa)	39.9	22	8.5	11.3	8.8	12.7
	67.4					
	94.9					
Angle of internal friction, Φ (Deg.)	39.9	6.22	5.2	4.7	3.6	2.5
	67.4					
	94.9					
Max. Shear stress, τ_{max}(kPa)	39.9	26	14	12	11.5	14.5
	67.4	30	10.8	20	13	16
	94.9	32	19	23	15	17
Max. Horizontal Dis.,Δx(mm)	39.9	12.5	12.5	10.5	11.5	12
	67.4	13	14	12	13	13.5
	94.9	14.5	16.5	13.5	15.5	14

IV. CONCLUSION

Leaching tests are performed in this study on three types of soils brought from Abu-Ghraib district, Al-Karma village and Al-Baladiyat region in Baghdad in order to find out the effect of leaching on the properties of soils:

1- For physical and chemical characteristics leaching process is not expected to affect the physical properties except the grain size distribution which slightly changes due to gypsum dissolution.

2- Leaching has an obvious effect on the chemical contents of the soil. The total soluble salts content reduces approximately to half its values before leaching due to the dissolution of salts especially during the seepage of water through the soil .

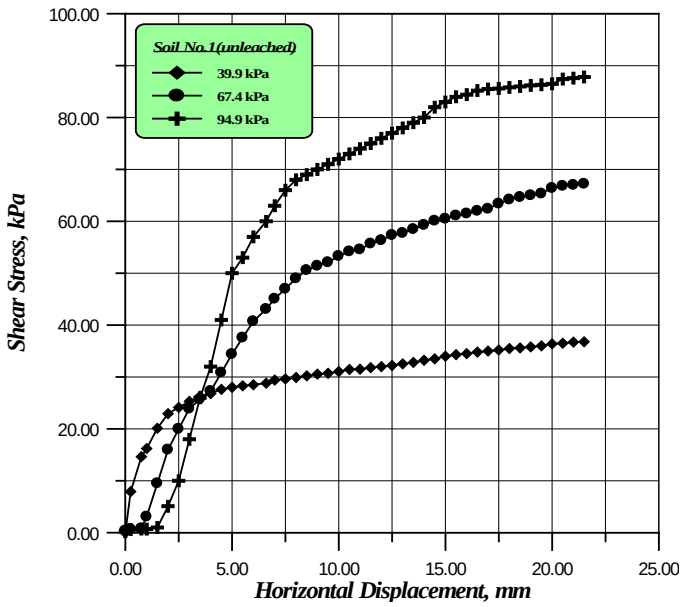

a-Shear Stress Vs. Horizontal Displacement

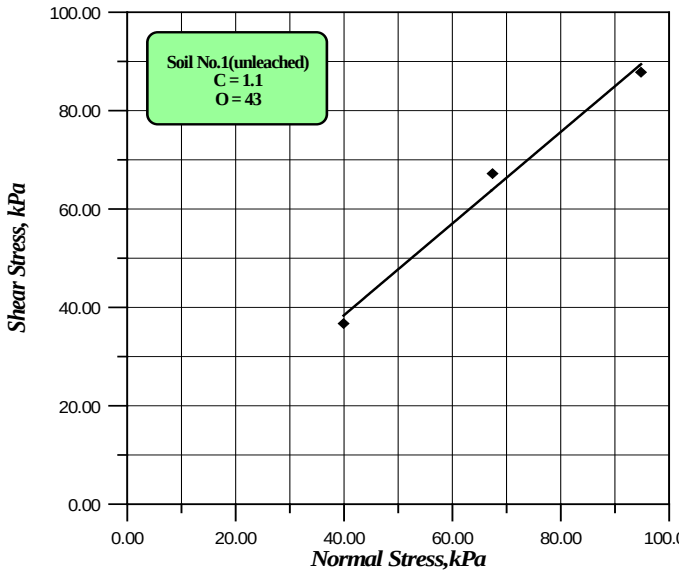

b- Shear Stress Vs. Normal Stress

Fig.19: Results of Direct Shear Test for Soil No.1 (unleached soil)

3- For compressibility characteristics: the total volumetric strain (εv)800 and the compression index (Cc) increases for the same soil type after the leaching process due to the dissolution of the gypsum and reduces the voids among the soil particles .

4-The swelling index (Cs) decreases after leaching process due to the removal of swelling salts like (SO3) and other soluble salts .

5- Soil Leaching Apparatus shows reliable results in tested gypseous soil when compared with conventional tests.

6- The collapse potential (Cp) of natural soils increases after leaching.

7- For leaching characteristics Soil Leaching Apparatus gives good results in studying behavior of gypseous soil during leaching process and confirms results obtained by Oedometer permeability-Leaching test.

8-In general, it can be concluded that the accumulative leaching strain and dissolved gypsum increase with time, while the permeability coefficient (k) decreases with the increase in time, leaching strain and dissolved gypsum.

9-Direction of flow through soil mass with the applied load shows sufficient effect on permeability coefficient (k).

10- For shear strength characteristics: Friction angle of natural soil (Ø) decreases after leaching process especially at downward flow (DWF). Also, sharp reduction is observed in cohesion (c) after leaching except the first soil which shows an increase in the cohesion (c) after leaching process .

REFERENCES

[1] Al-Azzawi, M.M.H: Leaching Effect on an Iraqi Soil. M.Sc. Thesis, Civil Engineering Department, Al-Nahrin University, 2005.

[2] Al-Mohammadi, N.M., Nashat,I.H. and Bako, G.Y.: Compressibility and Collapse of Gypseous Soils , proc.6th Asian Conference on Soil Mechanics, Tokyo,1987.

[3] Al-Abdullah, S.F.I. and Ibrahim, K.H.: Shear Strength Characteristics of Gypseous Soil during Leaching and Loading", The Iraqi Journal of Civil Engineering, Vol. 1.Special, June, pp.287-296, 2001.

[4] Al-Banna, L.A.K: Effect of Soaking and Leaching on the Dissolution of Al-Dour Gypseous Soils", M.Sc. Thesis, Building and Construction Engineering Department, University of Technology, Baghdad, 2004.

[5] Al-Kaisi, A., : Finite Element Analysis of Earth Structures Founded on Gypseous Soils ,Ph.D. Thesis, Building and Construction Dep., University of Technology, 1997.

[6] Ismael, N.F. and Mollah, M.A.: Leaching Effects on Properties of Cemented and Sands in Kuwait, Journal of Geotechnical and Geo-environmental Eng. Vol. 124, No. 10, pp. 997-1004. 1998.

[7] Al-Mufty, A.A. and Nashat, I.H.: Gypsum Content Determination in Gypseous Soils and Rock, 3rd International Jordanian Conference on Mining, p.p. 500-506, 2000.

[8] ASTM D-698: Standard Test Methods for Laboratory Compaction Characteristics of Soil Using Standard Effort (12 400 ft-lbf/ft3 (600 kN-m/m3)), Volume 04.08, pp.1-13.

[9] Clemence, S.P. and Finbarr, A.O: Design Consideration for Collapsible Soils, Journal of Geotechnical Engineering Division, proc. ASCE, Vol.107, No.GT3,pp.305-317. 1981.

[10] W.-K. Chen, Linear Networks and Systems (Book style). Belmont, CA: Wadsworth, 1993, pp. 123–135.

[11] H. Poor, An Introduction to Signal Detection and Estimation. New York: Springer-Verlag, 1985, ch. 4.

Improvement of Bearing Capacity of Footings on Soft Clay by Partial Soil Replacement Technique

Prof. Dr. Mohammed Y. Fattah, Assist. Prof. Dr. Mohammed A. Al-Neami,
and Ahmed Shamel Al-Suhaily.
Building and Construction Engineering Department, University of Technology, Baghdad, Iraq.

Abstract: **Remove and replace is widely used in construction practices and engineers have proved that it can be an effective technique. Further, several researchers have considered the mechanisms of remove and replace mitigation in the past. This study represents an investigation on the efficacy of remove and replace methods for mitigation of soft clays in that the analyses are based on fundamental stress -deformation principles.**

A total number of 8 models tests represents two series was carried out in models of soft clays of different values of undrained shear strength c_u varying from 7 to 17 kPa. The first series consists of 4 models of a square pattern of soil replacement; the second series consists of 4 models of a trench pattern of soil replacement both of the two series are carried out with different depths and widths of replacement, in addition to one model of untreated soil.

The bearing capacity of the soil improved by the soil replacement has been measured. It was noticed that ability of soft soil replacement by granular soil to improve the bearing capacity of footing on soil showed that the maximum degree of improvement is achieved when the soil is treated by partial replacement with a trench pattern of soil replacement of dimensions B (where B is the width of the footing) with extension of B/2 all sides to a depth of 1.5 B. Soil replacement method is more effective in improving the bearing capacity in case of the increasing the width of replacement compared with the increasing of the depth of replacement. It was found that the stone used as a replacement material help to increase the undrained shear strength of the soft soil by lowering the water content. The undrained shear strength is increased by about (5.5 – 15) % due to the implementation of soil replacement.

Index Terms: **Soft clay, bearing capacity, soil replacement, improvement.**

I. Introduction

DEVELOPMENTAL activities in cities have led to increased building construction. The availability of good quality land in developed areas has always been on the decline. Supporting high rise buildings on expensive deep foundations is justifiable. However, cost effective means of founding light residential buildings on such weak soils has always been a challenge. A number of ground improvement techniques have been used in practice. In the case of clay deposits, accelerating consolidation through installation of sand / band drains and chemical means have gained acceptance. In the case of loose sand deposits, densification through the installation of compaction sand piles is a widely adopted technique. The classical approach to ground improvement is replacement of weak soil by a better soil. However, replacing the entire weak zone is not practical given the high costs involved and the recent environmental restrictions on mining and reclamation. Selective replacement in the most desired zone is a feasible solution considering the above factors. The idea of such selective replacement in the form of a granular trench beneath the footing was pioneered by Madhav and Vitkar (1978) and was continued by Das (1988). The theoretical formulation provided by Madhav and Vitkar (1978) was experimentally verified by Hamed et al. (1986).

Fattah et al. (2010) provided a finite element procedure to model soft cohesive soil, granular trench soil, and the reinforcement material using a computer program called (SIGMA/W). The behavior of both cohesive and granular soils was simulated by nonlinear-elastic soil model (hyperbolic model), while the linear-elastic model was used to simulate the reinforcement material. The angle of friction of trench soil, modulus of elasticity of reinforcement martial, depth, width and shape of the granular trench, locations, and number of the reinforcement layers were varied. The sloped granular trench was analyzed in two cases; lined and unlined conditions. The results showed that the use of granular trench beneath foundation will increase the bearing capacity and reduce the settlement. Moreover, using of polymers as a reinforcement material has a significant effect on both bearing capacity and settlement. For both reinforced and unreinforced granular trenches, the depth ratio has an important effect on the settlement ratio, which decreases with the increase of depth ratio. The best practical value for the depth ratio was found to be equal to 2. Making a trench with a width (X) larger than the foundation width (B) also decreases the settlement, and the best effect occurs when the width ratio (X/B) equals to 0.65.

Influence of providing a granular trench (GT) below strip footings on loose sand deposits was explored by Unnikrishnan et al. (2011). The additional benefit of encapsulating such a granular trench with a geosynthetic was also studied. Such a system is christened as Encapsulated Granular Trench (EGT).

Load tests were conducted on laboratory model strip footings resting on granular trench and encapsulated granular trench. EGT supported strip footing was found to perform better than the footing on GT. The geosynthetic helps to redistribute the stresses within the granular trench and undergo self straining due to loading. In addition to this, the geosynthetic will also perform as a separator.

The reinforcement of the problematic soils with granular fill layers is one of the soil improvement techniques that are widely used. Problematic soil behavior can be improved by totally or partially replacing the inadequate soils with layers of compacted granular fill. Ornek et al. (2012a) presented the use of artificial neural networks (ANNs), and the multi-linear regression model (MLR) to predict the bearing capacity of circular shallow footings supported by layers of compacted granular fill over natural clay soil. The data used in running the network models have been obtained from an extensive series of field tests, including large-scale footing diameters. The field tests were performed using seven different footing diameters, up to 0.90 m, and three different granular fill layer thicknesses. The results indicated that the use of granular fill layers over natural clay soil has a considerable effect on the bearing capacity characteristics and that the ANN model serves as a simple and reliable tool for predicting the bearing capacity of circular footings in stabilized natural clay soil.

Numerical predictions of the scale effect for circular footings supported by partially replaced, compacted, layers on natural clay deposits were presented by Ornek et al. (2012b). The scale effect phenomenon was analyzed according to the footing sizes. Numerical analyses were carried out using an axisymmetric, two-dimensional, finite-element program. Before conducting the analysis, the validity of the constitutive model was validated using field tests performed by authors with seven different footing diameters up to 0.90 m and with three different partial replacement thicknesses. It was shown that the behavior of the circular footings on natural clay soil and the partial replacement system can be reasonably well represented by the Mohr Coulomb model. The Mohr-Coulomb model parameters were derived from the results of conventional laboratory and field tests. After achieving a good consistency between the results of the test and the numerical analysis, the numerical analyses were continued by increasing the footing diameter up to 25 m, considering the partial replacement thickness up to two times the footing diameter. The results of this parametric study showed that the stabilization had a considerable effect on the bearing capacity of the circular footings and for a given value of H/D the magnitude of the ultimate bearing capacity increases in a nonlinear manner with the footing diameter. The Bearing Capacity Ratio (BCR) was defined to evaluate the improved performance of the reinforced system. It was found, based on numerical and field-test results that the BCR of the partially replaced, natural clay deposits increased with an increase in the footing diameter and there was no significant scale effect of the circular footing resting on natural clay deposits.

Gueguin et al. (2015) addressed the geotechnical engineering problem of evaluating the ultimate bearing capacity of a strip foundation resting upon a reinforced soil, by means of the yield design homogenization approach. The analysis was notably focused on the determination of the macroscopic strength criterion of such reinforced soils, where both constituents are purely cohesive, which can be conveniently expressed through the notion of anisotropic cohesion. A comprehensive comparison was made between the classical configuration of reinforcing columns and the more original one of orthogonal reinforcing trenches. Among the most outstanding results of the analysis is the conclusion that the cross trench configuration is notably more efficient in terms of load bearing capacity than the reinforcement by columns, notably when significantly inclined loading is concerned.

The objective of the present study is to improve the bearing capacity of a footing resting on soft clay by partial replacement of the clay with a limited zone of granular material.

II. Procedure for Paper Submission

A. Experimental Work

A total number of 8 model tests representing two series was carried out in models of soft clays of different values of undrained shear strength c_u varying from 7 to 17 kPa. The first series consists of 4 models of a square pattern of soil replacement; the second series consists of 4 models of a trench pattern of soil replacement. Both of the two series are carried out with different depths and widths of replacement, in addition to one model of untreated soil.

B. Material Used

Soil used in this study was obtained from a site east of Baghdad city. The soil consists of 17% sand, 35% silt and 48% clay. According to the Unified Soil Classification System (USCS); the soil is classified as (CL). The crushed stone material which is used for the stone columns was obtained from a crushing stone factory. It is produced as a result of crushing massive stones, angular in shape. The crushed stone is of a uniform size, considered as poorly graded. Direct shear test was performed on samples prepared at a relative density of 73% according to (ASTM D-3080-2003). The test revealed that the angle of internal friction is 40^o.

C. Preparation of Model Test

The natural soil was first dried and crushed with a hammer to small sizes; further crushing was carried out using a crushing machine. The natural soil was mixed with enough quantity of water to get the desired consistency. The mixing operation was conducted using a large mixer (120 liter capacity) each 25 kg of dry soil was mixed separately till completing the whole quantity. After thorough mixing, the wet soil was kept inside tightened polythene bags for a period of 24 hours to get uniform moisture content.

The soil used for model tests was placed in a manufactured steel container in layers with a thickness ranging between (50-75) mm for each layer, each layer was leveled gently using a wooden tamper, and then the leveled layer was tamped gently with a metal hammer of 9.87 kg and dimensions of (150 x 150) mm in order to remove any entrapped air. This process continues for each layer till reaching a thickness of 300 mm of soil in the steel container.

After completing the final layer, the top surface was scraped and leveled to get as near as possible a flat surface, then covered with polythene sheet to prevent any loss of moisture. A wooden board of similar area to that of the surface area of bed soil (600 x 600) mm was placed on the bed of soil. The bed of soil was subjected to seating pressure of 5 kPa for 24 hours to regain part of its strength. The bed of soil was covered and left for a period of curing time of (five days) before the testing time.

The tests were carried out using a steel container with internal dimensions of (600 x 600 x 500 mm).

D. Loading assembly

A loading frame was designed and manufactured to apply static vertical load on the model footing in models of soil replacement. Details of the main features of the loading assembly are shown in Plate (1).

Implementation of soil replacement models

After preparing the bed of soft soil, the following steps were followed for implementation of soil replacement; Table (1) illustrates details of the soil replacement cases. The table shows that in four tests, the granular material was extended wider than the footing width (B) to a distance (b = 50 mm) from each side of the footing.

1. After the preparation of the bed of soft soil, the center of the footing and the boundaries of the replaced zone were located on the surface of the soil bed.
2. The undrained shear strength of the soil bed was measured in the center of the replaced zone at 100 mm or 150 mm depth (depending on the case) using the portable vane shear device.
3. The excavation was made by hand excavator till the required depth and width are reached.
4. The crushed stone was placed in the excavated zone by using a plastic cone in 2 layers for the 100 mm depth case and 3 layers for 150 mm depth, each layer is 60 mm thick and compacted by using a small hammer to maintain the desired dry unit weight of approximately 15.1 kN/m^3 as shown in Plate (3).
5. After finishing the implementation, the bed of soil was covered and left for a period of curing time of 24 hours before the testing day.

.

Testing procedure for the soil replacements

After the completion of the curing period, the following steps were followed:

1- The loading frame was placed in position so that the center of the footing coincides with the center of replaced soil.
2- Loads were applied through a loading disk in the form of load increments, Plate (2). Each load increment was left till the dial gauge nearly stopped or a penetration rate of 0.01 to 0.05 in. or 0.25 to 1.25 mm/min is reached according to (ASTM D-1143, 2000).
3- Dial gauge readings were recorded before the addition of the next load increment.
4- The load increments continued till failure was achieved.
5- After completion of the load test, the undrained shear strength of the soil bed was measured near and below replaced zone using the portable vane shear device.

Table (1)
Details of soil replacement models.

Plate (1) Loading assembly for soil replacement models

Type	*width of replacement (mm)*	*Depth of replacement (h) (mm)*
square	*100*	*100*
square	*100*	*150*
square	*200 (b = 50 mm)*	*100*
square	*200 (b = 50 mm)*	*150*
trench	*100*	*100*
trench	*100*	*150*
trench	*200 (b = 50 mm)*	*100*
trench	*200 (b = 50 mm)*	*150*

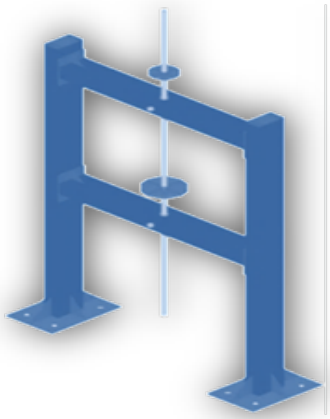

Plate (1) Loading assembly for soil replacement models

Plate (2) Loading of square footing on soil treated by replacement.

Plate (3) Trench of replaced soil 200 mm wide and 150 mm deep.

Results and Discussion

Eight model tests were performed with two different types of zone of soil replacement; square and trench, with footing dimensions of (100 x 100 mm) was used for both cases; square and trench. Table (2) illustrates the bearing capacity ratio (q_u/c_u) and the bearing improvement ratio ($q_{treated}/q_{untreated}$) of different cases of soil replacement while Figures (1) and (2) demonstrate the relationship between q_u/c_u and S/B. The undrained shear strength has been measured using portable vane shear before testing and after the failure of model. Table (3) shows the variation of the undrained shear strength. It can be noticed that the undrained shear strength is increased by about (5.5 – 15) % due to the implementation of soil replacement. The histogram in Figure (3) shows the variation of improvement ratio of the bearing capacity of both square and trench soil replacement.

Table (2) The bearing capacity ratio (q_u/c_u) and the bearing improvement ratio ($q_{treated}/q_{untreated}$) of different cases of soil replacement.

Table (3) Variation of the undrained shear strength before and after testing.

Case	Type	c_u before testing (kPa)	q_u/c_u after testing (kPa)	$q_{treated}/q_{untreated}$ Percentage of increase (%)
b=0 h=10 mm	Trench	3.5	16.5	4.9
b=0 h=15 mm	Trench	2.5	18.5	5.5
b=5 h=10 mm	Trench	3.5	24.5	7.3
B=10 b=0 h=10	Trench	15	16.5	9.09
b=5 h=15 mm	Trench	3.5	30.1	8.9
B=10 b=0 h=15	Trench	17	18	5.56
b=0 h=10 mm	Square	4	13.2	3.9
B=10 b=5 h=10	Trench	15	16	6.25
b=0 h=15 mm	Square	3.5	15.3	4.5
B=10 b=5 h=15	Trench	15.5	17	8.82
b=5 h=10 mm	Square	3.5	18.2	5.4
B=10 b=0 h=10	Square	7	8	12.50
b=5 h=15 mm	Square	3.5	28	8.12
B=10 b=0 h=15	Square	8.5	10	15.00
B=10 b=5 h=10	Square	11	12	8.33
B=10 b=5 h=15	Square	11.5	13	11.54

It can be noticed that with the provision of soil replacement in soft clay bed, the bearing capacity of foundation bed can be improved by (4.9 - 8.9) times for the trench soil replacement and (3.9 - 8.1) times for the square soil replacement. It can be noticed that the undrained shear strength is increased by about (5.5 – 15) % due to the implementation of soil replacement.

To some extent, the strain in the clay cannot develop around the replaced zone because of the presence of granular material in the trench. This constrained strain results in a higher stress state in the clay and thus in a higher confinement on the granular material. As settlement increases, the stone packing is rearranged and the stone packing is progressively destabilized (so-called yielding) resulting in a decrease in bearing capacity.

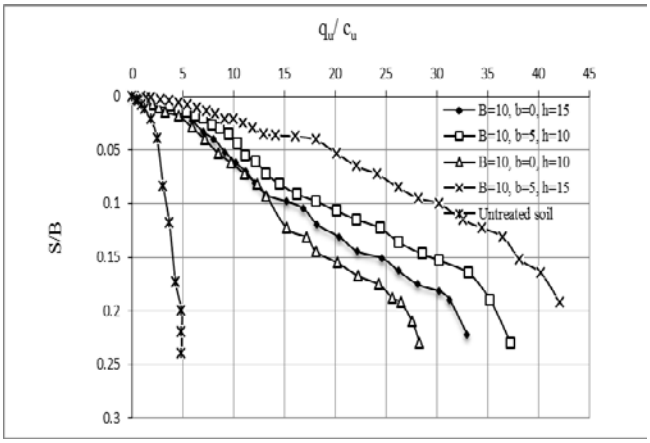

Figure (1) Pressure –settlement curves for a footing resting on soft clay treated by square soil replacement with different dimensions.

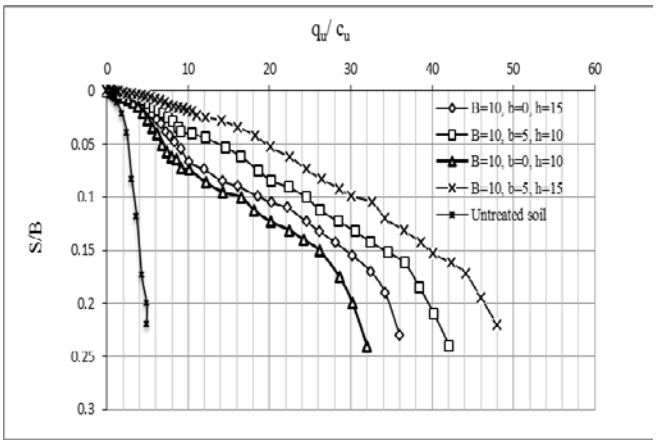

Figure (2) Pressure –settlement curves for a footing resting on soft clay treated by trench of soil replacement with different dimensions.

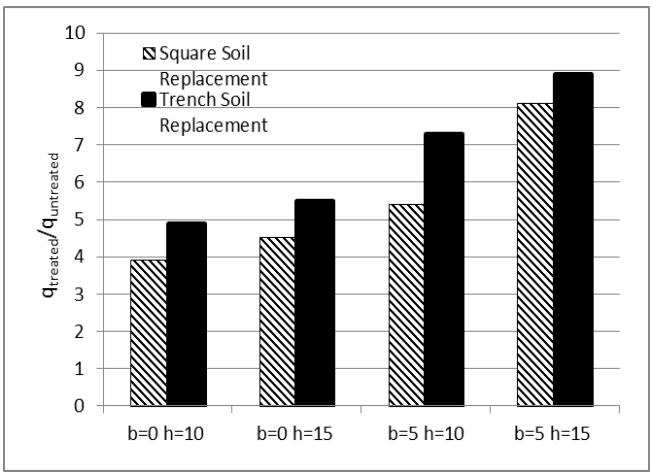

Figure (3) Variation of bearing capacity improvement ratio of square footing and strip over a trench of replaced soil.

It can be concluded that applying the load through a rigid foundation over a replaced area greater than the footing area (b > 0) increases the vertical and lateral strength in the surrounding soft soil. The larger bearing area together with the additional support of the replaced soil below the footing result in less bulging and a greater ultimate load capacity.

Conclusions

From the experimental work carried out, the following points have been concluded:

1- The ability of soft soil replacement by granular soil to improve the bearing capacity of footing on soil showed that the maximum degree of improvement is achieved when the soil is treated by partial replacement with a trench pattern (strip) of soil replacement of dimensions B with extension of B/2 all sides to a depth of 1.5 B.

2- Soil replacement method is more effective in improving the bearing capacity in case of the increasing the width of replacement compared with the increasing of the depth of replacement.

3- The stone used as a replacement material help to increase the undrained shear strength of the soft soil by lowering the water content. The undrained shear strength is increased by about (5.5 – 15) % due to the implementation of soil replacement.

4- The improvement ratio of trench soil replacement is higher than the square soil replacement by about (10 - 20) %.

REFERENCES

[1] ASTM D 3080-98: "Standard test method for direct shear test of soils unconsolidated undrained conditions", American Society for Testing and Materials.

[2] ASTM D1143-81 (1994), "Standard Test Method for Piles under Static Axial Compressive Load", American Society for Testing and Materials.

[3] Das, B. M. (1988). Bearing Capacity of Shallow Foundation on a Granular Trench in Clay. Proc. Fifth Australia-New Zealand Conference on Geomechanics: Barton, ACT:Institution of Engineers, Australia. pp. 278-282.

[4] Fattah, M. Y., Al-Baghdadi, W., Omar, M., Shanableh, A., (2010), "Analysis of Strip Footings Resting on Reinforced Granular Trench by the Finite Element Method", International Journal for Geotechnical Engineering, Vol. 4, Issue 4, October, 2010, pp. 471-482, J. Ross Publishing, Inc.

[5] Gueguin, M., Hassen, G., de Buhan, P., (2015), "Ultimate Bearing Capacity of a Foundation Reinforced by Columns or Cross Trenches under Inclined Loads: A Homogenization Approach", International Journal for Numerical and Analytical Methods in Geomechanics, Vol. 39, 3, pp. 277–294, DOI: 10.1002/nag.2307.

[6] Hamed, J. T., Das, B. M., and Echelberger, W. F. (1986). Bearing capacity of a strip foundation on granular trench in soft clay. Civil Engineering for Practicing and Design Engineers, Pergamon Press, 5(5), 359XXXXXX,

[7] Madhav, M. R., and Vitkar, P. P. (1978). "Strip Footing on Weak Clay Stabilized with a Granular Trench or Pile", Canadian Geotechnical Journal, Vol. 15, pp. 605–609.

[8] Ornek, M., Laman, M., Demirc, A., Yildiz, A. (2012a), "Prediction of Bearing Capacity of Circular Footings on Soft Clay Stabilized with Granular Soil", Soils and Foundations, Vol. 52(1), pp. 69–80.

[9] Ornek, M., Demir, A., Laman, M., Yildiz, A. (2012b), "Numerical Analysis of Circular Footings on Natural Clay Stabilized With A Granular Fill", Acta Geotechnica Slovenica, 1, pp. 61-75.

[10] Unnikrishnan, N., Rajan, S., Johnson, A. S., (2011). "Bearing Capacity of Strip Footings on Encapsulated Granular Trenches", Proceedings of Indian Geotechnical Conference, December 15-17, 2011, Kochi, Paper No.D-141, pp. 191-194.

Behavior of Modeling Piled-Raft System in Sandy Soil under Vertical Load

Kais T. Shlash[1], Hussein H. Karim[2], and Hussein H. Hussein[3]

***Abstract*—The piled raft system is a geotechnical complex structure composed of three elements; soil, piles and raft. The foundations of piled raft provide an economical foundation where the raft isolated does not satisfy the requirements of design. Under these situations, the addition of a limited number of piles may increase the ultimate load capacity and decrease the settlement of piled raft system. The study discusses the behavior of load-settlement of piled-raft foundation on sandy soil under vertical load by means of both full scale tests and finite element analysis. The effects of number of piles, ground water level, spacing between piles and raft thickness are discussed. The full scale test (compression loading) for piled raft 1.8m×1.8m × 0.6m contains 4 piles of 6 m length. A vertical load of 500 tons (simulated as a uniform surface load) and a pile spacing of 3 pile diameters have been used in this study for verification purpose using PLAXIS-3D software to show compatibility of the numerical analysis with field test results. 9 finite element models have been prepared and run on the basis of the analyses performed with verifications. It is noticed that the bearing capacity of piled raft system increases with increasing the number of piles and spacing without any significant effect of the raft thickness. The presence of water is found to increase settlement.**

***Index* Terms—Piled raft, Pile foundation, Bearing capacity, Settlement, Plaxis-3D**

I. Introduction

PILED raft foundations are composite structures unlike classical foundation where the building load is either transferred by the raft or the piles alone. The piles transfer is a portion of the building loads to the deeper and more severe than the soil layers, and thus allows reducing the total and differential settlement in areas very economical way. Piles are used up to a load level which can be the same order of size and load carrying capacity of a single pile similar to or greater than that level [1].

Manuscript received July 21, 2015; accepted August 23, 2015.

[1] Professor, Civil Engineering Department, Al-Esraa University College, Baghdad, Iraq. (e-mail: ktishlash1@yahoo.com)

[2] Professor, Building and Construction Engineering Department, University of Technology, Baghdad, Iraq. (e-mail: husn_irq@yahoo.com).

[3]Ph.D in Geotechnical Engineering, Building and Construction Engineering Department, University of Technology, Baghdad, Iraq. (corresponding author: e-mail: enghhhpile@yahoo.com)

The adoption of piled raft foundations concept in the design of pile groups is by no means new, and has been described by several authors (including [2] – [7] among many others). In the first years and because of the limited availability of processing speed and computer memory, the use of numerical methods was limited for simple problems. But, with the rapid growth in the computer technology, numerical methods are often utilized for full three dimensional techniques to solve the complex problems [8].

The design of conventional pile philosophy is depended on that piles carrying the entire load which are recognized as a group, and no contribution is made through the raft to the maximum load capacity. The new trend in foundation engineering is to combine pile and raft foundations. Combined system can be based on a different design philosophy [9].

The study considers developing a numerical model for analyzing piled-raft systems based on the finite element program PLAXIS-3D [10]. The validity of the developed numerical model is examined by comparing its results with the results of full scale tests. This paper deals with studying the effect of some important design parameters related to piles and raft dimension.

II. Soil Stratification of the Site

The site soil profile was specified according to the geotechnical investigations results on two boreholes with their Cone Penetration test (CPT) and standard penetration tests (SPT). The stratigraphy of soil consists of two major layers. The higher layer consists of a very dense yellowish to brown sandy silt soil (from 0 to -5) m and the second layer consisting of medium dense light brown to brownish yellow sand from (-5 m to -15). Laboratory tests involved triaxial and direct shear tests were carried out on Shelby tube samples. The main properties of the soil of every soil layer, derived through geotechnical investigations, the evaluation tests of the situ and laboratory are shown in Table 1.

Table 1. A summary of soil properties of the study site.

Property	Value
Upper layer	
Very dense dry sand from 0 to -5 m	
Unight weight (kN/m^3)	20
Angle of the Friction φ	41
Angle of the Dilatancy ψ	11
Cohesion (kPa)	0.1
Lower layer	
Medium dense drysand from -5 to -15 m	
Unight weight (kN/m^3)	20
angle of the Friction φ	35
angle of the Dilatancy ψ	5
Cohesion (kPa)	0.1

III. Static Load Test

A full real test was conducted and applied on Karbala soil by load testing according to [11] in order to obtain real results. The dimension of the piled raft foundation was (1.8 m×1.8m × 0.6 m) and the piles are distributed in the same manner maintaining a typical spacing (three times pile width = 0.9 m) between every two adjacent piles with 6 m pile length.

The compressive load was applied using from one to three hydraulic jacks having a capability of 500 tons for each that placed among the head of cap and the main steel beam. An appropriate square reinforced concrete cap was casted on the head of the test foundation to enable the transfer of the applied load uniformly. In addition, 25 mm thick steel plates were installed on the cap head. The settlements versus the vertical applied loads are shown in Fig. 1. This Figure illustrates curve representing the load settlement behavior of piled raft foundation (PRF). Fig. 2 shows the entire load frame and load concrete blocks. While, Fig. 3 shows setting the hydraulic jacks and displacement gages over the cap.

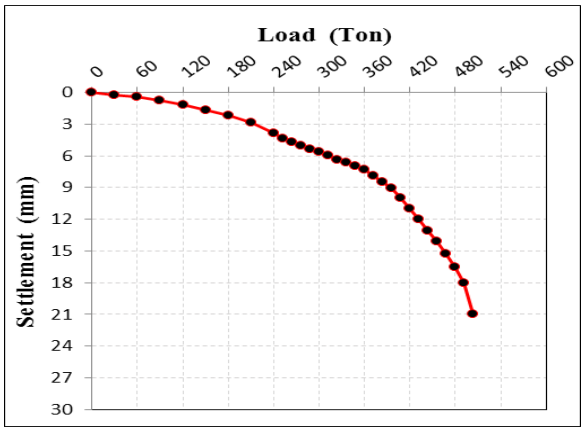

Fig. 1. The load settlement behavior of pile raft foundation.

Fig. 2. The entire load frame in the present study site.

Fig. 3. Setting hydraulic jacks dial gages in the present study site.

IV. Verification with Field Piled Raft Test

As explained in static load test in previous section, a real scale model for foundation of piled raft has been executed and tested in the Karbala soil. The raft and piles are made of concrete, while the soil was dry sand. The results of (2×2) piled raft foundation (Fig. 4) depicts the layout of the piled-raft foundation considered in this analysis as a reference for checking the numerical solution implemented by PLAXIS 3D program. The model sand ground was modeled during utilizing the (HS small) model having the parameters listed in the Table 2. Fig. 5 shows the quarter of the problem analyzed by PLAXIS 3D program. While, Fig. 6 presents the mesh of the finite element of the vertical loading, taking into account the elastic behavior of the piled raft and the ealsto-plastic behavior of sandy soil by incorporating the (HS small) model.

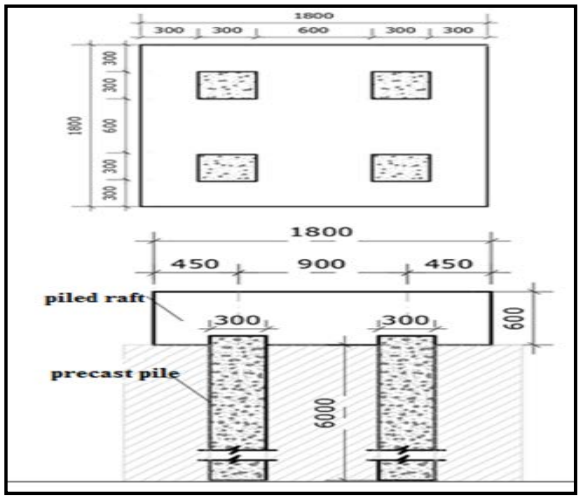

Fig. 4. The Problems of piled-raft (2×2) used for verification (all dimensions are in mm).

Table 2. Material properties of the sand adopting soil model (HS small).

	Very Dense Sand	Medium Dense Sand
Unit weight (kN.m^{-3})	20	20
Drainage type	Drained	Drained
$E_{50,ref}$ (kPa)	60000	35000
$E_{oed,ref}$ (kPa)	60000	35000
$E_{ur,ref}$ (kPa)	180000	105000
m	0.4	0.5
ν_{ur}	0.15	0.15
p_{ref} (kPa)	100	100
γ0.7	0.15E-4	0.15E-4
$G_{0,ref}$ (kPa)	130000	100000
Cohesion c (kPa)	0.1	0.1
Friction angle φ	41	35
Dilatancy angle ψ	11	5
Tension cut-off (kPa)	0	0
K_{0NC} = 1- sin φ	0.344	0.426
$K_{0ini} = K_{0NC}$	0.344	0.426

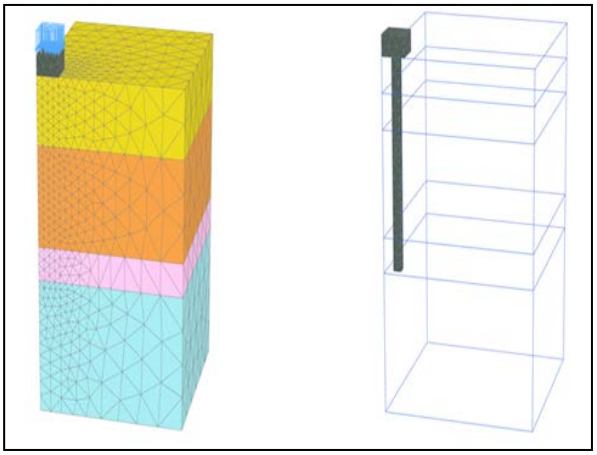

Fig. 5. Quarter of the problem of piled raft (2×2) as executed by PLAXIS-3D.

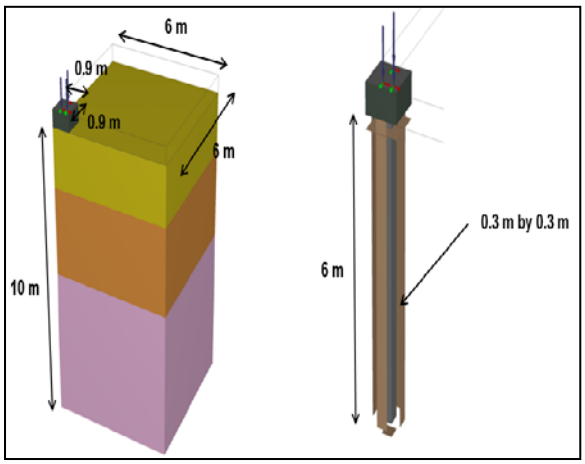

Fig. 6. Mesh of the finite element of piled raft model (2×2) for vertical loading.

By plotting a load-settlement curve for the results, it can be realized that there is a very good matching (93%) between the finite element and experimental results. This indicates that these results agreement. Fig. 7 presents load-settlement curve behavior for the piled raft foundation with a comparison between the experimental and PLAXIS-3D results for the case (2×2).

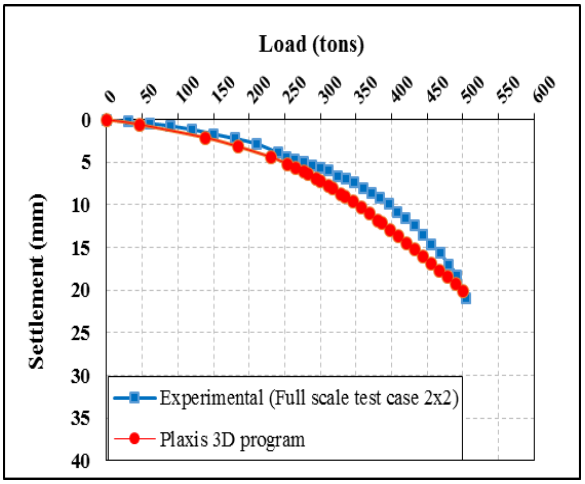

Fig. 7. Load-settlement curve showing a comparison between experimental and PLAXIS-3D results for case (2×2) PRF.

Parametric Study

The behavior of piled raft foundation is influenced by several parameters in the design of piled raft. It is important to take into consideration these parameters to achieve the objective of economic construction with a satisfactory performance. The parametric study presented in this paper was carried out with a computer program based on the finite element method. The reliability of the numerical simulation by PLAXIS-3D was verified by real scale tests as shown in Fig.

8. Based on these results, this work presents the influences of the parametric study for investigating the optimum design for a piled raft foundation. The piled raft model is considered to be subjected to vertical load. The study investigates the effects of changing the parameters on the load-settlement behavior such as: number of piles, raft thickness, the spacing between piles and water table depth. This study will help practicing engineers in recognizing the preeminent and economical qualities of optimizing pile arrangement in designing piled raft.

Influence of Pile Spacing

The effect of the pile spacing (3d to 7d) on the piled raft behavior is studied for the settlement of the piled raft for a value of intensity of loading as 500 tons. In this analysis, the raft thickness is 0.6 m and the dimension of the raft will increase with increasing pile spacing. The piles are 30cm×30cm in dimension and 6m in length. Numerical analysis output of PLAXIS-3D for the pile spacing ranging from 3d to 7d have been presented in the load settlement behavior as shown in Fig. 8. The output shows:

1. Increasing the spacing of piles from 3d, 5d and 7d leads the decrease the total Settlement of the piled raft foundation by 54.7% and 34.2% respectively.
2. This parameter is not safe because duo the increasing of spacing between piles, the load transformed the soil beneath the raft will be increased.

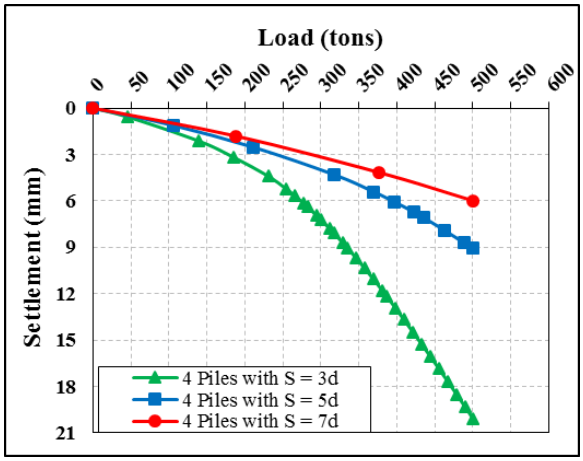

Fig. 8. Influence of pile spacing on load settlement behavior.

The present study shows that the maximum spacing of piled raft system be 5d must because for any increase more than this distance will cause a differential settlement with transmission of carrying loads from piles to raft. This will cause an increase in the displacement at the top of raft with a decrease around the piles as shown in Figs. 9 to 11.

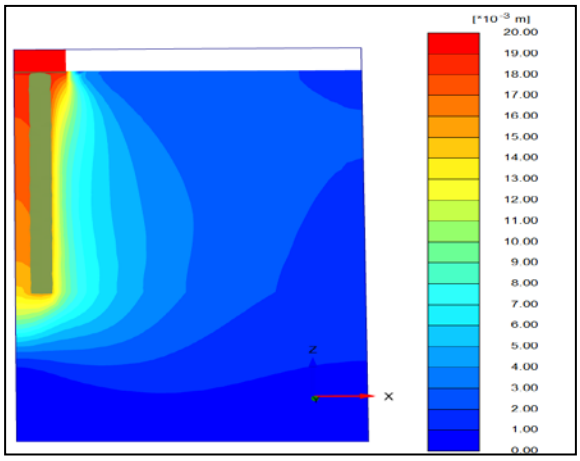

Fig. 9. The distribution of deformation of pile spacing 3d between piles.

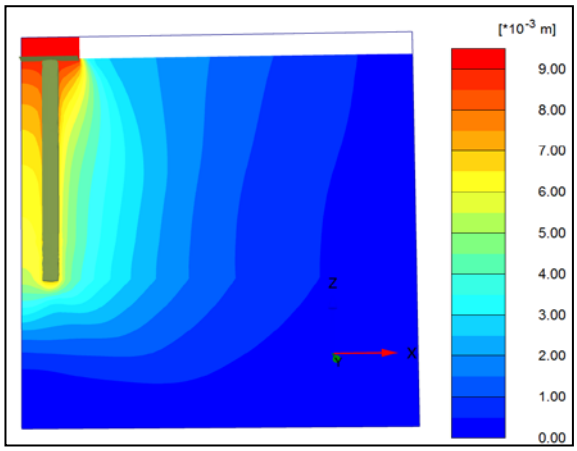

Fig. 10. The distribution of deformation of pile spacing 5d between piles.

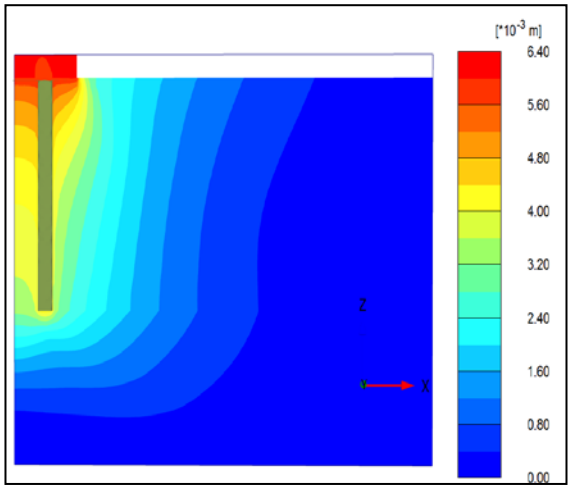

Fig. 11. The distribution of deformation of pile spacing 7d between piles.

Effects of the Number of Piles

Increasing the number of piles is another option that is used commonly in design to reduce the total and differential settlements. This section investigates the effects of increasing the number of piles on reducing the settlements of piled rafts subjected to maximum loads 500 tons. For piled raft models, the raft thickness is 0.6 m and pile length is 6.0 m. The numerical analysis output of PLAXIS-3D for the number of piles 4, 9 and 25 have been presented in the load settlement behavior as shown in Fig. 12. From this figure it can be observed that when the settlement is 20 mm, the ultimate loads at the number of piles 4, 9 and 25 are 500, 800 and 1450 tons respectively. But this effect is due to an increase number of piles as well as due to increasing raft dimensions. The general trend explains that increasing the number of piles will decrease the settlements of a piled raft. However, increasing the number of piles also adversely affects the economical design and it should be carefully minimized.

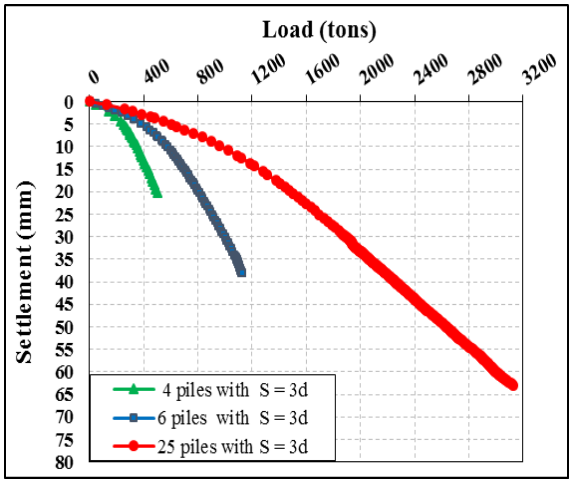

Fig. 12. Influence of the number of piles on load settlement behavior.

Influence of the Raft Thickness

A piled raft system with 25 piles supporting rafts have been investigated to the raft thickness influences on pile raft foundation behavior with the following characteristics: varying thicknesses (0.45, 0.6 and 0.9 m) with piles sizes of 30×30 cm, length of piles of 6 m, spacing of piles is 3d for a maximum load 3125 tons applied as uniform distributed load on square rafts of 22.5×22.5 m with different thicknesses. Quarter of the problem is analyzed using the finite element program PLAXIS. Fig. 13 shows the raft center settlement for various raft thickness in this study. It was found that the raft thickness has no effect on the load settlement relationship of piled-raft foundations. Other researchers reported the similar observations regarding the effect of raft thickness. "Reference [12] reported that raft thickness has little effect on the maximum settlement of piled-raft foundations on sand soil." While, "reference [13] reported finite element analyses of piled-raft foundations and showed that the raft thickness has little effect on maximum settlement in soft cohesive soils." From the present results, it can be concluded that increasing the raft thickness is effective primarily in reducing the differential settlement.

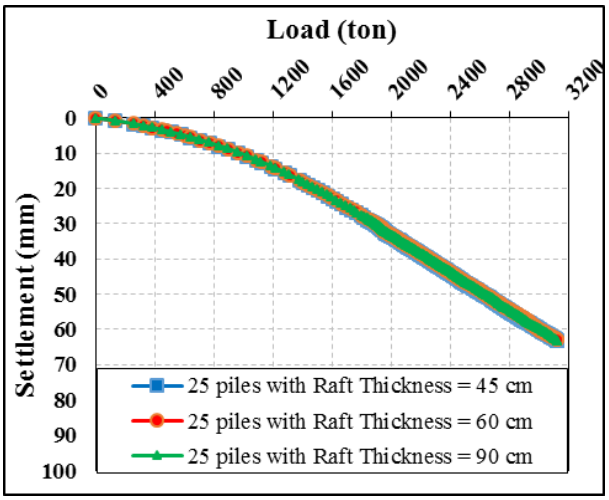

Fig. 13. Influence of the raft thickness on load settlement behavior applying uniform load.

Effects of the Water Table Level

A piled raft system with 4 piles supporting rafts with piles sizes of 30×30 cm length of piles of 6 m, spacing of piles is 3d and varying water depth (0.0, -3, and -10 m) for a maximum load 500 tons applied as uniform distributed load on square rafts of 1.8×1.8 m have been investigated to the water table depth influences on pile raft foundation behavior. Quarter of the problem is analyzed using the finite element program PLAXIS-3D. Fig. 14 shows the maximum piled raft settlement at center for various water depths. From this study, it was found that the water table has an effect on the load settlement relationship of piled-raft foundations in the case of fully saturated. The output shows:

- In the absence of water, (dry case) the maximum settlement is 20.1 mm at total applied load 500 tons. When the water level is lifted up to half the length of piles (partially saturated), note the slightly change in the maximum settlement to 23.1 mm applying the same load.
- When the water is on the ground surface (fully saturation), the total and differential settlement of the piled raft foundation increases by about 53.3% compared with dry condition due to increase in shear stress as shown in Fig. 15.

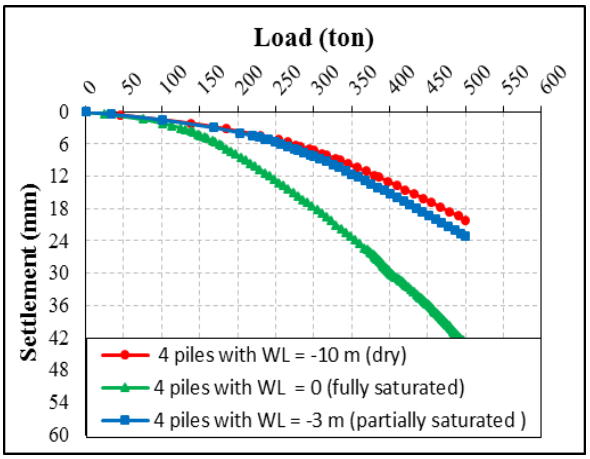

Fig. 14. Influence of the water table on load settlement behavior.

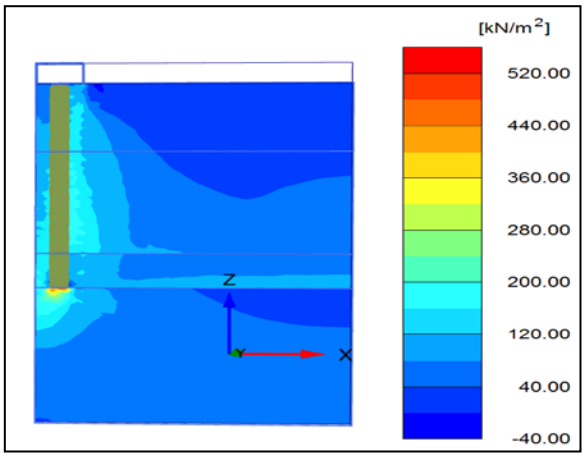

Fig. 15. Shear stress distribution duo to water level at surface.

V. Conclusion

In the light of full scale tests and finite element analysis, the following conclusions can be drawn:

1. Increasing the spacing of piles from 3d to 5d and 7d decreases the maximum settlement of the piled raft foundation by about 54% and 34%, respectively. Increasing piles spacing > 5d is not safe as the load transferred with a considerable increase from the pile to the raft foundation, therefore, the maximum spacing between the piles must be not exceed 5d to improve the piled raft system.
2. The total settlement of the piled raft decreases due to increasing the number of piles when the settlement is 20 mm, the ultimate loads at the number of piles 4, 9 and 25 are 500, 800 and 1450 tons respectively. This parameter is considered uneconomic because the gain in bearing capacity is small.
3. The thickness of the raft (pile cap) has no effect on the bearing capacity of the piled raft foundation. When the raft thickness is increased from 45, 60, 90 and 180 cm, for example, the maximum settlement of the piled raft foundation increases by 1.6%, 0.2% and 1.25% respectively. This slight increase of settlement is due to the increase of the dead loads of cap.
4. When the water approaches the ground surface, the total and differential settlement of the piled raft foundation increases by about 53.3% compared with dry condition therefore, the piled raft system is not advisable to be used in the saturated soils and water treatment plants even if the soil is dry for fear of water leak in the future.

REFERENCES

[1] F. Hartman, and P. Jahn, "Boundary element analysis of raft foundations on piles," Kluwer Academic Publishers, and Netherlands, *Meccanica*, vol. 3, 2001, pp. 351–366.

[2] J. Hooper, "Observations on the behavior of a piled-raft foundation on London clay," *Proc. Inst. Civ. Engrs.*, vol. 55, No. 2, 1973, pp. 855-877.

[3] E. Davis, and H. Poulos, *Pile foundation analysis and design*, Wiley, 1980.

[4] *J. B. Burland, B. B. Brooms, and V. F. B. De Mello*, Behavior of foundations and structures, in *Proc. of the 9th International Conference on Soil Mechanics and Foundation Engineering*, Tokyo, Japan, vol. 2, 1977, pp. 495-546.

[5] Prakoso, W.A. and Kulhawy, F.H., "Contribution to piled raft foundation design," *J. Geotechnical and Geoenvironmental Engineering*, vol. 127, No. 1, 2001, pp. 17-24.

[6] O. Reul, and M. F. Randolph, "Piled rafts in over consolidated clay: Comparison of In situ Measurements and Numerical Analyses," *Geotechnique*, vol. 53, No. 3, 2003, pp. 301-315.

[7] R. Katzenbach, U. Arslan, C. Moormann, and O. Reul, "Piled raft foundation interaction between piles and raft," *Darmstadt Geotechnics*, Darmstadt Univ. of Technology, No. 4, 1998, pp. 279-296.

[8] M. W. O'Neill,"Piled Rafts in Geotechnical Practice – An international perspective," *Proc. 10th. International Conference on Piling and Deep Foundations*, Amsterdam, 2006, pp. 197-208.

[9] H. G. Poulos, "Methods of analysis of piled raft foundations," *A report prepared on behalf of Technical Committee TC18 on piled foundations*, 2001.

[10] *PLAXIS, Vermeer and Brinkgreve:* Manual, 2004.

[11] *ASTM D1143*: Standard test method for piles under static axial compressive load, American Society of Testing and Materials, 2007.

[12] E.Y. N. Oh, M. Huang, C. Surrak, R. Adamec, and A .S. Balasurbamaniam, "Finite element modelling for piled raft foundation in sand," *Eleventh East Asia-Pacific Conference on Structural Engineering & Construction (EASEC-11)*, Building Sustainable Environment, Taiwan, 2008, pp. 1-8.

[13] A. K. Singh, and A. N. Singh,"Experimental study of piled raft foundation," *Proc. of Indian Geotechnical Conference*, December 15-17, 2011, Kochi (Paper No. D-378), 2011.

Prof. Dr. kais Taha Ismael Al-Shallash received the B.Sc. Civil Engineering, 1971, University of Baghdad, College of Engineering , M.Sc. degrees in Civil Engineering (Soil Mechanics & Foundation Engineering), 1974, University of Baghdad, College of Engineering, and the Ph.D degree in Geotechnical Engineering, 1979, University of Sheffield, England. Since 1996, he has been a Professor.

From 1974 to 1976 he was Piling Engineer, Piling Division, State Constructional Contracting Company, Baghdad. From 1979 to date is a consultant into a number of companies such as (Al-Mansur, Al-

Rasheed, and Idrisi Center). Since 1979 to 2014, he has been a lecture with the Building & Construction Engineering Department/ University of Technology. He is the supervisor of more than 53 post graduate (M.Sc. and Ph.D.) students, He has published more than 140 scientific research and two patents.

Prof. kais selecting a member of the Authority Foundation for the University of Uruk l in Baghdad and is now currently teaching at the College of Isra University - Department of Civil Engineering.

Prof. Dr. Hussein Hameed Karim received the B.S. and M.S. degrees in Earth Science/ Geophysics from the University of Baghdad, in 1978 and 1982 respectively, and the Ph.D. degree in Engineering Geophysics from University of Baghdad in 1996, Iraq.

From 1983 to 1997 he was within the academic staff of University of Basrah and graduated from Asst. lecturer to Asst. Professor. Since 1997 he is within the academic staff of University of Technology. Since 2000, he has been a Professor with the Building & Construction Engineering Department/ University of Technology. He is the supervisor of more than 45 post graduate (M.Sc. and Ph.D) students, the author of 5 books, and one under preparation, more than 100 scientific researches, more than 100 scientific articles, and two patents. His research interests include Engineering Geophysics, Soil & Rock Mechanics, Site Investigation, and Geomatics Engineering.

Prof. Karim was chosen by the Committee of University of Technology as the 1st Professor in the University of Technology for the academic year (2010-2011). Prof. Karim's awards and honors include training session to Bordeaux University- France (4 months, 1984); Visiting Professor to University of Hodeidah University- Yemen (3 months, 2002); Visiting Professor (one month, 2010) to Malaya University- Kuala Lumpur, Malaysia; and 3 Professor Visits sponsored by DAAD (Germany), Bauhaus University- Weimar 2006, Rhur University – Bochum 2010 and 2014 (3-months for each).

Dr. Hussein Hadi Hussein holds the B.Sc. and M.Sc. degrees in Civil Engineering from Building & Construction Dept. University of Technology, Baghdad, Iraq in 2002 and 2008 respectively, and the Ph.D degree in Geotechnical Engineering from University of Technology in 2015, Iraq. He is a member of Iraqi Engineers Union IEU, American Society of Civil Engineers ASCE and American Institute of Steel Construction AISC.

From 2000 to present he was within the staff of Al-Tariq Bureau for Engineering Consultation and Pile Tests, he has done papers and studies related to the foundations.

Dr. Hussein participated in several specialized courses outside of Iraq in the field of the foundations and piles engineering such as: Pile Driving Analyzer® (PAX), Pile Integrity Tester (PIT), PDA-W®, CAPWAP®, PIT-W® Professional, October 2011, Turkey.
Pundit Lab (+) operator training course, 20th December. Proceq Middle East, UAE. Advanced two courses on PLAXIS software, Computational Geotechnics held on 14-16 October 2014 & 29-31 March at American University in Dubai, United Arab Emirates.

An Experimental Investigation of Relation between Bearing Capacity of Fiber Reinforced Polymer Piled Raft and Stress Distribution of Sandy Soil

Hüseyin Suha AKSOY and Mesut GÖR

***Abstract*—Engineers are use piled raft as foundation for centuries. Driven piles are generally used for transmit building loads to the stiff soil layer. Moreover they can be used as friction pile. Because of long life in water, wooden piles are preferred for centuries. In 20th century steel used as pile material, because of advances of pile driving technology and economical difficulties. Nowadays, decreasing natural resources prompt to discover alternative pile materials. Fiber-reinforced polymer (FRP) is a economic material and it has very long life span in harsh environment. In this study, FRP model piles are vertically loaded in sand soils which prepared 10%, 40% and 65% relative density. As a result of the experiments conducted, bearing capacity and settlement graphics of the FRP piled raft foundation were obtained. Also, stress variations occured within the soil mass with loads and settlements were determined.**

***Index Terms*— Bearing Capacity, FRP, Relative Density, Piled Raft, Pressure Bulb**

I. Introduction

PILED foundation is a foundation system used since Romans. Wooden piles are still in-service even after centuries. Wood to have almost an infinite life under water is the most important reason for the preference of wooden piles. The use of wooden piles decreased because of environmental and economical reasons. In our day, driven piles are generally manufactured from steel. However, steel is an expensive material and it is quickly destroyed in the sea water or if the ground water contains harmful substances. This destruction is due to the presence of oxygen. Therefore, such piles often have short life spans in sandy soils.

The bearing capacity of a pile consists of the sum of two quantities. These are toe strength and frictional resistance due to adhesion and friction along the peripheral surface of pile. Piles are practically divided into two:

1. End-bearing piles where a great part of the load is transferred to a stiff soil layer;
2. Friction or floating piles where toe strength is at an insignificant level and the load is carried by the frictional resistance to a large extent.

Experimental studies performed showed that theoretical calculation methods used in the designs of piles were not valid for all types of soil and different calculation methods were needed for stratified soils.

Natural resources are not endless and it is known that they will run out one day in case they are not used well. Solid waste storage creates environmental and economic problems with each passing day. Therefore, recycling and reuse of wastes are important for the environment and economy in order to prevent waste of resources and energy crises. Having all these in mind, it is inevitable plastic material to be used in pile manufacture due to its feature of waste recycling and it is economic and long-lasting even under adverse conditions such as sea water [1]. Plastics are flexible (ubreakable) owing to their chemical structures. However, their mechanic strength is low. Therefore, plastics are reinforced with glass fiber and the like materials on the purpose of enhancing their mechanical properties. Fiber-reinforced polymer (FRP) is obtained by moulding of reinforced material (glassfiber) together with carring matrix (resin). Polyester resins are polymerized by a chemical reaction and transformed into a hard, nonsoluble and non-melting substance and take the shape they are moulded. FRP elements are used in aircraft industry since 1940s due to their advantages such as strength, lightness, high corrosion and chemical resistance and fatigue strength [2]. FRP's specific strength value σ_{max}/γ is 60 times higher than the specific strength value of high-strength steel [3].

It is seen that the plastic material has started to be used increasingly in the solution of soil problems in recent years. For example; plastics are used as geogrid, curtain of sheet piling, anchorage and pile materials. Plastic is a very cheap material comparing to steel. Sections obtained from products similar to FRP, which is named as reinforced plastic, can be used as end bearing piles due to they have sufficient strength. Besides, due to they have a higher frictional strength, they can be used as friction pile as well.

H. S. Aksoy is with Dep. Civil Engineering, Faculty of Engineering, Firat University, Elazığ, 23100 Turkey. (e-mail: aksoy.suha@gmail.com).

M. Gör is with Dep. Civil Engineering, Faculty of Engineering, Firat University, Elazığ, 23100 Turkey. (e-mail: mesutgor@gmail.com).

There were a lot of studies about piled raft in the literature. Sawwaf worked on the determination of the bearing capacities of piled raft foundations loaded eccentrically. He performed model tests using piles mounted and unmounted to raft and determined that the increase of density of sand was very effective in raising the bearing capacity of piled rafts especially in short piles. He reported that the short piles placed close to the raft edge decreased both settlements and rotations of rafts more efficiently and the settlement performances of piles mounted to raft were much higher than the unmounted ones [4]. Ashford and Jakrapiyanun compared the penetrabilities of FRP tube filled with steel and concrete, FRP and plastic covered steel piles manufactured with two different methods. The performed tests showed that all FRP piles had bearing capacities similar to steel and reinforced concrete piles. Authors suggested the use of FRP covered piles especially in regions exposed to harsh environment conditions [5]. Piles bear loads via point bearing and skin friction. It is known that the pile material can change the bearing capacity especially in friction piles. Gireesha and Muthukkumaran examined the interface frictions of sand soils with wooden, steel and concrete materials. They stated that the increase in relative density increased the angle of interface friction [6]. Besides, Acar et al. determined that the friction angle increased with relative density. They obtained the following results given in Figure 1 [7]. Sakr et al. modelled the driving pile by filling a FRP tube with thinning section (from large to small diameter) with self-compacting concrete. They modelled the driving pile numerically and compared it with the test results and stated that the FRP tube piles could be used safely in stiff sands, piles with downwardly thinning sections could be driven more easily comparing to cylindrical piles, FRP piles showed driving behavior similar to steel and reinforced concrete piles and buckling - torsion behaviors could be seen in case of the use of empty FRP tubes [8]. In addition, many researchers performed both experimental and numerical studies on the geometries and bearing capacities of pile groups and the bearing capacities of piled raft. Studies on piled raft still continue in our day. [9-12].

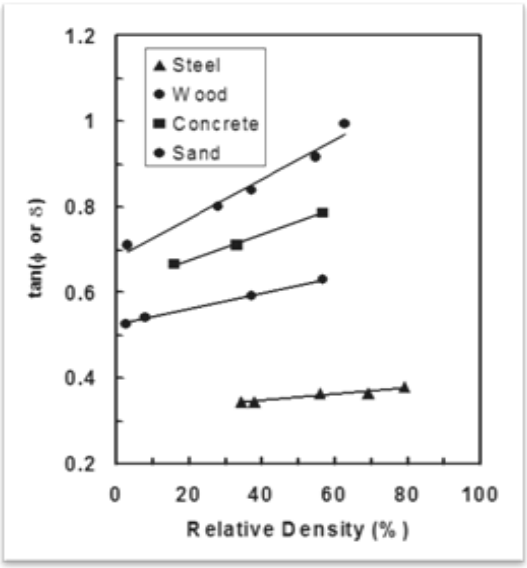

Fig. 1. Relative density and skin friction angle relationhip [7].

In this study, model tests were performed on the purpose of determining the bearing capacities of 3x3 FRP piled raft foundation on soils prepared in different relative densities. It was determined how the bearing capacity of FRP piled raft foundation was affected in soils with different relative densities.

II. MATERIAL AND METHOD

River sand to be used in model tests performed in the laboratory was provided and prepared in appropriate granulometry by being washed and sieved. The total volume of the prepared sand was $2m^3$. 350mm long (L) and 10mm diameter (D) FRP bars were provided for the modelling of piles and a 150x150mm raft suitable for these bars was produced in CNC counter. Due to positive reasons below, FRP was chosen as the pile material instead of conventional pile materials (e.g. steel, wood).

1. It was taken into consideration the increasing costs of wooden materials and that natural resources such as steel could deplete.
2. FRP is an economic material.
3. FRP is long-lasting under adverse conditions such as sea water.
4. Before FRP is preferred as the pile material, loading tests were performed on steel piles under same conditions and sizes with FRP piles in the laboratory. In these preliminary tests performed, it was seen that the pile raft foundations made of FRP had 15% to 25 % more bearing capacities comparing to the piled raft made of steel piles in the same sizes.

The stress variations within the soil mass were measured through transducers (pressure gauges). The test results were computerized by using digital data logger.

A. Properties of the Soil Used in Tests

River sand provided from the sand pit established in Elazığ Province Murat River Basin was used in the laboratory tests. The river sand material was basaltic and in black tones. The particle size distribution curve of the soil used in tests is seen in Figure 2. Thus, it was determined that this soil is a poor graded sand (SP).

The piles and pile cap (raft) used in the tests were manufactured respectively from FRP material and steel. The sub-ground layer, where pile toes would be driven, was prepared at 90% relative density and the upper layers were prepared at 10%, 40% and 65% relative densities in order to determine the bearing capacity variations in soils with different relative densities. Thus, the bearing capacities of the FRP friction piles driven to stiff soil and to soils in different densities were determined and compared. Transducers were placed within the soil at certain intervals while forming the sand layers.

As a result of the tests performed conforming to ASTM

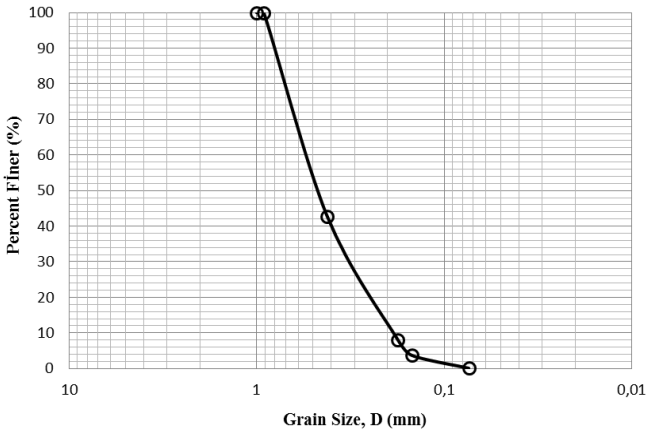

Fig. 2. Particle size distribution curve.

C127-15, ASTM D854-14 and ASTM D422-63(2007)e2 standards on the soil used in the experiments, the index properties of this soil were obtained and shown in Table 1 [13-15].

TABLE I
INDEX PROPERTIES OF THE SOIL

Specific Gravity, G_s	2.67
D10 (mm)	0.18
D50 (mm)	0.45
Maximum – Minimum Grain Size, D_{max}-D_{min} (mm)	1 - 0.074
Maximum Unit Weight (kN/m^3)	17.5
Minimum Unit Weight (kN/m^3)	14.3
Minimum Void Ratio, e_{min}	0.553
Maximum Void Ratio, e_{max}	0.903

B. Properties of FRP Piles and Raft

Propetries of the FRP piles used in the experiments were received from the manufacturer and shown in Table 2.

TABLE II
PROPERTIES OF THE FRP PILES USED IN THE EXPERIMENTS

Compressive Strength (MPa)	200
Tensile Strength (MPa)	240
Tensile Elasticity Module (GPa)	23
Density (gr/cm^3)	1.8
Glass Fiber Rate (%)	50

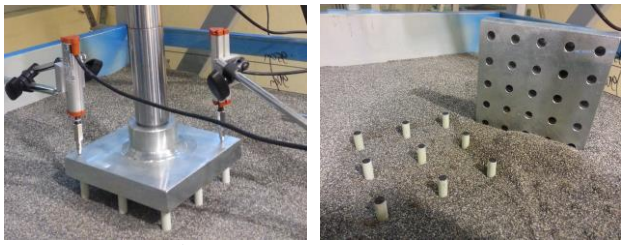

Plate 1. Pile Cap (Raft) and FRP Piles

Pile cap (raft) dimensions were 150x150x25mm and it was manufactured from st37 steel material on CNC counter and covered with galvanic for preventing corrosion. Pile cap and FRP piles are seen in Plate 1.

C. Properties of the Test System

In the model experiments, stress-deformation relation was observed with 150x150mm raft plate and 350mm long (L) and 10mm diameter (D) piles within in the sand tank having the sizes of 750x750x1000mm. Tank sizes were determined in a way to provide semi-infinite media in pile loading tests to be performed. Studies in the literature show that width of square foundation (B) to be 1/5 of the tank dimensions would be enough to create a semi-infinite media [16-19]. Due to pile length was 350mm and the height of the sand in the tank was 900mm, the remaining distance as from the pile toe would be 600mm. This distance is approximately 2L and it is enough to create a semi-infinite media. [16, 18, 20, 21]. The sand soil was placed within the sand tank in 100mm layers and desired

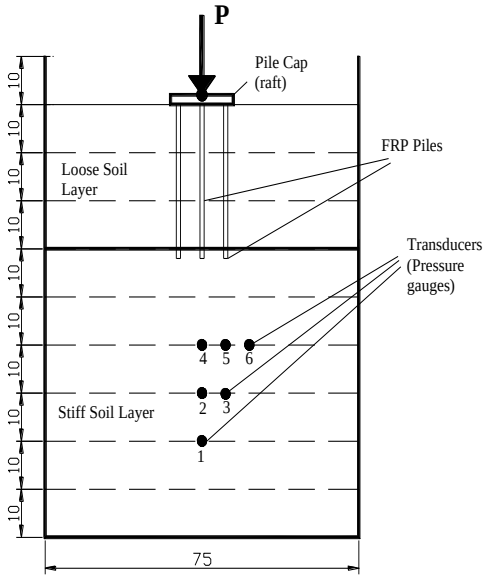

(a)

(b)

Fig. 3. Test System

relative densities. The transducers were put between the sand layers, into the places shown in Figure 3a. The loading was made in a way to create 2.0mm/min mean deformation rate in the experiments. Transducers were placed in different points within the soil mass. By means of these transducers, the stress variations in different points within the soil mass are computerized during the test. Deformations, load and values received from the transducers placed within the soil mass were computerized using a data logger in a way to become 2 data sets per second. The details of the test system are shown in Figure 3b.

III. RESULTS AND DISCUSSION

The sublayer inside the sand tank was prepared by soil with 90% relative density and 600mm height in all tests. Many relative flow tests were performed by pouring sands from various heights in order to obtain the stiffest substrate layer within the tank before performing the pile loading tests. 90% of relative density could be obtained as the stiffest sublayer; so, it was chosen as the relative density of the sublayer. One of the tests performed for relative density is seen in the Plate 2. Sand soils having 300mm of heights and 10%, 40% and 65% relative densities were laid on this layer. The FRP piled raft placed in 3x3 order was loaded within this sand tank in the tests. The piles were placed with 6D of intervals (from pile

Plate 2. Test of Relative Density

center to pile center). The layout of the piles was shown in the Figure 4. Settlements in piled raft plate were measured by 2 strain meters (potentiometers) placed on the raft plate seen in Plate 1. These two potentiometers were placed diagonally to the corners of the foundation plate and the resulting settlement values were averaged. The resulting settlement values were

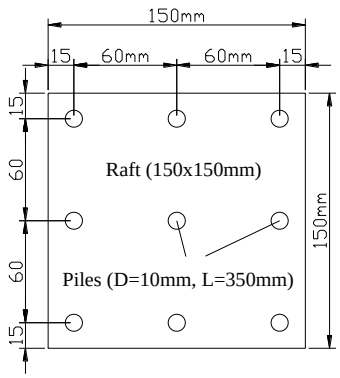

Fig. 4. Design of 3x3 FRP Piled Raft

computerized through the data logger during the tests. Measured loads in the tests performed and the variation of settlements are seen in Figure 5.

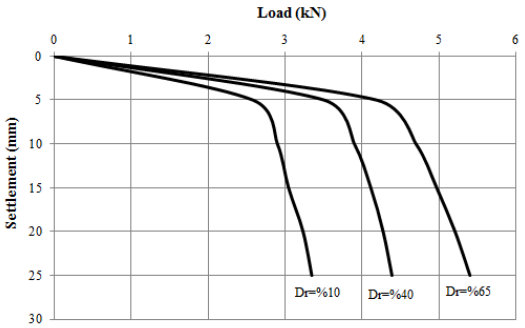

Fig. 5. Load-Settlement Curves

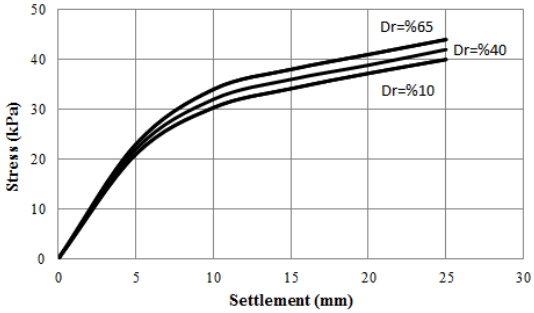

Fig. 6. Variation of Settlements and the Measured Stress by the Nearest Pressure Gauge to the Pile Ends (Number 4)

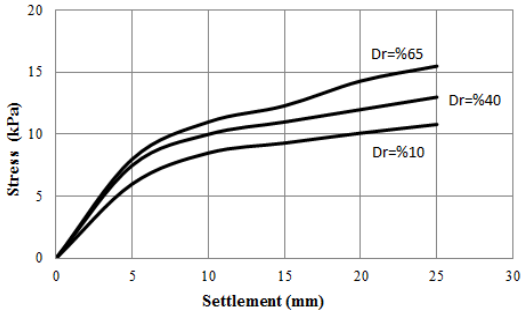

Fig. 7. Variation of Settlements and the Measured Stress by the Furthest Pressure Gauge to the Pile Ends (Number 1)

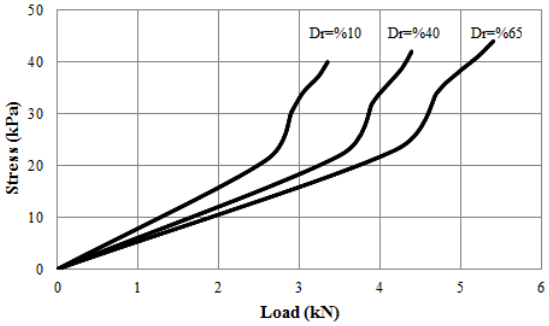

Fig. 8. Variation of the Applied Load and the Measured Stress by the Nearest (Number 4) Pressure Gauge to the Pile Toes

6 pressure gauges (transducer) were placed inside the soil mass. Variation of the stress values recorded by the nearest

(number 4) and the furthest (number 1) pressure gauges to the pile toes and the settlements of the piled raft are seen in Figure 6 and Figure 7, respectively. The variation of the applied loads and the measured stress are seen in Figure 8 and Figure 9, respectively.

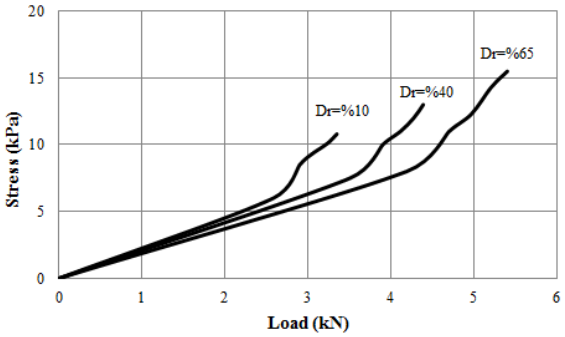

Fig. 9. Measured Stress Values by the Furthest Pressure Gauge (Number 1) to the Pile Toes in Different Relative Density Soils

IV. Conclusion

As a result of the model tests performed, it was seen that the increase in the relative density of the soil increased the bearing capacity of FRP piled raft foundation. It is seen that the bearing capacities of the piled rafts are 2.6kN, 3.5kN and 4.2kN respectively for the relative densities of 10%, 40% and 65% during 5mm settlement in piled raft. Similarly, these values are respectively 2.8kN, 3.8kN and 4.7kN in case of the settlement is 10mm. Maximum stresses occuring in soil mass showed very little increase with the increasing relative density of soil in regions close to pile toes. However, it was determined that the stresses measured with increasing relative densities at the furthest point to pile toes showed a bit more increase. Due to pressure bulb, stresses decreased in all tests as they become more distant from pile toes. Stress transmission within the soil mass became easier owing to grains close up as the relative density increased. So, considering the points where settlements are the same, it is seen that the measured stress values increased with the increase of relative density.

Acknowledgment

The authors are grateful to Firat University, Scientific Research Projects Administration Unit for the support of this project under the Project No: MF.14.19.

References

[1] R.B. Taylor, "Composite recycled plastic marine piling and timber: An alternate to traditional wood products for marine use," *Proceedings, Ports '95, Tampa, FL*,1995, pp. 711-722.

[2] S. Alampalli, J. O'Connor, A.P. Yannotti and K.T. Luu, "FRPs for bridge construction and rehabilitation in New York," *Materials and construction: Exploring the connection, ASCE*, Reston, VA, 1999, pp. 345-350.

[3] *USACE ETL 1110-2-548*, "Engineering and Design: Composite Materials for Civil Engineering Structures," Washington D.C., 31 March 1997.

[4] M.E. Sawwaf, " Experimental study of eccentrically loaded raft with connected and unconnected short piles," *J. Geotech. Geoenviron. Eng., ASCE*, vol. 136, pp. 1394-1402, 2010.

[5] S.A. Ashford and W. Jakrapiyanu, "Drivability of glass FRP composite piling," *Journal of Composites for Construction*, vol. 5, no. 1, pp. 58-60, 2001.

[6] N.T. Gireesha and K. Muthukkumaran, "Study on soil structure ınterface strength property," *Int. J. Earth Sciences and Engineering*, vol. 04, no. 06, pp. 89-93, 2011.

[7] Y.B. Acar, H.T. Durgunoğlu and M.T. Tumay, "Interface properties of sand," *Journal of Geotechnical Engineering, ASCE*, vol. 108, no. 4, pp. 648-654, 1982.

[8] M. Sakr, M.H.E. Naggar and M. Nehdi, "Wave equation analyses of tapered frp–concrete piles in dense sand," *Soil Dynamics and Earthquake Engineering*, vol. 27, issue. 2, pp. 166-182, 2007.

[9] O. Reul, "Numerical study of the bearing behavior of piled rafts," *International Journal of Geomechanics*, vol. 4, no. 2, pp. 59-68, 2004.

[10] B. McCabe and B. Sheil, "Pile group settlement estimation: Suitability of nonlinear interaction factors," *Int. Journal* of Geomechanics, vol. 15, no. 3, 04014056, 2015.

[11] M.Y. Fattah, M.A. Yousif and S.M.K. Al-Tameemi, "Effect of pile group geometry on bearing capacity of piled raft foundations," *Structural Engineering and Mechanics*, vol. 54, no. 5, pp. 829-853, 2015.

[12] Y.S. Unsever, T. Matsumoto and M.Y. Özkan, "Numerical analyses of load tests on model foundations in dry sand," *Computers and Geotechnics*, vol. 63, pp. 255-266, 2015.

[13] *ASTM C127-15*, Standard Test Method for Relative Density (Specific Gravity) and Absorption of Coarse Aggregate, ASTM International, West Conshohocken, PA, 2015, www.astm.org.

[14] *ASTM D854-14*, Standard Test Methods for Specific Gravity of Soil Solids by Water Pycnometer, ASTM International, West Conshohocken, PA, 2014, www.astm.org.

[15] *ASTM D422-63(2007)e2*, Standard Test Method for Particle-Size Analysis of Soils, ASTM International, West Conshohocken, PA, 2007, www.astm.org.

[16] M. El Sawwaf, "Experimental study of eccentrically loaded raft with connected and unconnected short piles," *Journal of Geotechnical and Geoenvironmental Engineering*, vol. 136, no. 10, pp. 1394-1402, 2010.

[17] J. Sadrekerimi andA. Asem, "The effect of pile spacing on bearing capacity of pile groups*," From Research to Design in European Practice*, Bratislava, Slovak Republic, 2010.

[18] B. Yılmaz, "An analytical and experimental study on piled raft foundations," *M.Sc. Thesis*, Graduate School of Natural and Applied Sciences, Middle East Technical University, Ankara, Turkey, 119p, 2010.

[19] B. Bagriacik and M. Laman, "Investigation of the size effect at different geometries on stress distribution of sandy soils," *International Balkans Conference on Challenges of Civil Engineering, BCCCE*, Paper No. 14, Epoka University, Tirana, Albania, 19-21 May 2011.

[20] S. Gök, "Design of piled raft foundations," *PhD Thesis*, Istanbul Technical University, Graduate School of Science Engineering and Technology, İstanbul, Turkey, 101p, 2007.

[21] E. Uncuoğlu, "The behaviour of the piles subjected to lateral load and overturning moment founded in cohesionless soils," *PhD Thesis*, Department of Civil Engineering, Institute of Natural and Applied Sciences, University of Çukurova, Adana, Turkey, 277p, 2009.

Hüseyin Suha AKSOY was born at 1970 in Elazig city (Turkey). He is working as assistant professor in Firat University Elazig-Turkey. He graduated Istanbul Technical University Civil Engineering Dept. at 1992. In 1995 he started to work as a research assistant at Firat University .He graduated MSc at 1996. He earns PhD degree at 2004 from Graduate School of Science Engineering and Technology of Istanbul Technical University. His main research areas are geotechnical engineering and foundation engineering.

Mesut Gör was born at 1983 in Hakkari city (Turkey). He is working as research assistant in Firat University Elazig-Turkey since 2009. He graduated Firat University Civil Engineering Dept. at 2005.He graduated MSc at 2011. He continues his PhD study at Graduate School of Science Engineering and Technology of Firat University (Division of Geotechnical Engineering). His main research areas are geotechnical engineering and foundation engineering.

Prediction of Unconfined Compressive Strength of Soil Using Artificial Neural Network

Dr. Mohammed A. Mahmoud Al-Neami, ***Assistant Professor - Building and Construction Engineering Department-University of Technology***

Abstract— **The limiting shear resistance beyond which the soil collapses or becomes unstable is called the ultimate bearing capacity (UBC). This is also referred to as soil shear failure and results in distortions in the superstructure leading to collapse. The foundation sinks into the ground as if there is no resistance from the soil below. This type of failure is also called bearing capacity failure.**

Therefore, in this paper, Artificial Neural Networks (ANNs) are used in an attempt to predict unconfined compressive strength of clayey soil based on a database comprising a total 150 case records of laboratory measurements for unconfined compressive strength of Iraqi soils which are considered more relevant to cohesive soils.

Three parameters are fed to ANN models which have the most significant impact on (UCS). These include the (liquid limit, dry unit weight and clay percentage), hence they represent the model inputs. On the other hand, the model output is UCS.

The comparison between results obtained from neural network model and the actual results of USC of cohesive soil showed clear superiority and accuracy of neural network technique to predict UCS of cohesive soils. Results also proved that the liquid limit has a significant impact on USC

Index Terms— **Keywords: Artificial Neural Network, ANN, cohesive soil, compressive strength, bearing capacity.**

I. INTRODUCTION

The soil which is supporting the loads transmitted by the foundation should be capable enough so that the structure–foundation–soil system is safe and stable besides being serviceable without excessive settlements.

The unconfined compression test (also called the UCC test) is more relevant to cohesive soils. This is a special case of the unconsolidated undrained triaxial test with no cell pressure (that is, $\sigma 3 = 0$). Hence, it is called unconfined compression test since the vertical compression stress, $\Delta\sigma 1$, is applied until failure. [15].

II. AIM OF STUDY

Sometimes it is difficult to collect undisturbed samples during soil boring process, in addition, preparation of soil samples in laboratory somewhat similar to the original soil accompanied by a lot of difficulties causing changing in properties and behavior of soil need to study. So, the empirical formulas and relationships are used to determine the soil properties such as compressibility of soil. Theses relations don't take into consideration all the variables acting on this property. The aim of this paper was to determine whether neural networks could more closely approximate the relationship between physical properties and unconfined compressive strength than models developed with multiple-linear regression (MLR).

The engineering properties for rock and soil are varied and exhibit unexpected behaviour because the complexity of physical processes related with formation of these materials. [11].

III. EVALUATION OF BEARING CAPACITY

The damages may occur due to foundation failure "collapse" or from excessive settlement. Two important criteria must be considered in calculating bearing capacity of foundation:

1. Foundation must be safe against soil shear failure.
2. Foundation shouldn't undergo excessive settlement.

Unconfined compressive strength of (UCS) of clayey soil or plastic silt is approximately equal to the net allowable bearing capacity as shown in equations below:

$$q_{ult} = C.Nc + \gamma.D_f \quad \text{for } \phi = 0 \qquad (1)$$

$(q_{net})_{ult}$ is defined as the maximum allowable net load intensity (surcharge) on the soil allowing for both shear and settlement. So:

$$q_{ult})_{net} = q_{ult} - \gamma.D_f = C.Nc + \gamma D_f - \gamma D_f \qquad (2)$$

$$q_{ult})_{net} = C.Nc \qquad (3)$$

Taking F.O.S. = 3

$$q_{all})_{net} = C.Nc/3 \qquad (4)$$

$$c = q_{unconfined}/2 \text{ , usually Nc =5.14} \approx 6 \qquad (5)$$

So $$q_{all})_{net} = q_{unconfined} \times 6/2 \times 3 \qquad (6)$$

So $q_{all} = q_{unconfined}$ (7)

Therefore, this study was built on the values of unconfined compressive determined by laboratory testing.

IV. Brief Introduction in Artificial Neural Network

Artificial Intelligence "AI" is simulating biological structure of human brain by software or hardware and artificial neural network "ANN" is a part of Artificial Intelligence "AI", while it has ability of learning to recognize relationship of non-linear input–output. Generally, artificial neural network is a software, or code which learns (train) from a certain data pack (patterns) including inputs data, and outputs data. (ANN) is primarily a multilayer feed forward network under the back propagation learning algorithm used extensively for pattern recognition. [18].

Definition of inputs of the ANN is very important, that affects the results and solution time.

Definition of inputs of the ANN is very important, that affects the results and solution time. Create

V. Application of ANN

The use of (ANNs) has applied and increased in many applications of foundation engineering and soil mechanics. Previous literature shows that artificial neural network have been used to solve various problems in geo-mechanical and have demonstrated more degree of success. Artificial neural network have been used to predict bearing capacity of pile and shallow footing [1] and [6]. Estimation of lateral movements of wall in braced cut [10], predication settlement of structures [16], analysis slope stability [14], used in tunneling design and underground openings[17], determination soil liquefaction phenomena [7], finding the hydraulic conductivity and permeability of soil and [4], determination compaction characteristics [13], predication swelling value of soil [13] , ANN used in a laboratory leaching modeling in gypseous soils [2] and determination delayed compression of gypseous soils [3].

VI. Neural network model

A neural network (NN) provides a method for modelling complex or nonlinear relationships between data. Neural networks were thus trained to predict (UCS) based on experimental data. Data for developing the (NN) are taken from previous site investigation reports. The collected data covers a wide range of soil types and properties. 150 individual cases of Iraqi soils shown in Table 1 are represents a total database used in this study. These data are divided into three groups 97 records for training, 30 records testing and 23 records to validation.

In this study, "back-propagation neural network" is considered. The term back propagation network actually refers to more than one input (a multi layered) feed-forward neural network trained using an error-back propagation algorithm.

TABLE1.

DATABASE USED FOR ANN MODEL DEVELOPMENT.

Location	No. of Cases	Location	No. of Cases
Baquba General Hospital	8	Al-Exindriah treatment plant	13
Communication Towers (Al-Falluja, Anbar, Al-Taji)	7	Al-Mahmoudyah sewage	25
Al-Madaean water project	14	Al-Haswa sewage project	7
Al-Hindyah Barrage	6	Al-Zaafaraniah city	9
Al-Musaib sewage project	19	Baghdad Airport Medical Center	5
Al-Exindriah pumping station	18	Al-Nassiryah anchorages	5
Al-Sweara city	6	Al-Kazamiah Hotel (Baghdad)	8
Total	150		

According to Caudill [5], number of hidden layer nodes must equal to twice number of inputs plus one. Therefore, seven nodes represent the maximum number of nodes in hidden layer needed to create any continuous function for a neural network for three inputs. After examined 7 nodes in hidden layer, non-significant change was observed, so that, one hidden layers was used to build NN in this study.

Neusciences, 2004 software package is used to simulate ANN operation. It was founded that the momentum rate of (0.8) and learning rate of (0.2) and with (0.05) training error represent the best values and suitable to estimate UCS by neural network. These values is compatible with recommendations stated by several researchers have used this program in their research.

VII. Model of input and output

A back propagation ANN architecture is a summation of nodes distributed over a three layers (i. input layer, ii. hidden layer(s), and iii. output layer). Variables of problems are fed in input layer while the output layer includes output variables, or what is being modelled. In statistical terms, independent variables represent in the input layer and dependent variables represent in output layer. The nodes in ANN layers are connected by links and each is carried a weight that shows quantitatively the strength of that connection. Therefore, the strength of each node in network has effect on the other nodes.

The model inputs used include liquid limit (L.L.), dry unit weight (γd), and clay percentage (particles smaller than 5μm) as these variables are considered to have the greatest effect on (UCS). The model output is unconfined compressive strength. Figure (1) represents the input and output models and also shows the transform function used for scaling data in input layer (linear), hidden layer (sigmoid) and output layer (sigmoid).

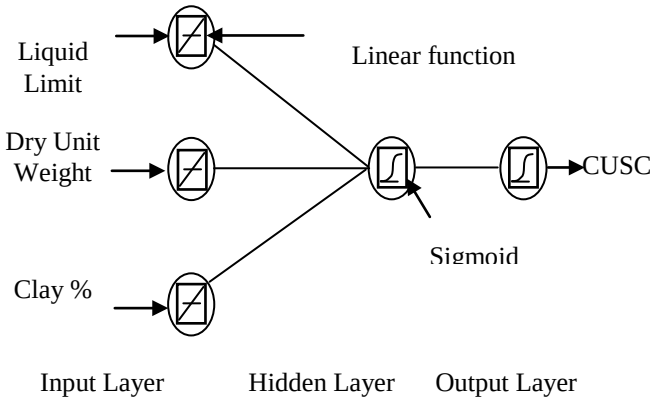

Fig. 1. Input and output models and transform function in ANN layers.

VIII. Analyses and Discussions

Random fashion was implemented to dividing the statistics data in sets of training, testing and validation and where the subsets statistics are taken into account as shown in Table 2. The statistical parameters used include the mean, standard deviation, maximum, minimum and range.

After concerning the neural network model, the performance of the models developed using the data sets whose statistics is shown in Table 2 is checked.

TABLE 2
STATISTICAL PARAMETERS OF INPUT AND OUTPUT USED FOR ANN MODELLING.

Variables / Stat. parameters	Liquid Limit (%)	Dry Unit Weight (kN/m^3)	Clay Content (%)	UCS (kPa)
Maximum	85	18.5	78	191
Minimum	26	13.05	18	4
Mean	52.43	15.48	48.19	62.08
Standard div.	13.83	1.03	12.72	42.37
range	59	5.45	60	187

A comparison between the results of the network and the laboratory is made. Figure 2 gives the plot of the testing set results of estimated versus measured unconfined compressive strength obtained from the neural network model. The plot in this figure shows that the predicted values from the neural networks are closer to those obtained from experimental values (R^2 = 86.75%).

A linear transfer function for the input nodes was employed in network used, where the nodal output is the sum of the nodal input and the bias, and a sigmoid transfer function for hidden and output nodes, Table 3 presents the results obtained by ANN approach.

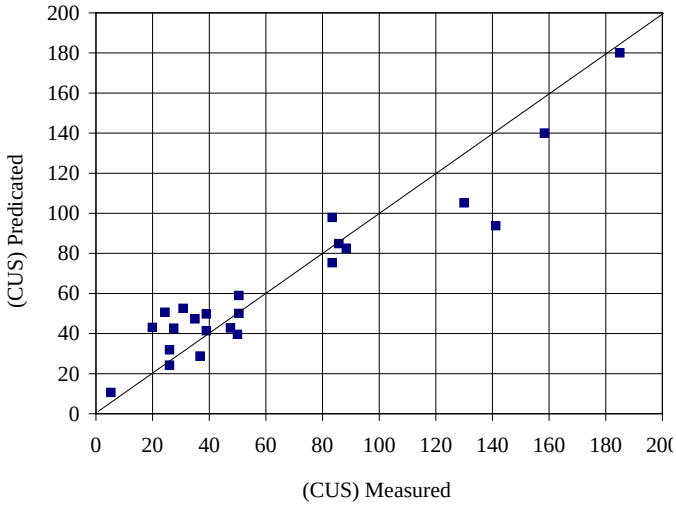

Fig. 2. Comparison between predicted and measured unconfined compressive strengths.

TABLE 3
WEIGHTS AND THRESHOLDS LEVELS OF ANN

Transfer function	Nodes	Weights	Bias
Linear	Input layer to hidden layer		8.26
	Liquid Limit → hidden	-8.45	
	Dry Unit weight → hidden	-3.67	
	Clay % → hidden	-7.10	
Sigmoid	Output layer		-0.23
	Hidden node →Unconfined compressive strength	-0.99	

So that, to translate the relationship between the nodal output and the weighted sum of the nodal inputs into formula where the bias is treated as a constant input, the above connection weights and bias are listed in Table 3. It will be collected together into sigmoid formula to predicate UCS as follows:

$$output = 1/[1+\exp(-\sum weights.x \quad input)] \tag{8}$$

$$CUS = 1/[1+e^{0.23-0.99\tanh x}] \tag{9}$$

where:

$$\chi = 8.26 - 8.45L.L - 3.67\gamma_d - 7.1clay\% \tag{10}$$

It should be noted that, Equation (9) is scaled between (0.0) and (1.0) and in order to calculate the actual values of unconfined compressive strength (UCS) has to be rescaled using the data ranges in the ANN model training tabulated in Table 2 and the following equation:

$$x_n = (x - x_{\min})/(x_{\max} - x_{\min}) \tag{11}$$

Where: χ = input variable - χ_{max} = maximum value of input variable (χ), χ_{min} = minimum value of input variable (χ) , and χ_n = scaled value of input variable (χ).

So, after rescaling and substituting the values of weights and thresholds, Eqs. 9 and 10 become:

$$CUS = \left[{}^{241}\!/_{(1+e^{0.23-0.99\tanh x})} \right] + 4 \qquad (12)$$

where:

$$\chi = 22.547 - 0.14L.L - 0.66d - 0.119\,\text{clay}\% \qquad (13)$$

The ANN model developed in this work is based on limited data records, therefore like all empirical equations, ANN model can be used successfully within the range of data listed in Table (2).

To improve the model developed in this work, Equation (12) was simplified and converted to the number of charts as shown in Figures (3) to (8).

These curves are plotted by taking six values of dry unit weight (13, 14, 15, 16, 17 and 18 kN/m^3) (minimum to maximum values). For each value, the clay percent stilling unchanged while the liquid limit was changed. The numbers on curves represents the percentage of clay.

It is worth mentioning that when the allowable bearing capacity of soil is needed the value of UCS calculated either by Equation (12) or charts must be multiplied by two because qall is twice (Cu).

To clarify the significant impact of input on the UCS; a sensitivity analysis has been evaluated on the results of ANN models using a simple technique proposed by Garson [8] and followed by Al-Janabi [2] and Al-Neami [3]. The results indicate that the liquid limit has the most significant effect on the UCS followed by the clay percent with relative importance 43.7 and 37.4% respectively, while the dry unit weight has the smallest impact (18.9). The results are presented in Figure 9.

These results are conjugates with nature of soil (increasing in liquid limit leads to increase the cohesion due to increase bonding between soil particles.

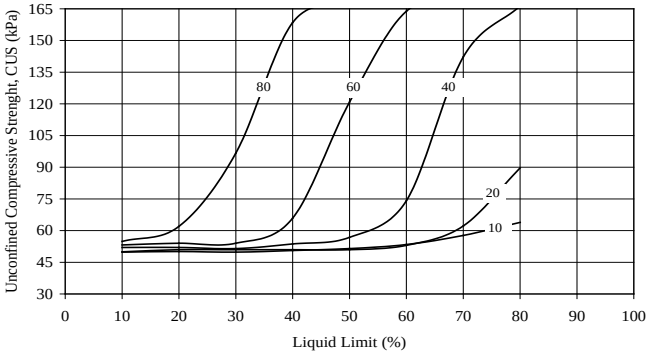

Fig. 3. UCS with L.L. at (13 kN/m^3) dry unit weight.

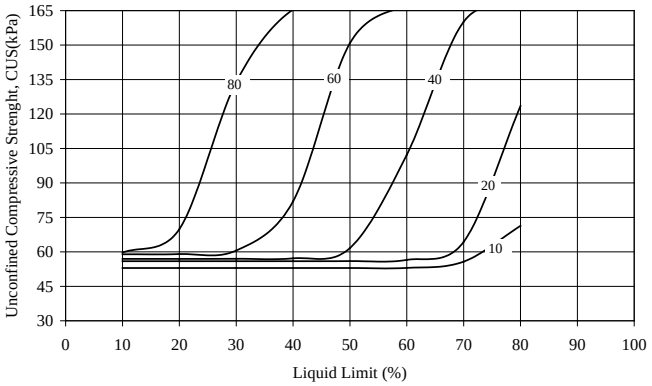

Fig. 4. UCS with L.L. at (14 kN/m3) dry unit weight.

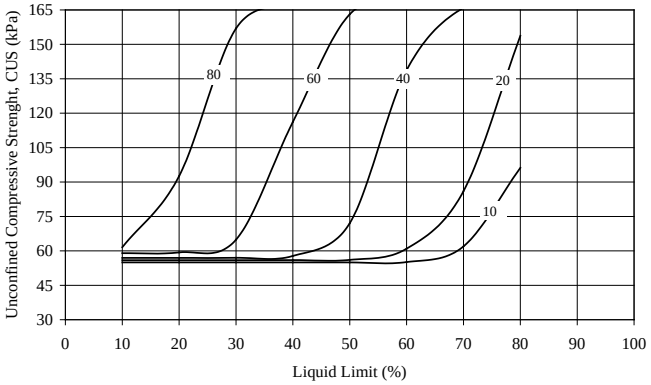

Fig. 5. UCS with L.L. at (15 kN/m^3) dry unit weight.

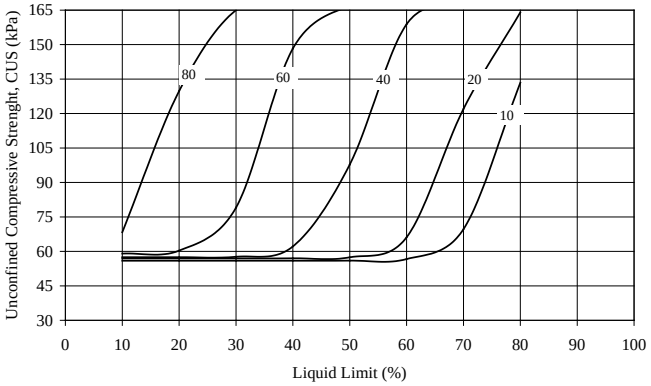

Fig. 6. UCS with liquid limit at (16 kN/m^3) dry unit weight.

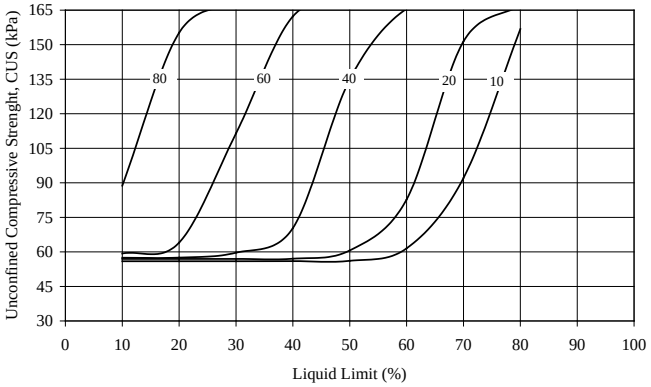

Fig. 7. UCS with L.L. at (17 kN/m^3) dry unit weight.

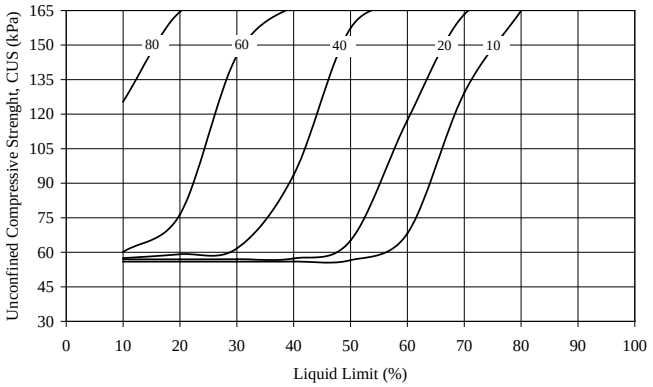

Fig. 8. UCS with liquid limit at (18 kN/m^3) dry unit weight.

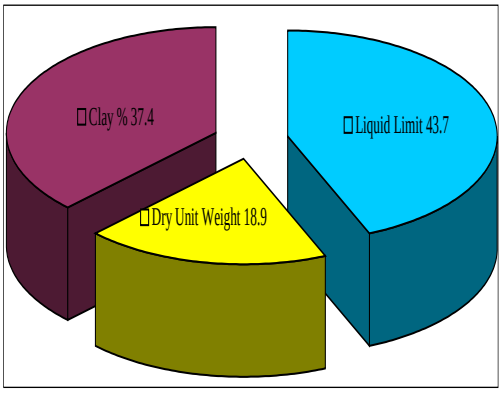

Fig. 9. Relative importance Relative importance.

IX. Conclusions

Based on the results of the study presented in this paper, the following conclusions can be derived:

1) The study conducted that the use of Artificial Neural Networks for predicting the parametric value of unconfined compressive strength is viable. This research advocated that Back-Propagation Algorithm Model has the powerful looming of predicting the (UCS).
2) The division of data on sets (training, testing, and validation) have a significant effect on the performance of network model.
3) Liquid limit and clay percentage showed a largest significant impact on USC while the dry unit weight has the smallest importance effect.
4) NN model provided a good predictive performance when compared the values of UCS obtained by ANN with values of unconfined compressive strength obtained by experience way.
5) Improvements in predictive accuracy may be possible through selection of inputs to maximize nonlinear model performance.

X. References

[1] Abu-Kiefa, M. A. (1998), "General Regression Neural Networks for Driven Piles in Cohesionless Soils", Journal of Geotechnical & Geoenvironmental Eng., ASCE, 124(12), 1177-1185.

[2] Al-Janabi, K.R.M., (2006), "Laboratory Leaching Modelling in Gypseous Soils Using Artificial Neural Network (ANN) ", Ph.D. Thesis, Building and Construction Department, University of technology, Baghdad.

[3] Al-Neami, M.A.M., (2006), "Evaluation of Delayed Compression of Gypseous Soils with Emphases on Neural Network Approach" Ph.D. Thesis, Department of Civil Eng., Al-Rasheed College of Engineering and Science., University of Technology., Baghdad.

[4] Basheer, I. A., Reddi, L. N., and Najjar, Y. M. (1996), "Site Characterization by Neuronets: An Application to the Landfill Sitting Problem", Ground Water, 34, 610-617.

[5] Caudill, M. (1988),"Neural Network Primer, Part III", AI Expert, 3(6), pp.53-59.

[6] Emam, Mohamed Ali and S. Shaaban, (2007), "Prediction of Bearing Capacity of the Soil Using Artificial Neural Networks", Journal of Geotechnical, Helwan University.

[7] Garcia, S.R., Romo, M.P, and Sarmiento, N., (2003), "Modelling Ground Motion in Mexico City Using Artificial Neural Network", Geofisica International, Vol. 42, No.2, pp. 173-183.

[8] Garson, G.D. (1991), "Interpreting Neural – Network Connection Weights", AI Expert 6 (7), 47-51.

[9] Goh, A.T.C. (1996b), "Pile Driving Records Reanalyzed using Neural Networks", Journal of Geotechnical Engineering – ASCE. Vol. 122, No. 6, pp 492-495.

[10] Goh, A. T. C., Wong, K. S., and Broms, B. B. (1995), "Estimation of Lateral Wall Movements in Braced Excavation Using Neural Networks", Canadian Geotechnical Journal, 32, 1059-1064.

[11] Jaksa, M. B. (1995), "The influence of Spatial Variability on The Geotechnical Design Properties of a Stiff, Overconsolidated Clay", Ph.D thesis, The University of Adelaide.

[12] Najjar, Y. M., Basheer, I. A., and McReynolds, R. (1996a), "Neural modeling of Kansan Soil Swelling", Transportation Research Record No. 1526, 14-19.

[13] Najjar, Y. M., Basheer, I. A., and Naouss, W. A. (1996b), "On the Identification of Compaction Characteristics by Neuronets", Journal of Computers and Geotechnical, 18(3), 167-187.

[14] Ni, S. H., Lu, P. C., and Juang, C. H. (1996), "A Fuzzy Neural Network Approach To Evaluation of Slope Failure Potential", Journal of Microcomputers in Civil Engineering, 11, 59-66.

[15] Rao, N. S. V. Kameswara, (2011), "Foundation Design: Theory and Practice", first edition, John Wiley & Sons (Asia) Pte Ltd.

[16] Shahin, M.A., (2003), "Use of Artificial Neural Networks for Predicating Settlement of Shallow Foundations on Cohesionless Soils", Ph. D. Thesis, Department of Civil and Environmental Eng., University of Adelaide.

[17] Shi, J., Ortigao, J. A. R., and Bai, J. (1998),"Modular Neural Networks for Predicting Settlement during Tunneling", Journal of Geotechnical & Geoenvironmental Eng., ASCE, 124(5), 389-395.

[18] Yoru, Yilmaz, T.Hikmet Karakoc, and Arif Hepbasli, (2010), "Application of Artificial Neural Network (ANN) Method to Exergy Analysis of Thermodynamic Systems", Int. Symp. On heat transfer in gas turbine systems, Antalya, Turkey.

رقم الايداع في دار الكتب والوثائق 159 لسنة 2016

المؤتمر الدولي الثاني لهندسة البناء والإنشاءات والبيئة

17-18 تشرين الأول 2015

بيروت - لبنان

الجزء 3: محور الهندسة الجيولوجية والهندسة الجيوتيكنيكية